On the way to columnar liquid quasi crystals – X-shaped bolapolyphiles with branched side chains

Dissertation

zur Erlangung des

Doktorgrades der Naturwissenschaften (Dr. rer. nat.)

Der

Naturwissenschaftlichen Fakultät II
Chemie, Physik und Mathematik

Der Martin-Luther-Universität
Halle-Wittenberg,

vorgelegt

von Herrn Christian Anders

Gutachter:

1. Prof. Dr. Carsten Tschierske
2. Prof. Dr. Rebecca Waldecker
3. Prof. Dr. Torsten Hegmann

Datum der Verteidigung: 14.05.2025

Abstract

Liquid crystalline phases represent an interesting state of matter that exhibits long-range orientational order in combination with molecular mobility. Recently, there have been just a few examples of LCs exhibiting quasiperiodic translational symmetry. This highlights the importance of understanding the quasiperiodic configurations that underpin the mediation of diverse orders and complexities within material structures. This doctoral thesis investigates the design, synthesis, and self-assembly behavior of X-shaped bolapolyphiles as molecular frameworks for inducing quasicrystalline phases. By integrating mathematical analysis and calculations with bespoke synthetic strategies, this work establishes a systematic approach to guiding molecular design toward the emergence of liquid quasicrystals.

The research was conducted as part of a collaborative project between chemists and mathematicians, employing mathematical tools such as the analysis of symmetry groups and molecular structures to predict a molecular design conducive to liquid quasicrystalline order. These insights inform the molecular design of X-shaped bolapolyphiles, whose amphiphilic architecture and anisotropic symmetry are precisely tuned at the triangle-square transition to promote self-assembly into quasiperiodic structures. The synthetic strategies emphasize modularity, thereby facilitating controlled variation in side chain volume, spacer length, and side chain modification.

Experimental studies employing polarized optical microscopy (POM), differential scanning calorimetry (DSC), and small-angle X-ray scattering (SAXS) substantiate the emergence of liquid crystalline phases exhibiting distinct symmetries, including intricate patterns of potential liquid quasi-crystalline and approximant structures.

This work not only advances the fundamental understanding of the formation of liquid quasicrystals but also establishes a robust framework for their rational design. The combination of mathematical analysis and strategic synthesis provides avenues for the design of soft materials with tailored quasiperiodic structures.

Acknowledgment

Here, I would like to express my appreciation for people's help, support, and encouragement. Without them, it would have not been possible to finish this work.

First of all, I would like to thank my supervisor, Prof. Dr. Carsten Tschierske for giving me the opportunity to work under his supervision. It was a great honor. He gave me plenty of scientific knowledge and ideas through countless discussions.

I want to express my appreciation to Prof. Dr. R. Waldecker and Prof. Dr. M. Alaasar for their moral and professional support throughout the work.

Prof. Dr. F. Liu and Dr. Yu Cao, State Kay Laboratory for Mechanical Behavior of Materials, Xi'an Jiaotong University, I would like to thank for the 3-month stay, which led to a deepening of my expertise in the field of structural analysis of liquid crystalline materials, as well as for the synchrotron XRD experiments and GISAXS measurements.

I would like to express my gratitude to the "Deutsche Forschungsgemeinschaft" for providing funding for this project, which this work was a part of. I also would like to thank all the people involved in GRK2670 for their numerous contributions during the workshops.

The in-house X-ray examinations allowed me to perform a thorough characterization of my compounds. I am grateful to Dr. Busse for teaching me how to operate the X-ray equipment and for providing useful insights during several discussions about the data.

I would like to express my gratitude to Mr. R. Gyger for his invaluable contribution to the differential calorimetric studies. I also extend my thanks to Ms. S. Tanner and M. Sc. V. Adjedje from the Macromolecular Chemistry group, under the supervision of Prof. Dr. Binder, for their assistance in preparing the ESI-MS spectra.

I thank Dr. Ströhl and his team for producing several NMR spectra.

I would like to thank Ms. V. M. Fischer for her continuous support, the good cooperation, and professional discussions during the entire work.

Finally, I extend my sincere gratitude to my fellow students, friends, and family for their ongoing support throughout my studies and this thesis.

Table of Contents

List of abbreviations

Abbreviations for solvents and reagents

Et$_3$N	Triethylamine
DMF	*N,N*-Dimethylformamide
DMSO	Dimethyl sulfoxide
DCM	Dichloromethane
Et$_2$O	Diethyl ether
MeOH	Methanol
THF	Tetrahydrofuran
PPTS	Pyridinium *p*-toluenesulfonate
Pd/C	Palladium on activated carbon
TBAI	Tetrabutylammonium iodine
TBABr	Tetrabutylammonium bromine
TMS	Tetramethylsilane
TMSA	Trimethylsilylacetylene
DDQ	2,3-Dichloro-5,6-dicyano-1,4-benzoquinone
PPh$_3$	Triphenylphosphine
Pd(PPh$_3$)$_4$	Tetrakis(triphenylphosphine)palladium(0)
PhI)OCOCF$_3$)$_2$	[Bis(trifluoroacetoxy)iodo]benzene

Abbreviations of the different methods

TLC	Thin layer chromatography
XRD	X-Ray diffraction
SAXS	Small angle X-ray scattering
WAXS	Wide angle X-ray scattering
GISAXS	Grazing-incidence small angle X-ray scattering
POM	Polarization microscopy
DSC	Dynamic differential scanning calorimetry

Abbreviations for mesophases

Col	Columnar mesophase
Col$_{hex}$	Hexagonal columnar mesophase
Col$_{rec}$	Rectangular columnar mesophase
Col$_{squ}$	Square columnar mesophase
N	Nematic mesophase
Sm	Smectic mesophase
SmA	Non-tilted Smectic mesophase
SmC	Tilted Smectic mesophase
HT-phase	High-temperature phase
LT-phase	Low-temperature phase
Cr	Crystalline phase
M	Mesophase of unknown structure
Iso	Isotropic liquid
Cub	Cubic mesophase
Cub$_{net}$	Network cubic mesophase
Cub$_{sph}$	Micellar cubic mesophase
Cub$_{bi}$	Bicontinuous cubic mesophase
LC	Liquid crystal
LQC	Liquid quasi crystal
CLQC	Columnar liquid quasi-crystal

Abbreviations for structural parameter

a,b	Lattice parameter of the respective phase
h	Height of the crystallographic unit cell
V_{Mol}	Molecular volume
V_{Cell}	Cell volume
V_C	Chain volume
L_C	Chain length
L_{Wall}	Length of a honeycomb wall
L_{Mol}	Length of a molecule
$n_{cell,LC}$	Number of molecules per crystallographic unit cell calculated in the LC state
n_{Wall}	Number of molecules per wall segment of the honeycomb structure
n_{Bundle}	Number of molecules per bundle like arrangements in the *rod-bundle-like* cubic phase
$n_{Cell,cr}$	Number of molecules per crystallographic unit cell calculated in the crystalline state
$n_{Cell,liq}$	Number of molecules per crystallographic unit cell calculated in the liquid state
q	Scattering vector
β	Angle included within the columnar phase between the OPE rod and the normal to the longitudinal axis of the column

d Distance between planes of atoms
Δn Birefringence

Abbreviations for NMR-spectra

δ   Chemical shift
s   Singlet
d   Doublet
t   Triplet
m   Multiplet
dd   Doublet of doublets
q   Quartet
J   Coupling constant
ppm   Parts per million

Other abbreviations

OPE   Oligo (*p*-phenylene ethynylene)
FOPE   Fluorinate oligo (*p*-phenylene ethynylene)
EDM   Electron density map
ED   Electron density
Calc.   Calculated
Obs.   Observed
SDS   Sodium dodecyl sulfate
RT   Room temperature

Abbreviations for atomic groups

Tos   *p*-Toluenesulfonyl group
Bnz   Benzyl group
TMS   Trimethylsilyl group
Hal   Halogenide

1 Introduction and motivation

"We may lay it down as an incontestable axiom, …, nothing is created, … nothing takes place beyond changes and modification…." [1]

[Elements of Chemistry by Antoine Lavoisier]

This quote from Antoine Lamarck's book, "Elements of Chemistry," expresses the principle of conservation of mass in chemical reactions. While this principle is typically associated with chemical reactions, it can also be applied to other fields, such as the topic of periodic and quasi-periodic structures, as explored in the context of liquid crystals. The quote suggests that matter can change in form or appearance, but not in essence. Quasi-crystalline structures found in liquid crystalline materials are examples of ordering principles that have unusual and complex arrangements of atoms and molecules. Nevertheless, they are still composed of the same building blocks as their periodic counterparts. They show that matter can transform into different shapes and patterns, but the only things we need to understand are the principles behind the formation.

Nowadays, the basic principle of these organizing processes is the generally applicable process of self-assembly. This process is responsible for forming complex biological systems such as multienzyme complexes,[2] ribosomes,[3] nucleosomes,[4] fibrils,[5] and membranes.[6] This raises the question of the driving forces behind the formation of simple and complex structures by self-assembly. The field of supramolecular chemistry is trying to find an answer to this question. In this field, scientists are trying to describe the formation processes based on identical and different molecules as a function of their inter- and intramolecular interactions. A special area in this wide field of structural research on self-assembly materials belongs to liquid crystals.

1.1 The liquid crystalline state

Besides the commonly known states of matter - solid, liquid, and gaseous - some materials exhibit several other states in between them. One such state is the liquid crystalline (LC) state, which exists between the solid and liquid states of matter, combining fluidity and order. In this state, the molecules are orientationally or positionally ordered in 1D, 2D, or 3D space over long distances. Through a combination of non-covalent interactions, such as hydrogen bonds, dispersion forces, Coulomb interactions, π-π-stacking, and dispersion interactions, this material possesses an outstanding ability to respond to external influences, serving as a perfect subject for the study of the basic principles of this process.

Based on these properties, liquid crystals serve not only as systems for basic research, additionally they show a wide range in the field of applications in our daily life. Smartphone[7] and television displays,[8,9] sensors,[10,11] photovoltaics,[12] and optoelectronics[13] made huge use of liquid crystalline materials. All these examples give an insight into the enormous potential of liquid crystalline materials, which were first discovered and described by Reinitzer[14] and Lehmann[15] in 1888.

Nowadays, various types of liquid crystalline phases are known depending on their structure. First, lyotropic systems,[16] where LC phase formation is strongly dependent on the solvent, temperature, and concentration of an amphiphile. Examples include aqueous solutions of SDS or DNA in water. Second, thermotropic LC systems,[16] where LC phase formation is controlled only by the

temperature change in the pure substance. Finally, the barotropic LC phase[17] is induced by applying pressure to the pure substance, resulting in the formation of the LC state.

The majority of liquid crystals rely on two fundamental concepts: shape anisotropy and amphiphilicity of the mesomorphic materials. The term anisometry refers to the varying geometric shapes of the rigid structural units in all three spatial dimensions. Therefore, molecules can be differentiated by their different shapes, such as calamitic (rod-like)[18], discotic (disk-like),[19,20,21] banana-shaped (bent),[22,23,24] sanidic,[25] and several other structures.[26]
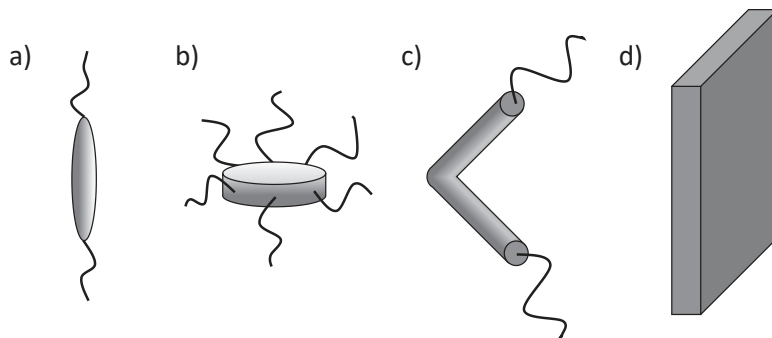

Figure 1.1-1. *Common molecular design of liquid crystalline materials: a) calamitic-, b) discotic-, c) bent-shaped-, and d) board-shaped mesogen.*

They all share the characteristic that their shape gives rise to various types of dispersion forces and steric distraction forces, which are essential driving forces to create a long-range orientation in the liquid crystal phase.[27,28] One type of long-range ordered system is the nematic phase, which is mainly found for calamitic and discotic mesogens. It is characterized by a one-dimensional, long-range orientation order with mesogens aligned parallel along a common direction described by director $\hat{n}$.[29] The alignment of molecules in a side-by-side configuration effectively minimizes the free space while maximizing the attractive interaction forces between them.[30] Modifying this simple phase to generate more complex structures can be achieved by increasing the amphiphilicity of the molecules. Introducing an incompatible molecular structure covalently bonded to the rigid core unit can induce nanodomain formation through a nanosegregation of the incompatible units.[31] In this way, the introduction of flexible alkyl chains leads to segregation into different domains of the flexible alkyl chains and the rigid cores. These segregation processes can be extended by covalent bonding of several different segments, e.g., polar/apolar parts, or aliphatic/perfluoroaliphatic parts, resulting in several different nanodomains.[31] The nature of the interfaces between these domains is determined by the volume ratios of the incompatible molecular parts.[29] This leads to positional ordering, resulting in various phases with one-dimensional (Sm = smectic phase), two-dimensional (Col = columnar phase), or three-dimensional (Cub = cubic phase) lattice.[29] Additionally, these phases can be further differentiated into subgroups based on the arrangement of the mesogens. For instance, smectic phases, which are mostly found in calamitic mesogens, can be arranged in layers with different tilts with respect to the layer normal. A molecule orientation perpendicular to the layer planes indicates a SmA phase, while a tilt angle with respect to the layer normal 0° is typical for SmC phases.
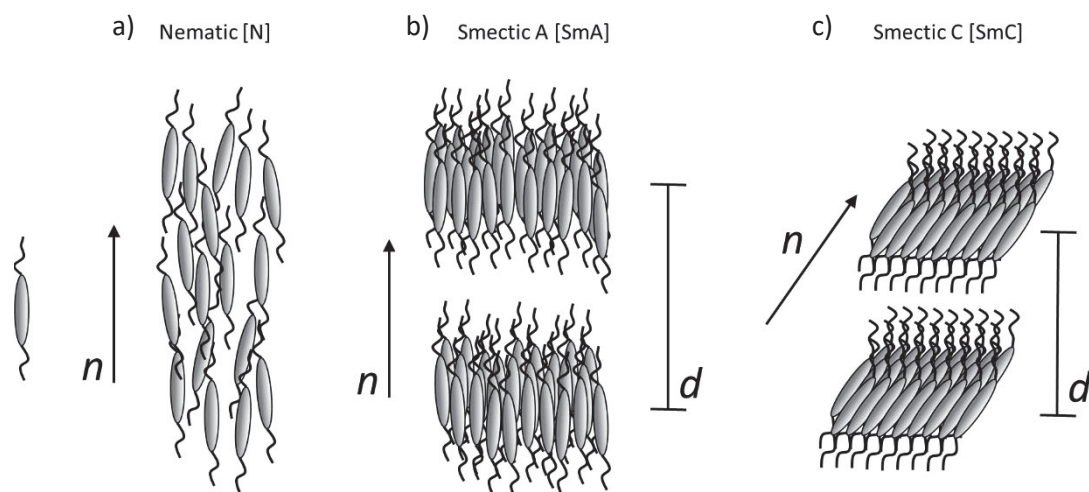
Figure 1.1-2. *Selected liquid crystalline phases of rod-like (calamitic) mesogens: a) nematic phase, b) Smectic A (SmA) phase, and c) Smectic C (SmC) phase.*

Columnar structures, such as those found in discotic mesogens, exhibit a two-dimensional positional order, depending on the interface curvature of the interfaces between columns and alkyl chains, in which molecules arrange in rectangular, square, oblique, or hexagonal 2D lattices. These lattices can be classified into different plane groups.[20] However, columnar phases are not exclusive to discotic mesogens. Mesogens that consist of a rod-like core, with a varying number of covalently bonded flexible chains, can also form columnar structures.[29,32,33]

Increasing the interface curvature of the different molecular nanodomains, e.g., at the transition between lamellar and columnar phases, leads to the formation of different intermediate cubic phases.[34,35] In this case, bi-continuous cubic phases (Cub$_{bi}$), consisting of low-volume compartments filling the networks and the high-volume compartments filling the continuum. With further increase of the interface curvature, columnar phases are formed, with the columnar aggregates formed by the low-volume compartments in the continuum filled by the high-volume compartments.[36] Last, at the maximum interface curvature, micellar cubic phases (Cub$_{sph}$) are formed by spherical aggregates arranged on a cubic lattice in the continuum of the high-volume compartment.[37]

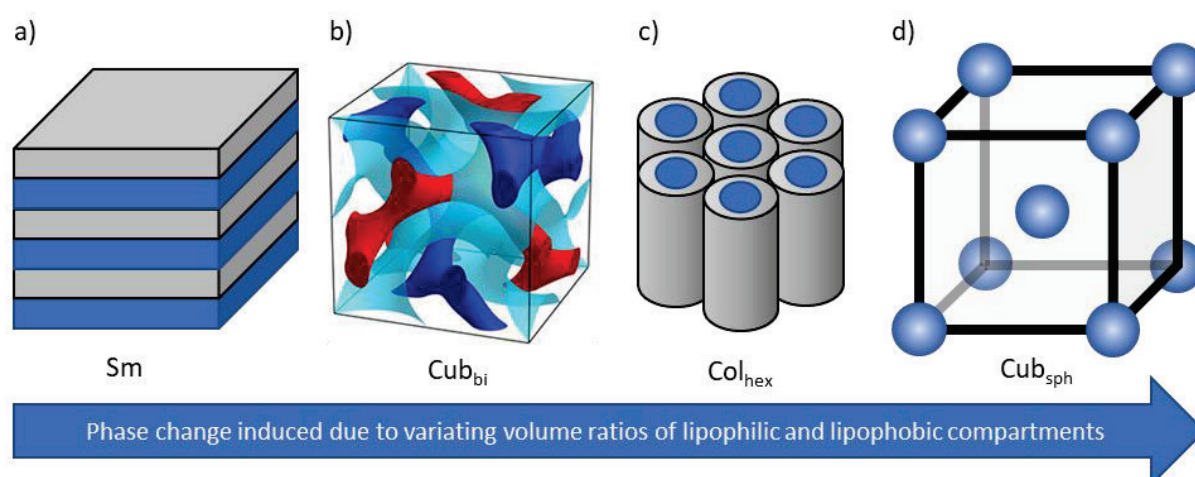***Figure 1.1-3.*** *Typical mesophase sequence of binary amphiphiles due to the variation of the different molecular compartments. a) Sm – smectic phase, b) Cub$_{bi}$ – bicontinuous cubic phase,[48] c) Col$_{hex}$ – hexagonal columnar phase, d) Cub$_{sph}$ – micellar cubic phase.*

Thermotropic liquid crystals, which are based on a combination of the principles of shape anisotropy and amphiphilicity, are the scope of this work.

1.2   Polyphiles by combination of anisotropy and amphiphilicity

The combination of anisotropy and amphiphilicity can lead to mesogens that combine more than two incompatible molecular parts, resulting in polyphiles[38] showing a variety of complex liquid crystalline phases similar to the morphologies of multiblock-co-polymers.[39,40]
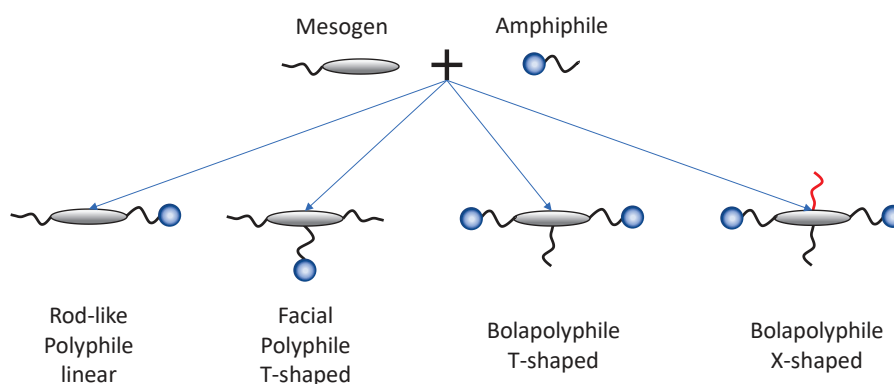

Figure 1.2-1. *Selected combinations of anisometric and amphiphilic segments. Black line – flexible hydrophobic chains, gray ellipsoid – rigid aromatic cores, blue circle - hydrophilic group, red line – flexible fluorophilic chain.*

The resulting mesogens can be distinguished according to the way the polar part is combined with the rigid-apolar core, as well as the number and position of the flexible chains.[31] A linear combination of the different molecular entities results in rod-like polyphiles with predominantly smectic multilayer structures as a result of the separation of the incompatible compartments into separate domains.[41,42] By locating the polar group perpendicular to the rigid core and increasing the number of flexible apolar chains, facial polyphilic mesogens are generated.[43] However, if the mesogen has two covalently bonded polar groups in the terminal positions, the so-called bolapolyphiles are obtained, which can be distinguished according to the number and position of the lateral chains, such as X-,[44] T-,[45] or Pi-shaped[46] bolapolyphiles, where three (triphilic) or more incompatible segments (polyphilie) are combined. Aromatic π-systems, including biphenyl,[38] *p*-terphenyl,[47] bistolane,[48] and oligo (*p*-phenylene ethynylene) units[49,50] have demonstrated their effectiveness as rigid cores in this type of mesogen. Polar groups were mainly glycerol groups, but also amides, carboxylic acids, carbohydrates, and single hydroxy groups have been investigated, which strongly contribute to the self-assembly due to the intermolecular hydrogen bonding. The flexible and non-polar side chains used also include a variety of structures, including linear[49] or branched alkyl chains (R_H), carbosilane,[51] siloxane,[52] and semiperfluorinated alkyl chains (R_F).[52]

A very extensively studied thermotropic phase behavior is described by Tschierske et al. for T-shaped bolapolyphiles consisting of a biphenylene core and lateral *n*-alkyl chains. In particular, the influence of length variation of the alkyl chains contributes to the complex mesomorphic properties shown in **Figure 1.2-2**.[29]

For bolapolyphiles with no or very short lateral chains, the molecules self-assemble into non-tilted alternating (SmA) layered structures. The anisometric units are mainly organized parallel to each other with an orientation perpendicular to the layer planes (SmA, **Figure 1.2-2a**).[53] A slight elongation of the chains results in a distortion of the layered structure (SmA+) due to the segregation of the side chains into (disordered) separate domains between the aromatic rods (SmA+, **Figure 1.2-2b**).[53]

By further increasing the chain length, the layered structures gradually disassemble, and the segregated nanodomains of alkyl chains, aromatic cores, and polar groups combine into columnar structures (Col_{rec}, Col_{hex}, Col_{squ}, **Figure 1.2-2c-h**). The aggregates are arranged as two-dimensional nets, forming three-dimensional honeycomb structures. This results in columnar mesophases that are described by different wallpaper groups. The compartments of the bolapolyphiles are segregated from each other in these structures, and the inner volume of the columns is filled with the lateral chains. The walls of the prismatic cells are built by two biphenyl cores arranged back-to-back to each other, and the long axis of the aromatic units is perpendicular to the longitudinal axis of the columns and separates the inner apolar prismatic cells. The honeycombs are stabilized by the sigma-cooperative hydrogen bridges of the glycerol groups, which act as the edges of the honeycombs. Depending on the lateral chain length, different prismatic cells are formed, ranging from triangular (Col_{hex})[53] to square (Col_{squ}),[54] pentagonal (Col_{rec}),[53] and hexagonal (Col_{hex})[53] honeycomb structures (**Figure 1.2-2c-g**).

Further increase in chain length results in expanded honeycomb structures, where some or all walls consist of molecular pairs coupled at their ends, doubling the wall length of the honeycomb. This leads to non-regular pentagonal or hexagonal wallpaper patterns (**Figure 1.2-2i-k**).[55,56,57]

Upon further increase of the side chain volume, a reduction of the interface curvature occurs, resulting in lamellar structures where the orientation of aromatic units is parallel to the layer planes, thus being inverted with respect to the SmA phase structure discussed above (see **Figure 1.2-2l-n**).[56]

For molecules with very large alkyl chain lengths, the formation of a hexagonal columnar and cubic phase can be observed. Here, the aromatic units are arranged in bundles parallel to the column long-axis, so-called rod-bundle phases (**Figure 1.2-2n-o**).[57,58,59] Infinitely long strings of coaxial rod-bundles in the $Col_{hex}^{\#}$ phase and networks of branched bundles in the cubic network phases.
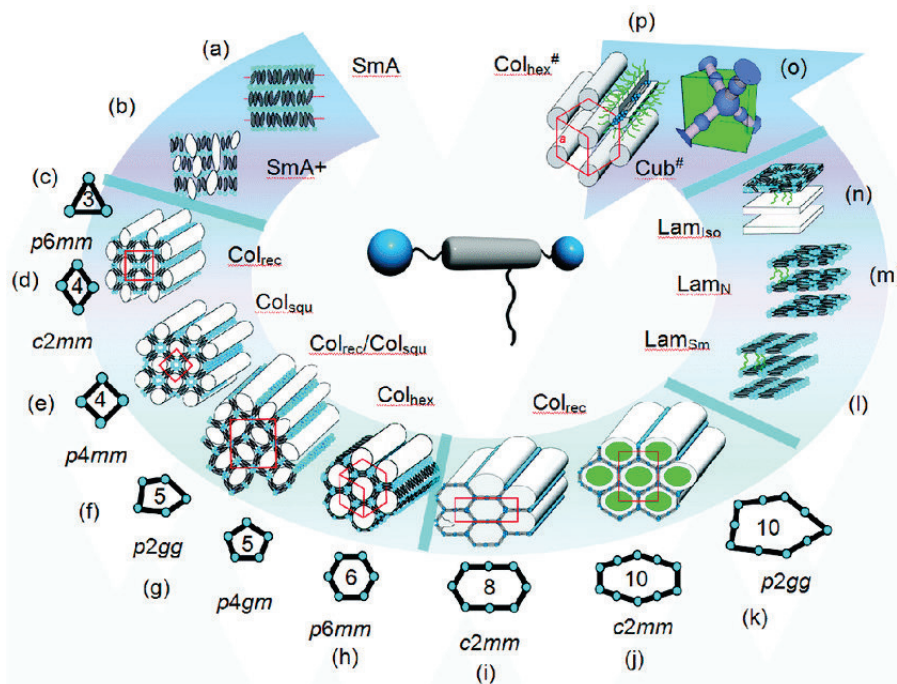
Figure 1.2-2. *Lateral volume dependent mesophase transition of T-shaped bolapolyphiles.[29,60]*

In addition to the studies of chain elongation leading to the mesophase transition from triangular to hexagonal structures, the elongation of the rod length at constant chain length was also studied. An inverse trend, i.e., a transition from larger to smaller honeycomb cells, was observed for the honeycomb structures at constant chain length when the rod length increases from biphenylene

(hexagonal/Col_{hex})[38] through terphenylene (pentagonal/Col_{rec})[47] and bistolane (square/Col_{squ})[48] to oligo(p-phenylene ethynylene) (triangular/Col_{hex}).[49,50]

Later on, the self-assembly processes of X-shaped bolapolyphilic molecules with oligo(p-phenylene ethynylene) core have become the focus of interest, where both sides of the aromatic unit are substituted with alkyl chains. The investigations have focused on the triangular-to-square transition, examining the use of two equal and two different incompatible (R_F, R_H) linear side chains.[38,49,61] By using two different incompatible chains, complex multicolor wallpaper patterns were achieved. Due to the side chains' incompatibility, multicolor tilings of triangular, square, and hexagonal structures were observed where the incompatible side-chains fill different altering prismatic cells. Due to emerging geometric frustration also tiles with mixed chains could also be observed, especially for patterns consisting of hexagonal tiles and for tilings combining triangles and square cells. In some cases, by changing from ternary to quaternary structures, a mixture of different color tilings with trigonal, square, and rhombohedral cells could be observed illustrated in **Figure 1.2-3**.
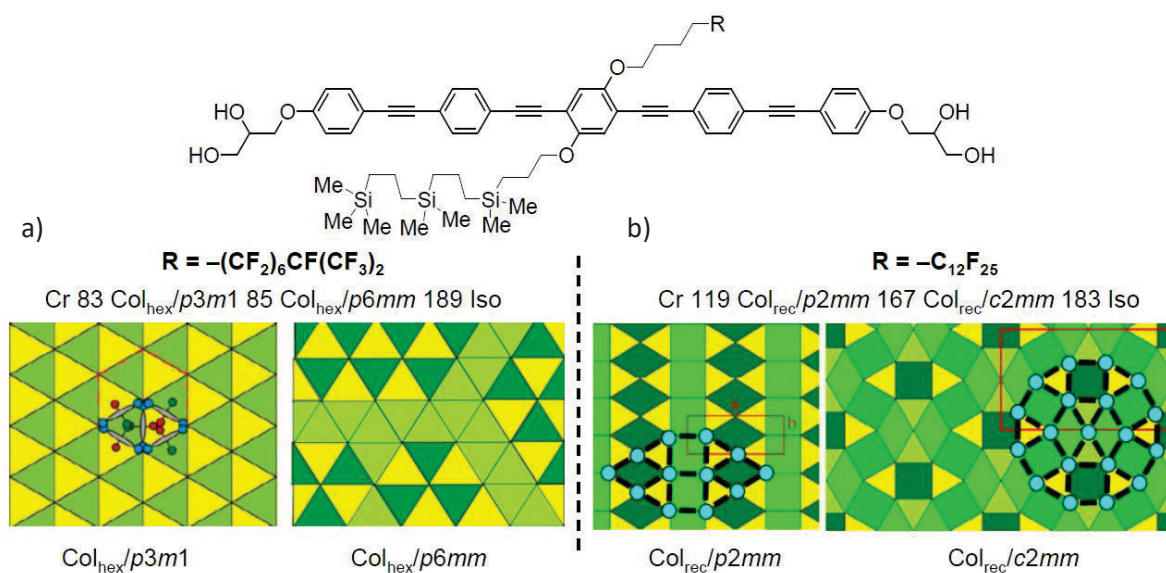

Figure 1.2-3. *Selected mesophases of OPE-based bolapolyphiles with different linear side chains. a) short semiperfluorinated side chain leading to completely mixed and fully segregated triangular mesophase structures, b) long semiperfluorinated side chain leading to mesophase structures composed of triangles, squares, and rhombs.*[38] *Used with the kind permission of Prof. C. TSCHIERSKE.*

Further prospects for wallpaper patterns with mixed triangular and square structures can be achieved by using a variation of alkyl chains with different lengths and volume distributions, as well as by using partial fluorinated rigid cores. In order to preserve the basic rod-like structure of the rigid core, an aromatic oligo (p-phenylene ethynylene) unit substituted in various positions of the benzene rings was explored. Glycerol units located in the terminal position served as polar groups. Replacing linear with branched side chains leads to lattices formed by supertilings combining different cells and expanding the lattice parameters (see, for example, **Figure 1.2-3**).[50,51,62] The focus of this work is the investigation of OPEs with chain volume at the triangle-square transition.

1.3   Preliminary studies and objectives

1.3.1   Preliminary studies

This thesis is based on the above-mentioned previous research in the group of Prof. Dr. C. Tschierske. [38,44,46,63,64,65] The focus of their work was on molecules with different linear or branched alkyl chains. It turned out that the branched chains can lead to a hexagonal superlattice formed by hexagonal supertiles and to different cubic network structures combining sphere packing with polyhedral rod-packing (see **Figure 1.3-1**), depending on the type of chain used, as well as side chain length and volume. . [44,51,61,62]
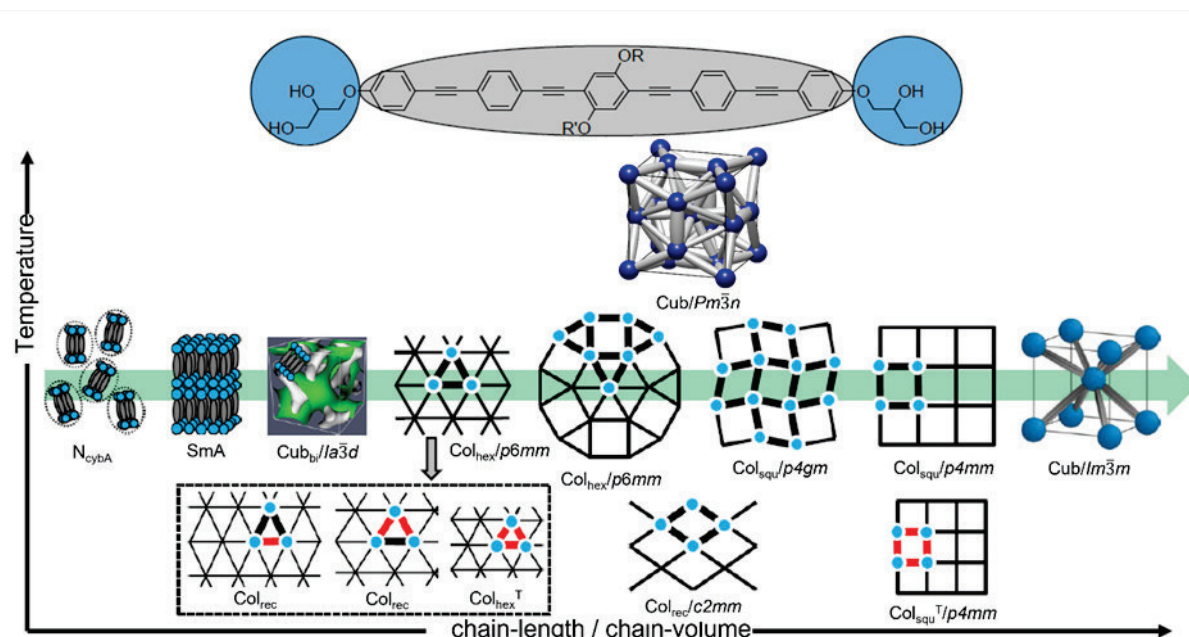

Figure 1.3-1. Mesophase sequence of OPE-based bolapolyphiles depending on side chain length or volume and temperature.[44]

The achievement of the dodecagonal super-tiling raises questions about the formation conditions and principles of this special type of honeycomb structure. Moreover, these dodecagonal supertiles are also capable of forming other 2D lattices and even quasiperiodic columnar LC with 12-fold rotational symmetry. Quasiperiodic tessellations, such as the renowned Penrose tiling initially conceptualized by the mathematician Roger Penrose[66] and various other quasiperiodic tessellations, e.g., by dodecagonal supertiles, can encompass a plane with nonoverlapping polygons that exhibit no gaps and lack translational symmetry. These structures were initially regarded as conceptual constructs devoid of tangible existence. Subsequently, Dan Shechtman demonstrated the existence of quasicrystalline structures in solid-state metal alloys. [67] Consequently, research interest shifted towards such materials, which exhibited distinctive physical properties, including high thermal and electrical resistance, high hardness, and anti-corrosion properties.[68]

Subsequently, self-assembled quasicrystalline and approximant structures have been identified in soft-matter systems formed by dendrimers,[69] nanoparticles,[70] or block copolymers,[71] which all represent packings of spherical micelles. Currently, there are additional two-dimensional quasiperiodic structures, as found in block copolymer morphologies[72] and including the first example of a columnar liquid quasicrystal with a honeycomb structure and dodecagonal symmetry observed in a T-shaped facial polyphile.[73] Despite the substantial research interest in these structures, the formation processes and driving forces behind them remain a challenge. This is despite the fact that, for example, trapezoidal structures[74] are known to support their formation.

1.3.2   Objectives

The objective of this work was to design, synthesize, and analyze X-shaped oligo (*p*-phenylene ethynylene)-based (OPE-based) bolapolyphiles with a focus on the possible formation of columnar liquid quasi-crystalline (CLQC) and approximant structures. The primary objective was to identify a precise design formalism for the lateral chain and rigid core type used in comparison to other OPE-based structures. Different influences on the formation of the CLQC phase were studied. Firstly, the impact of different core types on the expected CLQC structures was investigated by subdividing the rigid OPE core into two types: non-fluorinated (X = H, OPE) and partially core-fluorinated (X = F, FOPE). Secondly, the influence of the side chains on the formation of the liquid crystalline (LC) and potentially liquid quasi-crystalline structures (LQC) was investigated. Therefore, the studies investigated the influence of various highly branched carbosilane-based (**Figure 1.3-2a**), branched alkyl-, and branched partially fluorinated side chains, see **Figure 1.3-2b**.
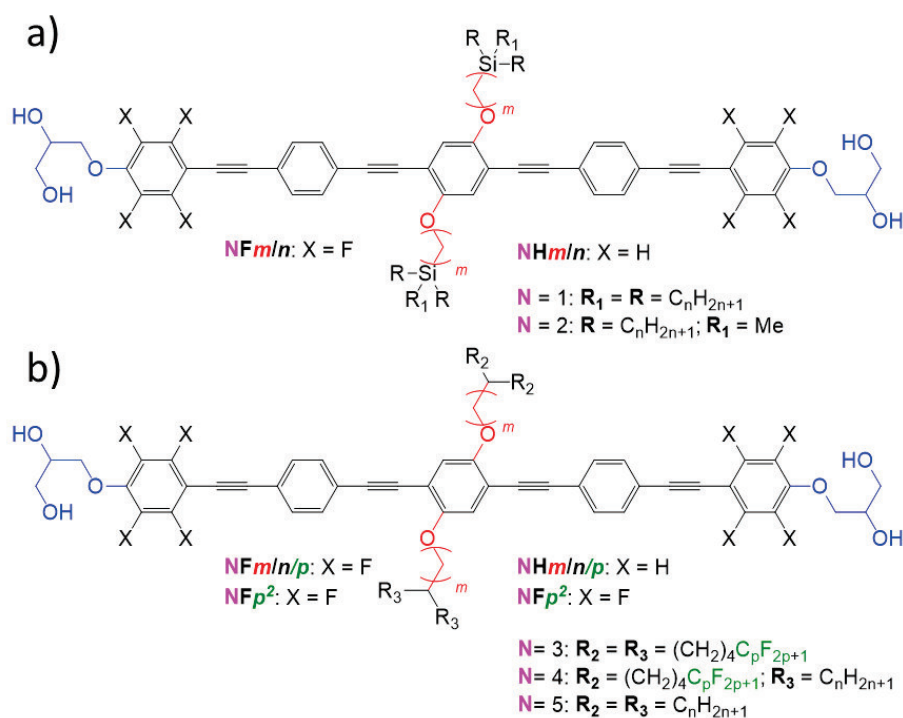

Figure 1.3-2. Chemical structures of the target materials; N represents an arbitrarily chosen compound number.

Additionally, we can investigate the influence of chain volume at various distances from the rigid core unit by variation of the spacer length *m* of the oligomethylene unit connecting the chain branching point with the OPE core, as well as the influence of chain length *n* and volume itself. The influence of fluorination of the lateral chain and its effect on phase formation was also investigated. The use of fluorinated chains, along with other immiscible chains, was also within the scope of this work to examine their impact on the formation of possible multi-colored CLQC structures. Finally, the effect of uniform chirality of the stereogenic centers in the glycerol units was investigated for a few examples.

The results obtained throughout the investigation process were further used in mathematical studies and calculations carried out by our cooperation partners from the Institute of Mathematics at the Martin-Luther University Halle Wittenberg (Virginia-Marie Fischer, Ph.D. Thesis under preparation). Through mathematical abstraction and simplification of chemical structures, as well as physical interaction with a simple geometric problem, allowed specific synthesis planning targeted towards CLQC and approximant structures.

2 Synthesis

The primary focus of this work was not only the study of mesophase structures but also the synthesis of new bolapolyphilic compounds that fit exactly into the triangular-square transition of liquid crystalline materials. Based on the work of Dr. Marco Poppe[44] and Dr. Helge Ebert[64] on bolapolyphilic molecules with a rod-like OPE core, further structural variations were carried out. As shown in **Schema 2-1,** the synthesis was conducted by reaction of 2,5-diiodohydroquinonediethers with two equivalents of the ethynyl-substituted tolane moieties **25H**, **26F**, **27H***, or **28F*** by a SONOGASHIRA cross-coupling reaction.[88] The resulting acetonides **1X*n/m*A** - **5X*n/m*A** were subsequently deprotected with pyridinium *p*-toluenesulfonate (PPTS) to yield the bolapolyphiles **1X*m/n* – 5X*m/n*** in only two synthetic steps.[75] The compounds **25H** and **26F** were synthesized from racemic rac-1,2-O-isopropylidene glycerol, and therefore **NH*m/n*** and **NF*m/n*** represent racemic mixtures of two diastereomers (*R,S*) meso forms, and the racemic mixtures (*R,R*) as well (*S,S*). For the compounds **27H*** and **28F*** (*R*)-2,3-*O*-isopropylidene glycerol was used, resulting in compounds ***NH*m/n*** and ***NF*m/n*** representing compounds with (*S,S*) configuration. The synthesis of most compounds is described in detail in the supporting information to publications A – C. Here we shortly summarize the applied syntheses. Those that are not included in publications A – C are outlined in the experimental part. The following sections will describe the synthesis of the intermediates.
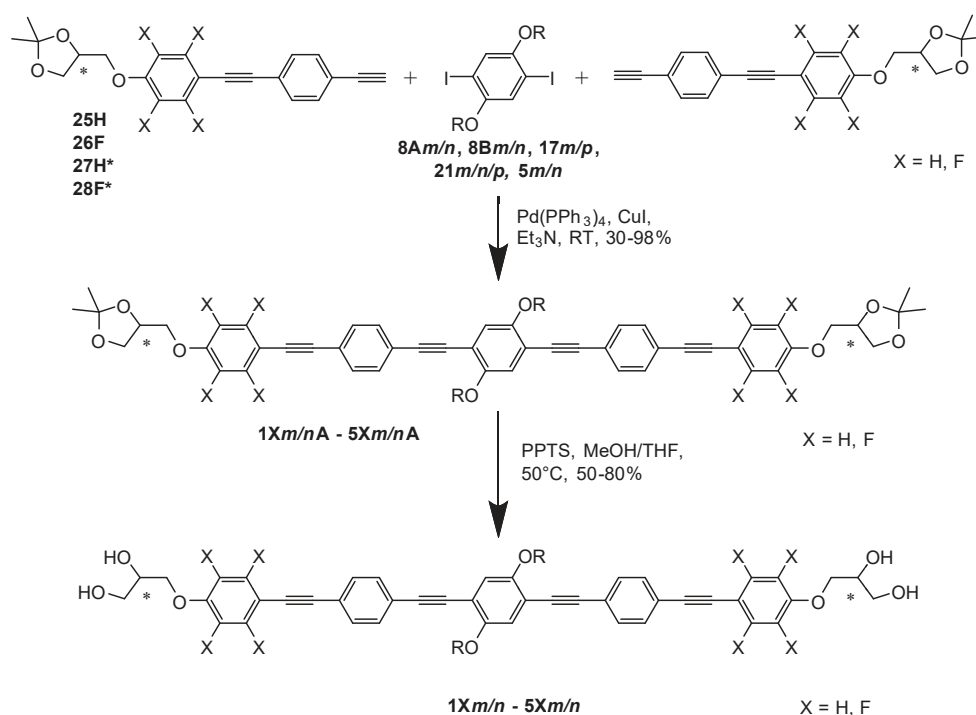
Scheme 2-1: *Synthesis of the bolapolyphiles **1Xm/n – 5Xm/n***

2.1. Syntheses of dialkylated 2,5-diiodohydroquinones

The synthesis of dialkylated 2,5-diiodohydroquinones was, in most cases, achieved by Williamson etherification of 2,5-diiodohydroquinone with two equivalents of branched alkylbromides. Four different types of such alkylbromides were used, resulting in five different types of 2,5-diiodohydroquinone ethers depending on certain combinations, and leading to 2,5-diiodohydroquinone ethers with branched carbosilane, branched alkyl, and branched partially fluorinated side chains. Also, 2,5-diiodohydroquinone ethers with two different side chains (compare

21*m/n/p*) were prepared as described in Pub. C (see **Scheme 2-2**). In the following sections, we will describe the synthesis of the respective central units according to the side chains that are used. Carbosilane-based compounds with a propylene spacer will be covered separately because their synthesis strategy differs from the usual ones with *n* > 3.


a)

8A*m/n*: $R_1 = (C_nH_{2n+1})_3$

8B*m/n*: R_1 = Me

b)

17*m/p*

c)

21*m/n/p*

d)

5*m/n*
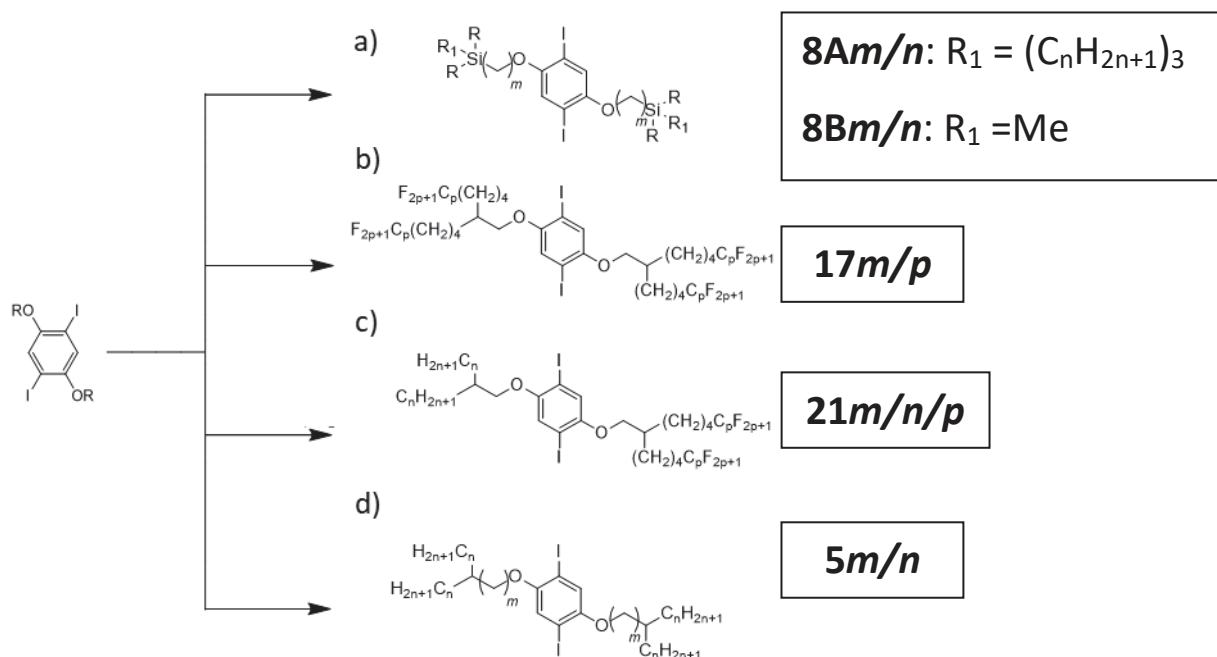
Scheme 2-2. *Depiction of the dialkylated 2,5-diiodohydroquinones used as a)* **8A*m/n*** *triple-branched carbosilane side chains with equal alkyl chains;* **8B*m/n*** *triple-branched carbosilane-based side chains with a methyl group and two equal alkyl chains; b)* **17*m/p*** *branched partially fluorinated alkyl chains; c)* **21*m/n/p*** *non-symmetric substituted 2,5-diiodohydroquinone ethers with a branched alkyl chain and a branched partially fluorinated alkyl chain; d)* **5*m/n*** *branched alkyl chains.*

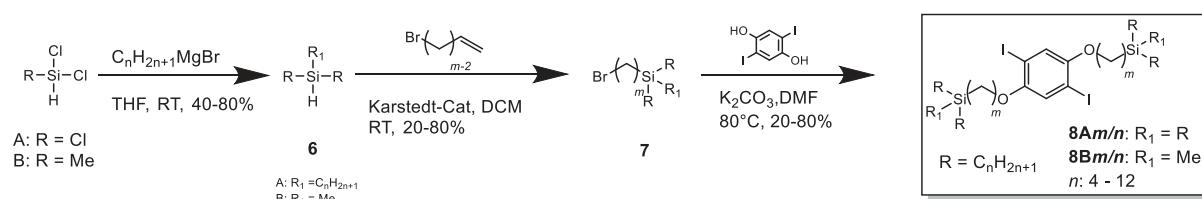## 2.1.1. Synthesis of 2,5-diiodohydroquinone ethers with branched alkyl chains 5*m/n*

The alkyl bromides used for compounds with 2,5-diiodohydroquinone ethers **5*m/n*** were branched in the 2- or 4-position of the alkyl chain. Compounds **5*m/n*** with identical substituted side chains and branching in the 2-position were mainly used to study the influence of enantiomerically pure stereogenic centers in the glycerol units on mesophase formation compared to their racemic analogs. In contrast, compounds with branching in the 4-position were used to investigate the volume shift away from the rigid-core unit compared to their 2-position branched analogs. The syntheses of both species were carried out in an analogous manner. These branched alkylbromides were synthesized using the malonic ester synthesis method (see **Scheme 2-3**).[44] Using two equivalents of a linear *n*-alkyl bromide resulted in branched side chains in the 2-position, while using only one equivalent of an alkyl chain already branched in the 2-position led to alkylbromides having the branching point at the 4-position. The intermediate malonic acid ester derivatives **1** were subjected to a dealkoxycarbonylation reaction according to Krapcho.[76] This was followed by a reduction of the obtained branched carboxylic acid esters with lithium aluminum hydride to give the corresponding alcohols **3**.[77] The reaction cascade to the branched alkyl bromides was completed by brominating the alcohols **3**.[78] The resulting bromide **4** was used for the alkylation of 2,5-diiodohydroquinone to complete the reaction to obtain the 1,4-dialkylated 2,5-diiodohydroquinone derivatives **5**.[79]
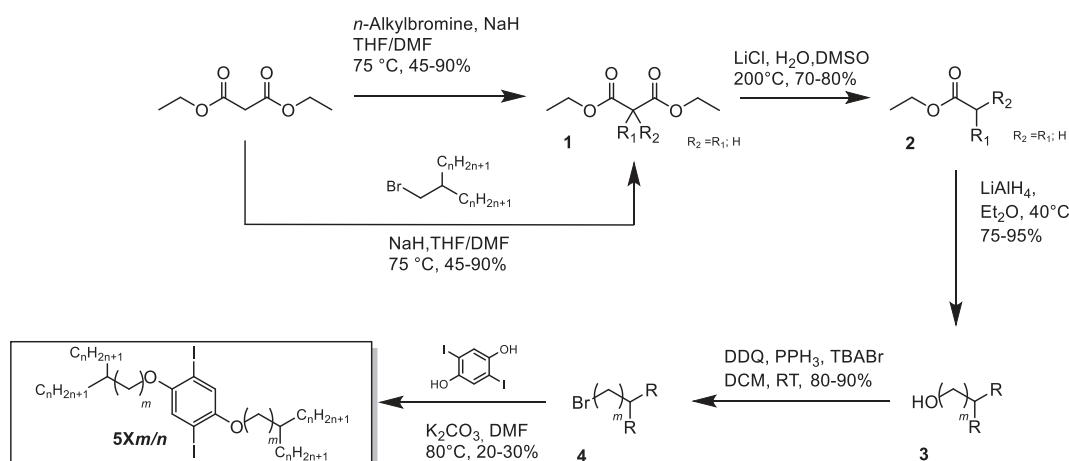
Scheme 2-3. *Synthesis of the 2,5-diiodohydroquinone ethers **5m/n** with identically branched alkyl chains and branching point in 2- or 4-position of the alkyl chain.*
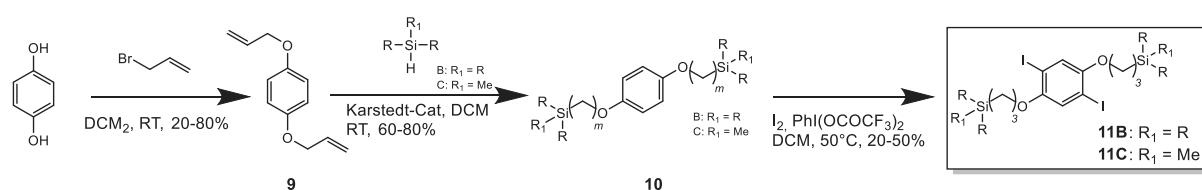
2.1.2. Synthesis of 2,5-diiodohydroquinone ethers with carbosilane chains 8AX*m/n*, 8BX*m/n*

The syntheses of compounds **1X*m/n*** and **2X*m/n*** with spacer units ≥ 4 started with either trichlorosilane or dichlormethylsilane, which were alkylated using a certain Grignard reagent to obtain the branched carbosilanes **6** (see **Scheme 2-4**).[80] The reaction of **6** with ω-bromo-*n*-alkenes was conducted by a hydrosilylation reaction with Karstedt's catalyst and resulted in the bromides **7**.[81] In the following alkylation, similar to that described for the compounds in section 2.1.1, we were able to produce 2,5-diiodohydroquinone ethers of type **8A*m/n*, 8B*m/n***.[79]

Scheme 2-4. *Synthesis of **8Am/n, 8Bm/n**, the 2,5-diiodohydroquinone ethers with branched carbosilane chains and spacer units n ≥ 4.*

As it turned out that carbosilane-based alkylbromides with spacers < 4 do not undergo double alkylation of 2,5-diiodohydroquinone or 2,5-dibromohydroquinone, an alternative synthesis strategy for producing 2,5-diiodohydroquinone ethers of type **11B*m/n*** and **11C*m/n*** with a spacer unit of *n* = 3 was required. This issue was resolved as shown in **Scheme 2-5** by first reacting hydroquinone with allyl bromide to obtain 1,4-bis(allyloxy)benzene **9** via alkylation.[82] Subsequently, **9** was subjected to a hydrosilylation reaction with the corresponding tri- and dialkylmethylsilanes to yield **10**.[81] Following, an iodination reaction using I₂ and PhI(OCOCF₃)₂ led to the 2,5-diiodohydroquinone ethers **11B3/*n*** and **11C3/*n***.[83]

Scheme 2-5. *Synthesis 2,5-diiodohydroquinone ethers **11B3/n, 11C3/n** with branched carbosilane chains and spacer units n = 3.*

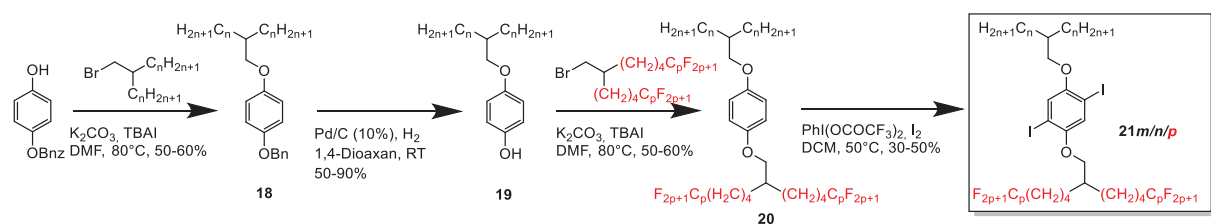## 2.1.3. Synthesis of 2,5-diiodohydroquinone ethers with branched partially fluorinated side chains 17*m/p*

The reaction of two equivalents of 4-bromobut-1-ene with malonic acid ester to obtain the desired diolefin with **13** resulted in only low yields. The reaction procedure was modified, as shown in **Scheme 2-6**, to a step-wise alkylation with 4-bromobut-1-ene to yield the desired compound **13**. The next reaction step was the dealkoxycarbonylation according to Krapcho to obtain **14**. The resulting diolefin **14** was subjected to a radical addition of linear perfluoroalkyl iodide supported by Pd(PPh$_3$)$_4$, followed by a reduction reaction with LiAlH$_4$ to synthesize the branched perfluorinated alcohols **15**.[84] The alcohols were then brominated by using DDQ, PPh$_3$, and TBABr to obtain the desired bromides **16**.[78] Subsequently, the bromides were subject to Williamson's etherification with 2,5-diiodohydroquinone to produce the 2,5-diiodohydroquinone ethers **17*m/p***.[79]
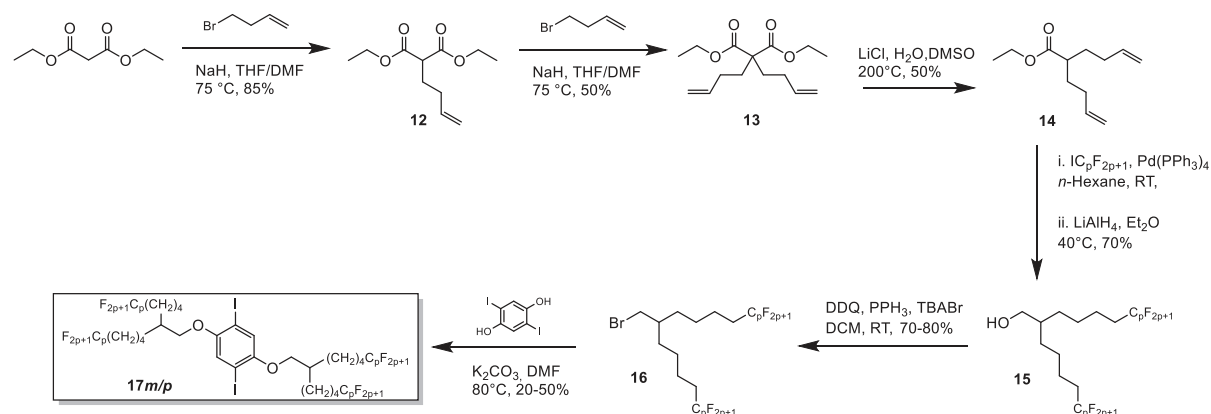
Scheme 2-6: *Synthesis of the 2,5-diiodohydroquinone ethers* **17m/p** *with branched partially fluorinated side chains.*

2.1.4. Synthesis of non-symmetric substituted 2,5-diiodohydroquinone ethers 21*m/n/p*

To obtain the 2,5-diiodohydroquinone ethers **21*m/n/p*** with two different chains 4-(benzyloxy)phenol was first alkylated with our previously synthesized branched alkyl bromide **14** to give the benzyl ether **18**.[79] Hydrogenolytic deprotection[85] of the benzyl group leads to the phenol **19** which was alkylated with the branched partially fluorinated alkyl bromide **16** to yield the non-symmetric hydroquinone ethers **20**.[79] The final step was an iodination reaction with hypervalent iodine to yield compounds **21** (see **Scheme 2-7**).[83]

Scheme 2-7: *Synthesis of 2,5-diiodohydroquinone ethers* **21m/n/p** *combining a branched carbosilane chain with a branched partially fluorinated chain.*

2.2. Synthesis of the 4'-ethynyl-4-(2,3-O-isopropylidene-2-glycerol) bistolanes 25H – 28F*

The Synthesis of the bistolane derivatives **25H** to **28F*** was conducted as outlined in **Scheme 2-8**.[50,86] The synthesis was, in most cases, conducted with racemic 2,3-O-isopropylidene glycerol to yield the racemic mixtures. Using (R)-2,3-O-isopropylidene glycerol leads to the enantiomerically pure compounds with (R)-conformation. Moreover, the benzene rings besides the (protected) glycerol group can be either non-fluorinated (**25H**, **27H***) or perfluorinated in positions 2,3,5, and 6 (**26F**, **28F***). The synthesis of the non-fluorinated compounds **25H** and **27H*** starts with a tosylation of 2,3-O-isopropylidene glycerol, respectively, (R)-2,3-O-isopropylidene glycerol with tosyl chloride, yielding in the tosylate **22**.[87] By an etherification with 4-bromophenol compounds **23H / 23H*** could be synthesized.[79] For the corresponding fluorinated compounds, a nucleophilic substitution of pentafluoroiodobenzene with 2,3-O-isopropylidene glycerol or (R)-2,3-O-isopropylidene glycerol was used, leading to the compound **23F / 23F***.[79] The acetylene compounds **24X** were achieved by the use of a Sonogashira cross-coupling reaction of the aryl halides **23X** with trimethylsilylacetylene, followed by desilylation with KF.[88,89] In the final step, we synthesized diverse isopropylidene-functionalized tolane derivatives (**25H**, **27H***, **26F**, and **28F***) through a Sonogashira reaction between the acetylenes **24X** and (4-bromophenylethynyl)trimethylsilane, followed by desilylation. [88,89]
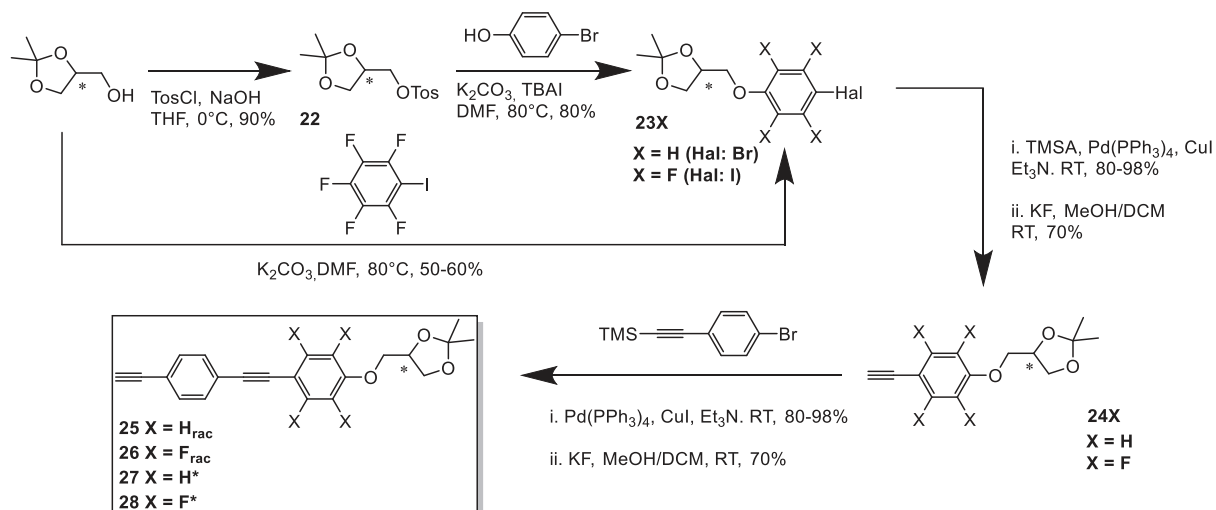
*Scheme 2-8. Synthesis of the racemic and enantiomerically pure non-fluorinated acetylide **25H**, **27H***, respectively, the 2,3,5,6 fluorinated acetylide **26F**, **28F***.*

2.3. Final consideration of the syntheses

The bolapolyphiles **1X*m/n*** – **5X*m/n***, which vary in the structure of the laterally attached alkyl chains, were synthesized successfully as shown in **Scheme 2-1** by Sonogashira Cross-coupling and deprotection of the isopropylidene groups. For the previously published compounds, the synthesis procedures and analytical data are recorded in the Supporting Information files of the respective publications A – C.

3   Soft self-assembly of bolapolyphiles with trialkylsilyl substituted side chains

Publications A – C are dedicated to the examination of the self-assembly of X-shaped OPE-based bolapolyphiles with two carbosilane chains, with a view to providing a comprehensive account of recent progress in this field.[73,90,91,92,93,94] The discussion will commence with an overview of the findings presented in Publications A–C, which will then be supplemented by including unpublished results at a later stage.

Here we use the compound abbreviation explained in **Scheme 1.3-2**. Each compound has a number N, which indicates the compound class defined by the structure of the side chains (carbosilanes, branched alkyl chains, branched semiperfluorinated chains, etc.). The following letter (X) indicates either a non-fluorinated OPE core (H) or a fluorinated one (F). The first number *m* defines the length of the spacer between the chain branching point and the ether oxygens at the aromatic core, while *n* gives the length of the individual *n*-alkyl chains connected with the branching point. The expression **NX*m/n*** is used throughout the thesis, while in the publications, short names were used.

For example, in Pub A, compounds **1H*m*/7** and **1F*m*/7** are abbreviated as **H/*n*** and **F/*n***. (Note that in Pub A, *n* instead of *m* was used to identify the spacer length) In Pub B, the abbreviations **H*m/n*** and **F*m/n*** were used (without the initial compound number N). For the chain fluorinated compounds, an additional letter *p* indicates the lengths of the perfluoroalkyl segments, which are decoupled from the branching point by butylene units in all cases. Thus, the compounds combining a fluorinated with a non-fluorinated side chain are abbreviated herein as **4H1*n/p*** and **4F1*n/p***, while **H*n/p*** and **F*n/p*** were used in ref. C. For the two compounds **3** with two semiperfluorinated side chains, the abbreviations **3H*p*²** and **3F*p*²** (specifically **3H8²** and **3F8²**) were used, being the same as in Publication C.

3.1   Effects of spacer length– Publication A

In publication A,[95] the effect of spacer length on the LC self-assembly of compounds with triple-branched side chains where silicon acts as a branching point was examined for the soft self-assembly of the OPE-based bolapolyphiles **1X*m/n*** with *n* = 7. Additionally, the chain volumes were selected to fit into the triangle-square transition region. The results of the molecules with equally long chains at the branching point and variable spacers *m* are summarized in the bar charts of **Figure 3.1-1**.
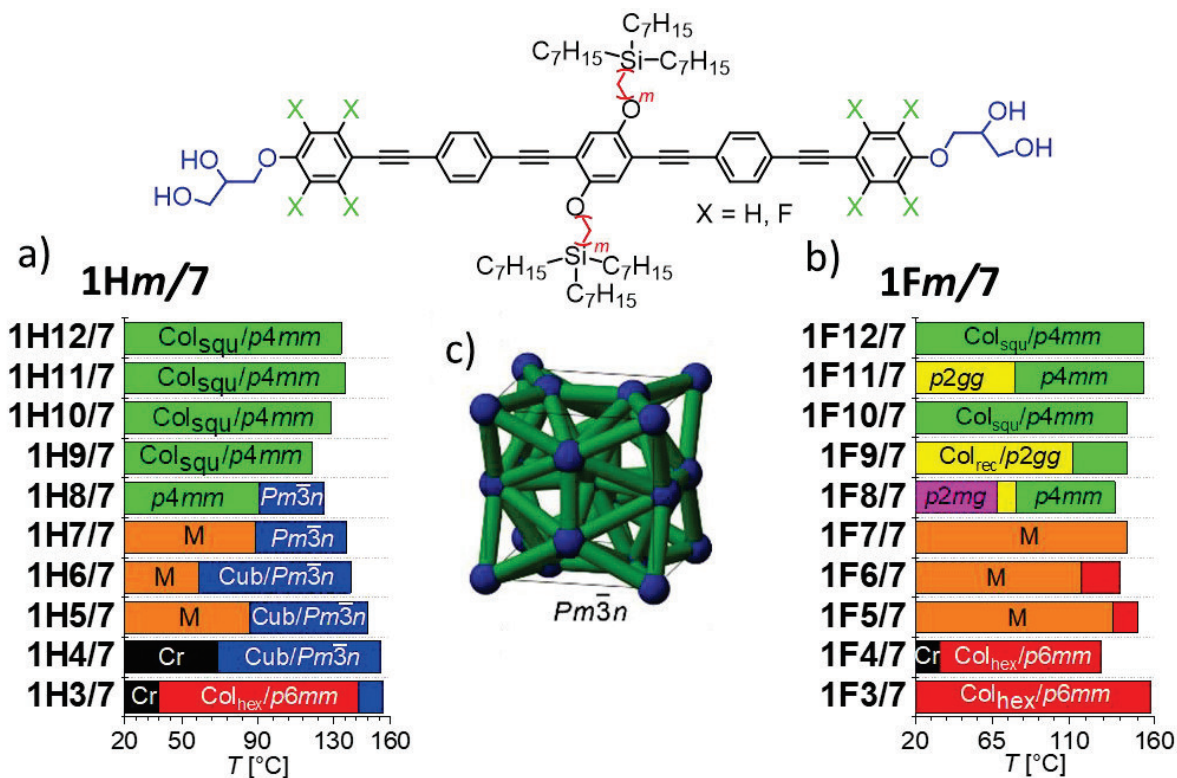

*Figure 3.1-1: Molecular structure and LC phases of a) **1Hm/7** and b) **1Fm/7** depending on the spacer length m = 3 … 12, c) schematic illustration of the organization of the molecules in the Pm3̄n phase. Bar diagrams showing the mesophase ranges of compounds **1Hm/7** and **1Fm/7**. Abbreviations: Cr = crystalline solid, Col$_{squ}$/p4mm = square honeycomb, Col$_{hex}$/p6mm = hexagonal honeycomb, Col$_{rec}$/p2gg = rhombic honeycomb; Col$_{rec}$/p2mg = honeycomb formed by non-regular triangle cells, M = unknown mesophase, Cub$_{net}$/Pm3̄n = cubic network phase (A15-Type Frank Kasper Phase); note that in Ref. 95 the compound numbers were shortened to **Hm** and **Fm**.*

In both cases, an elongation of the spacer *m* induces a transition from hexagonal columnar phases (Col$_{hex}$/*p6mm*), composed of triangular honeycombs, to square columnar phases (Col$_{squ}$/*p4mm*). A significant difference can be observed in the manner in which the transition between these two phases is achieved with the formation of intermediate phases.

In the case of the non-fluorinated series **1H*m/7***, an optically isotropic A15-type cubic network phase (Cub/*Pm3̄n*), composed of tetrahedra of rod-bundles, is observed as a new intermediate phase between the triangular and square honeycombs (see **Figure 3.1-1a,c**). In this phase type, the network is formed by rod-bundles of 5-6 parallel arranged molecules, interconnected at the junctions by spheres or oblate or spheroids involving the polar glycerol groups, while the continuum is filled by the side chains. In the unit cell, the spheres are positioned at the edges, in the center, and in pairs on the six faces, which corresponds to the observed structure in the A15 Frank-Kasper phase.[96] This represents a dense packing of tetrahedra formed by bundles of rods interconnected by the glycerol spheres/spheroids.

In contrast, the peripheral core fluorination of the fluorinated series (**1F*m/7***) has been observed to suppress the formation of the *Pm3̄n* network, thereby expanding the range of the triangular honeycomb phase with a *p6mm* plane group. Additionally, deformation of the square

honeycomb structure is observed for $n > 8$. The lattice of the rhombic honeycombs is composed of angularly distorted squares, leading to a *c2mm* space group (**Figure 3.1-2a**), while for **F8** it has *p2mg* plane group symmetry and is formed by rhombs divided into two triangles (**Figure 3.1-2b**).
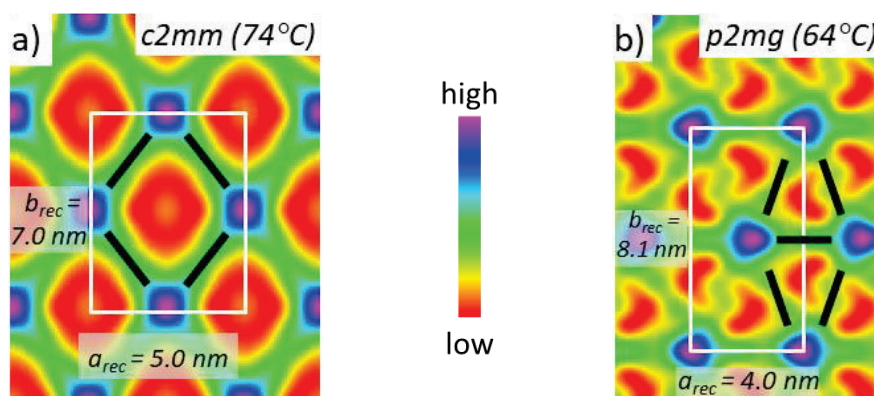

*Figure 3.1-2: Reconstructed EDMs of the honeycomb phases of a) Col$_{rec}$/c2mm – phase, b) Col$_{rec}$/p2mg – phase of compound **F8** with the molecular organization (black), crystallographic unit cell (white), polar glycerol groups (High ED, blue), aromatic cores (medium ED, green), and carbosilane chains (low ED, red). (Publication 95)*

3.2 Effects of side chain length and volume on $Pm\overline{3}n$ phase formation – Publication B

In publication B[97], a wider library of OPE-based bolapolyphiles with highly branched carbosilane chains (**Figure 3.2-1**) was used to study the soft self-assembly and the conditions for A15-type cubic network phase formation as a function of side chain volume, side chain length, and molecular packing. The focus is on compounds with two branched side chains with three identical branches (**1X*m/n***), where **X = H** indicates a non-fluorinated OPE core and **F** indicates a FOPE core with perfluorinated benzene rings at the peripheries besides the two glycerol groups. Here, the numbers ***m/n*** represent the spacer length ***m*** and the alkyl chain length ***n*** in each branch.

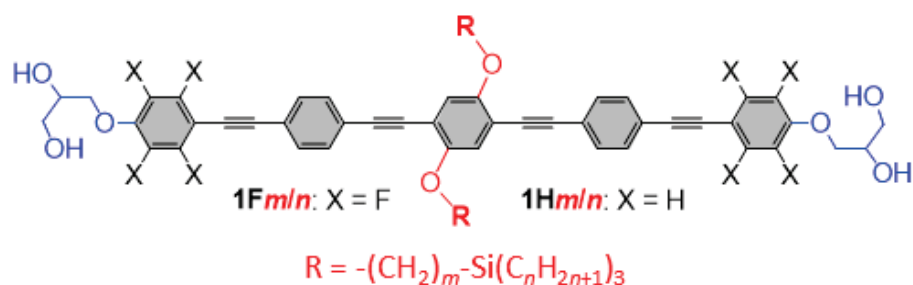*Figure 3.2-1: OPE core structure of compounds 1Hm/n and 1Fm/n.*

In the majority of cases, an optical isotropic mesophase is formed as the only mesophase or above one of the honeycomb phases for the **1H*m/n*** compounds. This phase corresponds to the A15-type cubic network phase (Cub$_{net}$/$Pm\overline{3}n$) described in Publication A. When considering the chain volume V_C =2(m + 3n) = 42 − 68, an overall sequence of phases from Col$_{hex}$/$p6mm$ V_C = 42 − 48 → Cub$_{net}$/$Pm\overline{3}n$ (V_C = 48 − 68) → Col$_{squ}$/$p4mm$ (V_C = 58 − 68) can be observed. However, the ordering of the phases according to the chain volume was not strict because some compounds did not have the expected phase, e.g., **1H3/8** (V_C = 54, Col$_{hex}$), **1H9/4** (V_C = 60, Col$_{squ}$) (See **Table 3.2-1**).

Table 3.2-1: LC phase overview of the compounds 1Hm/n ordered according to the chain volume V_C with V_C = 2(m + 3n).

Comp.	3/6	3/7	6/6	4/7	8/6	3/8	6/7	9/6	4/8	5/8	8/7	11/6	3/9	6/8	9/7	4/9	10/7	11/7	3/10	6/9	4/10
Phase																					
V_C	42	48	48	50	52	54	56	56	56	58	58	58	60	60	60	62	62	64	66	66	68

Color-code represents the formed LC phases with: red = Col$_{hex}$/$p6mm$, green = Col$_{squ}$/$p4mm$ and blue = Cub$_{net}$/$Pm\overline{3}n$

This leads to the conclusion that the honeycomb structure is simultaneously affected by the side chain length L_C = m + n + 1, where triangular honeycombs require shorter L_C, and otherwise, square honeycombs require longer L_C.[1] As noted above, the cubic $Pm\overline{3}n$ structure serves as an intermediate structure at the transition between triangular and square honeycombs. It is insufficient for the chain volume to fit with the cell volume; the chain must also be sufficiently long to efficiently fill the most distant spaces in the selected structure. Thereby, an increase in the spacer length ***m*** primarily affects the increase in L_C, while an increase in the length of the three branches predominantly influences V_C. The LC phases of compounds **1H*m/n*** are summarized in the bar graphs in **Figure 3.2-2**. The ordering of the compounds **1X*m/n*** is by side chain length with L_C = m + n + 1, while compounds with identical side chain length are further sorted by increasing spacer length ***m***.

---

[1] The number of C and Si atoms is used as approximate (dimensionless) measure for side chain volume and side chain length abbreviated here as V_C and L_C.

Figure 3.2-2: *Mesophase sequences of compounds* ***1Hm/n*** *on cooling (cooling rate: 10K/min). The numerical transition temperatures can be found in Publication B (Table 1). Bar diagrams showing the mesophase ranges of compounds* ***1Hm/n***. *Abbreviations: Cr = crystalline solid; Col_{squ}/p4mm = square honeycomb; Col_{hex}/p6mm = hexagonal honeycomb, M = unknown mesophase; Cub/Pm$\bar{3}$n = cubic network phase (A15-Type Frank Kasper Phase). (Publication 97)*

By core-fluorination of the benzene ring at the peripheries besides the two glycerol groups, the compounds **Fm/n** with almost the same chain volume range $V_C = 43 - 66$, showed a clear trend to suppress the formation of the $Pm\bar{3}n$ phase. Additionally, the ranges of the *p6mm* and *p4mm* phases are significantly expanded. Only two compounds (**1F4/9** and **1F3/10**) show a $Pm\bar{3}n$ phase in a small range, indicating a much narrower existence range of this cubic network phase. Moreover, it has a considerably reduced stability, if compounds with those found in series **1Hm/n**. In contrast, there appears to be a general stabilizing of core-fluorination for honeycomb phases (see **Figure 3.2-3**). Here, also a mesophase stabilization can be observed for compounds with optimal space filling in the prismatic cells ($V_C = 10$ for *p6mm* and $V_C > 16$ for *p4mm*). All other compounds between these limits experience steric frustration, leading to a decrease of the LC → Iso transition temperature upon fluorination. This leads to a reduced stability of the triangular and square honeycombs and also allows alternative modes of self-assembly to take place. In particular, deformed square honeycomb phases can be observed. One is the rhombic honeycomb phase with angular deformed squares observed for the low-temperature Col_{rec}/c2mm phase, and has an inner angle of 71 – 81° for compounds with long odd-number spacers (m = 9,11). The other phase is a rectangular honeycomb low-temperature with Col_{rec}/p2mm lattice, which avoids the tight vertices.
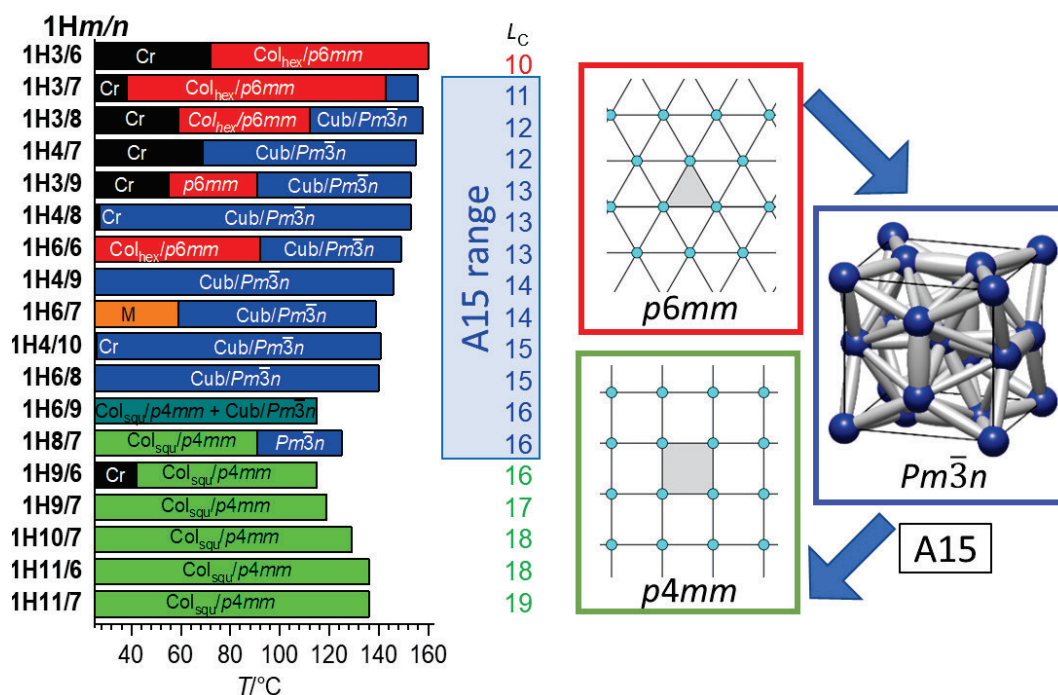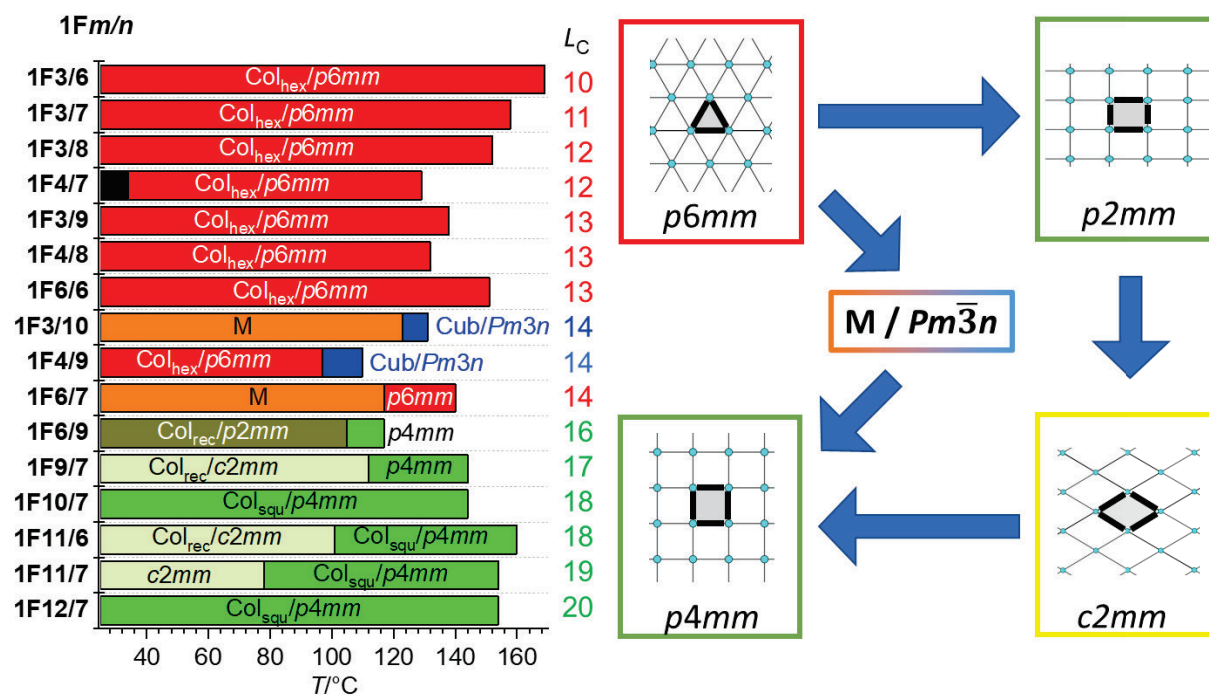
*Figure 3.2-3: Mesophase sequence of compounds **1Fm/n** on cooling (cooling rate: 10K/min). The numerical transition temperatures can be found in Publication B (Table 2). Bar diagrams showing the mesophase ranges of compounds **1Fm/n**. Abbreviations: Cr = crystalline solid; Col_{squ}/p4mm = square honeycomb; Col_{hex}/p6mm = hexagonal honeycomb; Col_{rec}/p2mm = rectangular honeycomb; Col_{rec}/c2mm = honeycomb formed by rhombic cells; M = unknown mesophase; Cub_{net}/Pm$\overline{3}$n = cubic network phase (A15-Type Frank Kasper Phase). (Publication 97)*

Moreover, a possible explanation for the packing modes of the series **1Hm/n** and **1Fm/n** (see **Figure 3.2-4**) is given in Publication B. The **1Fm/n** compounds have an increased face-to-face π-stacking interaction between neighboring FOPE cores indicated by an additional diffuse wide-angle scattering shoulder around $d = 0.36 – 0.39$ nm. In contrast, the electron-rich OPE compounds **1Hm/n** do not show such a shoulder. Accordingly, there is more rotational disorder around the OPE long axis, and edge-to-face interaction becomes more dominant for the FOPE cores.

The face-to-face interactions between the FOPE cores along the honeycomb walls contribute to the mesophase stabilizing effect of core fluorination. Moreover, this face-to-face stacking of the **1Fm/n** compounds provides distinct energetic minima and maxima for the longitudinal shift. One minimum is expected for the side-by-side packing resulting from the electron deficit perfluorinated benzene in a packing without longitudinal shift (see A in **Figure 3.2-4f**). The other minimum B is likely to result from the donor-acceptor packing of the fluorinated benzenes besides the π-electron-rich acetylene or benzene units of neighboring molecules, leading to a strong shift of adjacent molecules.
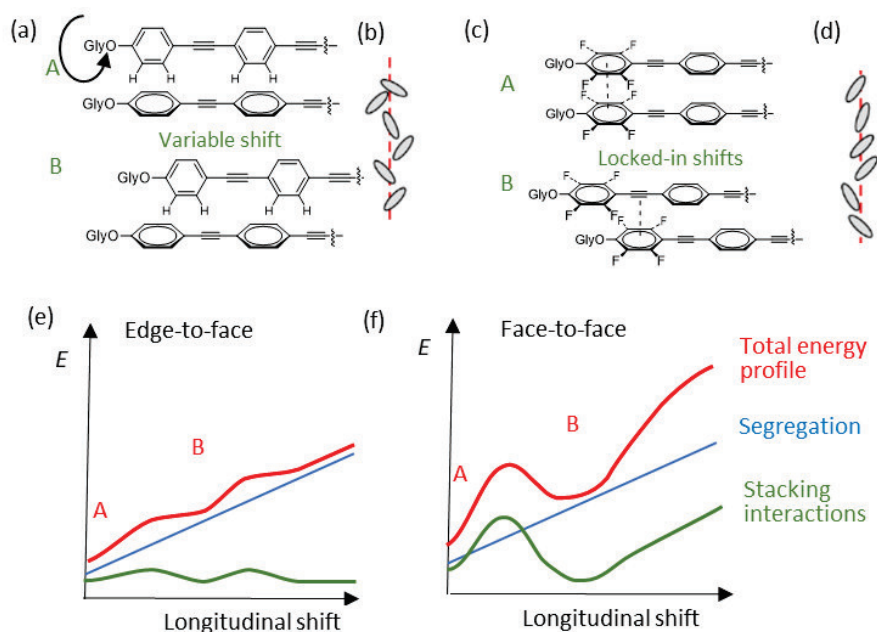
Figure 3.2-4*: (a-d) Schematics of the rod-packing and (e,f) sketches of their tentative energy profiles depending on longitudinal shift (a-d) views on the packing of the rods in the honeycombs (a, c) view along a short axis (only the two outer rings at one end of the molecules are shown) and (b, d) side-views along the long axes of the rod-like (F)OPE cores, and (e, f) the effects of stacking interactions and glycerol-(F)OPE segregation on the energy profiles of the longitudinal shift between neighboring molecules; (a, b, e) there is an easy sliding of the rotationally less ordered non-fluorinated OPE cores due to larger core-core distances (only edge-to-face packing is shown although also face-to-face and other arrangements contribute) while (c, d, f) for the FOPEs there are distinct preferred geometries for the distinct face-to-face stacking motifs; Gly = glycerol end groups. (Publication 97)*

In contrast, the loose packing of the **1H*m/n*** compounds allows an easy longitudinal shift of adjacent OPE cores. The non-regular tetrahedral packing of the rod bundles of the networks of the *Pm$\bar{3}$n* phase requires a length ratio of the rod bundles of 1 : 1.12 : 1.21 which requires a slight longitudinal shift of the polyaromatic rod in the bundles of the Cub$_{net}$/*Pm$\bar{3}$n* phase. This is easily possible for the OPE cores, while the locked-in mode of the FOPE cores of compounds **1F*m/n*** cannot provide the required length ratios. Therefore, the *Pm$\bar{3}$n* phase is suppressed, and honeycombs are retained. For compounds **1F4/9** and **1F3/10** with short spacers *m* the face-to-face packing is disturbed by the bulky R$_3$Si groups, thus reducing the locked-in behavior and allowing *Pm$\bar{3}$n* formation at high temperatures, while reducing the temperature supports denser packing, which favors locked-in behavior and the triangular honeycomb is retained.

3.3 M-Phases of bolapolyphiles with trialkylsilyl groups – Additions to Publication A and B

While Publication A[95] and B[97] have focused on the $Pm\overline{3}n$ phase, there are numerous additional compounds with birefringent mesophases showing complicated XRD patterns, which in most cases have not yet been indexed and which are summarized as M-Phase. These additional compounds and their mesophase sequences are summarized in **Table 3.3-1**.

*Table 3.3-1: Mesophases and phase transition temperatures of compounds **1Xm/n** with X = H, F, containing compounds with M-phase from publications A and B, and not published compounds. All transition temperatures were taken from the peak temperatures of the transition peaks at a heating and cooling rate of 10K/min. The transition enthalpies were determined from the peak areas given in kJ/mol.*

1X*m/n*	*m*	*n*	Phase Sequence *T* [°C] and Δ*H* [kJ/mol]	V_C	L_C
1H5/7	5	7	H: Cr 50 [3.3] M 96 [2.2] Cub/$Pm\overline{3}n$ 155 [1.3] Iso C: Iso 148 [-0.9] Cub/$Pm\overline{3}n$ 86 [-2.9] M < 20 Cr	*52*	*13*
1H5/8[b,c]	5	8	H: Cr 74 [5.2] M 104 [4.4] Cub/$Pm\overline{3}n$ 157 [1.6] Iso C: Iso 151 [-1.4] Cub/$Pm\overline{3}n$ 90 [-4.5] M 14 [-4.5] Cr	*58*	14
1H6/7	6	7	H: Cr 54 [16.3] M 85 [1.1] Cub/$Pm\overline{3}n$ 146 [0.5] Iso C: Iso 139 [-0.4] Cub/$Pm\overline{3}n$ 59 [-0.7] M < 20 Cr	*54*	*14*
1H7/7	7	7	H: Cr 77 [8.0] M 105 [2.9] Cub/$Pm\overline{3}n$ 145 [0.8] Iso C: Iso 137 [-0.4] Cub/$Pm\overline{3}n$ 89 [-2.6] M < 20 Cr	*56*	*15*
1H8/6[b,c]	8	6	H: Cr 67 [23.4] M 107 [2.2] Cub/$Pm\overline{3}n$ 139 [0.5] Iso C: Iso 127 [-0.4] Cub/$Pm\overline{3}n$ 93 [-2.1] M < 20 Cr	*52*	15
1H9/5[b,c]	9	5	H: Cr 62 [4.0] M 135 [3.3] Iso C: Iso 127 [-3.1] M < 20 Cr	48	15
1F5/7	5	7	H: Cr < 20 M 142 [1.6] Col$_{hex}$/$p6mm$ 154 [5.4] Iso C: Iso 150 [-5.0] Col$_{hex}$/$p6mm$ 136 [-1.9] M < 20 Cr	52	13
1F3/10	3	10	H: Cr 105 [3.3] M 118 [0.8] M 129 [6.8] Cub/$Pm\overline{3}n$ 139 [1.1] Iso C: Iso 131 [-0.6] Cub/$Pm\overline{3}n$ 123 [-6.9] M < 20 Cr	66	14
1F5/8[b,c]	5	8	H: Cr 110 [-] M 151 [9.4] Iso C: Iso 144 [-8.9] M < 20 Cr	58	14
1F6/7	6	7	H: Cr < 20 M 131 [0.3] Col$_{hex}$/$p6mm$ 146 [5.4] Iso C: Iso 140 [-5.3] Col$_{hex}$/$p6mm$ 117 [-0.7] M < 20 Cr	54	14
1F4/10[a,b,c]	4	10	H: Cr < 20 M 83 [3.5] Cub/$Pm\overline{3}n$ 130 [-] Iso C: Iso 130 [-] Cub/$Pm\overline{3}n$ 68 [-2.0] M < 20 Cr	68	15
1F6/8[b,c]	6	8	H: Cr 93 [1.9] M 129 [5.4] Iso C: Iso 123 [-5.4] M < 20 Cr	60	15
1F7/7	7	7	H: Cr < 20 M 150 [5.7] Iso C: Iso 144 [-5.7] M < 20 Cr	56	15
1F8/6[a,b,c]	8	6	H: Cr 98 [-] M 132 [4.3] Iso C: Iso 130 [-1.8] M < 20 Cr	52	15
1F9/5[a,b,c]	9	5	H: Cr 96 [11.4] Col$_{hex}$/$p6mm$ 105 [-] $c2mm$ 137 [-] M 158 [4.7] Iso C: Iso 151 [-4.4] M + Col$_{rec}$/$c2mm$ + Col$_{hex}$/$p6mm$ < 20 Cr	48	15
1F9/6[a,b,c]	9	6	H: Cr 101 [-] Col$_{rec}$/$c2mm$ 145 [-] M 156 [7.8] Iso C: Iso 153 [-7.3] Col$_{rec}$/$c2mm$ + M < 20 Cr	54	16

[a] Transition temperatures were determined by optical polarization microscopy; [b] Additional unpublished compounds **1X*m/n***, DSC traces can be found in the Appendix-2: Unpublished DSC-data; The red-indicated compound will be further described as a first investigated example of a possible M-phase structure. [c] Unpublished compounds which were already investigated by Synchrotron radiation.[100]

*Table 3.3-2. Structural data for Col$_{hex}$/p6mm and Col$_{rec}$/c2mm phases of compounds **1Fm/n**.*

Comp.	Phase (T/°C)	a [nm]	V_{Cell} [nm³]	$n_{Cell, LC}$	n_{Wall}	L_{Wall} [nm]
1F9/5	*p6mm* (55)	4.55	8.07	3.34	1.1	4.6
1F9/5	*c2mm* (119)	a = 4.66 b = 7.40	15.52	6.42	1.6	4.4
1F9/6	*c2mm* (119)	a = 4.89 b = 7.00	15.40	5.96	1.5	4.3

$V_{Cell} = \frac{\sqrt{3}}{2} a_{hex}^2 h$ for hexagonal phases and $V_{Cell} = a_{rec} \cdot b_{rec} \cdot h$ for the rectangular phases, where h represents the height of the unit cell and is assumed to be 0.45 nm. V_{Mol} = volume of the molecule as determined by the crystal volume increments.[98] $n_{Cell,cr}$ = number of molecules per unit cell in the crystalline state, calculated according to $n_{Cell,cr} = V_{Cell}/V_{Mol}$ (average packing coefficient in the crystal is k = 0.7). $n_{Cell,liq}$ = the number of molecules in the unit cell of an isotropic liquid with an average packing coefficient k = 0.55, calculated according to $n_{Cell,liq}$ = 0.55/0.7. $n_{Cell,LC}$ = number of molecules in the unit cell in the LC state as estimated from the average of $n_{Cell,cr}$, and $n_{Cell,liq}$ [99] n_{Wall} = the number of molecules in the cross-section of the honeycomb walls, calculated as $n_{Wall} = \frac{n_{cell,LC}}{3}$, calculated as $n_{Wall} = \frac{n_{cell,LC}}{4}$ for c2mm cells, L_{wall} is the side length of the polygonal cells.

*Table 3.3-3. Structural data for the Cub/Pm$\overline{3}$n phases of the **1Hm/n** and **1Fm/n** compounds.*

Comp.	Phase (T/°C)	a_{cub} [nm]	V_{Cell} [nm³]	$n_{Cell, LC}$	n_{Bundle}
1H5/8	*Pm$\overline{3}$n* (119)	9.06	744	279	5.2
1H8/6	*Pm$\overline{3}$n* (119)	9.13	761	305	5.6
1F4/10	*Pm$\overline{3}$n* (92)	8.67	652	219	4.1

V_{Cell} = volume of the unit cell, calculated according to $V_{Cell} = a_{cub}^3$. $n_{Cell,cr}$ = number of molecules per unit cell in the crystalline state, calculated according to $n_{Cell,cr} = V_{Cell}/V_{mol}$ (average packing coefficient in the crystal is k = 0.7). $n_{Cell,liq}$ = the number of molecules in the unit cell of an isotropic liquid with an average packing coefficient k = 0.55, calculated according to $n_{cell,liq}$ = 0.55/0.7. $n_{Cell,LC}$ = number of molecules in the unit cell in the LC state as estimated from the average of $n_{cell,cr}$, and $n_{cell,liq}$. n_{Bundle} = number of molecules per bundle in the cubic organization as $n_{Bundle} = n_{Cell,LC}/54$.
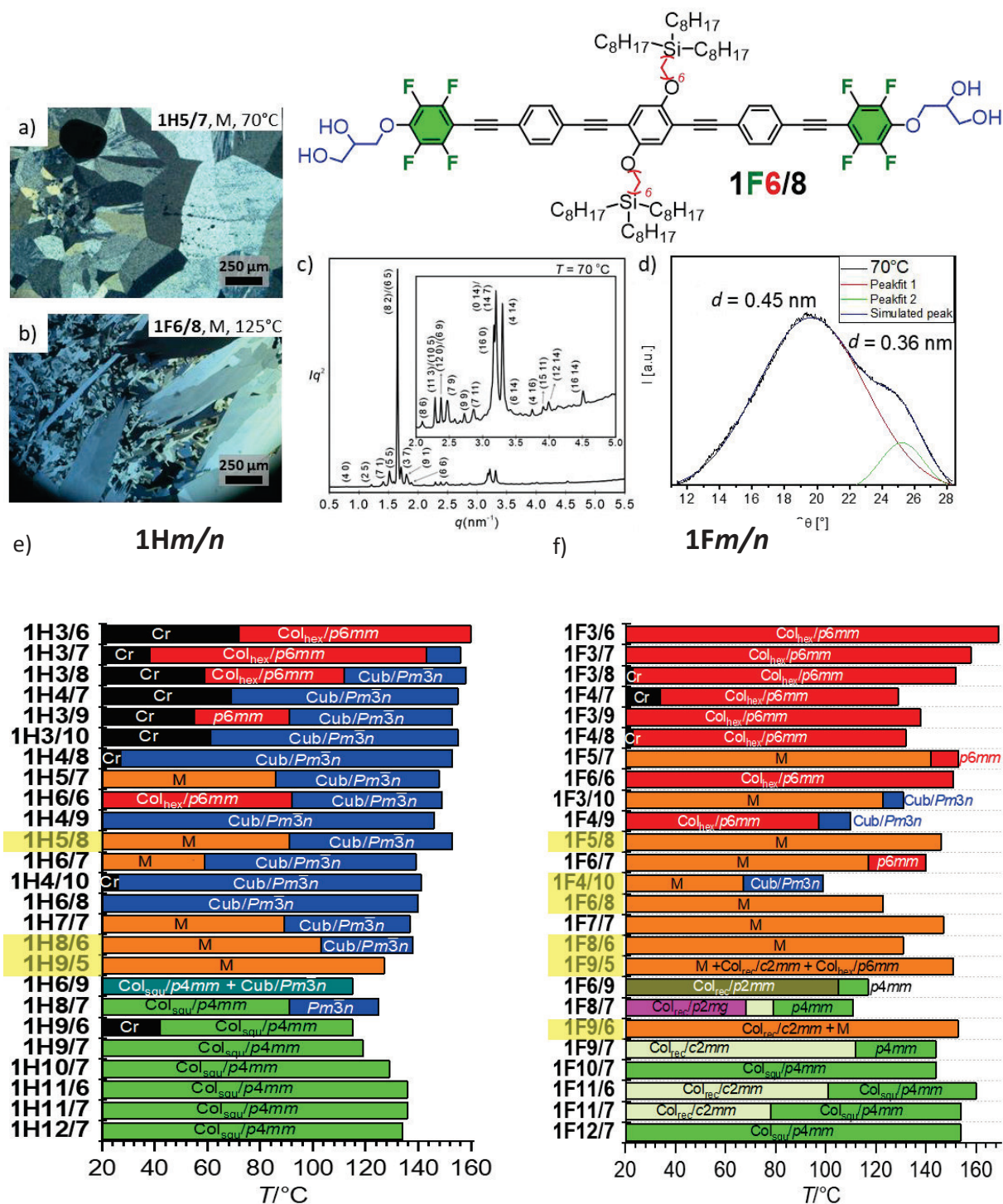
Figure 3.3-1. *Molecular structure of compound* **1F6/8**. *a) mosaic-like texture for the OPE compound* **1H5/7** *recorded on cooling at T = 70°C, b) mosaic-like texture of the FOPE compound* **1F6/8** *recorded on cooling from the isotropic liquid at T = 125°C, c) SAXS diffraction pattern of* **1F6/8** *recorded on cooling at T = 70°C,[100] d) WAXS diffraction pattern recorded at T = 70°C, e, f) mesophase behaviors of compounds* **1Hm/n** *and* **1Fm/n** *on cooling from the isotropic liquid, showing all synthesized compounds, including those from publication A and B. Bar diagrams showing the mesophase ranges of compounds* **1Hm/n** *and* **1Fm/n**. *Abbreviations: Cr = crystalline solid, Col_{squ}/p4mm = square honeycomb; Col_{hex}/p6mm = hexagonal honeycomb; Col_{rec}/c2mm = honeycomb formed by angular distorted squares; Col_{rec}/p2mm = rectangular honeycomb; Col_{rec}/p2mg = honeycomb formed by non-regular triangle cells; M = unknown mesophase; Cub_{net}/Pm$\overline{3}$n = cubic network phase (A15-Type Frank Kasper Phase). Yellow highlighted compounds depict unpublished compounds. Yellow-marked compounds have not yet been published.*

For all **1X*m/n*** compounds, clearing temperatures between T = 130 – 150°C can be observed (**Figure 3.3-1e, f**). The differences in the mesophase stabilities were already described by the odd-even effect of the spacer length ***m*** in Publication A, as well as by the non-perfect filling of triangular and square honeycombs in Publication B. For all M-phases of compounds **1X*m/n*,** a birefringent mosaic-like texture can be observed between crossed polarizers during cooling **(Figure 3.3-1a, b)**. The main difference between the formed M-phases of FOPE and OPE compounds is the nature of the high-temperature (HT) phase. In the case of the non-fluorinated compounds **1H*m/n*,** most of the M-phases are formed during cooling and form an optically isotropic HT phase with a cubic network structure and $Pm\overline{3}n$ symmetry (**Figure 3.3-1a**). In contrast, the formation of the M-phases in the **1F*m/n*** compounds takes place in most cases upon cooling from a birefringent honeycomb phase or directly from the isotropic liquid **(Figure 3.3-1b)**, and only in two cases a $Pm\overline{3}n$ phase is formed. X-ray diffraction experiments showed in all cases with M-phase complex diffraction patterns[100] with reflexes at very small 2θ values, indicating huge lattice parameters (**Figure 3.3-1c**). Some of them might have a 12-fold symmetry, which, however, requires further confirmation. The wide-angle X-ray scattering shows always a diffuse scattering with a maximum at d = 0.45nm, confirming the liquid crystalline state of the investigated phases **(Figure 3.3-1d)**, which is additionally supported by the fluid-like behavior of the samples determined by shearing experiments. The complex XRD patterns[100] are different and indicate several different LC phases, which seem to depend on the spacer length ***m***, the side chain volume V_C, as well as the temperature T. In addition, for all core-fluorinated compounds, there is a diffuse shoulder at d = 0.36 nm, indicating the presence of face-to-face π-stacking interactions.

Only for compound **1F6/8,** all 40+ peaks in the small-angle X-ray diffractogram (**Figure 3.3-1c**) can be indexed to a giant 2D-superlattice with *p*2*gg* symmetry, with lattice parameters of a_{rec} = 31.7 nm, b_{rec} = 27.4 nm.[100] There are no additional BRAGG-reflexes indicating a 3D lattice. Based on the small-angle diffraction pattern, a reconstructed electron density map (EDM) was generated. According to the molecular dimensions, it can be interpreted as a columnar mesophase with a honeycomb structure (**Figure 3.3-2a**). In the EDM, different super-tiling motifs composed of triangular and square honeycombs can be recognized. Moreover, the structure shows angular deformation and side-length modifications, which are attributed to the tilt of the molecules in the honeycomb walls as well as deformation and fusion of some glycerol columns (**Figure 3.3-2b**). This tentative structure is formed by 126 walls. The number of molecules per unit cell with an assumed height of h = 0.45 nm is calculated to $n_{Cell,LC}$ = V_{Cell} / V_{Mol} = 141. Thus, the average number of molecules in the cross-section of each honeycomb wall can be calculated as 1.2 molecules. This is in line with a single-wall honeycomb structure where the side chains fill the inside of the honeycombs. It can be assumed that the filling of the polygonal tiles cannot be achieved in a perfect manner. This leads to a steric frustration, which is compensated by a tilted organization of the molecules in the honeycomb walls. The tilted organization of the molecules reduces the flexibility of the honeycombs and thus would be in line with the mosaic-like textures.
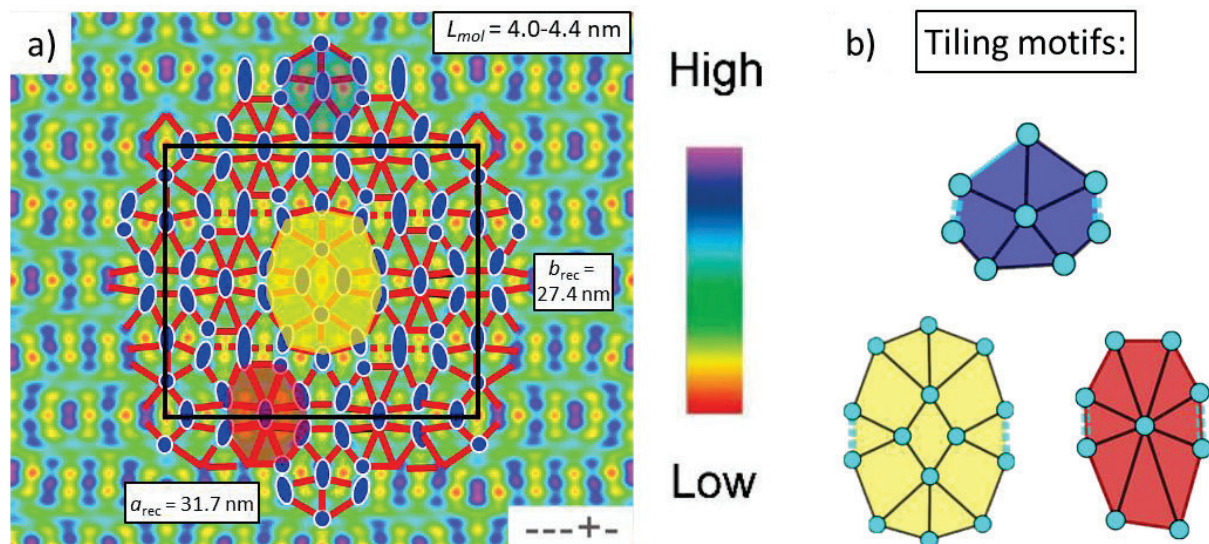
Figure 3.3-2. *a) Reconstructed electron density map (EDM) with inserted tentative tiling model, blue dots represent deformed glycerol columns, and red lines represent the honeycomb walls. The red, yellow, and blue patterns represent the tiling motifs inside the honeycomb structure;[100] b) reconstructed tiling motifs of the derivate dodecagonal, hexagonal, and pentagonal supertiles.[101]*

The structure formed by a mixture of non-regular triangular and tetraangular cells supports the hypothesis that the M-phase in the FOPE compounds could represent close approximants of a quasiperiodic lattice. The origin and structure of the M-phase in the other OPE compounds are still under investigation.

3.4   Bolapolyphiles with dialkylmethylsilyl groups

Besides the trialkylsilyl compounds in sections 3.1 to 3.3, where the spacer *m* between the (F)OPE core and the branching point, as well as the length *n* of the side chains, were modified which were mostly published in Publication A[95] and B[97], another modification of the side chains was conducted by using a dialkylmethylsilyl branching point in the side chains. These compounds have not yet been published and will be described here. The selection was, in this case, not strict with respect to the side chain length, but followed predictions based on a simple geometric model as explained in the next section. The compounds **2X*m/n*** were designed to obtain the largest possible number of M-phase compounds with the potential to form LQCs. Compared to the compounds **1X*m/n*** (**Figure 3.4-1a**), the **2X*m/n*** compounds (**Figure 3.4-1b**) are characterized by the replacement of one alkyl chain *R* by a methyl group, leading to bolapolyphiles with dialkylmethylsilyl substituted side chains. Thus, they represent an intermediate case between the compounds with two-way branched (swallow-tailed) alkyl side chains reported by M. Poppe[44] and the three-way branched carbosilanes **1X*m/n***. The resulting mesophase sequences of compounds **2X*m/n*** are summarized in **Table 3.4-1** sorted first, according to the side chain length L_C and secondly to the spacer length *m*.
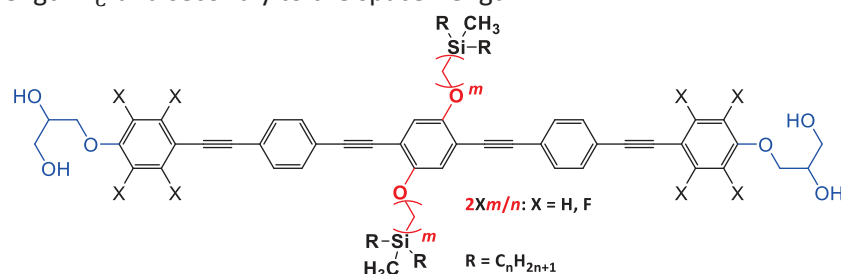

Figure 3.4-1. Molecular structure of compounds **2X*m/n***.

Table 3.4-1: Mesophases and phase transition temperatures of compounds **2X*m/n*** with X = H, F. All transition temperatures were taken from the peak temperatures of the transition peaks at a heating and cooling rate of 10K/min. The transition enthalpies were determined from the peak areas given in kJ/mol.

2X*m/n*	*m*	*n*	Phase Sequence T [°C] and ΔH [kJ/mol]	V_C	L_C
2H3/11[c,d]	3	11	H: Cr 90 [59.4] Col$_{hex}$/*p6mm* 137 [3.7] Cub/*Pm$\overline{3}$n* 151 [1.0] Iso C: Iso 145 [-0.7] Cub/*Pm$\overline{3}$n* 131 [-4.1] Col$_{hex}$/*p6mm* 44 [-36.1] Cr	52	15
2H4/10[c,d]	4	10	H: Cr 55 [21.1] Col$_{hex}$/*p6mm* 101 [2.0] Cub/*Pm$\overline{3}$n* 143 [1.0] Iso C: Iso 135 [-0.4] Cub/*Pm$\overline{3}$n* 90 [-2.0] Col$_{hex}$/*p6mm* < 20 Cr	50	15
2H5/9[c,b]	5	9	H: Cr 55 [22.8] Col$_{hex}$/*p6mm* 146 [4.4] Iso C: Iso 142 [-4.4] Col$_{hex}$/*p6mm* 16 [-16.9] Cr	48	15
2H3/12[a,b,c]	3	12	H: Cr 90 [48.6] M 101 [-] Col$_{hex}$/*p6mm* 111 [3.1] Cub/*Pm$\overline{3}$n* 144 [1.1] Iso C: Iso 141 [-0.9] Cub/*Pm$\overline{3}$n* 107 [-2.9] Col$_{hex}$/*p6mm* 101 [-] M 44 [-39.5] Cr	56	16
2H5/10[b,c]	5	10	H: Cr 55 [24.7] M 127 [3.7] Cub/*Pm$\overline{3}$n* 141 [0.6] Iso C: Iso 134 [-0.4] Cub/*Pm$\overline{3}$n* 121 [-3.8] M 7 [-3.4] Cr	52	16
2H4/12[b,c]	4	12	H: Cr 61 [5.6] Cub/*Pm$\overline{3}$n* 127 [0.6] Iso C: Iso 112 [-0.3] Cub/ *Pm$\overline{3}$n* < 20 Cr	58	17
2H6/10[a,b,c]	6	10	H: Cr 81 [30.0] M 110 [2.3] Cub/*Pm$\overline{3}$n* 135 [0.5] Iso C: Iso 130 [-] Cub/*Pm$\overline{3}$n* 95 [-2.6] M < 20 Cr	54	17
2H7/9[b,c]	7	9	H: Cr 56 [14.5] M 123 [3.7] Iso C: Iso 114 [-3.0] M < 20 Cr	52	17
2H3/14[a,b,c]	3	14	H: Cr 68 [26.4] M 83 [17.0] Cub/*Pm$\overline{3}$n* 143 [1.0] Iso C: Iso 135 [-] Cub/*Pm$\overline{3}$n* 65 [-4.1] M 39 [-20.6] Cr	64	18

[a] Transition temperatures were determined by optical polarization microscopy. [b] Compounds which were already investigated by Synchrotron radiation.[100] [c] Additional unpublished compounds **2X*m/n***, DSC traces can be found in Appendix-2: Unpublished DSC-data. [d] XRD-Data of the unpublished compounds measured with in-house XRD can be found in Appendix-3: Unpublished XRD-Data.

Table 3.4-1 (cont). *Mesophases and phase transition temperatures of compounds* **2Xm/n** *with X = H, F. All transition temperatures were taken from the peak temperatures of the transition peaks at a heating and cooling rate of 10K/min. The transition enthalpies were determined from the peak areas given in kJ/mol.*

2X*m/n*	*m*	*n*	Phase Sequence *T* [°C] and Δ*H* [kJ/mol]	V_C	L_C
2H7/10[b,c]	7	10	H: Cr 70 [3.4] Col$_{squ}$/*p4mm* 91 [1.4] Iso C: Iso 73 [-1.8] Col$_{squ}$/*p4mm* < 20 Cr	56	18
2H9/8[b,c]	9	8	H: Cr 95 [12.0] Col$_{squ}$/*p4mm* 123 [2.4] Iso C: Iso 116 [-2.2] Col$_{squ}$/*p4mm* 52 [-9.3] Cr	52	18
2H4/14[a,b,c]	4	14	H: Cr 69 [37.2] Cub/*Pm$\bar{3}$n* + M 84 [-] Cub/*Pm$\bar{3}$n* 113 [0.7] Iso C: Iso 110 [-] Cub/*Pm$\bar{3}$n* 65 [-] Cub/*Pm$\bar{3}$n* + Col$_{squ}$/*p4mm* 45[-8.7] Cr	66	19
2H6/12[a,b,c]	6	12	H: Cr 73 [9.1] Col$_{squ}$/*p4mm* 98 [3.7] Cub/*Pm$\bar{3}$n* 116 [0.3] Iso C: Iso 113 [-] Cub/*Pm$\bar{3}$n* 87 [-3.6] Col$_{squ}$/*p4mm* < 20 Cr	62	19
2H9/11[d,c]	9	11	H: Cr 81 [13.0] Col$_{squ}$/*p4mm* 127 [3.1] Iso C: Iso 121 [-3.3] Col$_{squ}$/*p4mm* < 20 Cr	64	21
2H11/11[b,c]	11	11	H: Cr 77 [14.1] Col$_{squ}$/*p4mm* 131 [6.8] Iso C: Iso 126 [-6.5] Col$_{squ}$/*p4mm* < 20 Cr	68	23
2F3/11[a,c,d]	3	11	H: Cr < 20 [-] Col$_{hex}$/*p6mm* 138 [1.1] M2 159 [9.3] Iso C: Iso 156 [-10.1] Col$_{hex}$/*p6mm* 119 [-] M < 20 Cr	52	15
2F4/10[a,c,d]	4	10	H: Cr < 20 [-] Col$_{hex}$/*p6mm* 155 [6.9] Iso C: Iso 151 [-6.5] Col$_{hex}$/*p6mm* < 20 Cr	50	15
2F5/9[b,c]	5	9	H: Cr < 20 Col$_{hex}$/*p6mm* 164 [9.9] Iso C: Iso 161 [-9.7] Col$_{hex}$/*p6mm* < 20 Cr	48	15
2F3/12[b,c]	3	12	H: Cr 55 [51.1] M 153 [10.3] Iso C: Iso 149 [-5.9] Col$_{hex}$/*p6mm* 145 [-2.4] M < 20 Cr	56	16
2F5/10[a,b,c]	5	10	H: Cr 110 [-] M 163 [10.4] Iso C: Iso 158 [-10.1] M < 20 Cr	52	16
2F4/12[a,b,c]	4	12	H: Cr 76 [1.3] M 108 [-] M 123 [4.0] Iso C: Iso 116 [-3.8] Col$_{hex}$/*p6mm* 106 [-] M 82 [-0.4] M < 20 Cr	58	17
2F6/10[a,b,c]	6	10	H: Cr 115 [-] M 145 [7.8] Iso C: Iso 141 [-7.1] M 87 [-] M < 20	54	17
2F7/9[a,b,c]	7	9	H: Cr 101 [-] M 148 [4.9] Iso C: Iso 142 [-5.7] M < 20 Cr	52	17
2F3/14[a,b,c]	3	14	H: Cr <20 Col$_{rec}$^{T}/*p2mm* 110 [-] Col$_{squ}$/*p4mm* 133 [9.1] Iso C: Iso 127 [-9.0] Col$_{squ}$/*p4mm* 110 [-] Col$_{rec}$^{T}/*p2mm* < 20 Cr	64	18
2F7/10[a,b,c]	7	10	H: Cr 101 [-] M 135 [3.5] Iso C: Iso 128 [-5.7] M < 20 Cr	56	18
2F9/8[a,b,c]	9	8	H: Cr < 20 [-] M 153 [6.8] Iso C: Iso 149 [-5.5] M < 20 Cr	52	18
2F4/14[b,c]	4	14	H: Cr 101 [0.7] Col$_{squ}$/*p4mm* 121 [7.6] Iso C: Iso 115 [-7.6] Col$_{squ}$/*p4mm* 98 [-0.7] Col$_{squ}$^{T}/*p4mm* < 20 Cr	66	19
2F6/12[b,c]	6	12	H: Cr 83 [0.2] Col$_{squ}$/*p4mm* 134 [8.5] Iso C: Iso 130 [-7.6] Col$_{squ}$^{T}/*p4mm* < 20 Cr	62	19
2F9/11[d,c]	9	11	H: Cr 69 [7.0] Col$_{squ}$/*p4mm* 154 [10.0] Iso C: Iso 150 [-9.1] Col$_{squ}$/*p4mm* < 20 Cr	64	21
2F11/11[b,c]	11	11	H: Cr 64 [3.0] Col$_{squ}$/*p4mm* 147 [8.3] Iso C: Iso 143 [-7.6] Col$_{squ}$/*p4mm* < 20 Cr	68	23

[a] Transition temperatures were determined by optical polarization microscopy. [b] Compounds which were already investigated by Synchrotron radiation.[100] [c] Additional unpublished compounds **2X*m/n***, DSC traces can be found in Appendix-2: Unpublished DSC-data. [d] XRD-Data of the unpublished compounds measured with in-house XRD can be found in Appendix-3: Unpublished XRD-Data.

In the case of **2H*m/n*** compounds, the optically isotropic A15-type cubic network phase (Cub$_{net}$/$Pm\overline{3}n$), the birefringent M-phase with mosaic-like textures, as well as the triangular and square honeycomb phases could be observed (**Figure 3.4-3a**) as they were also found in the **1H*m/n*** compounds. The observed M-phases in the **2H*m/n*** compounds show the same characteristics as mosaic-like textures and complex XRD patterns as described before in section 3.3 for the **1H*m/n*** compounds. In all **2H*m/n*** compounds, the M-phase forms either on heating or cooling as the LT phase below the $Pm\overline{3}n$ phase, and in one case directly below the isotropic liquid state. The mosaic-like texture (**Figure 3.4-2a**) and SAXS-diffractogram (**Figure 3.4-2b**) of **2H5/10** are depicted as representative examples. It can be seen that the diffuse reflex at *d* = 0.45 nm in the WAXS of the M-phase at the given temperature is still present, indicating the liquid crystalline state of the compounds. The SAXS shows again in all cases reflexes at very small *2θ* values, indicating huge lattice parameters in the M-phase of the **2H*m/n*** compounds. Some of them might have a 12-fold symmetry.[100] The complex XRD patterns are different and indicate several different LC phases, too. In the cases **2H*m/n***, it also seems that the M-phase structure depends on the spacer length *m*, the side chain volume *n*, and the temperature *T*.
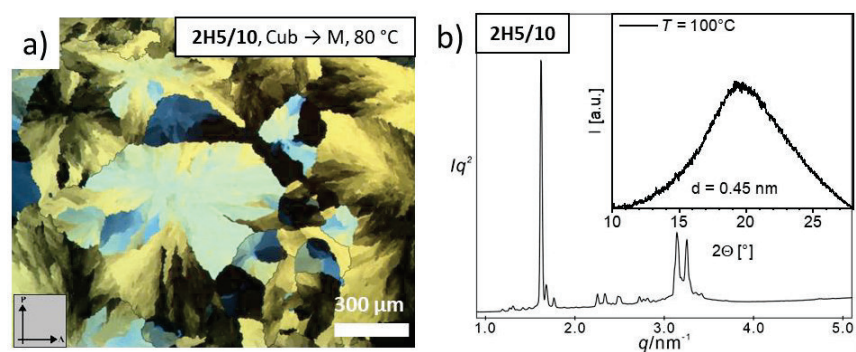

Figure 3.4-2. *Compound* ***2H5/10***. *a) Mosaic-like textures of the M-phase at given temperature between crossed polarizers (direction of the polarizers is indicated by arrows); b) SAXS diffractogram*[100] *of the M-phase with inset WAXS diffractogram.*

For compounds **2H*m/n*,** the general trend that with the low chain volume V_C and small chain length L_C Col$_{hex}$/$p6mm$ phases are stabilized, and Col$_{squ}$/$p4mm$ phases are supported by larger chain volume and long chain length, is present. However, in comparison to compounds **1H*m/n***, the *p6mm* phase is less pronounced, and the phase sequence of Col$_{hex}$/$p6mm$ → M + Cub$_{net}$/$Pm\overline{3}n$ → Col$_{squ}$/$p4mm$ can be found again. A smaller amount of the *p6mm* phases could be explained by the smaller number of synthesized compounds with shorter spacers and low chain volume compared to the **1H*m/n*** compounds.

For the fluorinated compounds **2F*m/n*,** again, the birefringent M-phase with mosaic-like texture and the triangular and square honeycomb phases can be observed as found in the **1F*m/n*** compounds; however, the $Pm\overline{3}n$ phase is completely missing among the synthesized compounds. Additionally, two further honeycomb phases, a rectangular and a tilted square phase, can be observed in the series of **2F*m/n*** compounds (**Figure 3.4-3b**) and will be described in the following by the example compounds **2F3/14** and **2F6/12**.
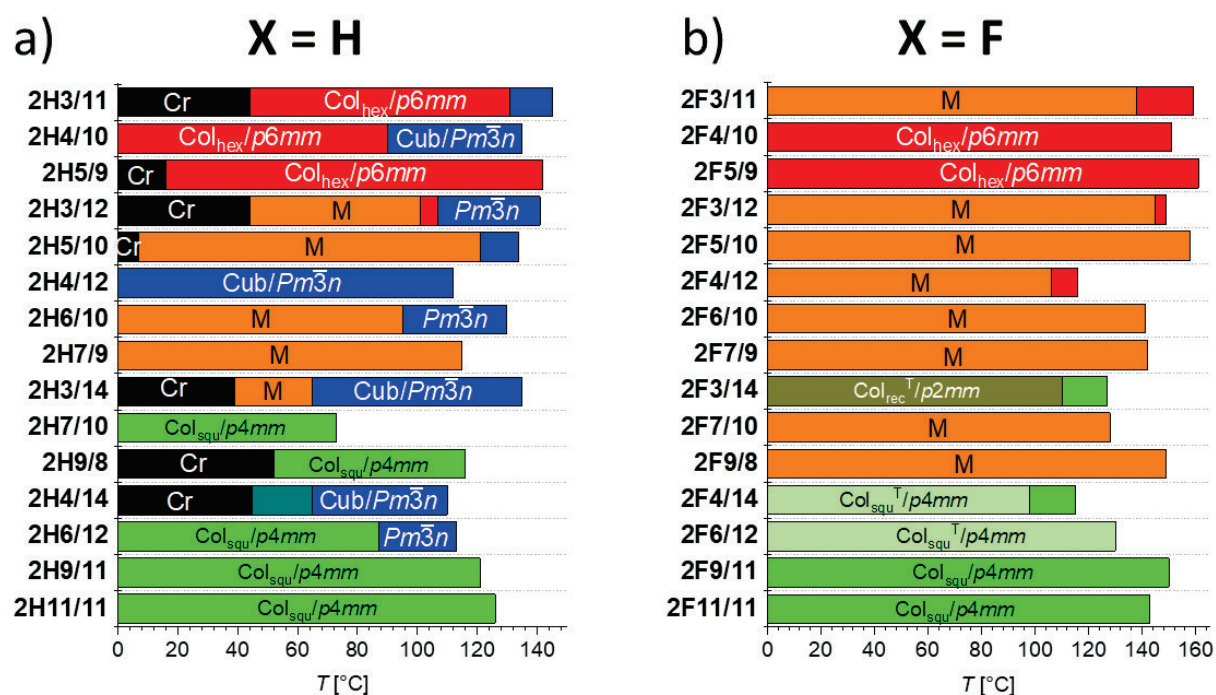
Figure 3.4-3. *Mesophase behavior of a) **2Hm/n** and b) **2Fm/n** compounds on cooling from the isotropic liquid. Bar diagrams showing the mesophase range of compounds **2Hm/n** and **2Fm/n**, abbreviations: Cr = crystalline solid; Col_{hex} and Col_{squ} = triangular and square LC honeycombs; Col_{squ}^{T}/p4mm. respectively; Col_{rec}^{T}/p2mm = tilings by rectangular honeycombs. respectively; Cub/Pm3̄n = cubic network phase with Pm3̄n space group (A15 phase); M = unknown LC phases; The isotropic liquid state is at the right side of the columns.*

Table 3.4-2. *Structural data for the Col_{hex}/p6mm phase of compounds **2Hm/n** and **2Fm/n**.*

Comp.	Phase (T/°C)	a [nm]	V_{Cell} [nm³]	$n_{Cell,LC}$	n_{Wall}	L_{Wall} [nm]
2H3/11	*p6mm* (70)	4.49	7.86	3.17	1.1	4.5
2H4/10	*p6mm* (70)	4.36	7.41	3.03	1.0	4.4
2H5/9	*p6mm* (110)	4.39	7.51	3.18	1.1	4.4
2H3/12	*p6mm* (101)	4.35	7.37	2.85	1.0	4.4
2F3/11	*p6mm* (145)	4.33	7.31	2.89	1.0	4.3
2F4/10	*p6mm* (100)	4.40	7.21	2.91	1.0	4.4
2F5/9	*p6mm* (92)	4.55	8.07	3.34	1.1	4.6
2F3/12	*p6mm* (143)	4.39	7.51	2.84	0.9	4.4

$V_{Cell} = \frac{\sqrt{3}}{2} a_{hex}^2 h$, where h represents the height of the unit cell and is assumed to be 0.45 nm. V_{Mol} = volume of the molecule as determined by the crystal volume increments.[98] $n_{Cell,cr}$ = number of molecules per unit cell in the crystalline state, calculated according to $n_{Cell,cr} = V_{cell}/V_{mol}$ (average packing coefficient in the crystal is k = 0.7). $n_{Cell,liq}$ = the number of molecules in the unit cell of an isotropic liquid with an average packing coefficient k = 0.55, calculated according to $n_{Cell,liq}$ = 0.55/0.7. $n_{Cell,LC}$ = number of molecules in the unit cell in the LC state as estimated from the average of $n_{Cell,cr}$, and $n_{Cell,Liq}$ [99] n_{Wall} = the number of molecules in the cross-section of the honeycomb walls, calculated as $n_{Wall} = \frac{n_{Cell,LC}}{3}$. Blue indicates compounds which were only measured with in-house XRD at MLU University.

Table 3.4-3. Structural data for the Cub/Pm$\bar{3}$n phases of the *2Hm/n* and *2Fm/n*.

Comp.	Phase (T/°C)	a_{cub} [nm]	V_{Cell} [nm³]	$n_{Cell,LC}$	n_{Bundle}
2H3/11	Pm$\bar{3}$n (140)	9.05	741	299	5.5
2H4/10	Pm$\bar{3}$n (120)	8.75	670	277	5.1
2H3/12	Pm$\bar{3}$n (128)	8.89	703	272	5.0
2H5/10	Pm$\bar{3}$n (128)	9.03	736	297	5.5
2H4/12	Pm$\bar{3}$n (92)	8.94	715	270	5.0
2H6/10	Pm$\bar{3}$n (115)	9.10	754	298	5.5
2H3/14	Pm$\bar{3}$n (84)	9.06	744	265	4.9
2H4/14	Pm$\bar{3}$n (92)	8.86	696	243	4.5
2H6/12	Pm$\bar{3}$n (105)	9.16	769	279	5.2

V_{Cell} = volume of the unit cell, calculated according to $V_{Cell} = a_{cub}^3$. V_{Mol} = volume of the molecule as determined by the crystal volume increments.[98] $n_{Cell,cr}$ = number of molecules per unit cell in the crystalline state, calculated according to $n_{Cell,cr} = V_{Cell}/V_{Mol}$ (average packing coefficient in the crystal is k = 0.7). $n_{Cell,liq}$ = the number of molecules in the unit cell of an isotropic liquid with an average packing coefficient k = 0.55, calculated according to $n_{Cell,liq}$ = 0.55/0.7. $n_{Cell,LC}$ = number of molecules in the unit cell in the LC state as estimated from the average of $n_{Cell,cr}$, and $n_{Cell,liq}$. n_{Bundle} = number of molecules per bundle in the cubic organization as $n_{Bundle} = n_{Cell,LC}/54$. Blue indicates compounds that were only measured with in-house XRD at MLU University.

Table 3.4-4. Structural data for Col$_{squ}$/p4mm and Col$_{rec}$/p2mm phases of compounds *2Hm/n* and *2Fm/n*.

Comp.	Phase (T/°C)	a,b [nm]	V_{Cell} [nm³]	$n_{Cell, LC}$	n_{Wall}	L_{Wall} [nm]
2H7/10	p4mm (37)	4.11	7.60	2.94	1.5	4.1
2H9/8	p4mm (105)	4.14	7.71	3.11	1.6	4.1
2H4/14	p4mm (55)	4.00	7.20	2.51	1.3	4.0
2H6/12	p4mm (83)	4.16	7.79	2.83	1.4	4.2
2H9/11	p4mm (100)	4.49	8.95	3.19	1.6	4.5
2H11/11	p4mm (87)	4.27	8.20	2.81	1.4	4.3
2F3/14	p4mm (119)	4.02	7.27	2.54	1.3	4.0
	p2mm (101)	a = 4.08 b = 3.57	6.55	2.29	1.1	4.1 3.6
	p2mm^T (37)	a = 3.91 b = 3.37	5.93	2.07	1.0	3.9 3.4
2F4/14	p4mm (110)	4.08	7.49	2.57	1.3	4.1
	p4mm^T (42)	3.37	5.11	1.75	0.9	3.4
2F6/12	p4mm^T (42)	3.39	5.17	1.84	0.9	3.4
2F9/11	p4mm (120)	4.20	8.59	3.00	1.5	4.4
2F11/11	p4mm (92)	4.27	8.20	2.76	1.4	4.3

V_{Cell} was determined according to $V_{Cell} = a_{squ}^2 \cdot h$ for the square and $a_{rec} \cdot b_{rec} \cdot h$ for the rectangular, where h represents the height of the unit cell, which was assumed to be 0.45 nm. $n_{Cell,cr}$ = number of molecules per unit cell in the crystalline state, calculated according to $n_{Cell,cr} = V_{Cell}/V_{Mol}$ (average packing coefficient in the crystal is k = 0.7). $n_{Cell,liq}$ = the number of molecules in the unit cell of an isotropic liquid with an average packing coefficient k = 0.55, calculated according to $n_{Cell,liq}$ = 0.55/0.7. $n_{Cell,LC}$ = number of molecules in the unit cell in the LC state as estimated from the average of $n_{Cell,cr}$, and $n_{Cell,Liq}$. n_{Wall} = the number of molecules in the cross-section of the honeycomb walls, calculated as $n_{Wall} = \frac{n_{Cell,LC}}{2}$ for p4mm and p2mm cells, L_{Wall} is the side length of the polygonal cells. Blue indicates compounds that were only measured with in-house XRD at MLU University.

Compound **2F3/14** shows, by polarization microscopic optical investigations on cooling from the isotropic liquid, the formation of spherulitic textures with optically isotropic areas (**Figure 3.4-4a**). The SAXS pattern (**Figure 3.4-4d**)[100] indicates a square lattice showing the typical ratio of d-spacing $1 : \frac{1}{\sqrt{2}} : \frac{1}{2} : \frac{1}{\sqrt{10}} : \frac{1}{\sqrt{13}}$: …with a lattice parameter of a_{squ} = 4.02 nm. This is in agreement with the molecular length of L_{mol} = 4.0 – 4.4 nm between the ends of the glycerols. On further cooling, the optical isotropic areas in the texture become birefringent, and a biaxial mesophase becomes the dominating LC phase at low temperature. The SAXS pattern[100] of the biaxial LT phase is indexed to a rectangular columnar phase with a $p2mm$ plane group and parameters of a_{rec} = 4.1 nm and b_{rec} = 3.57 nm at 101°C (**Figure 3.4-4f**). While a_{rec} corresponds almost with the full molecular length (L_{mol} = 4.0 – 4.4 nm), b_{rec} is significantly shorter, requiring a significant tilt of the FOPE cores of about $\beta = cos^{-1} \left(\frac{b_{rec}}{L_{mol}} = \frac{3.6\ nm}{4.4\ nm} \right) = $ 35° which is close to the "magic angle"[2] of 35.3°. This is in line with the fact that the birefringence of **2F3/14** decreases with decreasing temperature. Since only half of the walls are tilted, no inversion of the birefringence from negative to positive can be observed, which would be typical for crossing the magic angle. The diffuse WAXS pattern with its maximum at d = 0.45 nm confirms the LC state over the whole temperature range. A reconstruction of the EDMs (**Figure 3.4-4e, g**) shows that the molecular organization is in line with the assumed honeycomb structures for the $p4mm$ and $p2mm$ plane groups. The high ED (purple) represents the columns of the hydrogen bonding networks involving the glycerols, and medium electron density regions (green/blue) represent the positions of the FOPE cores, forming the honeycomb walls. The lowest ED (yellow/red) represents the filling of the resulting square and rectangular prismatic cells by the low ED flexible alkyl chains.

---

[2] "Magic angle": describes the boundary between negative and positive birefringence observed when the slow optical axis of the -conjugated rods assumes the magic angle of 54.7° with respect to the column long axis, i.e., 90°-57.7° = 35.3° tilt with respect to the lattice plane. Here we use the angle between the lattice plane and tilt direction as "magic angle".
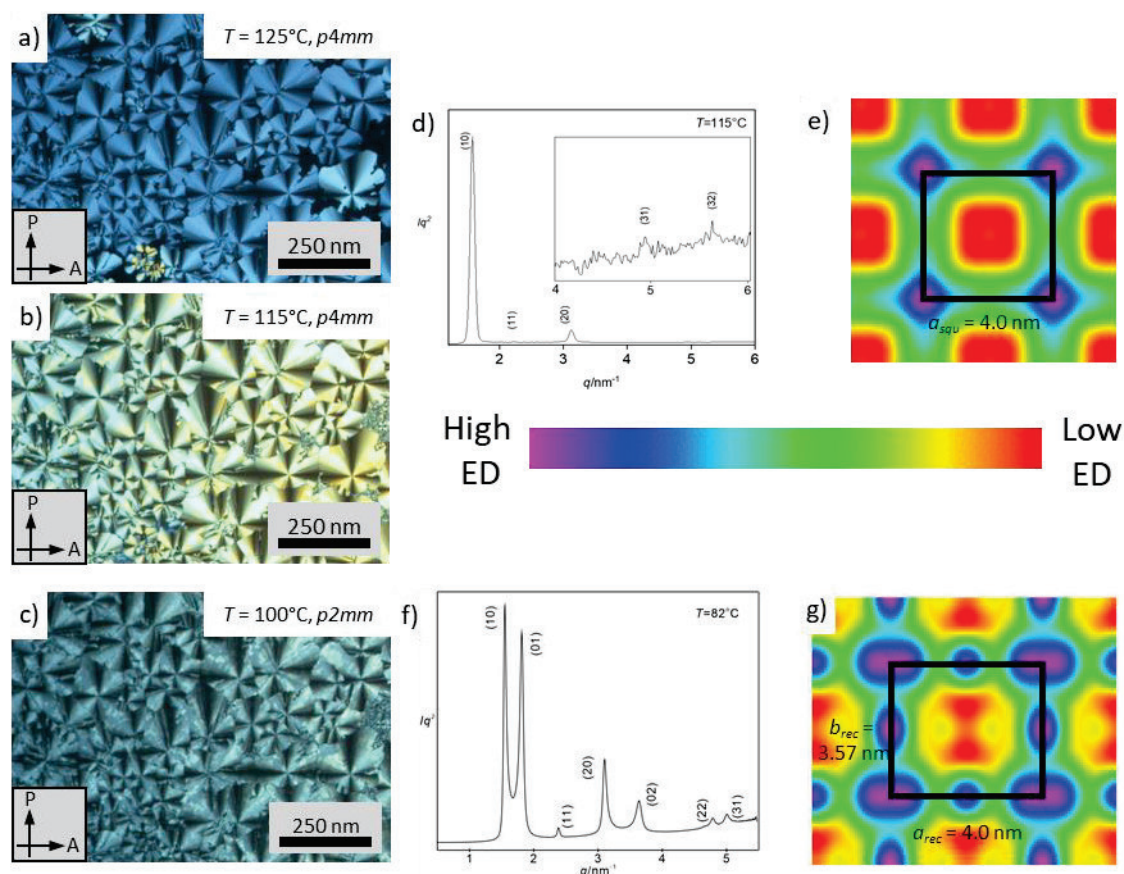
Figure 3.4-4. *Compound **2F3/14**. a – c) Texture between crossed polarizers (direction of the polarizers is indicated by arrows) in the a. b) HT Col$_{squ}$/p4mm phase and c) in the LT Col$_{rec}$/p2mm phase; d) SAXS diffractogram in the Col$_{squ}$ phase;[100] f) SAXS diffractogram in the Col$_{rec}$ phase;[100] e,g) reconstructed EDMs (red = low ED. blue/purple = high ED) d) the Col$_{squ}$ phase and g) the Col$_{rec}$ phase.[100]*

Also, for compound **2F6/12** during cooling from the isotropic liquid, a spherulitic-like texture is observed (**Figure 3.4-5a**), which is typical for a columnar phase. Also, in this case, XRD investigations[100] indicated the *d*-spacing of sharp reflections in the small angle region in a ratio of $1 : \frac{1}{\sqrt{2}} : \frac{1}{2} : \frac{1}{\sqrt{5}} : \frac{1}{\sqrt{8}} : \dots$ corroborating a square lattice with *p4mm* symmetry and a lattice parameter of a_{squ} = 4.12 nm at 124°C. During further cooling, a color change from yellow-green to blue-gray of the spherulites can be observed, indicated by a decrease of *Δn* (**Figure 3.4-5b**), being a first indication of the onset of a tilted organization of the FOPE-rod in the honeycomb walls of the LC phases. According to the XRD, the square lattice is retained in this case and the lattice parameter of the square *p4mm* continuously decreases to a_{squ} = 3.79 nm at *T* = 42°C becoming significantly smaller than the molecular length (**Figure 3.4-5c**) confirming a tilted organization of the rigid rod-like cores in all honeycomb walls (correspond to tilt of 30.5°).
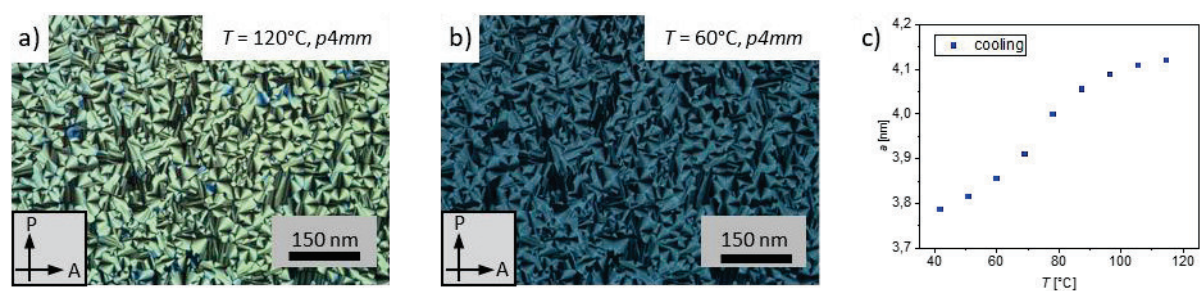
Figure 3.4-5. *Compound **2F6/12**. Textures of a) the Col$_{squ}$ and b) the Col$^T_{squ}$ phase between crossed polarizers. C) temperature-dependent lattice parameter plot of a$_{squ}$.*

Overall, similar to the previously observed phase sequence $Col_{hex}/p6mm \rightarrow$ M / $Cub_{net}/Pm\overline{3}n$ $\rightarrow Col_{squ}/p4mm$ for **1H*m/n*** compounds, the same sequence could be observed for the **2H*m/n*** compounds.

However, the number of compounds with triangular honeycombs decreased to only 4 compounds, probably due to the limited number of synthesized compounds **2H*m/n***. It appears that the Col_{hex} formation takes place in the same chain volume V_C = 48 – 56, but in a larger chain length LC range LC = 15 -16 than in the **1H*m/n*** compounds. Additionally, it appears that M-phase formation is a bit more supported by compounds **1H*m/n*** compared to **2H*m/n,*** while the cubic range seems to exist in the same V_C range of 50 – 66. The square honeycomb is already formed for a compound with V_C = 52, while for the series **1H*m/n,*** it starts for V_C = 56. The phases of the **2F*m/n*** compounds show, besides the previously reported triangular, rectangular, square, and unknown M honeycomb phases, an additional birefringent honeycomb phase with a tilted organization of the FOPE-rods in the square honeycomb phase (**Figure 3.4-3b)**. However, in contrast to the series **1F*m/n,*** no cubic phase can be found among the synthesized compounds, and the formation of the triangular honeycombs is also limited to only 4 compounds, again being in nearly the same chain volume range V_C: 44 – 58 as the compounds of series **1F*m/n***. The M-phase range in compounds **1H*m/n*** appears expanded, while compared to compounds **2H*m/n,*** nearly the same amount of M-phases can be observed in a lower number of synthesized compounds. Overall, because **2F*m/n*** has less number of synthesized compounds, it appears that there is a larger probability of M-phase (and hence potential LQC formation), and the influence of the chain volume on the mesophase type is a bit more important compared to the series **1X*m/n***. A comparison of the phase sequence of **2X*m/n*** with **1X*m/n*** indicates a different structure of the rectangular honeycombs in the *p2mm* phase formed in the two series. In the series **1X*m/n,*** the cell deformation results from an elliptical deformation of the glycerol columns, while in the series **2X*m/n,*** it is due to a tilting of the molecules in half of the honeycomb walls. In addition, the substitution of one alkyl chain at the Si branching point by methyl seems to shift the self-assembly processes away from a chain length-driven (L_C) arrangement to a more chain volume-influenced (V_C) self-assembly.

3.5   Geometric model for the prediction of M-phase formation

Parallel to the synthesis and investigation work on the compounds **1X*m/n* – 5X*m/n*,** mathematical analyses were conducted by V. M. Fischer and Prof. R. Waldecker, aiming to understand the mesophase sequences of the **1X*m/n*, 2X*m/n*,** and **5X*m/n*** compounds. The study combined the molecular dimensions of the synthesized compounds, ignoring intermolecular interactions. Conformational equilibria, and other details with the geometrical dimensions of the possible tilings in a simple geometric way. By abstracting side chain length (L_C) and side chain volume (V_C) and the dimensions of the (F)OPE cores, molecular parameters required for M-phase formation were determined, further optimized, and then experimentally verified (**Figure 3.5-1).** This gives the possibility for a more focused synthesis of compounds, potentially forming the M-phases. Further details of this geometric model can be found in the planned Ph.D. Thesis of Virginia-Marie Fischer. Most of the compounds **2X*m/n*** with $R_1 = CH_3$ (**Figure 3.5-1a**) were selected based on this simple model. The observed LC phases proved the efficiency of the proposed geometric model (**Table 3.4-1**, **Figure 3.5-2**, **3.5-3**). Therefore, using this mathematical model and depending on the molecular structural parameters i.e. V_{Core} = volume of the (F)OPE cores, V_{SC} = side chain volume, L_C = length of the side chain ($m+n$+1) (**Figure 3.5-1b**) we specifically synthesized the predicted molecules and successfully obtained a large number of **2X*m/n*** compounds exhibiting the predicted M-phase.
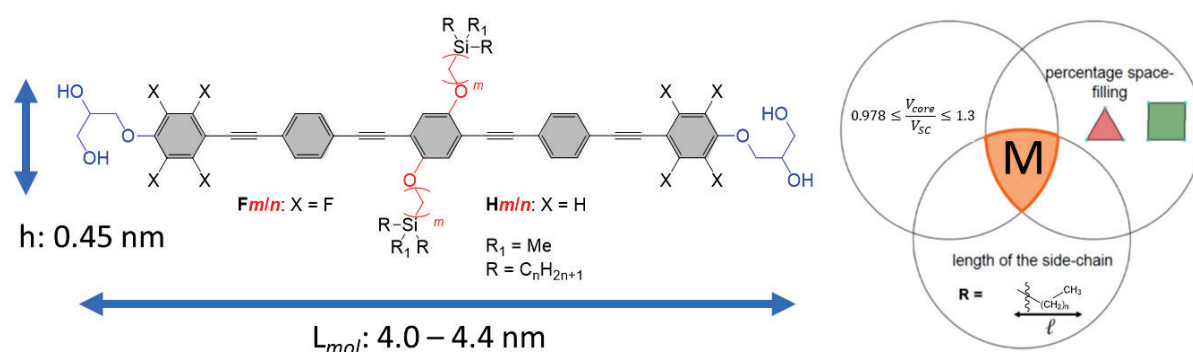
Figure 3.5-1: *a) Molecular structure with approximate length and height; b) simplified scheme of the developed geometric model with predictions of M-phase formation depending on molecular structural parameters (V_{Core} = volume of the (F)OPE cores; $^3V_{SC}$ = side chain volume; l = length of the side chain (m+n+1)).[101]*

However, only "ideal" triangle and square honeycombs with side lengths corresponding with the molecular length were considered and further details like tilted organizations (Section 3.4) and the formation of rhombic or rectangular honeycombs (Publication B and Section 3.4) were not considered in the scope of the geometric model due to the limitations imposed by the simplicity of the geometric restrictions and the focus on the M-phase. This geometric model was developed for the compounds with OPE and FOPE core based on a data set of 20 compounds each and was verified by 15 compounds synthesized for both series on the basis of these predictions. The M-phase was predicted for the **1X*m/n*** compounds (**Figure 3.5-2**) with a success rate of 77%. Furthermore, the formation of the anticipated M-phase in **2X*m/n*** compounds (**Figure 3.5-3**) could be achieved with an 80% success rate. A detailed description of the mathematical procedures, as well as a summary on a reduction for **2X*m/n*** compounds with possible M-phase, a detailed analysis, and error analyses can be found in the planned Ph.D. Thesis of Virginia-Marie Fischer.

---

[3] V_{SC} = side chain volume in the geometric model for just one side chain defined as $\sum 3n + m + 1$ with the values of the volumincremtnes for CH, CH$_2$, CH$_3$, Si groups according to IMMIRZI.[98]
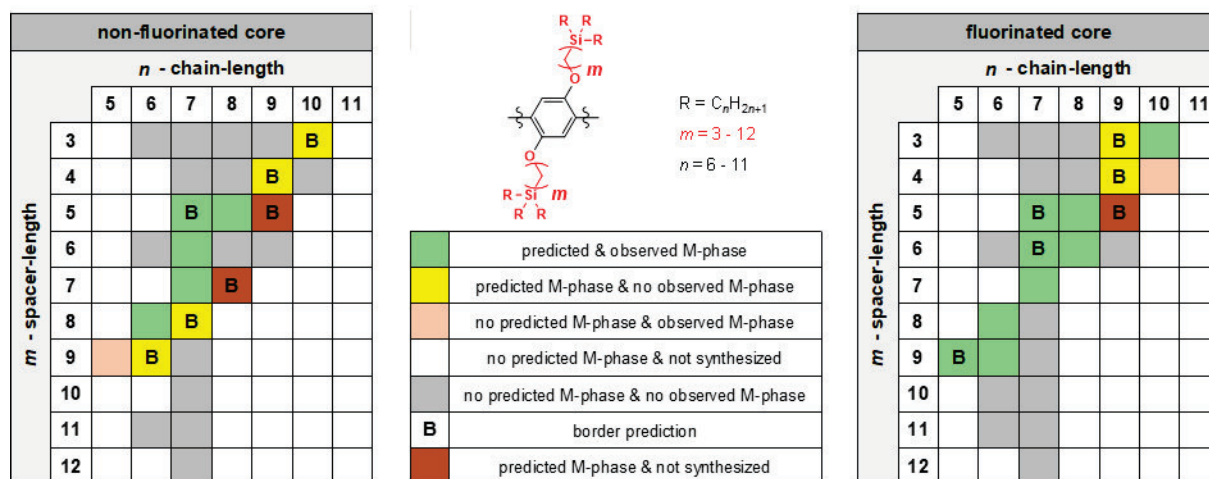
Figure 3.5-2. *Geometric model supported chain-spacer combinations for possible M-phase in the **1Xm/n** compounds (left: FOPE, right: OPE) with marked predictions, synthesis, success, and failure findings.*[101]
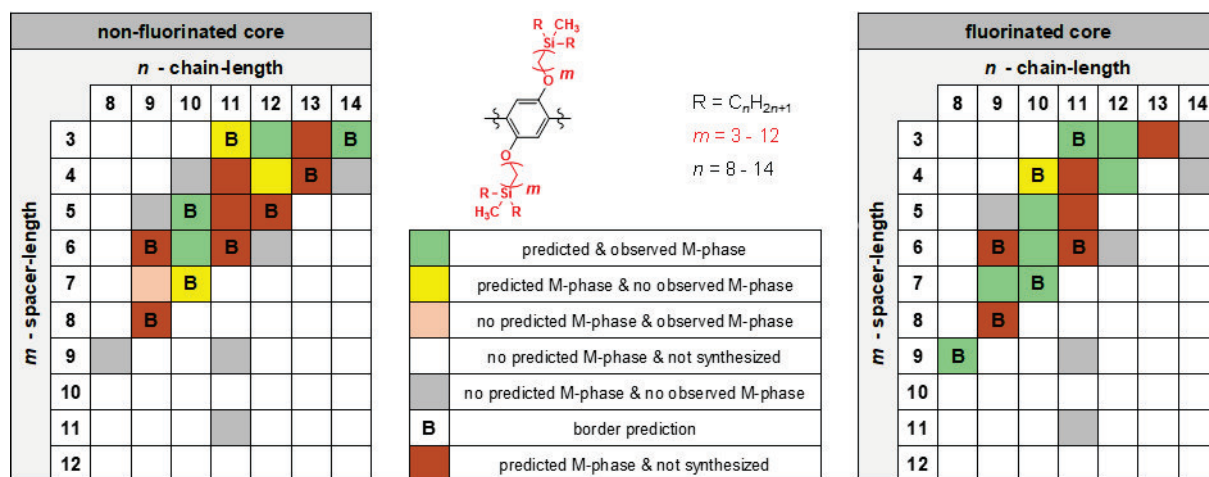

Figure 3.5-3. *Geometric model supported chain-spacer combinations for possible M-phase in the **2Xm/n** compounds (left: FOPE, right: OPE) with marked predictions, synthesis, success, and failure findings.*[101]

3.6 Bolapolyphiles with fluorinated side chains – Generating LC phase diversity and complexity by multi-color tilings – Publication C

In Publication C,[102] the understanding of the effects of π-stacking, nano-scale segregation, and volume effects on the formation of soft nanoscale patterns is demonstrated. This is provided by a class of tetraphilic compounds **4X1/*n/p*** based on rod-like (F)OPE cores having different branched chains on opposite sides, one being an alkyl chain (R_H) and the other one with perfluorinated ends (R_F) (**Figure 3.6-1a**). Furthermore, compounds **3X*p*²** (**Figure 3.6-1b**) with exclusively branched semiperfluorinated chains (R_F) at both sides were compared with the tetraphilic (F)OPEs compounds **4X*m/n/p***. Due to the fact that aromatic fluorination has a significant influence on the LC self-assembly, all compounds were synthesized with X =H and X = F to compare the influence induced by the perfluorination of the outer benzene rings.
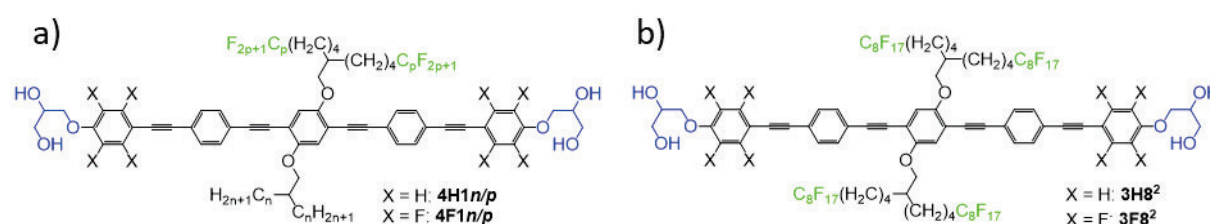
Figure 3.6-1. *Chemical structures of the target materials: a)* ***4X1/n/p*** *and b)* ***3Xp²***. *(Publication 102)*

Initially, the impact of partially fluorinated chains on both sides of the OPE core was investigated with the hydrocarbon compound **3H8²** (**Figure 3.6-2a**). The observation of birefringent optical textures and the temperature-dependent measurement of the lattice parameter in the XRD indicate that a direct transition occurs on cooling from the isotropic liquid to a square honeycomb phase. Further cooling results in a jump at 156°C to a smaller a_{squ}, further decreasing as the temperature decreases (**Figure 3.6-2c**). According to the reconstructed EDMs, low ED regions (red) with a not sufficiently dense packing of the relatively short and rigid fluorinated chains in the square cells were observed (**Figure 3.6-2b**). Decreasing temperatures lead to tilt-induced shrinkage of the square cells, allowing an improved packing of the R_F chains, but they still have difficulties filling the limited space in the corners of the square prismatic cells (**Figure 3.6-2d**) as indicated by the red low ED dots.
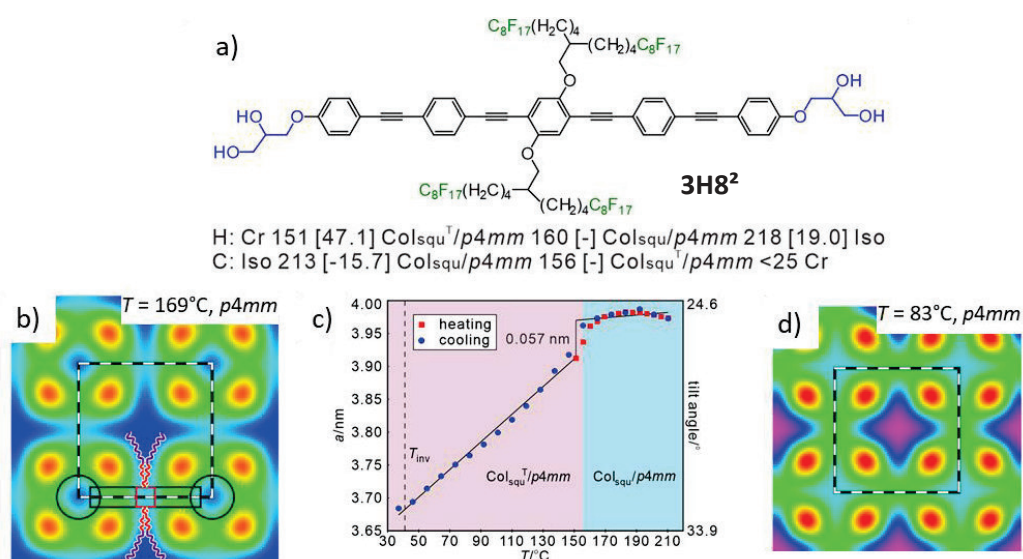

3H8²

H: Cr 151 [47.1] Col$_{squ}^{T}$/*p4mm* 160 [-] Col$_{squ}$/*p4mm* 218 [19.0] Iso
C: Iso 213 [-15.7] Col$_{squ}$/*p4mm* 156 [-] Col$_{squ}^{T}$/*p4mm* <25 Cr

Figure 3.6-2. *a) Formula of* ***3H8²*** *with transition temperatures (T/°C) and transition enthalpies (H/kJ mol-1); b, d) EDMs reconstructed from the SAXS patterns at the given temperatures, c) a_{squ} = f(T) plot, with transition between tilted/non-tilted squares as indicated. (Publication 102)*

The next steps to construct tunable multicolor tilings were to replace one of the semiperfluorinated chains with a longer alkyl chain of approximately the same volume, followed by a reduction of the side chain length of first the alkyl chain and secondly the semiperfluorinated side chain.

The replacement of one R_F chain of compound **3H8²** by a branched alkyl chain (R_H) leads to compound **4H1/8/16** showing a phase transition on cooling from a non-tilted to a tilted square chessboard tiling with alternating fluorine-rich and hydrocarbon-rich square cells, i.e., from $Col_{squ}/p4mm^L$ to $Col_{squ}^T/p4mm^L$. (In both phases, the superscript "L" indicates the by $\sqrt{2}$ larger square lattice of the chessboard tiling compared to the simple square tiling). The above-described problem of space-filling by the R_F chains can be removed by a partial mixing of R_F with R_H chains, resulting in a chessboard tiling with a core-shell structure of the tiles where pure R_F and R_H columns are surrounded by shells of medium ED mixed chains (**Figure 3.6-4**).

The reduction of the alkyl chain length retains the phase sequence $Col_{squ}/p4mm^L$ to $Col_{squ}^T/p4mm^L$, but on cooling, an additional three-color tiling by rhombic cells is observed between them. This indicates two options for the development of tilt, either out-of-plane tilt shrinking the square sides simultaneously and retaining square cells, or In-plane tilt deforming the squares to rhombs. (**Figure 3.6-3**). Both effects reducing the cell size compete with each other, but below a certain temperature, the out-of-plane tilt wins, leading to the formation of the $Col_{squ}^T/p4mm^L$ phase. The rhombic deformation is favored by the reduction of the side chain volume.
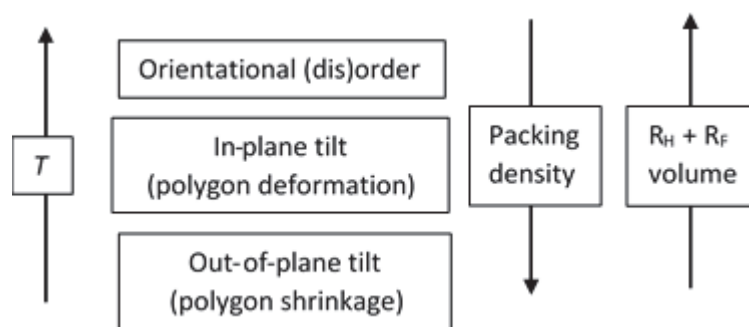

Figure 3.6-3. Development of different tilt modes of the rod-like cores in polygonal honeycomb LC phases, developing in order to adjust cell volumes to the side chain volume. (Publication 102)

Further reduction of the R_F chains leads to a $Col_{squ}/p4gm \rightarrow Col_{squ}^T/p4mm^L$ transition on cooling, where the honeycomb with *p4gm* plane group represents a tessellation by squares and rhombic cells in a dihedral tiling pattern (**Figure 3.6-4a**). The square cells contain the R_F chains, while the rhombic cells are filled with the alkyl chains. The rhomb formation takes place due to the reduced total chain volume supporting an In-plane tilt. Below a certain temperature, the rhomb-square tessellation of the *p4gm* phase becomes unstable, and a transition to a chessboard-type square honeycomb phase with a *p4mm* plane group and out-of-plane tilt of the molecules in the honeycomb walls takes place (**Figure 3.6-4d**).

The core fluorination of the outer benzene rings of the OPE cores results in the series of **4F1/n/p** compounds showing reduced LC-Iso transitions due to a distorted parallel rod alignment, a hindered hydrogen bonding of the glycerols, and a changed degree of incompatibility between the fluorinated FOPE cores and the R_H, R_F chains. The development of the high-temperature phase from $p4mm^L$ to *p4gm* with decreasing chain volume is the same as found in the **4H1/n/p** series, only shifted a bit towards larger side chain volume ($p4mm^T$ phase, **Figure 3.6-4e**). In contrast to the **4H1/n/p** compounds, the thermal range of the mesophase with out-of-plane tilt is relatively small, and the low-temperature phase becomes a rectangular columnar phase with *c2mm* plane group showing a two-color tiling by two types of rectangular tiles (**Figure 3.6-4g**). The fact that only two opposite walls being

tilted while the others have no uniform tilt indicates that the FOPE cores cannot assume any arbitrary tilt angle and prefer two modes of organization. As explained in Section 3.2, one is a non-shifted, and hence non-tilted organization favored by the face-to-face stacking of fluorinated rings. The other is a stacking interaction between the fluorinated benzenes and the electron-rich triple bonds of adjacent molecules, leading to a strong longitudinal shift and a tilt of around 35-50°. A closer packing of the FOPE by a face-to-face arrangement is also indicated by an additional diffuse shoulder in the WAXS with a distance at d = 0.38 nm, explaining the differences between the mesophase structures and sequences. Moreover, the effect of volume reduction leads to a shortening of the parameter b_{rec} (the shorter tilted side length) corresponding to a larger tilt angle of 50°, while the non-tilted side a_{rec} is only slightly affected.

In the case of compound **3F8²**, combining only fluorinated side chains with a fluorinated FOPE core, a phase sequence from Col_{squ}/$p4mm$ via $Col_{rec}^{T/2}$/$p2mm$ to Col_{squ}^{T}/$p4mm$ can be observed. Here, the rectangular honeycomb phase can be understood as a single-color version of the $Col_{rec}^{T/2}$/$c2mm$ phase formed by rectangular cells exclusively filled with R_F chains. This is the same rectangular honeycomb as fond for **2F3/14**, but in this case, filled with R_F instead of R_H chains. So, on cooling, starting from a square honeycomb phase, one of the sides b_{rec} starts to shrink while the other one is just slightly affected due to the previously described locked-in mode of the FOPE cores. However, on further cooling the thermal chain shrinkage requires the development of a stronger tilt which cannot be achieved by tilting only half of the molecules leading to a tilt in all honeycomb walls to adjust the cell size until a_{rec} and b_{rec} merge and become equal in the single-color square honeycomb phase with a tilt of all molecules around 30°. This effect and the absence of alkyl chains lead to favored square cells over rectangular cells. Overall, the investigation of the compounds with semiperfluorinated chains indicates the importance of π-stacking for the shape of the honeycomb cells. Moreover, combining R_H with R_F chains allows the formation of chessboard and related tilings as shown in **Figure 3.6-4**.
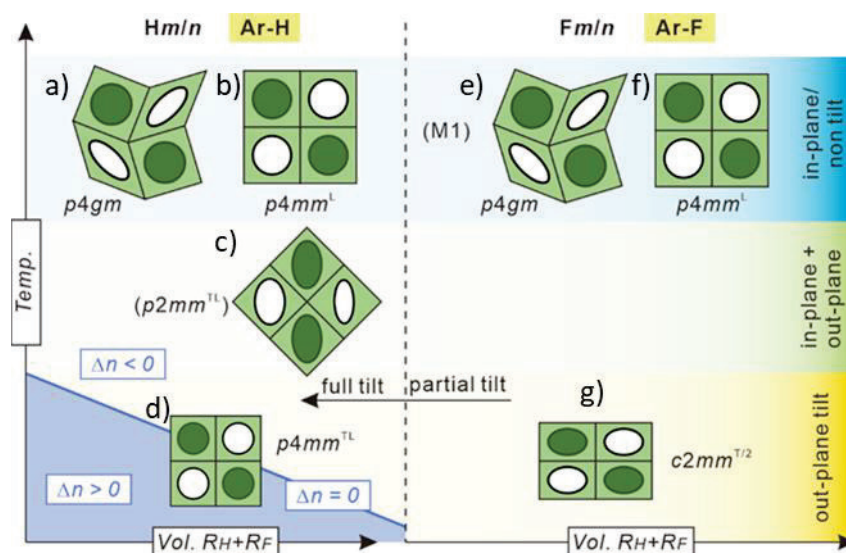

Figure 3.6-4. *LC-self-assembly of **4H1/n/p** and **4F1/n/p** compounds. Dependence of the mode of chessboard tiling and chessboard deformation on side chains volume, temperature, core-fluorination, and degree of tilt of the OPE cores in the honeycomb walls. Dark green areas indicate domains of R_F chains, white R_H chains, and plane green areas are mixed areas; phases in parentheses are metastable or coexisting phases. (Publication 102)*

## 3.7   Bolapolyphiles with branched alkyl side chains

Besides the studies of side chain volume and length effects on compounds **1X*m/n*** and **2X*m/n*** with trialkylsily- and dialkylmethylsilyl end groups, mostly published in Publications A and B and the structural studies of fluorinated side chain compounds **3X*m/n*** and **4X*m/n*** published in Publication C, another part of this work represents the synthesis and investigation of bolapolyphiles with branched alkyl side chain on both sides at the (F)OPE cores. These compounds **5X1/*n*** with n = 14, 16 have been synthesized by M. Poppe[44], while compounds with n = 15, **5X3/14** and the chiral compounds ***5X1/*n*** were synthesized and investigated in this work.

This section deals with the series **5X*m/n*** and their mesomorphic properties influenced by two different structural variations. The first variation was realized by the synthesis of compounds ***5X1/*n*** with uniform chiral centers in the glycerol units. The second was the study of the influence of spacer elongation from m =1 to 3 for the **5X*m/14*** compounds to compare them with compound **2X3/14** with dialkylmethylsilyl end groups in order to evaluate the effect of replacing CH with SiMe.

3.7.1 Effects of molecular chirality

The mesophase sequences of the enantiomerically pure *5X*m/n* compounds with (S,S) configuration and their racemic mixtures of diastereomers **5X**m/n*[44] are summarized in **Table 3.7-1**. Compounds with uniform (S,S) configuration are marked with *.

*Table 3.7-1: Phase transition temperatures T (°C), phase transition enthalpies H (kJ/mol) of the compounds *5X*m/n* and **5X**m/n*. All transition temperatures and enthalpies are from the first heating or cooling cycle with heat and cooling rates of 10 K/min. Enthalpies were determined by the peak areas.*

5X1/n
X = H / F
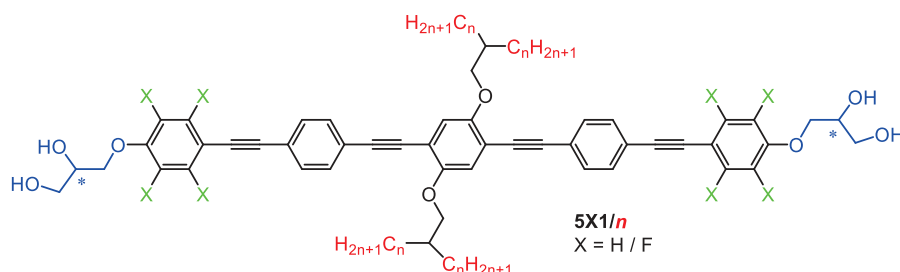
Comp.	n	Phase sequence T [°C] and ΔH [kJ/mol]	*	L_C	V_C
5H1/14[c]	14	H: Cr 120 [80.0] M 152 [2.1] Col$_{hex}$/*p6mm* 154 [7.5] Iso C: Iso 153 [-7.6] Col$_{hex}$/*p6mm* 145 [-1.6] M 89 [-103.6] Cr	rac.	16	58
***5H1/14**[a,b,c]	14	H: Cr 122 [77.2] M 151 [2.3] Col$_{hex}$/*p6mm* 155 [7.3] Iso C: Iso 153 [-7.0] Col$_{hex}$/*p6mm* 139 [-1.1] M 71 [-81.2] Cr	S,S	16	58
5H1/15[a,b,c]	15	H: Cr 127 [93.5] M 144 [8.6] Iso C: Iso 141 [-8.1] M 94 [-89.4] Cr	rac.	17	62
5H1/16[c]	16	H: Cr 137 [103.1] Iso C: Iso 133 [-8.7] M 114 [-92.7] Cr	rac.	18	66
***5H1/16**[a,b,c]	16	H: Cr 137 [93.5] Iso C: Iso 132 [-8.1] M 106 [-86.4] Cr	S,S	18	66
5F1/14[c]	14	H: Cr 77 [68.9] M 167 [14.7] Iso C: Iso 164 [-14.2] M 20 [-42.6] Cr	rac.	16	58
***5F1/14**[a,b,c]	14	H: Cr 97 [93.5] M 146 M 168 [16.6] Iso C: Iso 165 [-16.0] M 20 [-43.6] Cr	S,S	16	58
5F1/15[a,b,c]	15	H: Cr 121 [95.1] M 160 [13.3] Iso C: Iso 157 [-12.6] M 52 [-84.6] Cr	rac.	17	62
5F1/16[c]	16	H: Cr 99 [16.8] M 152 [14.2] Iso C: Iso 150 [-13.3] M 71 [-98.3] Cr	rac.	18	66
***5F1/16**[a,b,c]	16	H: Cr 125 [53.2] M 155 [13.0] Iso C: Iso 150 [-13.1] M 75 [-89.2] Cr	S,S	18	66

[a] Compounds which were already investigated by Synchrotron radiation.[100] [b] Additional unpublished compounds **5X**m/n* and ***5X**m/n*, DSC traces can be found in Appendix-2: Unpublished DSC-data. [c] Compounds which were already investigated by Synchrotron radiations.[100] *rac* = mixture of racemic (S,S)-diastereomer, (R,R)-diastereomer, and (R,S)-diastereomer

Most of the compounds **5X**m/n* and ***5X**m/n* show the formation of enantiotropic mesophases, except for ***5F1/16** and **5F1/16** showing a monotropic LC phase. A comparison of the melting and clearing temperatures of racemic compounds and their pure enantiomers indicates that the clearing temperatures are only slightly affected. The shift between the melting temperatures is more pronounced in the case of fluorinated compounds, e.g., **5F1/16** and ***5F1/16**, showing a deviation in the melting point of nearly 25°C. However, the deviation in the clearing point temperatures is negligible in all cases. Investigations with optical polarization microscopy show the formation of typical mosaic-like textures of the M-phase in all enantiomeric pure compounds as well as their racemic mixtures. The comparison of the XRD patterns of the formed mesophases also shows an identical complex M-phase pattern for all comparable pairs, which have not yet been indexed (see **Figure 3.7-1a,**

b). The different resolutions of the powder patterns of racemate and enantiomers might be due to different domain sizes of local alignments. In the high-temperature phase of ***5H1/14**, the SAXS pattern[100] can be indexed to a triangular honeycomb phase with a *p6mm* plane group with a lattice parameter determined to be a_{hex} = 4.29 nm, which is almost the same as the lattice parameter of the racemic compound **5H1/14** with an a_{hex} = 4.24 nm. The mesophase types of the ***5X*m/n*** compounds seem not to be affected by the molecular chirality due to the uniform configuration of the stereogenic centers in the glycerol units at the (F)OPE cores. A comparison between racemic **5X*m/n*** and enantiomeric pure compounds ***5X*m/n*** revealed no significant differences in mesophase type, molecular self-assembly, and physical properties. A related observation was recently made for K-shaped bolapolyphiles consisting of a *p*-terphenyl core with two polar glycerol end-groups and a swallow-tailed alkyl side chain.[103]
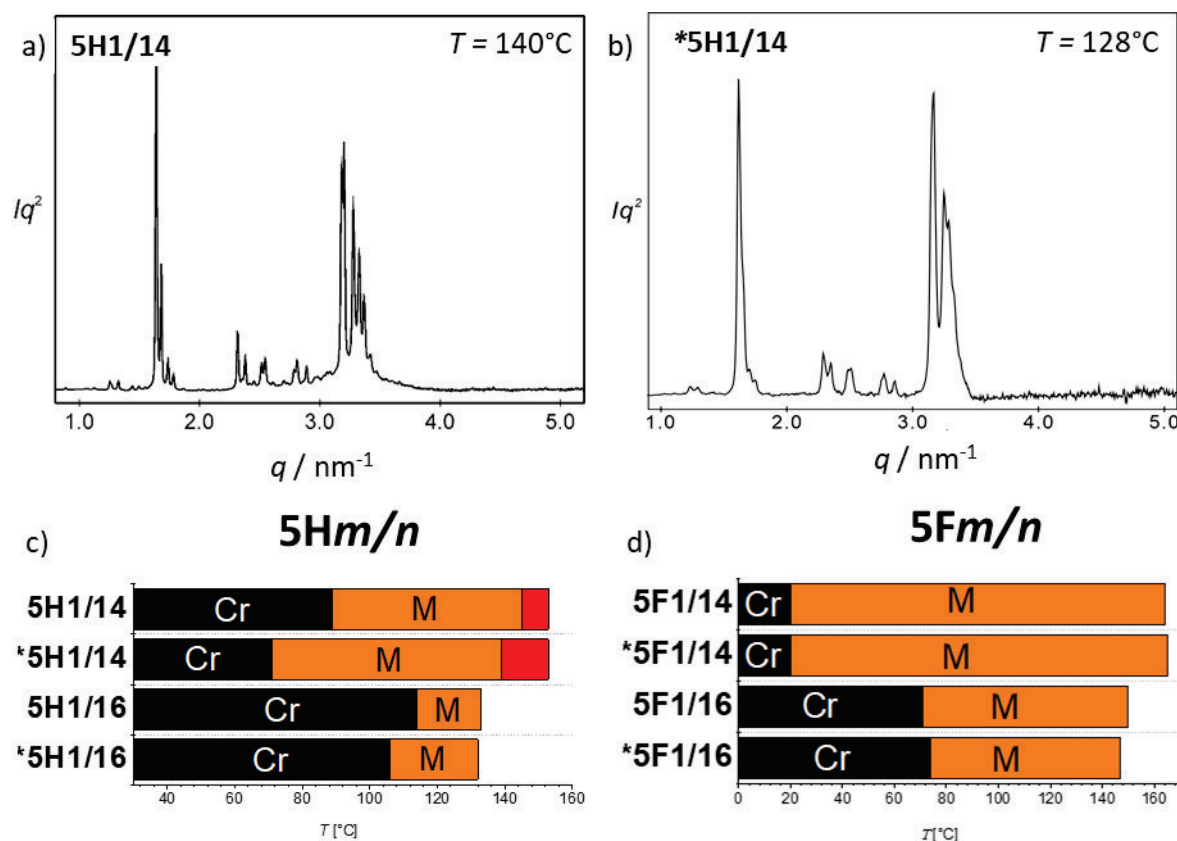
Figure 3.7-1. Comparison of **5X*m/n*** and ***5X*m/n*** compounds. a) SAXS powder pattern of **5H1/14** at given temperature;[100] b) SAXS powder pattern of ***5H1/14** at given temperature;[100] c,d) phase sequence of the **5H*m/n*** and **5F*m/n*** compounds where bar diagrams showing the mesophase range of compounds **5H*m/n*, *5H*m/n*, 5F*m/n*** and ***5F*m/n***, abbreviations: Cr = crystalline solid; red bar indicating a Col_{hex}/p6mm phase with triangular honeycombs; M = unknown LC phases; The isotropic liquid state is at the right side of the columns.

*Table 3.7-2. Mesophases and phase transition temperatures of compounds **5Xm/n** and **5Xm/n** with X = H, F. All transition temperatures were taken from the peak temperatures of the transition peaks at a heating and cooling rate of 10K/min. The transition enthalpies were determined from the peak areas given in kJ/mol.*
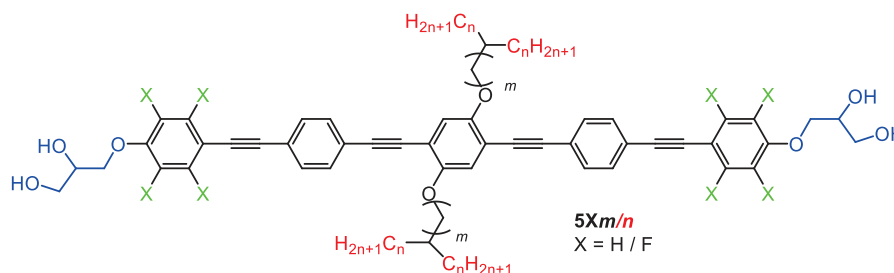
Comp.	m	n	Phase sequence T [°C] and ΔH [kJ/mol]	L_C	V_C
5H3/14[a,b,c]	3	14	H: Cr 84 [39.2] $Col_{squ}^T/p4mm$ 117 [1.4] M 124 [2.2] Cub/$Pm\overline{3}n$ 126 [-] Iso C: Iso 122 [-] Cub/$Pm\overline{3}n$ 119 [3.4] M 61 [4.5] $Col_{squ}^T/p4mm$ 44 [17.8] Cr	18	62
2H3/14[b]	3	14	H: Cr 68 [26.4] M 83.3 [17.0] Cub/$Pm\overline{3}n$ 143 [1.0] Iso C: Iso 135 [-] Cub/$Pm\overline{3}n$ 65 [-4.1] M 39 [-20.6] Cr	18	64
5F3/14[a,b,c]	3	14	H: Cr 95 [92.2] $Col_{rec}/p2mm$ 120 [-] $Col_{squ}/p4mm$ 159 [15.0] Iso C: Iso 155 [12.3] $Col_{squ}/p4mm$ 120 [-] $Col_{rec}/p2mm$ < 20 Cr	18	62
2F3/14[a,b]	3	14	H: Cr <20 $Col_{rec}^T/p2mm$ 110 [-] $Col_{squ}/p4mm$ 133 [9.1] Iso C: Iso 127 [-9.0] $Col_{squ}/p4mm$ 110 [-] $Col_{rec}^T/p2mm$ < 20 Cr	18	64

[a] Transition temperatures were determined by optical polarization microscopy. [b] Compounds which were already investigated by Synchrotron radiation.[100] [c] Additional unpublished compounds **5Xm/n**, DSC traces can be found in Appendix-2: Unpublished DSC-data.

*Table 3.7-3. Structural data for $Col_{hex}/p6mm$, Cub/$Pm\overline{3}n$, $Col_{squ}/p4mm$ $Col_{rec}/c2mm$ phases of compounds **5Xm/n** and ***5H1/14***.*

Comp.	Phase (T/°C)	a,b [nm]	V_{Cell} [nm³]	$n_{Cell,LC}$	n_{Wall}	n_{Bundle}	L_{Wall} [nm]
5H1/14	$p6mm$ (146)	4.29	7.17	2.75	0.9	-	4.3
5H3/14	$p4mm$ (54)	3.64	5.96	2.19	1.1	-	3.6
5F3/14	$p4mm$ (142)	4.16	7.79	2.81	1.4	-	4.2
	$p2mm$ (101)	a = 4.13 b = 3.48	6.47	2.33	1.2	-	4.1 3.5
5H3/14	$Pm\overline{3}n$ (125)	9.18	774	284	-	5.3	-

V_{Cell} was determined according to $V_{Cell} = a_{squ}^2 \cdot h$ for the square, $a_{rec} \cdot b_{rec} \cdot h$ for the rectangular, $\frac{\sqrt{3}}{2} a_{hex}^2 h$ for hexagonal, and a_{cub}^3 for cubic $Pm\overline{3}n$ phase, where h represents the height of the unit cell, which was assumed to be 0.45 nm. $n_{Cell,cr}$ = number of molecules per unit cell in the crystalline state, calculated according to $n_{Cell,cr} = V_{Cell}/V_{Mol}$ (average packing coefficient in the crystal is k = 0.7). $n_{Cell,liq}$ = the number of molecules in the unit cell of an isotropic liquid with an average packing coefficient k = 0.55, calculated according to $n_{Cell,liq}$ = 0.55/0.7. $n_{Cell,LC}$ = number of molecules in the unit cell in the LC state as estimated from the average of $n_{Cell,cr}$, and $n_{Cell,liq}$. n_{Wall} = the number of molecules in the cross-section of the honeycomb walls, calculated as $n_{Wall} = \frac{n_{cell,LC}}{2}$ for $p4mm$ and $p2mm$ cells, calculated as $n_{Wall} = \frac{n_{cell,LC}}{3}$ for $p6mm$ cells, L_{Wall} is the side length of the polygonal cells, n_{Bundle} = number of molecules per bundle in the cubic organization as $n_{Bundle} = n_{Cell,LC}/54$.

3.7.2   Effects of alkyl chain parity

Both compounds **5H1/15** and **5F1/15** show the formation of enantiotropic mesophases. An analysis of the clearing temperatures shows in series **5X1/n** a continuous temperature decrease with the length L_c and volume V_c increase of the side chains from n = 14 via 15 to 16 (see **Table 3.7-1**)

Recorded textures of the **5X1/15** compounds between crossed polarizers show that OPE and FOPE compounds tend to form mosaic-like textures (**Figure 3.7-2b**) during cooling from the isotropic liquid typically observed for compounds showing an M-phase. The XRD results[100] indicate that the formed phase is of the same type as for the compounds with m = 14, 16 (**Figure 3.7-2a**). A special influence of an odd-even effect of the chains can be excluded at the current state of investigation.
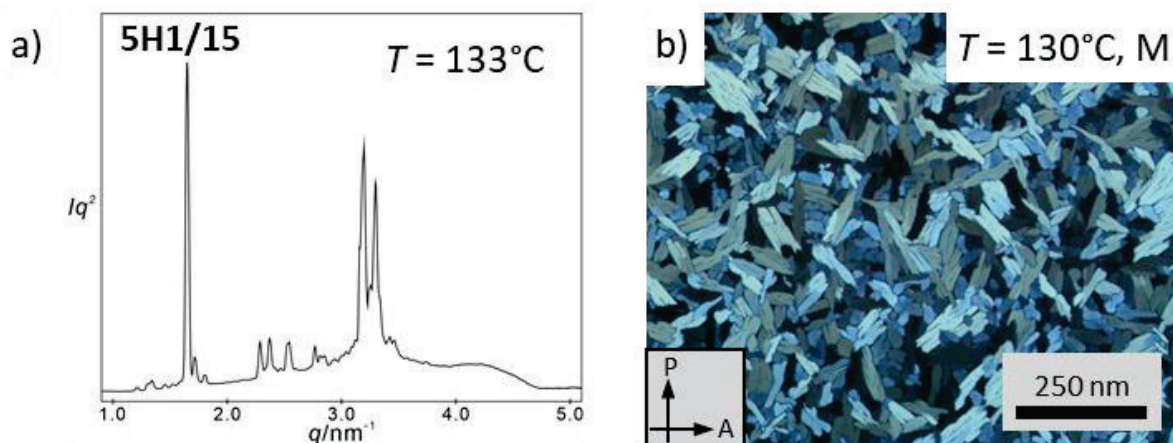
Figure 3.7-2. *a) SAXS powder pattern of **5H1/15** at given temperature;[100] b) optical mosaic-like texture observed between crossed polarizers of **5H1/15** at given temperature.*

3.7.3   Effects of the branching point structure – Carbon vs. Silicon

In contrast, the **5X3/14** compounds with a longer spacer (m = 3) show the formation of several other types of textures besides the mosaic-like ones during cooling from the isotropic liquid. **5H3/14** displays three different types of textures. First, an optical isotropic phase with high viscosity was identified, which indicated the presence of a cubic phase. On further cooling, a birefringent mosaic-like texture between crossed polarizers can be observed, typical for the M-phase (**Figure 3.7-3a**). On lowering the temperature, the birefringence starts to decrease and becomes nearly completely dark (optical isotropic) with low birefringent residues (**Figure 3.7-3b**) associated with a DSC peak at T = 61°C (**Figure 3.7-3c**).
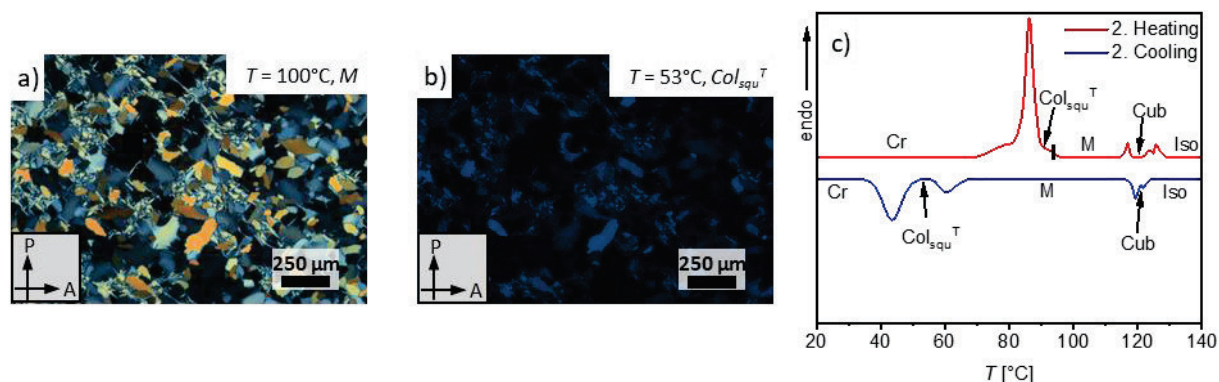
Figure 3.7-3. *Optical textures and DSC traces of **5H3/14**. a) Texture of the M-phase as observed on cooling at the given temperature; b) texture of the Col_{squ}^T/p4mm phase as observed on cooling at the given temperature; c) DSC trace showing recorded with heating and cooling rates of 10K/min.*

The SAXS pattern[100] of the isotropic high-temperature phase recorded at T = 125 °C shows three strong reflections which can be indexed to (200), (210), and (211) reflections of a cubic lattice with $Pm\bar{3}n$ space group. The remaining weaker reflections can also be indexed to this space group (**Figure 3.7-4a**). The structure of this cubic network phase is already described in detail in Publication A,[95] B,[97] and Section 3.3. The lattice parameter can be determined to a_{cub} = 9.18 nm, for which the length of the molecules in the bundles can be calculated by $0.5 \cdot a_{cub}$, $0.56 \cdot a_{cub}$, and $0.61 \cdot a_{cub}$ to 4.6 – 5.6 nm. Their length exceeds that of the individual compound **5H3/14** and can be attributed to the significant size of the glycerol spheres connecting the 12 and 14 rod-bundles with respect to some longitudinal shift of the OPE cores. The number of molecules per unit cell is calculated to 293, which are distributed to 54 struts interconnecting the spheres. This gives an average number of 5.4 molecules organized side-by-side in the bundles of parallel-aligned OPEs. This fits well with typical observations for the molecular organization in the observed cubic network phase of an A15-Frank-Kasper type. During further cooling, the SAXS pattern[100] becomes more complicated (**Figure 3.7-4b**) and turns at T = 117 °C into the typical complex pattern already observed for the M-phase in the former described **1Xm/n**, **2Xm/n**, and **5Xm/n** compounds. This result is in line with the observation of the formation of mosaic-like textures during optical investigations (**Figure 3.7-3a**). Finally, on further cooling the SAXS pattern[100] changes and the reflexes recorded at a temperature of T = 61°C can be indexed to a square honeycomb phase with a $p4mm$ plane group showing a typical ratio of a reciprocal d-spacing of $1:\sqrt{2}:$ $2:\sqrt{5}:8:\sqrt{9}$ … (**Figure 3.7-4c**). The determined lattice parameter of the Col$_{squ}$ phase is a_{squ} = 3.64 nm at T = 54 °C, which is significantly smaller than the molecular length L_{mol} = 4.0 – 4.4 nm between the two glycerol end-groups. This would lead to the assumption of a tilted organization of the molecules in the columnar phase with a tilt angle β = 34.2 ° according to $\beta = \cos^{-1}\left(\frac{a_{squ}}{L_{mol}}\right)$ which is close to the "magic angle" of 35.3°. This is in line with the observed low birefringent texture recorded at T = 53°C (**Figure 3.7-3b**). The WAXS pattern in all three mesophases of **5H3/14** is diffuse with a single maximum around 0.44 – 0.46 nm, indicating the absence of positional order between individual molecules, confirming the liquid crystalline state in all three phases.
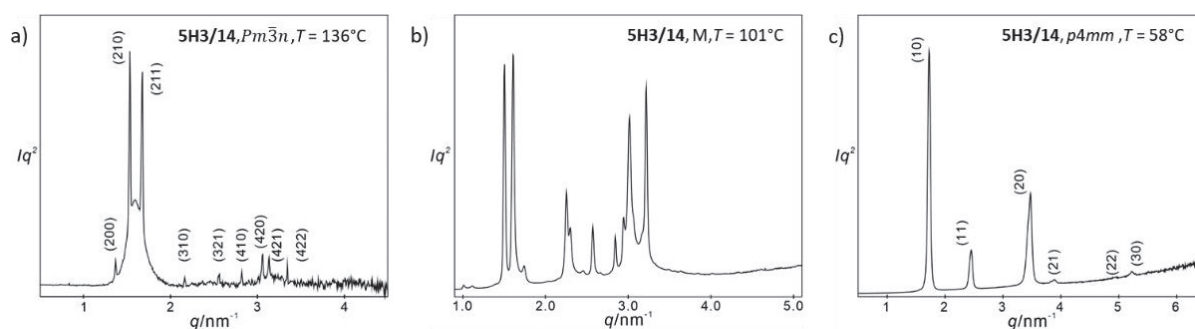

Figure 3.7-4. *SAXS powder pattern of **5H3/14**. a) Pattern of the Cub/$Pm\bar{3}n$ phase recorded at T = 136°C, b) pattern of the M-phase recorded at T = 101°C, c) pattern of the Col$_{squ}$/$p4mm^T$ phase recorded at 58°C.*[100]

For the core fluorinated compound **5F3/14** a different mesophase sequence can be observed during cooling from the isotropic liquid. First, a phase with spherulitic texture forms at around T = 155 °C (**Figure 3.7-5b**). Under shearing, a relatively high viscosity is observed, and considering the spherulitic-like texture, this could be a columnar phase. The indexation of the reflexes determined by SAXS experiments[100] displays BRAGG-reflexes of (10), (11), (20), and (21) with a reciprocal spacing ratio of $d = 1 : 2^{1/2} : 2 : 5^{1/2}$ which can be assigned to a square lattice with $p4mm$-plane group and a_{squ} = 4.16 nm at 142 °C (**Figure 3.7-5a**), which is in a good agreement with the molecular length (L_{mol} = 4.0 – 4.4 nm). The diffuse wide-angle scattering shows a broad scattering at d = 0.46 nm with an additional shoulder at d = 0.36 nm. The broad WAXS-reflex proves the liquid-like behavior of the sample, while the shoulder hints at the increased intermolecular *face-to-face* aromatic-aromatic interaction typically

found in FOPE compounds. The electron density map (**Figure 3.7-5c**) of the $Col_{squ}/p4mm$ phase reconstructed from the SAXS pattern at 142°C displays a square grid with dots of high ED (blue, purple) in the corners formed by the glycerol groups. The corners are connected by the medium electron density walls (green) of the FOPE cores, where the square low ED regions are filled by the aliphatic side chains separated by the medium ED walls.
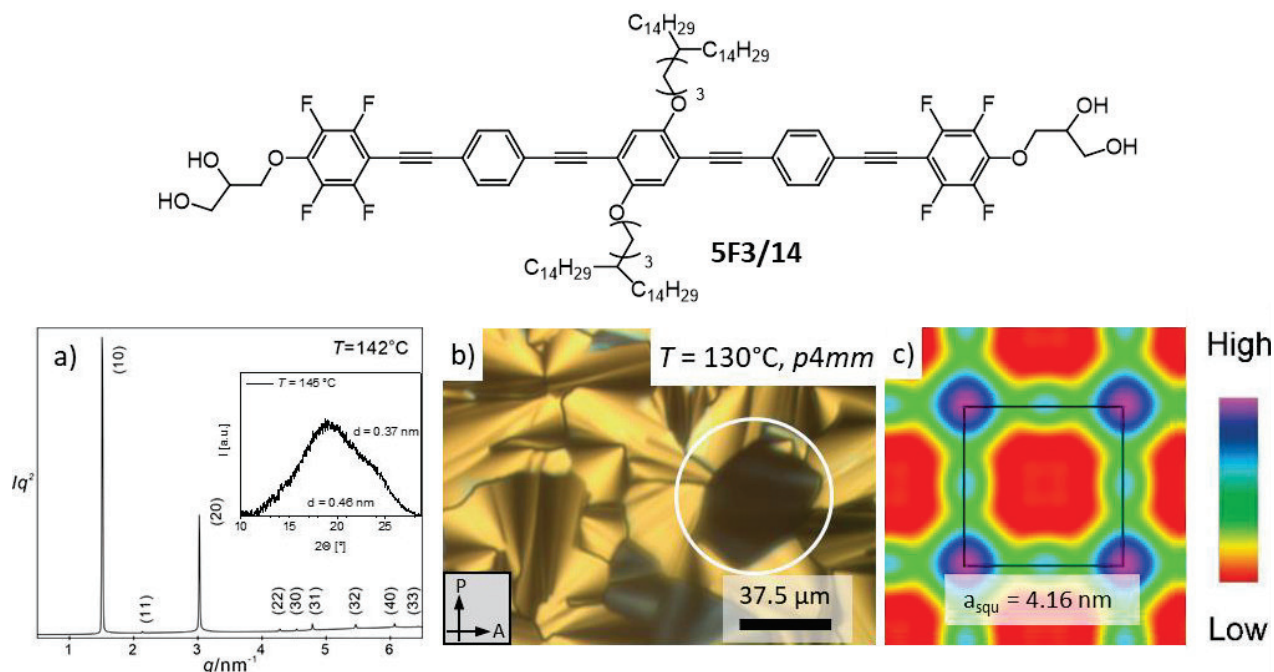

Figure 3.7-5. Chemical structure of **5F3/14** with a) SAXS diffractogram (WAXS inset),[100] b) optical texture of the $Col_{squ}/p4mm$ phase as observed on cooling at the given temperature, c) EDMs reconstructed from the SAXS pattern.[100]

On further cooling, a phase transition can be detected at around T = 120 °C with a change of the birefringence and a transformation to a biaxial phase (**Figure 3.7-6c**) without any additional peak in the DSC traces (**Figure 3.7-6a**). The emerging biaxiality is indicated by the development of birefringence in the dark homeotropic aligned regions in the texture (compare **Figure 3.7-5b** and **Figure 3.7-6c**). The biaxial phase shows a continuous decrease of the birefringence of the texture while decreasing the temperature(**Figure 3.7-6d, e**). The observed scatterings of the XRD pattern[100] can be assigned to a rectangular honeycomb phase with a $p2mm$ plane group with lattice parameters of a_{rec} = 4.13 nm and b_{rec} = 3.48 nm at T = 101 °C. While a_{rec} is in good agreement with the molecular length of L_{mol} = 4.0 – 4.4 nm, the length of b_{rec} is smaller than the molecular length, leading (together with the decreasing birefringence) to the assumption of a tilted arrangement of the FOPE cores along the b direction. During the cooling process in the XRD experiments, the rectangular $p2mm$ lattice is retained, but the parameter b_{rec} is decreasing continuously while the parameter a_{rec} decreases only marginally (see **Figure 3.7-6b**). The previously described wide-angle scattering remains completely diffuse, leading to the assumption that a uniform tilt of the FOPE cores in the honeycomb walls only along the direction of b takes place, which is in line with the observation of a decreased birefringence during cooling.
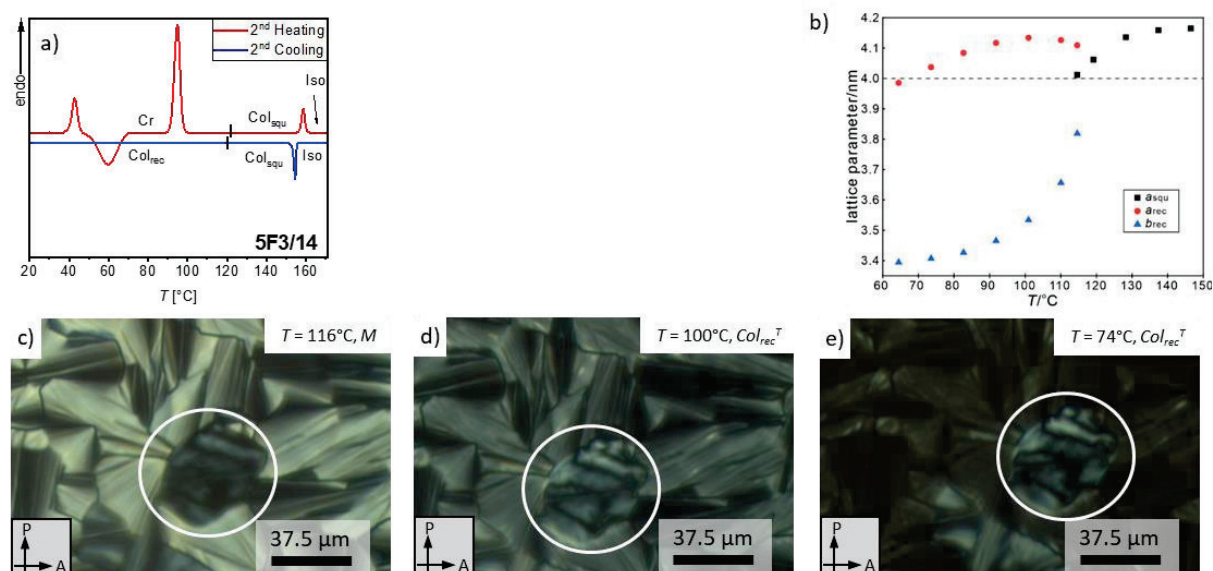
Figure 3.7-6. *a) DSC traces of compound **5F3/14** recorded with heat- and cooling rates of 10K/min, b) T-dependence of lattice parameters a_{squ}, a_{rec}, and b_{rec}, c-e) optical textures of the rectangular honeycomb phase during cooling.*

The replacement of the CH branching point by SiMe (compare **5H3/14** and **2H3/14** in **Table 3.7-2** and **Figure 3.7-7**) increases the clearing point temperatures (on heating) by nearly ΔT = 20K and decreases the melting point temperatures by about ΔT = 20 K. Additionally, a stabilization of the high-temperature Cub/$Pm\overline{3}n$ phase can be observed, while the stability of the M-phase is reduced by about ΔT = 32K, and the tilted square honeycomb structure observed for **5H3/14** is completely removed (**Figure 3.7-7**).

In contrast, for the pair **2F3/14** and **5F3/14**, replacing CH with SiMe decreases both the melting and clearing point temperatures. The phase sequence of Col$_{squ}$/$p4mm$ → Col$_{rec}^{T}$/$p2mm$ is retained in both compounds **AF3/14**. However, the LC phase range of **5F3/14** is narrower compared to the non-fluorinated compounds.

In general, it seems that the CH replacement by SiMe prefers a 3D-Cub$_{net}$ structure over an M and columnar phase, probably due to the increase of interface curvature by the additional CH$_3$ groups at the branching point. The effect of stabilized columnar phases supported by the interlocked π-π stacked FOPE-cores described in Publication C seems to be stronger for the branched hydrocarbon chains due to the absence of the distortion of π-stacking by the additional CH$_3$ group at the Si-branching point.
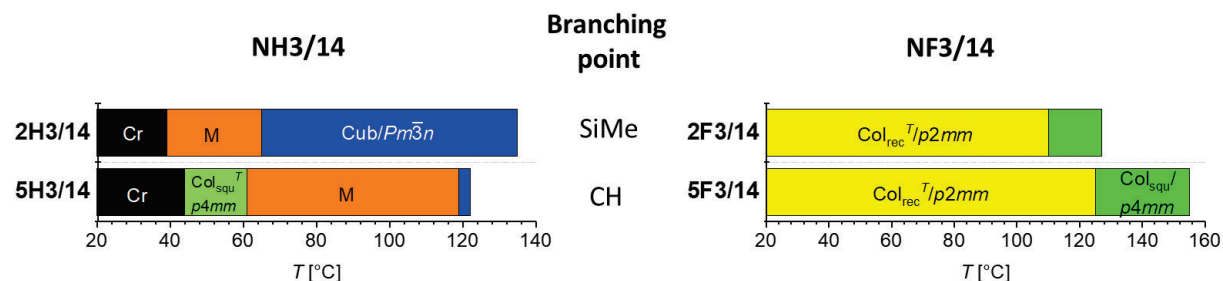

Figure 3.7-7. *Mesophase sequence of the a) **NH3/14** and b) **NF3/14** compounds on cooling from the isotropic liquid. Bar diagram showing the mesophase range of compound **NH3/14** and **NF3/14**; abbreviations: Cr = crystalline solid; Col$_{squ}$ = square LC honeycombs; Col$_{squ}^{T}$/$p4mm$ = square LC honeycombs with a tilted organization of the OPE cores. Respectively, Col$_{rec}^{T}$/$p2mm$ = tilings by rectangular honeycombs with tilted organization of the FOPE cores; Cub/$Pm\overline{3}n$ = cubic network phase with $Pm\overline{3}n$ space group (A15 phase); M = unknown LC phases; The isotropic liquid state is at the right side of the columns*

4 Summary

Bolapolyphilic molecules show a wide variety of liquid crystalline phases, and especially complex mesophase structures occurring at the triangular-square transition became the focus of interest in recent years due to the possibility of liquid quasi-crystal (LQC) and superlattice ("approximant") formation.

The focus of this work was on the design, synthesis, and analysis of the self-assembly of X-shaped OPE-based bolapolyphiles with a focus on the possible formation of columnar liquid quasi-crystalline (CLQC) and related approximant structures. Therefore, a variety of X-shaped OPE-based and FOPE-based bolapolyphiles with different side chain types were successfully synthesized (**Figure 4-1**) and their soft self-assembly processes were characterized. The side chain volume was chosen to fit into the range required for the triangular-square transition.
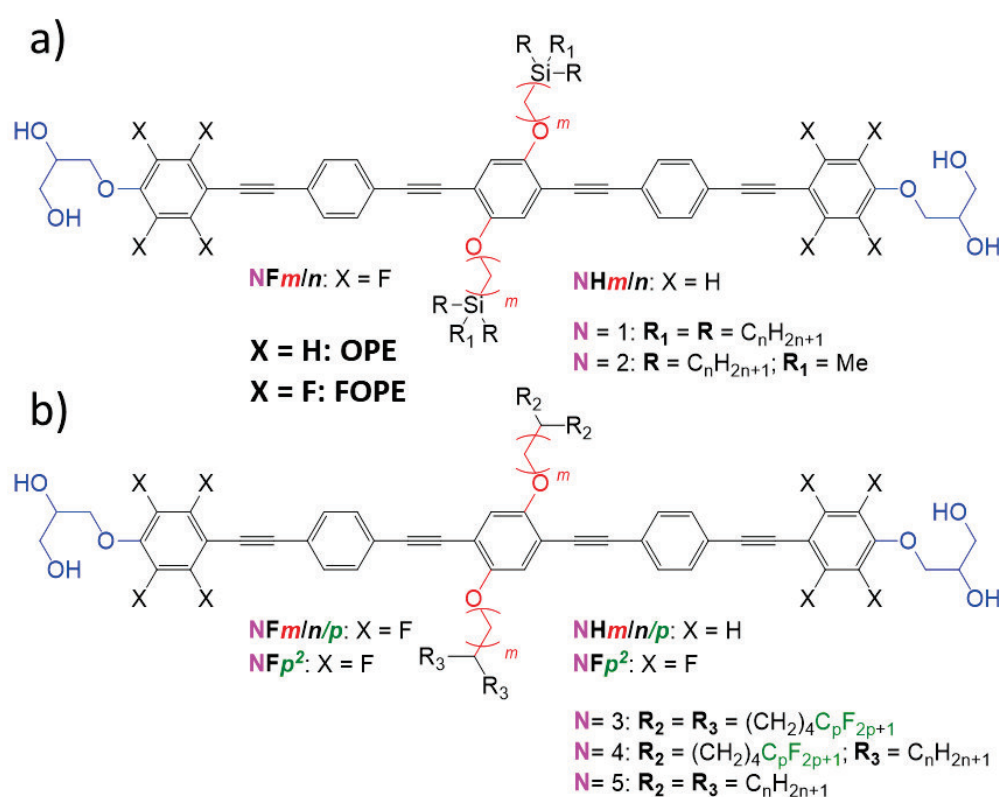
Figure 4-1. Molecular structure of the synthesized X-shaped (F)OPE-based bolapolyphiles; N represents an arbitrarily chosen compound number.

In Publication A and B, as well as for the unpublished compounds of the series **1Xm/n** and **2Xm/n** with trialkylsilyl and dialkylmethylsilyl groups at the end of the side chains (see **Figure 4-1a**), the effects of steric and geometric frustration at the triangular–square transition were investigated. The carbosilanes **1Hm/n** and **2Hm/n** show a phase sequence Col$_{hex}$/$p6mm$ → M / Cub$_{net}$/$Pm\bar{3}n$ → Col$_{squ}$/$p4mm$ (see **Fig. 4-2**) with growing chain volume V_C and chain length L_C. While the compounds of the analogous series **1Fm/n** and **2Fm/n** with partially fluorinated FOPE cores tend to show a phase sequence Col$_{hex}$/$p6mm$ → M → Col$_{rec}$ → Col$_{squ}$/$p4mm$ (see **Fig. 4-2**) and a strong suppression of the cubic phase, which exists in the series of compounds **1Fm/n** only in three cases and is not observed for the **2Fm/n** compounds. The cubic $Pm\bar{3}n$ phase represents a new type of Frank-Kasper phases where the polar glycerol end-groups form spheres which are interconnected by bundles of (F)OPE rods into segmented networks composed of non-regular tetrahedra (**see Fig 4-2a**).

It represents a new intermediate structure at the triangle-square transition competing with the mixed triangle-square tilings and honeycombs composed of non-regular triangles and square cells (for example, rhombic and rectangular, see **Fig. 4-2e,f**). $Pm\bar{3}n$ formation is favored at high *T*, while cell deformation is supported by low *T*. Core fluorination suppresses $Pm\bar{3}n$ phase formation and favors honeycomb cell deformation.

It is proposed that this is due to different core-core interactions between OPE and between FOPE cores. OPEs can easily shift with respect to each other, while FOPE shows locked-in behavior. Therefore, OPEs can assume any longitudinal shift and assume any tilt angle if the shift becomes uniform. In contrast, FOPEs cannot easily shift or assume a strong shift. Similarly, they do not tilt or assume a large tilt of around 30 – 40°.

This locked-in behavior of the FOPEs distorts $Pm\bar{3}n$ phase formation and supports honeycombs with strong tilt, rectangular phases with only half of the honeycomb walls being tilted (**see Fig. 4-2e**), or Col_{squ}^T phases with strong tilt in all walls (**Fig. 4-4**). 28 among the synthesized 80 compounds **1X*m/n*** and **2X*m/n*** show birefringent mesophases M with complex diffraction patterns. In only one case (**1F6/8**), the diffraction pattern of an M-phase was indexed, and the structure was solved. It shows a complex tiling pattern composed of different types of non-regular triangular and tetraangular tiles (**see Fig. 4-2d**), which is considered as a periodic approximant of a CLQC phase.

More of such approximant structures and most likely also the aperiodic CLQC structures can be expected for the remaining still unsolved M-phases, but their unambiguous confirmation requires additional investigations (e.g., small-angle neutron scattering) and computational work. This work will be continued with our collaboration partners F. Liu and Y. Cai at Xi'an Jiaotong University.
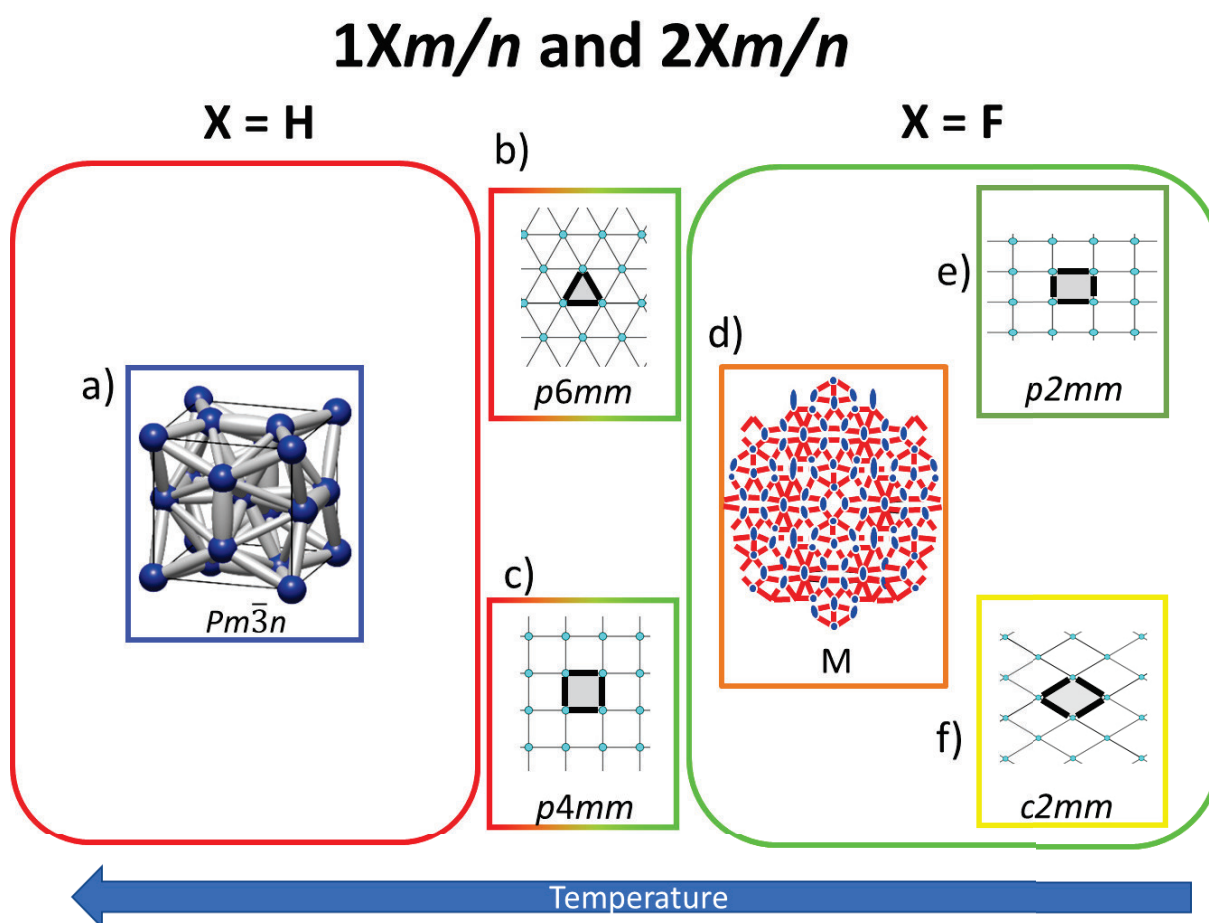

*Figure 4-2. Schematic phase sequence of the **1X*m/n*** and **2X*m/n*** compounds.*

The number of compounds **1X*m/n*** and **2X*m/n*** forming the M-phase was maximized by using a directed design based on a simple geometric model developed by our collaboration partners R. Waldecker and V.-M. Fischer at the Department of Mathematics at the MLU Halle (see **Fig. 4-3**). Using this geometric model led to success rates of 80% for the M-phase compounds.
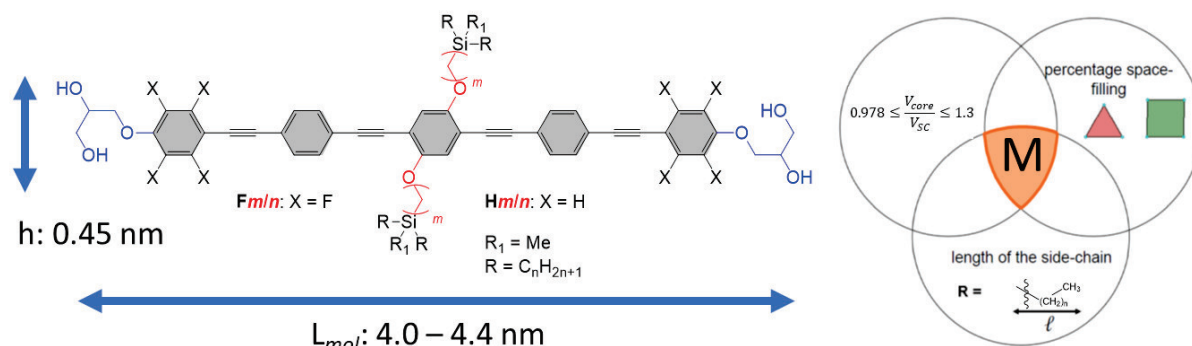

h: 0.45 nm

F*m/n*: X = F   **H*m/n*: X = H**

$R_1 = Me$
$R = C_nH_{2n+1}$

$L_{mol}: 4.0 - 4.4$ nm

$0.978 \leq \frac{V_{core}}{V_{SC}} \leq 1.3$

percentage space-filling

length of the side-chain

Figure 4-3. *a) Molecular structure with approximate length and height. b) simplified scheme of the developed geometric model with predictions of M-phase formation depending on molecular structural parameters (V_{Core} = volume of the (F)OPE cores; V_{SC} = side chain volume; l = length of the side chain (m+n+1)).*[101]

Publication C investigated the influence of side chain fluorination on the self-assembly of X-shaped (F)OPE-based bolapolyphiles **4X*m/n*,** with a chain volume again chosen to be located at the triangular-square transition. It was shown that the combination of semiperfluorinated and non-fluorinated side chains at opposite sides led to multicolor chessboard tilings, cell deformation, and tilting. The two-color rectangular "chessboard" tilings, the three-color rhomb tiling, and the mixed two-color rhomb square tiling represent new honeycomb LC phases (see **Fig. 4-4**). Again, for compounds **4H*m/n*** with a non-fluorinated OPE core, a continuously growing tilt could be observed where the square cells were retained by a tilting of all molecules simultaneously (see **Fig. 4-4a-d**). The core fluorinated compounds **4F*m/n*** could only assume no tilt or a large tilt angle due to the discrete face-to-face stacking modes of the FOPE cores, and this leads to the $c2mm^{T/2}$ phase with rectangular cells, as shown in **Fig. 4-4g**.
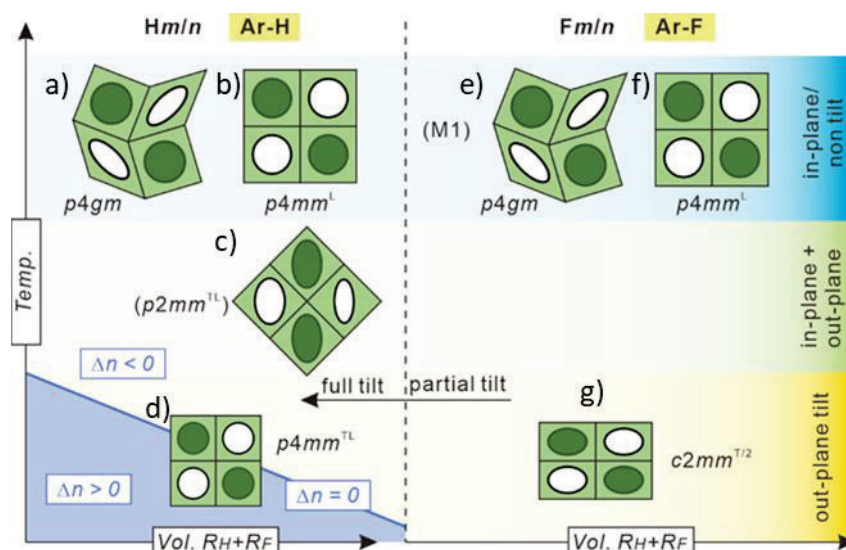

Figure 4-4. *Schematic phase sequence of the **4H1/m/p** and **4F1/m/p** compounds. (Publication 102)*

The final part of this work deals with the influence of stereogenic centers in the glycerol units attached to the (F)OPE-cores, as well as the effects of alkyl chain parity and branching point structure in the branched alkyl chains of compounds **5X*m/n***. It is shown that the uniform configuration of the

stereogenic centers has no significant influence on the mesophase type, molecular self-assembly, and physical properties. Especially, no indications of helical superstructures could be detected. Moreover, a special influence of an odd-even effect of the chain length could be excluded. Additionally, the replacement of the CH branching point by SiMe prefers the 3D-Cub$_{net}$ structure ($Pm\overline{3}n$) over the M-type and honeycomb phases for the OPE compounds, while in the FOPE compounds, the CH replacement by SiMe mainly leads to a decreased LC phase stability.

Overall, the presented X-shaped bolapolyphiles show a wide range of liquid crystalline phase structures at the triangular-square transition, among them the M-phases, which are considered as potential quasiperiodic and approximant structures.

Interestingly, the $Pm\overline{3}n$ Frank Kasper-type network phase competes with the M-type honeycomb mesophases at the triangular-square cross-over. This raises the question if in this frustration range, also a competition of quasiperiodic sphere packings and networks with quasiperiodic honeycombs (and their periodic approximants) could be found in future work.

5 Experimental Section

The synthetic data of the not-published materials and their analytical data are listed in the experimental section. The analytical data of the published compounds are summarized in the supporting information of the corresponding literature (Pub. A – C, see Appendix A.1).

5.1 Characterizing methods

The synthesized liquid crystalline materials were characterized using standard methods, including differential scanning calorimetry (DSC), polarization microscopy (POM), and X-ray diffraction (XRD) techniques. The structural parameters for the various mesophases were calculated according to established procedures.

5.1.1 Polarization microscopy (POM)

Optical investigations were carried out for all liquid crystalline materials by the use of a polarizing optical microscopy DMRXP (LAICA MICROSYSTEMS) in combination with a heating stage with sample holder FP 82-HAT (METLER). Optical textures were taken by a LAICA MC120 HD camera. Optical investigations were carried out by the preparation of the sample between two glass slides that were used without further treatment. A full wavelength retardation plate was used to determine the sign of birefringence.

5.1.2 Dynamic differential calorimetry (DSC)

Transition temperatures and enthalpies were determined as obtained from differential scanning calorimetry (DSC), which were recorded on a DSC-8000 (Perkin Elmer) in sealed 30 µL aluminum pans with heating and cooling rates of 10 K/min under an N_2 stream; peak temperatures are given in all tables. As reverence served an air-filled capsule.

5.1.3 X-ray diffraction investigations (XRD)

In-house X-ray investigations were carried out with an Incoatec (Geesthacht, Germany) IµS microfocus source with a monochromator for CuK_α radiation (λ = 0.154 nm), calibration with the powder pattern of $Pb(NO_3)_2$. A droplet of the sample was placed on a glass plate on a Linkam hot stage HFS-X350-GI (rate: 1 $Kmin^{-1}$ – 0.01 $Kmin^{-1}$). Exposure time was 5 min; the sample-detector distance was 9.00 cm for WAXS and 26.80 cm for SAXS. The diffraction patterns were recorded with a Vantec 500 area detector (Bruker AXS, Karlsruhe) and transformed into 1D plots using GADDS software.

5.1.4 Synchrotron-based X-ray scattering

High-resolution small-angle and wide-angle powder diffraction experiments were recorded on Beamline BL16B1 at the Shanghai Synchrotron Radiation Facility (SSRF) by Prof Dr. F. Liu and Dr. Y. Cao (University of Xi'an, P. R. China). Samples were held in evacuated 1 mm capillaries. A modified Linkam hot stage with thermal stability within 0.2 °C was used, with a hole for the capillary drilled through the silver heating block and mica windows attached to it on each side. A Pilatus 2M detector was used. q Calibration and linearization were verified using several orders of layer reflections from silver behenate and a series of n-alkanes. Experimental diffractograms are fitted using Gaussian-shaped peaks to determine the positions and intensities of the diffraction peaks. The diffraction peaks are indexed based on their peak positions, and the lattice parameters and the space groups are subsequently determined. More details on the investigation method can be read in the SI of Publication A – C.

5.1.5 Reconstruction of the electron density map (EDM)

Once the diffraction intensities are measured and the corresponding plane group determined, 2D electron density maps can be reconstructed based on the general formula.

$$E(xy) = \sum_{hk} F(hk)\, e^{[i2\pi(hx+ky)]} \tag{1}$$

Here $F(hk)$ is the structure factor of a diffraction peak with index (hk). It is normally a complex number, and the experimentally observed diffraction intensity is

$$I(xy) = K \cdot F(hk) = F * (hk) = K \cdot |F(hk)|^2 \tag{2}$$

Here K is a constant related to the sample volume, incident beam intensity etc. If the constant is equal to 1, then the electron density is

$$E(xy) = \sum_{hk} \sqrt{I(hk)}\, e^{[i2\pi(hx+ky)+\Phi_{hk}]} \tag{3}$$

As the observed diffraction intensity $I(hk)$ is only related to the amplitude of the structure factor $|F(hk)|$, the information about the phase of $F(hk)$, Φhk, cannot be determined directly from the experiment. However, the problem is much simplified when the structure of the ordered phase is centrosymmetric; hence, the structure factor $F(hk)$ is always real, and Φhk is either 0 or π. The case is essentially the same for the 3D centrosymmetric cubic phase.

This makes it possible for a trial-and-error approach, where candidate electron density maps are reconstructed for all possible phase combinations. The "correct" phase combination is then selected on the merit of the maps, helped by prior physical and chemical knowledge of the system. This is especially useful for the study of nanostructures, where typically only a limited number of diffraction peaks are observed.

5.2 Syntheses

5.2.1 General aspects

The used solvents were dried and cleaned up according to the general literature instructions. [104]

To purify the substances, column chromatography with silica gel 60 M (Corn size 0.04 – 0.63 nm, for column chromatography) sourced from MACHERY-NAGEL was utilized. The purity of the substances was evaluated using thin-layer chromatography with a silica gel-coated aluminum plate (silica gel 60 F254, supplied by MERCK). Substance detection was accomplished either by utilizing UV light (λ = 254 nm or 366 nm) or by applying Hanessian stain, prepared with 30 mL of concentrated sulfuric acid, 470 mL water, 240 g ammonium molybdate, and 1 g ceric ammonium molybdate the resulting stain was obtained through stirring the substances under heat. The listed yields pertain to the products after column chromatography and recrystallization.

The purity and identity of the synthesized substances were evaluated by ^{1}H-, ^{13}C-, ^{19}F-, and ^{29}Si-NMR spectroscopy. The VARIAN Gemini 2000 or Inova 500 instruments were used for this purpose. If no other information was given, the NMR-spectroscopic investigations were conducted at a temperature of 27 °C. Trimethylsilane (TMS) was used as a reference. The software MESTRENOVA 14.2.0 was utilized to analyze the NMR spectra received. Additionally, high-resolution mass spectra were obtained using HR-ESI-TOF-MS (Brucker). Melting point measurements were obtained using the DSC-8000 instrument.

5.2.2   General procedures

5.2.2.1   Alkylation of silanes (GP1)

Trialkylmagnesium bromide solution (3.5 eq.) in THF was cooled with stirring to 0 °C. LiCl (0.9 eq.) was added, followed by trichlorosilane (1 eq.), by adding with a syringe. The reaction is heated up to room temperature and stirred for 24 hours. Afterward, the reaction was quenched with water (1 ml / 1 ml THF), and the aqueous layers were extracted with Et_2O (3x50 ml). The combined organic layers were washed with water and brine. After drying over anhydrous Na_2SO_4, filtration, and evaporation of the solvent (850 mbar, 60°C), the crude product was purified by column chromatography.

5.2.2.2   Hydrosilylation of the (ω-bromoalkyl)trialkyl silanes (GP2)

Trialkylsilane (1 eq.), the appropriate ω-bromoalk-1-ene (1.5 eq), and Karstedt-cat. (3 mol%) were added to anhydrous DCM (20 mL/mmol) and stirred at RT for 3 days. Afterward, the solvent was evaporated, and the crude product was purified by column chromatography. (Eluent: *n*-hexane)

5.2.2.3   WILLIAMSON ether synthesis – monoalkylation (GP3)

Phenol (1 eq.), alkyl bromide (1 eq.), and potassium carbonate (2.5 eq.) were suspended in DMF (20 mL/10 mmol phenol). A small amount of TBAI (tip of a spatula) was added to the suspension, and the reaction mixture was stirred for 3 days at 80°C. TLC was used to monitor the reaction process. Once the reaction was complete, the mixture was diluted with water to twice its volume, followed by extraction of the aqueous phase with Et_2O (3 x 50 mL). The organic fractions were combined and washed with saturated LiCl solution, water, and brine. After drying over $MgSO_4$, the solvent was evaporated under reduced pressure (850 mbar), and the resulting crude product was purified by column chromatography (eluent: 1. *n*-hexane, 2. $CHCl_3$).

5.2.2.4   WILLIAMSON ether synthesis (GP4)

2,5-Diiodohydroquinone (1 eq.), alkyl bromide (2.2 eq.), and potassium carbonate (10 eq.) were suspended in DMF (20 mL/10 mmol phenol). A small amount of TBAI (tip of a spatula) was added to the suspension, and the reaction mixture was stirred for 3 days at 80°C. TLC was used to monitor the reaction process. Once the reaction was complete, the mixture was diluted with water to twice its volume, followed by extraction of the aqueous phase with Et_2O (3 x 50 mL). The organic fractions were combined and washed with saturated LiCl solution, water, and brine. After drying over $MgSO_4$, the solvent was evaporated under reduced pressure (850 mbar), and the resulting crude product was purified by column chromatography (eluent: 1. *n*-hexane, 2. $CHCl_3$).

5.2.2.5   Carbon-carbon cross coupling according to SONOGASHIRA (GP5)

The halide (1 eq.) and acetylene compounds (2.2 eq.) were dissolved in anhydrous Et_3N and degassed with argon for 30 minutes. Tetrakis(triphenylphosphine)palladium(0) (3 mol%) and copper(I)iodine (3 mol%) were then added to the solution. The suspension was stirred at room temperature for 24 hours. Upon completion of the reaction (checked by TLC), the solvent was evaporated under reduced pressure (250 mbar), and the crude product was purified by column chromatography (eluent $CHCl_3$).

5.2.2.6 Desilylation (GP6)

The TMS-protected acetylene compound (1 eq.) and potassium fluoride (2 eq.) were suspended in a mixture of DCM and MeOH (2:1) and stirred for 24 hours at room temperature. After completion of the reaction (checked by TLC), the reaction was diluted to twice the volume by adding water. The aqueous phase was extracted with DCM (3 x 50 mL), and the combined organic fractions were washed with brine, followed by drying with MgSO4. After evaporation of the solvent under reduced pressure (850 mbar), the crude product was purified using column chromatography (eluent: $CHCl_3$).

5.2.2.7 Iodination with hypervalent iodine (GP7)

The hydroquinone diether (1 eq), iodine (1.1 eq), and [bis(trifluoroacetoxy)iodo]benzene (1.1 eq) were dissolved in anhydrous DCM and stirred under reflux for 6 hours. Once the reaction was completed, a $Na_2S_2O_3$ solution was added to remove any excess iodine. The aqueous phase was extracted with DCM (3 x 50 mL). The combined organic fraction was washed with H_2O, then with brine, and finally dried with Mg_2SO_4. The solvent was then removed under reduced pressure (850 mbar), and the crude product was purified by column chromatography (eluent: n-hexane).

5.2.2.8 Hydrolysis of the isopropylidene protecting group (GP8)

The appropriate acetonide and PPTS (2 eq.) were dissolved in a mixture of THF and MeOH (1:1, 60 mL). The reaction was stirred at 55°C for 24 hours, and the progress was monitored by TLC. The solvent was evaporated under reduced pressure (300 mbar) after the reaction was completed, and the crude product was purified by column chromatography ($CHCl_3$ / MeOH, 9:1) followed by recrystallization from MeOH/THF.

5.2.2.9 Chemicals

The following chemicals were commercially available and were used without further purification.

3-Bromo-prop-1-ene (*Aldrich*)	4-Bromo-but-1-ene (*Aldrich*)
5-Bromo-pent-1-ene (*Aldrich*)	6-Bromo-hex-1-ene (*Aldrich*)
7-Bromo-hept-1-ene (*Aldrich*)	8-Bromo-oct-1-ene (*Aldrich*)
9-Bromo-non-1-ene (*Aldrich*)	10-Bromo-dec-1-ene (*Aldrich*)
11-Bromo-undec-1-ene (*Aldrich*)	

2,3-Dichloro-5,6-dicyano-1,4-benzoquinone (*Aldrich*)
Triphenylphosphine (*Aldrich*)
Karstedt-catalyst 1,1,3,3-tetramethyl-1,3-divinyl-disiloxane – 2% Pd in xylene (*Aldrich*)
Tetrakis(triphenylphosphine)palladium (0) (*TCI*)

5-Bromo-*n*-heptane (*Aldrich*)	6-Bromo-*n*-hexane (*Aldrich*)
8-Bromo-*n*-octane (*Aldrich*)	9-Bromo-*n*-nonane (*Aldrich*)
10-Bromo-*n*-decane (*Aldrich*)	11-Bromo-*n*-undecane (*Aldrich*)
12-Bromo-*n*-dodecane (*Aldrich*)	14-Bromo-*n*-tetradecane (*Aldrich*)
16-Bromo-*n*-hexadecane (*Aldrich*)	

Dodecanemagnesiumbromide-solution 1.0 M in THF (*Aldrich*)

Magnesium tunings (*Aldrich*)	Malonic acid diethyl ester (*Aldrich*)
Iodopentafluorobenzene (*Aldrich*)	Trimethylsilane (*Aldrich*)

(4-Bromophenylethinyl)trimethylsilane (*Aldrich*)
(*R*)-(-)2,3-O-Isopropylideneglycerol (95%) (*Aldrich*)
p-Toluenesulfonyl chloride (*Aldrich*)
Iodine (*Aldrich*)

[Bis(trifluoroacetoxy)iodo]benzene (*Aldrich*)   Hydroquinone (*Aldrich*)
2,5-Diiodo-1,4-benzenediol (*Aldrich*)   Lithium aluminum hydride (*Aldrich*)
Sodium hydride (60% in paraffin) (*Aldrich*)   Lithium chloride (*Aldrich*)
Sodium hydroxide (*Aldrich*)   Potassium fluoride (*Aldrich*)
Tetrabutylammonium iodide (*Aldrich*)   Tetrabutylammonium bromide (*Aldrich*)
Cupper-(I)-iodide (*Aldrich*)   Pyridinium *p*-toluenesulfonate (*Aldrich*)
Potassium carbonate (*Aldrich*)

The following chemicals were already present in the stock of the workgroup.

Dioctylmethylsilane was synthesized by Dr. M. Wagner during the work for his Ph.D thesis.[105]
16-(Bromomethyl)hentriacontane synthesized by Dr. M. Poppe during his work for his Ph. D. thesis.[44]

The synthesis and analytical data of the following chemicals were already published.

15-(Bromomethyl)nonacosane[106]
17-(Bromomethyl)tritriacontane[107]
1,4-Bis(allyloxy)benzene[82]
4-[4-(4-Ethynylphenylethynyl)phenoxymethyl]-2,2-dimethyl-1,3-dioxolane **25H**[50]
4-{[4-(4-ethynylphenylethynyl)-2,3,5,6-tetrafluorophenoxy]methyl}-2,2-dimethyl-1,3-dioxolane **26F**[86]

5.3 Syntheses and Analytical Data

The synthetic and analytical data of the described compounds and their intermediates of Publication A – C can be read in the supporting information of the respective publication. In the following section, the analytical data of the unpublished compounds and their intermediates will be described.

5.3.1 Intermediates

(*S*)-(2,2-Dimethyl-1,3-dioxolane-4-yl)methyl 4-methylbenzenesulfonate 22[108]
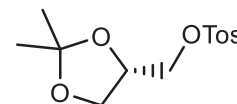
(*R*)-(2,2-Dimethyl-1,3-dioxolane-4-yl)methanol (1 eq., 21.2 g; 20 mL, 0.16 mol), NaOH (1.5 eq, 9.6 g, 0.24 mol) were added to a THF / H_2O mixture (4/1, 160 mL / 40 mL) and cooled to 0°C in an ice bath. Tosyl chloride (1.1 eq, 33.5 g, 0.18 mol) dissolved in THF (50 mL) is added to the mixture and stirred for 3 h at 0 °C. Afterward, the reaction was quenched with water and extracted with $CHCl_3$ (3x 100 mL). The combined organic layers were washed with $NaHCO_3$ and water and dried over Na_2SO_4. The solvent was evaporated (474 mbar, 60°C), and the crude product was purified by phase separation with *n*-pentane. A colorless liquid, $C_{13}H_{18}O_5S$ M = 286.34 g/mol, yield: 44.08 g (96 %), **^{1}H- NMR** (CDCl$_3$, 400 MHz): δ / ppm = 7.78 (d, $^3J_{H,H}$ = 8.2 Hz2H, Aryl-*H*), 7.33 (d, $^3J_{H,H}$ = 8.2 Hz, 2H, Aryl-*H*), 4.31 – 4.19 (m, 1H, -C*H*O-), 4.11 – 3.86 (m, 3H, -OCH$_A$C*H*$_B$-, -OCH$_A$C*H*$_B$-), 3.77 – 3.71 (m, 1H, -OCH$_A$C*H*$_B$-), 2.43 (s, 3H, Aryl-C*H*$_3$), 1.32 (s, 3H,-C*H*$_3$), 1.29 (s, 3H,-C*H*$_3$).

(*R*)-4-(4-Bromophenoxy)methyl-2,2-dimethyl-1,3-dioxolane 23H
Synthesized according to GP3 from (*S*)-(2,2-dimethyl-1,3-dioxolane-4-yl)methyl 4-methylbenzenesulfonate (1 eq, 44.0 g, 0.15 mol) 4-Bromophenol (1.1 eq, 29.2 g, 0.17 mol), K$_2$CO$_3$ (2.6 eq. 55.3 g, 0.40 mol), TBAI (50 mg, 0.1 mol) in anhydrous DMF (150 mL), purification by column chromatography (eluent: CHCl$_3$); white solid, yield: $C_{12}H_{15}BrO_3$ M = 287.15 g/mol, 32.6 g (81 %), *mp* = 94°C **^{1}H- NMR** (CDCl$_3$, 400 MHz): δ / ppm = 7.40 – 7.32 (m, 2H, Aryl-*H*), 6.82 – 6.74 (m, 2H, Aryl-*H*), 4.50 – 4.39 (m, 1H, -C*H*O-), 4.19 – 4.10 (m, 1H, -OCH$_A$C*H*$_B$-), 4.04 – 3.96 (m, 1H, -OCH$_A$C*H*$_B$-), 3.93 – 3.84 (m, 2H, -OCH$_A$C*H*$_B$-), 1.44 (s, 3H,-C*H*$_3$), 1.39 (s, 3H,-C*H*$_3$).
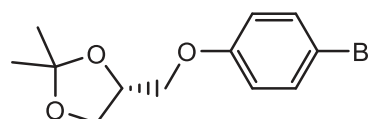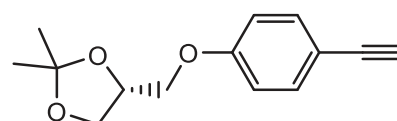
(*R*)-({4-[(2,2-Dimethyl-1,3-dioxolane-4-yl)methoxy]phenyl}ethynyl)trimethylsilane 24H-TMS
Synthesized according to GP5 from (*R*)-4-[(4-bromophenoxy)methyl]-2,2-dimethyl-1,3-dioxolane (1eq, 16.3 g, 26.0 mmol) TMSA (1.25 eq, 7.0 g, 9.8 mL, 71.0 mmol), Pd(PPh$_3$)$_4$ (0.9 g, 0.8 mmol), CuI (0.2 g, 0.2 mmol) in anhydrous Et$_3$N (150 mL), purification by column chromatography (eluent: CHCl$_3$); colorless liquid, yield: $C_{17}H_{24}O_3Si$ M = 304.46 g/mol, 17.1 g (98 %), **^{1}H- NMR** (CDCl$_3$, 400 MHz): δ / ppm = 7.42 – 7.36 (m, 2H, Aryl-*H*), 6.83 – 6.78 (m, 2H, Aryl-*H*), 4.49 – 4.39 (m, 1H, -C*H*O-), 4.18 – 4.11 (m, 1H, -OCH$_A$CH$_B$-), 4.05 – 3.99 (m, 1H, -OCH$_A$CH$_B$-), 3.95 – 3.83 (m, 2H, -OCH$_A$C*H*$_B$-), 1.45 (s, 3H,-C*H*$_3$), 1.39 (s,3H,-C*H*$_3$), 0.23 (s, 9H,-SiC*H*$_3$).
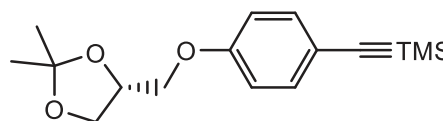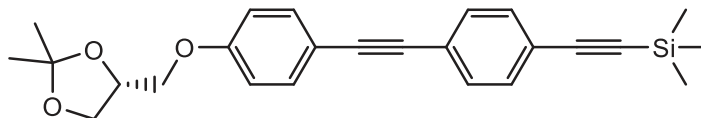
(*R*)-4-[(4-Ethynylphenoxy)methyl]-2,2-dimethyl-1,3-dioxolane 24H
Synthesized according to GP6 from (*R*)-({4-[(2,2-dimethyl-1,3-dioxolane-4-yl)methoxy]phenyl}ethynyl)trimethylsilane (1eq, 17.1 g, 56.2 mmol) KF (2 eq, 6.5 g, 112.4 mmol) in MeOH / DCM (50 mL / 100 mL), purification by column chromatography (eluent: CHCl$_3$); colorless liquid, yield: $C_{14}H_{16}O_3$ M = 232.28 g/mol, 8.9 g (68 %), **^{1}H- NMR** (CDCl$_3$, 400 MHz): δ / ppm = 7.48 – 7.36 (m, 2H, Aryl-*H*), 6.90 – 6.82 (m, 2H, Aryl-*H*), 4.53

– 4.39 (m, 1H, -CHO-), 4.18 – 4.12 (m, 1H, -OCH_ACH$_B$-), 4.07 – 4.01 (m, 1H, -OCH_ACH$_B$-), 3.97 – 3.85 (m, 2H, -OCH$_A$CH_B-), 3.00 (s, 1H, ≡CH), 1.45 (s, 3H,-CH_3), 1.39 (s, 3H,-CH_3).

### (*R*)-4-[4-(4-Ethynylpheylethynyl)phenoxymethyl]-2,2-dimethyl-1,3-dioxolane 25H-TMS

Synthesized according to GP5 from (*R*)-4-[(4-ethynylphenoxy)methyl]-2,2-dimethyl-1,3-dioxolane (1eq, 8.9 g, 38.3 mmol), (4-bromopheyl)ethenyltrimethylsilane (1.25 eq, 12.3 g, 48.5 mmol), Pd(PPh$_3$)$_4$ (1.3 g, 1.2 mmol), CuI (0.2 g, 1.1 mmol) in anhydrous Et$_3$N (150 mL), purification by column chromatography (eluent: CHCl$_3$); yellow solid, yield: C$_{25}$H$_{28}$O$_3$Si *M* = 404.57 g/mol, 13.6 g (87 %), *mp* = 107 °C, **^{1}H- NMR** (CDCl$_3$, 400 MHz): δ / ppm = 7.53 – 7.39 (m, 6H, Aryl-*H*), 6.92 – 6.83 (m, 2H, Aryl-*H*), 4.52 – 4.43 (m, 1H, -CHO-), 4.17 (dd, $^2J_{H,H}$ = 8.5, $^3J_{H,H}$ = 6.4 Hz, 1H, -OCH_ACH$_B$-), 4.07 (dd, $^2J_{H,H}$ = 9.7, $^3J_{H,H}$ = 6.4 Hz, 1H, -OCH_ACH$_B$-), 3.96 (dd, $^2J_{H,H}$ = 9.6, $^3J_{H,H}$ = 5.9 Hz, 1H, -OCH$_A$CH_B-), 3.91 (dd, $^2J_{H,H}$ = 8.5, $^3J_{H,H}$ = 5.9 Hz, 1H, -OCH$_A$CH_B-), 1.46 (s, 3H,-CH_3), 1.41 (s, 3H,-CH_3), 0.25 (s, 9H,-SiCH_3).

(*R*)-4-({4-[(4-Ethynylphenyl)ethynyl]phenoxy}methyl)-2,2-dimethyl-1,3-dioxolane 27H*
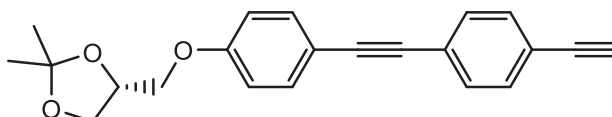
Synthesized according to GP6 from (*R*)-4-[4-(4-ethynylphenylethynyl)phenoxymethyl]-2,2-dimethyl-1,3-dioxolane (1eq, 13.6 g, 33.6 mmol) KF (2 eq, 3.9 g, 67.2 mmol) in MeOH / DCM (50 mL / 100 mL), purification by column chromatography (eluent: CHCl$_3$ / *n*-hexane (1 / 1)); yellow solid, yield: C$_{22}$H$_{20}$O$_3$ *M* = 332.40 g/mol, 5.8 g (51 %), *mp* = 131 °C, **^{1}H- NMR** (CDCl$_3$, 400 MHz): δ / ppm = 7.56 – 7.41 (m, 6H, Aryl-*H*), 6.93 – 6.85 (m, 2H, Aryl-*H*), 4.54 – 4.43 (m, 1H, -CHO-), 4.17 (dd, $^2J_{H,H}$ = 8.5, $^3J_{H,H}$ = 6.4 Hz, 1H, -OCH_ACH$_B$-), 4.07 (dd, $^2J_{H,H}$ = 9.4, $^3J_{H,H}$ = 5.5 Hz, 1H, -OCH_ACH$_B$-), 3.96 (dd, $^2J_{H,H}$ = 9.5, $^3J_{H,H}$ = 5.8 Hz, 1H, -OCH$_A$CH_B-), 3.91 (dd, $^2J_{H,H}$ = 8.5, $^3J_{H,H}$ = 5.8 Hz, 1H, -OCH$_A$CH_B-), 3.16 (s, 1H, ≡CH), 1.47 (s, 3H,-CH_3), 1.41 (s, 3H,-CH_3).
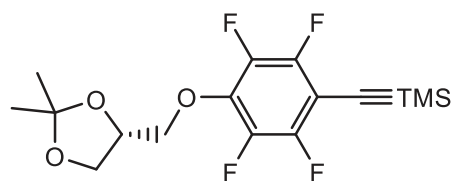
(*R*)-1,2-Isopropylidene-3-(2,3,5,6-tetrafluoro-4-iodophenyl)-glycerol 23F[109]
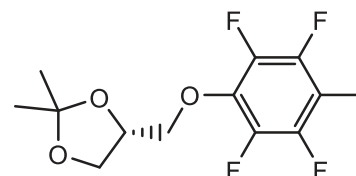
Synthesized according to GP3 from (*R*)-(2,2-dimethyl-1,3-dioxolane-4-yl)methanol (1 eq., 11.2 g; 10.5 mL, 85 mmol), pentafluoro-iodo-benzene (1 eq, 25.0 g, 85 mmol) in anhydrous DMF (150 mL), colorless liquid, C$_{12}$H$_{11}$F$_4$IO$_3$ *M* = 406.11 g/mol, yield: 25.0 g (72 %), **^{1}H- NMR** (CDCl$_3$, 400 MHz): δ / ppm = 4.47 – 4.37 (m, 1H, -CHO-), 4.28 (dd, $^2J_{H,H}$ = 10.2, $^3J_{H,H}$ = 5.1 Hz, 1H, -OCH_ACH$_B$-), 4.23 – 4.10 (m, 2H, -OCH_ACH$_B$-, -OCH$_A$CH_B-), 3.93 (dd, $^2J_{H,H}$ = 8.6, $^3J_{H,H}$ = 5.5 Hz, 1H, -OCH$_A$CH_B-), 1.41 (s, 3H,-CH_3), 1.36 (s, 3H,-CH_3). **^{19}F- NMR** (CDCl$_3$, 376 MHz): δ / ppm = -121.00 – -121.28 (m, C$_{Aryl}$-*F*), -154.04 – -154.36 (m, C$_{Aryl}$-*F*).

(R)-1,2-Isopropylidene-3-[2,3,5,6-tetrafluoro-4-(trimethylsilylethynyl)phenyl]-glycerol 24F-TMS

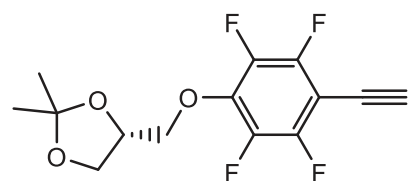Synthesized according to GP5 from (R)-1,2-isopropylidene-3-(2,3,5,6-tetrafluoro-4-iodophenyl)-glycerol (1eq, 25 g, 62.0 mmol) TMSA (1.25 eq, 7.6 g, 10.7 mL, 77.0 mmol), Pd(PPh$_3$)$_4$ (2.2 g, 1.9 mmol), CuI (0.4 g, 1.9 mmol) in anhydrous Et$_3$N (150 mL), purification by column chromatography (eluent: CHCl$_3$); colorless liquid, yield: C$_{17}$H$_{20}$F$_4$O$_3$Si M = 376.42 g/mol, 20.3 g (88 %), **^{1}H- NMR** (CDCl$_3$, 400 MHz): δ / ppm = 4.48 − 4.37 (m, 1H, -CHO-), 4.29 (dd, $^2J_{H,H}$ = 10.3, $^3J_{H,H}$ = 5.2 Hz, 1H, -OCH_ACH$_B$-), 4.20 (dd, $^2J_{H,H}$ = 10.2, $^3J_{H,H}$ = 5.6 Hz, 1H, -OCH_ACH$_B$-), 4.13 (dd, $^2J_{H,H}$ = 8.7, $^3J_{H,H}$ = 5.3 Hz, 1H, -OCH$_A$CH_B-), 3.93 (dd, $^2J_{H,H}$ = 8.7, $^3J_{H,H}$ = 5.6 Hz, 1H, -OCH$_A$CH_B-), 1.41 (s, 3H,-CH_3), 1.36 (s, 3H,-CH_3), 0.26 (s, 9H,-SiCH_3). **^{19}F- NMR** (CDCl$_3$, 376 MHz): δ / ppm = -137.42 − -137.66 (m, C$_{Aryl}$-F), -157.07 − -157.29 (m, C$_{Aryl}$-F).

(R)-3-(4-Ethynyl-2,3,5,6-tetrafluorophenyl)-1,2-isopropylidene-glycerol 24

Synthesized according to GP6 from (R)-1,2-isopropylidene-3-[2,3,5,6-tetrafluoro-4-(trimethylsilylethynyl)phenyl]-glycerol (1eq, 10.2 g, 27.0 mmol) KF (2 eq, 3.1 g, 54.0 mmol) in MeOH / DCM (50 mL / 100 mL), purification by column chromatography (eluent: CHCl$_3$); colorless liquid, yield: C$_{14}$H$_{12}$F$_4$O$_3$ M = 304.24 g/mol, 6.5 g (80 %), **^{1}H- NMR** (CDCl$_3$, 500 MHz): δ / ppm = 4.49 − 4.41 (m, 1H, -CHO-), 4.32 (dd, $^2J_{H,H}$ = 10.3, $^3J_{H,H}$ = 5.3 Hz, 1H, -OCH_ACH$_B$-), 4.23 (dd, $^2J_{H,H}$ = 10.3, $^3J_{H,H}$ = 5.6 Hz, 1H, -OCH_ACH$_B$-), 4.15 (dd, $^2J_{H,H}$ = 8.6, $^3J_{H,H}$ = 6.4 Hz, 1H, -OCH$_A$CH_B-), 3.95 (dd, $^2J_{H,H}$ = 8.6, $^3J_{H,H}$ = 5.6 Hz, 1H, -OCH$_A$CH_B-), 3.56 (s, 1H, ≡CH), 1.42 (s, 3H,-CH_3), 1.38 (s, 3H,-CH_3). **^{19}F- NMR** (CDCl$_3$, 470 MHz): δ / ppm = -137.40 − -137.65 (m, C$_{Aryl}$-F), -156.42 − -157.11 (m, C$_{Aryl}$-F).

(R)-3-{4-[4-(Trimethylsilylethynyl)phenylethynyl]-2,3,5,6-tetrafluorophenyl}-1,2-isopropylidene-glycerol 28F-TMS
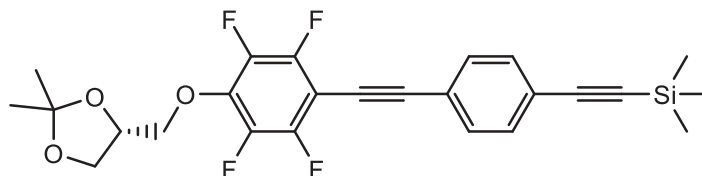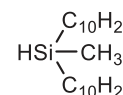
Synthesized according to GP5 from (R)-3-(4-ethynyl-2,3,5,6-tetrafluorophenyl)-1,2-isopropylidene-glycerol (1eq, 6.5g, 21.3 mmol), (4-bromopheyl)ethenyltrimethylsilane (1.25 eq, 5.9 g, 23.4 mmol), Pd(PPh$_3$)$_4$ (0.7 g, 0.6 mmol), CuI (0.1 g, 0.6 mmol) in anhydrous Et$_3$N (150 mL), purification by column chromatography (eluent: CHCl$_3$); yellow solid, yield: C$_{25}$H$_{24}$F$_4$O$_3$Si M = 476.54 g/mol, 4.4 g (43 %), mp = 126 °C, **^{1}H- NMR** (CDCl$_3$, 400 MHz): δ / ppm = 7.52 − 7.42 (m, 4H, Aryl-H), 4.49 − 4.41 (m, 1H, -CHO-), 4.32 (dd, $^2J_{H,H}$ = 10.2, $^3J_{H,H}$ = 5.2 Hz, 1H, -OCH_ACH$_B$-), 4.23 (dd, $^2J_{H,H}$ = 10.2, $^3J_{H,H}$ = 5.6 Hz, 1H, -OCH_ACH$_B$-), 4.15 (dd, $^2J_{H,H}$ = 8.6, $^3J_{H,H}$ = 6.4 Hz, 1H, -OCH$_A$CH_B-), 3.95 (dd, $^2J_{H,H}$ = 8.6, $^3J_{H,H}$ = 5.6 Hz, 1H, -OCH$_A$CH_B-), 1.43 (s, 3H,-CH_3), 1.38 (s, 3H,-CH_3), 0.26 (s, 9H,-SiCH_3). **^{19}F- NMR** (CDCl$_3$, 376 MHz): δ / ppm = -137.36 − -137.73 (m, C$_{Aryl}$-F), -156.58 − -156.95 (m, C$_{Aryl}$-F).

(R)-3-[4-(4-Ethynylphenylethynyl)-2,3,5,6-tetrafluorophenyl]-1,2-isopropylidene-glycerol 28F
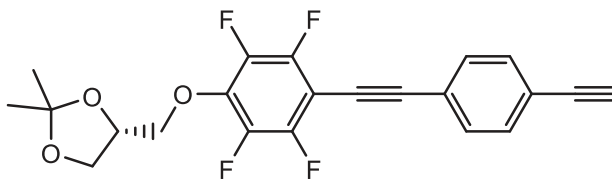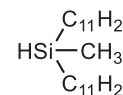

Synthesized according to GP6 from (R)-3-{4-[4-(trimethylsilylethynyl)phenylethynyl]-2,3,5,6-tetrafluorophenyl}-1,2-isopropylidene-glycerol (1eq, 3.3 g, 6.9 mmol) KF (2 eq, 0.8 g, 13.9 mmol) in MeOH / DCM (25 mL / 50 mL), purification by column chromatography (eluent: CHCl$_3$ / n-hexane (1 / 1)); yellow solid, yield: C$_{22}$H$_{16}$F$_4$O$_3$ M = 404.36 g/mol, 2.3 g (61 %), mp = 72 °C, **^{1}H- NMR** (CDCl$_3$, 400 MHz): δ / ppm = 7.66 − 7.48 (m, 4H, Aryl-H), 4.52 − 4.41 (m, 1H, -CHO-), 4.33 (dd, $^2J_{H,H}$ = 10.1, $^3J_{H,H}$ = 5.1 Hz, 1H, -OCH_ACH$_B$-), 4.23 (dd, $^2J_{H,H}$ = 10.1, $^3J_{H,H}$ = 5.6 Hz, 1H, -OCH_ACH$_B$-), 4.16 (dd, $^2J_{H,H}$ = 8.6, $^3J_{H,H}$ = 6.4 Hz, 1H, -OCH$_A$CH_B-), 3.95 (dd, $^2J_{H,H}$ = 8.6, $^3J_{H,H}$ = 5.5 Hz, 1H, -OCH$_A$CH_B-), 3.20 (s, 1H, ≡CH), 1.43 (s, 3H,-CH_3), 1.38 (s, 3H,-CH_3). **^{19}F- NMR** (CDCl$_3$, 376 MHz): δ / ppm = -137.41 − -137.54 (m), -156.80 − -156.93 (m).
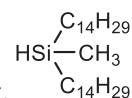
Dinonylmethylsilane
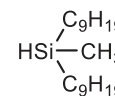
Synthesized according to GP1 from nonylmangnesium bromide solution, LiCl (1.0 g, 23.4 mmol), dichlormethylsilane (3.0 g, 2.7 mL, 26.0 mmol), purification by column chromatography (eluent: n-hexane); colorless liquid, yield: C$_{19}$H$_{42}$Si M = 298.63 g/mol, 5.65 g (73 %), **^{1}H- NMR** (CDCl$_3$, 400 MHz): δ / ppm = 3.80 − 3.71 (m, 1H, -SiH), 1.39 − 1.21 (m, 28H, -CH_2), 0.88 (t, $^3J_{H,H}$ = 6.8 Hz, 6H, -CH_3), 0.65 − 0.50 (m, 4H, -SiCH_2), 0.03 (d, $^3J_{H,H}$ = 3.7 Hz, 3H, -SiCH_3). **^{29}Si-NMR** (CDCl$_3$, 79 MHz): δ / ppm = -9.86 (Si).

Didecylmethylsilane

Synthesized according to GP1 from decylmangnesium bromide solution, LiCl (1.0 g, 23.4 mmol), dichlormethylsilane (3.0 g, 2.7 mL, 26.0 mmol, purification by column chromatography (eluent: n-hexane); colorless liquid, yield: C$_{21}$H$_{46}$Si M = 326.58 g/mol, 7.95 g (94 %), **^{1}H- NMR** (CDCl$_3$, 400 MHz): δ / ppm =3.77 − 3.71 (m, 1H, -SiH), 1.40 − 1.20 (m, 32H, -CH_2), 0.88 (t, $^3J_{H,H}$ = 6.4 Hz, 6H, -CH_3), 0.67 − 0.49 (m, 4H, -SiCH_2), 0.03 (d, $^3J_{H,H}$ = 3.7 Hz, 3H, -SiCH_3). **^{29}Si-NMR** (CDCl$_3$, 79 MHz): δ / ppm = -9.86 (Si).

Diundecylmethylsilane

Synthesized according to GP1 from undecylmangnesium bromide solution, LiCl (1.0 g, 23.4 mmol), dichlormethylsilane (3.0 g, 2.7 mL, 26.0 mmol), purification by column chromatography (eluent: n-hexane); colorless liquid, yield: C$_{23}$H$_{50}$Si M = 366.83 g/mol, 6.3 g (71 %), **^{1}H- NMR** (CDCl$_3$, 400 MHz): δ / ppm = 3.80 − 3.71 (m, 1H, -SiH), 1.44 − 1.16 (m, 36H, -CH_2), 0.88 (t, $^3J_{H,H}$ = 6.9 Hz, 6H, -CH_3), 0.67 − 0.45 (m, 4H, -SiCH_2), 0.03 (d, $^3J_{H,H}$ = 3.7 Hz, 3H, -SiCH_3). **^{29}Si-NMR** (CDCl$_3$, 79 MHz): δ / ppm = -9.86 (Si).

Didodecylmethylsilane
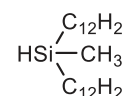
Synthesized according to GP1 from dodecylmangnesium bromide solution, LiCl (1.0 g, 23.4 mmol), dichlormethylsilane (3.0 g, 2.7 mL, 26.0 mmol), purification by column chromatography (eluent: n-hexane); colorless liquid, yield: C$_{25}$H$_{54}$Si M = 382.79 g/mol, 9.74 g (98 %), **^{1}H- NMR** (CDCl$_3$, 400 MHz): δ / ppm = 3.79 − 3.72 (m, 1H, -SiH), 1.41 − 1.18 (m, 40H, -CH_2), 0.89 (t, $^3J_{H,H}$ = 6.8 Hz, 6H, -

CH_3), 0.63 – 0.50 (m, 4H, -SiCH_2), 0.03 (d, $^3J_{H,H}$ = 3.7 Hz, 3H, -SiCH_3). **^{29}Si-NMR** (CDCl$_3$, 79 MHz): δ / ppm = -9.87 (*Si*).

Ditetradecylmethylsilane

Synthesized according to GP1 from tetradecylmangnesium bromide solution, LiCl (1.0 g, 23.4 mmol), dichlormethylsilane (3.0 g, 2.7 mL, 26.0 mmol), purification by column chromatography (eluent: *n*-hexane); colorless liquid, yield: C$_{29}$H$_{62}$Si *M* = 438.90 g/mol, 10.4 g (91 %), **^{1}H- NMR** (CDCl$_3$, 400 MHz): δ / ppm =3.81 – 3.73 (m, 1H, -Si*H*), 1.48 – 1.17 (m, 48H, -CH_2), 0.89 (t, $^3J_{H,H}$ = 6.8 Hz, 6H, -CH_3), 0.67 – 0.50 (m, 4H, -SiCH_2), 0.04 (d, $^3J_{H,H}$ = 3.7 Hz, 3H, -SiCH_3). **^{29}Si-NMR** (CDCl$_3$, 79 MHz): δ / ppm = -9.87 (*Si*).

Triheptylsilane
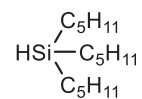
Synthesized according to GP1 from pentylmangnesium bromide solution, LiCl (0.6 g, 12.3 mmol), trichlorosilane (2.0 g, 1.5 mL, 14.8 mmol), purification by column chromatography (eluent: *n*-hexane), yield: colorless liquid, C$_{15}$H$_{34}$Si *M* = 242.52 g/mol, 2.61 g (73 %), **^{1}H- NMR** (CDCl$_3$, 400 MHz): δ / ppm = 3.70 – 3.65 (m, 1H, -Si*H*), 1.42 – 1.24 (m, 18H, -CH_2), 0.88 (t, $^3J_{H,H}$ = 6.7 Hz, 9H, -CH_3), 0.66 – 0.54 (m, 6H, -SiCH_2). **^{29}Si-NMR** (CDCl$_3$, 79 MHz): δ / ppm = -6.45 (*Si*).

### (9-Bromononyl)dioctylmethylsilane 6-1
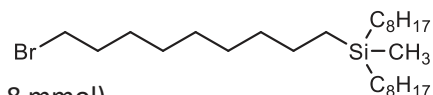
Synthesized according to GP2 from dioctylmethylsilane (4.0 g, 14.8 mmol), 9-bromonon-1-ene (4.6 g, 4.1 mL, 22.2 mmol), Karstedt-Cat (0.59 mL) in anhydrous DCM (20 mL), purification by column chromatography (eluent: *n*-hexane); colorless liquid, yield: C$_{26}$H$_{55}$SiBr *M* = 475.72 g/mol, 3.70 g (53 %), **^{1}H-NMR** (CDCl$_3$, 402 MHz): δ / ppm = 3.39 (t, $^3J_{H,H}$ = 6.9 Hz, 2H, BrCH_2-), 1.90 – 1.78 (m, 2H, BrCH$_2$CH_2-), 1.47 – 1.35 (m, 2H, BrCH$_2$CH$_2$CH_2-), 1.35 – 1.18 (m, 34H, -CH_2-), 0.87 (t, $^3J_{H,H}$ = 6.8 Hz, 6H, -CH_3), 0.49 – 0.41 (m, 6H, -SiCH_2-), -0.10 (s, 3H, -SiCH_3). **^{29}Si-NMR** (CDCl$_3$, 80 MHz): δ / ppm = 2.77 (*Si*).

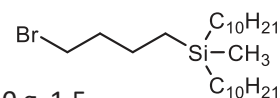### (5-Bromopentyl)dinonylmethylsilane 6-2
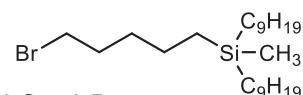
Synthesized according to GP2 from 1 (4.4 g, 8.2 mmol), 5-bromopent-1-ene (1.8 g, 1.5 mL, 12.3 mmol), Karstedt-Cat (0.33 mL) in anhydrous DCM (20 mL), purification by column chromatography (eluent: *n*-hexane); colorless liquid, yield: C$_{24}$H$_{51}$SiBr *M* = 447.66 g/mol, 2.10 g (57 %), **^{1}H-NMR** (CDCl$_3$, 402 MHz): δ / ppm = 3.38 (t, $^3J_{H,H}$ = 6.9 Hz, 2H, BrCH_2-), 1.92 – 1.77 (m, 2H, BrCH$_2$CH_2-), 1.48 – 1.38 (m, 2H, BrCH$_2$CH$_2$CH_2-), 1.35 – 1.19 (m, 30H, -CH_2-), 0.87 (t, $^3J_{H,H}$ = 6.7 Hz, 6H, -CH_3), 0.55 – 0.41 (m, 6H, -SiCH_2-), -0.10 (s, 3H, -SiCH_3). **^{29}Si-NMR** (CDCl$_3$, 80 MHz): δ / ppm = 2.82 (*Si*).

(7-Bromoheptyl)dinonylmethylsilane 6-3
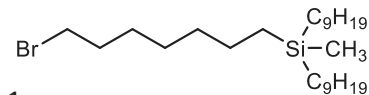
Synthesized according to GP2 from 1 (2.8 g, 9.42 mmol), 7-bromohept-1-ene (2.5 g, 2.2 mL, 14.1 mmol), Karstedt-Cat (0.38 mL) in anhydrous DCM (20 mL), purification by column chromatography (eluent: *n*-hexane); colorless liquid, yield: C$_{26}$H$_{55}$SiBr *M* = 475.72 g/mol, 2.99 g (67 %), **^{1}H-NMR** (CDCl$_3$, 400 MHz): δ / ppm = 3.40 (t, $^3J_{H,H}$ = 6.9 Hz, 2H, BrCH_2-), 1.91 – 1.80 (m, 2H, BrCH$_2$CH_2-), 1.46 – 1.36 (m, 2H, BrCH$_2$CH$_2$CH_2-), 1.36 – 1.19 (m, 34H, -CH_2-), 0.87 (t, $^3J_{H,H}$ = 7.1 Hz, 6H, -CH_3), 0.51 – 0.42 (m, 6H, -SiCH_2-), -0.09 (s, 3H, -SiCH_3) **^{29}Si-NMR** (CDCl$_3$, 79 MHz): δ / ppm = 2.79 (*Si*).

(4-Bromobutyl)didecylmethylsilane 6-4

Synthesized according to GP2 from 2 (3.1 g, 9.4 mmol), 4-bromobut-1-ene (2.0 g, 1.5 mL, 14.1 mmol), Karstedt-Cat (0.26 mL) in anhydrous DCM (20 mL), purification by column chromatography (eluent: n-hexane); colorless liquid, yield: $C_{25}H_{53}SiBr$ M = 461.68 g/mol, 1.95 g (45 %), **^{1}H-NMR** (CDCl$_3$, 500 MHz): δ / ppm = 3.43 (t, $^3J_{H,H}$ = 6.8 Hz, 2H), 1.93 – 1.83 (m, 2H), 1.49 – 1.37 (m, 2H), 1.36 – 1.20 (m, 12H), 0.89 (t, $^3J_{H,H}$ = 6.9 Hz, 6H), 0.54 – 0.46 (m, 6H), -0.05 (s, 3H). **^{29}Si-NMR** (CDCl$_3$, 99 MHz): δ / ppm = 3.01 (Si).

(5-Bromopentyl)didecylmethylsilane 6-5
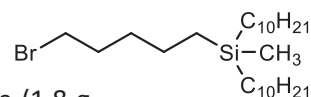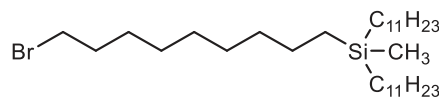
Synthesized according to GP2 from 2 (2.7 g, 8.1 mmol), 5-bromobut-1-ene (1.8 g, 1.4 mL, 12.2 mmol), Karstedt-Cat (0.32 mL) in anhydrous DCM (20 mL), purification by column chromatography (eluent: n-hexane); colorless liquid, yield: $C_{26}H_{55}SiBr$ M = 475.72 g/mol, 2.66 g (69 %), **^{1}H-NMR** (CDCl$_3$, 400 MHz): δ / ppm = 3.40 (t, $^3J_{H,H}$ = 6.9 Hz, 2H, BrCH_2-), 1.91 – 1.80 (m, 2H, BrCH$_2$CH_2-), 1.49 – 1.40 (m, 2H, BrCH$_2$CH$_2$CH_2-), 1.35 – 1.19 (m, 34H, -CH_2-), 0.88 (t, $^3J_{H,H}$ = 6.2 Hz, 6H, -CH_3), 0.52 – 0.42 (m, 6H, -SiCH_2-), -0.08 (s, 3H, -SiCH_3). **^{29}Si-NMR** (CDCl$_3$, 79 MHz): δ / ppm = 2.83 (Si).

(6-Bromohexyl)didecylmethylsilane 6-6
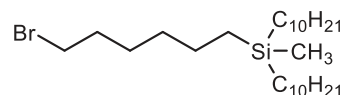
Synthesized according to GP2 from 2 (2.7 g, 8.1 mmol), 6-bromohex-1-ene (2.0 g, 1.6 mL, 12.1 mmol), Karstedt-Cat (0.32 mL) in anhydrous DCM (20 mL), purification by column chromatography (eluent: n-hexane); colorless liquid, yield: $C_{27}H_{57}SiBr$ M = 489.74 g/mol, 2.93 g (74 %), **^{1}H-NMR** (CDCl$_3$, 400 MHz): δ / ppm = 3.40 (t, $^3J_{H,H}$ = 6.9 Hz, 2H, BrCH_2-), 1.90 – 1.80 (m, 2H, BrCH$_2$CH_2-), 1.47 – 1.39 (m, 2H, BrCH$_2$CH$_2$CH_2-), 1.35 – 1.20 (m, 36H, -CH_2-), 0.89 (t, $^3J_{H,H}$ = 6.8 Hz, 6H, -CH_3), 0.52 – 0.42 (m, 6H, -SiCH_2-), -0.09 (s, 3H, -SiCH_3) **^{29}Si-NMR** (CDCl$_3$, 79 MHz): δ / ppm = 2.80 (Si).

(7-Bromoheptyl)didecylmethylsilane 6-7
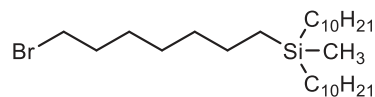
Synthesized according to GP2 from 2 (2.7 g, 8.1 mmol), 7-bromohept-1-ene (2.2 g, 1.9 mL, 12.2 mmol), Karstedt-Cat (0.32 mL) in anhydrous DCM (20 mL), purification by column chromatography (eluent: n-hexane); colorless liquid, yield: $C_{28}H_{59}SiBr$; M = 503.77 g/mol, 2.15 g (53 %), **^{1}H-NMR** (CDCl$_3$, 400 MHz): δ / ppm = 3.40 (t, $^3J_{H,H}$ = 6.9 Hz, 2H, BrCH_2-), 1.90 – 1.79 (m, 2H, BrCH$_2$CH_2-), 1.46 – 1.37 (m, 2H, BrCH$_2$CH$_2$CH_2-), 1.35 – 1.21 (m, 38H, -CH_2-), 0.88 (t, $^3J_{H,H}$ = 6.7 Hz, 6H, -CH_3), 0.50 – 0.43 (m, 6H, -SiCH_2-), -0.09 (s, 3H, -SiCH_3). **^{29}Si-NMR** (CDCl$_3$, 79 MHz): δ / ppm = 2.79 (Si).

(9-Bromononyl)diundecylmethylsilane 6-8

Synthesized according to GP2 from 3 (3.0 g, 8.1 mmol), 9-bromonon-1-ene (2.5 g, 2.3 mL, 12.2 mmol), Karstedt-Cat (0.49 mL) in anhydrous DCM (20 mL), purification by column chromatography (eluent: n-hexane); colorless liquid, yield: $C_{32}H_{67}SiBr$; M = 559.88 g/mol, 2.07 g (46 %), **^{1}H-NMR** (CDCl$_3$, 500 MHz): δ / ppm = 3.41 (t, $^3J_{H,H}$ = 6.9 Hz, 2H, BrCH_2-), 1.89 – 1.83 (m, 2H, BrCH$_2$CH_2-), 1.47 – 1.38 (m, 2H, BrCH$_2$CH$_2$CH_2-), 1.35 – 1.22 (m, 46H, -CH_2-), 0.89 (t, $^3J_{H,H}$ = 6.9 Hz, 6H, -CH_3), 0.51 – 0.45 (m, 6H, -SiCH_2-), -0.08 (s, 3H, -SiCH_3). **^{29}Si-NMR** (CDCl$_3$, 99 MHz): δ / ppm = 2.79 (Si).

(11-Bromoundecyl)diundecylmethylsilane 6-9
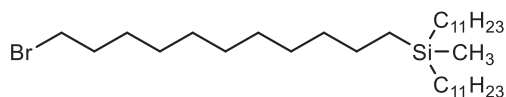
Synthesized according to GP2 from 3 (2.4 g, 6.8 mmol),
11-bromoundec-1-ene (2.4 g, 2.2 mL, 11.2 mmol), Karstedt-Cat (0.18 mL) in anhydrous DCM (20 mL),
purification by column chromatography (eluent: *n*-hexane); colorless liquid, yield: $C_{34}H_{71}SiBr$; M =
587.93 g/mol, 1.70 g (43 %), **^{1}H-NMR** (CDCl$_3$, 400 MHz): δ / ppm = 3.40 (t, $^3J_{H,H}$ = 6.9 Hz, 2H, Br*CH$_2$*-),
1.91 – 1.80 (m, 2H, BrCH$_2$*CH$_2$*-), 1.48 – 1.35 (m, 2H, BrCH$_2$CH$_2$*CH$_2$*-), 1.36 – 1.18 (m, 50H, -*CH$_2$*-), 0.88 (t,
$^3J_{H,H}$ = 6.8 Hz, 6H, -*CH$_3$*), 0.53 – 0.41 (m, 6H, -Si*CH$_2$*-), -0.09 (s, 3H, -Si*CH$_3$*). **^{29}Si-NMR** (CDCl$_3$, 79 MHz): δ
/ ppm = 2.79 (*Si*).

### (4-Bromobutyl)didodecylmethylsilane 6-10
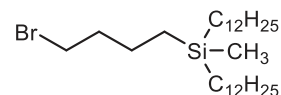
Synthesized according to GP2 from 4 (4.0 g, 10.5 mmol), 5-bromobut-1-ene
(2.1 g, 1.6 mL, 15.7 mmol), Karstedt-Cat (0.28 mL) in anhydrous DCM (20 mL), purification by column
chromatography (eluent: *n*-hexane); colorless liquid, yield: $C_{29}H_{61}SiBr$ M = 517.80 g/mol, 4.48 g (83 %),
^{1}H-NMR (CDCl$_3$, 400 MHz): δ / ppm = 3.42 (t, $^3J_{H,H}$ = 6.8 Hz, 2H, Br*CH$_2$*-), 1.92 – 1.80 (m, 2H, BrCH$_2$*CH$_2$*-
), 1.50 – 1.37 (m, 2H, BrCH$_2$CH$_2$*CH$_2$*), 1.36 – 1.19 (m, 40H, -*CH$_2$*-), 0.88 (t, $^3J_{H,H}$ = 6.8 Hz, 6H, -*CH$_3$*), 0.54 –
0.42 (m, 6H, -Si*CH$_2$*-), -0.09 (s, 3H, -Si*CH$_3$*). **^{29}Si-NMR** (CDCl$_3$, 79 MHz): δ / ppm = 2.80 (*Si*).

### (6-Bromohexyl)didodecylmethylsilane 6-11
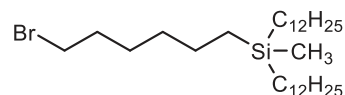
Synthesized according to GP2 from 4 (3.0g, 7.8mmol), 6-bromohex-1-
ene (1.9 g, 1.6 mL, 11.8 mmol), Karstedt-Cat (0.21 mL) in anhydrous DCM (20 mL), purification by
column chromatography (eluent: *n*-hexane); colorless liquid, yield: $C_{31}H_{65}SiBr$ M = 545.85 g/mol, 3.07
g (71 %), **^{1}H-NMR** (CDCl$_3$, 500 MHz): δ / ppm = 3.41 (t, $^3J_{H,H}$ = 6.9 Hz, 2H, Br*CH$_2$*-), 1.90 – 1.82 (m, 2H,
BrCH$_2$*CH$_2$*-), 1.47 – 1.40 (m, 2H, BrCH$_2$CH$_2$*CH$_2$*-), 1.37 – 1.21 (m, 44H, -*CH$_2$*-), 0.89 (t, $^3J_{H,H}$ = 6.8 Hz, 6H, -
CH$_3$), 0.51 – 0.46 (m, 6H, -Si*CH$_2$*-), -0.08 (s, 3H, -Si*CH$_3$*). **^{29}Si-NMR** (CDCl$_3$, 99 MHz): δ / ppm = 2.81 (*Si*).

### (4-Bromobutyl)ditetradecylmethylsilane 6-12
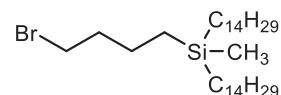
Synthesized according to GP2 from 5 (4.0 g, 9.1 mmol), 4-bromobut-1-ene
(1.9 g, 1.4 mL, 13.7 mmol), Karstedt-Cat (0.24 mL) in anhydrous DCM (20 mL), purification by column
chromatography (eluent: *n*-hexane); colorless liquid, yield: $C_{33}H_{69}SiBr$ M = 573.90 g/mol, 2.40 g (46 %),
^{1}H-NMR (CDCl$_3$, 400 MHz): δ / ppm = 3.42 (t, $^3J_{H,H}$ = 6.8 Hz, 2H, Br*CH$_2$*-), 1.91 – 1.81 (m, 2H, BrCH$_2$*CH$_2$*-
), 1.49 – 1.37 (m, 2H, BrCH$_2$CH$_2$*CH$_2$*-), 1.35 – 1.19 (m, 48H, -*CH$_2$*-), 0.87 (t, $^3J_{H,H}$ = 6.5 Hz, 6H, -*CH$_3$*), 0.55
– 0.42 (m, 6H, -Si*CH$_2$*-), -0.06 (s, 3H, -Si*CH$_3$*). **^{29}Si-NMR** (CDCl$_3$, 79 MHz): δ / ppm = 3.00 (*Si*).

(9-Bromononyl)tripentylsilane 6-13
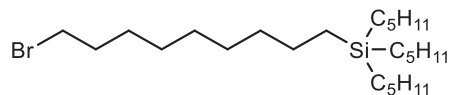
Synthesized according to GP2 from 6 (2.0 g, 8.1 mmol),
9-bromonon-1-ene (2.5 g, 2.3 mL, 12.2 mmol), Karstedt-Cat (0.33 mL) in anhydrous DCM (20 mL),
purification by column chromatography (eluent: *n*-hexane); colorless liquid, yield: $C_{24}H_{51}SiBr$ M =
447.66 g/mol, 1.32 g (36 %), **^{1}H-NMR** (CDCl$_3$, 400 MHz): δ / ppm = 3.40 (t, $^3J_{H,H}$ = 6.9 Hz, 2H, Br*CH$_2$*-),
1.92 – 1.79 (m, 2H, BrCH$_2$*CH$_2$*-), 1.46 – 1.37 (m, 2H, BrCH$_2$CH$_2$*CH$_2$*-), 1.37 – 1.20 (m, 28H, -*CH$_2$*-), 0.90 (t,
$^3J_{H,H}$ = 6.6 Hz, 9H, -*CH$_3$*), 0.55 – 0.41 (m, 8H, -Si*CH$_2$*-). **^{29}Si-NMR** (CDCl$_3$, 79 MHz): δ / ppm = 2.93 (*Si*).

(8-Bromooctyl)trihexylsilane 6-14
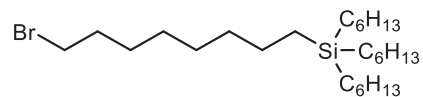
Synthesized according to GP2 from trihexylsilane (2.5 g, 8.7 mmol), 8-bromooct-1-ene (2.5 g, 2.2 mL, 13.1 mmol), Karstedt-Cat (0.35 mL) in anhydrous DCM (20 mL), purification by column chromatography (eluent: *n*-hexane); colorless liquid, yield: $C_{24}H_{55}SiBr$ M = 475.72 g/mol, 2.28 g (55 %), **^{1}H-NMR** (CDCl$_3$, 400 MHz): δ / ppm = 3.40 (t, $^3J_{H,H}$ = 6.9 Hz, 2H, BrC*H$_2$*-), 1.91 − 1.80 (m, 2H, BrCH$_2$C*H$_2$*-), 1.48 − 1.38 (m, 2H, BrCH$_2$CH$_2$C*H$_2$*-), 1.38 − 1.20 (m, 32H, -C*H$_2$*-), 0.89 (t, $^3J_{H,H}$ = 6.7 Hz, 9H, -C*H$_3$*), 0.56 − 0.43 (m, 8H, -SiC*H$_2$*-). **^{29}Si-NMR** (CDCl$_3$, 79 MHz): δ / ppm = 2.89 (*Si*).

(5-Bromopentyl)trioctylsilane 6-15
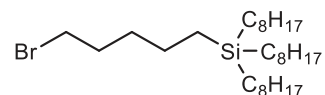
Synthesized according to GP2 from trioctylsilane (4.1 g, 11.2 mmol), 5-bromopent-1-ene (2.5 g, 1.99 mL, 16.8 mmol), Karstedt-Cat (0.45 mL) in anhydrous DCM (20 mL), purification by column chromatography (eluent: *n*-hexane); colorless liquid, yield: $C_{29}H_{61}SiBr$ M = 517.80 g/mol, 1.64 g (28 %), **^{1}H-NMR** (CDCl$_3$, 400 MHz): δ / ppm = 3.39 (t, $^3J_{H,H}$ = 6.9 Hz, 2H, BrC*H$_2$*-), 1.91 − 1.81 (m, 2H, BrCH$_2$C*H$_2$*-), 1.49 − 1.39 (m, 2H, BrCH$_2$CH$_2$C*H$_2$*-), 1.36 − 1.20 (m, 38H, -C*H$_2$*-), 0.88 (t, $^3J_{H,H}$ = 7.0 Hz, 9H, -C*H$_3$*), 0.61 − 0.43 (m, 8H, -SiC*H$_2$*-). **^{29}Si-NMR** (CDCl$_3$, 79 MHz): δ / ppm = 2.94 (*Si*).

2-Diethyl(2-tetradecylhexadecyl)malonate 1

NaH (1 or 2.5 eq., 60% in paraffin) is added to a DMF/THF mixture ((1:4), 20 mL / 10 mmol NaH) and degassed with argon for 30 minutes. Then, add diethylmalonate (1 equivalent) slowly to the reaction at 0°C and stir until no gas is observed. Afterward, slowly add the appropriate 15-(bromomethyl)nonacosane (1 eq, 12.3 g, 24.4 mmol), dissolved in a 20 mL DMF/THF mixture. Stir the reaction at 80°C for 8 hours, followed by an expansion of the volume with water addition. Extract the resulting solution with Et$_2$O (3 x 75 ml). The organic layers will be combined, washed with water and brine, and dried using MgSO$_4$. The solvent will be evaporated under reduced pressure (850 mbar), and the resulting crude product will be purified through column chromatography (eluent: 1. *n*-hexane, 2. CHCl$_3$). Yield: $C_{37}H_{72}O_4$ M = 580.98 g/mol, 8.92 g (63%), colorless liquid, **^{1}H-NMR** (CDCl$_3$, 500 MHz): δ / ppm = 4.24 − 4.16 (m, 4H, -OC*H$_2$*-), 3.41 (t, $^3J_{H,H}$ = 7.4 Hz, 1H, -C*H$_α$*-), 1.86 − 1.81 (m, 2H, -CH$_α$-C*H$_2$*-), 1.68 − 1.60 (m, 1H, -C*H*-), 1.33 − 1.19 (m, 58H, -C*H$_2$*-, -CH$_3$), 0.88 (t, $^3J_{H,H}$ = 6.9 Hz, 6H, -CH$_3$).
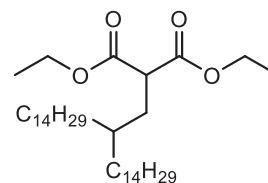
Ethyl 4-tetradecyloctadecanoate 2

1 (1 eq., 8.92g, 15.4 mmol), lithium chloride (2 eq., 1.3 g, 30.7 mmol), and water (1 eq., 0.4 mL, 20 mmol) are added to DMSO (40 mL / 10 mmol malonester). The reaction is stirred under reflux for 1 day. Afterward, the reaction is cooled to room temperature and diluted with water to twice the volume. The mixture undergoes extraction with Et$_2$O (3 x 75 mL), and the combined organic layers are washed with water and brine and dried over MgSO$_4$. The solvent will be evaporated at reduced pressure (850 mbar), and the resulting crude product will be purified through column chromatography (eluent: *n*-hexane: CHCl$_3$, 1:1). Yield: $C_{34}H_{68}O_4$ M = 508.92 g/mol, 6.76 g (84%), colorless liquid, **^{1}H-NMR** (CDCl$_3$, 400 MHz): δ / ppm = 4.11 (q, $^3J_{H,H}$ = 7.1 Hz, 2H, -OC*H$_2$*-), 2.28 − 2.23 (m, 2H, COO-C*H$_2$*-), 1.65 − 1.53 (m, 3H, -C*H$_2$*-, -C*H*-), 1.25 (s, 55H,-C*H$_2$*-, -CH$_3$), 0.87 (t, $^3J_{H,H}$ = 6.8 Hz, 6H, -CH$_3$).
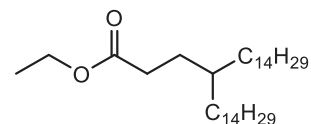
4-Tetradecyloctadecan-1-ol 3
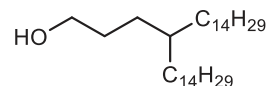
LiAlH$_4$ (1.5 eq., 0.8 g, 19.9 mmol) is suspended in anhydrous Et$_2$O (75 mL), then **2** solved in anhydrous Et$_2$O (75 mL) is added through a dropping funnel. The resulting suspension is stirred under reflux for 6 hours. Once the reaction is complete, any remaining LiAlH$_4$ is carefully hydrolyzed, and the residue is dissolved by the addition of diluted sulfuric acid (50%). The mixture is then extracted with Et$_2$O (3 x 75 mL). The combined organic layers are washed with a saturated solution of Na$_2$S$_2$O$_3$ until no precipitation is observed. After the solvent has been distilled under reduced pressure (850 mbar), the crude product is purified by column chromatography (eluent: CHCl$_3$). Yield: C$_{32}$H$_{66}$O$_4$ M = 466.88 g/mol, 5.86 g (94%), white solid, mp = 53 °C, **^{1}H-NMR** (CDCl$_3$, 400 MHz): δ / ppm = 3.62 (t, $^3J_{H,H}$ = 6.7 Hz, 2H, HOCH_2-), 1.58 – 1.49 (m, 2H, HOCH$_2$CH_2-), 1.46 – 1.40 (m, 1H, -CH-), 1.25 (s, 54H,-CH_2-), 0.87 (t, $^3J_{H,H}$ = 7.0 Hz, 6H, -CH$_3$).

15-(3-Bromopropyl)nonacosane 4
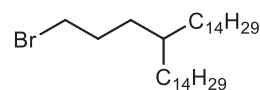
DDQ (1.2 eq., 3.4 g, 15.1 mmol) and PPh$_3$ (1.2 eq., 4.0 g, 15.1 mmol) were placed in a two-neck flask and degassed with argon for 5 minutes. Anhydrous DCM (25 mL) was slowly added to the materials until a yellow suspension was formed. TBAI (1.2 eq., 5.0 g, 15.1 mmol), dissolved in anhydrous DCM (25 mL), was then added to the suspension, followed by **3** (1 eq., 5.9 g, 12.6 mmol), also dissolved in anhydrous DCM (25 mL). The reaction was stirred for 24 hours at room temperature, filtered over silica gel through vacuum filtration, and then the solvent was distilled off under reduced pressure (850 mbar). The filter cake is rinsed three times with hot *n*-hexane (3 x 100 mL), added to the dried residue, and the solvent is evaporated under reduced pressure (335 mbar). The crude product is purified by column chromatography (eluent: *n*-hexane). Yield: C$_{32}$H$_{65}$Br M = 529.78 g/mol, 5.16 g (78 %), white solid, mp = 37 °C, **^{1}H-NMR** (CDCl$_3$, 400 MHz): δ / ppm = 3.38 (t, $^3J_{H,H}$ = 6.9 Hz, 2H, BrCH_2-), 1.88 – 1.77 (m, 2H, BrCH$_2$CH_2-), 1.42 – 1.17 (m, 55H,-CH_2-,-CH-), 0.88 (t, $^3J_{H,H}$ = 6.8 Hz, 6H, -CH$_3$).

1,4-Bis[3-(methyldiundecylsilyl)propyloxy]benzene 10-1
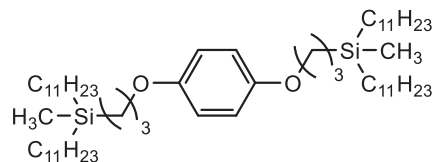
Synthesized according to GP2 from 1,4-bis(allyloxy)benzene (0.5 g, 2.6 mmol), diundecylmethylsilane (2.8 g, 5.8 mmol), Karstedt-Cat (0.07 mL) in anhydrous DCM (20 mL), purification column chromatography (eluent: *n*-hexane); colorless liquid, yield: C$_{58}$H$_{114}$O$_2$Si M = 899.72 g/mol, 1.28 g (54 %), **^{1}H-NMR** (CDCl$_3$, 502 MHz): δ / ppm = 6.81 (s, 4H, Aryl-H), 3.85 (t, $^3J_{H,H}$ = 6.9 Hz, 4H, -OCH_2-), 1.79 – 1.69 (m, 4H, -OCH$_2$CH_2-), 1.35 – 1.20 (m, 72H, -CH_2-), 0.89 (t, $^3J_{H,H}$ = 6.9 Hz, 12H, -CH_3), 0.62 – 0.55 (m, 4H, -SiCH_2-), 0.55 – 0.48 (m, 8H, -SiCH_2-), -0.04 (s, 6H, -SiCH_3). **^{29}Si-NMR** (CDCl$_3$, 100 MHz): δ / ppm = 3.42 (*Si*).

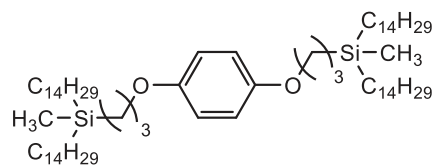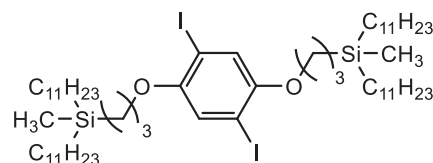### 1,4-Bis{3-[didodecyl(methyl)silyl]propyloxy}benzene 10-2
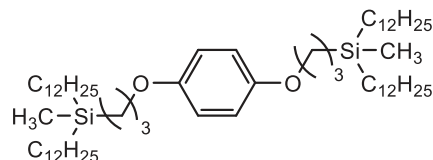
Synthesized according to GP2 from 1,4-bis(allyloxy)benzene (0.5 g, 2.6 mmol), didodecylmethylsilane (2.2 g, 5.8 mmol), Karstedt-Cat (0.07 mL) in anhydrous DCM (20 mL), purification by column chromatography (eluent: *n*-hexane); colorless liquid, yield: C$_{62}$H$_{122}$O$_2$Si M = 955.83 g/mol, 1.74 g (69 %), **^{1}H-NMR** (CDCl$_3$, 400 MHz): δ / ppm = 6.81 (s, 4H, Aryl-H), 3.85 (t, $^3J_{H,H}$ = 7.0 Hz, 4H, -OCH_2-), 1.79 – 1.69 (m, 4H, -OCH$_2$CH_2-), 1.33 – 1.21 (m, 80H, -CH_2-), 0.88 (t, $^3J_{H,H}$ = 7.1 Hz, 12H, -CH_3), 0.62 – 0.55 (m, 4H, -SiCH_2-), 0.54 – 0.47 (m, 8H, -SiCH_2-), -0.05 (s, 6H, -SiCH_3). **^{29}Si-NMR** (CDCl$_3$, 79 MHz): δ / ppm = 3.41 (*Si*).

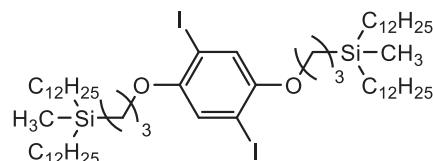### 1,4-Bis[3-(methylditetradecylsilyl)propyloxy]benzene 10-3

Synthesized according to GP2 from 1,4-bis(allyloxy)benzene (0.5 g, 2.6 mmol), ditetradecylmethylsilane (2.5 g, 5.8 mmol), Karstedt-Cat (0.04 mL) in anhydrous DCM (20 mL), purification by column chromatography (eluent: *n*-hexane); colorless liquid yield: $C_{70}H_{138}O_2Si$ M = 1068.04 g/mol, 1.14 g (41 %), **^{1}H-NMR** (CDCl$_3$, 400 MHz): δ / ppm = 6.81 (s, 4H, Aryl-*H*), 3.85 (t, $^3J_{H,H}$ = 6.9 Hz, 4H, -OC*H$_2$*-), 1.79 – 1.69 (m, 4H, -OCH$_2$C*H$_2$*-), 1.34 – 1.21 (m, 96H, -C*H$_2$*-), 0.88 (t, $^3J_{H,H}$ = 6.8 Hz, 12H, -C*H$_3$*), 0.62 – 0.55 (m, 4H, -SiC*H$_2$*-), 0.54 – 0.47 (m, 8H, -SiC*H$_2$*-), -0.05 (s, 6H, -SiC*H$_3$*). **^{29}Si-NMR** (CDCl$_3$, 79 MHz): δ / ppm = 3.42 (*Si*).

1,4-Bis[3-(methyldiundecylsilyl)propyloxy]-2,5-diiodobenzene 11C-1

Synthesized according to GP7 from **10-1** (1.3 g, 1.4 mmol), I$_2$ (0.5 g, 2.1 mmol), PhI(OCOCF$_3$)$_2$ (0.9 g, 2.1 mmol) in anhydrous DCM (50 mL), purification by column chromatography (eluent: *n*-hexane); colorless liquid, yield: $C_{58}H_{112}I_2O_2Si$ M = 1151.51 g/mol, 1.06 g (65 %), **^{1}H-NMR** (CDCl$_3$, 502 MHz): δ / ppm = 7.16 (s, 2H, Aryl-*H*), 3.88 (t, $^3J_{H,H}$ = 6.6 Hz, 4H, -OC*H$_2$*-), 1.83 – 1.71 (m, 4H, -OCH$_2$C*H$_2$*-), 1.35 – 1.21 (m, 72H, -C*H$_2$*-), 0.88 (t, $^3J_{H,H}$ = 6.9 Hz, 12H, -OC*H$_3$*), 0.69 – 0.62 (m, 4H, -SiC*H$_2$*-), 0.56 – 0.47 (m, 8H, -SiC*H$_2$*-), -0.03 (s, 6H, -SiC*H$_3$*). **^{29}Si-NMR** (CDCl$_3$, 100 MHz): δ / ppm = 3.44 (*Si*).

1,4-Bis{3-[didodecyl(methyl)silyl]propyloxy}-2,5-diiodobenzene 11C-2
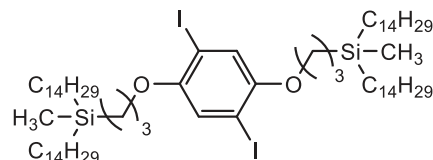
Synthesized according to GP7 from **10-2** (1.7 g, 1.8 mmol), I$_2$ (0.5 g, 2.0 mmol), PhI(OCOCF$_3$)$_2$ (0.9 g, 2.0 mmol) in anhydrous DCM (50 mL), purification by column chromatography (eluent: *n*-hexane); colorless liquid, yield: $C_{62}H_{120}I_2O_2Si$ M = 1207.62 g/mol, 0.67 g (31 %), **^{1}H-NMR** (CDCl$_3$, 400 MHz): δ / ppm = 7.16 (s, 2H, Aryl-*H*), 3.88 (t, $^3J_{H,H}$ = 6.6 Hz, 4H, -OC*H$_2$*-), 1.83 – 1.72 (m, 4H, -OCH$_2$C*H$_2$*-), 1.35 – 1.22 (m, 80H, -C*H$_2$*-), 0.88 (t, $^3J_{H,H}$ = 6.9 Hz, 12H, -C*H$_3$*), 0.67 – 0.62 (m, 4H, -SiC*H$_2$*-), 0.55 – 0.48 (m, 8H, -SiC*H$_2$*-), -0.03 (s, 6H, -SiC*H$_3$*). **^{29}Si-NMR** (CDCl$_3$, 79 MHz): δ / ppm = 3.43 (*Si*).

1,4-bis[3-(methylditetradecylsilyl)propyloxy]-2,5-diiodobenzene 11C-3

Synthesized according to GP7 from **10-3** (1.4 g, 1.1 mmol), I$_2$ (0.3 g, 1.2 mmol), PhI(OCOCF$_3$)$_2$ (0.5 g, 1.2 mmol) in anhydrous DCM (50 mL), purification by column chromatography (eluent: *n*-hexane); colorless liquid, yield: $C_{70}H_{136}I_2O_2Si$ M = 1319.84 g/mol, 360 mg (26 %), **^{1}H-NMR** (CDCl$_3$, 400 MHz): δ / ppm = 7.18 (s, 2H, Aryl-*H*), 3.89 (t, $^3J_{H,H}$ = 6.5 Hz, 4H, -OC*H$_2$*-), 1.84 – 1.74 (m, 4H, -OCH$_2$C*H$_2$*-), 1.38 – 1.20 (m, 96H, -C*H$_2$*-), 0.90 (t, $^3J_{H,H}$ = 7.1 Hz, 12H, -C*H$_3$*), 0.70 – 0.62 (m, 4H, -SiC*H$_2$*-), 0.58 – 0.49 (m, 8H, -SiC*H$_2$*-), -0.01 (s, 6H, -SiC*H$_3$*). **^{29}Si-NMR** (CDCl$_3$, 79 MHz): δ / ppm = 3.45 (*Si*).
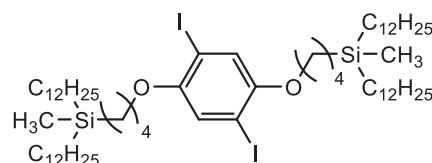
1,4-Bis[4-(methyldidecylylsilyl)butyloxy]-2,5-diiodobenzene 8C4/10

Synthesized according to GP4 from **6-4** (1.3 g, 2.8 mmol), 2,5-Diiodohydrochinone (0.5 g, 1.3 mmol), K_2CO_3 (1.8 g, 13.2 mmol), TBAI (0.9 mg, 2.5 mmol) in anhydrous DMF (20 mL), purification by column chromatography (eluent: *n*-hexane); colorless liquid, yield: $C_{56}H_{108}I_2O_2Si$ *M* = 1123.46 g/mol, 1.10 g (74 %), **¹H-NMR** (CDCl₃, 402 MHz): δ / ppm = 7.16 (s, 2H, Aryl-*H*), 3.92 (t, $^3J_{H,H}$ = 6.2 Hz, 4H, -OC*H₂*-), 1.85 – 1.73 (m, 4H, -OCH₂C*H₂*-), 1.56 – 1.44 (m, 4H, -OCH₂CH₂C*H₂*-), 1.34 – 1.19 (m, 64H, -C*H₂*-), 0.86 (t, $^3J_{H,H}$ = 6.8 Hz, 12H, -C*H₃*), 0.56 – 0.45 (m, 12H, -SiC*H₂*-), -0.07 (s, 6H, -SiC*H₃*). **²⁹Si-NMR** (CDCl₃, 80 MHz): δ / ppm = 2.95 (*Si*).
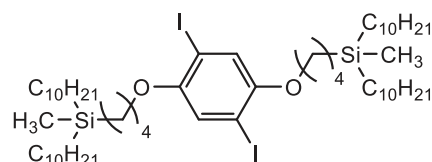
1,4-Bis[4-(methyldidodecylylsilyl)butyloxy]-2,5-diiodobenzene 8C4/12

Synthesized according to GP4 from **6-10** (1.6 g, 3.0 mmol), 2,5-Diiodohydrochinone (0.5 g, 1.4 mmol), K_2CO_3 (1.9 g, 13.8 mmol), TBAI (1.0 mg, 2.7 mmol) in anhydrous DMF (20 mL), purification by column chromatography (eluent: *n*-hexane); colorless liquid, yield: $C_{64}H_{124}I_2O_2Si$ *M* = 1235.67 g/mol, 0.52 g (30 %), **¹H-NMR** (CDCl₃, 400 MHz): δ / ppm = 7.17 (s, 2H, Aryl-*H*), 3.93 (t, $^3J_{H,H}$ = 6.2 Hz, 4H, -OC*H₂*-), 1.86 – 1.75 (m, 4H, -OCH₂C*H₂*-), 1.58 – 1.46 (m, 4H, -OCH₂CH₂C*H₂*-), 1.36 – 1.19 (m, 80H, -C*H₂*-), 0.88 (t, $^3J_{H,H}$ = 6.8 Hz, 12H, -C*H₃*), 0.59 – 0.45 (m, 12H, -SiC*H₂*-), -0.06 (s, 6H, -SiC*H₃*). **²⁹Si-NMR** (CDCl₃, 79 MHz): δ / ppm = 2.97 (*Si*).

1,4-Bis[4-(methylditetradecylsilyl)butyloxy]-2,5-diiodobenzene 8C4/14

Synthesized according to GP4 from **6-12** (1.7 g, 3.0 mmol), 2,5-Diiodohydrochinone (0.5 g, 1.4 mmol), K_2CO_3 (1.9 g, 13.8 mmol), TBAI (1.0 mg, 2.7 mmol) in anhydrous DMF (20 mL), purification by column chromatography (eluent: *n*-hexane); colorless liquid, yield: $C_{72}H_{140}I_2O_2Si$ *M* = 1347.89 g/mol, 1.40 g (75 %), **¹H-NMR** (CDCl₃, 400 MHz): δ / ppm = 7.17 (s, 2H, Aryl-*H*), 3.94 (t, $^3J_{H,H}$ = 6.2 Hz, 4H, -OC*H₂*-), 1.86 – 1.75 (m, 4H, -OCH₂C*H₂*-), 1.61 – 1.47 (m, 4H, -OCH₂CH₂C*H₂*-), 1.36 – 1.20 (m, 96H, -C*H₂*-), 0.88 (t, $^3J_{H,H}$ = 6.7 Hz, 12H, -C*H₃*), 0.59 – 0.45 (m, 12H, -SiC*H₂*-), -0.06 (s, 6H, -SiC*H₃*). **²⁹Si-NMR** (CDCl₃, 79 MHz): δ / ppm = 2.97 (*Si*).
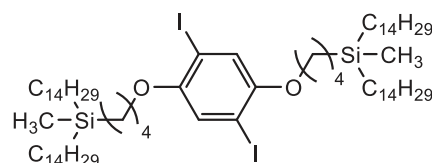
1,4-Bis[5-(methyldinonylsilyl)pentyloxy]-2,5-diiodobenzene 8C5/9

Synthesized according to GP4 from **6-2** (1.9 g, 4.3 mmol), 2,5-Diiodohydrochinone (0.5 g, 1.9 mmol), K_2CO_3 (2.7 g, 19.3 mmol), TBAI (1.4 mg, 3.9 mmol) in anhydrous DMF (20 mL), purification by column chromatography (eluent: *n*-hexane); colorless liquid, yield: $C_{54}H_{104}I_2O_2Si$ *M* = 1095.40 g/mol, 1.67 g (79 %), **¹H-NMR** (CDCl₃, 502 MHz): δ / ppm = 7.17 (s, 2H, Aryl-*H*), 3.92 (t, $^3J_{H,H}$ = 6.5 Hz, 4H, -OC*H₂*-), 1.85 – 1.75 (m, 4H, -OCH₂C*H₂*-), 1.57 – 1.46 (m, 4H, -OCH₂CH₂C*H₂*-), 1.40 – 1.21 (m, 60H, -C*H₂*-), 0.88 (t, $^3J_{H,H}$ = 6.7 Hz, 12H, -C*H₃*), 0.57 – 0.45 (m, 12H, -SiC*H₂*-), -0.07 (s, 6H, -SiC*H₃*). **²⁹Si-NMR** (CDCl₃, 100 MHz): δ / ppm = 2.84 (*Si*).
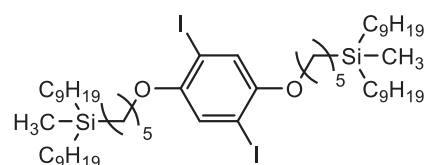
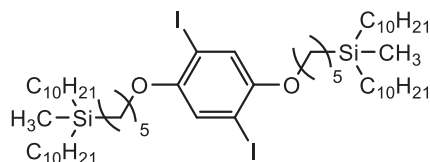### 1,4-Bis[5-(methyldidecylsilyl)pentyloxy]-2,5-diiodobenzene 8C5/10

Synthesized according to GP4 from **6-5** (2.0 g, 4.2 mmol), 2,5-Diiodohydrochinone (0.7 g, 1.9 mmol), K_2CO_3 (2.6 g, 1.9 mmol), TBAI (1.4 mg, 3.5 mmol) in anhydrous DMF (20 mL), purification by column chromatography (eluent: *n*-hexane); colorless liquid, yield: $C_{58}H_{112}I_2O_2Si$ *M* = 1151.51 g/mol, 1.82 g (83 %), **^{1}H-NMR** (CDCl$_3$, 400 MHz): δ / ppm = 7.17 (s, 2H, Aryl-*H*), 3.91 (t, $^3J_{H,H}$ = 6.4 Hz, 4H, -OC*H$_2$*-), 1.84 – 1.75 (m, 4H, -OCH$_2$C*H$_2$*-), 1.53 – 1.46 (m, 4H, -OCH$_2$CH$_2$C*H$_2$*-), 1.40 – 1.19 (m, 68H, -C*H$_2$*-), 0.88 (t, $^3J_{H,H}$ = 7.1 Hz, 12H, -C*H$_3$*), 0.55 – 0.43 (m, 12H, -SiC*H$_2$*-), -0.08 (s, 6H, -SiC*H$_3$*). **^{29}Si-NMR** (CDCl$_3$, 79 MHz): δ / ppm = 2.84 (*Si*).

1,4-Bis[6-(methyldidecylsilyl)hexyloxy]-2,5-diiodobenzene 8C6/10

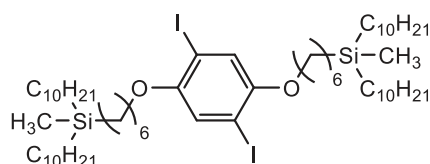Synthesized according to GP4 from **6-6** (2.0 g, 4.1 mmol), 2,5-Diiodohydrochinone (0.7 g, 1.9 mmol), K_2CO_3 (2.6 g, 18.6 mmol), TBAI (1.4 mg, 3.7 mmol) in anhydrous DMF (20 mL), purification by column chromatography (eluent: *n*-hexane); colorless liquid, yield: $C_{60}H_{116}I_2O_2Si$ *M* = 1179.57 g/mol, 1.54 g (70 %), **^{1}H-NMR** (CDCl$_3$, 400 MHz): δ / ppm = 7.17 (s, 2H, Aryl-*H*), 3.92 (t, $^3J_{H,H}$ = 6.4 Hz, 4H, -OC*H$_2$*-), 1.83 – 1.74 (m, 4H, -OCH$_2$C*H$_2$*-), 1.52 – 1.44 (m, 4H, -OCH$_2$CH$_2$C*H$_2$*-), 1.42 – 1.19 (m, 72H, -C*H$_2$*-), 0.88 (t, $^3J_{H,H}$ = 6.7 Hz, 12H, -C*H$_3$*), 0.53 – 0.43 (m, 12H, -SiC*H$_2$*-), -0.09 (s, 6H, -SiC*H$_3$*). **^{29}Si-NMR** (CDCl$_3$, 79 MHz): δ / ppm = 2.81 (*Si*).

1,4-Bis[6-(methyldidodecylsilyl)hexyloxy]-2,5-diiodobenzene 8C6/12

Synthesized according to GP4 from **6-11** (2.0 g, 3.7 mmol), 2,5-Diiodohydrochinone (0.6 g, 1.7 mmol), K_2CO_3 (2.3 g, 1.7 mmol), TBAI (1.2 mg, 3.3 mmol) in anhydrous DMF (20 mL), purification by column chromatography (eluent: *n*-hexane); colorless liquid, yield: $C_{68}H_{132}I_2O_2Si$ *M* = 1291.78 g/mol, 1.67 g (77 %), **^{1}H-NMR** (CDCl$_3$, 400 MHz): δ / ppm = 7.17 (s, 2H, Aryl-*H*), 3.92 (t, $^3J_{H,H}$ = 6.4 Hz, 4H, -OC*H$_2$*-), 1.82 – 1.74 (m, 4H, -OCH$_2$C*H$_2$*-), 1.55 – 1.45 (m, 4H, -OCH$_2$CH$_2$C*H$_2$*-), 1.42 – 1.20 (m, 88H, -C*H$_2$*-), 0.88 (t, $^3J_{H,H}$ = 6.8 Hz, 12H, -C*H$_3$*), 0.53 – 0.44 (m, 12H, -SiC*H$_2$*-), -0.08 (s, 6H, -SiC*H$_3$*). **^{29}Si-NMR** (CDCl$_3$, 79 MHz): δ / ppm = 2.81 (*Si*).

1,4-Bis[7-(methyldinonylsilyl)heptyloxy]-2,5-diiodobenzene 8C7/9

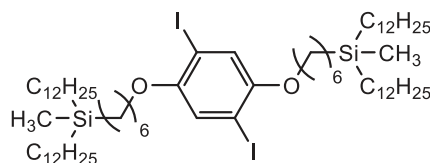Synthesized according to GP4 from **6-3** (2.0 g, 4.2 mmol), 2,5-Diiodohydrochinone (0.7 g, 1.9 mmol), K_2CO_3 (2.6 g, 19.1 mmol), TBAI (1.4 mg, 3.9 mmol) in anhydrous DMF (20 mL), purification by column chromatography (eluent: *n*-hexane); colorless liquid, yield: $C_{58}H_{112}I_2O_2Si$ *M* = 1151.51 g/mol, 1.66 g (76 %), **^{1}H-NMR** (CDCl$_3$, 400 MHz): δ / ppm = 7.17 (s, 2H, Aryl-*H*), 3.92 (t, $^3J_{H,H}$ = 6.4 Hz, 4H, -OC*H$_2$*-), 1.84 – 1.75 (m, 4H, -OCH$_2$C*H$_2$*-), 1.53 – 1.44 (m, 4H, -OCH$_2$CH$_2$C*H$_2$*-), 1.41 – 1.19 (m, 68H, -C*H$_2$*-), 0.88 (t, $^3J_{H,H}$ = 6.7 Hz, 12H, -C*H$_3$*), 0.52 – 0.43 (m, 12H, -SiC*H$_2$*-), -0.09 (s, 6H, -SiC*H$_3$*). **^{29}Si-NMR** (CDCl$_3$, 79 MHz): δ / ppm = 2.80 (*Si*).

1,4-Bis[7-(methyldidecylsilyl)heptyloxy]-2,5-diiodobenzene 8C7/10

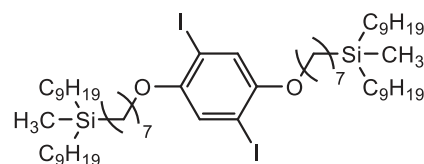Synthesized according to GP4 from **6-7** (2.0 g, 4.0 mmol), 2,5-Diiodohydrochinone (0.7 g, 1.8 mmol), K_2CO_3 (2.5 g, 18.0 mmol), TBAI (1.3 mg, 3.6 mmol) in anhydrous DMF (20 mL), purification by column chromatography (eluent: *n*-hexane); colorless liquid, yield: $C_{62}H_{120}I_2O_2Si$ M = 1207.62 g/mol, 1.67 g (77 %), **¹H-NMR** (CDCl₃, 400 MHz): δ / ppm = 7.17 (s, 2H, Aryl-*H*), 3.92 (t, $^3J_{H,H}$ = 6.4 Hz, 4H, -OC*H₂*-), 1.83 – 1.74 (m, 4H, -OCH₂C*H₂*-), 1.52 – 1.44 (m, 4H, -OCH₂CH₂C*H₂*-), 1.40 – 1.19 (m, 76H, -C*H₂*-), 0.87 (t, $^3J_{H,H}$ = 6.7 Hz, 12H, -C*H₃*), 0.51 – 0.43 (m, 12H, -SiC*H₂*-), -0.09 (s, 6H, -SiC*H₃*). **²⁹Si-NMR** (CDCl₃, 79 MHz): δ / ppm = 2.80 (*Si*).

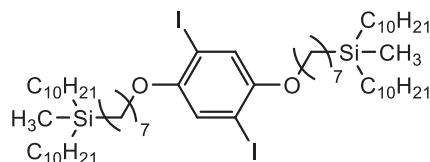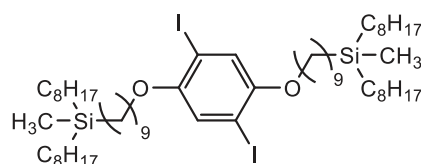## 1,4-Bis[9-(methyldioctylsilyl)nonyloxy]-2,5-diiodobenzene 8C9/8

Synthesized according to GP4 from 6-1 (2.0 g, 4.3 mmol), 2,5-Diiodohydrochinone (0.7 g, 1.9 mmol), K_2CO_3 (2.7 g, 19.3 mmol), TBAI (1.4 mg, 3.9 mmol) in anhydrous DMF (20 mL), purification by column chromatography (eluent: *n*-hexane); colorless liquid, yield: $C_{58}H_{112}I_2O_2Si$ M = 1151.51 g/mol, 1.09 g (49 %), **¹H-NMR** (CDCl₃, 502 MHz): δ / ppm = 7.17 (s, 2H, Aryl-*H*), 3.92 (t, $^3J_{H,H}$ = 6.4 Hz, 4H, -OC*H₂*-), 1.84 – 1.75 (m, 4H, -OCH₂C*H₂*-), 1.53 – 1.45 (m, 4H, -OCH₂CH₂C*H₂*-), 1.39 – 1.21 (m, 68H, -C*H₂*-), 0.86 (t, $^3J_{H,H}$ = 6.9 Hz, 12H, -C*H₃*), 0.50 – 0.44 (m, 12H, -SiC*H₂*-), -0.09 (s, 6H, -SiC*H₃*). **²⁹Si-NMR** (CDCl₃, 100 MHz): δ / ppm = 2.79 (*Si*).

1,4-Bis[9-(methyldiundecylsilyl)nonyloxy]-2,5-diiodobenzene 8C9/11

Synthesized according to GP4 from **6-8** (2.0 g, 3.6 mmol), 2,5-Diiodohydrochinone (0.6 g, 1.6 mmol), K_2CO_3 (2.2 g, 16.2 mmol), TBAI (1.2 mg, 3.2 mmol) in anhydrous DMF (20 mL), purification by column chromatography (eluent: *n*-hexane); colorless liquid, yield: $C_{70}H_{136}I_2O_2Si$ M = 1319.84 g/mol, 1.00 g (47 %), **¹H-NMR** (CDCl₃, 400 MHz): δ / ppm = 7.17 (s, 2H, Aryl-*H*), 3.92 (t, $^3J_{H,H}$ = 6.4 Hz, 4H, -OC*H₂*-), 1.83 – 1.75 (m, 4H, -OCH₂C*H₂*-), 1.52 – 1.44 (m, 4H, -OCH₂CH₂C*H₂*-), 1.40 – 1.19 (m, 92H, -C*H₂*-), 0.88 (t, $^3J_{H,H}$ = 6.2 Hz, 12H, -C*H₃*), 0.51 – 0.44 (m, 12H, -SiC*H₂*-), -0.09 (s, 6H, -SiC*H₃*). **²⁹Si-NMR** (CDCl₃, 79 MHz): δ / ppm = 2.79 (*Si*).
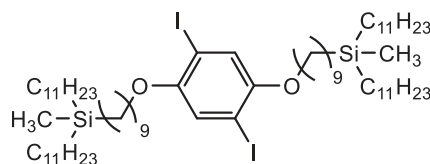
1,4-Bis[11-(methyldiundecylsilyl)undecyloxy]-2,5-diiodobenzene 8C11/11

Synthesized according to GP4 from **6-9** (0.9 g, 1.5 mmol), 2,5-Diiodohydrochinone (0.2 g, 0.7 mmol), K_2CO_3 (0.9 g, 6.6 mmol), TBAI (0.5 mg, 1.4 mmol) in anhydrous DMF (20 mL), purification by column chromatography (eluent: *n*-hexane); colorless liquid, yield: $C_{74}H_{144}I_2O_2Si$ M = 1375.94 g/mol, 0.53 g (58 %), **¹H-NMR** (CDCl₃, 400 MHz): δ / ppm = 7.17 (s, 2H, Aryl-*H*), 3.92 (t, $^3J_{H,H}$ = 6.4 Hz, 4H, -OC*H₂*-), 1.87 – 1.74 (m, 4H, -OCH₂C*H₂*-), 1.55 – 1.44 (m, 4H, -OCH₂CH₂C*H₂*-), 1.40 – 1.19 (m, 100H, -C*H₂*-), 0.88 (t, $^3J_{H,H}$ = 6.7 Hz, 12H, -C*H₃*), 0.53 – 0.41 (m, 12H, -SiC*H₂*-), -0.09 (s, 6H, -SiC*H₃*). **²⁹Si-NMR** (CDCl₃, 79 MHz): δ / ppm = 2.79 (*Si*).
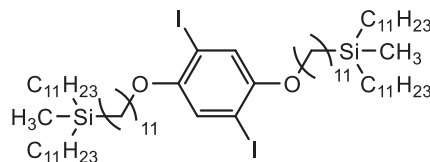
1,4-Bis[5-(trioctylsilyl)pentyloxy]-2,5-diiodobenzene 8B5/8

Synthesized according to GP4 from **6-15** (1.6 g, 3.2 mmol), 2,5-Diiodohydrochinone (0.5 g, 1.4 mmol), K_2CO_3 (2.0 g, 14.4 mmol), TBAI (1.1 mg, 2.7 mmol) in anhydrous DMF (20 mL), purification by column chromatography (eluent: *n*-hexane); colorless liquid, yield: $C_{64}H_{124}I_2O_2Si$ *M* = 1235.67 g/mol, 1.32 g (74 %), **¹H-NMR** (CDCl₃, 400 MHz): δ / ppm = 7.17 (s, 2H, Aryl-*H*), 3.91 (t, $^3J_{H,H}$ = 6.4 Hz, 4H, -OC*H₂*-), 1.85 − 1.74 (m, 4H, -OCH₂C*H₂*-), 1.56 − 1.47 (m, 4H, -OCH₂CH₂C*H₂*-), 1.40 − 1.19 (m, 76H, -C*H₂*-), 0.88 (t, $^3J_{H,H}$ = 6.8 Hz, 18H, -C*H₃*), 0.60 − 0.42 (m, 16H, -SiC*H₂*-). **²⁹Si-NMR** (CDCl₃, 79 MHz): δ / ppm = 2.94 (*Si*).
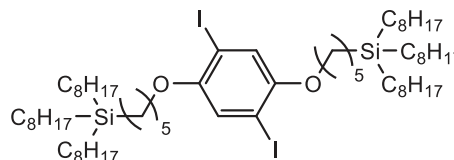
1,4-Bis[8-(trihexylsilyl)octyloxy]-2,5-diiodobenzene 8B8/6

Synthesized according to GP4 from **6-14** (2.0 g, 4.2 mmol), 2,5-Diiodohydrochinone (0.7 g, 1.9 mmol), K_2CO_3 (2.6 g, 19.4 mmol), TBAI (1.4 mg, 3.8 mmol) in anhydrous DMF (20 mL), purification by column chromatography (eluent: *n*-hexane); colorless liquid, yield: $C_{58}H_{112}I_2O_2Si$ *M* = 1151.51 g/mol, 1.41 g (64 %), **¹H-NMR** (CDCl₃, 400 MHz): δ / ppm = 7.17 (s, 2H, Aryl-*H*), 3.92 (t, $^3J_{H,H}$ = 6.4 Hz, 4H, -OC*H₂*-), 1.85 − 1.74 (m, 4H, -OCH₂C*H₂*-), 1.52 − 1.44 (m, 4H, -OCH₂CH₂C*H₂*-), 1.39 − 1.19 (m, 64H, -C*H₂*-), 0.87 (t, $^3J_{H,H}$ = 6.7 Hz, 18H, -C*H₃*), 0.53 − 0.42 (m, 16H, -SiC*H₂*-). **²⁹Si-NMR** (CDCl₃, 79 MHz): δ / ppm = 2.90 (*Si*).
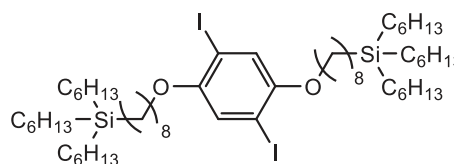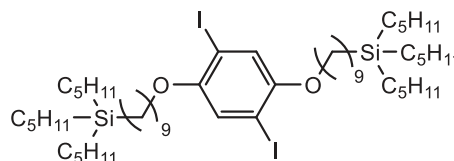
1,4-Bis[9-(tripentylsilyl)nonyloxy]-2,5-diiodobenzene 8B9/5

Synthesized according to GP4 from **6-13** (1.3 g, 3.0 mmol), 2,5-Diiodohydrochinone (0.5 g, 1.3 mmol), K_2CO_3 (1.9 g, 13.4 mmol), TBAI (1.0 mg, 2.7 mmol) in anhydrous DMF (20 mL), purification by column chromatography (eluent: *n*-hexane); colorless liquid, yield: $C_{54}H_{104}I_2O_2Si$ *M* = 1095.40 g/mol, 0.48 g (34 %), **¹H-NMR** (CDCl₃, 400 MHz): δ / ppm = 7.17 (s, 2H, Aryl-*H*), 3.92 (t, $^3J_{H,H}$ = 6.4 Hz, 4H, -OC*H₂*-), 1.84 − 1.74 (m, 4H, -OCH₂C*H₂*-), 1.56 − 1.44 (m, 4H, -OCH₂CH₂C*H₂*-), 1.40 − 1.21 (m, 56H, -C*H₂*-), 0.89 (t, $^3J_{H,H}$ = 6.8 Hz, 18H, -C*H₃*), 0.54 − 0.42 (m, 16H, -SiC*H₂*-). **²⁹Si-NMR** (CDCl₃, 79 MHz): δ / ppm = 2.93 (*Si*).

1,4-Bis(2-tetradecylhexadecyloxy)-2,5-diiodobenzene 5/1/14

Synthesized according to GP4 from 15-(Bromomethyl)nonacosane (2.4 g, 4.8 mmol), 2,5-Diiodohydrochinone (0.7 g, 1.9 mmol), K_2CO_3 (3.8 g, 27.6 mmol), TBAI (1.6 mg, 4.3 mmol) in anhydrous DMF (20 mL), purification by column chromatography (eluent: *n*-hexane); colorless solid, yield: $C_{66}H_{124}I_2O_2$ *M* = 1203.53 g/mol, 0.62 g (27 %), *mp* = 65 °C, **¹H-NMR** (CDCl₃, 500 MHz): δ / ppm = 7.16 (s, 2H, Aryl-*H*), 3.81 (d, $^3J_{H,H}$ = 5.4 Hz, 4H, -OC*H₂*-), 1.82 − 1.75 (m, 2H, -C*H*-), 1.56 − 1.25 (m, 104H, -C*H₂*-), 0.87 (t, $^3J_{H,H}$ = 6.5 Hz, 12H, -C*H₃*).

1,4-Bis(2-pentadecylheptadecyloxy)-2,5-diiodobenzene 5/1/15

Synthesized according to GP4 from 16-(Bromomethyl)hentriacontane (2.5 g, 4.7 mmol), 2,5-Diiodohydrochinone (2.2 g, 0.8 mmol), K_2CO_3 (3.0 g, 21.5 mmol), TBAI (1.6 mg, 4.2 mmol) in anhydrous DMF (20 mL), purification by column chromatography (eluent: *n*-hexane); colorless solid, yield: $C_{70}H_{132}I_2O_2$ *M* = 1259.63 g/mol, 0.70 g (26 %), *mp* = 70 °C, **¹H-NMR** (CDCl₃, 400 MHz): δ / ppm =

7.15 (s, 2H, Aryl-H), 3.79 (d, $^3J_{H,H}$ = 5.4 Hz, 4H, -OCH_2-), 1.82 – 1.73 (m, 2H, -CH-), 1.56 – 1.20 (m, 112H, -CH_2-), 0.87 (t, $^3J_{H,H}$ = 7.0 Hz, 12H, -CH_3).

1,4-Bis[2-hexadecyloctadecyloxy]-2,5-diiodobenzene 5/1/16

Synthesized according to GP4 from 17-(Bromomethyl)tritriacontane (2.3 g, 4.1 mmol), 2,5-Diiodohydrochinone (0.7 g, 1.9 mmol), K$_2$CO$_3$ (2.7 g, 19.3 mmol), TBAI (1.4 mg, 3.7 mmol) in anhydrous DMF (20 mL), purification by column chromatography (eluent: n-hexane); colorless solid, yield: C$_{74}$H$_{140}$I$_2$O$_2$ M = 1315.74 g/mol, 0.66 g (25 %), mp = 72 °C, ^{1}**H-NMR** (CDCl$_3$, 400 MHz): δ / ppm = 7.15 (s, 2H, Aryl-H), 3.80 (d, $^3J_{H,H}$ = 5.4 Hz, 4H, -OCH_2-), 1.83 – 1.70 (m, 2H, -CH-), 1.53 – 1.18 (m, 120H, -CH_2-), 0.87 (t, $^3J_{H,H}$ = 6.6 Hz, 12H, -CH_3).

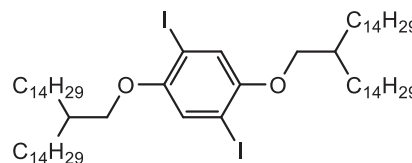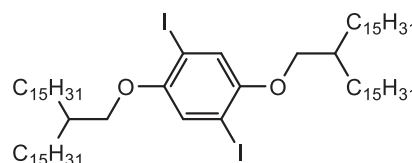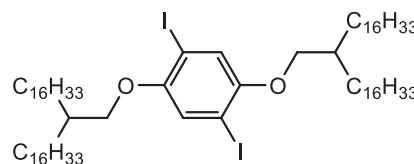**1,4-Bis[4-tetradecyloctadecyloxy]-2,5-diiodobenzene 5/3/14**

Synthesized according to GP4 from **4** (2.5 g, 4.7 mmol), 2,5-Diiodohydrochinone (0.8 g, 2.2 mmol), K$_2$CO$_3$ (3.0 g, 21.5 mmol), TBAI (1.6 mg, 4.2 mmol) in anhydrous DMF (20 mL), purification by column chromatography (eluent: n-hexane); colorless solid, yield: C$_{70}$H$_{132}$I$_2$O$_2$ M = 1259.63 g/mol, 1.11 g (41 %), mp = 79 °C, ^{1}**H-NMR** (CDCl$_3$, 400 MHz): δ / ppm = 7.16 (s, 2H, Aryl-H), 3.90 (t, $^3J_{H,H}$ = 6.3 Hz, 4H, -OCH_2-), 1.80 – 1.71 (m, 4H, -OCH$_2$CH_2-), 1.48 – 1.38 (m, 6H, -OCH$_2$CH$_2$CH_2-, -CH-), 1.37 – 1.20 (m, 104H, -CH_2-), 0.88 (t, $^3J_{H,H}$ = 6.5 Hz, 12H, -CH_3).
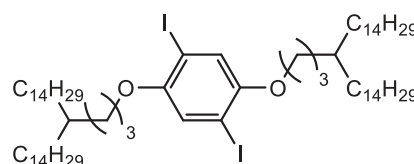
5.3.2 Analytical data of the acetonides NH*m/n*A and NF*m/n*A

1,4-Bis[3-(diundecylmethylsilyl)porpyloxy]-2,5-bis{4-[4-(2,3-isopropylidene-2,3-dihydroxyprop-1-yloxy)phenylethynyl]phenylethynyl}benzene 2H3/11A
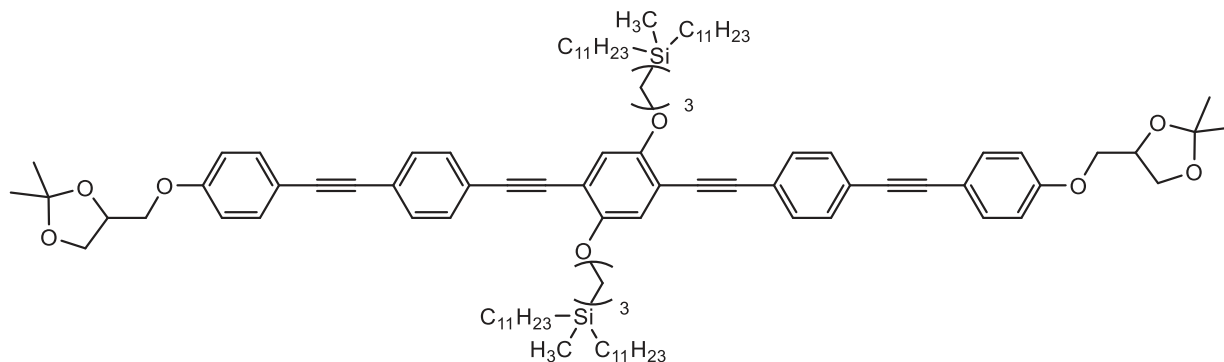
Synthesized according to GP5 from **11C-1** (250 mg, 0.22 mmol), **25H** (159 mg, 0.48 mmol), Pd(PPh$_3$)$_4$ (7.6 mg, 6.6 · 10^{-3} mmol), CuI (1.3 mg, 6.6 · 10^{-3} mmol) in anhydrous Et$_3$N (20 mL), purification by column chromatography (eluent: CHCl$_3$); yellow solid, yield: C$_{102}$H$_{150}$O$_8$Si$_2$ M = 1560.48 g/mol, 210 mg (62 %), mp = 118 °C, ^{1}**H-NMR** (CDCl$_3$, 402 MHz): δ / ppm = 7.51 – 7.40 (m, 12H, Aryl-H), 6.99 (s, 2H, Aryl-H), 6.92 – 6.84 (m, 4H, Aryl-H), 4.52 – 4.42 (m, 2H, -CHO-), 4.16 (dd, $^2J_{H,H}$ = 8.5, $^3J_{H,H}$ = 6.4 Hz, 2H, -OCH_AH$_B$-), 4.06 (dd, $^2J_{H,H}$ = 9.5, $^3J_{H,H}$ = 5.4 Hz, 2H, -OCH$_A$$H_B$-), 4.03 – 3.92 (m, 6H, -OCH_2-, ArOCH_AH$_B$-), 3.89 (dd, $^2J_{H,H}$ = 8.5, $^3J_{H,H}$ = 5.8 Hz, 2H, ArOCH$_A$$H_B$-), 1.88 – 1.76 (m, 4H, -CH_2-), 1.45 (s, 6H, -CH_3), 1.39 (s, 6H, -CH_3), 1.32 – 1.13 (m, 72H, -CH_2-), 0.85 (t, $^3J_{H,H}$ = 6.7 Hz, 12H, -CH_3), 0.73 – 0.64 (m, 4H, -SiCH_2-), 0.54 – 0.46 (m, 8H, -SiCH_2-), -0.05 (s, 6H, -SiCH_3). ^{29}**Si-NMR** (CDCl$_3$, 80 MHz): δ / ppm = 3.36 (*Si*).

1,4-Bis[3-(didodecylmethylsilyl)propyloxy]-2,5-bis{4-[4-(2,3-isopropylidene-2,3-dihydroxyprop-1-yloxy)phenylethynyl]phenylethynyl}benzene 2H3/12A
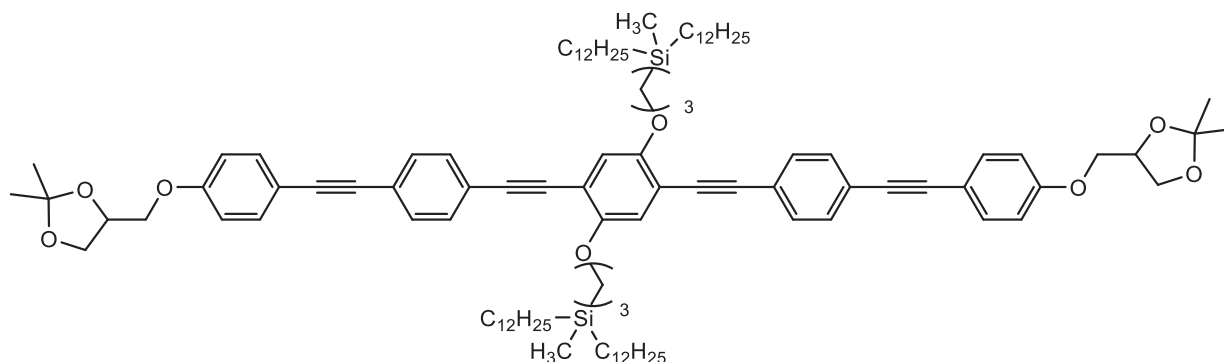
Synthesized according to GP5 from **11C-2** (200 mg, 0.17 mmol), **25H** (121 mg, 0.36 mmol), Pd(PPh$_3$)$_4$ (5.9 mg, $5.1 \cdot 10^{-3}$ mmol), CuI (1.0 mg, $5.1 \cdot 10^{-3}$ mmol) in anhydrous Et$_3$N (20 mL), purification by column chromatography (eluent: CHCl$_3$); yellow solid, yield: C$_{106}$H$_{158}$O$_8$Si$_2$ M = 1616.59 g/mol, 200 mg (75 %), *mp* = 99 °C, **^{1}H-NMR** (CDCl$_3$, 400 MHz): δ / ppm = 7.51 − 7.43 (m, 12H, Aryl-*H*), 7.00 (s, 2H, Aryl-*H*), 6.92 − 6.87 (m, 4H, Aryl-*H*), 4.52 − 4.43 (m, 2H, -C*H*O-), 4.17 (dd, $^2J_{H,H}$ = 8.5, $^3J_{H,H}$ = 6.4 Hz, 2H, -OC*H*$_A$H$_B$-), 4.07 (dd, $^2J_{H,H}$ = 8.8, $^3J_{H,H}$ = 5.6 Hz, 2H, -OCH$_A$*H*$_B$-), 3.99 (t, $^3J_{H,H}$ = 7.0 Hz, 4H, -OC*H*$_2$-), 3.91 (dd, $^2J_{H,H}$ = 8.5, $^3J_{H,H}$ = 5.8 Hz, 2H, -ArOC*H*$_A$H$_B$-), 3.86 (dd, $^2J_{H,H}$ = 11.4, $^3J_{H,H}$ = 3.8 Hz, 2H, -ArOCH$_A$*H*$_B$-), 1.96 − 1.72 (m, 4H, -C*H*$_2$-), 1.47 (s, 6H, -C*H*$_3$), 1.41 (s, 6H, -C*H*$_3$), 1.34 − 1.18 (m, 80H, -C*H*$_2$-), 0.86 (t, $^3J_{H,H}$ = 6.6 Hz, 12H, -C*H*$_3$), 0.74 − 0.66 (m, 4H, -SiC*H*$_2$-), 0.55 − 0.44 (m, 8H, -SiC*H*$_2$-), -0.03 (s, 6H, -SiC*H*$_3$). **^{29}Si-NMR** (CDCl$_3$, 79 MHz): δ / ppm = 3.37 (*Si*).

1,4-Bis[3-(ditetradecylmethylsilyl)propyloxy]-2,5-bis{4-[4-(2,3-isopropylidene-2,3-dihydroxyprop-1-yloxy)phenylethynyl]phenylethynyl}benzene 2H3/14A
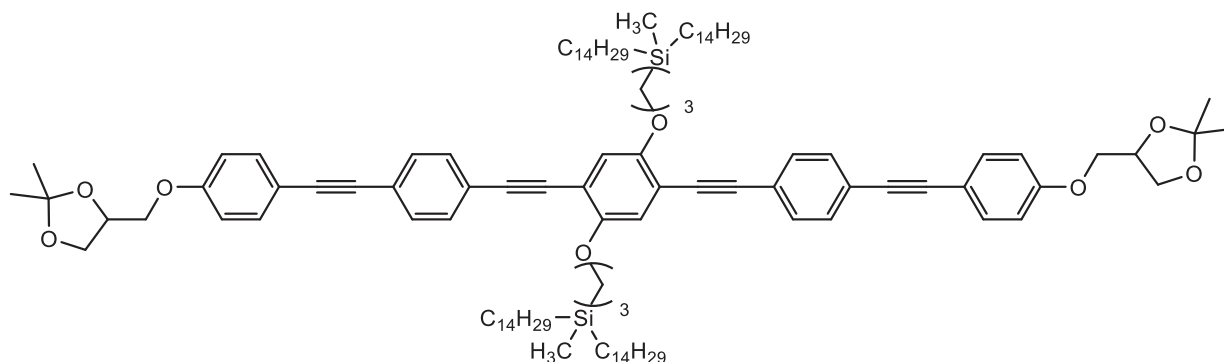

Synthesized according to GP5 from **11C-3** (210 mg, 0.16 mmol), **25H** (111 mg, 0.33 mmol), Pd(PPh$_3$)$_4$ (5.5 mg, $4.8 \cdot 10^{-3}$ mmol), CuI (0.9 mg, $4.8 \cdot 10^{-3}$ mmol) in anhydrous Et$_3$N (20 mL), purification by column chromatography (eluent: CHCl$_3$); yellow solid, yield: C$_{114}$H$_{174}$O$_8$Si$_2$ M = 1728.81 g/mol, 260 mg (95 %), *mp* = 97 °C, **^{1}H-NMR** (CDCl$_3$, 400 MHz): δ / ppm = 7.51 − 7.45 (m, 12H, Aryl-*H*), 7.00 (s, 2H, Aryl-*H*), 6.94 − 6.87 (m, 4H, Aryl-*H*), 4.52 − 4.45 (m, 2H, -C*H*O-), 4.18 (dd, $^2J_{H,H}$ = 8.5, $^3J_{H,H}$ = 6.4 Hz, 2H, -OC*H*$_A$H$_B$-), 4.07 (dd, $^2J_{H,H}$ = 8.4, $^3J_{H,H}$ = 6.6 Hz, 2H, -OCH$_A$*H*$_B$-), 3.99 (t, $^3J_{H,H}$ = 6.6 Hz, 4H, -OC*H*$_2$-), 3.91 (dd, $^2J_{H,H}$ = 8.5, $^3J_{H,H}$ = 5.8 Hz, 2H, -ArOC*H*$_A$H$_B$-), 3.86 (dd, $^2J_{H,H}$ = 11.4, $^3J_{H,H}$ = 3.8 Hz, 2H, -ArOCH$_A$*H*$_B$-), 1.89 − 1.77 (m, 4H, -C*H*$_2$-), 1.47 (s, 6H, -C*H*$_3$), 1.41 (s, 6H, -C*H*$_3$), 1.34 − 1.19 (m, 96H, -C*H*$_2$-), 0.87 (t, $^3J_{H,H}$ = 6.8 Hz, 12H, -C*H*$_3$), 0.75 − 0.66 (m, 4H, -SiC*H*$_2$-), 0.55 − 0.48 (m, 8H, -SiC*H*$_2$-), -0.03 (s, 6H, -SiC*H*$_3$). **^{29}Si-NMR** (CDCl$_3$, 79 MHz): δ / ppm = 3.38 (*Si*).

1,4-Bis[4-(didecylmethylsilyl)butyloxy]-2,5-bis{4-[4-(2,3-isopropylidene-2,3-dihydroxyprop-1-yloxy)phenylethynyl]phenylethynyl}benzene 2H4/10A
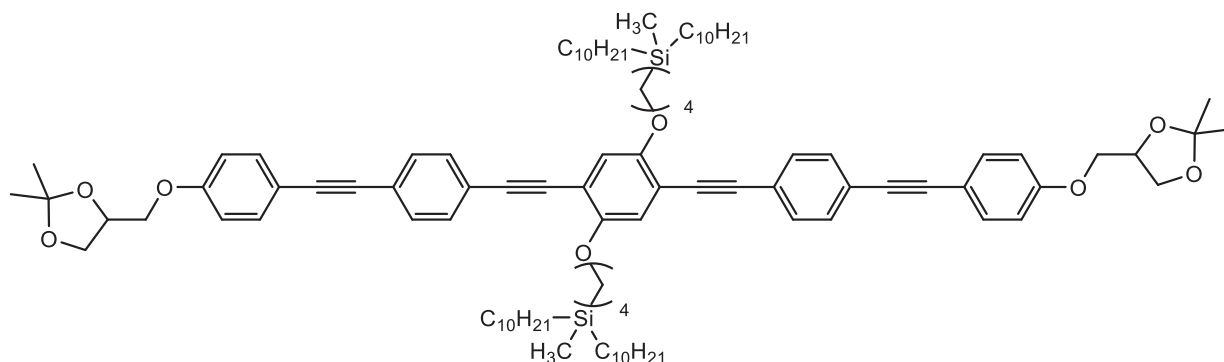

Synthesized according to GP5 from **8C4/10** (200 mg, 0.18 mmol), **25H** (130 mg, 0.39 mmol), Pd(PPh$_3$)$_4$ (6.2 mg, $5.4 \cdot 10^{-3}$ mmol), CuI (1.0 mg, $5.4 \cdot 10^{-3}$ mmol) in anhydrous Et$_3$N (20 mL), purification by column chromatography (eluent: CHCl$_3$); yellow solid, yield: C$_{100}$H$_{146}$O$_8$Si$_2$ M = 1532.43 g/mol, 240 mg (88 %), mp = 89 °C, **^{1}H-NMR** (CDCl$_3$, 402 MHz): δ / ppm = 7.50 − 7.40 (m, 12H, Aryl-H), 6.99 (s, 2H, Aryl-H), 6.92 − 6.84 (m, 4H, Aryl-H), 4.52 − 4.43 (m, 2H, -CHO-), 4.16 (dd, $^2J_{H,H}$ = 8.5, $^3J_{H,H}$ = 6.4 Hz, 2H, -OCH_AH$_B$-), 4.10 − 3.99 (m, 6H, -OCH_2-, -OCH$_A$$H_B$-), 3.95 (dd, $^2J_{H,H}$ = 9.5, $^3J_{H,H}$ = 5.9 Hz, 2H, -ArOCH_AH$_B$-), 3.89 (dd, $^2J_{H,H}$ = 8.5, $^3J_{H,H}$ = 5.8 Hz, 2H, ArOCH$_A$$H_B$-), 1.92 − 1.80 (m, 4H, -CH_2-), 1.59 − 1.47 (m, 4H, -CH_2-), 1.45 (s, 6H, -CH_3), 1.39 (s, 6H, -CH_3), 1.32 − 1.16 (m, 64H, -CH_2-), 0.85 (t, $^3J_{H,H}$ = 6.6 Hz, 12H, -CH_3), 0.59 − 0.51 (m, 4H, -SiCH_2-), 0.50 − 0.41 (m, 8H, -SiCH_2-), -0.10 (s, 6H, -CH_3). **^{29}Si-NMR** (CDCl$_3$, 80 MHz): δ / ppm = 2.89 (*Si*).

1,4-Bis[4-(didodecylmethylsilyl)butyloxy]-2,5-bis{4-[4-(2,3-isopropylidene-2,3-dihydroxyprop-1-yloxy)phenylethynyl]phenylethynyl}benzene 2H4/12A
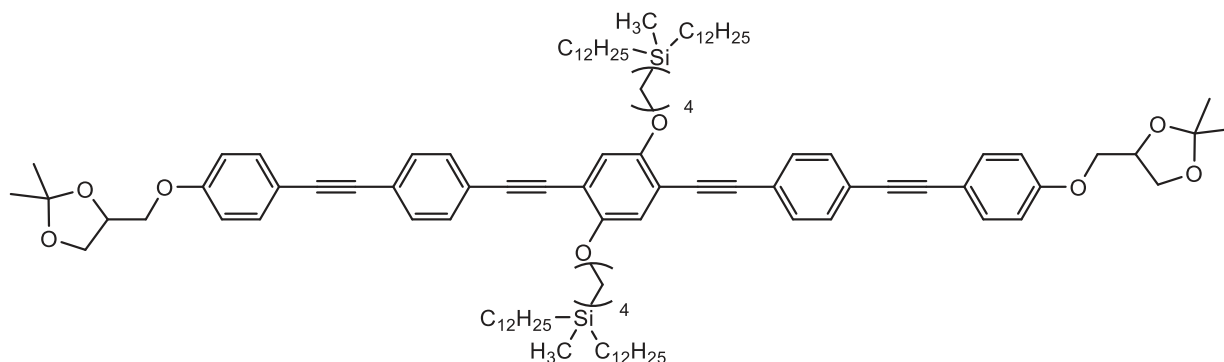

Synthesized according to GP5 from **5C4/12** (260 mg, 0.21 mmol), **25H** (154 mg, 0.46 mmol), Pd(PPh$_3$)$_4$ (7.3 mg, $6.3 \cdot 10^{-3}$ mmol), CuI (1.2 mg, $6.3 \cdot 10^{-3}$ mmol) in anhydrous Et$_3$N (20 mL), purification by column chromatography (eluent: CHCl$_3$); yellow solid, yield: C$_{108}$H$_{162}$O$_8$Si$_2$ M = 1644.65 g/mol, 320 mg (93 %), mp = 115 °C, **^{1}H-NMR** (CDCl$_3$, 400 MHz): δ / ppm = 7.53 − 7.43 (m, 12H, Aryl-H), 7.01 (s, 2H, Aryl-H), 6.93 − 6.86 (m, 4H, Aryl-H), 4.53 − 4.44 (m, 2H, -CHO-), 4.18 (dd, $^2J_{H,H}$ = 8.5, $^3J_{H,H}$ = 6.4 Hz, 2H, -OCH_AH$_B$-), 4.11 − 4.03 (m, 6H, -OCH_2-, -OCH$_A$$H_B$-), 3.97 (dd, $^2J_{H,H}$ = 9.6, $^3J_{H,H}$ = 5.9 Hz, 2H, ArOCH_AH$_B$-), 3.91 (dd, $^2J_{H,H}$ = 8.5, $^3J_{H,H}$ = 5.8 Hz, 2H, ArOCH$_A$$H_B$-), 1.94 − 1.81 (m, 4H, -CH_2-), 1.60 − 1.49 (m, 4H, -CH_2-), 1.47 (s, 6H, -CH_3), 1.41 (s, 6H, -CH_3), 1.35 − 1.17 (m, 80H, -CH_2-), 0.87 (t, $^3J_{H,H}$ = 6.7 Hz, 12H, -CH_2-), 0.62 − 0.53 (m, 4H, -SiCH_2-), 0.52 − 0.44 (m, 8H, -SiCH_2-), -0.08 (s, 6H, -SiCH_3). **^{29}Si-NMR** (CDCl$_3$, 79 MHz): δ / ppm = 2.91 (*Si*).

1,4-Bis[4-(ditetradeylmethylsilyl)butyloxy]-2,5-bis{4-[4-(2,3-isopropylidene-2,3-dihydroxyprop-1-yloxy)phenylethynyl]phenylethynyl}benzene 2H4/14A
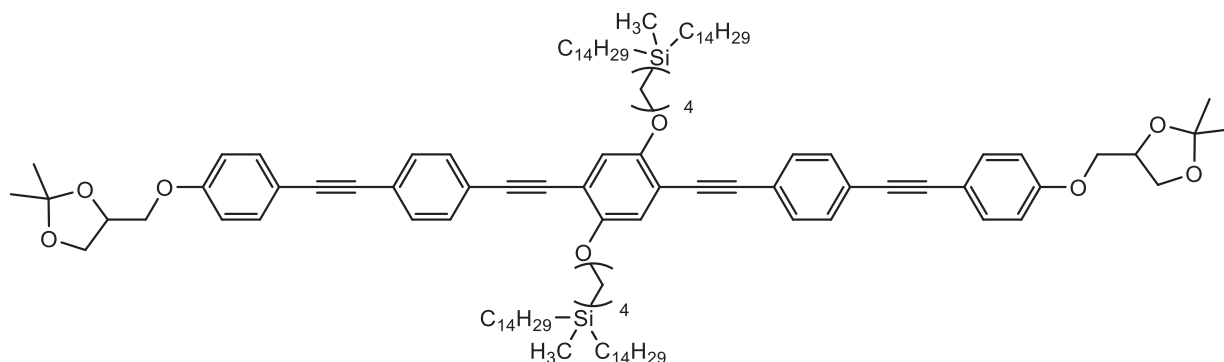

Synthesized according to GP5 from 8C4/14 (500 mg, 0.37 mmol), **25H** (271 mg, 0.82 mmol), Pd(PPh$_3$)$_4$ (12.8 mg, 11.1 · 10^{-3} mmol), CuI (2.1 mg, 11.1 · 10^{-3} mmol) in anhydrous Et$_3$N (20 mL), purification by column chromatography (eluent: CHCl$_3$); yellow solid, yield: C$_{116}$H$_{178}$O$_8$Si$_2$ M = 1756.86 g/mol, 640 mg (98 %), *mp* = 83 °C, **^{1}H-NMR** (CDCl$_3$, 400 MHz): δ / ppm = 7.53 − 7.43 (m, 12H, Aryl-*H*), 7.01 (s, 2H, Aryl-*H*), 6.93 − 6.86 (m, 4H, Aryl-*H*), 4.55 − 4.44 (m, 2H, -C*H*O-), 4.18 (dd, $^2J_{H,H}$ = 8.5, $^3J_{H,H}$ = 6.4 Hz, 2H, -OC*H*$_A$H$_B$-), 4.11 − 4.01 (m, 6H, -OC*H*$_2$-, -OCH$_A$*H*$_B$-), 3.97 (dd, $^2J_{H,H}$ = 9.5, $^3J_{H,H}$ = 5.9 Hz, 2H, -ArOC*H*$_A$H$_B$-), 3.91 (dd, $^2J_{H,H}$ = 8.5, $^3J_{H,H}$ = 5.8 Hz, 2H, ArOCH$_A$*H*$_B$-), 1.93 − 1.82 (m, 4H, -C*H*$_2$-), 1.59 − 1.50 (m, 4H, -C*H*$_2$-), 1.47 (s, 6H, -C*H*$_3$), 1.41 (s, 6H, -C*H*$_3$), 1.36 − 1.17 (m, 96H, -C*H*$_2$-), 0.88 (t, $^3J_{H,H}$ = 6.8 Hz, 12H, -C*H*$_3$), 0.64 − 0.54 (m, 4H, -SiC*H*$_2$-), 0.53 − 0.42 (m, 8H, -SiC*H*$_2$-), -0.07 (s, 6H, -SiC*H*$_3$). **^{29}Si-NMR** (CDCl$_3$, 79 MHz): δ / ppm = 2.91 (*Si*).

1,4-Bis[5-(dinonylmethylsilyl)pentyloxy]-2,5-bis{4-[4-(2,3-isopropylidene-2,3-dihydroxyprop-1-yloxy)phenylethynyl]phenylethynyl}benzene 2H5/9A
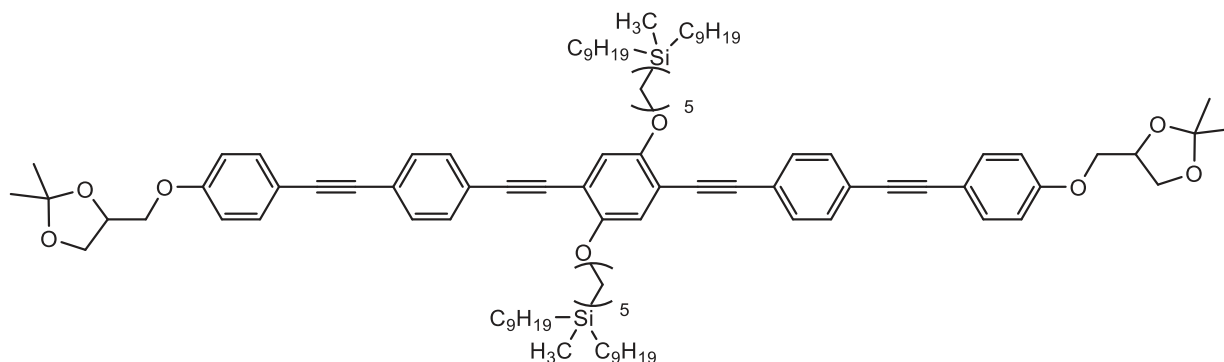

Synthesized according to GP5 from **8C5/9** (200 mg, 0.19 mmol), **25H** (134 mg, 0.40 mmol), Pd(PPh$_3$)$_4$ (6.6 mg, 5.7 · 10^{-3} mmol), CuI (1.1 mg, 5.7 · 10^{-3} mmol) in anhydrous Et$_3$N (20 mL), purification by column chromatography (eluent: CHCl$_3$); yellow solid, yield: C$_{98}$H$_{142}$O$_8$Si$_2$ M = 1504.38 g/mol, 250 mg (91 %), *mp* = 107 °C, **^{1}H-NMR** (CDCl$_3$, 502 MHz): δ / ppm = 7.53 − 7.43 (m, 12H, Aryl-*H*), 7.01 (s, 2H, Aryl-*H*), 6.93 − 6.87 (m, 4H, Aryl-*H*), 4.53 − 4.45 (m, 2H, -C*H*O-), 4.18 (dd, $^2J_{H,H}$ = 8.5, $^3J_{H,H}$ = 6.4 Hz, 2H, -OC*H*$_A$H$_B$-), 4.08 (dd, $^2J_{H,H}$ = 9.5, $^3J_{H,H}$ = 5.4 Hz, 2H, -OCH$_A$*H*$_B$-), 4.03 (t, $^3J_{H,H}$ = 6.5 Hz, 4H, -OC*H*$_2$-), 3.97 (dd, $^2J_{H,H}$ = 9.5, $^3J_{H,H}$ = 5.8 Hz, 2H, -ArOC*H*$_A$H$_B$-), 3.91 (dd, $^2J_{H,H}$ = 8.5, $^3J_{H,H}$ = 5.8 Hz, 2H, -ArOCH$_A$*H*$_B$-), 1.91 − 1.81 (m, 4H, -C*H*$_2$-), 1.61 − 1.51 (m, 4H, -C*H*$_2$-), 1.47 (s, 6H, -C*H*$_3$), 1.41 (s, 6H, -C*H*$_3$), 1.39 − 1.21 (m, 60H, -C*H*$_2$-), 0.87 (t, $^3J_{H,H}$ = 6.9 Hz, 12H, -C*H*$_3$), 0.56 − 0.44 (m, 12H, -SiC*H*$_2$-), -0.08 (s, 6H, -SiC*H*$_3$). **^{29}Si-NMR** (CDCl$_3$, 100 MHz): δ / ppm = 2.80 (*Si*).

1,4-Bis[5-(didecylmethylsilyl)pentyloxy]-2,5-bis{4-[4-(2,3-isopropylidene-2,3-dihydroxyprop-1-yloxy)phenylethynyl]phenylethynyl}benzene 2H5/10A
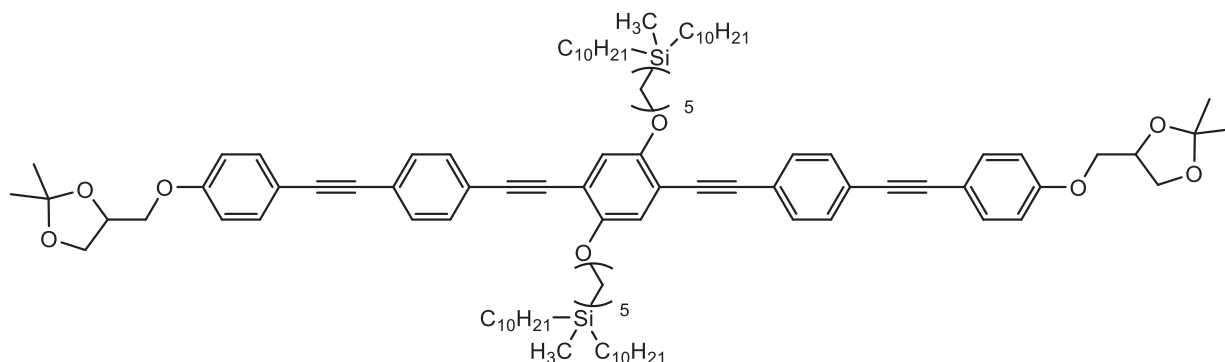

Synthesized according to GP5 from **8C5/10** (200 mg, 0.17 mmol), **25H** (127 mg, 0.38 mmol), Pd(PPh$_3$)$_4$ (5.9 mg, 5.1 · 10^{-3} mmol), CuI (1.0 mg, 5.1 · 10^{-3} mmol) in anhydrous Et$_3$N (20 mL), purification by column chromatography (eluent: CHCl$_3$); yellow solid, yield: C$_{102}$H$_{150}$O$_8$Si$_2$ M = 1560.48 g/mol, 260 mg (96 %), mp = 104 °C, **^{1}H-NMR** (CDCl$_3$, 400 MHz): δ / ppm = 7.52 − 7.43 (m, 12H, Aryl-*H*), 7.01 (s, 2H, Aryl-*H*), 6.93 − 6.85 (m, 4H, Aryl-*H*), 4.52 − 4.44 (m, 2H, -C*H*O-), 4.17 (dd, $^2J_{H,H}$ = 8.5, $^3J_{H,H}$ = 6.4 Hz, 2H, -OC*H$_A$*H$_B$-), 4.10 − 4.00 (m, 6H, -OC*H$_2$*-, -OC*H$_A$*H$_B$-), 3.97 (dd, $^2J_{H,H}$ = 9.5, $^3J_{H,H}$ = 5.9 Hz, 2H, -ArOC*H$_A$*H$_B$-), 3.91 (dd, $^2J_{H,H}$ = 8.5, $^3J_{H,H}$ = 5.8 Hz, 2H, ArOC*H$_A$*H$_B$-), 1.90 − 1.81 (m, 4H, -C*H$_2$*-), 1.61 − 1.51 (m, 4H, -C*H$_2$*-), 1.47 (s, 6H, -C*H$_3$*), 1.41 (s, 6H, -C*H$_3$*), 1.39 − 1.18 (m, 68H, -C*H$_2$*-), 0.86 (t, $^3J_{H,H}$ = 7.1 Hz, 12H, -C*H$_3$*), 0.55 − 0.43 (m, 12H, -SiC*H$_2$*-), -0.08 (s, 6H, -SiC*H$_3$*). **^{29}Si-NMR** (CDCl$_3$, 79 MHz): δ / ppm = 2.79 (*Si*).

1,4-Bis[6-(didecylmethylsilyl)hexyloxy]-2,5-bis{4-[4-(2,3-isopropylidene-2,3-dihydroxyprop-1-yloxy)phenylethynyl]phenylethynyl}benzene 2H6/10A
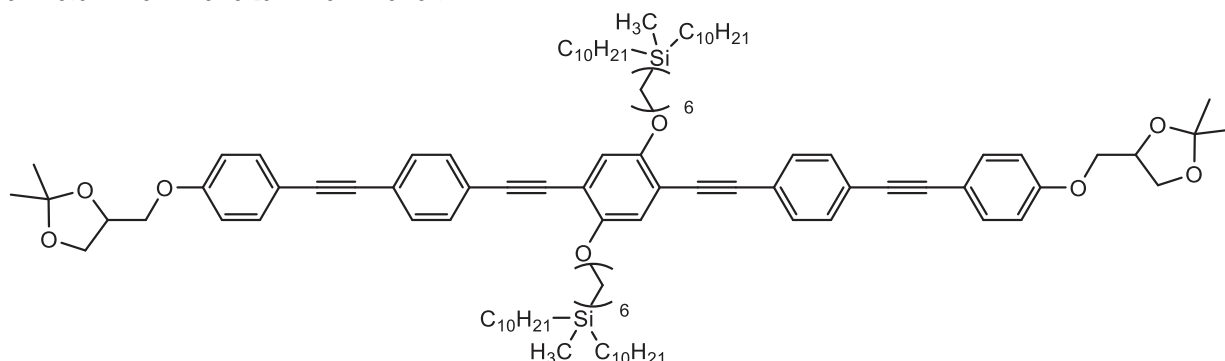

Synthesized according to GP5 from **8C6/10** (200 mg, 0.17 mmol), **25H** (123 mg, 0.38 mmol), Pd(PPh$_3$)$_4$ (5.9 mg, 5.1 · 10^{-3} mmol), CuI (1.0 mg, 5.1 · 10^{-3} mmol) in anhydrous Et$_3$N (20 mL), purification by column chromatography (eluent: CHCl$_3$); yellow solid, yield: C$_{104}$H$_{154}$O$_8$Si$_2$ M = 1588.54 g/mol, 270 mg (98 %), mp = 94 °C, **^{1}H-NMR** (CDCl$_3$, 400 MHz): δ / ppm = 7.52 − 7.42 (m, 12H, Aryl-*H*), 7.01 (s, 2H, Aryl-*H*), 6.93 − 6.87 (m, 4H, Aryl-*H*), 4.53 − 4.44 (m, 2H, -C*H*O-), 4.17 (dd, $^2J_{H,H}$ = 8.5, $^3J_{H,H}$ = 6.4 Hz, 2H, -OC*H$_A$*H$_B$-), 4.11 − 4.01 (m, 6H, -OC*H$_2$*-, -OC*H$_A$*H$_B$-), 3.97 (dd, $^2J_{H,H}$ = 9.5, $^3J_{H,H}$ = 5.9 Hz, 2H, -ArOC*H$_A$*H$_B$-), 3.91 (dd, $^2J_{H,H}$ = 8.5, $^3J_{H,H}$ = 5.8 Hz, 2H, ArOC*H$_A$*H$_B$-), 1.90 − 1.79 (m, 4H, -C*H$_2$*-), 1.60 − 1.50 (m, 4H, -C*H$_2$*-), 1.47 (s, 6H, -C*H$_3$*), 1.41 (s, 6H, -C*H$_3$*), 1.35 − 1.19 (m, 72H, -C*H$_2$*-), 0.87 (t, $^3J_{H,H}$ = 6.8 Hz, 12H, -C*H$_3$*), 0.52 − 0.42 (m, 12H, -SiC*H$_2$*-), -0.10 (s, 6H, -SiC*H$_3$*). **^{29}Si-NMR** (CDCl$_3$, 79 MHz): δ / ppm = 2.78 (*Si*).

1,4-Bis[6-(didodecylmethylsilyl)hexyloxy]-2,5-bis{4-[4-(2,3-isopropylidene-2,3-dihydroxyprop-1-yloxy)phenylethynyl]phenylethynyl}benzene 2H6/12A
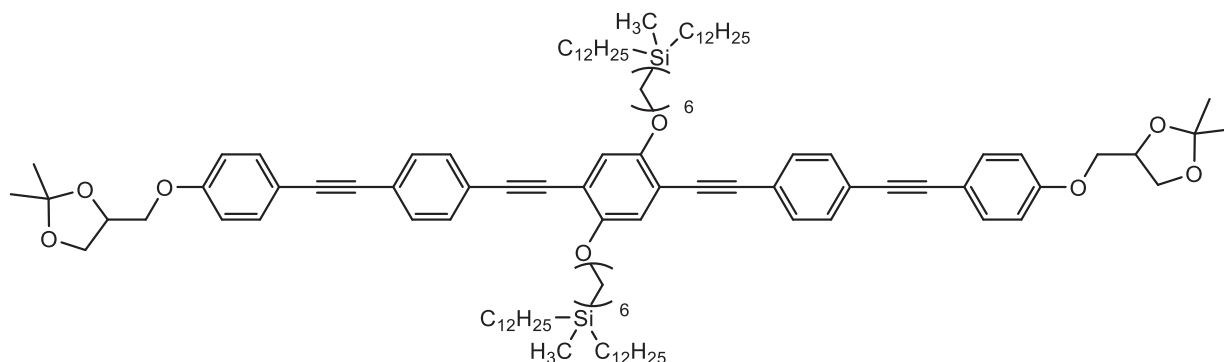
Synthesized according to GP5 from **8C6/12** (250 mg, 0.19 mmol), **25H** (142 mg, 0.43 mmol), Pd(PPh$_3$)$_4$ (6.6mg, $5.7 \cdot 10^{-3}$ mmol), CuI (1.1 mg, $5.7 \cdot 10^{-3}$ mmol) in anhydrous Et$_3$N (20 mL), purification by column chromatography (eluent: CHCl$_3$); yellow solid, yield: C$_{112}$H$_{170}$O$_8$Si$_2$ M = 1700.75 g/mol, 270 mg (82 %), mp = 89 °C, **^{1}H-NMR** (CDCl$_3$, 400 MHz): δ / ppm = 7.51 − 7.42 (m, 12H, Aryl-H), 7.00 (s, 2H, Aryl-H), 6.95 − 6.86 (m, 4H, Aryl-H), 4.53 − 4.44 (m, 2H, -CHO-), 4.17 (dd, $^2J_{H,H}$ = 8.5, $^3J_{H,H}$ = 6.4 Hz, 2H, -OCH_AH$_B$-), 4.12 − 4.01 (m, 6H, -OCH_2-, -OCH$_A$$H_B$-), 3.96 (dd, $^2J_{H,H}$ = 9.6, $^3J_{H,H}$ = 5.9 Hz, 2H, -ArOCH_AH$_B$-), 3.91 (dd, $^2J_{H,H}$ = 8.5, $^3J_{H,H}$ = 5.8 Hz, 2H, ArOCH$_A$$H_B$-), 1.91 − 1.76 (m, 4H, -CH_2-), 1.58 − 1.51 (m, 4H, -CH_2-), 1.47 (s, 6H, -CH_3), 1.41 (s, 6H, -CH_3), 1.35 − 1.15 (m, 88H, -CH_2-), 0.87 (t, $^3J_{H,H}$ = 6.8 Hz, 12H, -CH_3), 0.53 − 0.40 (m, 12H, -SiCH_2-), -0.10 (s, 6H, -SiCH_2-). **^{29}Si-NMR** (CDCl$_3$, 79 MHz): δ / ppm = 2.78 (*Si*).

1,4-Bis[7-(dinonylmethylsilyl)heptyloxy]-2,5-bis{4-[4-(2,3-isopropylidene-2,3-dihydroxyprop-1-yloxy)phenylethynyl]phenylethynyl}benzene 2H7/9A

Synthesized according to GP5 from **8C7/9** (200 mg, 0.17mmol), **25H** (127 mg, 0.38 mmol), Pd(PPh$_3$)$_4$ (5.9 mg, $5.1 \cdot 10^{-3}$ mmol), CuI (1.0 mg, $5.1 \cdot 10^{-3}$ mmol) in anhydrous Et$_3$N (20 mL), purification by column chromatography (eluent: CHCl$_3$); yellow solid, yield: C$_{102}$H$_{150}$O$_8$Si$_2$ M = 1560,48 g/mol, 270 mg (99 %), mp = 93 °C, **^{1}H-NMR** (CDCl$_3$, 402 MHz): δ / ppm = 7.51 − 7.41 (m, 12H, Aryl-H), 6.99 (s, 2H, Aryl-H), 6.91 − 6.85 (m, 4H, Aryl-H), 4.52 − 4.43 (m, 2H, -CHO-), 4.16 (dd, $^2J_{H,H}$ = 8.5, $^3J_{H,H}$ = 6.4 Hz, 2H, -OCH_AH$_B$-), 4.06 (dd, $^2J_{H,H}$ = 9.6, $^3J_{H,H}$ = 6.0 Hz, 2H, -OCH$_A$$H_B$-), 4.02 (t, $^3J_{H,H}$ = 6.5 Hz, 4H, -OCH_2-), 3.95 (dd, $^2J_{H,H}$ = 9.6, $^3J_{H,H}$ = 5.9 Hz, 2H, ArOCH_AH$_B$-), 3.89 (dd, $^2J_{H,H}$ = 8.5, $^3J_{H,H}$ = 5.8 Hz, 2H, ArOCH$_A$$H_B$-), 1.88 − 1.80 (m, 4H, -CH_2-), 1.57 − 1.48 (m, 4H, -CH_2-), 1.45 (s, 6H, -CH_3), 1.39 (s, 6H, -CH_3), 1.33 − 1.17 (m, 68H, -CH_2-), 0.85 (t, $^3J_{H,H}$ = 6.8 Hz, 12H, -CH_3), 0.50 − 0.40 (m, 12H, -SiCH_2-), -0.11 (s, 6H, -SiCH_3). **^{29}Si-NMR** (CDCl$_3$, 80 MHz): δ / ppm = 2.76 (*Si*).

1,4-Bis[7-(didecylmethylsilyl)heptyloxy]-2,5-bis{4-[4-(2,3-isopropylidene-2,3-dihydroxyprop-1-yloxy)phenylethynyl]phenylethynyl}benzene 2H7/10A
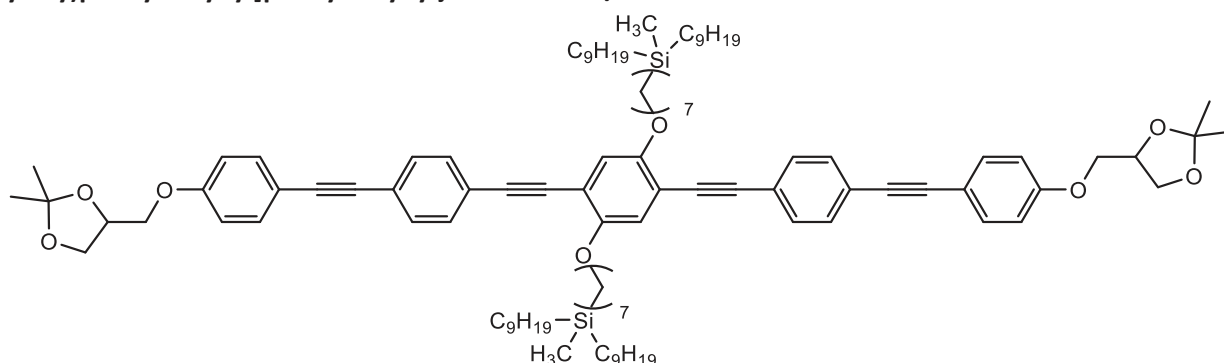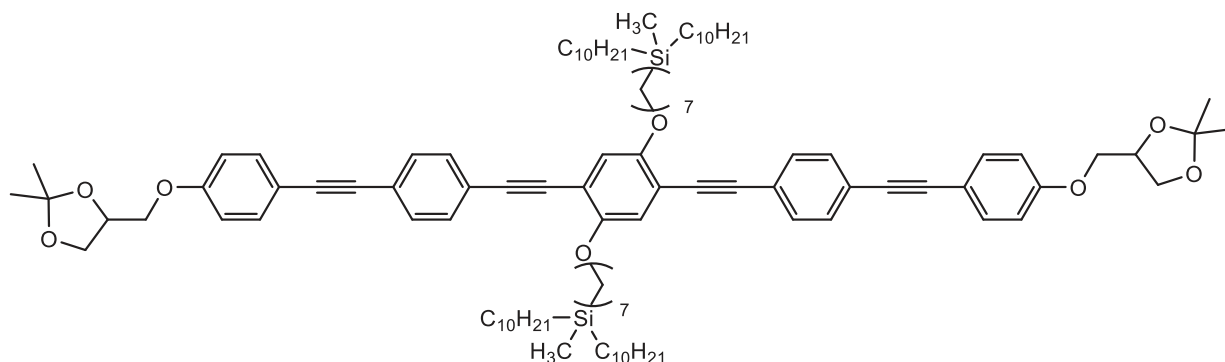

Synthesized according to GP5 from **8C7/10** (200 mg, 0.17mmol), **25H** (121 mg, 0.36 mmol), Pd(PPh$_3$)$_4$ (5.9 mg, $5.1 \cdot 10^{-3}$ mmol), CuI (1.0 mg, $5.1 \cdot 10^{-3}$ mmol) in anhydrous Et$_3$N (20 mL), purification by column chromatography (eluent: CHCl$_3$); yellow solid, yield: C$_{106}$H$_{158}$O$_8$Si$_2$ M = 1616.59 g/mol, 250 mg (93 %), mp = 97 °C, **^{1}H-NMR** (CDCl$_3$, 400 MHz): δ / ppm = 7.51 − 7.43 (m, 12H, Aryl-H), 7.01 (s, 2H, Aryl-H), 6.92 − 6.87 (m, 4H, Aryl-H), 4.53 − 4.45 (m, 2H, -CHO-), 4.17 (dd, $^2J_{H,H}$ = 8.5, $^3J_{H,H}$ = 6.4 Hz, 2H, -OCH_AH$_B$-), 4.09 − 4.00 (m, 6H, -OCH_2-, -OCH$_A$$H_B$-), 3.96 (dd, $^2J_{H,H}$ = 9.6, $^3J_{H,H}$ = 5.9 Hz, 2H, -ArOCH_AH$_B$-), 3.91 (dd, $^2J_{H,H}$ = 8.5, $^3J_{H,H}$ = 5.8 Hz, 2H, ArOCH$_A$$H_B$-), 1.91 − 1.81 (m, 4H, -CH_2-), 1.58 − 1.49 (m, 4H, -CH_2-), 1.47 (s, 6H, -CH_3), 1.41 (s, 6H, -CH_3), 1.39 − 1.18 (m, 76H, -CH_2-), 0.87 (t, $^3J_{H,H}$ = 6.5 Hz, 12H, -CH_3), 0.50 − 0.42 (m, 12H, -SiCH_2-), -0.10 (s, 6H, -SiCH_2-) **^{29}Si-NMR** (CDCl$_3$, 79 MHz): δ / ppm = 2.77 (Si).

1,4-Bis[9-(dioctylmethylsilyl)nonyloxy]-2,5-bis{4-[4-(2,3-isopropylidene-2,3-dihydroxyprop-1-yloxy)phenylethynyl]phenylethynyl}benzene 2H9/8A
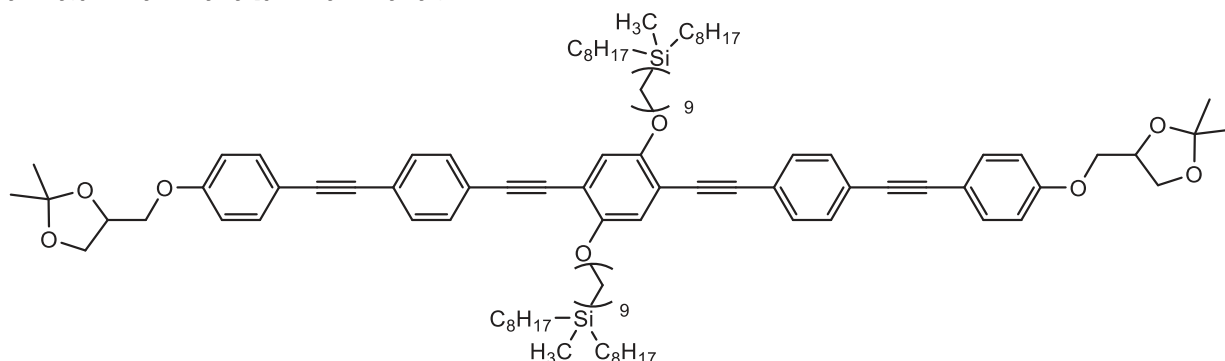

Synthesized according to GP5 from **8C9/8** (200 mg, 0.17mmol), **25H** (127 mg, 0.38 mmol), Pd(PPh$_3$)$_4$ (5.9 mg, $5.1 \cdot 10^{-3}$ mmol), CuI (1.0 mg, $5.1 \cdot 10^{-3}$ mmol) in anhydrous Et$_3$N (20 mL), purification by column chromatography (eluent: CHCl$_3$); yellow solid, yield: C$_{102}$H$_{150}$O$_8$Si$_2$ M = 1560.48 g/mol, 250 mg (92 %), mp = 94 °C, **^{1}H-NMR** (CDCl$_3$, 402 MHz): δ / ppm = 7.51 − 7.40 (m, 12H, Aryl-H), 6.99 (s, 2H, Aryl-H), 6.92 − 6.84 (m, 4H, Aryl-H), 4.52 − 4.40 (m, 2H, -OCH-), 4.16 (dd, $^2J_{H,H}$ = 8.5, $^3J_{H,H}$ = 6.4 Hz, 2H, -OCH_AH$_B$-), 4.07 − 3.98 (m, 6H, -OCH_2-, -OCH$_A$$H_B$-), 3.95 (dd, $^2J_{H,H}$ = 9.4, $^3J_{H,H}$ = 5.7 Hz, 2H, -ArOCH_AH$_B$-), 3.89 (dd, $^2J_{H,H}$ = 8.3, $^3J_{H,H}$ = 6.1 Hz, 2H, -ArOCH$_A$$H_B$-), 1.90 − 1.78 (m, 4H, -CH_2-), 1.58 − 1.47 (m, 4H, -CH_2-), 1.45 (s, 6H, -CH_3), 1.39 (s, 6H, -CH_3), 1.32 − 1.16 (m, 68H, -CH_2-), 0.85 (t, $^3J_{H,H}$ = 6.5 Hz, 12H, -CH_3), 0.49 − 0.40 (m, 12H, -SiCH_2-), -0.11 (s, 6H, -SiCH_3). **^{29}Si-NMR** (CDCl$_3$, 80 MHz): δ / ppm = 2.76 (Si).

1,4-Bis[9-(diundecylmethylsilyl)nonyloxy]-2,5-bis{4-[4-(2,3-isopropylidene-2,3-dihydroxyprop-1-yloxy)phenylethynyl]phenylethynyl}benzene 2H9/11A
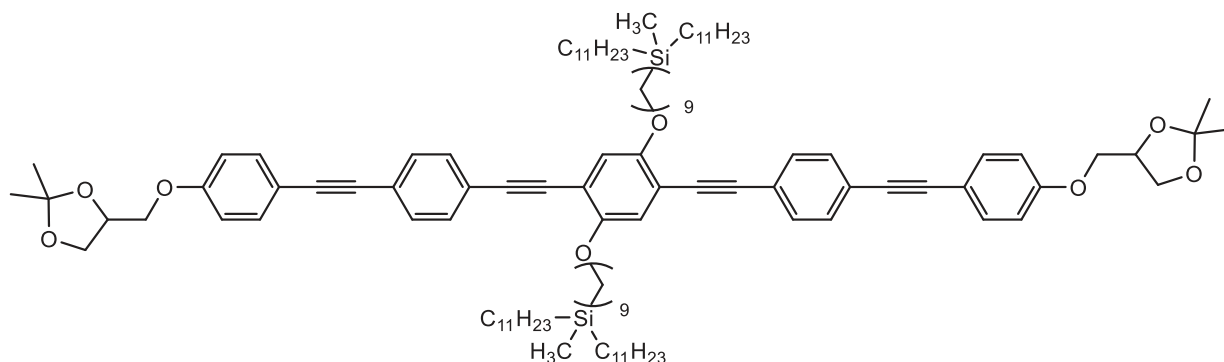

Synthesized according to GP5 from **8C9/11** (250 mg, 0.19 mmol), **25H** (138 mg, 0.42 mmol), Pd(PPh$_3$)$_4$ (6.6 mg, 5.7 · 10^{-3} mmol), CuI (1.1 mg, 5.7 · 10^{-3} mmol) in anhydrous Et$_3$N (20 mL), purification by column chromatography (eluent: CHCl$_3$); yellow solid, yield: C$_{114}$H$_{174}$O$_8$Si$_2$ M = 1728.81 g/mol, 300 mg (92 %), mp = 92 °C, **^{1}H-NMR** (CDCl$_3$, 400 MHz): δ / ppm = 7.53 − 7.43 (m, 12H, Aryl-H), 7.00 (s, 2H, Aryl-H), 6.93 − 6.86 (m, 4H, Aryl-H), 4.53 − 4.44 (m, 2H), 4.17 (dd, $^2J_{H,H}$ = 8.5, $^3J_{H,H}$ = 6.4 Hz, 2H, -OCH_AH$_B$-), 4.11 − 4.00 (m, 6H, -OCH_2-, -OCH$_A$$H_B$-), 3.97 (dd, $^2J_{H,H}$ = 9.6, $^3J_{H,H}$ = 5.9 Hz, 2H, -ArOCH_AH$_B$-), 3.91 (dd, $^2J_{H,H}$ = 8.5, $^3J_{H,H}$ = 5.8 Hz, 2H, -ArOCH$_A$$H_B$-), 1.91 − 1.82 (m, 4H, -CH_2-), 1.59 − 1.50 (m, 4H, -CH_2-), 1.47 (s, 6H, -CH_3), 1.41 (s, 6H, -CH_3), 1.39 − 1.20 (m, 92H, -CH_2-), 0.87 (t, $^3J_{H,H}$ = 6.8 Hz, 12H, -CH_3), 0.51 − 0.41 (m, 12H, -SiCH_2-), -0.10 (s, 6H, -SiCH_3). **^{29}Si-NMR** (CDCl$_3$, 79 MHz): δ / ppm = 2.77 (*Si*).

1,4-Bis[11-(diundecylmethylsilyl)undecyloxy]-2,5-bis{4-[4-(2,3-isopropylidene-2,3-dihydroxyprop-1-yloxy)phenylethynyl]phenylethynyl}benzene 2H11/11A
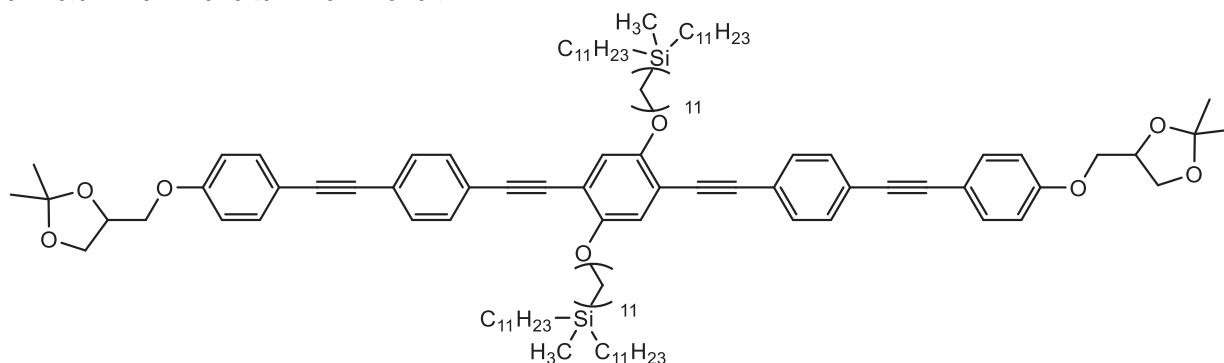

Synthesized according to GP5 from **8C11/11** (300 mg, 0.22 mmol), **25H** (159 mg, 0.48 mmol), Pd(PPh$_3$)$_4$ (16.4 mg, 14.4 · 10^{-3} mmol), CuI (2.7 mg, 14.4 · 10^{-3} mmol) in anhydrous Et$_3$N (20 mL), purification by column chromatography (eluent: CHCl$_3$); yellow solid, yield: C$_{118}$H$_{182}$O$_8$Si$_2$ M = 1784.92 g/mol, 370 mg (95 %), mp = 75 °C, **^{1}H-NMR** (CDCl$_3$, 400 MHz): δ / ppm = 7.56 − 7.43 (m, 12H, Aryl-H), 7.01 (s, 2H, Aryl-H), 6.93 − 6.87 (m, 4H, Aryl-H), 4.54 − 4.44 (m, 2H, -CHO-), 4.18 (dd, $^2J_{H,H}$ = 8.5, $^3J_{H,H}$ = 6.4 Hz, 2H, -OCH_AH$_B$-), 4.07 (dd, $^2J_{H,H}$ = 9.4, $^3J_{H,H}$ = 4.0 Hz, 2H, -OCH$_A$$H_B$-), 4.03 (t, $^3J_{H,H}$ = 6.5 Hz, 4H, -OCH_2-), 3.97 (dd, $^2J_{H,H}$ = 9.5, $^3J_{H,H}$ = 5.9 Hz, 2H, ArOCH_AH$_B$-), 3.91 (dd, $^2J_{H,H}$ = 8.5, $^3J_{H,H}$ = 5.8 Hz, 2H, ArOCH$_A$$H_B$-), 1.92 − 1.78 (m, 4H, -CH_2-), 1.60 − 1.49 (m, 4H, -CH_2-), 1.47 (s, 6H, -CH_3), 1.41 (s, 6H, -CH_3), 1.35 − 1.16 (m, 100H, -CH_2-), 0.88 (t, $^3J_{H,H}$ = 6.8 Hz, 12H, -CH_3), 0.50 − 0.42 (m, 12H, -SiCH_2-), -0.10 (s, 6H, -SiCH_3). **^{29}Si-NMR** (CDCl$_3$, 79 MHz): δ / ppm = 2.77 (*Si*).

1,4-Bis[5-(trioctylsilyl)pentyloxy]-2,5-bis{4-[4-(2,3-isopropylidene-2,3-dihydroxyprop-1-yloxy)phenylethynyl]phenylethynyl}benzene 1H5/8A
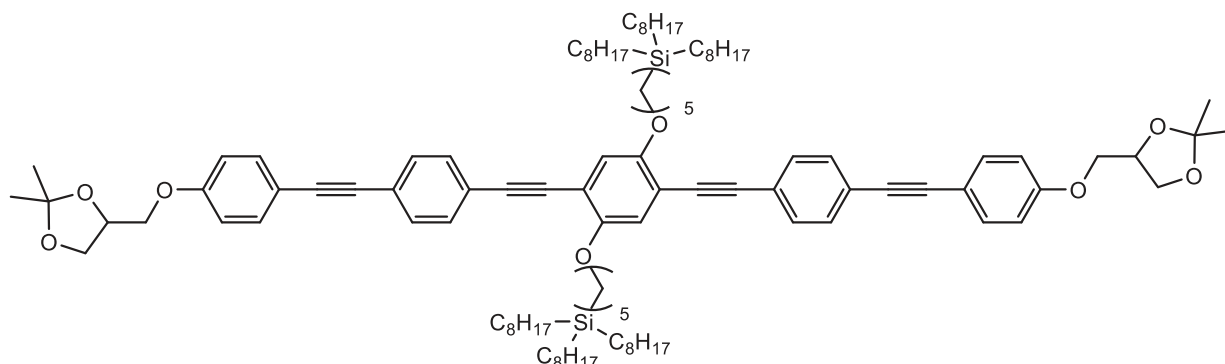

Synthesized according to GP5 from **8B5/8** (200 mg, 0.16 mmol), **25H** (115 mg, 0.36 mmol), Pd(PPh$_3$)$_4$ (5.5 mg, 4.8 · 10^{-3} mmol), CuI (0.9 mg, 4.8 · 10^{-3} mmol) in anhydrous Et$_3$N (20 mL), purification by column chromatography (eluent: CHCl$_3$); yellow solid, yield: C$_{108}$H$_{162}$O$_8$Si$_2$ M = 1643.18g/mol, 220 mg (83 %), mp = 108 °C, **^{1}H-NMR** (CDCl$_3$, 402 MHz): δ / ppm = 7.50 − 7.42 (m, 12H, Aryl-*H*), 6.99 (s, 2H, Aryl-*H*), 6.91 − 6.84 (m, 4H, Aryl-*H*), 4.51 − 4.43 (m, 2H, -C*H*O-), 4.17 (dd, $^2J_{H,H}$ = 8.8, $^3J_{H,H}$ = 6.3 Hz, 2H, -OC*H*$_A$H$_B$-), 4.06 (dd, $^2J_{H,H}$ = 9.4, $^3J_{H,H}$ = 5.0 Hz, 2H, -OCH$_A$*H*$_B$-), 4.01 (t, $^3J_{H,H}$ = 6.4 Hz, 4H, -OC*H*$_2$-), 3.95 (dd, $^2J_{H,H}$ = 9.6, $^3J_{H,H}$ = 5.9 Hz, 2H, -ArOC*H*$_A$H$_B$-), 3.89 (dd, $^2J_{H,H}$ = 8.5, $^3J_{H,H}$ = 5.8 Hz, 2H, -ArOCH$_A$*H*$_B$-), 1.88 − 1.79 (m, 4H, -C*H*$_2$-), 1.61 − 1.50 (m, 4H, -C*H*$_2$-), 1.45 (s, 6H, -C*H*$_3$), 1.39 (s, 6H, -C*H*$_3$), 1.31 − 1.18 (m, 76H, -C*H*$_2$-), 0.85 (t, $^3J_{H,H}$ = 6.7 Hz, 18H, -C*H*$_3$), 0.54 − 0.42 (m, 16H, -SiC*H*$_2$-). **^{29}Si-NMR** (CDCl$_3$, 80 MHz): δ / ppm = 2.88 (*Si*).

1,4-Bis[8-(trihexylsilyl)octyloxy]-2,5-bis{4-[4-(2,3-isopropylidene-2,3-dihydroxyprop-1-yloxy)phenylethynyl]phenylethynyl}benzene 1H8/6A
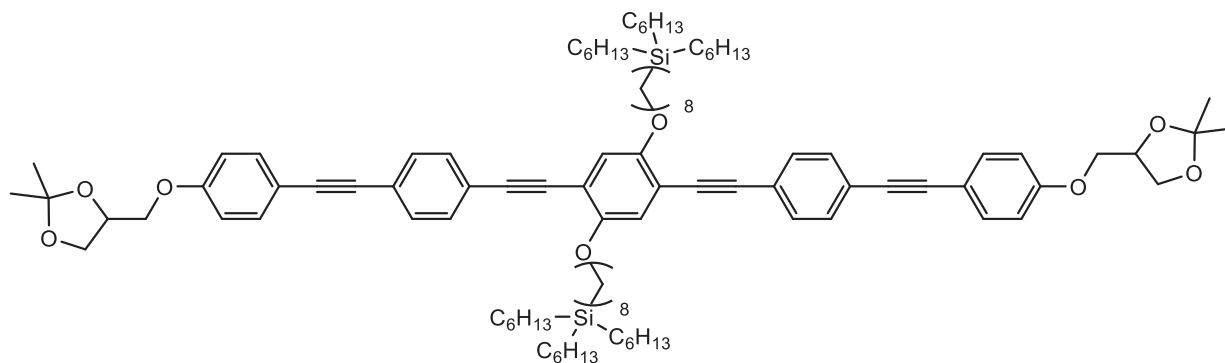

Synthesized according to GP5 from **8B8/6** (200 mg, 0.17 mmol), **25H** (127 mg, 0.38 mmol), Pd(PPh$_3$)$_4$ (5.9 mg, 5.1 · 10^{-3} mmol), CuI (1.0 mg, 5.9 · 10^{-3} mmol) in anhydrous Et$_3$N (20 mL), purification by column chromatography (eluent: CHCl$_3$); yellow solid, yield: C$_{102}$H$_{150}$O$_8$Si$_2$ M = 1560.48 g/mol, 230 mg (85 %), mp = 92 °C, **^{1}H-NMR** (CDCl$_3$, 400 MHz): δ / ppm = 7.51 − 7.44 (m, 12H, Aryl-*H*), 7.01 (s, 2H, Aryl-*H*), 6.92 − 6.86 (m, 4H, Aryl-*H*), 4.53 − 4.44 (m, 2H, -C*H*O-), 4.17 (dd, $^2J_{H,H}$ = 8.5, $^3J_{H,H}$ = 6.4 Hz, 2H, -OC*H*$_A$H$_B$-), 4.08 − 4.00 (m, 6H, -OC*H*$_2$-, -OCH$_A$*H*$_B$-), 3.96 (dd, $^2J_{H,H}$ = 9.5, $^3J_{H,H}$ = 5.9 Hz, 2H, -ArOC*H*$_A$H$_B$-), 3.91 (dd, $^2J_{H,H}$ = 8.5, $^3J_{H,H}$ = 5.8 Hz, 2H, -ArOCH$_A$*H*$_B$-), 1.93 − 1.80 (m, 4H, -C*H*$_2$-), 1.59 − 1.50 (m, 4H, -C*H*$_2$-), 1.47 (s, 6H, -C*H*$_3$), 1.41 (s, 6H, -C*H*$_3$), 1.39 − 1.17 (m, 64H, -C*H*$_2$-), 0.88 (t, $^3J_{H,H}$ = 6.2 Hz, 18H, -C*H*$_3$), 0.52 − 0.41 (m, 16H, -SiC*H*$_2$-). **^{29}Si-NMR** (CDCl$_3$, 79 MHz): δ / ppm = 2.88 (*Si*).

1,4-Bis[9-(tripentylsilyl)nonyloxy]-2,5-bis{4-[4-(2,3-isopropylidene-2,3-dihydroxyprop-1-yloxy)phenylethynyl]phenylethynyl}benzene 1H9/5A
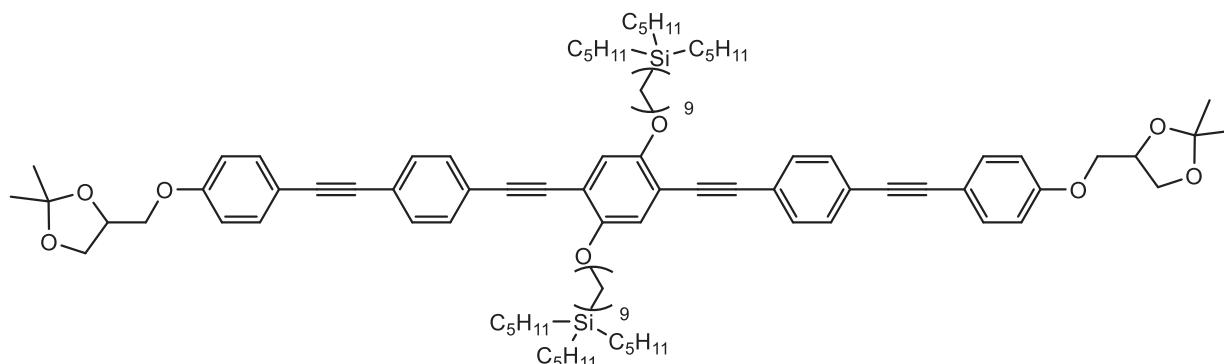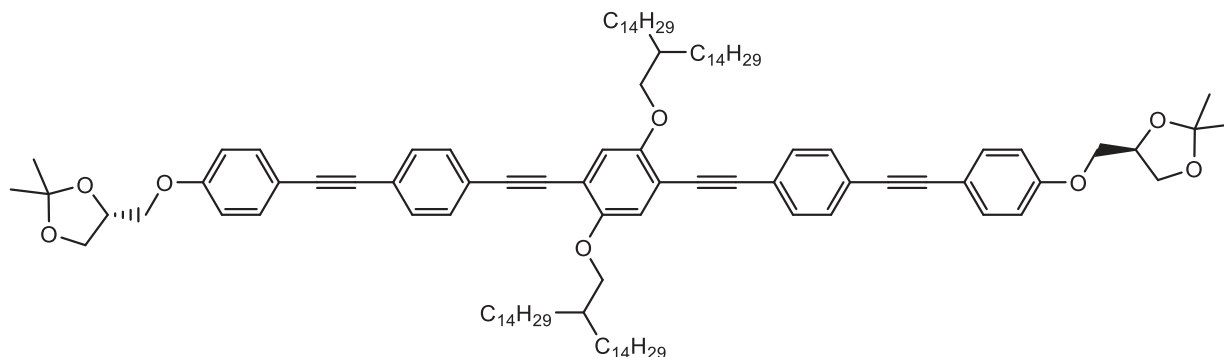

Synthesized according to GP5 from **8B9/5** (200 mg, 0.18 mmol), **25H** (134 mg, 0.40 mmol), Pd(PPh$_3$)$_4$ (6.2 mg, $5.4 \cdot 10^{-3}$ mmol), CuI (1.0 mg, $5.4 \cdot 10^{-3}$ mmol) in anhydrous Et$_3$N (20 mL), purification by column chromatography (eluent: CHCl$_3$); yellow solid, yield: C$_{98}$H$_{142}$O$_8$Si$_2$ M = 1504.38 g/mol, 220 mg (80 %), mp = 103 °C, **^{1}H-NMR** (CDCl$_3$, 400 MHz): δ / ppm = 7.51 − 7.44 (m, 12H, Aryl-H), 7.01 (s, 2H, Aryl-H), 6.92 − 6.87 (m, 4H, Aryl-H), 4.52 − 4.44 (m, 2H, -CHO-), 4.17 (dd, $^2J_{H,H}$ = 8.5, $^3J_{H,H}$ = 6.4 Hz, 2H, -OCH_AH$_B$-), 4.07 (dd, $^2J_{H,H}$ = 9.5, $^3J_{H,H}$ = 5.4 Hz, 2H, -OCH$_A$$H_B$-), 4.03 (t, $^3J_{H,H}$ = 6.5 Hz, 4H, -OCH_2-), 3.97 (dd, $^2J_{H,H}$ = 9.5, $^3J_{H,H}$ = 5.8 Hz, 2H, -ArOCH_AH$_B$-), 3.91 (dd, $^2J_{H,H}$ = 8.5, $^3J_{H,H}$ = 5.8 Hz, 2H, -ArOCH$_A$$H_B$-), 1.90 − 1.81 (m, 4H, -CH_2-), 1.59 − 1.50 (m, 4H, -CH_2-), 1.47 (s, 6H, -CH_3), 1.41 (s, 6H, -CH_3), 1.35 − 1.20 (m, 56H, -CH_2-), 0.88 (t, $^3J_{H,H}$ = 7.0 Hz, 18H, -CH_3), 0.50 − 0.42 (m, 16H, -SiCH_2-). **^{29}Si-NMR** (CDCl$_3$, 79 MHz): δ / ppm = 2.92 (*Si*).

(R,R)-1,4-Bis(2-tetradecylhexadecyloxy)-2,5-bis{4-[4-(2,3-isopropylidene-2,3-dihydroxyprop-1-yloxy)phenylethynyl]phenylethynyl}benzene *5H1/14A

Synthesized according to GP5 from **5/1/14** (310 mg, 0.26 mmol), **27H*** (189 mg, 0.57 mmol), Pd(PPh$_3$)$_4$ (9.0 mg, $7.8 \cdot 10^{-3}$ mmol), CuI (1.5 mg, $7.8 \cdot 10^{-3}$ mmol) in anhydrous Et$_3$N (20 mL), purification by column chromatography (eluent: CHCl$_3$); yellow solid, yield: C$_{110}$H$_{162}$O$_8$Si$_2$ M = 1612.50 g/mol, 275 mg (67 %), mp = 118 °C, **^{1}H-NMR** (CDCl$_3$, 400 MHz): δ / ppm = 7.53 − 7.43 (m, 12H, Aryl-H), 7.00 (s, 2H, Aryl-H), 6.92 − 6.86 (m, 4H, Aryl-H), 4.54 − 4.44 (m, 2H, -CHO-), 4.18 (dd, $^2J_{H,H}$ = 8.5, $^3J_{H,H}$ = 6.4 Hz, 2H, -OCH_AH$_B$-), 4.08 (dd, $^2J_{H,H}$ = 9.0, $^3J_{H,H}$ = 5.7 Hz, 2H, -OCH$_A$$H_B$-), 3.97 (dd, $^2J_{H,H}$ = 9.6, $^3J_{H,H}$ = 5.9 Hz, 2H, -ArOCH_AH$_B$-), 3.94 − 3.89 (m, 6H, -OCH_2-, -OCH$_A$$H_B$-), 1.90 − 1.80 (m, 2H, -CH-), 1.62 − 1.50 (m, 8H, -CH_2-), 1.47 (s, 6H, -CH_3), 1.41 (s, 6H, -CH_3), 1.39 − 1.16 (m, 96H, -CH_2-), 0.87 (t, $^3J_{H,H}$ = 6.8 Hz, 12H, -CH_3).

1,4-Bis(2-pentadecylheptadecyloxy)-2,5-bis{4-[4-(2,3-isopropylidene-2,3-dihydroxyprop-1-yloxy)phenylethynyl]phenylethynyl}benzene 5H1/15A
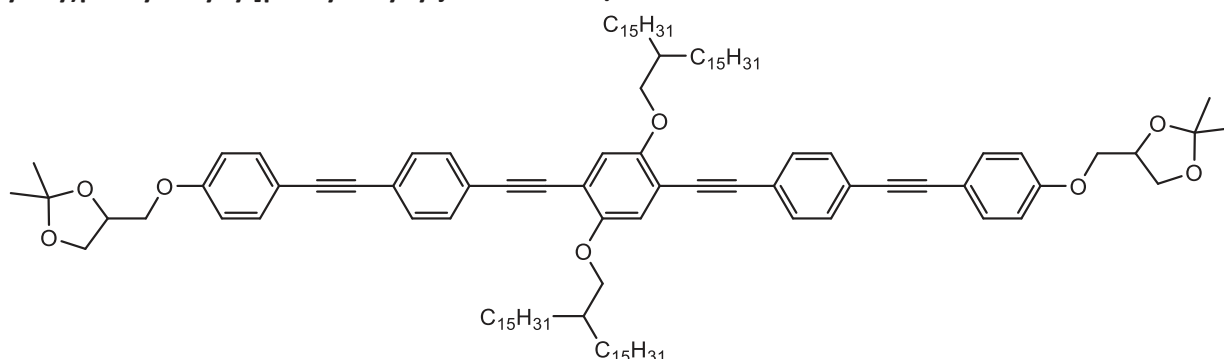
Synthesized according to GP5 from **5/1/15** (200 mg, 0.16 mmol), **25H** (116 mg, 0.25 mmol), Pd(PPh$_3$)$_4$ (5.5 mg, $4.8 \cdot 10^{-3}$ mmol), CuI (0.9 mg, $4.8 \cdot 10^{-3}$ mmol) in anhydrous Et$_3$N (20 mL), purification by column chromatography (eluent: CHCl$_3$); yellow solid, yield: C$_{114}$H$_{170}$O$_8$Si$_2$ M = 1668.61 g/mol, 170 mg (64 %), mp = 117 °C, **^{1}H-NMR** (CDCl$_3$, 400 MHz): δ / ppm = 7.49 − 7.43 (m, 12H, Aryl-*H*), 6.99 (s, 2H, Aryl-*H*), 6.92 − 6.87 (m, 4H, Aryl-*H*), 4.52 − 4.45 (m, 2H, -C*H*O-), 4.17 (dd, $^2J_{H,H}$ = 8.5, $^3J_{H,H}$ = 6.4 Hz, 2H, -OC*H$_A$*H$_B$-), 4.07 (dd, $^2J_{H,H}$ = 9.5, $^3J_{H,H}$ = 5.7 Hz, 2H, -OCH$_A$*H$_B$*-), 3.96 (dd, $^2J_{H,H}$ = 9.6, $^3J_{H,H}$ = 5.9 Hz, 2H, -ArOC*H$_A$*H$_B$-), 3.93 − 3.88 (m, 6H, -OC*H$_2$*-, -ArOCH$_A$*H$_B$*-), 1.90 − 1.80 (m, 2H, -C*H*-), 1.66 − 1.58 (m, 8H, -C*H$_2$*-), 1.47 (s, 6H, -C*H$_3$*), 1.41 (s, 6H, -C*H$_3$*), 1.32 − 1.19 (m, 104H, -C*H$_2$*-), 0.87 (t, $^3J_{H,H}$ = 6.7 Hz, 12H, -C*H$_3$*).

(*R*,*R*)-1,4-Bis(2-hexadecyloctadecyloxy)-2,5-bis{4-[4-(2,3-isopropylidene-2,3-dihydroxyprop-1-yloxy)phenylethynyl]phenylethynyl}benzene *5H1/16A
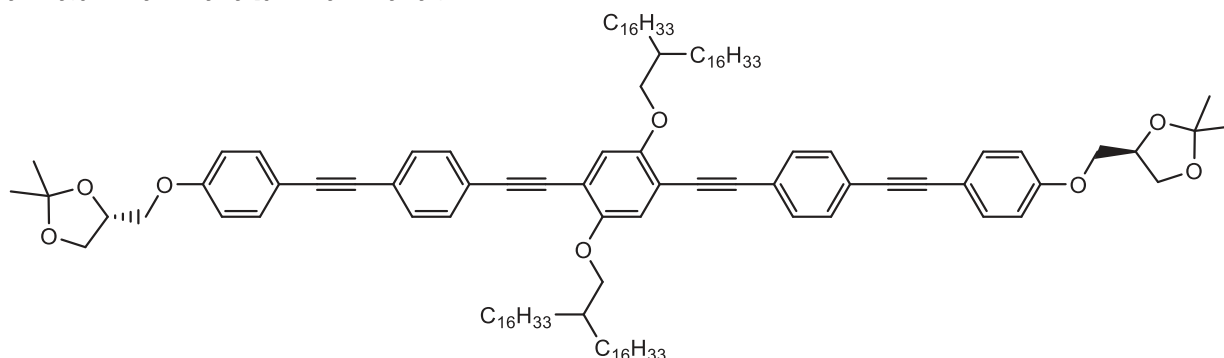

Synthesized according to GP5 from **5/1/16** (440 mg, 0.33 mmol), **27H*** (240 mg, 0.72 mmol), Pd(PPh$_3$)$_4$ (11.4 mg, $9.9 \cdot 10^{-3}$ mmol), CuI (1.9 mg, $9.9 \cdot 10^{-3}$ mmol) in anhydrous Et$_3$N (20 mL), purification by column chromatography (eluent: CHCl$_3$); yellow solid, yield: C$_{118}$H$_{178}$O$_8$Si$_2$ M = 1724.71 g/mol, 330 mg (57 %), mp = 122 °C, **^{1}H-NMR** (CDCl$_3$, 500 MHz): δ / ppm = 7.51 − 7.43 (m, 12H, Aryl-*H*), 7.00 (s, 2H, Aryl-*H*), 6.93 − 6.87 (m, 4H, Aryl-*H*), 4.52 − 4.45 (m, 2H, -C*H*O-), 4.18 (dd, $^2J_{H,H}$ = 9.1, $^3J_{H,H}$ = 5.4 Hz, 2H, -OC*H$_A$*H$_B$-), 4.08 (dd, $^2J_{H,H}$ = 9.5, $^3J_{H,H}$ = 5.4 Hz, 2H, -OCH$_A$*H$_B$*-), 3.97 (dd, $^2J_{H,H}$ = 9.5, $^3J_{H,H}$ = 5.9 Hz, 2H, -ArOC*H$_A$*H$_B$-), 3.94 − 3.88 (m, 6H, -OC*H$_2$*-, -ArOCH$_A$*H$_B$*-), 1.90 − 1.79 (m, 2H, -C*H*-), 1.61 − 1.50 (m, 8H, -C*H$_2$*-), 1.47 (s, 6H, -C*H$_3$*), 1.41 (s, 6H, -C*H$_3$*), 1.38 − 1.19 (m, 112H, -C*H$_2$*-), 0.87 (t, $^3J_{H,H}$ = 6.9 Hz, 12H, -C*H$_3$*).

1,4-Bis(4-tetradecyloctadecyloxy)-2,5-bis{4-[4-(2,3-isopropylidene-2,3-dihydroxyprop-1-yloxy)phenylethynyl]phenylethynyl}benzene 5H3/14A
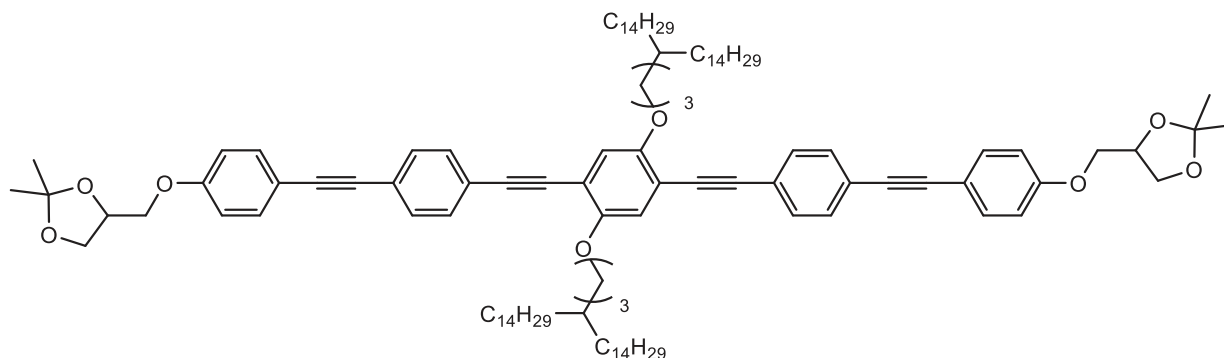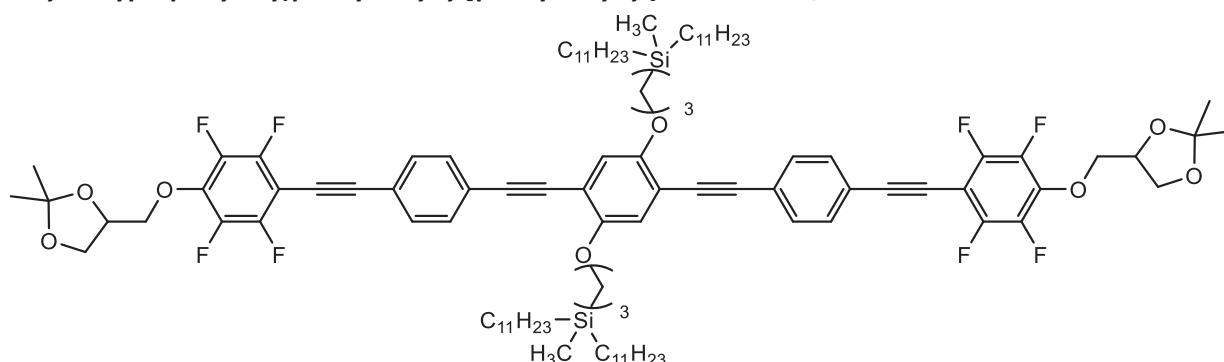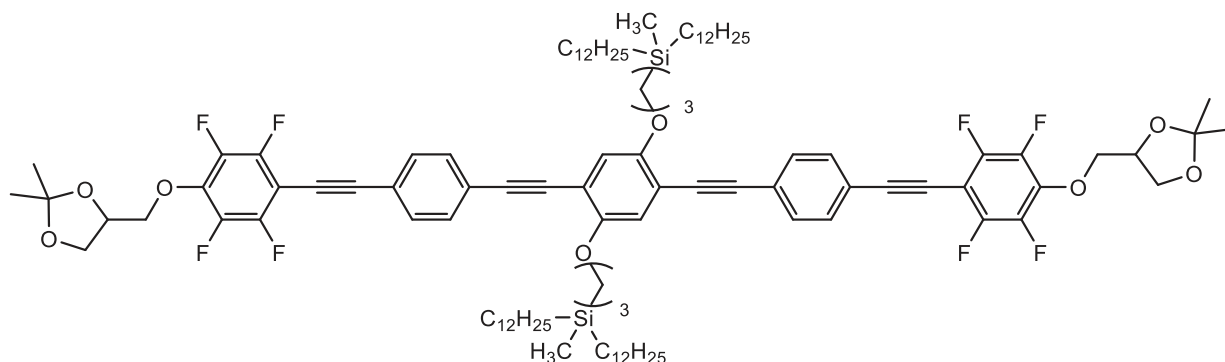

Synthesized according to GP5 from **5/3/14** (360 mg, 0.41 mmol), **25H** (207 mg, 0.82 mmol), Pd(PPh$_3$)$_4$ (14.2 mg, 12.3 · 10^{-3} mmol), CuI (2.3 mg, 12.3 · 10^{-3} mmol) in anhydrous Et$_3$N (20 mL), purification by column chromatography (eluent: CHCl$_3$); yellow solid, yield: C$_{114}$H$_{170}$O$_8$Si$_2$ *M* = 1668.61 g/mol, 251 mg (77 %), *mp* = 120 °C, **^{1}H-NMR** (CDCl$_3$, 400 MHz): δ / ppm 7.53 − 7.42 (m, 12H, Aryl-*H*), 7.00 (s, 2H, Aryl-*H*), 6.93 − 6.86 (m, 4H, Aryl-*H*), 4.52 − 4.45 (m, 2H, -C*H*O-), 4.17 (dd, $^2J_{H,H}$ = 8.5, $^3J_{H,H}$ = 6.4 Hz, 2H, -OC*H*$_A$H$_B$-), 4.07 (dd, $^2J_{H,H}$ = 9.5, $^3J_{H,H}$ = 5.4 Hz, 2H, -OCH$_A$*H*$_B$-), 4.02 (t, $^3J_{H,H}$ = = 6.3 Hz, 4H, -OC*H*$_2$-), 3.96 (dd, $^2J_{H,H}$ = 9.6, $^3J_{H,H}$ = 5.9 Hz, 2H, -ArOC*H*$_A$H$_B$-), 3.91 (dd, $^2J_{H,H}$ = 8.5, $^3J_{H,H}$ = 5.8 Hz, 2H, -ArOCH$_A$*H*$_B$-), 1.87 − 1.78 (m, 4H, -C*H*$_2$-), 1.47 (s, 6H, -C*H*$_3$), 1.41 (s, 6H, -C*H*$_3$), 1.38 − 1.33 (m, 2H, -C*H*-), 1.24 (s, 108H, -C*H*$_2$-), 0.87 (t, $^3J_{H,H}$ = = 6.7 Hz, 12H, -C*H*$_3$).

1,4-Bis[3-(diundecylmethylsilyl)porpyloxy]-2,5-bis{4-[2,3,5,6-tetrafluoro-4-(2,3-isopropylidene-2,3-dihydroxyprop-1-yloxy)phenylethynyl]phenylethynyl}benzene 2F3/11A

Synthesized according to GP5 from **11C-1** (250 mg, 0.22 mmol), **26F** (193 mg, 0.48 mmol), Pd(PPh$_3$)$_4$ (7.6 mg, 6.6 · 10^{-3} mmol), CuI (1.3 mg, 6.6 · 10^{-3} mmol) in anhydrous Et$_3$N (20 mL), purification by column chromatography (eluent: CHCl$_3$); yellow solid, yield: C$_{102}$H$_{142}$F$_8$O$_8$Si$_2$ *M* = 1704.41 g/mol, 360 mg (97 %), *mp* = 58 °C, **^{1}H-NMR** (CDCl$_3$, 502 MHz): δ / ppm = 7.58 − 7.50 (m, 8H, Aryl-*H*), 7.01 (s, 2H, Aryl-*H*), 4.49 − 4.44 (m, 2H, -C*H*O-), 4.33 (dd, $^2J_{H,H}$ = 10.2, $^3J_{H,H}$ = 5.1 Hz, 2H, -OC*H*$_A$H$_B$-), 4.24 (dd, $^2J_{H,H}$ = 10.2, $^3J_{H,H}$ = 5.6 Hz, 2H, -OCH$_A$*H*$_B$-), 4.16 (dd, $^2J_{H,H}$ = 8.6, $^3J_{H,H}$ = 6.4 Hz, 2H, -ArOC*H*$_A$H$_B$-), 4.03 − 3.93 (m, 6H, -OC*H*$_2$-, ArOCH$_A$*H*$_B$-), 1.88 − 1.80 (m, 4H, -C*H*$_2$-), 1.44 (s, 6H, -C*H*$_3$), 1.39 (s, 6H, -C*H*$_3$), 1.34 − 1.18 (m, 72H, -C*H*$_2$-), 0.87 (t, $^3J_{H,H}$ = 7.2 Hz, 12H, -C*H*$_3$), 0.74 − 0.67 (m, 4H, -SiC*H*$_2$-), 0.56 − 0.45 (m, 8H, -SiC*H*$_2$-), -0.03 (s, 6H, -SiC*H*$_3$). **^{19}F-NMR** (CDCl$_3$, 473 MHz): δ / ppm = -137.40 − -137.58 (m, Aryl-F), -156.82 − -156.99 (m, Aryl-F). **^{29}Si-NMR** (CDCl$_3$, 100 MHz): δ / ppm = 3.44 (*Si*).

1,4-Bis[3-(didodecylmethylsilyl)propyloxy]-2,5-bis{4-[2,3,5,6-tetrafluoro-4-(2,3-isopropylidene-2,3-dihydroxyprop-1-yloxy)phenylethynyl]phenylethynyl}benzene 2F3/12A

Synthesized according to GP5 from **11C-2** (200 mg, 0.17 mmol), **26F** (147 mg, 0.36 mmol), Pd(PPh$_3$)$_4$ (5.9 mg, 5.1 · 10^{-3} mmol), CuI (1.0 mg, 5.1 · 10^{-3} mmol) in anhydrous Et$_3$N (20 mL), purification by column chromatography (eluent: CHCl$_3$); yellow solid, yield: C$_{106}$H$_{150}$F$_8$O$_8$Si$_2$ M = 1760.52 g/mol, 285 mg (98 %), mp = 72 °C, **^{1}H-NMR** (CDCl$_3$, 400 MHz): δ / ppm = 7.56 − 7.52 (m, 8H, Aryl-*H*), 7.01 (s, 2H, Aryl-*H*), 4.50 − 4.42 (m, 2H, -C*H*O-), 4.33 (dd, $^2J_{H,H}$ = 10.1, $^3J_{H,H}$ = 5.1 Hz, 2H, -OC*H$_A$*H$_B$-), 4.23 (dd, $^2J_{H,H}$ = 10.1, $^3J_{H,H}$ = 5.6 Hz, 2H, -OCH$_A$*H$_B$*-), 4.16 (dd, $^2J_{H,H}$ = 8.6, $^3J_{H,H}$ = 6.4 Hz, 2H, -ArOC*H$_A$*H$_B$-), 4.03 − 3.93 (m, 6H, -OC*H$_2$*-, ArOCH$_A$*H$_B$*-), 1.89 − 1.79 (m, 4H, -C*H$_2$*-), 1.43 (s, 6H, -C*H$_3$*), 1.38 (s, 6H, -C*H$_3$*), 1.34 − 1.18 (m, 80H, -C*H$_2$*-), 0.87 (t, $^3J_{H,H}$ = 6.8 Hz, 12H, -C*H$_3$*), 0.74 − 0.67 (m, 4H, -SiC*H$_2$*-), 0.55 − 0.46 (m, 8H, -SiC*H$_2$*-), -0.03 (s, 6H, -SiC*H$_3$*). **^{19}F-NMR** (CDCl$_3$, 376 MHz): δ / ppm = -137.30 − -137.74 (m, Aryl-*F*), -156.65 − -157.08 (m, Aryl-*F*). **^{29}Si-NMR** (CDCl$_3$, 79 MHz): δ / ppm = 3.37 (*Si*).

1,4-Bis[3-(ditetradecylmethylsilyl)propyloxy]-2,5-bis{4-[2,3,5,6-tetrafluoro-4-(2,3-isopropylidene-2,3-dihydroxyprop-1-yloxy)phenylethynyl]phenylethynyl}benzene 2F3/14A
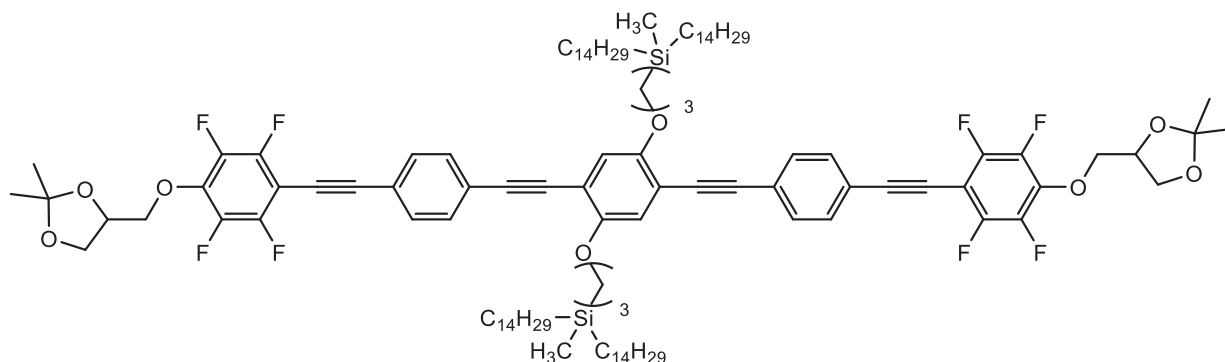

Synthesized according to GP5 from **11C-3** (360 mg, 0.27 mmol), **26F** (243 mg, 0.60 mmol), Pd(PPh$_3$)$_4$ (9.4 mg, 8.1 · 10^{-3} mmol), CuI (1.5 mg, 8.1 · 10^{-3} mmol) in anhydrous Et$_3$N (20 mL), purification by column chromatography (eluent: CHCl$_3$); yellow solid, yield: C$_{114}$H$_{166}$F$_8$O$_8$Si$_2$ M = 1872.73 g/mol, 370 mg (72 %), mp = 41 °C, **^{1}H-NMR** (CDCl$_3$, 500 MHz): δ / ppm = 7.57 − 7.53 (m, 8H, Aryl-*H*), 7.03 (s, 2H, Aryl-*H*), 4.51 − 4.44 (m, 2H, -C*H*O-), 4.35 (dd, $^2J_{H,H}$ = 10.2, $^3J_{H,H}$ = 5.0 Hz, 2H, -OC*H$_A$*H$_B$-), 4.25 (dd, $^2J_{H,H}$ = 10.2, $^3J_{H,H}$ = 5.6 Hz, 2H, -OCH$_A$*H$_B$*-), 4.17 (dd, $^2J_{H,H}$ = 8.6, $^3J_{H,H}$ = 6.4 Hz, 2H, -ArOC*H$_A$*H$_B$-), 4.04 − 3.95 (m, 6H, -OC*H$_2$*-, ArOCH$_A$*H$_B$*-), 1.90 − 1.82 (m, 4H, -C*H$_2$*-), 1.44 (s, 6H, -C*H$_3$*), 1.40 (s, 6H, -C*H$_3$*), 1.34 − 1.20 (m, 96H, -C*H$_2$*-), 0.89 (t, $^3J_{H,H}$ = 7.1 Hz, 12H, -C*H$_3$*), 0.76 − 0.70 (m, 4H, -SiC*H$_2$*-), 0.58 − 0.46 (m, 8H, -SiC*H$_2$*-), -0.01 (s, 6H, -SiC*H$_3$*). **^{19}F-NMR** (CDCl$_3$, 470 MHz): δ / ppm = -137.36 − -137.59 (m, Aryl-*F*), -156.80 − -156.98 (m, Aryl-*F*). **^{29}Si-NMR** (CDCl$_3$, 99 MHz): δ / ppm = 3.39 (*Si*).

1,4-Bis[4-(didecylmethylsilyl)butyloxy]-2,5-bis{4-[2,3,5,6-tetrafluoro-4-(2,3-isopropylidene-2,3-dihydroxyprop-1-yloxy)phenylethynyl]phenylethynyl}benzene 2F4/10A
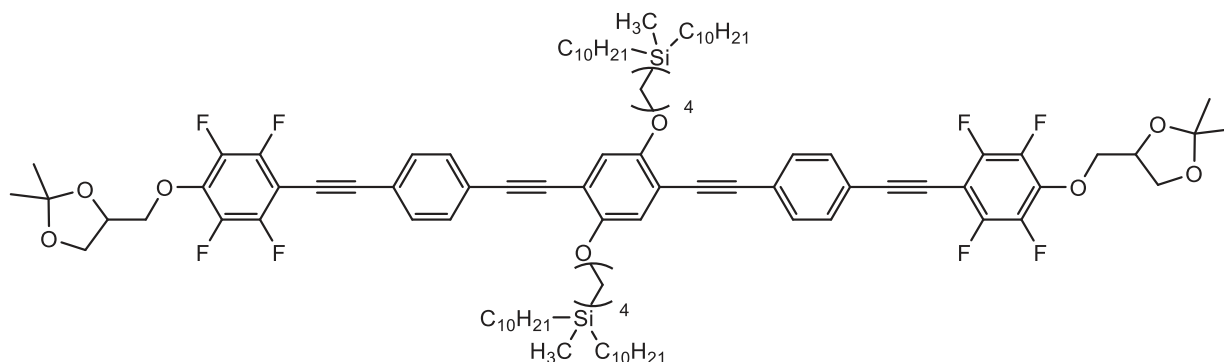

Synthesized according to GP5 from **8C4/10** (200 mg, 0.18 mmol), **26F** (158 mg, 0.39 mmol), Pd(PPh$_3$)$_4$ (6.2 mg, 5.4 · 10^{-3} mmol), CuI (1.0 mg, 5.4 · 10^{-3} mmol) in anhydrous Et$_3$N (20 mL), purification by column chromatography (eluent: CHCl$_3$); yellow solid, yield: C$_{100}$H$_{138}$F$_8$O$_8$Si$_2$ M = 1676.35 g/mol, 250 mg (84 %), mp = 42 °C, **^{1}H-NMR** (CDCl$_3$, 402 MHz): δ / ppm = 7.58 – 7.46 (m, 8H, Aryl-*H*), 7.00 (s, 2H, Aryl-*H*), 4.47 – 4.40 (m, 2H, -C*H*O-), 4.29 (dd, $^2J_{H,H}$ = 9.4, $^3J_{H,H}$ = 5.8 Hz, 2H, -OC*H*$_A$H$_B$-), 4.22 (dd, $^2J_{H,H}$ = 10.5, $^3J_{H,H}$ = 5.3 Hz, 2H, -OCH$_A$*H*$_B$-), 4.14 (dd, $^2J_{H,H}$ = 8.6, $^3J_{H,H}$ = 6.5 Hz, 2H, -ArOC*H*$_A$H$_B$-), 4.03 (t, $^3J_{H,H}$ = 6.3 Hz, 4H, -OC*H*$_2$-), 3.94 (dd, $^2J_{H,H}$ = 8.6, $^3J_{H,H}$ = 5.6 Hz, 2H, -ArOCH$_A$*H*$_B$-), 1.92 – 1.81 (m, 4H, -C*H*$_2$-), 1.56 – 1.49 (m, 4H, -C*H*$_2$-), 1.42 (s, 6H, -C*H*$_3$), 1.37 (s, 6H, -C*H*$_3$), 1.31 – 1.15 (m, 64H, -C*H*$_2$-), 0.85 (t, $^3J_{H,H}$ = 6.4 Hz, 12H, -C*H*$_3$), 0.60 – 0.51 (m, 4H, -SiC*H*$_2$-), 0.50 – 0.41 (m, 8H, -SiC*H*$_2$-), -0.10 (s, 6H, -SiC*H*$_3$). **^{19}F-NMR** (CDCl$_3$, 378 MHz): δ / ppm = -137.46 – -137.59 (m, Aryl-*F*), -156.87 – -157.04 (m, Aryl-*F*). **^{29}Si-NMR** (CDCl$_3$, 80 MHz): δ / ppm = 2.89 (*Si*).

1,4-Bis[4-(didodecylmethylsilyl)butyloxy]-2,5-bis{4-[2,3,5,6-tetrafluoro-4-(2,3-isopropylidene-2,3-dihydroxyprop-1-yloxy)phenylethynyl]phenylethynyl}benzene F4/12A
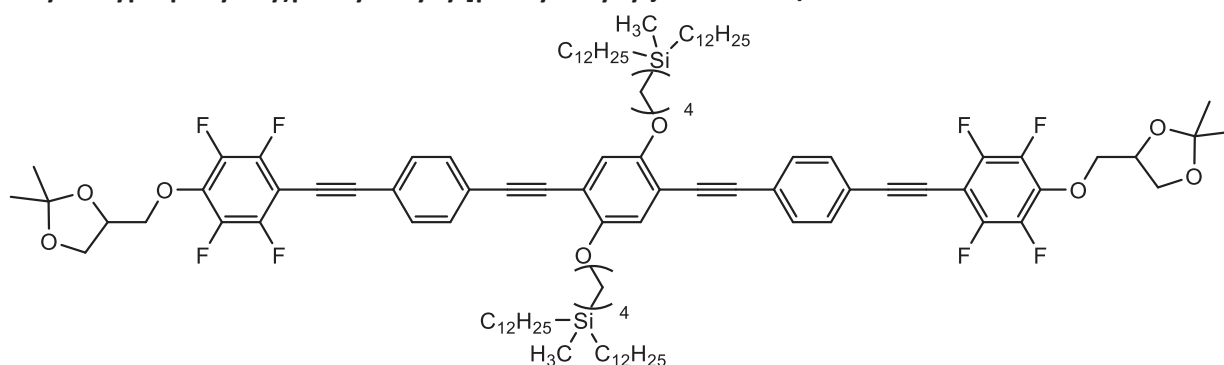

Synthesized according to GP5 from **8C4/12** (260 mg, 0.21 mmol), **26F** (187 mg, 0.46 mmol), Pd(PPh$_3$)$_4$ (7.3 mg, 6.3 · 10^{-3} mmol), CuI (1.2 mg, 6.3 · 10^{-3} mmol) in anhydrous Et$_3$N (20 mL), purification by column chromatography (eluent: CHCl$_3$); yellow solid, yield: C$_{108}$H$_{154}$F$_8$O$_8$Si$_2$ M = 1788.57 g/mol, 310 mg (83 %), mp = 110 °C, **^{1}H-NMR** (CDCl$_3$, 400 MHz): δ / ppm = 7.58 – 7.50 (m, 8H, Aryl-*H*), 7.02 (s, 2H, Aryl-*H*), 4.50 – 4.42 (m, 2H, -C*H*O-), 4.35 (dd, $^2J_{H,H}$ = 10.2, $^3J_{H,H}$ = 4.8 Hz, 2H, -OC*H*$_A$H$_B$-), 4.24 (dd, $^2J_{H,H}$ = 10.1, $^3J_{H,H}$ = 5.7 Hz, 2H, -OCH$_A$*H*$_B$-), 4.16 (dd, $^2J_{H,H}$ = 8.6, $^3J_{H,H}$ = 6.4 Hz, 2H, -ArOC*H*$_A$H$_B$-), 4.05 (t, $^3J_{H,H}$ = 6.4 Hz, 4H, -OC*H*$_2$-), 3.96 (dd, $^2J_{H,H}$ = 8.6, $^3J_{H,H}$ = 5.6 Hz, 2H, -ArOCH$_A$*H*$_B$-), 1.93 – 1.81 (m, 4H, -C*H*$_2$-), 1.60 – 1.48 (m, 4H, -C*H*$_2$-), 1.43 (s, 6H, -C*H*$_3$), 1.39 (s, 6H, -C*H*$_3$), 1.33 – 1.15 (m, 80H, -C*H*$_2$-), 0.87 (t, $^3J_{H,H}$ = 6.8 Hz, 12H, -C*H*$_3$), 0.64 – 0.53 (m, 4H, -SiC*H*$_2$-), 0.52 – 0.42 (m, 8H, -SiC*H*$_2$-), -0.08 (s, 6H, -SiC*H*$_3$). **^{19}F-NMR** (CDCl$_3$, 376 MHz): δ / ppm = -137.36 – -137.61 (m, Aryl-*F*), -156.79 – -157.01 (m, Aryl-*F*). **^{29}Si-NMR** (CDCl$_3$, 79 MHz): δ / ppm = 2.91 (*Si*).

1,4-Bis[4-(ditetradeylmethylsilyl)butyloxy]-2,5-bis{4-[2,3,5,6-tetrafluoro-4-(2,3-isopropylidene-2,3-dihydroxyprop-1-yloxy)phenylethynyl]phenylethynyl}benzene 2F4/14A
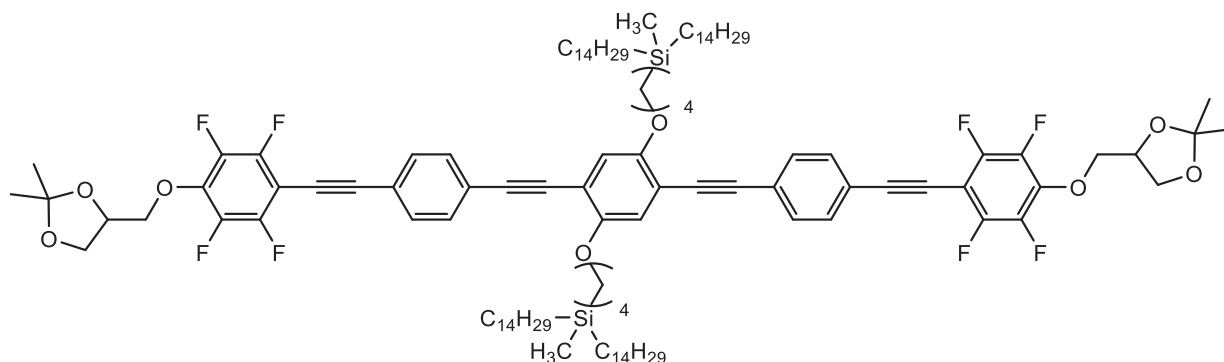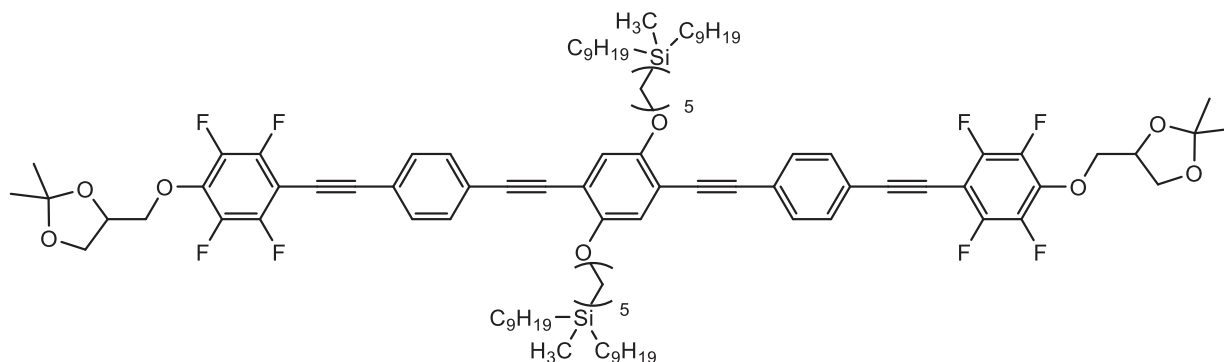

Synthesized according to GP5 from **8C4/14** (200 mg, 0.15 mmol), **26F** (132 mg, 0.33 mmol), Pd(PPh$_3$)$_4$ (5.2 mg, 4.5 · 10^{-3} mmol), CuI (0.9 mg, 4.5 · 10^{-3} mmol) in anhydrous Et$_3$N (20 mL), purification by column chromatography (eluent: CHCl$_3$); yellow solid, yield: C$_{116}$H$_{170}$F$_8$O$_8$Si$_2$ M = 1900.79 g/mol, 170 mg (60 %), mp = 97 °C, **^{1}H-NMR** (CDCl$_3$, 500 MHz): δ / ppm = 7.58 − 7.50 (m, 8H, Aryl-H), 7.02 (s, 2H, Aryl-H), 4.50 − 4.43 (m, 2H, -CHO-), 4.34 (dd, $^2J_{H,H}$ = 10.1, $^3J_{H,H}$ = 5.1 Hz, 2H, -OCH_AH$_B$-), 4.25 (dd, $^2J_{H,H}$ = 10.2, $^3J_{H,H}$ = 5.6 Hz, 2H, -OCH$_A$$H_B$-), 4.17 (dd, $^2J_{H,H}$ = 8.6, $^3J_{H,H}$ = 6.4 Hz, 2H, -ArOCH_AH$_B$-), 4.06 (t, $^3J_{H,H}$ = 6.4 Hz, 4H, -OCH_2-), 3.97 (dd, $^2J_{H,H}$ = 8.6, $^3J_{H,H}$ = 5.6 Hz, 2H, -ArOCH$_A$$H_B$-), 1.94 − 1.85 (m, 4H, -CH_2-), 1.60 − 1.51 (m, 4H, -CH_2-), 1.44 (s, 6H, -CH_3), 1.39 (s, 6H, -CH_3), 1.34 − 1.20 (m, 96H, -CH_2-), 0.88 (t, $^3J_{H,H}$ = 6.9 Hz, 12H, -CH_3), 0.62 − 0.55 (m, 4H, -SiCH_2-), 0.52 − 0.44 (m, 8H, -SiCH_2-), -0.07 (s, 6H, -SiCH_3). **^{19}F-NMR** (CDCl$_3$, 470 MHz): δ / ppm = -136.55 − -138.35 (m, Aryl-F), -156.00 − -157.86 (m, Aryl-F). **^{29}Si-NMR** (CDCl$_3$, 99 MHz): δ / ppm = 2.92 (Si).

1,4-Bis[5-(dinonylmethylsilyl)pentyloxy]-2,5-bis{4-[2,3,5,6-tetrafluoro-4-(2,3-isopropylidene-2,3-dihydroxyprop-1-yloxy)phenylethynyl]phenylethynyl}benzene 2F5/9A

Synthesized according to GP5 from **8C5/9** (200 mg, 0.18 mmol), **26F** (162 mg, 0.40 mmol), Pd(PPh$_3$)$_4$ (6.2 mg, 5.4 · 10^{-3} mmol), CuI (1.0 mg, 5.4 · 10^{-3} mmol) in anhydrous Et$_3$N (20 mL), purification by column chromatography (eluent: CHCl$_3$); yellow solid, yield: C$_{98}$H$_{134}$F$_8$O$_8$Si$_2$ M = 1648.30 g/mol, 280 mg (93 %), mp = 54 °C, **^{1}H-NMR** (CDCl$_3$, 502 MHz): δ / ppm = 7.57 − 7.50 (m, 8H, Aryl-H), 7.02 (s, 2H, Aryl-H), 4.50 − 4.42 (m, 2H, -CHO-), 4.33 (dd, $^2J_{H,H}$ = 10.1, $^3J_{H,H}$ = 5.2 Hz, 2H, -OCH_AH$_B$-), 4.24 (dd, $^2J_{H,H}$ = 10.1, $^3J_{H,H}$ = 5.6 Hz, 2H, -OCH$_A$$H_B$-), 4.16 (dd, $^2J_{H,H}$ = 8.6, $^3J_{H,H}$ = 6.4 Hz, 2H, -ArOCH_AH$_B$-), 4.04 (t, $^3J_{H,H}$ = 6.5 Hz, 4H, -OCH_2-), 3.96 (dd, $^2J_{H,H}$ = 8.6, $^3J_{H,H}$ = 5.6 Hz, 2H, -ArOCH$_A$$H_B$-), 1.91 − 1.82 (m, 4H, -CH_2-), 1.61 − 1.52 (m, 4H, -CH_2-), 1.44 (s, 6H, -CH_3), 1.39 (s, 6H, -CH_3), 1.32 − 1.19 (m, 60H, -CH_2-), 0.87 (t, $^3J_{H,H}$ = 6.9 Hz, 12H, -CH_3), 0.57 − 0.43 (m, 12H, -SiCH_2-), -0.08 (s, 6H, -SiCH_3). **^{19}F-NMR** (CDCl$_3$, 287 MHz): δ / ppm = 137.19 − -137.36 (m, Aryl-F), -157.05 − -157.27 (m, Aryl-F). **^{29}Si-NMR** (CDCl$_3$, 100 MHz): δ / ppm = 2.79 (Si).

1,4-Bis[5-(didecylmethylsilyl)pentyloxy]-2,5-bis{4-[2,3,5,6-tetrafluoro-4-(2,3-isopropylidene-2,3-dihydroxyprop-1-yloxy)phenylethynyl]phenylethynyl}benzene 2F5/10A
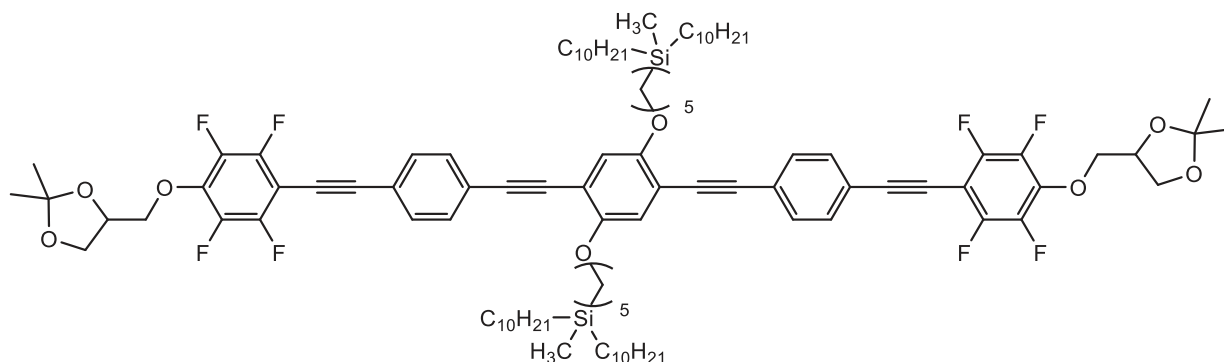
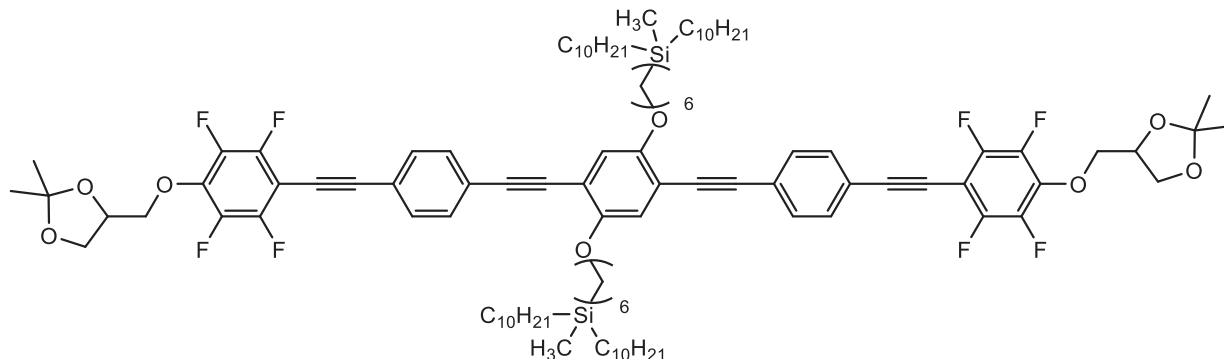

Synthesized according to GP5 from **8C5/10** (200 mg, 0.17 mmol), **26F** (155 mg, 0.38 mmol), Pd(PPh$_3$)$_4$ (5.9 mg, 5.1 · 10^{-3} mmol), CuI (1.0 mg, 5.1 · 10^{-3} mmol) in anhydrous Et$_3$N (20 mL), purification by column chromatography (eluent: CHCl$_3$); yellow solid, yield: C$_{102}$H$_{142}$F$_8$O$_8$Si$_2$ M = 1704.41 g/mol, 280 mg (94 %), *mp* = 58 °C, **^{1}H-NMR** (CDCl$_3$, 400 MHz): δ / ppm = 7.57 − 7.49 (m, 8H, Aryl-*H*), 7.01 (s, 2H, Aryl-*H*), 4.50 − 4.42 (m, 2H, -C*H*O-), 4.33 (dd, $^2J_{H,H}$ = 10.1, $^3J_{H,H}$ = 5.1 Hz, 2H, -OC*H*$_A$H$_B$-), 4.23 (dd, $^2J_{H,H}$ = 10.1, $^3J_{H,H}$ = 5.6 Hz, 2H, -OCH$_A$*H*$_B$-), 4.16 (dd, $^2J_{H,H}$ = 8.6, $^3J_{H,H}$ = 6.4 Hz, 2H, -ArOC*H*$_A$H$_B$-), 4.03 (t, $^3J_{H,H}$ = 6.5 Hz, 4H, -OC*H*$_2$-), 3.96 (dd, $^2J_{H,H}$ = 8.6, $^3J_{H,H}$ = 5.5 Hz, 2H, -ArOCH$_A$*H*$_B$-), 1.92 − 1.82 (m, 4H, -C*H*$_2$-), 1.62 − 1.51 (m, 4H, -C*H*$_2$-), 1.43 (s, 6H, -C*H*$_3$), 1.38 (s, 6H, -C*H*$_3$), 1.31 − 1.17 (m, 68H, -C*H*$_2$-), 0.86 (t, $^3J_{H,H}$ = 6.7 Hz, 12H, -C*H*$_3$), 0.55 − 0.42 (m, 12H, -SiC*H*$_2$-), -0.08 (s, 6H, -SiC*H*$_2$-). **^{19}F-NMR** (CDCl$_3$, 376 MHz): δ / ppm = -137.41 − -137.61 (m, Aryl-*F*), -157.11 − -157.31 (m, Aryl-*F*). **^{29}Si-NMR** (CDCl$_3$, 79 MHz): δ / ppm = 2.79 (*Si*).

1,4-Bis[6-(didecylmethylsilyl)hexyloxy]-2,5-bis{4-[2,3,5,6-tetrafluoro-4-(2,3-isopropylidene-2,3-dihydroxyprop-1-yloxy)phenylethynyl]phenylethynyl}benzene 2F6/10A
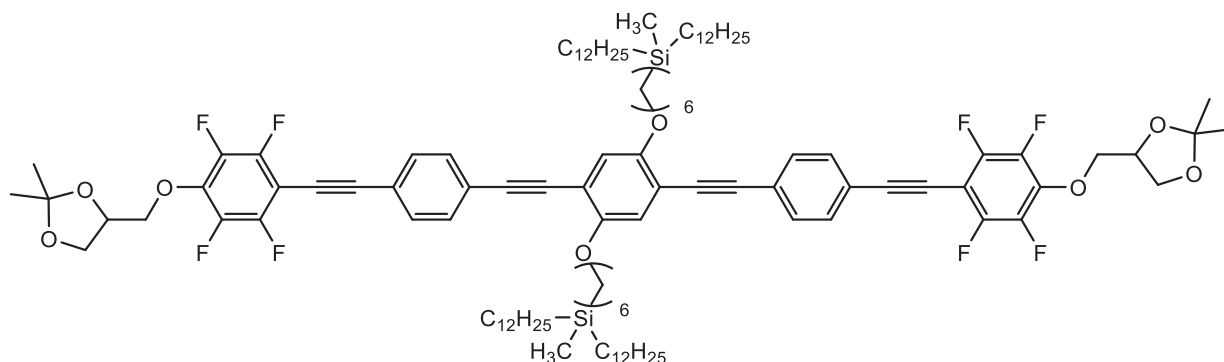

Synthesized according to GP5 from **8C6/10** (200 mg, 0.17 mmol), **26F** (155 mg, 0.38 mmol), Pd(PPh$_3$)$_4$ (5.9 mg, 5.1 · 10^{-3} mmol), CuI (1.0 mg, 5.1 · 10^{-3} mmol) in anhydrous Et$_3$N (20 mL), purification by column chromatography (eluent: CHCl$_3$); yellow liquid, yield: C$_{104}$H$_{146}$F$_8$O$_8$Si$_2$ M = 1732.46 g/mol, 295 mg (98 %), **^{1}H-NMR** (CDCl$_3$, 400 MHz): δ / ppm = 7.57 − 7.49 (m, 8H, Aryl-*H*), 7.01 (s, 2H, Aryl-*H*), 4.49 − 4.42 (m, 2H, -C*H*O-), 4.33 (dd, $^2J_{H,H}$ = 10.1, $^3J_{H,H}$ = 5.1 Hz, 2H, -OC*H*$_A$H$_B$-), 4.23 (dd, $^2J_{H,H}$ = 10.1, $^3J_{H,H}$ = 5.6 Hz, 2H, -OCH$_A$*H*$_B$-), 4.16 (dd, $^2J_{H,H}$ = 8.6, $^3J_{H,H}$ = 6.4 Hz, 2H, -ArOC*H*$_A$H$_B$-), 4.04 (t, $^3J_{H,H}$ = 6.4 Hz, 4H, -OC*H*$_2$-), 3.96 (dd, $^2J_{H,H}$ = 8.6, $^3J_{H,H}$ = 5.5 Hz, 2H, -ArOCH$_A$*H*$_B$-), 1.91 − 1.80 (m, 4H, -C*H*$_2$-), 1.60 − 1.49 (m, 4H, -C*H*$_2$-), 1.43 (s, 6H, -C*H*$_3$), 1.38 (s, 6H, -C*H*$_3$), 1.36 − 1.16 (m, 72H, -C*H*$_2$-), 0.86 (t, $^3J_{H,H}$ = 6.8 Hz, 12H, -C*H*$_3$), 0.52 − 0.41 (m, 12H, -SiC*H*$_2$-), -0.10 (s, 6H, -SiC*H*$_3$). **^{19}F-NMR** (CDCl$_3$, 376 MHz): δ / ppm = -137.38 − -137.64 (m, Aryl-*F*), -156.73 − -157.03 (m, Aryl-*F*). **^{29}Si-NMR** (CDCl$_3$, 79 MHz): δ / ppm = 2.77 (*Si*).

1,4-Bis[6-(didodecylmethylsilyl)hexyloxy]-2,5-bis{4-[2,3,5,6-tetrafluoro-4-(2,3-isopropylidene-2,3-dihydroxyprop-1-yloxy)phenylethynyl]phenylethynyl}benzene 2F6/12A
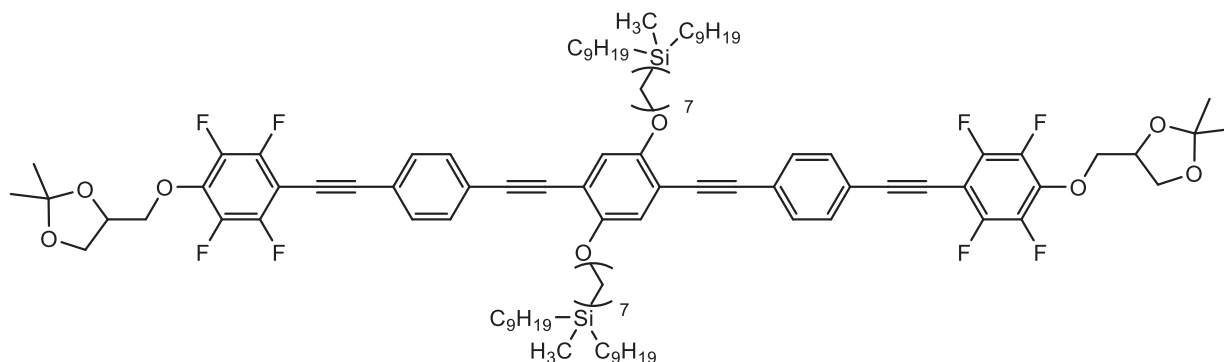

Synthesized according to GP5 from **8C6/12** (250 mg, 0.19 mmol), **26F** (172 mg, 0.43 mmol), Pd(PPh$_3$)$_4$ (6.6 mg, $5.7 \cdot 10^{-3}$ mmol), CuI (1.1 mg, $5.7 \cdot 10^{-3}$ mmol) in anhydrous Et$_3$N (20 mL), purification by column chromatography (eluent: CHCl$_3$); yellow liquid, yield: C$_{112}$H$_{162}$F$_8$O$_8$Si$_2$ M = 1844.68 g/mol, 230 mg (64 %), **^{1}H-NMR** (CDCl$_3$, 400 MHz): δ / ppm = 7.55 − 7.50 (m, 8H, Aryl-*H*), 7.01 (s, 2H, Aryl-*H*), 4.49 − 4.41 (m, 2H, -C*H*O-), 4.33 (dd, $^2J_{H,H}$ = 10.2, $^3J_{H,H}$ = 5.1 Hz, 2H, -OC*H*$_A$H$_B$-), 4.23 (dd, $^2J_{H,H}$ = 10.1, $^3J_{H,H}$ = 5.6 Hz, 2H, -OCH$_A$*H*$_B$-), 4.16 (dd, $^2J_{H,H}$ = 8.6, $^3J_{H,H}$ = 6.4 Hz, 2H, -ArOC*H*$_A$H$_B$-), 4.04 (t, $^3J_{H,H}$ = 6.4 Hz, 4H, -OC*H*$_2$-), 3.96 (dd, $^2J_{H,H}$ = 8.6, $^3J_{H,H}$ = 5.6 Hz, 2H, -ArOCH$_A$*H*$_B$-), 1.90 − 1.81 (m, 4H, -C*H*$_2$-), 1.61 − 1.47 (m, 4H, -C*H*$_2$-), 1.43 (s, 6H, -C*H*$_3$), 1.38 (s, 6H, -C*H*$_3$), 1.34 − 1.19 (m, 88H, -C*H*$_2$-), 0.87 (t, $^3J_{H,H}$ = 6.8 Hz, 12H, -C*H*$_3$), 0.52 − 0.41 (m, 12H, -SiC*H*$_2$-), -0.10 (s, 6H, -SiC*H*$_3$). **^{19}F-NMR** (CDCl$_3$, 376 MHz): δ / ppm = -137.39 − -137.65 (m, Aryl-*F*), -156.81 − -157.04 (m, Aryl-*F*). **^{29}Si-NMR** (CDCl$_3$, 79 MHz): δ / ppm = 2.78 (*Si*).

1,4-Bis[7-(dinonylmethylsilyl)heptyloxy]-2,5-bis{4-[2,3,5,6-tetrafluoro-4-(2,3-isopropylidene-2,3-dihydroxyprop-1-yloxy)phenylethynyl]phenylethynyl}benzene 2F7/9A

Synthesized according to GP5 from **8C7/9** (200 mg, 0.17 mmol), **26F** (155 mg, 0.38 mmol), Pd(PPh$_3$)$_4$ (5.9 mg, $5.1 \cdot 10^{-3}$ mmol), CuI (1.0 mg, $5.1 \cdot 10^{-3}$ mmol) in anhydrous Et$_3$N (20 mL), purification by column chromatography (eluent: CHCl$_3$); yellow liquid, yield: C$_{102}$H$_{142}$F$_8$O$_8$Si$_2$ M = 1704.41 g/mol, 290 mg (98 %), **^{1}H-NMR** (CDCl$_3$, 402 MHz): δ / ppm = 7.56 − 7.47 (m, 8H, Aryl-*H*), 7.00 (s, 2H, Aryl-*H*), 4.48 − 4.41 (m, 2H, -C*H*O-), 4.32 (dd, $^2J_{H,H}$ = 10.2, $^3J_{H,H}$ = 5.2 Hz, 2H, -OC*H*$_A$H$_B$-), 4.22 (dd, $^2J_{H,H}$ = 10.2, $^3J_{H,H}$ = 5.7 Hz, 2H, -OCH$_A$*H*$_B$-), 4.14 (dd, $^2J_{H,H}$ = 8.7, $^3J_{H,H}$ = 6.4 Hz, 2H, -ArOC*H*$_A$H$_B$-), 4.02 (t, $^3J_{H,H}$ = 6.4 Hz, 4H, -OC*H*$_2$-), 3.94 (dd, $^2J_{H,H}$ = 8.6, $^3J_{H,H}$ = 5.6 Hz, 2H, -ArOCH$_A$*H*$_B$-), 1.90 − 1.80 (m, 4H, -C*H*$_2$-), 1.58 − 1.48 (m, 4H, -C*H*$_2$-), 1.42 (s, 6H, -C*H*$_3$), 1.37 (s, 6H, -C*H*$_3$), 1.33 − 1.15 (m, 68H, -C*H*$_2$-), 0.85 (t, $^3J_{H,H}$ = 6.8 Hz, 12H, -C*H*$_3$), 0.51 − 0.39 (m, 12H, -SiC*H*$_2$-), -0.11 (s, 6H, -SiC*H*$_3$). **^{19}F-NMR** (CDCl$_3$, 378 MHz): δ / ppm = -137.36 − -137.90 (m, Aryl-*F*), -156.64 − -157.11 (m, Aryl-*F*). **^{29}Si-NMR** (CDCl$_3$, 80 MHz): δ / ppm = 2.75 (*Si*).

1,4-Bis[7-(didecylmethylsilyl)heptyloxy]-2,5-bis{4-[2,3,5,6-tetrafluoro-4-(2,3-isopropylidene-2,3-dihydroxyprop-1-yloxy)phenylethynyl]phenylethynyl}benzene 2F7/10A
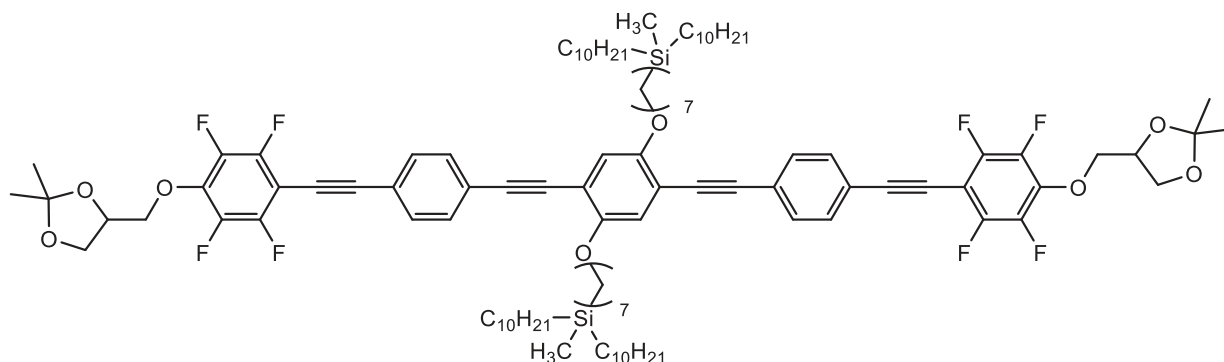
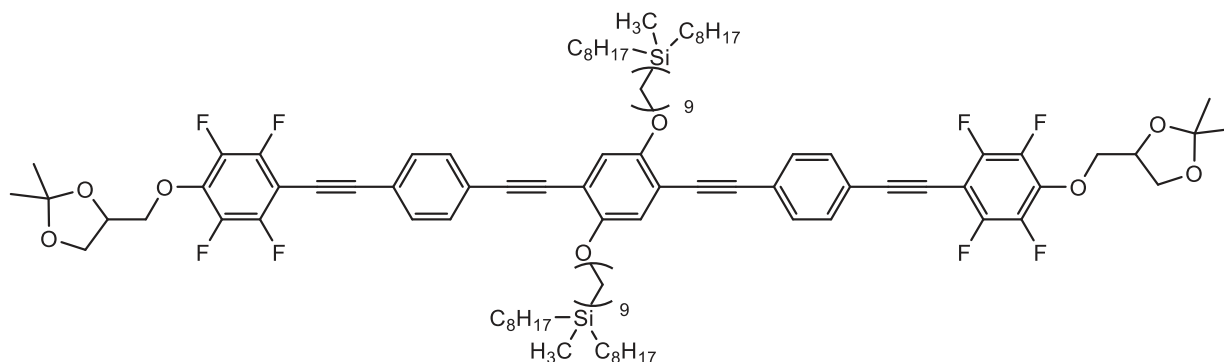

Synthesized according to GP5 from **8C7/10** (200 mg, 0.17 mmol), **26F** (147 mg, 0.36 mmol), Pd(PPh$_3$)$_4$ (5.9 mg, 5.1 · 10^{-3} mmol), CuI (1.0 mg, 5.1 · 10^{-3} mmol) in anhydrous Et$_3$N (20 mL), purification by column chromatography (eluent: CHCl$_3$); yellow liquid, yield: C$_{106}$H$_{150}$F$_8$O$_8$Si$_2$ M = 1760.52 g/mol, 285 mg (98 %), **^{1}H-NMR** (CDCl$_3$, 400 MHz): δ / ppm = 7.57 − 7.50 (m, 8H, Aryl-*H*), 7.01 (s, 2H, Aryl-*H*), 4.49 − 4.42 (m, 2H, -C*H*O-), 4.32 (dd, $^2J_{H,H}$ = 10.3, $^3J_{H,H}$ = 5.2 Hz, 2H, -OC*H$_A$*H$_B$-), 4.23 (dd, $^2J_{H,H}$ = 10.1, $^3J_{H,H}$ = 5.6 Hz, 2H, -OCH$_A$*H$_B$*-), 4.16 (dd, $^2J_{H,H}$ = 8.6, $^3J_{H,H}$ = 6.4 Hz, 2H, -ArOC*H$_A$*H$_B$-), 4.03 (t, $^3J_{H,H}$ = 6.5 Hz, 4H, -OC*H$_2$*-), 3.96 (dd, $^2J_{H,H}$ = 8.6, $^3J_{H,H}$ = 5.6 Hz, 2H, -ArOCH$_A$*H$_B$*-), 1.91 − 1.81 (m, 4H, -C*H$_2$*-), 1.60 − 1.48 (m, 4H, -C*H$_2$*-), 1.43 (s, 6H, -C*H$_3$*), 1.38 (s, 6H, -C*H$_3$*), 1.36 − 1.15 (m, 76H, -C*H$_2$*-), 0.87 (t, $^3J_{H,H}$ = 6.9 Hz, 12H, -C*H$_3$*), 0.51 − 0.41 (m, 12H, -SiC*H$_2$*-), -0.10 (s, 6H, -C*H$_2$*-). **^{19}F-NMR** (CDCl$_3$, 376 MHz): δ / ppm = -137.40 − -137.61 (m, Aryl-*F*), -156.79 − -157.02 (m, Aryl-*F*). **^{29}Si-NMR** (CDCl$_3$, 79 MHz): δ / ppm = 2.77 (*Si*).

1,4-Bis[9-(dioctylmethylsilyl)nonyloxy]-2,5-bis{4-[2,3,5,6-tetrafluoro-4-(2,3-isopropylidene-2,3-dihydroxyprop-1-yloxy)phenylethynyl]phenylethynyl}benzene 2F9/8A

Synthesized according to GP5 from **8C9/8** (200 mg, 0.17 mmol), **26F** (155 mg, 0.38 mmol), Pd(PPh$_3$)$_4$ (5.9 mg, 5.1 · 10^{-3} mmol), CuI (1.0 mg, 5.1 · 10^{-3} mmol) in anhydrous Et$_3$N (20 mL), purification by column chromatography (eluent: CHCl$_3$); yellow solid, yield: C$_{102}$H$_{142}$F$_8$O$_8$Si$_2$ M = 1532.43 g/mol, 280 mg (94 %), *mp* = 59 °C, **^{1}H-NMR** (CDCl$_3$, 402 MHz): δ / ppm = 7.59 − 7.46 (m, 8H, Aryl-*H*), 7.00 (s, 2H, Aryl-*H*), 4.47 − 4.39 (m, 2H, -C*H*O-), 4.30 (dd, $^2J_{H,H}$ = 10.4, $^3J_{H,H}$ = 5.5 Hz, 2H, -OC*H$_A$*H$_B$-), 4.22 (dd, $^2J_{H,H}$ = 10.2, $^3J_{H,H}$ = 5.6 Hz, 2H, -OCH$_A$*H$_B$*-), 4.14 (dd, $^2J_{H,H}$ = 8.6, $^3J_{H,H}$ = 6.4 Hz, 2H, -ArOC*H$_A$*H$_B$-), 4.02 (t, $^3J_{H,H}$ = 6.4 Hz, 4H, -OC*H$_2$*-), 3.94 (dd, $^2J_{H,H}$ = 8.6, $^3J_{H,H}$ = 5.6 Hz, 2H, -ArOCH$_A$*H$_B$*-), 1.90 − 1.78 (m, 4H, -C*H$_2$*-), 1.59 − 1.47 (m, 4H, -C*H$_2$*-), 1.42 (s, 6H, -C*H$_3$*), 1.37 (s, 6H, -C*H$_3$*), 1.32 − 1.17 (m, 68H, -C*H$_2$*-), 0.85 (t, $^3J_{H,H}$ = 7.2 Hz, 12H, -C*H$_3$*), 0.48 − 0.39 (m, 12H, -SiC*H$_2$*-), -0.12 (s, 6H, -SiC*H$_3$*). **^{19}F-NMR** (CDCl$_3$, 387 MHz): δ / ppm = -137.39 − -137.58 (m, Aryl-*F*), -156.85 − -156.98 (m, Aryl-*F*). **^{29}Si-NMR** (CDCl$_3$, 80 MHz): δ / ppm = 2.75 (*Si*).

1,4-Bis[9-(diundecylmethylsilyl)nonyloxy]-2,5-bis{4-[2,3,5,6-tetrafluoro-4-(2,3-isopropylidene-2,3-dihydroxyprop-1-yloxy)phenylethynyl]phenylethynyl}benzene 2F9/11A
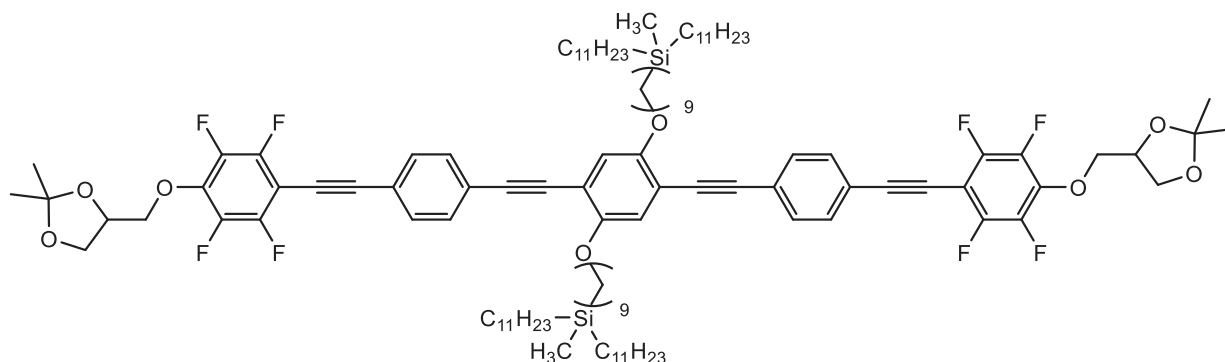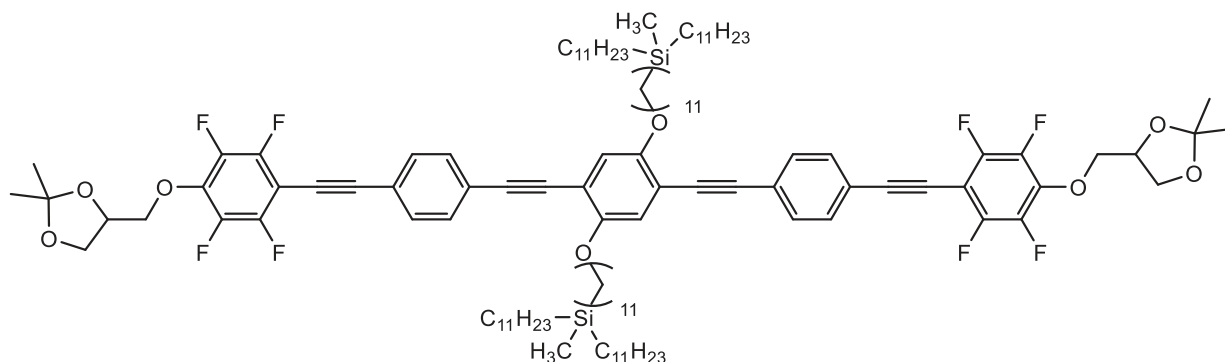

Synthesized according to GP5 from **8C9/11** (250 mg, 0.19 mmol), **26F** (169 mg, 0.42 mmol), Pd(PPh$_3$)$_4$ (6.6 mg, $5.7 \cdot 10^{-3}$ mmol), CuI (1.1 mg, $5.7 \cdot 10^{-3}$ mmol) in anhydrous Et$_3$N (20 mL), purification by column chromatography (eluent: CHCl$_3$); yellow liquid, yield: C$_{114}$H$_{166}$F$_8$O$_8$Si$_2$ M = 1872.73 g/mol, 300 mg (85 %), **^{1}H-NMR** (CDCl$_3$, 400 MHz): δ / ppm = 7.57 – 7.50 (m, 8H, Aryl-*H*), 7.01 (s, 2H, Aryl-*H*), 4.50 – 4.42 (m, 2H, -C*H*O-), 4.33 (dd, $^2J_{H,H}$ = 10.6, $^3J_{H,H}$ = 4.9 Hz, 2H, -OC*H$_A$H$_B$*-), 4.23 (dd, $^2J_{H,H}$ = 10.1, $^3J_{H,H}$ = 5.6 Hz, 2H, -OCH$_A$*H$_B$*-), 4.16 (dd, $^2J_{H,H}$ = 8.6, $^3J_{H,H}$ = 6.4 Hz, 2H, -ArOC*H$_A$H$_B$*-), 4.03 (t, $^3J_{H,H}$ = 6.5 Hz, 4H, -OC*H$_2$*-), 3.96 (dd, $^2J_{H,H}$ = 8.6, $^3J_{H,H}$ = 5.6 Hz, 2H, -ArOCH$_A$*H$_B$*-), 1.91 – 1.81 (m, 4H, -C*H$_2$*-), 1.59 – 1.49 (m, 4H, -C*H$_2$*-), 1.43 (s, 6H, -C*H$_3$*), 1.38 (s, 6H, -C*H$_3$*), 1.34 – 1.19 (m, 92H, -C*H$_2$*-), 0.87 (t, $^3J_{H,H}$ = 6.5 Hz, 12H, -C*H$_3$*), 0.50 – 0.41 (m, 12H, -SiC*H$_2$*-), -0.10 (s, 6H, -SiC*H$_3$*). **^{19}F-NMR** (CDCl$_3$, 376 MHz): δ / ppm = -137.35 – -137.66 (m, Aryl-*F*), -156.79 – -157.03 (m, Aryl-*F*). **^{29}Si-NMR** (CDCl$_3$, 79 MHz): δ / ppm = 2.76 (*Si*).

1,4-Bis[11-(diundecylmethylsilyl)undecyloxy]-2,5-bis{4-[2,3,5,6-tetrafluoro-4-(2,3-isopropylidene-2,3-dihydroxyprop-1-yloxy)phenylethynyl]phenylethynyl}benzene 2F11/11A
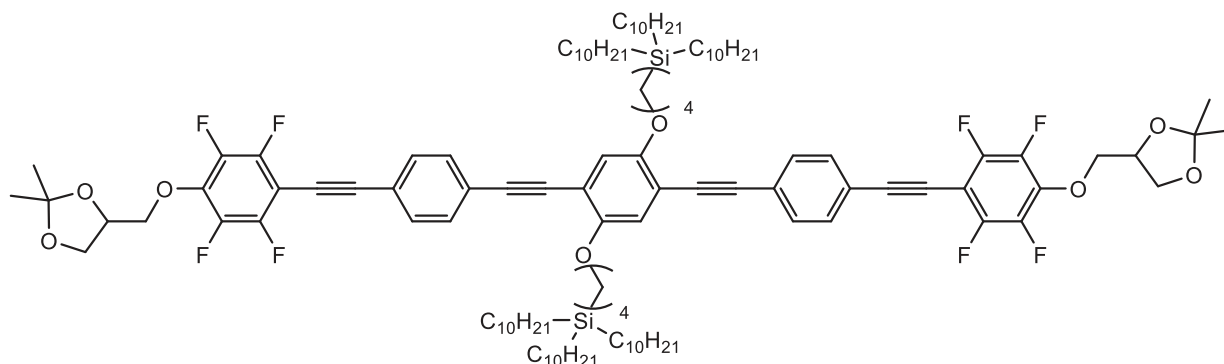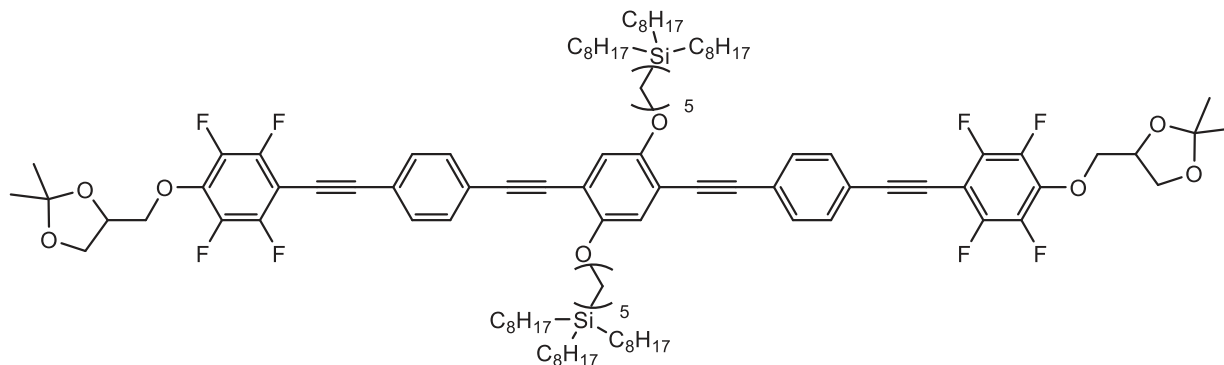

Synthesized according to GP5 from **8C11/11** (212 mg, 0.15 mmol), **26F** (137 mg, 0.34 mmol), Pd(PPh$_3$)$_4$ (5.2 mg, $4.5 \cdot 10^{-3}$ mmol), CuI (0.9 mg, $4.5 \cdot 10^{-3}$ mmol) in anhydrous Et$_3$N (20 mL), purification by column chromatography (eluent: CHCl$_3$); yellow liquid, yield: C$_{118}$H$_{174}$F$_8$O$_8$Si$_2$ M = 1928.84 g/mol, 220 mg (74 %), **^{1}H-NMR** (CDCl$_3$, 400 MHz): δ / ppm = 7.57 – 7.50 (m, 8H, Aryl-*H*), 7.02 (s, 2H, Aryl-*H*), 4.50 – 4.42 (m, 2H, -C*H*O-), 4.33 (dd, $^2J_{H,H}$ = 10.1, $^3J_{H,H}$ = 5.2 Hz, 2H, -OC*H$_A$H$_B$*-), 4.24 (dd, $^2J_{H,H}$ = 10.1, $^3J_{H,H}$ = 5.6 Hz, 2H, -OCH$_A$*H$_B$*-), 4.16 (dd, $^2J_{H,H}$ = 8.6, $^3J_{H,H}$ = 6.4 Hz, 2H, -ArOC*H$_A$H$_B$*-), 4.04 (t, $^3J_{H,H}$ = 6.5 Hz, 4H, -OC*H$_2$*-), 3.96 (dd, $^2J_{H,H}$ = 8.6, $^3J_{H,H}$ = 5.6 Hz, 2H, -OArCH$_A$*H$_B$*-), 1.91 – 1.80 (m, 4H, -C*H$_2$*-), 1.60 – 1.49 (m, 4H, -C*H$_2$*-), 1.43 (s, 6H, -C*H$_3$*), 1.39 (s, 6H, -C*H$_3$*), 1.35 – 1.18 (m, 100H, -C*H$_2$*-), 0.87 (t, $^3J_{H,H}$ = 6.8 Hz, 12H, -C*H$_3$*), 0.50 – 0.41 (m, 12H, -SiC*H$_2$*-), -0.10 (s, 6H, -SiC*H$_3$*). **^{19}F-NMR** (CDCl$_3$, 376 MHz): δ / ppm = -137.39 – -137.59 (m, Aryl-*F*), -156.82 – -156.96 (m, Aryl-*F*). **^{29}Si-NMR** (CDCl$_3$, 79 MHz): δ / ppm = 2.77 (*Si*).

1,4-Bis[4-(tridecylsilyl)butyloxy]-2,5-bis{4-[2,3,5,6-tetrafluoro-4-(2,3-isopropylidene-2,3-dihydroxyprop-1-yloxy)phenylethynyl]phenylethynyl}benzene 1F4/10A

$C_{10}H_{21}$
$C_{10}H_{21}$—Si—$C_{10}H_{21}$
O 4

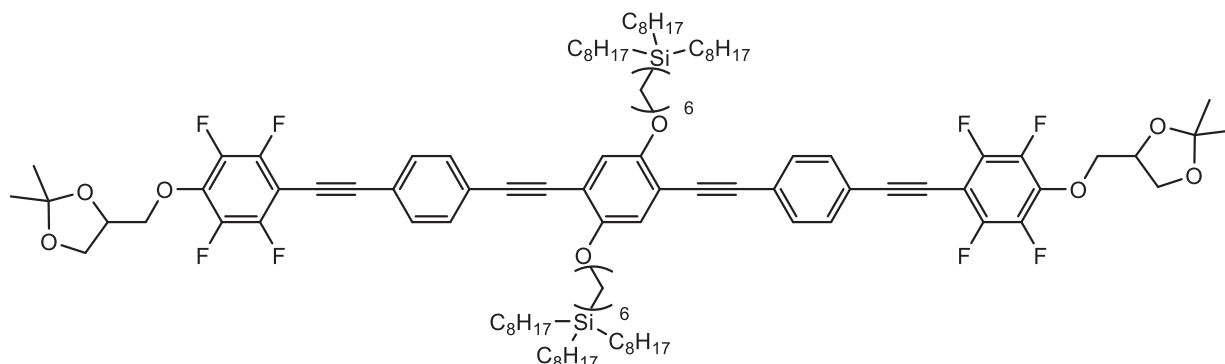$C_{10}H_{21}$—Si—$C_{10}H_{21}$
$C_{10}H_{21}$
O 4

Synthesized according to GP5 from **8B4/10** (220 mg, 0.16 mmol), **26F** (136 mg, 0.34 mmol), Pd(PPh₃)₄ (5.5 mg, 4.8 · 10⁻³ mmol), CuI (0.9 mg, 4.8 · 10⁻³ mmol) in anhydrous Et₃N (20 mL), purification by column chromatography (eluent: CHCl₃); yellow solid, yield: $C_{118}H_{174}F_8O_8Si_2$ M = 1928.84 g/mol, 300 mg (97 %), mp = 42 °C, **¹H-NMR** (CDCl₃, 400 MHz): δ / ppm = 7.58 − 7.50 (m, 8H, Aryl-*H*), 7.03 (s, 2H, Aryl-*H*, -OC*H*ₐ*H*ᵦ-), 4.52 − 4.42 (m, 2H, -C*H*O-), 4.34 (dd, $^2J_{H,H}$ = 10.1, $^3J_{H,H}$ = 5.1 Hz, 2H, -OC*H*ₐHᵦ-), 4.25 (dd, $^2J_{H,H}$ = 10.1, $^3J_{H,H}$ = 5.7 Hz, 2H, -OC*H*ₐHᵦ-), 4.17 (dd, $^2J_{H,H}$ = 8.6, $^3J_{H,H}$ = 6.4 Hz, 2H, ArOC*H*ₐHᵦ-), 4.06 (t, $^3J_{H,H}$ = 6.4 Hz, 4H, -OC*H₂*-), 3.97 (dd, $^2J_{H,H}$ = 8.6, $^3J_{H,H}$ = 5.6 Hz, 2H, -ArOC*H*ₐHᵦ-), 1.95 − 1.84 (m, 4H, -C*H₂*-), 1.62 − 1.49 (m, 4H, -C*H₂*-), 1.44 (s, 6H, -C*H₃*), 1.39 (s, 6H, -C*H₃*), 1.35 − 1.18 (m, 96H, -C*H₂*-), 0.88 (t, $^3J_{H,H}$ = 6.7 Hz, 18H, -C*H₃*), 0.63 − 0.55 (m, 4H, -SiC*H₂*-), 0.54 − 0.43 (m, 12H, -SiC*H₂*-). **¹⁹F-NMR** (CDCl₃, 376 MHz): δ / ppm = -137.38 − -137.59 (m), -156.82 − -157.03 (m). **²⁹Si-NMR** (CDCl₃, 79 MHz): δ / ppm = 3.02 (*Si*).

1,4-Bis[5-(trioctylsilyl)pentyloxy]-2,5-bis{4-[2,3,5,6-tetrafluoro-4-(2,3-isopropylidene-2,3-dihydroxyprop-1-yloxy)phenylethynyl]phenylethynyl}benzene 1F5/8A

C_8H_{17}
C_8H_{17}—Si—C_8H_{17}
O 5

C_8H_{17}—Si—C_8H_{17}
C_8H_{17}
O 5

Synthesized according to GP5 from **8C5/8** (200 mg, 0.16 mmol), **26F** (144 mg, 0.36 mmol), Pd(PPh₃)₄ (5.5 mg, 4.8 · 10⁻³ mmol), CuI (0.9 mg, 4.8 · 10⁻³ mmol) in anhydrous Et₃N (20 mL), purification by column chromatography (eluent: CHCl₃); yellow solid, yield: $C_{108}H_{154}F_8O_8Si_2$ M = 1788.57 g/mol, 250 mg (86 %), mp = 55 °C, **¹H-NMR** (CDCl₃, 402 MHz): δ / ppm = 7.55 − 7.49 (m, 8H, Aryl-*H*), 7.00 (s, 2H, Aryl-*H*), 4.49 − 4.38 (m, 2H, -C*H*O-), 4.32 (dd, $^2J_{H,H}$ = 10.1, $^3J_{H,H}$ = 5.2 Hz, 2H, -OC*H*ₐHᵦ-), 4.22 (dd, $^2J_{H,H}$ = 10.1, $^3J_{H,H}$ = 5.6 Hz, 2H, -OC*H*ₐHᵦ-), 4.15 (dd, $^2J_{H,H}$ = 8.6, $^3J_{H,H}$ = 6.4 Hz, 2H, -ArOC*H*ₐHᵦ-), 4.02 (t, $^3J_{H,H}$ = 6.4 Hz, 4H, -OC*H₂*-), 3.94 (dd, $^2J_{H,H}$ = 8.6, $^3J_{H,H}$ = 5.6 Hz, 2H, -ArOC*H*ₐHᵦ-), 1.90 − 1.78 (m, 4H, -C*H₂*-), 1.63 − 1.50 (m, 4H, -C*H₂*-), 1.42 (s, 6H, -C*H₃*), 1.37 (s, 6H, -C*H₃*), 1.31 − 1.17 (m, 76H, -C*H₂*-), 0.85 (t, $^3J_{H,H}$ = 6.8 Hz, 18H, -C*H₃*), 0.55 − 0.42 (m, 16H, -SiC*H₂*-). **¹⁹F-NMR** (CDCl₃, 378 MHz): δ / ppm = -137.32 − -137.75 (m, Aryl-*F*), -156.83 − -157.05 (m, Aryl-*F*). **²⁹Si-NMR** (CDCl₃, 80 MHz): δ / ppm = 2.88 (*Si*).

1,4-Bis[6-(trioctylsilyl)pentyloxy]-2,5-bis{4-[2,3,5,6-tetrafluoro-4-(2,3-isopropylidene-2,3-dihydroxyprop-1-yloxy)phenylethynyl]phenylethynyl}benzene 1F6/8A
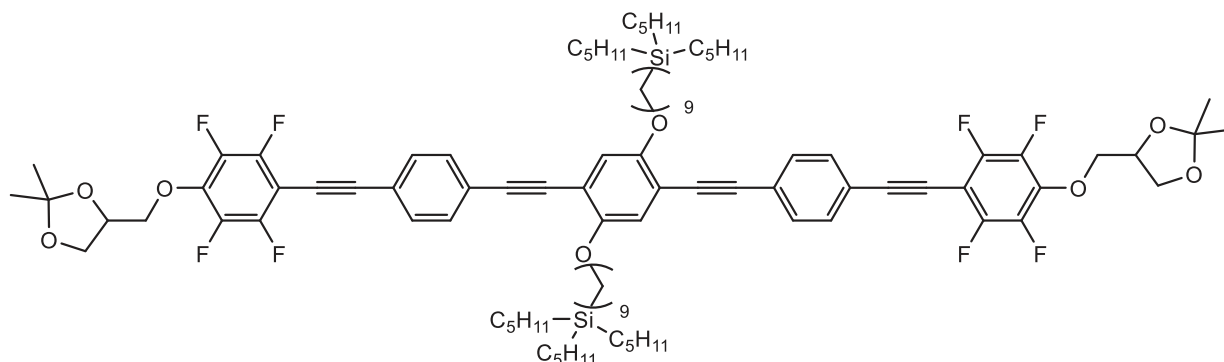

Synthesized according to GP5 from **8B6/8** (200 mg, 0.16 mmol), **26F** (142 mg, 0.35 mmol), Pd(PPh$_3$)$_4$ (5.5 mg, 4.8 · 10^{-3} mmol), CuI (0.9 mg, 4.8 · 10^{-3} mmol) in anhydrous Et$_3$N (20 mL), purification by column chromatography (eluent: CHCl$_3$); yellow solid, yield: C$_{110}$H$_{158}$F$_8$O$_8$Si$_2$ M = 1816.62 g/mol, 220 mg (76 %), *mp* = 51 °C, **^{1}H-NMR** (CDCl$_3$, 500 MHz): δ / ppm = 7.59 − 7.52 (m, 8H, Aryl-*H*), 7.03 (s, 2H, Aryl-*H*), 4.51 − 4.43 (m, 2H, -C*H*O-), 4.35 (dd, $^2J_{H,H}$ = 10.1, $^3J_{H,H}$ = 5.1 Hz, 2H, -OC*H*$_A$H$_B$-), 4.25 (dd, $^2J_{H,H}$ = 10.2, $^3J_{H,H}$ = 5.6 Hz, 2H, -OC*H*$_A$*H*$_B$-), 4.18 (dd, $^2J_{H,H}$ = 8.6, $^3J_{H,H}$ = 6.4 Hz, 2H, -ArOC*H*$_A$H$_B$-), 4.06 (t, $^3J_{H,H}$ = 6.4 Hz, 4H, -OC*H*$_2$-), 3.98 (dd, $^2J_{H,H}$ = 8.6, $^3J_{H,H}$ = 5.6 Hz, 2H, -ArOC*H*$_A$*H*$_B$-), 1.92 − 1.82 (m, 4H, -C*H*$_2$-), 1.62 − 1.52 (m, 4H, -C*H*$_2$-), 1.45 (s, 6H, -C*H*$_3$), 1.40 (s, 6H, -C*H*$_3$), 1.37 − 1.21 (m, 80H, -C*H*$_2$-), 0.88 (t, $^3J_{H,H}$ = 6.9 Hz, 18H, -C*H*$_3$), 0.56 − 0.44 (m, 16H, -SiC*H*$_2$-). **^{19}F-NMR** (CDCl$_3$, 470 MHz): δ / ppm = -137.27 − -137.67 (m, Aryl-*F*), -156.82 − -157.04 (m, Aryl-*F*). **^{29}Si-NMR** (CDCl$_3$, 99 MHz): δ / ppm = 2.91 (*Si*).

1,4-Bis[8-(trihexylsilyl)octyloxy]-2,5-bis{4-[2,3,5,6-tetrafluoro-4-(2,3-isopropylidene-2,3-dihydroxyprop-1-yloxy)phenylethynyl]phenylethynyl}benzene 1F8/6A
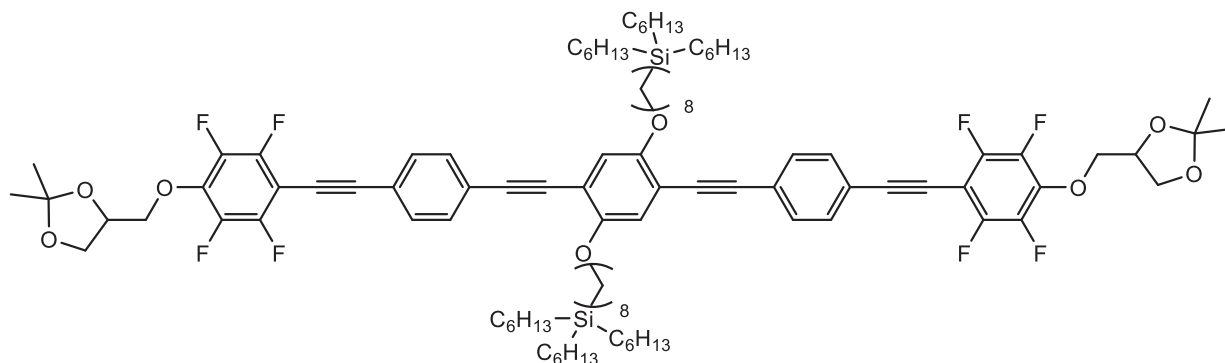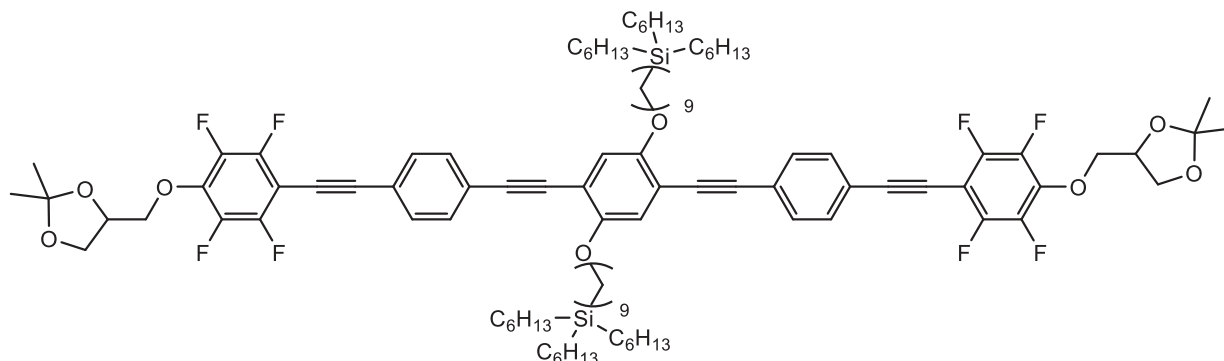

Synthesized according to GP5 from **8B8/6** (200 mg, 0.17 mmol), **26F** (155 mg, 0.38 mmol), Pd(PPh$_3$)$_4$ (5.9 mg, 5.1 · 10^{-3} mmol), CuI (1.0 mg, 5.1 · 10^{-3} mmol) in anhydrous Et$_3$N (20 mL), purification by column chromatography (eluent: CHCl$_3$); yellow solid, yield: C$_{102}$H$_{142}$F$_8$O$_8$Si$_2$ M = 1704.41 g/mol, 290 mg (98 %), *mp* = 73 °C, **^{1}H-NMR** (CDCl$_3$, 400 MHz): δ / ppm = 7.57 − 7.50 (m, 8H, Aryl-*H*), 7.01 (s, 2H, Aryl-*H*), 4.50 − 4.41 (m, 2H, -C*H*O-), 4.33 (dd, $^2J_{H,H}$ = 10.2, $^3J_{H,H}$ = 5.1 Hz, 2H, -OC*H*$_A$H$_B$-), 4.23 (dd, $^2J_{H,H}$ = 10.2, $^3J_{H,H}$ = 5.6 Hz, 2H, -OC*H*$_A$*H*$_B$-), 4.16 (dd, $^2J_{H,H}$ = 8.6, $^3J_{H,H}$ = 6.4 Hz, 2H, -ArOC*H*$_A$H$_B$-), 4.04 (t, $^3J_{H,H}$ = 6.4 Hz, 4H, -OC*H*$_2$-), 3.96 (dd, $^2J_{H,H}$ = 8.6, $^3J_{H,H}$ = 5.6 Hz, 2H, -ArOC*H*$_A$*H*$_B$-), 1.91 − 1.82 (m, 4H, -C*H*$_2$-), 1.61 − 1.48 (m, 4H, -C*H*$_2$-), 1.43 (s, 6H, -C*H*$_3$), 1.38 (s, 6H, -C*H*$_3$), 1.35 − 1.19 (m, 64H, -C*H*$_2$-), 0.87 (t, $^3J_{H,H}$ = 6.6 Hz, 18H, -C*H*$_3$), 0.53 − 0.41 (m, 16H, -SiC*H*$_2$-). **^{19}F-NMR** (CDCl$_3$, 376 MHz): δ / ppm = -137.06 − -137.65 (m, Aryl-*F*), -156.75 − -157.27 (m, Aryl-*F*). **^{29}Si-NMR** (CDCl$_3$, 79 MHz): δ / ppm = 2.88 (*Si*).

1,4-Bis[9-(tripentylsilyl)nonyloxy]-2,5-bis{4-[2,3,5,6-tetrafluoro-4-(2,3-isopropylidene-2,3-dihydroxyprop-1-yloxy)phenylethynyl]phenylethynyl}benzene 1F9/5A

Synthesized according to GP5 from **8B9/5** (200 mg, 0.18 mmol), **26F** (162 mg, 0.40 mmol), Pd(PPh$_3$)$_4$ (6.2 mg, $5.4 \cdot 10^{-3}$ mmol), CuI (1.0 mg, $5.4 \cdot 10^{-3}$ mmol) in anhydrous Et$_3$N (20 mL), purification by column chromatography (eluent: CHCl$_3$); yellow solid, yield: C$_{98}$H$_{134}$F$_8$O$_8$Si$_2$ M = 1648.30 g/mol, 290 mg (96 %), mp = 93 °C, **^{1}H-NMR** (CDCl$_3$, 400 MHz): δ / ppm = 7.57 − 7.50 (m, 8H, Aryl-*H*), 7.01 (s, 2H, Aryl-*H*), 4.48 − 4.42 (m, 2H, -C*H*O-), 4.33 (dd, $^2J_{H,H}$ = 10.1, $^3J_{H,H}$ = 5.2 Hz, 2H, -OC*H*$_A$H$_B$-), 4.23 (dd, $^2J_{H,H}$ = 10.1, $^3J_{H,H}$ = 5.6 Hz, 2H, -OCH$_A$*H$_B$*-), 4.16 (dd, $^2J_{H,H}$ = 8.6, $^3J_{H,H}$ = 6.4 Hz, 2H, -ArOC*H$_A$*H$_B$-), 4.04 (t, $^3J_{H,H}$ = 6.4 Hz, 4H, -OC*H$_2$*-), 3.96 (dd, $^2J_{H,H}$ = 8.6, $^3J_{H,H}$ = 5.6 Hz, 2H, -ArOCH$_A$*H$_B$*-), 1.90 − 1.81 (m, 4H, -C*H$_2$*-), 1.61 − 1.49 (m, 4H, -C*H$_2$*-), 1.43 (s, 6H, -C*H$_3$*), 1.38 (s, 6H, -C*H$_3$*), 1.35 − 1.19 (m, 56H, -C*H$_2$*-), 0.88 (t, $^3J_{H,H}$ = 7.1 Hz, 18H, -C*H$_3$*), 0.55 − 0.38 (m, 16H, -SiC*H$_2$*-). **^{19}F-NMR** (CDCl$_3$, 376 MHz): δ / ppm = -137.40 − -137.68 (m, Aryl-*F*), -156.60 − -157.24 (m, Aryl-*F*). **^{29}Si-NMR** (CDCl$_3$, 79 MHz): δ / ppm = 2.91 (*Si*).

1,4-Bis[9-(trigexylsilyl)nonyloxy]-2,5-bis{4-[2,3,5,6-tetrafluoro-4-(2,3-isopropylidene-2,3-dihydroxyprop-1-yloxy)phenylethynyl]phenylethynyl}benzene 1F9/6A
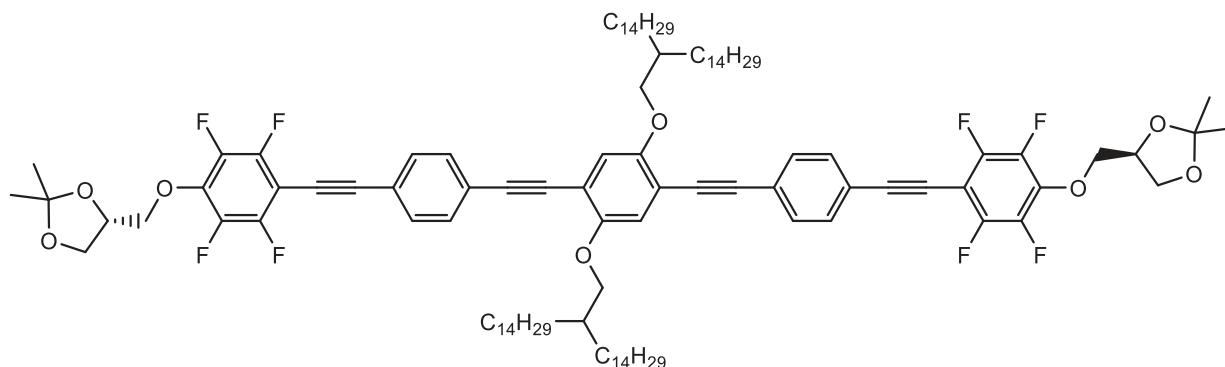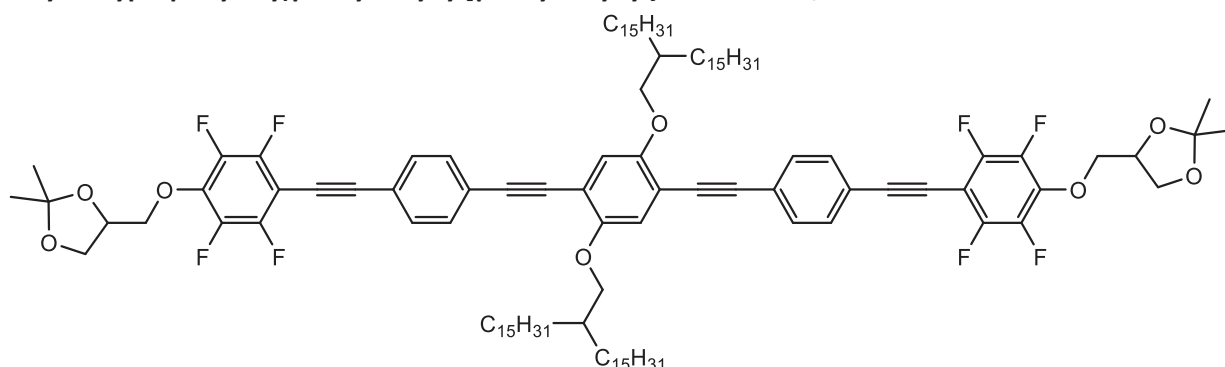

Synthesized according to GP5 from **8B9/6** (200 mg, 0.17 mmol), **26F** (151 mg, 0.37 mmol), Pd(PPh$_3$)$_4$ (5.9 mg, $5.1 \cdot 10^{-3}$ mmol), CuI (1.0 mg, $5.1 \cdot 10^{-3}$ mmol) in anhydrous Et$_3$N (20 mL), purification by column chromatography (eluent: CHCl$_3$); yellow solid, yield: C$_{104}$H$_{148}$F$_8$O$_8$Si$_2$ M = 1732.46 g/mol, 260 mg (89 %), mp = 58 °C, **^{1}H-NMR** (CDCl$_3$, 402 MHz): δ / ppm = 7.55 − 7.49 (m, 8H, Aryl-*H*), 7.00 (s, 2H, Aryl-*H*), 4.48 − 4.40 (m, 2H, -C*H*O-), 4.32 (dd, $^2J_{H,H}$ = 10.1, $^3J_{H,H}$ = 5.2 Hz, 2H, -OC*H*$_A$H$_B$-), 4.22 (dd, $^2J_{H,H}$ = 10.1, $^3J_{H,H}$ = 5.6 Hz, 2H, -OCH$_A$*H$_B$*-), 4.15 (dd, $^2J_{H,H}$ = 8.6, $^3J_{H,H}$ = 6.4 Hz, 2H, -ArOC*H$_A$*H$_B$-), 4.02 (t, $^3J_{H,H}$ = 6.5 Hz, 4H, -OC*H$_2$*-), 3.95 (dd, $^2J_{H,H}$ = 8.6, $^3J_{H,H}$ = 5.6 Hz, 2H, -ArOCH$_A$*H$_B$*-), 1.89 − 1.80 (m, 4H, -C*H$_2$*-), 1.56 − 1.48 (m, 4H, -C*H$_2$*-), 1.42 (s, 6H, -C*H$_3$*), 1.37 (s, 6H, -C*H$_3$*), 1.33 − 1.15 (m, 68H, -C*H$_2$*-), 0.86 (t, $^3J_{H,H}$ = 6.3 Hz, 18H, -C*H$_3$*), 0.49 − 0.41 (m, 16H, -SiC*H$_2$*-). **^{19}F-NMR** (CDCl$_3$, 378 MHz): δ / ppm = -137.30 − -137.65 (m, Aryl-*F*), -156.74 − -157.08 (m, Aryl-*F*). **^{29}Si-NMR** (CDCl$_3$, 80 MHz): δ / ppm = 2.86 (*Si*).

(_R_,_R_)-1,4-Bis(2-tetradecylhexadecyloxy)-2,5-bis{4-[2,3,5,6-tetrafluoro-4-(2,3-isopropylidene-2,3-dihydroxyprop-1-yloxy)phenylethynyl]phenylethynyl}benzene *5F1/14A

Synthesized according to GP5 from **5/1/14** (310 mg, 0.26 mmol), **28F*** (229 mg, 0.57 mmol), Pd(PPh$_3$)$_4$ (9.0 mg, 7.8 · 10^{-3} mmol), CuI (1.5 mg, 7.8 · 10^{-3} mmol) in anhydrous Et$_3$N (20 mL), purification by column chromatography (eluent: CHCl$_3$); yellow solid, yield: C$_{110}$H$_{154}$O$_8$F$_8$ _M_ = 1756.42 g/mol, 312 mg (69 %), _mp_ = 73 °C, **^{1}H-NMR** (CDCl$_3$, 400 MHz): δ / ppm = 7.57 − 7.50 (m, 8H, Aryl-_H_), 7.00 (s, 2H, Aryl-_H_), 4.50 − 4.41 (m, 2H, -C_H_O-), 4.33 (dd, $^2J_{H,H}$ = 10.2, $^3J_{H,H}$ = 5.1 Hz, 2H, -OC_H_$_A$H$_B$-), 4.24 (dd, $^2J_{H,H}$ = 10.0, $^3J_{H,H}$ = 5.7 Hz, 2H, -OCH$_A$_H_$_B$-), 4.15 (dd, $^2J_{H,H}$ = 8.6, $^3J_{H,H}$ = 6.6 Hz, 2H, -ArOC_H_$_A$H$_B$-), 4.00 − 3.87 (m, 6H, -ArOCH$_A$_H_$_B$-, -OC_H$_2$-), 1.90 − 1.80 (m, 2H, -C_H_-), 1.43 (s, 6H, -C_H$_3$), 1.38 (s, 6H, -C_H$_3$), 1.33 − 1.17 (m, 104H, -C_H$_2$-), 0.87 (t, $^3J_{H,H}$ = 7.1 Hz, 12H, -C_H$_3$). **^{19}F-NMR** (CDCl$_3$, 376 MHz): δ / ppm = -137.37 − -137.74 (m), -156.65 − -157.15 (m).

1,4-Bis(2-pentadecylheptadecyloxy)-2,5-bis{4-[2,3,5,6-tetrafluoro-4-(2,3-isopropylidene-2,3-dihydroxyprop-1-yloxy)phenylethynyl]phenylethynyl}benzene 5F1/15A
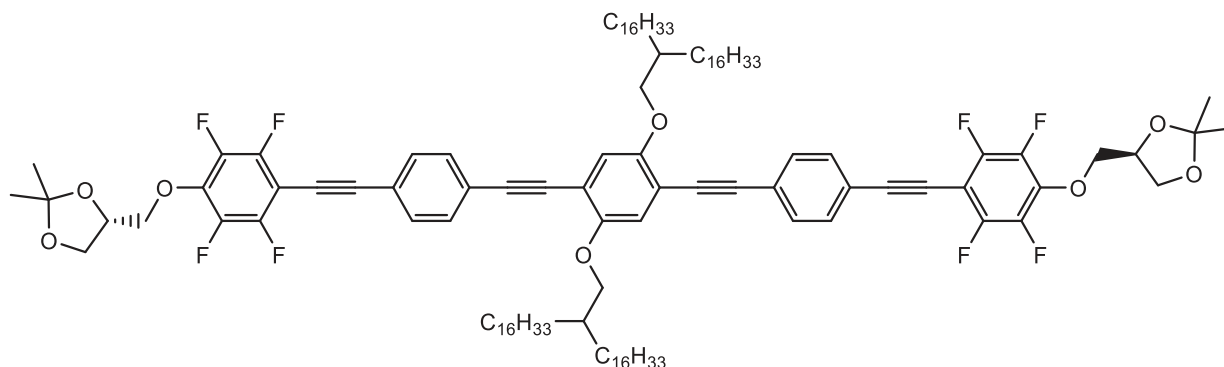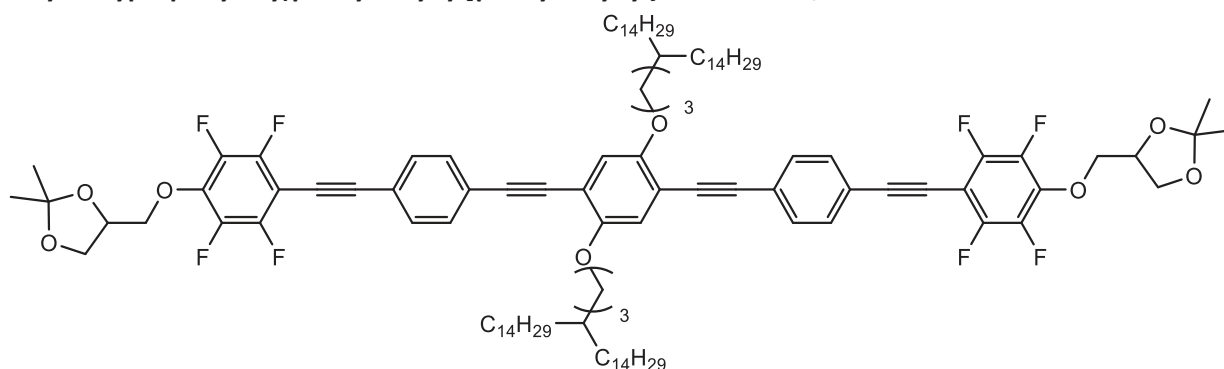

Synthesized according to GP5 from **5/1/15** (200 mg, 0.16 mmol), **26F** (141 mg, 0.35 mmol), Pd(PPh$_3$)$_4$ (5.5 mg, 4.8 · 10^{-3} mmol), CuI (0.9 mg, 4.8 · 10^{-3} mmol) in anhydrous Et$_3$N (20 mL), purification by column chromatography (eluent: CHCl$_3$); yellow solid, yield: C$_{114}$H$_{162}$O$_8$F$_8$ _M_ = 1812.53 g/mol, 220 mg (76 %), _mp_ = 95 °C, **^{1}H-NMR** (CDCl$_3$, 400 MHz): δ / ppm = 7.56 − 7.49 (m, 8H, Aryl-_H_), 7.00 (s, 2H, Aryl-_H_), 4.49 − 4.41 (m, 2H, -C_H_O-), 4.33 (dd, $^2J_{H,H}$ = 10.1, $^3J_{H,H}$ = 5.2 Hz, 2H, -OC_H_$_A$H$_B$-), 4.23 (dd, $^2J_{H,H}$ = 10.1, $^3J_{H,H}$ = 5.6 Hz, 2H, -OCH$_A$_H_$_B$-), 4.16 (dd, $^2J_{H,H}$ = 8.6, $^3J_{H,H}$ = 6.4 Hz, 2H, -ArOC_H_$_A$H$_B$-), 3.96 (dd, $^2J_{H,H}$ = 8.6, $^3J_{H,H}$ = 5.6 Hz, 2H, -ArOCH$_A$_H_$_B$-), 3.91 (d, $^3J_{H,H}$ = 5.6 Hz, 4H, -OC_H$_2$-), 1.90 − 1.80 (m, 2H, -C_H_-), 1.43 (s, 6H, -C_H$_3$), 1.38 (s, 6H, -C_H$_3$), 1.31 − 1.17 (m, 112H, -C_H$_2$-), 0.87 (t, $^3J_{H,H}$ = 6.8 Hz, 12H, -C_H$_3$). **^{19}F-NMR** (CDCl$_3$, 376 MHz): δ / ppm = -137.33 − -137.67 (m, Aryl-_F_), -156.78 − -157.09 (m, Aryl-_F_).

(R,R)-1,4-Bis(2-hexadecyloctadecyloxy)-2,5-bis{4-[2,3,5,6-tetrafluoro-4-(2,3-isopropylidene-2,3-dihydroxyprop-1-yloxy)phenylethynyl]phenylethynyl}benzene *5H1/16A

Synthesized according to GP5 from **5/1/16** (300 mg, 0.23 mmol), **28F*** (194 mg, 0.48 mmol), Pd(PPh$_3$)$_4$ (8.0 mg, 6.9 · 10^{-3} mmol), CuI (1.3 mg, 6.9 · 10^{-3} mmol) in anhydrous Et$_3$N (20 mL), purification by column chromatography (eluent: CHCl$_3$); yellow solid, yield: C$_{118}$H$_{170}$O$_8$F$_8$ M = 1868.64 g/mol, 290 mg (68 %), mp = 114 °C, **^{1}H-NMR** (CDCl$_3$, 400 MHz): δ / ppm =7.56 − 7.50 (m, 8H, Aryl-H), 7.00 (s, 2H, Aryl-H), 4.50 − 4.41 (m, 2H, -CHO-), 4.33 (dd, $^2J_{H,H}$ = 10.1, $^3J_{H,H}$ = 5.2 Hz, 2H, -OCH_AH$_B$-), 4.24 (dd, $^2J_{H,H}$ = 10.1, $^3J_{H,H}$ = 5.7 Hz, 2H, -OCH$_A$$H_B$-), 4.16 (dd, $^2J_{H,H}$ = 8.6, $^3J_{H,H}$ = 6.4 Hz, 2H, -ArOCH_AH$_B$-), 3.96 (dd, $^2J_{H,H}$ = 8.6, $^3J_{H,H}$ = 5.6 Hz, 2H, -ArOCH$_A$$H_B$-), 3.91 (d, $^3J_{H,H}$ = 5.6 Hz, 4H, -OCH_2-), 1.90 − 1.80 (m, 2H, -CH-), 1.43 (s, 6H, -CH_3), 1.39 (s, 6H, -CH_3), 1.33 − 1.19 (m, 120H, -CH_2-), 0.87 (t, $^3J_{H,H}$ = 6.8 Hz, 12H, -CH_3). **^{19}F-NMR** (CDCl$_3$, 376 MHz): δ / ppm = -137.38 − -137.69 (m, Aryl-F), -156.69 − -157.12 (m, Aryl-F).

1,4-Bis(4-tetradecyloctadecyloxy)-2,5-bis{4-[2,3,5,6-tetrafluoro-4-(2,3-isopropylidene-2,3-dihydroxyprop-1-yloxy)phenylethynyl]phenylethynyl}benzene 5F3/14A
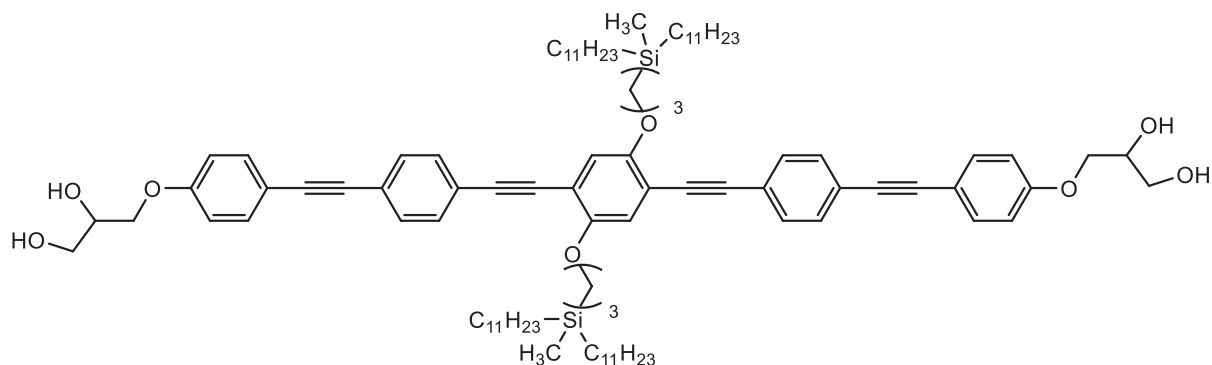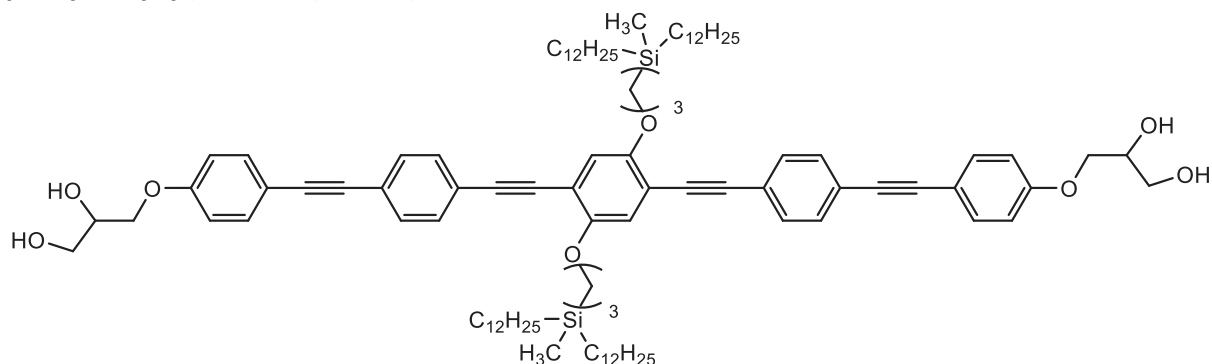

Synthesized according to GP5 from **5/3/14** (200 mg, 0.16 mmol), **26F** (141 mg, 0.35 mmol), Pd(PPh$_3$)$_4$ (5.5 mg, 4.8 · 10^{-3} mmol), CuI (0.9 mg, 4.8 · 10^{-3} mmol) in anhydrous Et$_3$N (20 mL), purification by column chromatography (eluent: CHCl$_3$); yellow solid, yield: C$_{114}$H$_{162}$O$_8$F$_8$ M = 1812.53 g/mol, 280 mg (97 %), mp = 95 °C, **^{1}H-NMR** (CDCl$_3$, 400 MHz): δ / ppm = 7.57 − 7.50 (m, 8H, Aryl-H), 7.01 (s, 2H, Aryl-H), 4.50 − 4.41 (m, 2H, -CHO-), 4.33 (dd, $^2J_{H,H}$ = 10.1, $^3J_{H,H}$ = 5.2 Hz, 2H, -OCH_AH$_B$-), 4.23 (dd, $^2J_{H,H}$ = 10.1, $^3J_{H,H}$ = 5.6 Hz, 2H, -OCH$_A$$H_B$-), 4.16 (dd, $^2J_{H,H}$ = 8.6, $^3J_{H,H}$ = 6.4 Hz, 2H, -ArOCH_AH$_B$-), 4.02 (t, $^3J_{H,H}$ = 6.3 Hz, 4H, -OCH_2-), 3.96 (dd, $^2J_{H,H}$ = 8.6, $^3J_{H,H}$ = 5.6 Hz, 2H, -ArOCH$_A$$H_B$-), 1.87 − 1.77 (m, 4H, -CH_2-), 1.54 − 1.45 (m, 4H, -CH_2-), 1.43 (s, 6H, -CH_3), 1.38 (s, 6H, -CH_3), 1.37 − 1.33 (m, 2H, -CH-), 1.31 − 1.17 (m, 104H, -CH_2-), 0.87 (t, $^3J_{H,H}$ = 6.8 Hz, 12H, -CH_3). **^{19}F-NMR** (CDCl3, 376 MHz): δ / ppm = -137.37 − -137.65 (m), -156.79 − -157.05 (m).

5.3.3 Analytical data of selected bolapolyphiles NX*n/m*

1,4-Bis[3-(diundecylmethylsilyl)propyloxy]-2,5-bis{4-[4-(2,3-dihydroxyprop-1-yloxy)phenylethynyl]-phenyl-ethynyl}benzene (2H3/11):

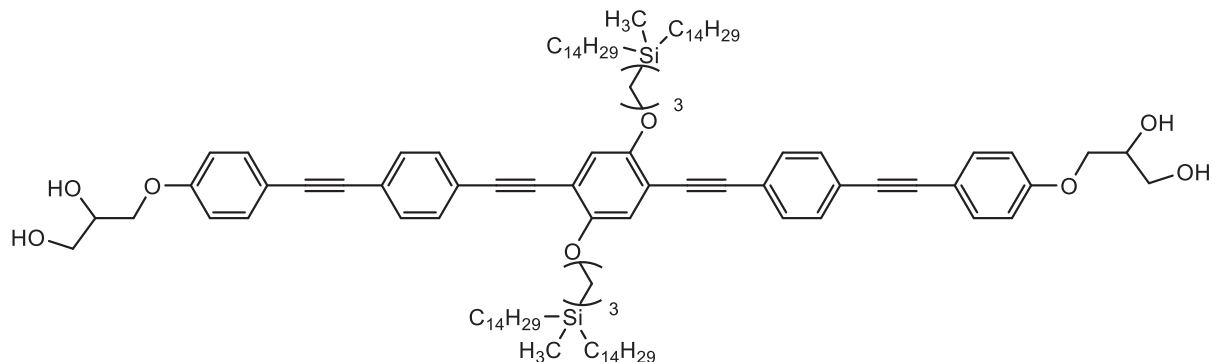Synthesized according to GP8 from **2H3/11A** (210 mg, 0.14 mmol),PPTS (68 mg, 0.27 mmol) in MeOH/THF (1:1; 30 mL : 30 mL), purification by column chromatography (eluent: CHCl$_3$); yellow solid, yield: C$_{96}$H$_{142}$O$_8$Si$_2$ M = 1480.35 g/mol, 136.3 mg (68 %), *mp* = 90 °C, **^{1}H-NMR** (402 MHz, Pyridine-*d*$_5$): δ / ppm = 7.78 (d, $^3J_{H,H}$ = 8.6 Hz, 4H, Aryl-*H*), 7.72 (d, $^3J_{H,H}$ = 8.6 Hz, 4H, Aryl-*H*), 7.65 (d, $^3J_{H,H}$ = 8.7 Hz, 4H, Aryl-*H*), 7.54 (s, 2H, Aryl-*H*), 7.12 (d, $^3J_{H,H}$ = 8.9 Hz, 4H, Aryl-*H*), 7.02 (s, 2H, -O*H*), 6.53 (s, 2H, -O*H*), 4.61 – 4.54 (m, 2H, -C*H*OH), 4.52 (dd, $^2J_{H,H}$ = 9.6, $^3J_{H,H}$ = 4.3 Hz, 2H, -ArOC*H*$_A$H$_B$), 4.43 (dd, $^2J_{H,H}$ = 9.6, $^3J_{H,H}$ = 6.3 Hz, 2H, -ArOCH$_A$*H*$_B$), 4.26 – 4.15 (m, 8H, -C*H*$_2$OH, -OC*H*$_2$-), 2.06 – 1.96 (m, 4H, -C*H*$_2$-), 1.52 – 1.20 (m, 72H, -C*H*$_2$-), 0.99 – 0.92 (m, 4H, -SiC*H*$_2$-), 0.89 (t, $^3J_{H,H}$ = 7.2 Hz, 12H, -C*H*$_3$), 0.73 – 0.65 (m, 8H, -SiC*H*$_2$-), 0.15 (s, 6H, -SiC*H*$_3$). **^{13}C NMR** (101 MHz, Pyridine-*d*$_5$) δ / ppm = 160.77, 154.81 (*C*$_{Aryl}$-O), 134.07, 132.53, 132.43 (*C*$_{Aryl}$-H), 124.68, 123.41 (*C*$_{Aryl}$-*quart*), 118.08, 115.87(*C*$_{Aryl}$-H), 115.67, 115.11 (*C*$_{Aryl}$-*quart*), 95.89, 93.15, 89.65, 88.99 (-*C*≡*C*-), 72.84, 71.81, 71.56, 64.73 (-O*C*H-, -O*C*H$_2$-), 34.63, 32.62, 30.54, 30.47, 30.44, 30.17, 30.12, 24.89, 24.78, 23.42 (-*C*H$_2$-), 14.76 (-*C*H$_3$), 14.60, 10.78 (-Si*C*H$_2$-), -4.47 (-Si*C*H$_3$). **^{29}Si-NMR** (80 MHz, Pyridine-*d*$_5$): δ / ppm = 3.30 (*Si*). **HRMS** (m/z): [M]+Cl$^-$ calc. for C$_{96}$H$_{142}$O$_8$Si$_2$Cl: 1514.9957, found: 1514.9976.

1,4-Bis[3-(didodecylmethylsilyl)propyloxy]-2,5-bis{4-[4-(2,3-dihydroxyprop-1-yloxy)phenylethynyl]-phenyl-ethynyl}benzene (2H3/12):

Synthesized according to GP8 from **2H3/12A** (200 mg, 0.12 mmol),PPTS (62 mg, 0.25 mmol) in MeOH/THF (1:1; 30 mL : 30 mL), purification by column chromatography (eluent: CHCl$_3$); yellow solid, yield: C$_{100}$H$_{150}$O$_8$Si$_2$ M = 1536.46 g/mol, 83.6 mg (44 %), *mp* = 90 °C, **^{1}H-NMR** (402 MHz, Pyridine-*d*$_5$): δ / ppm = 7.78 (d, $^3J_{H,H}$ = 7.9 Hz, 4H, Aryl-*H*), 7.72 (d, $^3J_{H,H}$ = 8.0 Hz, 4H, Aryl-*H*), 7.66 (d, $^3J_{H,H}$ = 8.5 Hz, 4H, Aryl-*H*), 7.54 (s, 2H, Aryl-*H*), 7.12 (d, $^3J_{H,H}$ = 8.4 Hz, 4H, Aryl-*H*), 6.95 (s, 2H, -O*H*), 6.53 (s, 2H, -O*H*), 4.63 – 4.54 (m, 2H, -C*H*OH), 4.52 (dd, $^2J_{H,H}$ = 9.5, $^3J_{H,H}$ = 4.4 Hz, 2H, -ArOC*H*$_A$H$_B$), 4.43 (dd, $^2J_{H,H}$ = 9.5, $^3J_{H,H}$ = 6.3 Hz, 2H, -ArOCH$_A$*H*$_B$), 4.30 – 4.14 (m, 8H, -C*H*$_2$OH, -OC*H*$_2$-), 2.08 – 1.96 (m, 4H, -C*H*$_2$-), 1.53 – 1.19 (m, 80H, -C*H*$_2$-), 0.99 – 0.92 (m, 4H, -SiC*H*$_2$-), 0.89 (t, $^3J_{H,H}$ = 6.5 Hz, 12H, -C*H*$_3$), 0.78 – 0.61 (m, 8H, -SiC*H*$_2$-), 0.15 (s, 6H, -SiC*H*$_3$). **^{13}C NMR** (101 MHz, Pyridine-*d*$_5$) δ / ppm = 160.76, 154.81 (*C*$_{Aryl}$-O), 134.07, 132.52,

132.43 (C_{Aryl}-H), 124.68, 123.42 (C_{Aryl}-*quart*), 118.07, 115.86 (C_{Aryl}-H), 115.67, 115.11 (C_{Aryl}-*quart*), 95.89, 93.15, 89.65, 88.99 (-*C*≡*C*-), 72.84, 71.80, 71.55, 64.72 (-O*C*H-, -O*C*H$_2$-), 34.64, 32.62, 30.56, 30.51, 30.49, 30.44, 30.19, 30.13, 24.90, 24.78, 23.43 (-*C*H$_2$-), 14.76 (-*C*H$_3$), 14.61, 10.79 (-Si*C*H$_2$-), -4.46 (-Si*C*H$_3$). **^{29}Si-NMR** (80 MHz, Pyridine-d_5): δ / ppm = 3.36 (*Si*). **HRMS** (m/z): [M]+Cl$^-$ calc. for C$_{100}$H$_{150}$O$_8$Si$_2$Cl: 1571.0583, found: 1571.0569.

1,4-Bis[3-(ditetradecylmethylsilyl)propyloxy]-2,5-bis{4-[4-(2,3-dihydroxyprop-1-yloxy)phenylethynyl]-phenyl-ethynyl}benzene (2H3/14):

Synthesized according to GP8 from **2H3/14A** (260 mg, 0.15 mmol), PPTS (76 mg, 0.30 mmol) in MeOH/THF (1:1; 30 mL : 30 mL), purification by column chromatography (eluent: CHCl$_3$); yellow solid, yield: C$_{108}$H$_{166}$O$_8$Si$_2$ *M* = 1648.68 g/mol, 143.8 mg (58 %), *mp* = 68 °C, **^{1}H-NMR** (400 MHz, Pyridine-d_5): δ / ppm = 7.78 (d, $^3J_{H,H}$ = 8.1 Hz, 4H, Aryl-*H*), 7.72 (d, $^3J_{H,H}$ = 8.2 Hz, 4H, Aryl-*H*), 7.65 (d, $^3J_{H,H}$ = 8.6 Hz, 4H, Aryl-*H*), 7.53 (s, 2H, Aryl-*H*), 7.11 (d, $^3J_{H,H}$ = 8.5 Hz, 4H, Aryl-*H*), 6.94 (s, 2H, -O*H*), 6.53 (s, 2H, -O*H*), 4.61 – 4.54 (m, 2H, -C*H*OH), 4.51 (dd, $^2J_{H,H}$ = 9.6, $^3J_{H,H}$ = 4.3 Hz, 2H, -ArOC*H$_A$*H$_B$), 4.42 (dd, $^2J_{H,H}$ = 9.5, $^3J_{H,H}$ = 6.2 Hz, 2H, -ArOCH$_A$*H$_B$*), 4.25 – 4.16 (m, 8H, -C*H$_2$*OH, -OC*H$_2$*-), 2.08 – 1.96 (m, 4H, -C*H$_2$*-), 1.54 – 1.20 (m, 96H, -C*H$_2$*-), 0.98 – 0.92 (m, 4H, -SiC*H$_2$*-), 0.89 (t, $^3J_{H,H}$ = 6.7 Hz, 12H, -C*H$_3$*), 0.74 – 0.65 (m, 8H, -SiC*H$_2$*-), 0.15 (s, 6H, -SiC*H$_3$*). **^{13}C NMR** (101 MHz, Pyridine-d_5) δ / ppm = 160.77, 154.81 (C_{Aryl}-O), 134.07, 132.53, 132.44 (C_{Aryl}-H), 124.69, 123.43 (C_{Aryl}-*quart*), 118.09, 115.87 (C_{Aryl}-H), 115.68, 115.12 (C_{Aryl}-*quart*), 95.90, 93.16, 89.66, 88.99 (-*C*≡*C*-), 72.84, 71.81, 71.56, 64.74 (-O*C*H-, -O*C*H$_2$-), 34.63, 34.53, 32.61, 30.56, 30.53, 30.50, 30.49, 30.42, 30.18, 30.11, 24.89, 24.78, 23.42 (-*C*H$_2$-), 14.76 (-*C*H$_3$), 14.61, 10.79 (-Si*C*H$_2$-), -4.45 (-Si*C*H$_3$). **^{29}Si-NMR** (79 MHz, Pyridine-d_5): δ / ppm = 3.35 (*Si*). **HRMS** (m/z): [M]+Cl$^-$ calc. for C$_{108}$H$_{166}$O$_8$Si$_2$Cl: 1683.1835, found: 1683.1880.

1,4-Bis[4-(didecylmethylsilyl)butyloxy]-2,5-bis{4-[4-(2,3-dihydroxyprop-1-yloxy)phenylethynyl]-phenyl-ethynyl}benzene (2H4/10):
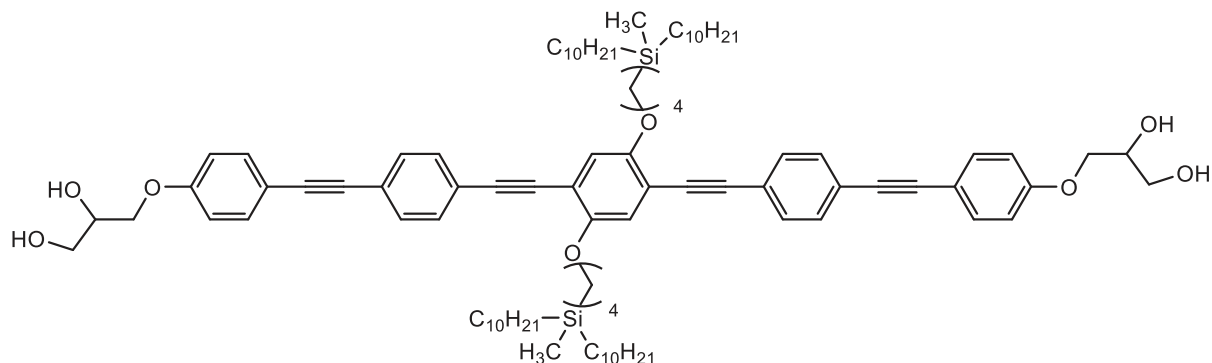
Synthesized according to GP8 from **2H4/10A** (240 mg, 0.16 mmol), PPTS (79 mg, 0.31 mmol) in MeOH/THF (1:1; 30 mL : 30 mL), purification by column chromatography (eluent: CHCl$_3$); yellow solid, yield: C$_{94}$H$_{138}$O$_8$Si$_2$ *M* = 1452.30 g/mol, 156.3 mg (69 %), *mp* = 55 °C, **^{1}H-NMR** (402 MHz, Pyridine-d_5): δ / ppm = 7.79 (d, $^3J_{H,H}$ = 8.4 Hz, 4H, Aryl-*H*), 7.72 (d, $^3J_{H,H}$ = 8.4 Hz, 4H, Aryl-*H*), 7.65 (d, $^3J_{H,H}$ = 8.7 Hz, 4H, Aryl-*H*), 7.51 (s, 2H, Aryl-*H*), 7.11 (d, $^3J_{H,H}$ = 8.8 Hz, 4H, Aryl-*H*), 4.60 – 4.54 (m, 2H, -C*H*OH), 4.52 (dd,

$^2J_{H,H}$ = 9.5, $^3J_{H,H}$ = 4.3 Hz, 2H, -ArOCH_AH$_B$), 4.43 (dd, $^2J_{H,H}$ = 9.5, $^3J_{H,H}$ = 6.3 Hz, 2H, -ArOCH$_A$H$_B$), 4.27 – 4.17 (m, 8H, -CH_2OH, -OCH_2-), 2.07 – 1.95 (m, 4H, -CH_2-), 1.83 – 1.70 (m, 4H, -CH_2-), 1.52 – 1.22 (m, 64H, -CH_2-), 0.89 (t, $^3J_{H,H}$ = 7.5 Hz, 12H, -CH_3), 0.78 – 0.71 (m, 4H, -SiCH_2-), 0.71 – 0.63 (m, 8H, -SiCH_2-), 0.13 (s, 6H, -SiCH_3). ^{13}**C NMR** (101 MHz, Pyridine-d_5) δ / ppm = 160.76, 154.79 (C_{Aryl}-O), 134.07, 132.55, 132.46 (C_{Aryl}-H), 124.66, 123.41 (C_{Aryl}-quart), 117.87, 115.87 (C_{Aryl}-H), 115.67, 114.98 (C_{Aryl}-quart), 95.90, 93.13, 89.62, 89.02 (-C≡C-), 71.81, 71.56, 69.73, 64.73 (-OCH-, -OCH$_2$-), 34.63, 34.00, 32.63, 30.48, 30.46, 30.19, 30.13, 24.81, 23.43, 21.35 (-CH$_2$-), 14.76 (-CH$_3$), 14.61, 14.36 (-SiCH$_2$-), -4.43 (-SiCH$_3$). ^{29}**Si-NMR** (80 MHz, Pyridine-d_5): δ / ppm = 2.89 (Si). **HRMS** (m/z): [M]+Cl$^-$ calcd. for C$_{94}$H$_{138}$O$_8$Si$_2$Cl: 1486.9644, found: 1486.9633.

1,4-Bis[4-(didodecylmethylsilyl)butyloxy]-2,5-bis{4-[4-(2,3-dihydroxyprop-1-yloxy)phenylethynyl]-phenyl-ethynyl}benzene (2H4/12):
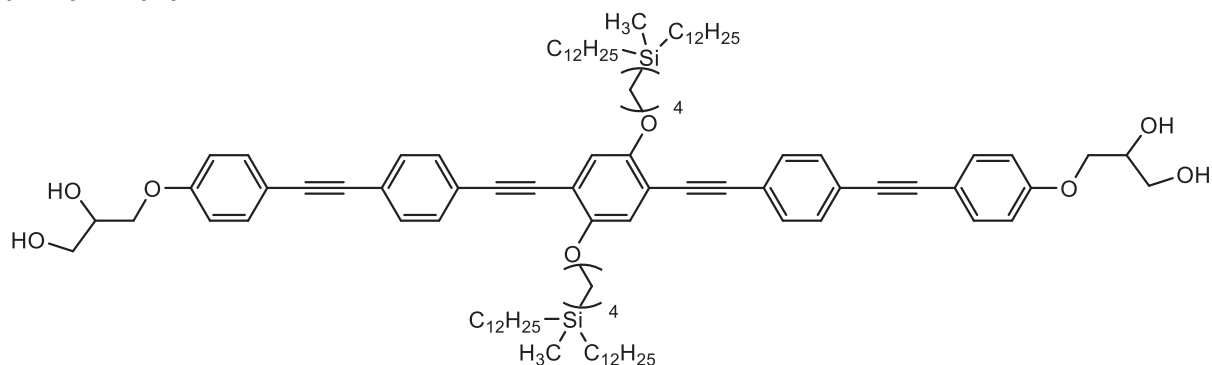
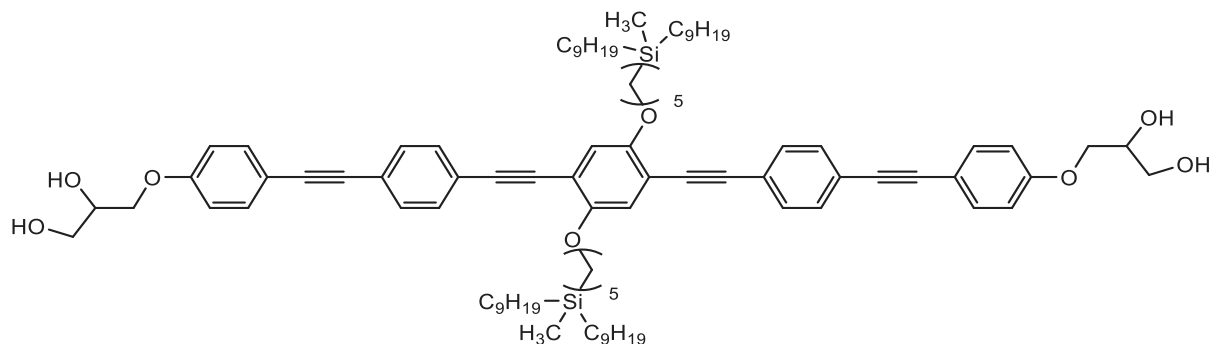

Synthesized according to GP8 from **2H4/12A** (320 mg, 0.20 mmol),PPTS (98 mg, 0.39 mmol) in MeOH/THF (1:1; 30 mL : 30 mL), purification by column chromatography (eluent: CHCl$_3$); yellow solid, yield: C$_{102}$H$_{154}$O$_8$Si$_2$ M = 1564.52 g/mol, 181.5 mg (60 %), mp = 61 °C, ^{1}**H-NMR** (400 MHz, Pyridine-d_5): δ / ppm = 7.79 (d, $^3J_{H,H}$ = 8.2 Hz, 4H, Aryl-H), 7.73 (d, $^3J_{H,H}$ = 8.2 Hz, 4H, Aryl-H), 7.65 (d, $^3J_{H,H}$ = 8.7 Hz, 4H, Aryl-H), 7.51 (s, 2H, Aryl-H), 7.11 (d, $^3J_{H,H}$ = 8.8 Hz, 4H, Aryl-H), 6.92 (s, 2H, -OH), 6.53 (s, 2H, -OH), 4.62 – 4.54 (m, 2H, -CHOH), 4.52 (dd, $^2J_{H,H}$ = 9.6, $^3J_{H,H}$ = 4.3 Hz, 2H, -ArOCH_AH$_B$), 4.43 (dd, $^2J_{H,H}$ = 9.6, $^3J_{H,H}$ = 6.3 Hz, 2H, -ArOCH$_A$H$_B$), 4.26 – 4.18 (m, 8H, -CH_2OH, -OCH_2-), 2.07 – 1.96 (m, 4H, -CH_2-), 1.85 – 1.70 (m, 4H, -CH_2-), 1.55 – 1.20 (m, 80H, -CH_2-), 0.90 (t, $^3J_{H,H}$ = 7.2 Hz, 12H, -CH_3), 0.79 – 0.72 (m, 4H, -SiCH_2-), 0.71 – 0.63 (m, 8H, -SiCH_2-), 0.14 (s, 6H, -SiCH_3). ^{13}**C NMR** (101 MHz, Pyridine-d_5) δ / ppm = 160.76, 154.79 (C_{Aryl}-O), 134.06, 132.54, 132.46 (C_{Aryl}-H), 124.66, 123.41 (C_{Aryl}-quart), 117.87, 115.86 (C_{Aryl}-H), 115.68, 114.99 (C_{Aryl}-quart), 95.89, 93.13, 89.62, 89.02 (-C≡C-), 71.80, 71.55, 69.73, 64.73 (-OCH-, -OCH$_2$-), 34.63, 34.00, 32.62, 30.54, 30.49, 30.47, 30.43, 30.20, 30.11, 24.81, 23.42, 21.35 (-CH$_2$-), 14.76 (-CH$_3$), 14.61, 14.36 (-SiCH$_2$-), -4.42 (-SiCH$_3$). ^{29}**Si-NMR** (79 MHz, Pyridine-d_5): δ / ppm = 2.92 (Si). **HRMS** (m/z): [M]+Cl$^-$ calc. for C$_{102}$H$_{154}$O$_8$Si$_2$Cl: 1599.0896, found: 1599.0871.

1,4-Bis[4-(ditetradecylmethylsilyl)butyloxy]-2,5-bis{4-[4-(2,3-dihydroxyprop-1-yloxy)phenylethynyl]-phenyl-ethynyl}benzene (2H4/14):
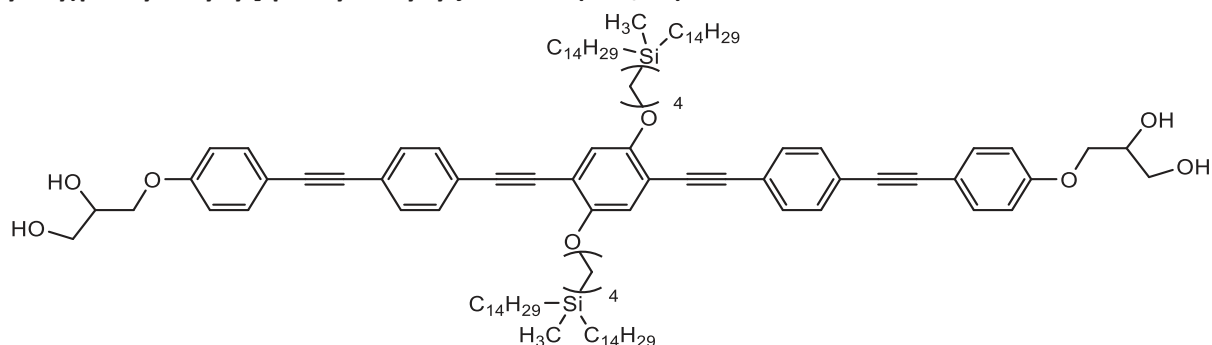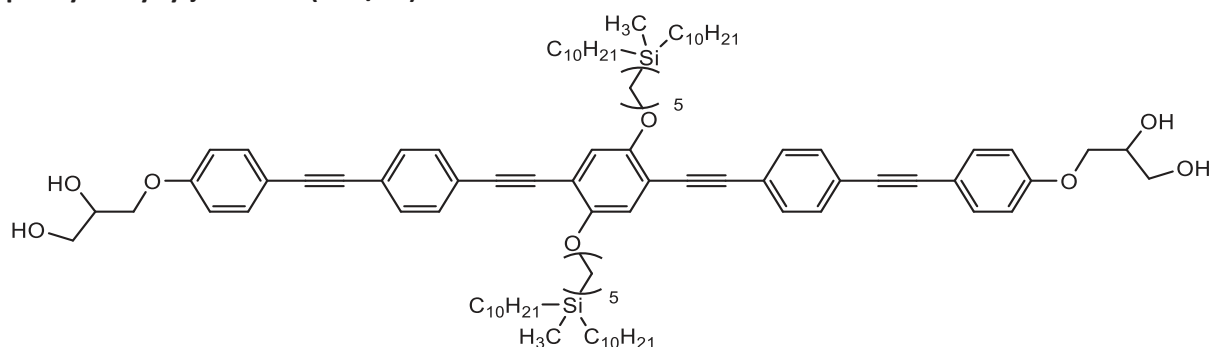
Synthesized according to GP8 from **2H4/14A** (600 mg, 0.34 mmol),PPTS (172 mg, 0.68 mmol) in MeOH/THF (1:1; 30 mL : 30 mL), purification by column chromatography (eluent: CHCl$_3$); yellow solid, yield: C$_{110}$H$_{170}$O$_8$Si$_2$ *M* = 1676.73 g/mol, 359.8 mg (63 %), *mp* = 69 °C, **^{1}H-NMR** (400 MHz, Pyridine-*d*$_5$): δ / ppm = 7.80 (d, $^3J_{H,H}$ = 8.3 Hz, 4H, Aryl-*H*), 7.73 (d, $^3J_{H,H}$ = 8.2 Hz, 4H, Aryl-*H*), 7.65 (d, $^3J_{H,H}$ = 8.6 Hz, 4H, Aryl-*H*), 7.52 (s, 2H, Aryl-*H*), 7.12 (d, $^3J_{H,H}$ = 8.8 Hz, 4H, Aryl-*H*), 6.95 (s, 2H, -O*H*), 6.54 (s, 2H, -O*H*), 4.62 – 4.55 (m, 2H, -C*H*OH), 4.52 (dd, $^2J_{H,H}$ = 9.6, $^3J_{H,H}$ = 4.3 Hz, 2H, -ArOC*H*$_A$H$_B$), 4.43 (dd, $^2J_{H,H}$ = 9.5, $^3J_{H,H}$ = 6.3 Hz, 2H, -ArOCH$_A$*H*$_B$), 4.26 – 4.19 (m, 8H, -C*H*$_2$OH, -OC*H*$_2$-), 2.06 – 1.97 (m, 4H, -C*H*$_2$-), 1.84 – 1.71 (m, 4H, -C*H*$_2$-), 1.52 – 1.21 (m, 96H, -C*H*$_2$-), 0.89 (t, $^3J_{H,H}$ = 7.1 Hz, 12H, -C*H*$_3$), 0.78 – 0.72 (m, 4H, -SiC*H*$_2$-), 0.72 – 0.65 (m, 8H, -SiC*H*$_2$-), 0.14 (s, 6H, -SiC*H*$_3$). **^{13}C NMR** (126 MHz, Pyridine-*d*$_5$) δ / ppm = 160.76, 154.79 (*C*$_{Aryl}$-O), 134.06, 132.54, 132.46 (*C*$_{Aryl}$-H), 124.66, 123.51 (*C*$_{Aryl}$-*quart*), 117.87, 115.86 (*C*$_{Aryl}$-H), 115.68, 114.99 (*C*$_{Aryl}$-*quart*), 95.89, 93.13, 89.62, 89.02 (-*C*≡*C*-), 71.80, 71.55, 69.73, 64.72 (-O*C*H-, -O*C*H$_2$-), 34.63, 33.99, 32.61, 30.55, 30.51, 30.50, 30.48, 30.42 [2x C], 30.20, 30.10, 24.81, 23.41, 21.34 (-*C*H$_2$-), 14.75 (-*C*H$_3$), 14.61, 14.35 (-Si*C*H$_2$-), -4.42 (-Si*C*H$_3$). **^{29}Si-NMR** (79 MHz, Pyridine-*d*$_5$): δ / ppm = 2.93 (*Si*). **HRMS** (m/z): [M]+Cl$^-$ calc. for C$_{110}$H$_{170}$O$_8$Si$_2$Cl: 1711.2148, found: 1711.2127.

1,4-Bis[5-(dinonylmethylsilyl)pentyloxy]-2,5-bis{4-[4-(2,3-dihydroxyprop-1-yloxy)phenylethynyl]-phenyl-ethynyl}benzene (2H5/9):
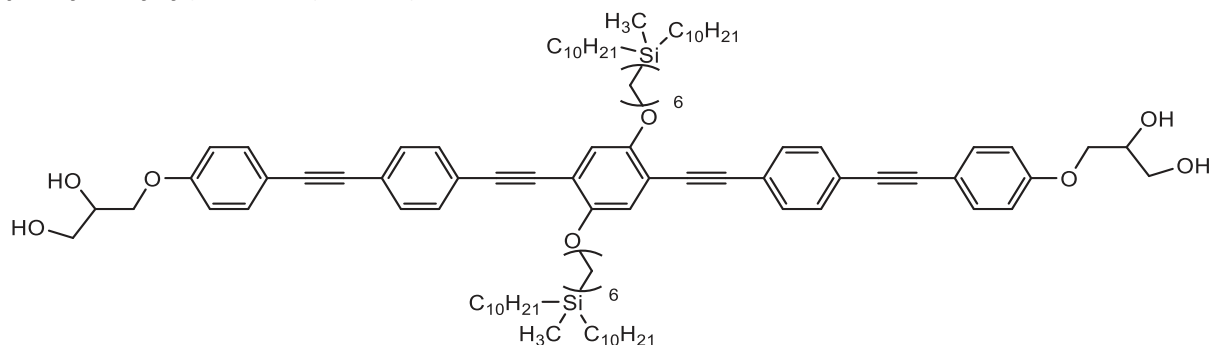

Synthesized according to GP8 from **2H5/9A** (250 mg, 0.17 mmol),PPTS (84 mg, 0.34 mmol) in MeOH/THF (1:1; 30 mL : 30 mL), purification by column chromatography (eluent: CHCl$_3$); yellow solid, yield: C$_{92}$H$_{134}$O$_8$Si$_2$ *M* = 1424.25 g/mol, 181.9 mg (77 %), *mp* = 55 °C, **^{1}H-NMR** (402 MHz, Pyridine-*d*$_5$): δ / ppm = 7.78 (d, $^3J_{H,H}$ = 8.4 Hz, 4H, Aryl-*H*), 7.70 (d, $^3J_{H,H}$ = 8.4 Hz, 4H, Aryl-*H*), 7.65 (d, $^3J_{H,H}$ = 8.7 Hz, 4H, Aryl-*H*), 7.50 (s, 2H, Aryl-*H*), 7.11 (d, $^3J_{H,H}$ = 8.9 Hz, 4H, Aryl-*H*), 4.61 – 4.54 (m, 2H, -C*H*OH), 4.52 (dd, $^2J_{H,H}$ = 9.5, $^3J_{H,H}$ = 4.3 Hz, 2H, -ArOC*H*$_A$H$_B$), 4.43 (dd, $^2J_{H,H}$ = 9.5, $^3J_{H,H}$ = 6.3 Hz, 2H, -ArOCH$_A$*H*$_B$), 4.28 – 4.15 (m, 8H, -C*H*$_2$OH, -OC*H*$_2$-), 2.04 – 1.92 (m, 4H, -C*H*$_2$-), 1.81 – 1.67 (m, 4H, -C*H*$_2$-), 1.60 – 1.21 (m, 60H, -C*H*$_2$-), 0.90 (t, $^3J_{H,H}$ = 7.1 Hz, 12H, -C*H*$_3$), 0.76 – 0.62 (m, 12H, -SiC*H*$_2$-), 0.12 (s, 6H, -SiC*H*$_3$). **^{13}C NMR** (101 MHz, Pyridine-*d*$_5$) δ / ppm = 160.76, 154.84 (*C*$_{Aryl}$-O), 134.07, 132.53, 132.44 (*C*$_{Aryl}$-H), 124.66, 123.43 (*C*$_{Aryl}$-*quart*), 118.02, 115.87 (*C*$_{Aryl}$-H), 115.67, 115.08 (*C*$_{Aryl}$-*quart*), 95.89, 93.14, 89.65, 89.00 (-*C*≡*C*-), 71.81, 71.56, 70.26, 64.73 (-O*C*H-, -O*C*H$_2$-), 34.61, 32.63, 31.02, 30.39, 30.16, 30.15, 29.92, 24.80, 24.61, 23.42 (-*C*H$_2$-), 14.76 (-*C*H$_3$), 14.64 (2x -Si*C*H$_2$-), -4.38 (-Si*C*H$_3$). **^{29}Si-NMR** (80 MHz, Pyridine-*d*$_5$): δ / ppm = 2.77 (*Si*). **HRMS** (m/z): [M]+Cl$^-$ calc. for C$_{92}$H$_{134}$O$_8$Si$_2$Cl: 1458.9331, found: 1458.9319.

1,4-Bis[5-(didecylmethylsilyl)pentyloxy]-2,5-bis{4-[4-(2,3-dihydroxyprop-1-yloxy)phenylethynyl]-phenyl-ethynyl}benzene (2H5/10):

Synthesized according to GP8 from **2H5/10A** (260 mg, 0.17 mmol),PPTS (84 mg, 0.34 mmol) in MeOH/THF (1:1; 30 mL : 30 mL), purification by column chromatography (eluent: CHCl$_3$); yellow solid, yield: C$_{96}$H$_{142}$O$_8$Si$_2$ M = 1480.35 g/mol, 180.4 mg (73 %), mp = 55 °C, **^{1}H-NMR** (400 MHz, Pyridine-d_5): δ / ppm = 7.78 (d, $^3J_{H,H}$ = 8.3 Hz, 4H, Aryl-H), 7.70 (d, $^3J_{H,H}$ = 8.3 Hz, 4H, Aryl-H), 7.65 (d, $^3J_{H,H}$ = 8.7 Hz, 4H, Aryl-H), 7.49 (s, 2H, Aryl-H), 7.11 (d, $^3J_{H,H}$ = 8.9 Hz, 4H, Aryl-H), 4.61 − 4.54 (m, 2H, -CHOH), 4.52 (dd, $^2J_{H,H}$ = 9.6, $^3J_{H,H}$ = 4.3 Hz, 2H, -ArOCH_AH$_B$), 4.43 (dd, $^2J_{H,H}$ = 9.6, $^3J_{H,H}$ = 6.2 Hz, 2H, -ArOC$H_A$$H_B$), 4.25 − 4.14 (m, 8H, -CH_2OH, -OCH_2-), 2.05 − 1.94 (m, 4H, -CH_2-), 1.81 − 1.71 (m, 4H, -CH_2-), 1.60 − 1.19 (m, 68H, -CH_2-), 0.90 (t, $^3J_{H,H}$ = 7.6 Hz, 12H, -CH_3), 0.74 − 0.62 (m, 12H, -SiCH_2-), 0.13 (s, 6H, -SiCH_3). **^{13}C NMR** (101 MHz, Pyridine-d_5) δ / ppm = 160.76, 154.85 (C_{Aryl}-O), 134.08, 132.54, 132.45 (C_{Aryl}-H), 124.67, 123.43 (C_{Aryl}-quart), 118.02, 115.87 (C_{Aryl}-H), 115.69, 115.09 (C_{Aryl}-quart), 95.89, 93.15, 89.66, 89.01 (-C≡C-), 71.81, 71.56, 70.26, 64.73 (-OCH-, -OCH$_2$-), 34.63, 32.63, 31.03, 30.48, 30.46, 30.19, 30.14, 29.93, 24.82, 24.62, 23.44 (-CH$_2$-), 14.77 (-CH$_3$), 14.66 (2x -SiCH$_2$-), -4.36 (-SiCH$_3$). **^{29}Si-NMR** (79 MHz, Pyridine-d_5): δ / ppm = 2.79 (Si). **HRMS** (m/z): [M]+Cl$^-$ calc. for C$_{96}$H$_{142}$O$_8$Si$_2$Cl: 1514.9957, found: 1514.9967.

1,4-Bis[6-(didecylmethylsilyl)hexyloxy]-2,5-bis{4-[4-(2,3-dihydroxyprop-1-yloxy)phenylethynyl]-phenyl-ethynyl}benzene (2H6/10):

Synthesized according to GP8 from **2H6/10A** (270 mg, 0.17 mmol),PPTS (85 mg, 0.34 mmol) in MeOH/THF (1:1; 30 mL : 30 mL), purification by column chromatography (eluent: CHCl$_3$); yellow solid, yield: C$_{98}$H$_{146}$O$_8$Si$_2$ M = 1508.41 g/mol, 185.1 mg (72 %), mp = 81 °C, **^{1}H-NMR** (402 MHz, Pyridine-d_5): δ / ppm = 7.78 (d, $^3J_{H,H}$ = 8.4 Hz, 4H, Aryl-H), 7.71 (d, $^3J_{H,H}$ = 8.3 Hz, 4H, Aryl-H), 7.65 (d, $^3J_{H,H}$ = 8.8 Hz, 4H, Aryl-H), 7.49 (s, 2H, Aryl-H), 7.11 (d, $^3J_{H,H}$ = 9.0 Hz, 4H, Aryl-H), 4.60 − 4.54 (m, 2H, -CHOH), 4.52 (dd, $^2J_{H,H}$ = 9.5, $^3J_{H,H}$ = 4.3 Hz, 2H, -ArOCH_AH$_B$), 4.43 (dd, $^2J_{H,H}$ = 9.6, $^3J_{H,H}$ = 6.2 Hz, 2H, -ArOC$H_A$$H_B$), 4.25 − 4.20 (m, 4H, -CH_2OH), 4.17 (t, $^3J_{H,H}$ = 6.4 Hz, 4H, -OCH_2-), 2.00 − 1.90 (m, 4H, -CH_2-), 1.76 − 1.66 (m, 4H, -CH_2-), 1.60 − 1.21 (m, 72H, -CH_2-), 0.90 (t, $^3J_{H,H}$ = 7.1 Hz, 12H, -CH_3), 0.70 − 0.64 (m, 12H, -SiCH_2-), 0.12 (s, 6H, -SiCH_3). **^{13}C NMR** (101 MHz, Pyridine-d_5) δ / ppm = 160.75, 154.80 (C_{Aryl}-O), 134.06, 132.51, 132.45 (C_{Aryl}-H), 124.66, 123.42 (C_{Aryl}-quart), 117.94, 115.86 (C_{Aryl}-H), 115.68, 115.05 (C_{Aryl}-quart), 95.90, 93.15, 89.63, 89.01 (-C≡C-), 71.80, 71.55, 70.24, 64.72 (-OCH-, -OCH$_2$-), 34.61, 34.31, 32.61, 30.46, 30.43, 30.17, 30.13, 30.11, 26.64, 24.85, 24.80, 23.42 (-CH$_2$-), 14.75 (-CH$_3$), 14.64 (2x -SiCH$_2$-), -4.39 (-SiCH$_3$).

^{29}**Si-NMR** (80 MHz, Pyridine-d_5): δ / ppm = 2.83 (*Si*). **HRMS** (m/z): [M]+Cl$^-$ calc. for $C_{98}H_{146}O_8Si_2Cl$: 1543.0270, found: 1543.0281.

1,4-Bis[6-(didodecylmethylsilyl)hexyloxy]-2,5-bis{4-[4-(2,3-dihydroxyprop-1-yloxy)phenylethynyl]-phenyl-ethynyl}benzene (2H6/12):
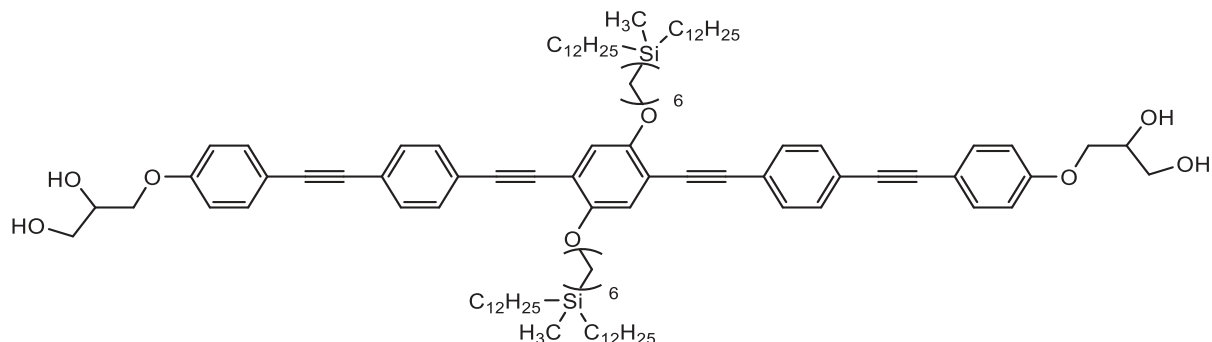
Synthesized according to GP8 from **2H6/12A** (270 mg, 0.16 mmol),PPTS (80 mg, 0.32 mmol) in MeOH/THF (1:1; 30 mL : 30 mL), purification by column chromatography (eluent: CHCl$_3$); yellow solid, yield: $C_{106}H_{162}O_8Si_2$ *M* = 1620.62 g/mol, 170.0 mg (66 %), *mp* = 73 °C, ^{1}**H-NMR** (400 MHz, Pyridine-d_5): δ / ppm = 7.78 (d, $^3J_{H,H}$ = 8.4 Hz, 4H, Aryl-*H*), 7.71 (d, $^3J_{H,H}$ = 8.3 Hz, 4H, Aryl-*H*), 7.65 (d, $^3J_{H,H}$ = 8.7 Hz, 4H, Aryl-*H*), 7.48 (s, 2H, Aryl-*H*), 7.11 (d, $^3J_{H,H}$ = 8.8 Hz, 4H, Aryl-*H*), 4.60 − 4.54 (m, 2H, -C*H*OH), 4.51 (dd, $^2J_{H,H}$ = 9.5, $^3J_{H,H}$ = 4.3 Hz, 2H, -ArOC*H$_A$*H$_B$), 4.42 (dd, $^2J_{H,H}$ = 9.5, $^3J_{H,H}$ = 6.2 Hz, 2H, -ArOCH$_A$*H$_B$*), 4.24 − 4.21 (m, 4H, -C*H$_2$*OH), 4.18 (t, $^3J_{H,H}$ = 6.3 Hz, 4H, -OC*H$_2$*-), 2.00 − 1.91 (m, 4H, -C*H$_2$*-), 1.77 − 1.67 (m, 4H, -C*H$_2$*-), 1.59 − 1.22 (m, 88H, -C*H$_2$*-), 0.90 (t, $^3J_{H,H}$ = 7.1 Hz, 12H, -C*H$_3$*), 0.74 − 0.63 (m, 12H, -SiC*H$_2$*-), 0.13 (s, 6H, -SiC*H$_3$*). ^{13}**C NMR** (101 MHz, Pyridine-d_5) δ / ppm = 160.76, 154.82 (C_{Aryl}-O), 134.08, 132.52, 132.46 (C_{Aryl}-H), 124.68, 123.45 (C_{Aryl}-*quart*), 117.95, 115.87 (C_{Aryl}-H), 115.70, 115.07 (C_{Aryl}-*quart*), 95.91, 93.16, 89.65, 89.02 (-*C≡C*-), 71.81, 71.56, 70.25, 64.74 (-*O*CH-, -*O*CH$_2$-), 34.63, 34.33, 32.63, 30.55, 30.50, 30.46, 30.44, 30.20, 30.15, 30.12, 26.66, 24.88, 24.83, 23.44 (-*C*H$_2$-), 14.78 (-*C*H$_3$), 14.66 (2x -Si*C*H$_2$-), -4.36 (-Si*C*H$_3$). ^{29}**Si-NMR** (79 MHz, Pyridine-d_5): δ / ppm = 2.80 (*Si*). **HRMS** (m/z): [M]+Cl$^-$ calc. for $C_{106}H_{162}O_8Si_2Cl$: 1655.1522, found: 1655.1511.

1,4-Bis[7-(dinonylmethylsilyl)heptyloxy]-2,5-bis{4-[4-(2,3-dihydroxyprop-1-yloxy)phenylethynyl]-phenyl-ethynyl}benzene (2H7/9):
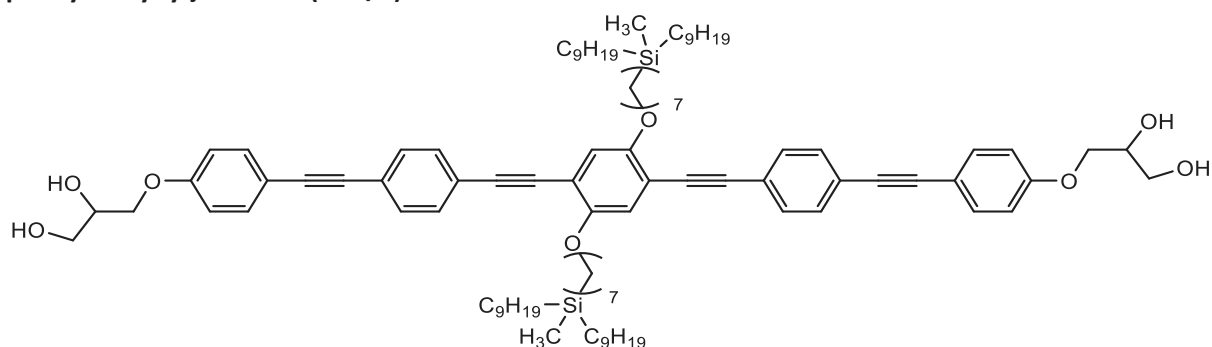
Synthesized according to GP8 from **2H7/9A** (270 mg, 0.17 mmol),PPTS (87 mg, 0.35 mmol) in MeOH/THF (1:1; 30 mL : 30 mL), purification by column chromatography (eluent: CHCl$_3$); yellow solid, yield: $C_{96}H_{142}O_8Si_2$ *M* = 1480.35 g/mol, 148.1 mg (58 %), *mp* = 75 °C, ^{1}**H-NMR** (402 MHz, Pyridine-d_5): δ / ppm 7.81 − 7.74 (m, 4H, Aryl-*H*), 7.70 (d, $^3J_{H,H}$ = 8.3 Hz, 4H, Aryl-*H*), 7.65 (d, $^3J_{H,H}$ = 8.7 Hz, 4H, Aryl-*H*), 7.48 (d, $^3J_{H,H}$ = 1.2 Hz, 2H, Aryl-*H*), 7.11 (d, $^3J_{H,H}$ = 8.8 Hz, 4H, Aryl-*H*), 4.60 − 4.54 (m, 2H, -C*H*OH), 4.51 (dd, $^2J_{H,H}$ = 9.5, $^3J_{H,H}$ = 4.4 Hz, 2H, -ArOC*H$_A$*H$_B$), 4.43 (dd, $^2J_{H,H}$ = 9.5, $^3J_{H,H}$ = 6.2 Hz, 2H, -ArOCH$_A$*H$_B$*), 4.26 − 4.20 (m, 4H, -C*H$_2$*OH), 4.16 (t, $^3J_{H,H}$ = 6.4 Hz, 4H, -OC*H$_2$*-), 1.99 − 1.90 (m, 4H, -C*H$_2$*-), 1.74 − 1.62 (m, 4H, -C*H$_2$*-), 1.54 − 1.20 (m, 68H, -C*H$_2$*-), 0.90 (t, $^3J_{H,H}$ = 7.7 Hz, 12H, -C*H$_3$*), 0.71 − 0.62 (m, 12H, -SiC*H$_2$*-), 0.13 (s, 6H, -SiC*H$_3$*). ^{13}**C NMR** (101 MHz, Pyridine-d_5) δ / ppm = 160.75, 154.81 (C_{Aryl}-O), 134.06, 132.51,

132.45 (C_{Aryl}-H), 124.66, 123.43 (C_{Aryl}-*quart*), 117.96, 115.86 (C_{Aryl}-H), 115.68, 115.05 (C_{Aryl}-*quart*), 95.89, 93.14, 89.62, 89.00 (-*C*≡*C*-), 71.80, 71.54, 70.26, 64.72 (-O*C*H-, -O*C*H$_2$-), 34.67, 34.59, 32.62, 30.36, 30.19, 30.15, 30.14, 29.90, 26.94, 24.80, 24.77, 23.42 (-*C*H$_2$-), 14.75 (-*C*H$_3$), 14.73, 14.65 (-Si*C*H$_2$-), -4.36 (-Si*C*H$_3$). ^{29}**Si-NMR** (80 MHz, Pyridine-d_5): δ / ppm = 2.77 (*Si*). **HRMS** (m/z): [M]+Cl⁻ calc. for C$_{96}$H$_{142}$O$_8$Si$_2$Cl: 1514.9957, found: 1514.9971.

1,4-Bis[7-(didecylmethylsilyl)heptyloxy]-2,5-bis{4-[4-(2,3-dihydroxyprop-1-yloxy)phenylethynyl]-phenyl-ethynyl}benzene (2H7/10):
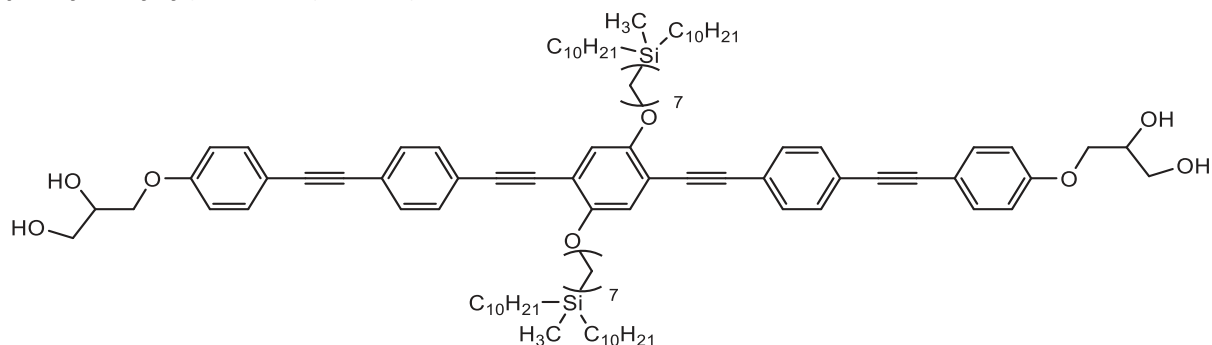
Synthesized according to GP8 from **2H7/10A** (250 mg, 0.16 mmol),PPTS (78 mg, 0.32 mmol) in MeOH/THF (1:1; 30 mL : 30 mL), purification by column chromatography (eluent: CHCl$_3$); yellow solid, yield: C$_{100}$H$_{150}$O$_8$Si$_2$ *M* = 1536.46 g/mol, 84.5 mg (36 %), *mp* = 70 °C, ^{1}**H-NMR** (402 MHz, Pyridine-d_5): δ / ppm = 7.78 (d, $^3J_{H,H}$ = 8.4 Hz, 4H, Aryl-*H*), 7.71 (d, $^3J_{H,H}$ = 8.2 Hz, 4H, Aryl-*H*), 7.65 (d, $^3J_{H,H}$ = 8.9 Hz, 4H, Aryl-*H*), 7.48 (s, 2H, Aryl-*H*), 7.11 (d, $^3J_{H,H}$ = 8.7 Hz, 4H, Aryl-*H*), 4.60 − 4.54 (m, 2H, -C*H*OH), 4.51 (dd, $^2J_{H,H}$ = 9.5, $^3J_{H,H}$ = 4.3 Hz, 2H, -ArOC*H*$_A$H$_B$), 4.43 (dd, $^2J_{H,H}$ = 9.5, $^3J_{H,H}$ = 6.2 Hz, 2H, -ArOCH$_A$*H*$_B$), 4.25 − 4.20 (m, 4H, -C*H*$_2$OH), 4.16 (t, $^3J_{H,H}$ = 6.4 Hz, 4H, -OC*H*$_2$-), 1.99 − 1.90 (m, 4H, -C*H*$_2$-), 1.74 − 1.62 (m, 4H, -C*H*$_2$-), 1.59 − 1.21 (m, 76H, -C*H*$_2$-), 0.90 (t, $^3J_{H,H}$ = 7.0 Hz, 12H, -C*H*$_3$), 0.71 − 0.63 (m, 12H, -SiC*H*$_2$-), 0.13 (s, 6H, -SiC*H*$_3$). ^{13}**C NMR** (101 MHz, Pyridine-d_5) δ / ppm = 160.75, 154.82 (C_{Aryl}-O), 134.06, 132.51, 132.45 (C_{Aryl}-H), 124.66, 123.41 (C_{Aryl}-*quart*), 117.96, 115.86 (C_{Aryl}-H), 115.68, 115.05 (C_{Aryl}-*quart*), 95.90, 93.14, 89.62, 89.01 (-*C*≡*C*-), 71.80, 71.54, 70.26, 64.72 (-O*C*H-, -O*C*H$_2$-), 34.67, 34.61, 32.61, 30.45, 30.42, 30.19, 30.16, 30.11, 29.90, 26.94, 24.81, 24.77, 23.42 (-*C*H$_2$-), 14.76 (-*C*H$_3$), 14.73, 14.66 (-Si*C*H$_2$-), -4.35 (-Si*C*H$_3$). ^{29}**Si-NMR** (80 MHz, Pyridine-d_5): δ / ppm = 2.77 (*Si*). **HRMS** (m/z): [M]+Cl⁻ calc. for C$_{100}$H$_{150}$O$_8$Si$_2$Cl: 1571.0583, found: 1571.0579.

1,4-Bis[9-(dioctylmethylsilyl)nonyloxy]-2,5-bis{4-[4-(2,3-dihydroxyprop-1-yloxy)phenylethynyl]-phenyl-ethynyl}benzene (2H9/8):
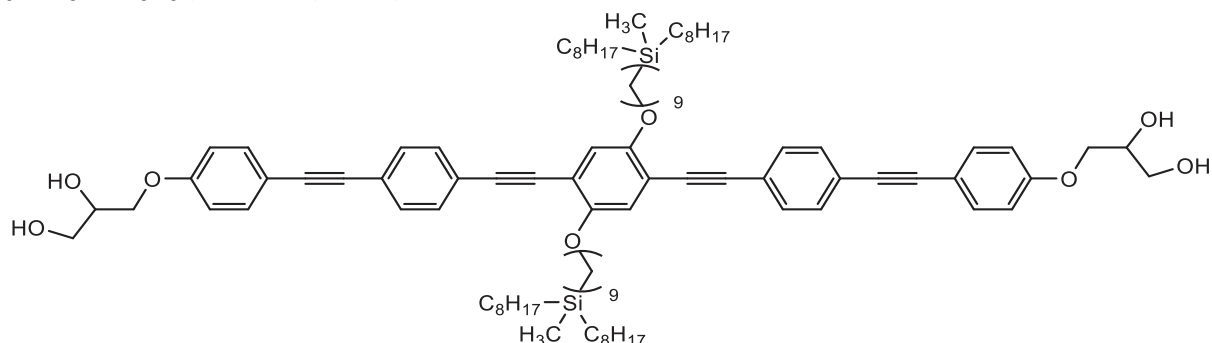
Synthesized according to GP8 from **2H9/8A** (250 mg, 0.16 mmol),PPTS (80 mg, 0.32 mmol) in MeOH/THF (1:1; 30 mL : 30 mL), purification by column chromatography (eluent: CHCl$_3$); yellow solid, yield: C$_{96}$H$_{142}$O$_8$Si$_2$ *M* = 1480.35 g/mol, 142.0 mg (60 %), *mp* = 95 °C, ^{1}**H-NMR** (502 MHz, Pyridine-d_5): δ / ppm = 7.78 (d, $^3J_{H,H}$ = 8.3 Hz, 4H, Aryl-*H*), 7.70 (d, $^3J_{H,H}$ = 8.3 Hz, 4H, Aryl-*H*), 7.65 (d, $^3J_{H,H}$ = 8.7 Hz, 4H, Aryl-*H*), 7.49 (s, 2H, Aryl-*H*), 7.11 (d, $^3J_{H,H}$ = 8.8 Hz, 4H, Aryl-*H*), 4.60 − 4.54 (m, 2H, -C*H*OH), 4.52 (dd,

$^2J_{H,H}$ = 9.6, $^3J_{H,H}$ = 4.4 Hz, 2H, -ArOCH_AH$_B$), 4.43 (dd, $^2J_{H,H}$ = 9.5, $^3J_{H,H}$ = 6.2 Hz, 2H, -ArOCH_AH$_B$), 4.25 – 4.20 (m, 4H, -CH_2OH), 4.15 (t, $^3J_{H,H}$ = 6.4 Hz, 4H, -OCH_2-), 1.96 – 1.87 (m, 4H, -CH_2-), 1.70 – 1.60 (m, 4H, -CH_2-), 1.51 – 1.23 (m, 68H, -CH_2-), 0.90 (t, $^3J_{H,H}$ = 6.7 Hz, 12H, -CH_3), 0.70 – 0.62 (m, 12H, -SiCH_2-), 0.13 (s, 6H, -SiCH_3). ^{13}**C NMR** (126 MHz, Pyridine-d_5) δ / ppm = 160.75, 154.81 (C_{Aryl}-O), 134.06, 132.51, 132.44 (C_{Aryl}-H), 124.66, 123.51 (C_{Aryl}-quart), 117.98, 115.86 (C_{Aryl}-H), 115.67, 115.05 (C_{Aryl}-quart), 95.89, 93.15, 89.61, 89.01 (-C≡C-), 71.80, 71.55, 70.25, 64.72 (-OCH-, -OCH$_2$-), 34.62, 34.57, 32.64, 30.43, 30.20, 30.13, 30.10, 30.08, 30.03, 26.92, 24.81, 24.78, 23.41 (-CH$_2$-), 14.74 (-CH$_3$), 14.69, 14.65 (-SiCH$_2$-), -4.35 (-SiCH$_3$). ^{29}**Si-NMR** (100 MHz, Pyridine-d_5): δ / ppm = 2.76 (Si). **HRMS** (m/z): [M]+Cl$^-$ calc. for $C_{96}H_{142}O_8Si_2Cl$: 1514.9957, found: 1514.9926.

1,4-Bis[9-(diundecylmethylsilyl)nonyloxy]-2,5-bis{4-[4-(2,3-dihydroxyprop-1-yloxy)phenylethynyl]-phenyl-ethynyl}benzene (2H9/11):
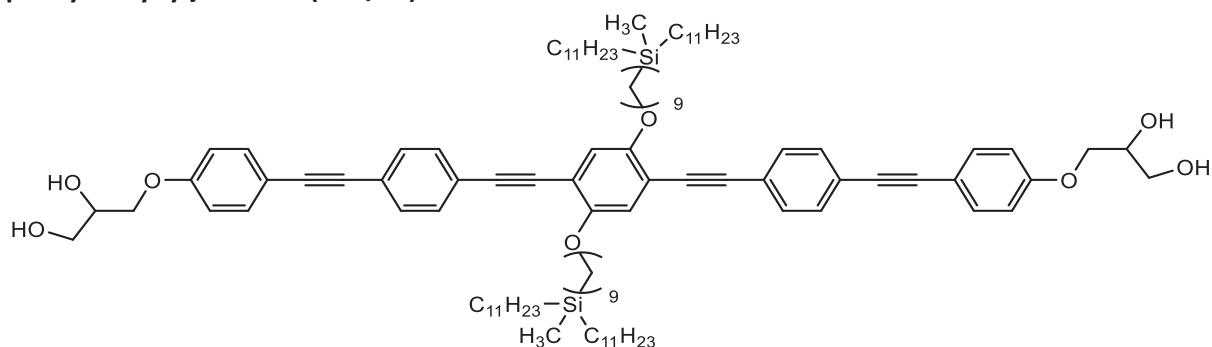
Synthesized according to GP8 from **2H9/11A** (300 mg, 0.17 mmol),PPTS (87 mg, 0.35 mmol) in MeOH/THF (1:1; 30 mL : 30 mL), purification by column chromatography (eluent: CHCl$_3$); yellow solid, yield: $C_{108}H_{166}O_8Si_2$ M = 1648.68 g/mol, 213.6 mg (75 %), mp = 66 °C, ^{1}**H-NMR** (500 MHz, Pyridine-d_5): δ / ppm = 7.78 (d, $^3J_{H,H}$ = 8.3 Hz, 4H, Aryl-H), 7.70 (d, $^3J_{H,H}$ = 8.3 Hz, 4H, Aryl-H), 7.65 (d, $^3J_{H,H}$ = 8.7 Hz, 4H, Aryl-H), 7.49 (s, 2H, Aryl-H), 7.11 (d, $^3J_{H,H}$ = 8.8 Hz, 4H, Aryl-H), 4.61 – 4.54 (m, 2H, -CHOH), 4.51 (dd, $^2J_{H,H}$ = 9.6, $^3J_{H,H}$ = 4.4 Hz, 2H, -ArOCH_AH$_B$), 4.43 (dd, $^2J_{H,H}$ = 9.5, $^3J_{H,H}$ = 6.3 Hz, 2H, -ArOCH_AH$_B$), 4.25 – 4.21 (m, 4H, -CH_2OH), 4.15 (t, $^3J_{H,H}$ = 6.4 Hz, 4H, -OCH_2-), 1.97 – 1.88 (m, 4H, -CH_2-), 1.70 – 1.61 (m, 4H, -CH_2-), 1.52 – 1.21 (m, 92H, -CH_2-), 0.90 (t, $^3J_{H,H}$ = 6.9 Hz, 12H, -CH_3), 0.71 – 0.64 (m, 12H, -SiCH_2-), 0.14 (s, 6H, -SiCH_3). ^{13}**C NMR** (126 MHz, Pyridine-d_5) δ / ppm = 160.76, 154.82 (C_{Aryl}-O), 134.07, 132.52, 132.45 (C_{Aryl}-H), 124.67, 123.54 (C_{Aryl}-quart), 117.98, 115.87 (C_{Aryl}-H), 115.69, 115.06 (C_{Aryl}-quart), 95.90, 93.16, 89.62, 89.02 (-C≡C-), 71.81, 71.55, 70.26, 64.73 (-OCH-, -OCH$_2$-), 34.64, 34.60, 32.62, 30.51, 30.45, 30.42 [3xC], 30.22, 30.16, 30.11 [2xC], 26.94, 24.83, 24.81, 23.43 (-CH$_2$-), 14.77 (-CH$_3$), 14.72, 14.68 (-SiCH$_2$-), -4.31 (-SiCH$_3$). ^{29}**Si-NMR** (99 MHz, Pyridine-d_5): δ / ppm = 2.78 (Si). **HRMS** (m/z): [M]+Cl$^-$ calc. for $C_{108}H_{166}O_8Si_2Cl$: 1683.1835, found: 1683.1814.

1,4-Bis[11-(diundecylmethylsilyl)undecyloxy]-2,5-bis{4-[4-(2,3-dihydroxyprop-1-yloxy)phenylethynyl]-phenyl-ethynyl}benzene (2H11/11):
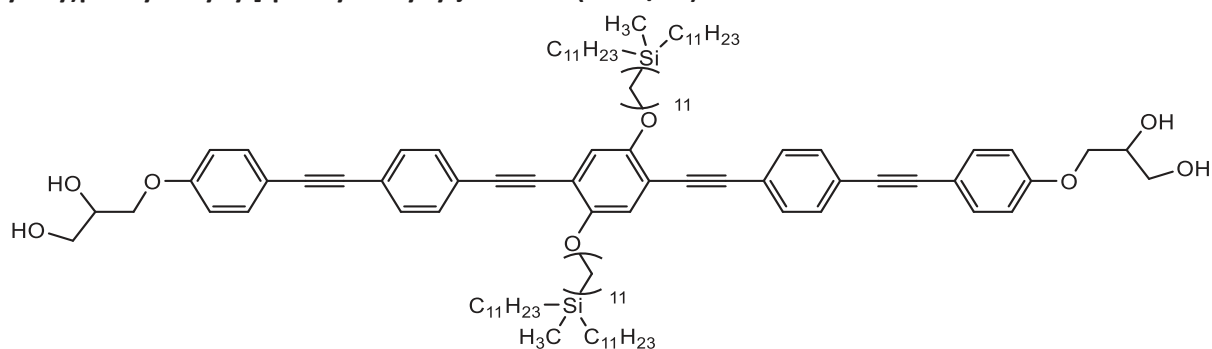
Synthesized according to GP8 from **2H11/11A** (400 mg, 0.22 mmol),PPTS (113 mg, 0.45 mmol) in MeOH/THF (1:1; 30 mL : 30 mL), purification by column chromatography (eluent: CHCl$_3$); yellow solid,

yield: $C_{112}H_{174}O_8Si_2$ M = 1704.79 g/mol, 134.7 mg (35 %), *mp* = 77 °C, **¹H-NMR** (400 MHz, Pyridine-d_5): δ / ppm = 7.78 (d, $^3J_{H,H}$ = 8.4 Hz, 4H, Aryl-*H*), 7.70 (d, $^3J_{H,H}$ = 8.3 Hz, 4H, Aryl-*H*), 7.66 (d, $^3J_{H,H}$ = 8.7 Hz, 4H, Aryl-*H*), 7.50 (s, 2H, Aryl-*H*), 7.12 (d, $^3J_{H,H}$ = 8.8 Hz, 4H, Aryl-*H*), 6.98 (s, 2H, -O*H*), 6.54 (s, 2H, -O*H*), 4.61 – 4.54 (m, 2H, -C*H*OH), 4.52 (dd, $^2J_{H,H}$ = 9.5, $^3J_{H,H}$ = 4.3 Hz, 2H, -ArOC*H*$_A$H$_B$), 4.43 (dd, $^2J_{H,H}$ = 9.5, $^3J_{H,H}$ = 6.2 Hz, 2H, -ArOCH$_A$*H*$_B$), 4.27 – 4.20 (m, 4H, -C*H*$_2$OH), 4.15 (t, $^3J_{H,H}$ = 6.4 Hz, 4H, -OC*H*$_2$-), 1.98 – 1.84 (m, 4H, -C*H*$_2$-), 1.72 – 1.58 (m, 4H, -C*H*$_2$-), 1.58 – 1.19 (m, 100H, -C*H*$_2$-), 0.89 (t, $^3J_{H,H}$ = 7.2 Hz, 12H, -C*H*$_3$), 0.72 – 0.62 (m, 12H, -SiC*H*$_2$-), 0.13 (s, 6H, -SiC*H*$_3$). **¹³C NMR** (126 MHz, Pyridine-d_5) δ / ppm = 160.76, 154.81 (C_{Aryl}-O), 134.07, 132.52, 132.44 (C_{Aryl}-H), 124.66 (C_{Aryl}-*quart*), 117.99, 115.87 (C_{Aryl}-H), 115.67, 115.05 (C_{Aryl}-*quart*), 95.89, 93.14, 89.61, 89.01 (-*C*≡*C*-), 71.80, 71.55, 70.24, 64.72 (-O*C*H-, -O*C*H$_2$-), 34.61, 34.57, 32.60, 30.49 [2xC], 30.47, 30.44, 30.40 [2xC], 30.17, 30.15, 30.14, 30.09, 26.90, 24.90, 24.81, 24.79, 23.41 (-*C*H$_2$-), 14.74 (-*C*H$_3$), 14.69, 14.66 (-Si*C*H$_2$-), -4.33 (-Si*C*H$_3$). **²⁹Si-NMR** (79 MHz, Pyridine-d_5): δ / ppm = 2.80 (*Si*). **HRMS** (m/z): [M]+Cl⁻ calc. for $C_{112}H_{174}O_8Si_2Cl$: 1739.2461, found: 1739.2456.

1,4-Bis[5-(trioctylsilyl)pentyloxy]-2,5-bis{4-[4-(2,3-dihydroxyprop-1-yloxy)phenylethynyl]-phenylethynyl}benzene (1H5/9):
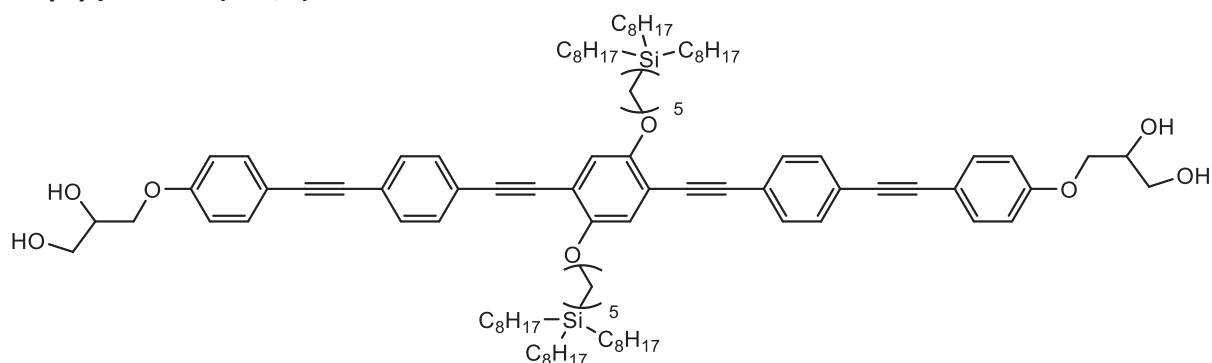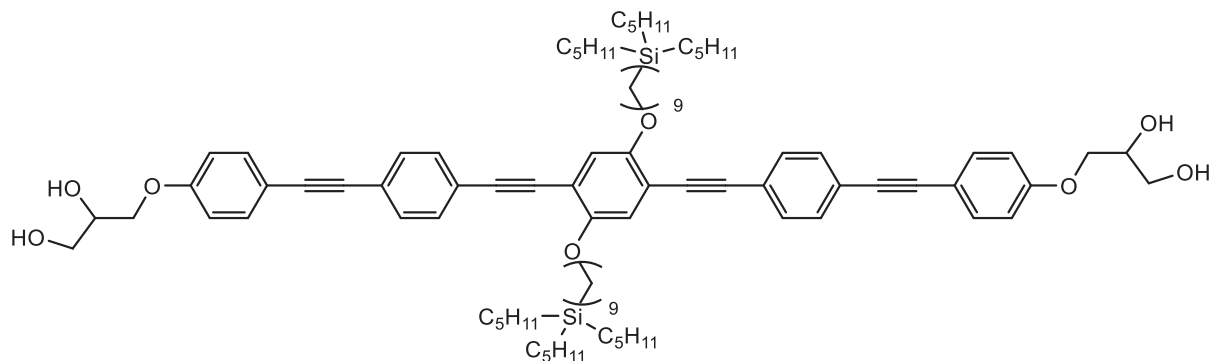

Synthesized according to GP8 from **1H5/8A** (220 mg, 0.13 mmol),PPTS (67 mg, 0.27 mmol) in MeOH/THF (1:1; 30 mL : 30 mL), purification by column chromatography (eluent: CHCl$_3$); yellow solid, yield: $C_{102}H_{154}O_8Si_2$ M = 1563.12 g/mol, 131.3 mg (63 %), *mp* = 73 °C, **¹H-NMR** (502 MHz, Pyridine-d_5): δ / ppm = 7.78 (d, $^3J_{H,H}$ = 8.2 Hz, 4H, Aryl-*H*), 7.71 (d, $^3J_{H,H}$ = 8.2 Hz, 4H, Aryl-*H*), 7.65 (d, $^3J_{H,H}$ = 8.6 Hz, 4H, Aryl-*H*), 7.49 (s, 2H, Aryl-*H*), 7.11 (d, $^3J_{H,H}$ = 9.4 Hz, 4H, Aryl-*H*), 4.59 – 4.54 (m, 2H, -C*H*OH), 4.51 (dd, $^2J_{H,H}$ = 9.5, $^3J_{H,H}$ = 4.4 Hz, 2H, -ArOC*H*$_A$H$_B$), 4.43 (dd, $^2J_{H,H}$ = 9.5, $^3J_{H,H}$ = 6.2 Hz, 2H, -ArOCH$_A$*H*$_B$), 4.24 – 4.18 (m, 8H, -C*H*$_2$OH, -OC*H*$_2$-), 2.05 – 1.98 (m, 4H, -C*H*$_2$-), 1.83 – 1.75 (m, 4H, -C*H*$_2$-), 1.66 – 1.26 (m, 76H, -C*H*$_2$-), 0.91 (t, $^3J_{H,H}$ = 7.2 Hz, 18H, -C*H*$_3$), 0.80 – 0.69 (m, 16H, -SiC*H*$_2$-). **¹³C NMR** (126 MHz, Pyridine-d_5) δ / ppm = 160.76, 154.86 (C_{Aryl}-O), 134.06, 132.52, 132.44 (C_{Aryl}-H), 124.66, 123.53 (C_{Aryl}-*quart*), 118.01, 115.86 (C_{Aryl}-H), 115.70, 115.11 (C_{Aryl}-*quart*), 95.88, 93.13, 89.65, 88.99 (-*C*≡*C*-), 71.80, 71.55, 70.26, 64.72 (-O*C*H-, -O*C*H$_2$-), 34.73, 32.69, 31.17, 30.10 [2xC], 29.90, 24.86, 24.67, 23.46 (-*C*H$_2$-), 14.78 (-*C*H$_3$), 13.51, 13.35 (-Si*C*H$_2$-). **²⁹Si-NMR** (100 MHz, Pyridine-d_5): δ / ppm = 3.02 (*Si*). **HRMS** (m/z): [M]+Cl⁻ calc. for $C_{102}H_{154}O_8Si_2Cl$: 1599.0896, found: 1599.0913.

1,4-Bis[8-(trihexylsilyl)octyloxy]-2,5-bis{4-[4-(2,3-dihydroxyprop-1-yloxy)phenylethynyl]-phenyl-ethynyl}benzene (1H8/6):
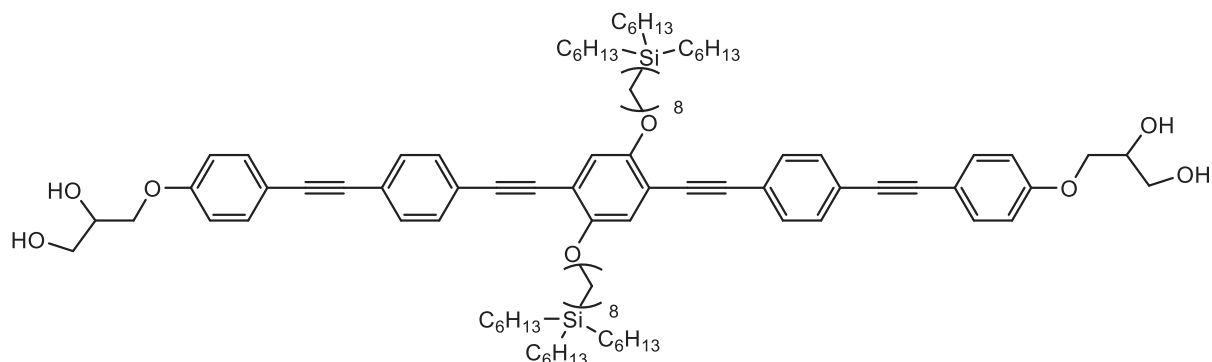
Synthesized according to GP8 from **1H8/6A** (230 mg, 0.15 mmol), PPTS (74 mg, 0.30 mmol) in MeOH/THF (1:1; 30 mL : 30 mL), purification by column chromatography (eluent: CHCl$_3$); yellow solid, yield: C$_{96}$H$_{142}$O$_8$Si$_2$ M = 1480.35 g/mol, 99.3 mg (46 %), *mp* = 67 °C, **^{1}H-NMR** (502 MHz, Pyridine-*d$_5$*): δ / ppm = 7.78 (d, $^3J_{H,H}$ = 8.1 Hz, 4H, Aryl-*H*), 7.70 (d, $^3J_{H,H}$ = 7.8 Hz, 4H, Aryl-*H*), 7.65 (d, $^3J_{H,H}$ = 9.3 Hz, 4H, Aryl-*H*), 7.48 (s, 2H, Aryl-*H*), 7.12 (d, $^3J_{H,H}$ = 8.6 Hz, 4H, Aryl-*H*), 4.60 − 4.54 (m, 2H, -C*H*OH), 4.51 (dd, $^2J_{H,H}$ = 9.6, $^3J_{H,H}$ = 4.3 Hz, 2H, -ArOC*H$_A$*H$_B$), 4.43 (dd, $^2J_{H,H}$ = 9.5, $^3J_{H,H}$ = 6.3 Hz, 2H, -ArOCH$_A$*H$_B$*), 4.21 (d, $^3J_{H,H}$ = 5.6 Hz, 4H, -C*H$_2$*OH), 4.15 (t, $^3J_{H,H}$ = 6.4 Hz, 4H, -OC*H$_2$*-), 1.97 − 1.89 (m, 4H, -C*H$_2$*-), 1.71 − 1.61 (m, 4H, -C*H$_2$*-), 1.52 − 1.29 (m, 64H, -C*H$_2$*-), 0.93 (t, $^3J_{H,H}$ = 6.3 Hz, 18H, -C*H$_3$*), 0.72 − 0.66 (m, 16H, -SiC*H$_2$*-). **^{13}C NMR** (126 MHz, Pyridine-*d$_5$*) δ / ppm = 160.76, 154.80 (*C$_{Aryl}$*-O), 134.07, 132.52, 132.44 (*C$_{Aryl}$*-H), 124.67, 123.52 (*C$_{Aryl}$*-*quart*), 117.96, 115.87 (*C$_{Aryl}$*-H), 115.70, 115.04 (*C$_{Aryl}$*-*quart*), 95.89, 93.15, 89.62, 89.01 (-*C*≡*C*-), 71.81, 71.55, 70.21, 68.31 (-O*C*H-, -O*C*H$_2$-), 64.73, 34.66, 34.37, 32.30, 30.15 [3xC], 26.96, 24.86, 24.80, 23.41 (-*C*H$_2$-), 14.81 (-*C*H$_3$), 13.36, 13.34 (-Si*C*H$_2$-). **^{29}Si-NMR** (100 MHz, Pyridine-*d$_5$*): δ / ppm = 3.03 (*Si*). **HRMS** (m/z): [M]+Cl$^-$ calc. for C$_{96}$H$_{142}$O$_8$Si$_2$Cl: 1514.9957, found: 1514.9962.

1,4-Bis[9-(tripentylsilyl)nonyloxy]-2,5-bis{4-[4-(2,3-dihydroxyprop-1-yloxy)phenylethynyl]-phenyl-ethynyl}benzene (1H9/5):

Synthesized according to GP8 from **1H9/5A** (220 mg, 0.15 mmol),PPTS (74 mg, 0.30 mmol) in MeOH/THF (1:1; 30 mL : 30 mL), purification by column chromatography (eluent: CHCl$_3$); yellow solid, yield: C$_{92}$H$_{134}$O$_8$Si$_2$ M = 1424.25 g/mol, 157.7 mg (76 %), *mp* < 20 °C, **^{1}H-NMR** (402 MHz, Pyridine-*d$_5$*): δ / ppm = 7.77 (d, $^3J_{H,H}$ = 8.3 Hz, 4H, Aryl-*H*), 7.70 (d, $^3J_{H,H}$ = 8.3 Hz, 4H, Aryl-*H*), 7.65 (d, $^3J_{H,H}$ = 8.7 Hz, 4H, Aryl-*H*), 7.48 (s, 2H, Aryl-*H*), 7.11 (d, $^3J_{H,H}$ = 8.8 Hz, 4H, Aryl-*H*), 6.93 (s, 2H, -O*H*), 6.52 (s, 2H, -O*H*), 4.61 − 4.54 (m, 2H, -C*H*OH), 4.51 (dd, $^2J_{H,H}$ = 9.5, $^3J_{H,H}$ = 4.3 Hz, 2H, -ArOC*H$_A$*H$_B$), 4.42 (dd, $^2J_{H,H}$ = 9.5, $^3J_{H,H}$ = 6.2 Hz, 2H, -ArOCH$_A$*H$_B$*), 4.26 − 4.19 (m, 4H, -C*H$_2$*OH), 4.15 (t, $^3J_{H,H}$ = 6.4 Hz, 4H, -OC*H$_2$*-), 1.97 − 1.87 (m, 4H, -C*H$_2$*-), 1.70 − 1.60 (m, 4H, -C*H$_2$*-), 1.52 − 1.31 (m, 56H, -C*H$_2$*-), 0.96 (t, $^3J_{H,H}$ = 7.1 Hz, 18H, -C*H$_3$*), 0.71 − 0.62 (m, 16H, -SiC*H$_2$*-). **^{13}C NMR** (101 MHz, Pyridine-*d$_5$*) δ / ppm = 160.75, 154.81 (*C$_{Aryl}$*-O), 134.07, 132.52, 132.44 (*C$_{Aryl}$*-H), 124.66 (*C$_{Aryl}$*-*quart*), 117.97, 115.86 (*C$_{Aryl}$*-H), 115.68, 115.05 (*C$_{Aryl}$*-*quart*), 95.89, 93.15, 89.61, 89.01 (-*C*≡*C*-), 71.80, 71.55, 70.25, 64.73 (-O*C*H-, -O*C*H$_2$-), 36.85, 34.72, 30.45, 30.21, 30.14, 30.07, 26.94, 24.83, 24.43, 23.06 (-*C*H$_2$-), 14.71 (-*C*H$_3$), 13.31, 13.22 (-Si*C*H$_2$-). **^{29}Si-NMR** (80 MHz,

Pyridine-d_5): δ / ppm = 3.03 (*Si*). **HRMS** (m/z): [M]+Cl⁻ calc. for $C_{92}H_{134}O_8Si_2Cl$: 1458.9331, found: 1458.9327.

(*S*,*S*)-1,4-Bis(2-tetradecylhexadecyl-1-oxy)-2,5-bis{4-[4-(2,3-dihydroxyprop-1-yloxy)phenylethynyl]phenylethynyl}benzene *5H1/14:
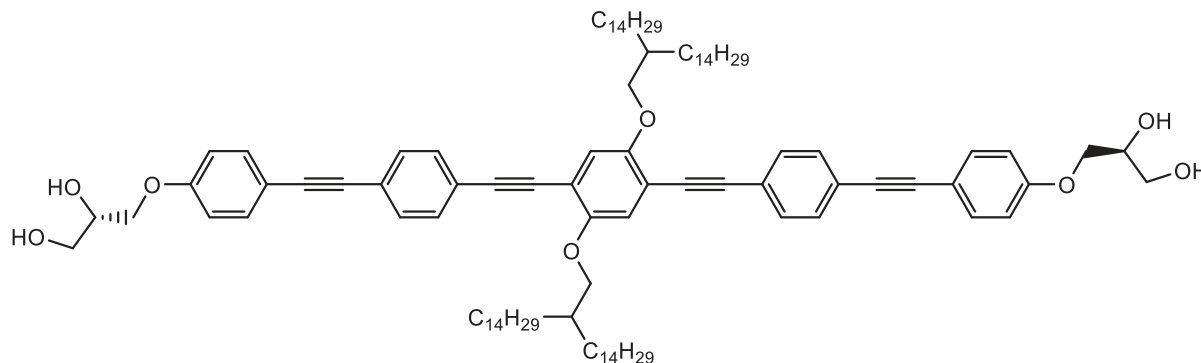
Synthesized according to GP8 from ***5H1/14A** (275 mg, 0.17 mmol),PPTS (86 mg, 0.34 mmol) in MeOH/THF (1:1; 30 mL : 30 mL), purification by column chromatography (eluent: CHCl₃); yellow solid, yield: $C_{104}H_{154}O_8$ M = 1532.37 g/mol, 196.6 mg (75 %), *mp* = 122 °C, **¹H-NMR** (400 MHz, Pyridine-d_5): δ / ppm = 7.83 (d, $^3J_{H,H}$ = 8.3 Hz, 4H, Aryl-*H*), 7.74 (d, $^3J_{H,H}$ = 8.3 Hz, 4H, Aryl-*H*), 7.65 (d, $^3J_{H,H}$ = 8.7 Hz, 4H, Aryl-*H*), 7.57 (s, 2H, Aryl-*H*), 7.12 (d, $^3J_{H,H}$ = 8.8 Hz, 4H, Aryl-*H*), 4.62 − 4.54 (m, 4H, -C*H*OH), 4.52 (dd, $^2J_{H,H}$ = 9.5, $^3J_{H,H}$ = 4.3 Hz, 2H, -ArOC*H*_A*H*_B), 4.43 (dd, $^2J_{H,H}$ = 9.5, $^3J_{H,H}$ = 6.2 Hz, 2H, -ArOC*H*_A*H*_B), 4.23 (d, $^3J_{H,H}$ = 5.3 Hz, 4H, -C*H*₂OH), 4.15 (d, $^3J_{H,H}$ = 5.5 Hz, 4H, -OC*H*₂-), 2.10 − 1.99 (m, 2H, -C*H*-), 1.84 − 1.73 (m, 4H, -C*H*₂-), 1.70 − 1.18 (m, 98H, -C*H*₂-), 0.89 (t, $^3J_{H,H}$ = 7.4 Hz, 12H, -C*H*₃). **¹³C NMR** (101 MHz, Pyridine-d_5) δ / ppm = 160.77, 155.05 (*C*_Aryl-O), 134.08, 132.53, 132.50 (*C*_Aryl-H), 124.72, 123.43 (*C*_Aryl-*quart*), 117.76, 115.87 (*C*_Aryl-H), 115.69, 115.01 (*C*_Aryl-*quart*), 95.95, 93.16, 89.64, 89.01 (-*C*≡*C*-), 73.09, 71.82, 71.56, 64.74 (-O*C*H-, -O*C*H₂-), 39.10 (-*C*H-), 32.62, 32.43, 30.95, 30.52 [4xC], 30.50, 30.46, 30.43, 30.11, 27.79, 23.42 (-*C*H₂-), 14.76 (-*C*H₃). **HRMS** (m/z): [M]+Cl⁻ calc. for $C_{104}H_{154}O_8Cl$: 1567.1361, found: 1567.1555.

1,4-Bis(2-pentadecylheptadecyl-1-oxy)-2,5-bis{4-[4-(2,3-dihydroxyprop-1-yloxy)phenylethynyl]phenylethynyl}benzene 5H1/15:
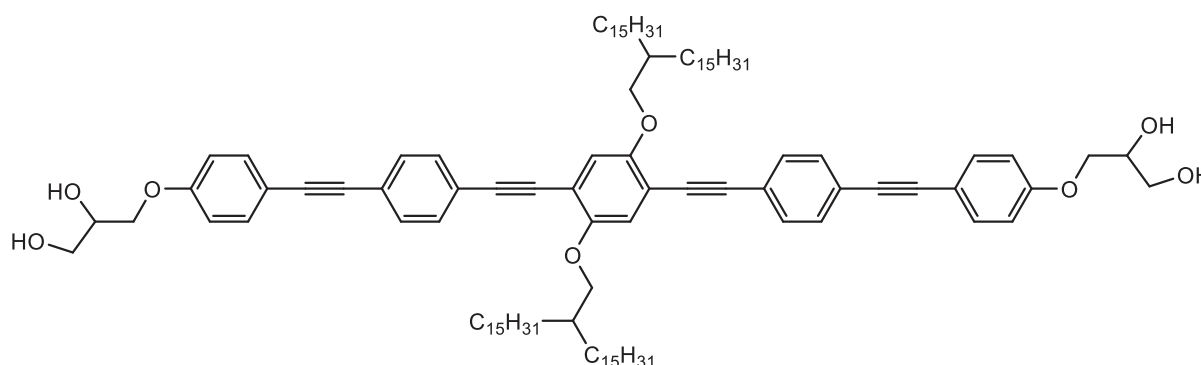
Synthesized according to GP8 from **5H1/15A** (170 mg, 0.10 mmol),PPTS (51 mg, 0.20 mmol) in MeOH/THF (1:1; 30 mL : 30 mL), purification by column chromatography (eluent: CHCl₃); yellow solid, yield: $C_{108}H_{162}O_8$ M = 1588.48 g/mol, 144.5 mg (89 %), *mp* = 127 °C, **¹H-NMR** (400 MHz, Pyridine-d_5): δ / ppm = 7.83 (d, $^3J_{H,H}$ = 8.2 Hz, 4H, Aryl-*H*), 7.74 (d, $^3J_{H,H}$ = 8.2 Hz, 4H, Aryl-*H*), 7.66 (d, $^3J_{H,H}$ = = 9.1 Hz, 4H, Aryl-*H*), 7.57 (s, 2H, Aryl-*H*), 7.12 (d, $^3J_{H,H}$ = 8.8 Hz, 4H, Aryl-*H*), 4.61 − 4.54 (m, 2H, -C*H*OH), 4.52 (dd, $^2J_{H,H}$ = 9.5, $^3J_{H,H}$ = 4.3 Hz, 2H, -ArOC*H*_A*H*_B), 4.43 (dd, $^2J_{H,H}$ = 9.6, $^3J_{H,H}$ = 6.3 Hz, 2H, -ArOC*H*_A*H*_B), 4.23 (d, $^3J_{H,H}$ = 5.3 Hz, 4H, -C*H*₂OH), 4.14 (d, $^3J_{H,H}$ = 5.5 Hz, 4H, -OC*H*₂-), 2.09 − 1.98 (m, 2H, -C*H*-), 1.84 − 1.73 (m,

4H, -CH_2-), 1.70 – 1.20 (m, 108H, -CH_2-), 0.89 (t, $^3J_{H,H}$ = 6.9 Hz, 12H, -CH_2-) ^{13}**C NMR** (101 MHz, Pyridine-d_5) δ / ppm = 160.76, 155.04 (C_{Aryl}-O), 134.07, 132.52, 132.49 (C_{Aryl}-H), 124.71, 123.40 (C_{Aryl}-quart), 117.74, 115.86 (C_{Aryl}-H), 115.68, 115.00 (C_{Aryl}-quart), 95.94, 93.16, 89.64, 89.01 (-$C{\equiv}C$-), 73.10, 71.81, 71.56, 64.73 (-OCH-, -OCH$_2$-), 39.09 (-CH-), 32.61, 32.42, 30.94, 30.52 [4xC], 30.49, 30.48, 30.46, 30.42, 30.10, 27.78, 23.42 (-CH$_2$-), 14.75 (-CH$_3$). **HRMS** (m/z): [M]+Cl$^-$ calc. for $C_{108}H_{162}O_8Cl$: 1623.1987, found: 1623.2036.

(S,S)-1,4-Bis(2-hexadecyloctadecyl-1-oxy)-2,5-bis{4-[4-(2,3-dihydroxyprop-1-yloxy)phenylethynyl]phenylethynyl}benzene *5H1/16:
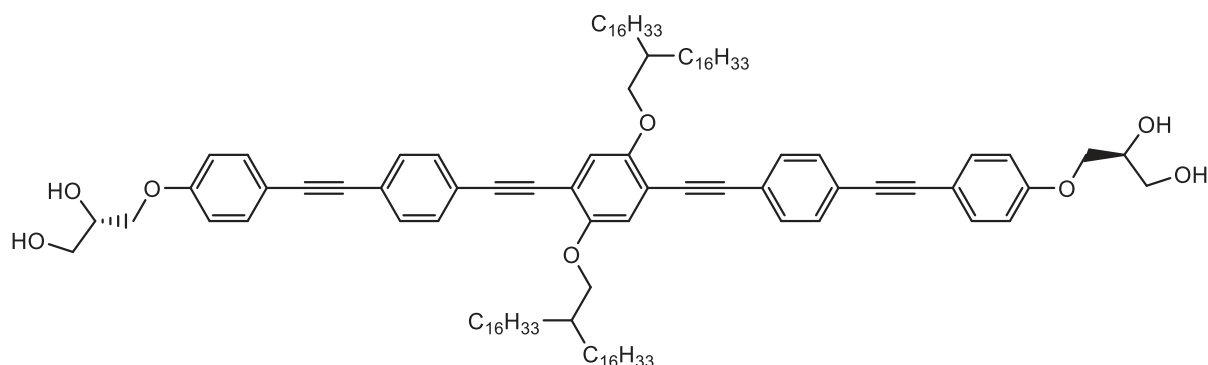
Synthesized according to GP8 from ***5H1/16A** (330 mg, 0.19 mmol),PPTS (95 mg, 0.38 mmol) in MeOH/THF (1:1; 30 mL : 30 mL), purification by column chromatography (eluent: CHCl$_3$); yellow solid, yield: $C_{112}H_{170}O_8$ M = 1644.58 g/mol, 228.3 mg (74 %), *mp* = 137 °C, ^{1}**H-NMR** (400 MHz, Pyridine-d_5): δ / ppm = 7.83 (d, $^3J_{H,H}$ = 8.1 Hz, 4H, Aryl-*H*), 7.75 (d, $^3J_{H,H}$ = 8.1 Hz, 4H, Aryl-*H*), 7.65 (d, $^3J_{H,H}$ = 8.6 Hz, 4H, Aryl-*H*), 7.57 (s, 2H, Aryl-*H*), 7.12 (d, $^3J_{H,H}$ = 8.6 Hz, 4H, Aryl-*H*), 4.61 – 4.54 (m, 2H, -C*H*OH), 4.52 (dd, $^2J_{H,H}$ = 9.5, $^3J_{H,H}$ = 4.3 Hz, 2H, -ArOC*H*$_A$H$_B$), 4.43 (dd, $^2J_{H,H}$ = 9.5, $^3J_{H,H}$ = 6.3 Hz, 2H, -ArOCH$_A$*H*$_B$), 4.23 (d, $^3J_{H,H}$ = 5.3 Hz, 4H, -C*H$_2$*OH), 4.15 (d, $^3J_{H,H}$ = 5.5 Hz, 4H, -OC*H$_2$*-), 2.12 – 1.98 (m, 2H, -C*H*-), 1.84 – 1.73 (m, 4H, -C*H$_2$*-), 1.70 – 1.18 (m, 116H, -C*H$_2$*-), 0.89 (t, $^3J_{H,H}$ = 6.7 Hz, 12H, -C*H$_3$*). ^{13}**C NMR** (101 MHz, Pyridine-d_5) δ / ppm = 160.77, 155.05 (C_{Aryl}-O), 134.07, 132.52, 132.49 (C_{Aryl}-H), 124.71, 123.43 (C_{Aryl}-quart), 117.76, 115.87 (C_{Aryl}-H), 115.69, 115.00 (C_{Aryl}-quart), 95.95, 92.63, 87.82, 85.07 (-$C{\equiv}C$-), 71.81, 71.56, 69.29, 64.73 (-OCH-, -OCH$_2$-), 32.60, 32.42, 30.94, 30.51 [4xC], 30.49, 30.48, 30.45, 30.41, 30.10, 27.77, 23.41 (-CH$_2$-), 14.75 (-CH$_3$). **HRMS** (m/z): [M]+Cl$^-$ calc. for $C_{112}H_{170}O_8Cl$: 1679.2613, found: 1679.2603.

1,4-Bis[3-(diundecylmethylsilyl)pentyloxy]-2,5-bis{4-[2,3,5,6-tetrafluoro-4-(2,3-dihydroxyprop-1-yloxy)phenylethynyl]phenylethynyl}benzene (2F3/11):
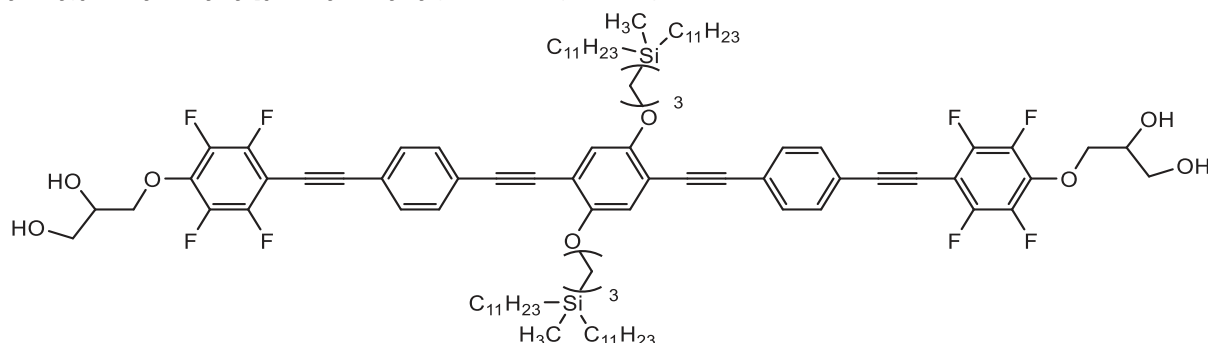
Synthesized according to GP8 from **2F3/11A** (360 mg, 0.21 mmol),PPTS (106 mg, 0.42 mmol) in MeOH/THF (1:1; 30 mL : 30 mL), purification by column chromatography (eluent: CHCl$_3$); yellow solid, yield: $C_{96}H_{134}F_8O_8Si_2$ M = 1624.28 g/mol, 165.7 mg (48 %), *mp* < 20 °C, ^{1}**H-NMR** (402 MHz, Pyridine-d_5): δ / ppm = 7.80 (d, $^3J_{H,H}$ = 8.3 Hz, 4H, Aryl-*H*), 7.74 (d, $^3J_{H,H}$ = 8.3 Hz, 4H, Aryl-*H*), 7.55 (s, 2H, Aryl-*H*), 4.90 (dd, $^2J_{H,H}$ = 10.1, $^3J_{H,H}$ = 4.0 Hz, 2H, -Ar$_F$OC*H*$_A$H$_B$), 4.80 (dd, $^2J_{H,H}$ = 10.2, $^3J_{H,H}$ = 6.2 Hz, 2H, -Ar$_F$OCH$_A$*H*$_B$),
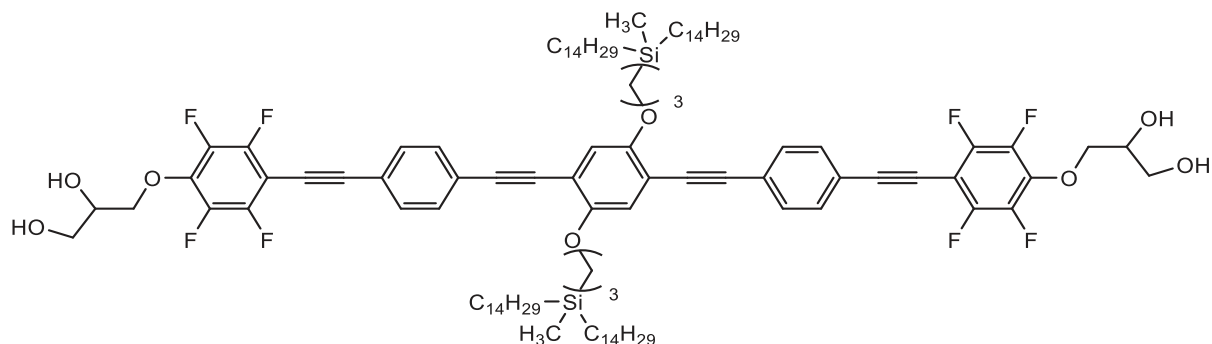
4.61 – 4.51 (m, 2H, -CHOH), 4.25 – 4.16 (m, 8H, -CH_2OH, -OCH_2-), 2.08 – 1.96 (m, 4H, -CH_2-), 1.52 – 1.21 (m, 72H, -CH_2-), 0.98 – 0.92 (m, 4H, -SiCH_2-), 0.89 (t, $^3J_{H,H}$ = 7.2 Hz, 12H, -CH_3), 0.74 – 0.65 (m, 8H, -SiCH_2-), 0.16 (s, 6H, -SiCH_3). ^{13}**C NMR** (101 MHz, Pyridine-d_5) δ / ppm = 154.85 (C_{Aryl}-O), 147.13 – 146.57, 143.23 – 142.81 (m, C_{Aryl}-F), 140.79 – 140.37 (m, C_{ArylF}-O), 132.82, 132.59 (C_{Aryl}-H), 125.51, 122.56 (C_{Aryl}-quart), 118.10 (C_{Aryl}-H), 115.06 (C_{Aryl}-quart), 100.65 (-C≡C-), 98.19 – 97.64 (m, C$_{ArylF}$-quart.), 95.60, 90.37 (-C≡C-), 78.28 (t, $^4J_{C,F}$ = 3.2 Hz, C$_{ArylF}$-O-CH$_2$-), 77.11 (t, $^3J_{C,F}$ = 4.1 Hz, -C≡C-)), 72.84, 72.42, 64.22 (-OCH-, -OCH$_2$-), 34.63, 32.63, 30.54, 30.47, 30.45, 30.18, 30.12, 24.87, 24.78, 23.42 (-CH$_2$-), 14.74 (-CH$_3$), 14.60, 10.77 (-SiCH$_2$-), -4.47 (-SiCH$_3$). ^{19}**F-NMR** (378 MHz, Pyridine-d_5): δ / ppm = -138.50 – -138.88 (m, C$_{Aryl}$-F), -156.73 – -157.14 (m, C$_{Aryl}$-F). ^{29}**Si-NMR** (80 MHz, Pyridine-d_5): δ / ppm = 3.30 (*Si*). **HRMS** (m/z): [M]+Cl⁻ calc. for C$_{96}$H$_{134}$F$_8$O$_8$Si$_2$Cl: 1658.9203, found: 1658.9153.

1,4-Bis[3-(didodecylmethylsilyl)propyloxy]-2,5-bis{4-[2,3,5,6-tetrafluoro-4-(2,3-dihydroxyprop-1-yloxy)phenylethynyl]phenylethynyl}benzene (2F3/12):
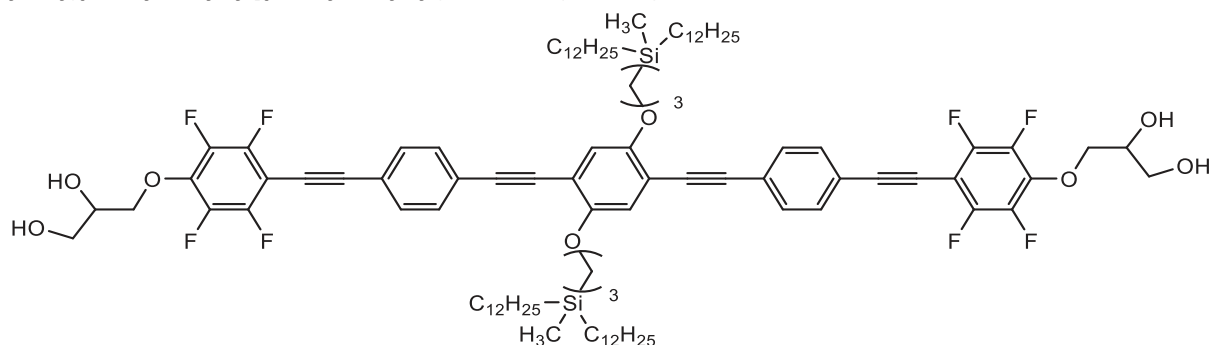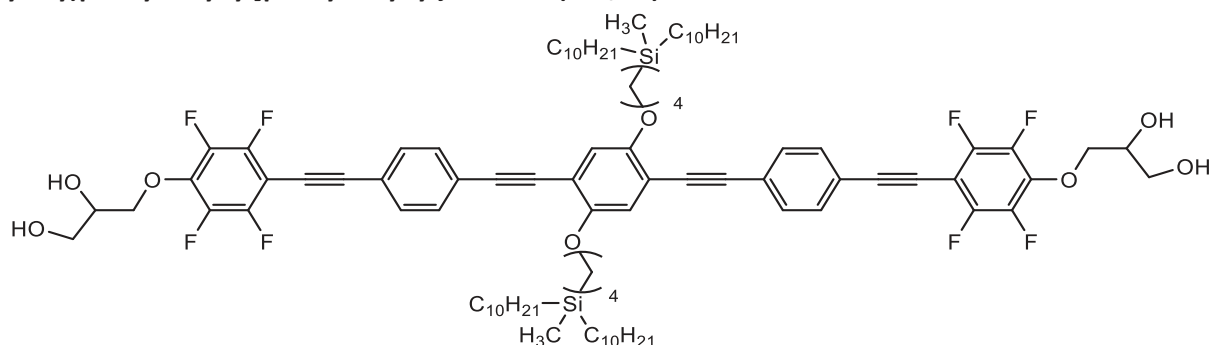

Synthesized according to GP8 from **2F3/12A** (285 mg, 0.16 mmol),PPTS (82 mg, 0.32 mmol) in MeOH/THF (1:1; 30 mL : 30 mL), purification by column chromatography (eluent: CHCl$_3$); yellow solid, yield: C$_{100}$H$_{142}$F$_8$O$_8$Si$_2$ M = 1680.39 g/mol, 170.9 mg (63 %), *mp* = 55 °C, ^{1}**H-NMR** (402 MHz, Pyridine-d_5): δ / ppm = 7.79 (d, $^3J_{H,H}$ = 8.6 Hz, 4H, Aryl-H), 7.74 (d, $^3J_{H,H}$ = 8.4 Hz, 4H, Aryl-H), 7.55 (s, 2H, Aryl-H), 4.90 (dd, $^2J_{H,H}$ = 10.1, $^3J_{H,H}$ = 4.2 Hz, 2H, -Ar$_F$OCH_AH$_B$), 4.80 (dd, $^2J_{H,H}$ = 10.0, $^3J_{H,H}$ = 5.9 Hz, 2H, -Ar$_F$OCH$_A$$H_B$), 4.60 – 4.52 (m, 2H, -CHOH), 4.24 – 4.17 (m, 8H, -CH_2OH, -OCH_2-), 2.07 – 1.96 (m, 4H, -CH_2-), 1.53 – 1.19 (m, 80H, -CH_2-), 0.98 – 0.93 (m, 4H, -SiCH_2-), 0.89 (t, $^3J_{H,H}$ = 7.2 Hz, 12H, -CH_3), 0.73 – 0.65 (m, 8H, -SiCH_2-), 0.16 (s, 6H, -SiCH_3). ^{13}**C NMR** (101 MHz, Pyridine-d_5) δ / ppm = 154.85 (C_{Aryl}-O), 147.16 – 146.52, 143.28 – 142.73 (m, C_{Aryl}-F), 140.91 – 140.22 (m, C_{ArylF}-O), 132.82, 132.59 (C_{Aryl}-H), 125.52, 122.56 (C_{Aryl}-quart), 118.11 (C_{Aryl}-H), 115.06 (C_{Aryl}-quart), 100.66 (-C≡C-), 98.27 – 97.67 (m, C$_{ArylF}$-quart.), 95.60, 90.37 (-C≡C-), 78.28 (t, $^4J_{C,F}$ = 3.4 Hz, C$_{ArylF}$-O-CH$_2$-), 77.11 (t, $^3J_{C,F}$ = 4.5 Hz, -C≡C-), 72.84, 72.42, 64.22 (-OCH-, -OCH$_2$-), 34.63, 32.62, 30.55, 30.51, 30.48, 30.43, 30.19, 30.12, 24.87, 24.78, 23.42 (-CH$_2$-), 14.74 (-CH$_3$), 14.60, 10.77 (-SiCH$_2$-), -4.47 (-SiCH$_3$). ^{19}**F-NMR** (378 MHz, Pyridine-d_5): δ / ppm = -138.47 – -138.75 (m, C$_{Aryl}$-F), -156.56 – -157.20 (m, C$_{Aryl}$-F). ^{29}**Si-NMR** (80 MHz, Pyridine-d_5): δ / ppm = 3.36 (*Si*). **HRMS** (m/z): [M]+Cl⁻ calc. for C$_{100}$H$_{142}$F$_8$O$_8$Si$_2$Cl: 1714.9829, found: 1714.9789.

1,4-Bis[3-(ditetradecylmethylsilyl)propyloxy]-2,5-bis{4-[2,3,5,6-tetrafluoro-4-(2,3-dihydroxyprop-1-yloxy)phenylethynyl]phenylethynyl}benzene (2F3/14):

Synthesized according to GP8 from **2F3/14A** (370 mg, 0.20 mmol),PPTS (100 mg, 0.40 mmol) in MeOH/THF (1:1; 30 mL : 30 mL), purification by column chromatography (eluent: CHCl$_3$); yellow solid, yield: C$_{108}$H$_{158}$F$_8$O$_8$Si$_2$ M = 1792.60 g/mol, 224.5 mg (68 %), mp = 50 °C, **^{1}H-NMR** (500 MHz, Pyridine-d_5): δ / ppm = 7.80 (d, $^3J_{H,H}$ = 8.2 Hz, 4H, Aryl-H), 7.74 (d, $^3J_{H,H}$ = 8.3 Hz, 4H, Aryl-H), 7.56 (s, 2H, Aryl-H), 4.90 (dd, $^2J_{H,H}$ = 10.1, $^3J_{H,H}$ = 4.1 Hz, 2H, -Ar$_F$OCH_AH$_B$), 4.80 (dd, $^2J_{H,H}$ = 10.2, $^3J_{H,H}$ = 6.3 Hz, 2H, -Ar$_F$OCH$_A$$H_B$), 4.59 − 4.53 (m, 2H, -CHOH), 4.25 − 4.18 (m, 8H, -CH_2OH, -OCH_2-), 2.07 − 1.98 (m, 4H, -CH_2-), 1.53 − 1.22 (m, 96H, -CH_2-), 0.98 − 0.93 (m, 4H, -SiCH_2-), 0.90 (t, $^3J_{H,H}$ = 6.8 Hz, 12H, -CH_3), 0.73 − 0.67 (m, 8H, -SiCH_2-), 0.16 (s, 6H, -SiCH_3). **^{13}C NMR** (126 MHz, Pyridine-d_5) δ / ppm = 154.85 (C_{Aryl}-O), 147.38 − 146.91, 142.90 − 142.59 (m, C_{Aryl}-F), 140.98 − 140.62 (m, C_{ArylF}-O), 132.82, 132.60 (C_{Aryl}-H), 125.52, 122.56 (C_{Aryl}-quart), 118.11 (C_{Aryl}-H), 115.07 (C_{Aryl}-quart), 100.64 (-C≡C-), 95.60, 90.37 (-C≡C-), 78.28 (t, $^4J_{C,F}$ = 3.3 Hz, C$_{ArylF}$-O-CH$_2$-), 77.12 (t, $^3J_{C,F}$ = 4.5 Hz, -C≡C-), 72.84, 72.42, 64.22 (-OCH-, -OCH$_2$-), 34.63, 32.61, 30.56, 30.52, 30.49, 30.49, 30.48, 30.42, 30.18, 30.10, 24.87, 24.78, 23.41 (-CH$_2$-), 14.74 (-CH$_3$), 14.60, 10.77 (-SiCH$_2$-), -4.46 (-SiCH$_3$). **^{19}F-NMR** (470 MHz, Pyridine-d_5): δ / ppm = -138.54 − -138.82 (m, C$_{Aryl}$-F), -156.81 − -157.03 (m, C$_{Aryl}$-F). **^{29}Si-NMR** (99 MHz, Pyridine-d_5): δ / ppm = 3.32 (*Si*). **HRMS** (m/z): [M]+Cl$^-$ calc. for C$_{108}$H$_{158}$F$_8$O$_8$Si$_2$Cl: 1827.1082, found: 1827.1045.
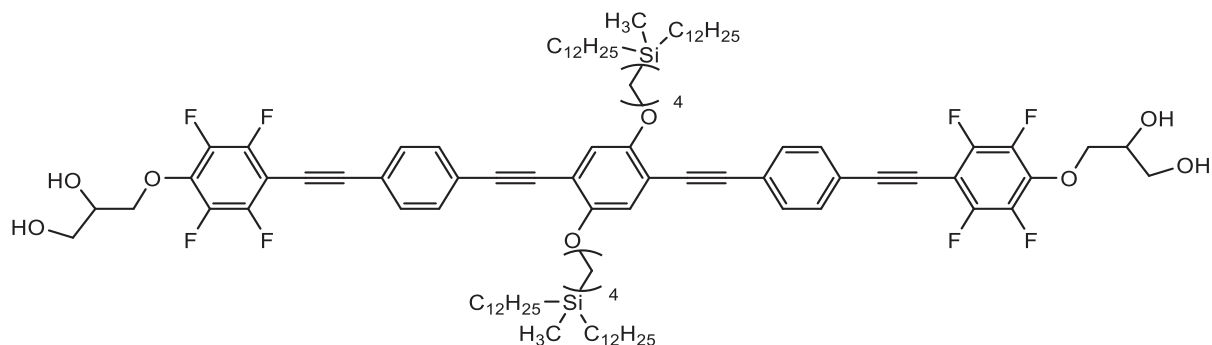
1,4-Bis[4-(didecylmethylsilyl)butyloxy]-2,5-bis{4-[2,3,5,6-tetrafluoro-4-(2,3-dihydroxyprop-1-yloxy)phenylethynyl]phenylethynyl}benzene (2F4/10):

Synthesized according to GP8 from **2F4/10A** (250 mg, 0.15 mmol),PPTS (75 mg, 0.30 mmol) in MeOH/THF (1:1; 30 mL : 30 mL), purification by column chromatography (eluent: CHCl$_3$); yellow solid, yield: C$_{94}$H$_{130}$F$_8$O$_8$Si$_2$ M = 1596.22 g/mol, 210.3 mg (88 %), mp < 20 °C, **^{1}H-NMR** (402 MHz, Pyridine-d_5): δ / ppm = 7.81 (d, $^3J_{H,H}$ = 8.4 Hz, 4H, Aryl-H), 7.74 (d, $^3J_{H,H}$ = 8.4 Hz, 4H, Aryl-H), 7.53 (s, 2H, Aryl-H), 4.90 (dd, $^2J_{H,H}$ = 10.1, $^3J_{H,H}$ = 4.1 Hz, 2H, -Ar$_F$OCH_AH$_B$), 4.80 (dd, $^2J_{H,H}$ = 10.2, $^3J_{H,H}$ = 6.2 Hz, 2H, -Ar$_F$OCH$_A$$H_B$), 4.61 − 4.51 (m, 2H, -CHOH), 4.26 − 4.19 (m, 8H, -CH_2OH, -OCH_2-), 2.08 − 1.96 (m, 4H, -CH_2-), 1.83 − 1.71 (m, 4H, -CH_2-), 1.51 − 1.21 (m, 64H, -CH_2-), 0.90 (t, $^3J_{H,H}$ = 7.1 Hz, 12H, -CH_3), 0.79 − 0.71 (m, 4H, -SiCH_2-), 0.71 − 0.63 (m, 8H, -SiCH_2-), 0.13 (s, 6H, -SiCH_3). **^{13}C NMR** (101 MHz, Pyridine-d_5) δ / ppm = 154.85 (C_{Aryl}-O), 147.21 − 146.54, 143.30 − 142.80 (m, C_{Aryl}-F), 140.75 − 140.33 (m, C_{ArylF}-O), 132.85, 132.61 (C_{Aryl}-H), 125.55, 122.54 (C_{Aryl}-quart), 117.86 (C_{Aryl}-H), 114.93 (C_{Aryl}-quart), 100.68 (-C≡C-), 98.22 − 97.64 (m, C$_{ArylF}$-quart.), 95.63, 90.35 (-C≡C-), 78.28 (t, $^4J_{C,F}$ = 3.5 Hz, C$_{ArylF}$-O-CH$_2$-), 77.10 (t, $^3J_{C,F}$ = 4.0 Hz, -C≡C-
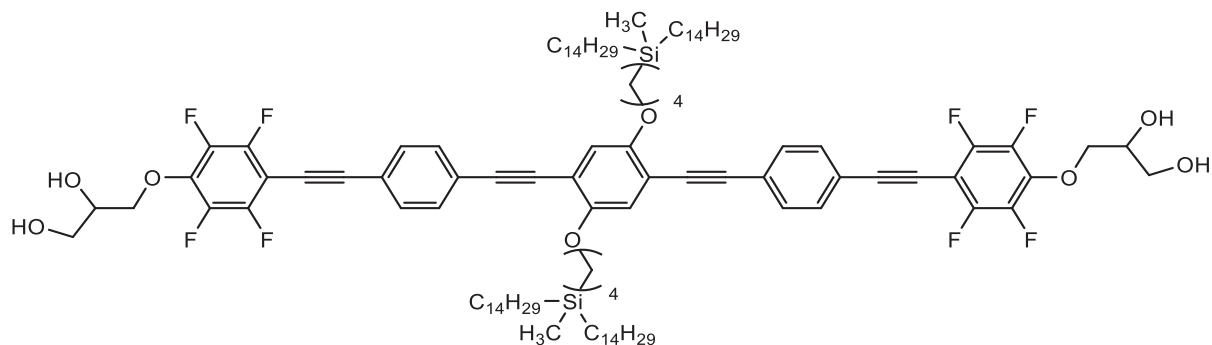
), 72.42, 69.73, 64.22 (-OCH-, -OCH_2-), 34.64, 33.98, 32.64, 30.48, 30.46, 30.20, 30.13, 24.81, 23.43, 21.35 (-CH_2-), 14.77 (-CH_3), 14.61, 14.36 (-SiCH_2-), -4.43 (-SiCH_3). **^{19}F-NMR** (378 MHz, Pyridine-d_5): δ / ppm = -138.62 – -138.78 (m, C_{Aryl}-F), -156.86 – -157.00 (m, C_{Aryl}-F). **^{29}Si-NMR** (80 MHz, Pyridine-d_5): δ / ppm = 2.90 (Si). **HRMS** (m/z): [M]+Cl$^-$ calc. for $C_{94}H_{130}F_8O_8Si_2Cl$: 1630.8890, found: 1630.8907.

1,4-Bis[4-(didodecylmethylsilyl)butyloxy]-2,5-bis{4-[2,3,5,6-tetrafluoro-4-(2,3-dihydroxyprop-1-yloxy)phenylethynyl]phenylethynyl}benzene (2F4/12):

Synthesized according to GP8 from **2F4/12A** (310 mg, 0.17 mmol),PPTS (87 mg, 0.35 mmol) in MeOH/THF (1:1; 30 mL : 30 mL), purification by column chromatography (eluent: CHCl$_3$); yellow solid, yield: $C_{102}H_{146}F_8O_8Si_2$ M = 1708.44 g/mol, 129.1 mg (44 %), mp < 20 °C, **^{1}H-NMR** (500 MHz, Pyridine-d_5): δ / ppm = 7.80 (d, $^3J_{H,H}$ = 8.0 Hz, 4H, Aryl-H), 7.74 (d, $^3J_{H,H}$ = 8.0 Hz, 4H, Aryl-H), 7.51 (s, 2H, Aryl-H), 4.89 (dd, $^2J_{H,H}$ = 10.1, $^3J_{H,H}$ = 4.0 Hz, 2H, -Ar$_F$OCH_AH_B, -Ar$_F$OCH_AH_B), 4.79 (dd, $^2J_{H,H}$ = 10.2, $^3J_{H,H}$ = 6.3 Hz, 2H), 4.60 – 4.51 (m, 2H, -CHOH), 4.27 – 4.17 (m, 8H, -CH_2OH, -OCH_2-), 2.07 – 1.98 (m, 4H, -CH_2-), 1.84 – 1.70 (m, 4H, -CH_2-), 1.53 – 1.21 (m, 80H, -CH_2-), 0.91 (t, $^3J_{H,H}$ = 6.7 Hz, 12H, -CH_3), 0.81 – 0.72 (m, 4H, -SiCH_2-), 0.72 – 0.64 (m, 8H, -SiCH_2-), 0.14 (s, 6H, -SiCH_3). **^{13}C NMR** (126 MHz, Pyridine-d_5) δ / ppm = 154.86 (C_{Aryl}-O), 147.23 – 146.99, 142.95 – 142.69 (m, C_{Aryl}-F), 141.03 – 140.75 (m, C_{ArylF}-O), 132.85, 132.62 (C_{Aryl}-H), 125.58, 122.55 (C_{Aryl}-quart), 117.87 (C_{Aryl}-H), 114.95 (C_{Aryl}-quart), 100.68 (-$C{\equiv}C$-), 98.24 – 97.76 (m, C_{ArylF}-quart.), 95.63, 90.35 (-$C{\equiv}C$-), 78.27 (t, $^4J_{C,F}$ = 3.3 Hz, C_{ArylF}-O-CH_2-), 77.10 (t, $^3J_{C,F}$ = 3.9 Hz, -$C{\equiv}C$-), 72.42, 69.75, 64.22 (-OCH-, -OCH_2-), 34.66, 34.01, 32.66, 30.58, 30.53, 30.51, 30.47, 30.23, 30.15, 24.84, 23.45, 21.36 (-CH_2-, 14.77 (-CH_3), 14.63, 14.38 (-SiCH_2-), -4.41 (-SiCH_3). **^{19}F-NMR** (470 MHz, Pyridine-d_5): δ / ppm = -138.41 – -138.90 (m, C_{Aryl}-F), -156.69 – -157.16 (m, C_{Aryl}-F). **^{29}Si-NMR** (99 MHz, Pyridine-d_5): δ / ppm = 2.91 (Si). **HRMS** (m/z): [M]+Cl$^-$ calc. for $C_{102}H_{146}F_8O_8Si_2Cl$: 1743.0142, found: 1743.0217.

1,4-Bis[4-(ditetradecylmethylsilyl)butyloxy]-2,5-bis{4-[2,3,5,6-tetrafluoro-4-(2,3-dihydroxyprop-1-yloxy)phenylethynyl]phenylethynyl}benzene (2F4/14):

Synthesized according to GP8 from **2F4/14A** (170 mg, 0.09 mmol),PPTS (45 mg, 0.18 mmol) in MeOH/THF (1:1; 30 mL : 30 mL), purification by column chromatography (eluent: CHCl$_3$); yellow solid, yield: $C_{110}H_{162}F_8O_8Si_2$ M = 1820.66 g/mol, 64 mg (39 %), mp = 101 °C, **^{1}H-NMR** (400 MHz, Pyridine-d_5): δ / ppm = 7.82 (d, $^3J_{H,H}$ = 8.3 Hz, 4H, Aryl-H), 7.75 (d, $^3J_{H,H}$ = 8.3 Hz, 4H, Aryl-H), 7.53 (s, 2H, Aryl-H), 4.90
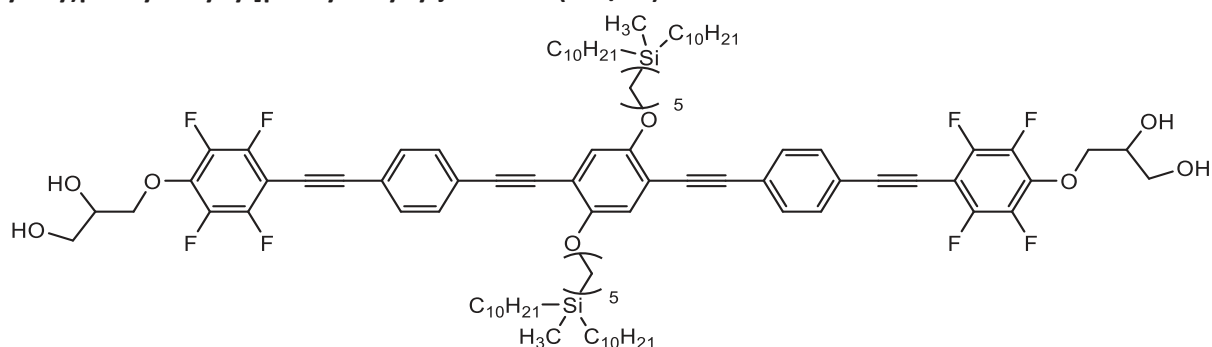
(dd, $^2J_{H,H}$ = 10.1, $^3J_{H,H}$ = 4.1 Hz, 2H, -Ar$_F$OCH_AH$_B$), 4.80 (dd, $^2J_{H,H}$ = 10.1, $^3J_{H,H}$ = 6.3 Hz, 2H, -Ar$_F$OCH$_A$$H_B$), 4.62 – 4.52 (m, 2H, -CHOH), 4.27 – 4.19 (m, 8H, -CH_2OH, -OCH_2-), 2.08 – 1.97 (m, 4H, -CH_2-), 1.85 – 1.71 (m, 4H, -CH_2-), 1.52 – 1.22 (m, 96H, -CH_2-), 0.90 (t, $^3J_{H,H}$ = 7.3 Hz, 12H, -CH_3), 0.81 – 0.73 (m, 4H, -SiCH_2-), 0.72 – 0.63 (m, 8H, -SiCH_2-), 0.14 (s, 6H, -SiCH_3). **^{13}C NMR** (101 MHz, Pyridine-d_5) δ / ppm = 154.87 (C$_{Aryl}$-O), 147.31 – 146.63, 143.63 – 142.46 (m, C$_{Aryl}$-F), 140.98 – 140.27 (m, C$_{ArylF}$-O), 132.87, 132.63 (C$_{Aryl}$-H), 125.57, 122.55 (C$_{Aryl}$-quart), 117.89 (C$_{Aryl}$-H), 114.96 (C$_{Aryl}$-quart), 100.70 (-C≡C-), 98.30 – 97.66 (m, C$_{ArylF}$-quart.), 95.64, 90.36 (-C≡C-), 78.28 (t, $^4J_{C,F}$ = 3.2 Hz, C$_{ArylF}$-O-CH$_2$-), 77.11 (t, $^3J_{C,F}$ = 4.3 Hz, -C≡C-), 72.43, 69.74, 64.23 (-OCH-, -OCH$_2$-), 34.64, 33.98, 32.63, 30.57, 30.53, 30.52, 30.50, 30.49, 30.44, 30.22, 30.12, 24.83, 23.43, 21.36 (-CH$_2$-), 14.76 (-CH$_3$), 14.62, 14.36 (-SiCH$_2$-), -4.40 (-SiCH$_3$). **^{19}F-NMR** (376 MHz, Pyridine-d_5): δ / ppm = -138.55 – -138.79 (m, C$_{Aryl}$-F), -156.80 – -157.00 (m, C$_{Aryl}$-F). **^{29}Si-NMR** (79 MHz, Pyridine-d_5): δ / ppm = 2.93 (*Si*). **HRMS** (m/z): [M]+Cl⁻ calc. for C$_{110}$H$_{162}$F$_8$O$_8$Si$_2$Cl: 1855.1395, found: 1855.1402.

1,4-Bis[5-(dinonylmethylsilyl)pentyloxy]-2,5-bis{4-[2,3,5,6-tetrafluoro-4-(2,3-dihydroxyprop-1-yloxy)phenylethynyl]phenylethynyl}benzene (2F5/9):
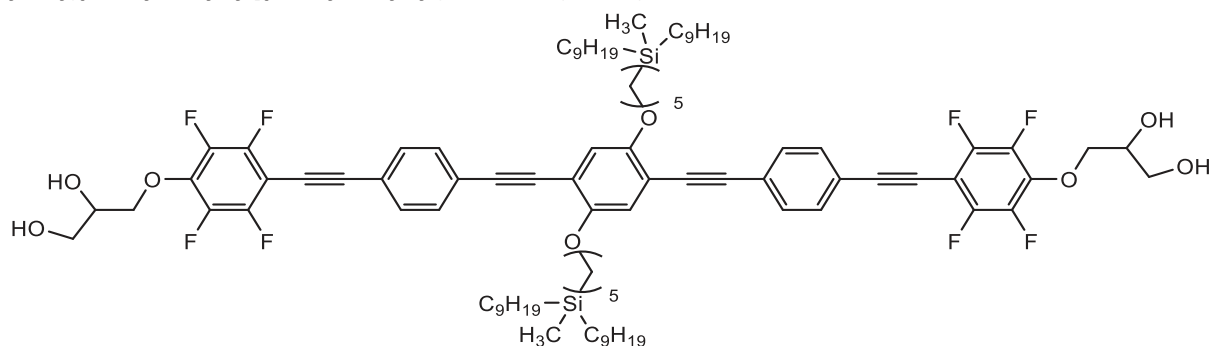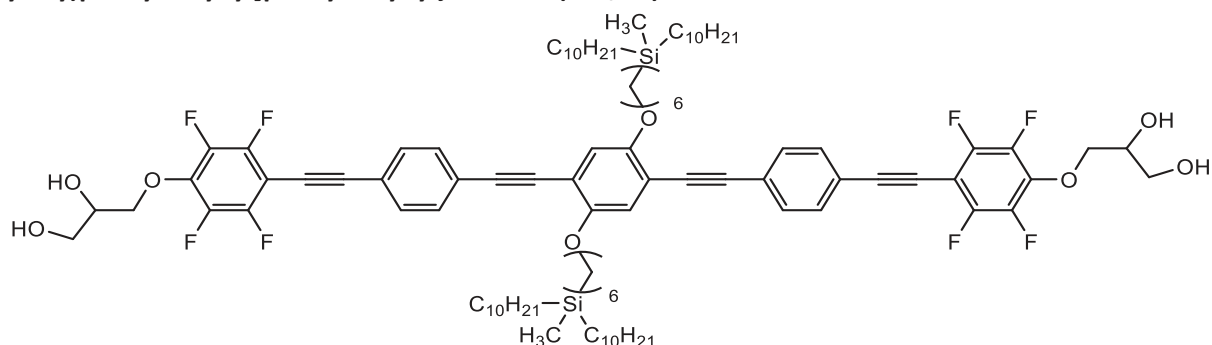

Synthesized according to GP8 from **2F5/9A** (280 mg, 0.17 mmol), PPTS (85 mg, 0.34 mmol) in MeOH/THF (1:1; 30 mL : 30 mL), purification by column chromatography (eluent: CHCl$_3$); yellow solid, yield: C$_{92}$H$_{126}$F$_8$O$_8$Si$_2$ *M* = 1568.17 g/mol, 185.9 mg (78 %), *mp* < 20 °C, **^{1}H-NMR** (502 MHz, Pyridine-d_5): δ / ppm = 7.80 (d, $^3J_{H,H}$ = 8.3 Hz, 4H, Aryl-H), 7.72 (d, $^3J_{H,H}$ = 8.4 Hz, 4H, Aryl-H), 7.52 (s, 2H, Aryl-H), 4.90 (dd, $^2J_{H,H}$ = 10.3, $^3J_{H,H}$ = 4.4 Hz, 2H, -Ar$_F$OCH_AH$_B$), 4.80 (dd, $^2J_{H,H}$ = 10.1, $^3J_{H,H}$ = 6.4 Hz, 2H, -Ar$_F$OCH$_A$$H_B$), 4.61 – 4.53 (m, 2H, -CHOH), 4.25 – 4.17 (m, 8H, -CH_2OH, -OCH_2-), 2.03 – 1.94 (m, 4H, -CH_2-), 1.80 – 1.71 (m, 4H, -CH_2-), 1.62 – 1.23 (m, 60H, -CH_2-), 0.89 (t, $^3J_{H,H}$ = 6.9 Hz, 12H, -CH_3), 0.74 – 0.63 (m, 12H, -SiCH_2-), 0.13 (s, 6H, -SiCH_3). **^{13}C NMR** (126 MHz, Pyridine-d_5) δ / ppm = 154.91 (C$_{Aryl}$-O), 147.39 – 146.93, 143.11 – 142.57 (m, C$_{Aryl}$-F), 141.07 – 140.64 (m, C$_{ArylF}$-O), 132.82, 132.59 (C$_{Aryl}$-H), 125.53, 122.52 (C$_{Aryl}$-quart), 118.00 (C$_{Aryl}$-H), 115.04 (C$_{Aryl}$-quart), 100.66 (-C≡C-), 98.16 – 97.66 (m, C$_{ArylF}$-quart.), 95.62, 90.36 (-C≡C-), 78.28 (t, $^4J_{C,F}$ = 3.4 Hz, C$_{ArylF}$-O-CH$_2$-), 77.09 (t, $^3J_{C,F}$ = 4.4 Hz, -C≡C-), 72.42, 70.26, 64.22 (-OCH-, -OCH$_2$-), 34.60, 32.62, 31.03, 30.38, 30.15, 30.14, 29.91, 24.80, 24.62, 23.42 (-CH$_2$-), 14.79 (-CH$_3$), 14.73, 14.64 (-SiCH$_2$-), -4.40 (-SiCH$_3$). **^{19}F-NMR** (473 MHz, Pyridine-d_5): δ / ppm = -138.44 – -138.87 (m, C$_{Aryl}$-F), -156.75 – -157.16 (m, C$_{Aryl}$-F). **^{29}Si-NMR** (100 MHz, Pyridine-d_5): δ / ppm = 2.76 (*Si*). **HRMS** (m/z): [M]+Cl⁻ calc. for C$_{92}$H$_{126}$F$_8$O$_8$Si$_2$Cl: 1602.8577, found: 1602.8621.

1,4-Bis[5-(didecylmethylsilyl)pentyloxy]-2,5-bis{4-[2,3,5,6-tetrafluoro-4-(2,3-dihydroxyprop-1-yloxy)phenylethynyl]phenylethynyl}benzene (2F5/10):

Synthesized according to GP8 from **2F5/10A** (280 mg, 0.16 mmol),PPTS (83 mg, 0.33 mmol) in MeOH/THF (1:1; 30 mL : 30 mL), purification by column chromatography (eluent: CHCl$_3$); yellow solid, yield: C$_{96}$H$_{134}$F$_8$O$_8$Si$_2$ M = 1624.28 g/mol, 209.7 mg (79 %), mp = 110 °C, **^{1}H-NMR** (400 MHz, Pyridine-d_5): δ / ppm = 7.80 (d, $^3J_{H,H}$ = 8.3 Hz, 4H, Aryl-H), 7.72 (d, $^3J_{H,H}$ = 8.3 Hz, 4H, Aryl-H), 7.51 (s, 2H, Aryl-H), 4.90 (dd, $^2J_{H,H}$ = 10.2, $^3J_{H,H}$ = 4.0 Hz, 2H, -Ar$_F$OCH_AH$_B$), 4.80 (dd, $^2J_{H,H}$ = 10.1, $^3J_{H,H}$ = 6.4 Hz, 2H, -Ar$_F$OCH$_A$$H_B$), 4.60 − 4.52 (m, 2H, -CHOH), 4.25 − 4.17 (m, 8H, -CH_2OH, -OCH_2-), 2.05 − 1.95 (m, 4H, -CH_2-), 1.82 − 1.71 (m, 4H, -CH_2-), 1.61 − 1.23 (m, 68H, -CH_2-), 0.90 (t, $^3J_{H,H}$ = 6.9 Hz, 12H, -CH_3), 0.75 − 0.63 (m, 12H, -SiCH_2-), 0.13 (s, 6H, -SiCH_3). **^{13}C NMR** (101 MHz, Pyridine-d_5) δ / ppm = 154.92 (C_{Aryl}-O), 147.17 − 146.63, 143.27 − 142.80 (m, C_{Aryl}-F), 140.78 − 140.44 (m, C_{ArylF}-O), 132.83, 132.61 (C_{Aryl}-H), 125.56, 122.54 (C_{Aryl}-quart), 118.00 (C_{Aryl}-H), 115.05 (C_{Aryl}-quart), 100.68 (-C≡C-), 98.23 − 97.69 (m, C$_{ArylF}$-quart.), 95.63, 90.37 (-C≡C-), 78.28 (t, $^4J_{C,F}$ = 3.3 Hz, C$_{ArylF}$-O-CH$_2$-), 77.11 (t, $^3J_{C,F}$ = 4.5 Hz, -C≡C-), 72.43, 70.27, 64.23 (-OCH-, -OCH$_2$-), 34.64, 32.65, 31.05, 30.49, 30.47, 30.20, 30.15, 29.93, 24.83, 24.64, 23.45 (-CH$_2$-), 14.81 (-SiCH$_2$-), 14.76 (-CH$_3$), 14.66 (-SiCH_2-), -4.37 (-SiCH_3). **^{19}F-NMR** (376 MHz, Pyridine-d_5): δ / ppm = -138.49 − -138.81 (m, C$_{Aryl}$-F), -156.69 − -157.11 (m, C$_{Aryl}$-F). **^{29}Si-NMR** (79 MHz, Pyridine-d_5): δ / ppm = 2.79 (*Si*). **HRMS** (m/z): [M]+Cl$^-$ calc. for C$_{96}$H$_{134}$F$_8$O$_8$Si$_2$Cl: 1658.9203, found: 1658.9206.

1,4-Bis[6-(didecylmethylsilyl)hexyloxy]-2,5-bis{4-[2,3,5,6-tetrafluoro-4-(2,3-dihydroxyprop-1-yloxy)phenylethynyl]phenylethynyl}benzene (2F6/10):

Synthesized according to GP8 from **2F6/10A** (300 mg, 0.17 mmol),PPTS (87 mg, 0.34 mmol) in MeOH/THF (1:1; 30 mL : 30 mL), purification by column chromatography (eluent: CHCl$_3$); yellow solid, yield: C$_{98}$H$_{138}$F$_8$O$_8$Si$_2$ M = 1652.33 g/mol, 229.4 mg (80 %), mp = 115 °C, **^{1}H-NMR** (402 MHz, Pyridine-d_5): δ / ppm = 7.80 (d, $^3J_{H,H}$ = 8.3 Hz, 4H, Aryl-H), 7.73 (d, $^3J_{H,H}$ = 8.3 Hz, 4H, Aryl-H), 7.50 (s, 2H, Aryl-H), 4.90 (dd, $^2J_{H,H}$ = 10.1, $^3J_{H,H}$ = 4.1 Hz, 2H, -Ar$_F$OCH_AH$_B$), 4.80 (dd, $^2J_{H,H}$ = 6.4, $^3J_{H,H}$ = 3.8 Hz, 2H, -Ar$_F$OCH$_A$$H_B$), 4.60 − 4.52 (m, 2H, -CHOH), 4.24 − 4.15 (m, 8H, -CH_2OH, -OCH_2-), 2.01 − 1.92 (m, 4H, -CH_2-), 1.78 − 1.67 (m, 4H, -CH_2-), 1.62 − 1.21 (m, 72H, -CH_2-), 0.91 (t, $^3J_{H,H}$ = 6.9 Hz, 12H, -CH_3), 0.72 − 0.63 (m, 12H, -SiCH_2-), 0.13 (s, 6H, -SiCH_3). **^{13}C NMR** (101 MHz, Pyridine-d_5) δ / ppm = 154.88 (C_{Aryl}-O), 147.00 − 146.75, 143.27 − 142.83 (m, C_{Aryl}-F), 140.78 − 140.38 (m, C_{ArylF}-O), 132.84, 132.58 (C_{Aryl}-H), 125.54, 122.54 (C_{Aryl}-quart), 117.92 (C_{Aryl}-H), 115.01 (C_{Aryl}-quart), 100.69 (-C≡C-), 98.18 − 97.73 (m, C$_{ArylF}$-quart.), 95.63, 90.35

(-*C*≡*C*-), 78.27 (t, $^4J_{C,F}$ = 3.3 Hz, C_{ArylF}-O-*C*H$_2$-), 77.11 (t, $^3J_{C,F}$ = 4.5 Hz, -*C*≡*C*-), 72.42, 70.25, 64.22 (-O*C*H-, -O*C*H$_2$-), 34.62, 34.35, 32.63, 30.48, 30.45, 30.18, 30.15, 30.13, 26.67, 24.89, 24.81, 23.43 (-*C*H$_2$-), 14.75 (-*C*H$_3$), 14.66, 14.64 (-Si*C*H$_2$-), -4.40 (-Si*C*H$_3$). **^{19}F-NMR** (378 MHz, Pyridine-d_5): δ / ppm = -138.47 − -138.78 (m, C_{Aryl}-*F*), -156.67 − -156.97 (m, C_{Aryl}-*F*). **^{29}Si-NMR** (80 MHz, Pyridine-d_5): δ / ppm = 2.82 (*Si*). **HRMS** (m/z): [M]+Cl$^-$ calc. for C$_{98}$H$_{138}$F$_8$O$_8$Si$_2$Cl: 1686.9516, found: 1686.9533.

1,4-Bis[6-(didodecylmethylsilyl)hexyloxy]-2,5-bis{4-[2,3,5,6-tetrafluoro-4-(2,3-dihydroxyprop-1-yloxy)phenylethynyl]phenylethynyl}benzene (2F6/12):
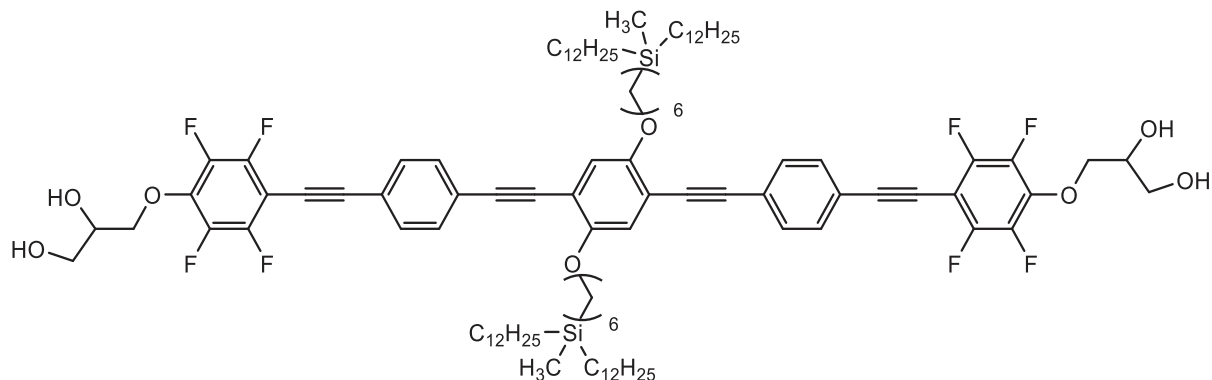
Synthesized according to GP8 from **2F6/12A** (230 mg, 0.13 mmol),PPTS (63 mg, 0.26 mmol) in MeOH/THF (1:1; 30 mL : 30 mL), purification by column chromatography (eluent: CHCl$_3$); yellow solid, yield: C$_{106}$H$_{154}$F$_8$O$_8$Si$_2$ *M* = 1764.55 g/mol, 208.4 mg (95 %), *mp* = 83 °C, **^{1}H-NMR** (400 MHz, Pyridine-d_5): δ / ppm = 7.80 (d, $^3J_{H,H}$ = 8.3 Hz, 4H, Aryl-*H*), 7.73 (d, $^3J_{H,H}$ = 8.3 Hz, 4H, Aryl-*H*), 7.50 (s, 2H, Aryl-*H*), 4.90 (dd, $^2J_{H,H}$ = 10.1, $^3J_{H,H}$ = 4.1 Hz, 2H, -Ar$_F$OC*H$_A$*H$_B$-), 4.80 (dd, $^2J_{H,H}$ = 10.2, $^3J_{H,H}$ = 6.2 Hz, 2H, -Ar$_F$OCH$_A$*H$_B$*), 4.59 − 4.52 (m, 2H, -C*H*OH), 4.24 − 4.16 (m, 8H, -C*H$_2$*OH, -OC*H$_2$*-), 2.02 − 1.91 (m, 4H, -C*H$_2$*-), 1.78 − 1.68 (m, 4H, -C*H$_2$*-), 1.60 − 1.22 (m, 88H, -C*H$_2$*-), 0.91 (t, $^3J_{H,H}$ = 6.8 Hz, 12H, -C*H$_3$*), 0.73 − 0.63 (m, 12H, -SiC*H$_2$*-), 0.13 (s, 6H, -SiC*H$_3$*). **^{13}C NMR** (101 MHz, Pyridine-d_5) δ / ppm = 154.88 (C_{Aryl}-O), 147.03 − 146.73, 143.20 − 142.87 (m, C_{Aryl}-F), 140.75 − 140.49 (m, C_{ArylF}-O), 132.84, 132.57 (C_{Aryl}-H), 125.55, 122.54 (C_{Aryl}-quart), 117.92 (C_{Aryl}-H), 115.01 (C_{Aryl}-quart), 100.69 (-*C*≡*C*-), 98.19 − 97.74 (m, C_{ArylF}-quart.), 95.63, 90.36 (-*C*≡*C*-), 78.27 (t, $^4J_{C,F}$ = 3.4 Hz, C_{ArylF}-O-*C*H$_2$-), 77.11 (t, $^3J_{C,F}$ = 4.5 Hz, -*C*≡*C*-), 72.41, 70.25, 64.22 (-O*C*H-, -O*C*H$_2$-), 34.63, 34.35, 32.63, 30.55, 30.51, 30.47, 30.44, 30.20, 30.15, 30.13, 26.68, 24.89, 24.82, 23.44 (-*C*H$_2$-), 14.76 (-*C*H$_3$), 14.67, 14.65 (-Si*C*H$_2$-), -4.39 (-Si*C*H$_3$). **^{19}F-NMR** (376 MHz, Pyridine-d_5): δ / ppm = -138.44 − -138.68 (m, C_{Aryl}-*F*), -156.68 − -157.11 (m, C_{Aryl}-*F*). **^{29}Si-NMR** (79 MHz, Pyridine-d_5): δ / ppm = 2.80 (*Si*). **HRMS** (m/z): [M]+Cl$^-$ calc. for C$_{106}$H$_{154}$F$_8$O$_8$Si$_2$Cl: 1799.0768, found: 1799.0746.

1,4-Bis[7-(dinonylmethylsilyl)heptyloxy]-2,5-bis{4-[2,3,5,6-tetrafluoro-4-(2,3-dihydroxyprop-1-yloxy)phenylethynyl]phenylethynyl}benzene (2F7/9):
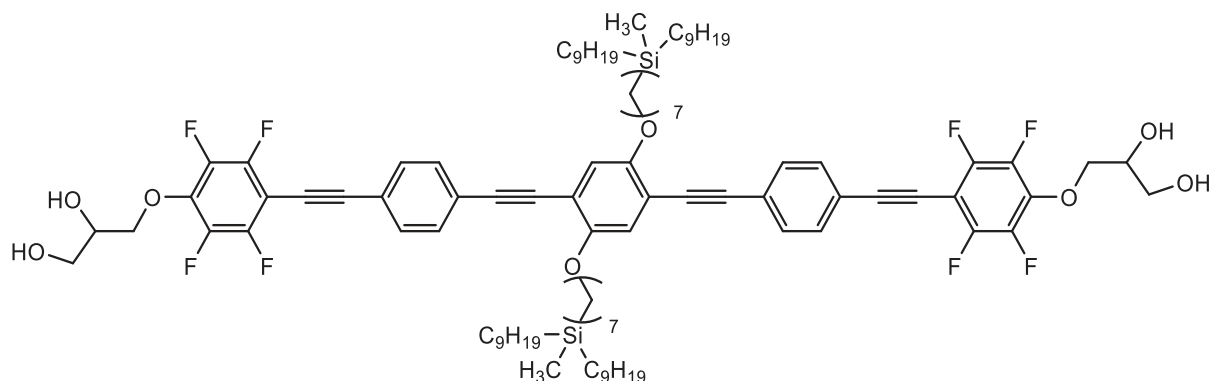
Synthesized according to GP8 from **2F7/9A** (290 mg, 0.17 mmol),PPTS (86 mg, 0.34 mmol) in MeOH/THF (1:1; 30 mL : 30 mL), purification by column chromatography (eluent: CHCl$_3$); yellow solid, yield: C$_{96}$H$_{134}$F$_8$O$_8$Si$_2$ *M* = 1624.28 g/mol, 135.1 mg (49 %), *mp* = 101 °C, **^{1}H-NMR** (402 MHz, Pyridine-

d_5): δ / ppm = 7.80 (d, $^3J_{H,H}$ = 8.2 Hz, 4H, Aryl-*H*), 7.71 (d, $^3J_{H,H}$ = 8.2 Hz, 4H, Aryl-*H*), 7.50 (s, 2H, Aryl-*H*), 4.90 (dd, $^2J_{H,H}$ = 10.4, $^3J_{H,H}$ = 4.3 Hz, 2H, -Ar$_F$OC*H$_A$*H$_B$), 4.80 (dd, $^2J_{H,H}$ = 9.8, $^3J_{H,H}$ = 4.2 Hz, 2H, -Ar$_F$OCH$_A$*H$_B$*), 4.60 – 4.53 (m, 2H, -C*H*OH), 4.22 (d, $^3J_{H,H}$ = 5.7 Hz, 4H, -C*H$_2$*OH), 4.17 (t, $^3J_{H,H}$ = 6.4 Hz, 4H, -OC*H$_2$*-), 2.00 – 1.90 (m, 4H, -C*H$_2$*-), 1.74 – 1.63 (m, 4H, -C*H$_2$*-), 1.53 – 1.22 (m, 68H, -C*H$_2$*-), 0.89 (t, $^3J_{H,H}$ = 7.2 Hz, 12H, -C*H$_3$*), 0.71 – 0.61 (m, 12H, -SiC*H$_2$*-), 0.13 (s, 6H, -SiC*H$_3$*) **^{13}C NMR** (101 MHz, Pyridine-d_5) δ / ppm = 154.88 (*C$_{Aryl}$*-O), 147.06 – 146.75, 143.16 – 142.83 (m, *C$_{Aryl}$*-F), 140.68 – 140.35 (m, *C$_{ArylF}$*-O), 132.84, 132.58 (*C$_{Aryl}$*-H), 125.52, 122.53 (*C$_{Aryl}$*-quart), 117.96 (*C$_{Aryl}$*-H), 115.01 (*C$_{Aryl}$*-quart), 100.67 (-*C≡C*-), 98.21 – 97.71 (m, C$_{ArylF}$-quart.), 95.63, 90.33 (-*C≡C*-), 78.28 (t, $^4J_{C,F}$ = 3.5 Hz, C$_{ArylF}$-O-*C*H$_2$-), 77.09 (t, $^3J_{C,F}$ = 4.5 Hz, -*C≡C*-), 72.42, 70.27, 64.22 (-O*C*H-, -O*C*H$_2$-), 34.69, 34.59, 32.62, 30.37 [2xC], 30.18, 30.15 [2xC], 29.91, 26.96, 24.80, 23.42 (-*C*H$_2$-), 14.74 (-*C*H$_3$), 14.64 (2x -Si*C*H$_2$-), -4.38 (-Si*C*H$_3$). **^{19}F-NMR** (378 MHz, Pyridine-d_5): δ / ppm = -138.52 – -138.78 (m, C$_{Aryl}$-*F*), -156.72 – -156.93 (m, C$_{Aryl}$-*F*). **^{29}Si-NMR** (80 MHz, Pyridine-d_5): δ / ppm = 2.81 (*Si*). **HRMS** (m/z): [M]+Cl$^-$ calc. for C$_{96}$H$_{134}$F$_8$O$_8$Si$_2$Cl: 1658.9203, found: 1658.9260.

1,4-Bis[7-(didecylmethylsilyl)heptyloxy]-2,5-bis{4-[2,3,5,6-tetrafluoro-4-(2,3-dihydroxyprop-1-yloxy)phenylethynyl]phenylethynyl}benzene (2F7/10):
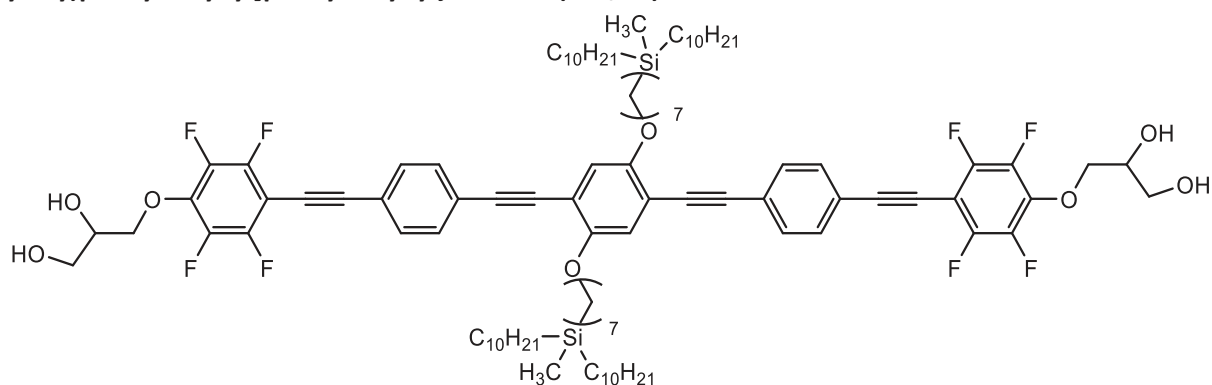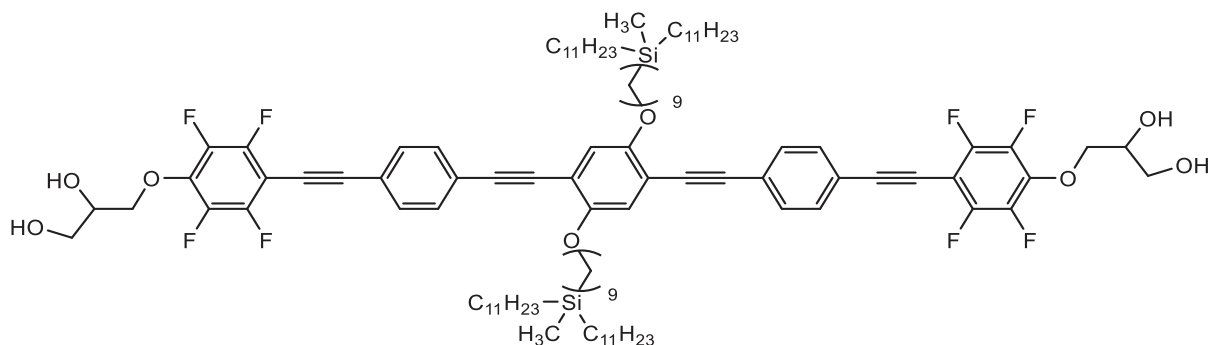

Synthesized according to GP8 from **2F7/10A** (285 mg, 0.16 mmol), PPTS (81 mg, 0.32 mmol) in MeOH/THF (1:1; 30 mL : 30 mL), purification by column chromatography (eluent: CHCl$_3$); yellow solid, yield: C$_{100}$H$_{142}$F$_8$O$_8$Si$_2$ *M* = 1680.39 g/mol, 198.2 mg (73 %), *mp* = 101 °C, **^{1}H-NMR** (402 MHz, Pyridine-d_5): δ / ppm = 7.80 (d, $^3J_{H,H}$ = 8.3 Hz, 4H, Aryl-*H*), 7.72 (d, $^3J_{H,H}$ = 8.3 Hz, 4H, Aryl-*H*), 7.50 (s, 2H, Aryl-*H*), 4.90 (dd, $^2J_{H,H}$ = 10.1, $^3J_{H,H}$ = 4.1 Hz, 2H, -Ar$_F$OC*H$_A$*H$_B$), 4.80 (dd, $^2J_{H,H}$ = 10.2, $^3J_{H,H}$ = 6.2 Hz, 2H, -Ar$_F$OCH$_A$*H$_B$*), 4.59 – 4.53 (m, 2H, -C*H*OH), 4.22 (d, $^3J_{H,H}$ = 5.5 Hz, 4H, -C*H$_2$*OH), 4.17 (t, $^3J_{H,H}$ = 6.4 Hz, 4H, -OC*H$_2$*-), 2.01 – 1.91 (m, 4H, -C*H$_2$*-), 1.74 – 1.64 (m, 4H, -C*H$_2$*-), 1.58 – 1.21 (m, 76H, -C*H$_2$*-), 0.90 (t, $^3J_{H,H}$ = 7.0 Hz, 12H, -C*H$_3$*), 0.72 – 0.63 (m, 12H, -SiC*H$_2$*-), 0.13 (s, 6H, -SiC*H$_3$*). **^{13}C NMR** (101 MHz, Pyridine-d_5) δ / ppm = 154.88 (*C$_{Aryl}$*-O), 147.06 – 146.70, 143.22 – 142.89 (m, *C$_{Aryl}$*-F), 140.73 – 140.40 (m, *C$_{ArylF}$*-O), 132.83, 132.58 (*C$_{Aryl}$*-H), 125.53, 122.53 (*C$_{Aryl}$*-quart), 117.94 (*C$_{Aryl}$*-H), 115.00 (*C$_{Aryl}$*-quart), 100.67 (-*C≡C*-), 98.19 – 97.72 (m, C$_{ArylF}$-quart.), 95.62, 90.33 (-*C≡C*-), 78.27 (t, $^4J_{C,F}$ = 3.5 Hz, C$_{ArylF}$-O-*C*H$_2$-), 77.09 (t, $^3J_{C,F}$ = 4.1 Hz, -*C≡C*-), 72.41, 70.26, 64.21 (-O*C*H-, -O*C*H$_2$-), 34.69, 34.61, 32.62, 30.46, 30.43, 30.19, 30.17, 30.12, 29.92, 26.96, 24.81, 24.79, 23.43 (-*C*H$_2$-), 14.75 (-*C*H$_3$), 14.65 (2x -Si*C*H$_2$-), -4.38 (-Si*C*H$_3$). **^{19}F-NMR** (378 MHz, Pyridine-d_5): δ / ppm = -137.01 – -137.32 (m, C$_{Aryl}$-*F*), -155.18 – -155.53 (m, C$_{Aryl}$-*F*). **^{29}Si-NMR** (80 MHz, Pyridine-d_5): δ / ppm = 2.81 (*Si*). **HRMS** (m/z): [M]+Cl$^-$ calc. for C$_{100}$H$_{142}$F$_8$O$_8$Si$_2$Cl: 1714.9829, found: 1714.9842.

1,4-Bis[9-(dioctylmethylsilyl)nonyloxy]-2,5-bis{4-[2,3,5,6-tetrafluoro-4-(2,3-dihydroxyprop-1-yloxy)phenylethynyl]phenylethynyl}benzene (2F9/8):
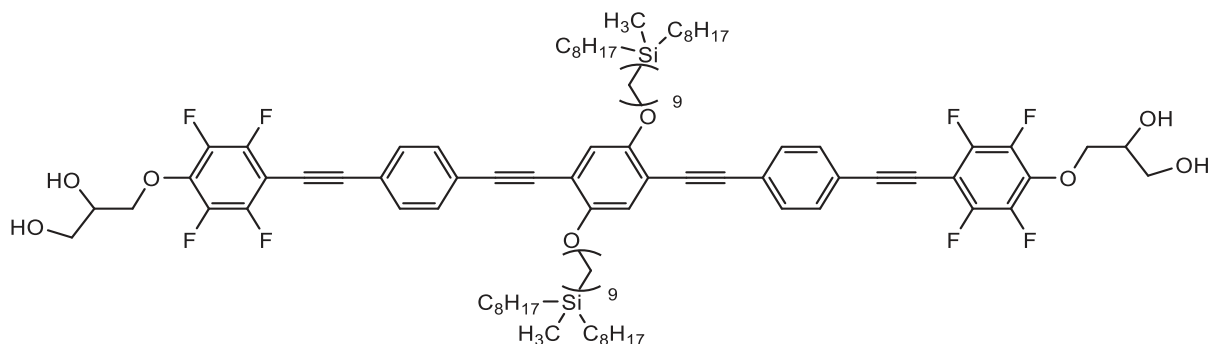
Synthesized according to GP8 from **2F9/8A** (280 mg, 0.16 mmol),PPTS (82 mg, 0.32 mmol) in MeOH/THF (1:1; 30 mL : 30 mL), purification by column chromatography (eluent: CHCl$_3$); yellow solid, yield: C$_{96}$H$_{134}$F$_8$O$_8$Si$_2$ M = 1624.28 g/mol, 179.0 mg (69 %), mp < 20 °C, **^{1}H-NMR** (502 MHz, Pyridine-d_5): δ / ppm = 7.79 (d, $^3J_{H,H}$ = 8.5 Hz, 4H, Aryl-*H*), 7.72 (d, $^3J_{H,H}$ = 8.5 Hz, 4H, Aryl-*H*), 7.51 (s, 2H, Aryl-*H*), 4.90 (dd, $^2J_{H,H}$ = 10.1, $^3J_{H,H}$ = 4.0 Hz, 2H, -Ar$_F$OC*H*$_A$H$_B$), 4.80 (dd, $^2J_{H,H}$ = 10.0, $^3J_{H,H}$ = 6.3 Hz, 2H, -Ar$_F$OCH$_A$*H*$_B$), 4.60 – 4.52 (m, 2H, -C*H*OH), 4.23 (d, $^3J_{H,H}$ = 5.7 Hz, 4H, -C*H*$_2$OH), 4.16 (t, $^3J_{H,H}$ = 6.4 Hz, 4H, -OC*H*$_2$-), 1.97 – 1.88 (m, 4H, -C*H*$_2$-), 1.71 – 1.61 (m, 4H, -C*H*$_2$-), 1.52 – 1.21 (m, 68H, -C*H*$_2$-), 0.90 (t, $^3J_{H,H}$ = 7.3 Hz, 12H, -C*H*$_3$), 0.70 – 0.60 (m, 12H, -SiC*H*$_2$-), 0.12 (d, $^3J_{H,H}$ = 3.6 Hz, 6H, -SiC*H*$_3$). **^{13}C NMR** (126 MHz, Pyridine-d_5) δ / ppm = 154.88 (*C*$_{Aryl}$-O), 147.27 – 146.95, 142.93 – 142.62 (m, *C*$_{Aryl}$-F), 141.01 – 140.73 (m, *C*$_{ArylF}$-O), 132.83, 132.58 (*C*$_{Aryl}$-H), 125.51, 122.53 (*C*$_{Aryl}$-quart), 117.97 (*C*$_{Aryl}$-H), 115.00 (*C*$_{Aryl}$-quart), 100.68 (-*C*≡C-), 98.14 – 97.76 (m, C$_{ArylF}$-quart.), 95.63, 90.32 (-*C*≡C-), 78.27 (t, $^4J_{C,F}$ = 3.3 Hz, C$_{ArylF}$-O-CH$_2$-), 77.10 (t, $^3J_{C,F}$ = 4.2 Hz, -*C*≡C-), 72.42, 70.25, 64.22 (-O*C*H-, -O*C*H$_2$-), 34.64, 34.58, 32.65, 30.46, 30.22, 30.13, 30.11, 30.08, 30.04, 26.94, 24.82, 24.78, 23.42 (-*C*H$_2$-), 14.74 (-*C*H$_3$), 14.69, 14.64 (-Si*C*H$_2$-), -4.38 (-Si*C*H$_3$). **^{19}F-NMR** (473 MHz, Pyridine-d_5): δ / ppm = -138.57 – -138.74 (m, C$_{Aryl}$-*F*), -156.80 – -156.93 (m, C$_{Aryl}$-*F*). **^{29}Si-NMR** (80 MHz, Pyridine-d_5): δ / ppm = 2.80 (*Si*). **HRMS** (m/z): [M]+Cl$^-$ calc. for C$_{96}$H$_{134}$F$_8$O$_8$Si$_2$Cl: 1658.9203, found: 1658.9162.

1,4-Bis[9-(diundecylmethylsilyl)nonyloxy]-2,5-bis{4-[2,3,5,6-tetrafluoro-4-(2,3-dihydroxyprop-1-yloxy)phenylethynyl]phenylethynyl}benzene (2F9/11):

Synthesized according to GP8 from **2F9/11A** (300 mg, 0.16 mmol),PPTS (81 mg, 0.32 mmol) in MeOH/THF (1:1; 30 mL : 30 mL), purification by column chromatography (eluent: CHCl$_3$); yellow solid, yield: C$_{108}$H$_{158}$F$_8$O$_8$Si$_2$ M = 1792.60 g/mol, 234.6 mg (82 %), mp = 69 °C, **^{1}H-NMR** (500 MHz, Pyridine-d_5): δ / ppm = 7.80 (d, $^3J_{H,H}$ = 8.3 Hz, 4H, Aryl-*H*), 7.72 (d, $^3J_{H,H}$ = 8.3 Hz, 4H, Aryl-*H*), 7.51 (s, 2H, Aryl-*H*), 4.90 (dd, $^2J_{H,H}$ = 10.1, $^3J_{H,H}$ = 4.0 Hz, 2H, -Ar$_F$OC*H*$_A$H$_B$), 4.80 (dd, $^2J_{H,H}$ = 10.1, $^3J_{H,H}$ = 6.3 Hz, 2H, -Ar$_F$OCH$_A$*H*$_B$), 4.62 – 4.52 (m, 2H, -C*H*OH), 4.23 (d, $^3J_{H,H}$ = 5.5 Hz, 4H, -C*H*$_2$OH), 4.17 (t, $^3J_{H,H}$ = 6.4 Hz, 4H, -OC*H*$_2$-), 1.98 – 1.88 (m, 4H, -C*H*$_2$-), 1.71 – 1.63 (m, 4H, -C*H*$_2$-), 1.51 – 1.22 (m, 92H, -C*H*$_2$-), 0.90 (t, $^3J_{H,H}$ = 7.4 Hz, 12H, -C*H*$_3$), 0.68 (t, $^3J_{H,H}$ = 7.8 Hz, 12H, -SiC*H*$_2$-), 0.14 (s, 6H, -SiC*H*$_3$). **^{13}C NMR** (126 MHz, Pyridine-d_5) δ / ppm = 154.88 (*C*$_{Aryl}$-O), 147.38 – 146.89, 143.04 – 142.62 (m, *C*$_{Aryl}$-F), 140.95 – 140.75 (m, *C*$_{ArylF}$-O), 132.84, 132.58 (*C*$_{Aryl}$-H), 125.52, 122.54 (*C*$_{Aryl}$-quart), 117.96 (*C*$_{Aryl}$-H), 115.01 (*C*$_{Aryl}$-quart), 100.68 (-*C*≡C-), 98.21

– 97.66 (m, C_{ArylF}-quart.), 95.63, 90.33 (-$C\equiv C$-), 78.27 (t, $^4J_{C,F}$ = 3.3 Hz, C_{ArylF}-O-CH_2-), 77.11 (t, $^3J_{C,F}$ = 4.0 Hz, -$C\equiv C$-), 72.42, 70.25, 64.22 (-OCH-, -OCH_2-), 34.64, 34.60, 32.62, 30.51, 30.46, 30.42 [2xC], 30.22, 30.16, 30.14, 30.11, 30.10, 26.95, 24.83, 24.80, 23.42 (-CH_2-), 14.75 (-CH_3), 14.70, 14.66 (-SiCH_2-), -4.36 (-SiCH_3). ^{19}**F-NMR** (470 MHz, Pyridine-d_5): δ / ppm = -138.52 – -138.78 (m), -156.72 – -156.93 (m).^{29}**Si-NMR** (99 MHz, Pyridine-d_5): δ / ppm = 2.78 (*Si*). **HRMS** (m/z): [M]+Cl$^-$ calc. for $C_{108}H_{158}F_8O_8Si_2Cl$: 1927.1082, found: 1827.1044.

1,4-Bis[11-(diundecylmethylsilyl)undecyloxy]-2,5-bis{4-[2,3,5,6-tetrafluoro-4-(2,3-dihydroxyprop-1-yloxy)phenylethynyl]phenylethynyl}benzene (2F11/11):
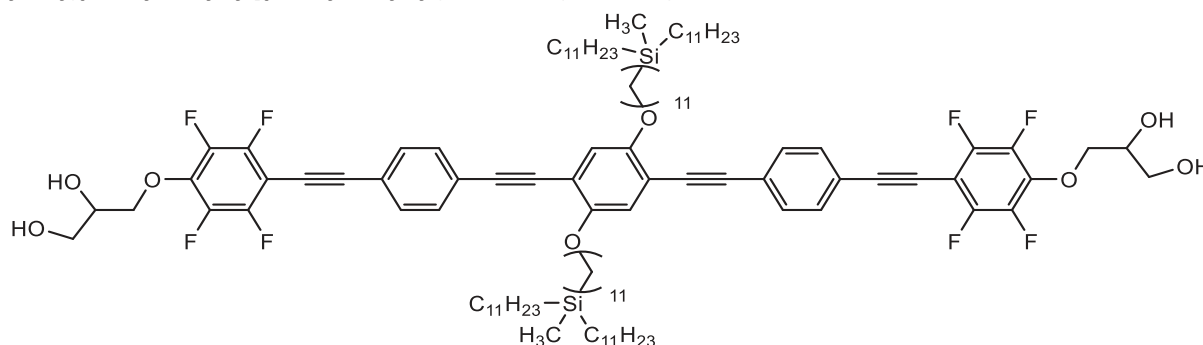
Synthesized according to GP8 from **2F11/11A** (200 mg, 0.11 mmol),PPTS (57 mg, 0.23 mmol) in MeOH/THF (1:1; 30 mL : 30 mL), purification by column chromatography (eluent: CHCl$_3$); yellow solid, yield: $C_{112}H_{166}F_8O_8Si_2$ *M* = 1848.71 g/mol, 191.3 mg (91 %), *mp* = 64 °C, ^{1}**H-NMR** (400 MHz, Pyridine-d_5): δ / ppm = 7.80 (d, $^3J_{H,H}$ = 8.2 Hz, 4H, Aryl-*H*), 7.72 (d, $^3J_{H,H}$ = 8.2 Hz, 4H, Aryl-*H*), 7.51 (s, 2H, Aryl-*H*), 4.91 (dd, $^2J_{H,H}$ = 10.2, $^3J_{H,H}$ = 4.1 Hz, 2H, -Ar$_F$OCH_AH$_B$), 4.81 (dd, $^2J_{H,H}$ = 10.2, $^3J_{H,H}$ = 6.3 Hz, 2H, -Ar$_F$OCH$_A$H$_B$), 4.60 – 4.52 (m, 2H, -C*H*OH), 4.23 (d, $^3J_{H,H}$ = 5.6 Hz, 4H, -CH_2OH), 4.17 (t, $^3J_{H,H}$ = 6.3 Hz, 4H, -OCH_2-), 2.00 – 1.88 (m, 4H, -CH_2-), 1.73 – 1.58 (m, 4H, -CH_2-), 1.55 – 1.20 (m, 100H, -CH_2-), 0.90 (t, $^3J_{H,H}$ = 6.1 Hz, 12H, -CH_3), 0.72 – 0.63 (m, 12H, -SiCH_2-), 0.13 (s, 6H, -SiCH_3). ^{13}**C NMR** (101 MHz, Pyridine-d_5) δ / ppm = 154.89 (C_{Aryl}-O), 147.06 – 146.59, 143.20 – 142.76 (m, C_{Aryl}-F), 140.65 – 140.26 (m, C_{ArylF}-O), 132.85, 132.60 (C_{Aryl}-H), 125.53, 122.55 (C_{Aryl}-quart), 117.99 (C_{Aryl}-H), 115.02 (C_{Aryl}-quart), 100.68 (-$C\equiv C$-), 95.64, 90.33 (-$C\equiv C$-), 78.28 (t, $^4J_{C,F}$ = 3.6 Hz, C_{ArylF}-O-CH_2-), 77.11 (t, $^3J_{C,F}$ = 4.3 Hz, -$C\equiv C$-), 72.43, 70.27, 64.23 (-OCH-, -OCH_2-), 34.64, 34.60, 32.63, 30.52 [2xC], 30.47, 30.43 [2xC], 30.20, 30.16 [2xC], 30.14, 30.12 [2xC], 26.94, 24.83, 24.81, 23.43 (-CH_2-), 14.76 (-CH_3), 14.70, 14.68 (-SiCH_2-), -4.35 (-SiCH_3). ^{19}**F-NMR** (376 MHz, Pyridine-d_5): δ / ppm = -138.55 – -138.92 (m), -156.79 – -157.04 (m). ^{29}**Si-NMR** (79 MHz, Pyridine-d_5): δ / ppm = 2.80 (*Si*). **HRMS** (m/z): [M]+Cl$^-$ calc. for $C_{112}H_{166}F_8O_8Si_2Cl$: 1883.1708, found: 1883.1637.

1,4-Bis[4-(tridecylsilyl)butyloxy]-2,5-bis{4-[2,3,5,6-tetrafluoro-4-(2,3-dihydroxyprop-1-yloxy)phenylethynyl]phenylethynyl}benzene (1F4/10):
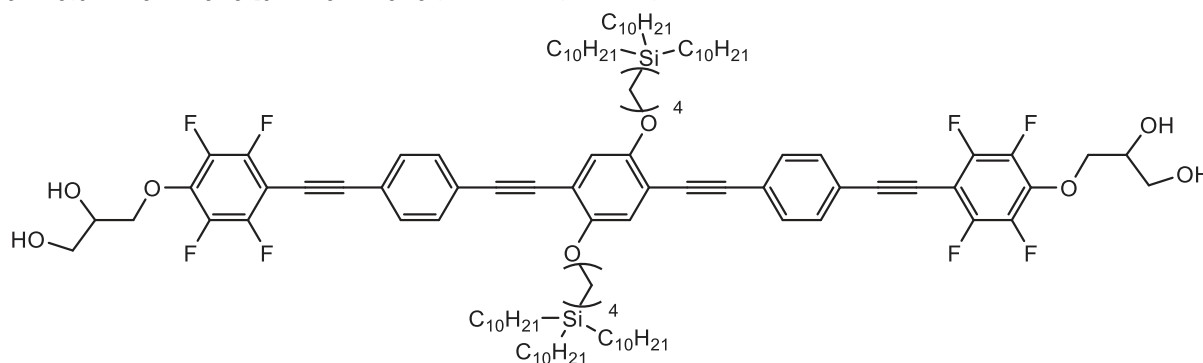
Synthesized according to GP8 from **1F4/10A** (300 mg, 0.16 mmol),PPTS (78 mg, 0.32 mmol) in MeOH/THF (1:1; 30 mL : 30 mL), purification by column chromatography (eluent: CHCl$_3$); yellow solid,

yield: $C_{112}H_{166}F_8O_8Si_2$ M = 1848.71 g/mol, 207.5 mg (72 %), *mp* < 20 °C, **^{1}H-NMR** (400 MHz, Pyridine-d_5): δ / ppm = 7.82 (d, $^3J_{H,H}$ = 8.3 Hz, 4H, Aryl-*H*), 7.76 (d, $^3J_{H,H}$ = 8.3 Hz, 4H, Aryl-*H*), 7.53 (s, 2H, Aryl-*H*), 4.90 (dd, $^2J_{H,H}$ = 10.1, $^3J_{H,H}$ = 4.1 Hz, 2H, -Ar$_F$OC*H$_A$*H$_B$), 4.80 (dd, $^2J_{H,H}$ = 10.2, $^3J_{H,H}$ = 6.3 Hz, 2H, -Ar$_F$OCH$_A$*H$_B$*), 4.61 − 4.52 (m, 2H, -C*H*OH), 4.26 (t, $^3J_{H,H}$ = 6.2 Hz, 4H, -OC*H$_2$*-), 4.22 (d, $^3J_{H,H}$ = 5.5 Hz, 4H, -C*H$_2$*OH), 2.13 − 2.00 (m, 4H, -C*H$_2$*-), 1.90 − 1.78 (m, 4H, -C*H$_2$*-), 1.58 − 1.21 (m, 96H, -C*H$_2$*-), 0.91 (t, $^3J_{H,H}$ = 6.4 Hz, 18H, -C*H$_3$*), 0.86 − 0.80 (m, 4H, -SiC*H$_2$*-), 0.78 − 0.71 (m, 12H). **^{13}C NMR** (101 MHz, Pyridine-d_5) δ / ppm = 154.86 (C_{Aryl}-O), 147.16 − 146.57, 143.35 − 142.80 (m, C_{Aryl}-F), 140.86 − 140.24 (m, C_{ArylF}-O), 132.86, 132.62 (C_{Aryl}-H), 125.59, 122.54 (C_{Aryl}-quart), 117.84 (C_{Aryl}-H), 114.94 (C_{Aryl}-quart), 100.70 (-*C*≡C-), 98.25 − 97.80 (m, C_{ArylF}-quart.), 95.64, 90.38 (-*C*≡C-), 78.29 (t, $^4J_{C,F}$ = 3.2 Hz, C_{ArylF}-O-CH$_2$-), 77.09 (t, $^3J_{C,F}$ = 4.2 Hz, -*C*≡C-), 72.42, 69.64, 64.22 (-O*C*H-, -O*C*H$_2$-), 34.76, 34.06, 32.65, 30.50, 30.48, 30.18, 30.15, 24.88, 23.44, 21.37 (-*C*H$_2$-), 14.76 (-*C*H$_3$), 13.32, 13.03 (-Si*C*H$_2$-). **^{19}F-NMR** (376 MHz, Pyridine-d_5): δ / ppm = -138.54 − -138.81 (m, C_{Aryl}-F), -156.76 − -157.04 (m, C_{Aryl}-F). **^{29}Si-NMR** (79 MHz, Pyridine-d_5): δ / ppm = 3.16 (*Si*). **HRMS** (m/z): [M]+Cl$^-$ calc. for $C_{112}H_{166}F_8O_8Si_2Cl$: 1883.1708, found: 1883.1750.

1,4-Bis[5-(trioctylsilyl)pentyloxy]-2,5-bis{4-[2,3,5,6-tetrafluoro-4-(2,3-dihydroxyprop-1-yloxy)phenylethynyl]phenylethynyl}benzene (1F5/8):
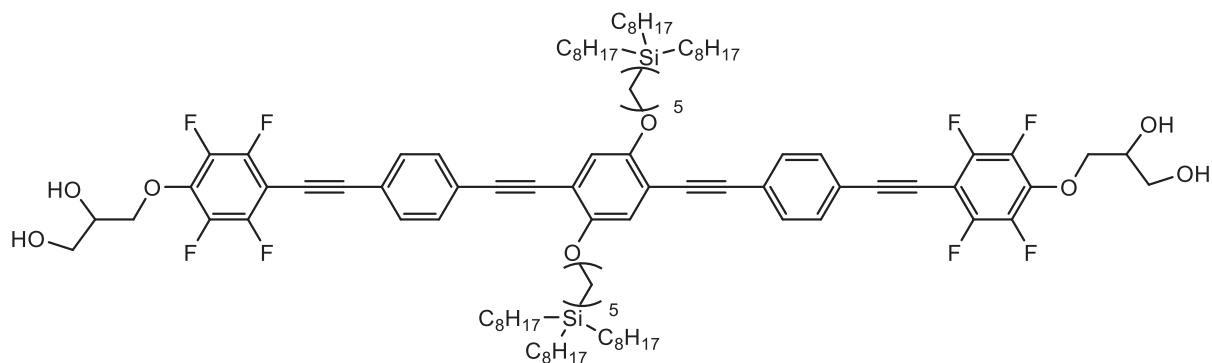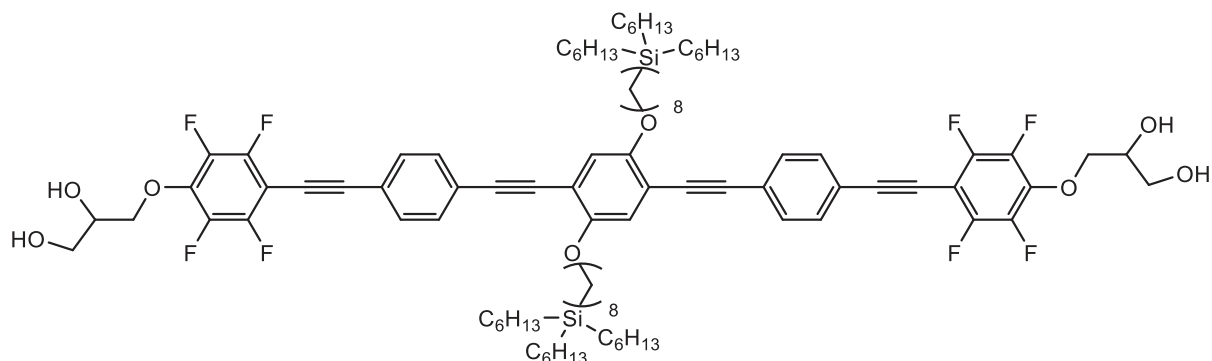

Synthesized according to GP8 from **1F5/8A** (250 mg, 0.14 mmol), PPTS (70 mg, 0.28 mmol) in MeOH/THF (1:1; 30 mL : 30 mL), purification by column chromatography (eluent: CHCl$_3$); yellow solid, yield: $C_{102}H_{146}F_8O_8Si_2$ M = 1708.44 g/mol, 159.2 mg (67 %), *mp* = 110 °C, **^{1}H-NMR** (502 MHz, Pyridine-d_5): δ / ppm = 7.80 (d, $^3J_{H,H}$ = 8.1 Hz, 4H, Aryl-*H*), 7.72 (d, $^3J_{H,H}$ = 7.9 Hz, 4H, Aryl-*H*), 7.51 (s, 2H, Aryl-*H*), 7.08 (s, 2H, -O*H*), 6.62 (s, 2H, -O*H*), 4.90 (dd, $^2J_{H,H}$ = 10.1, $^3J_{H,H}$ = 4.2 Hz, 2H, -Ar$_F$OC*H$_A$*H$_B$), 4.80 (dd, $^2J_{H,H}$ = 10.1, $^3J_{H,H}$ = 6.2 Hz, 2H, -Ar$_F$OCH$_A$*H$_B$*), 4.59 − 4.52 (m, 2H, -C*H*OH), 4.25 − 4.16 (m, 8H, -C*H$_2$*OH, -OC*H$_2$*-), 2.05 − 1.97 (m, 4H, -C*H$_2$*-), 1.86 − 1.75 (m, 4H, -C*H$_2$*-), 1.66 − 1.56 (m, 4H, -C*H$_2$*-), 1.55 − 1.24 (m, 72H, -C*H$_2$*-), 0.91 (t, $^3J_{H,H}$ = 6.7 Hz, 18H, -C*H$_3$*), 0.82 − 0.66 (m, 16H, -SiC*H$_2$*-). **^{13}C NMR** (126 MHz, Pyridine-d_5) δ / ppm = 154.93 (C_{Aryl}-O), 147.38 − 146.90, 142.95 − 142.54 (m, C_{Aryl}-F), 140.97 − 140.68 (m, C_{ArylF}-O), 132.82, 132.58 (C_{Aryl}-H), 125.56, 122.53 (C_{Aryl}-quart), 117.99 (C_{Aryl}-H), 115.06 (C_{Aryl}-quart), 100.64 (-*C*≡C-), 98.22 − 97.72 (m, C_{ArylF}-quart.), 95.61, 90.37 (-*C*≡C-), 78.28 (t, $^4J_{C,F}$ = 3.3 Hz, C_{ArylF}-O-CH$_2$-), 77.09 (t, $^3J_{C,F}$ = 4.2 Hz, -*C*≡C-), 72.42, 70.26, 64.22 (-O*C*H-, -O*C*H$_2$-), 34.73, 32.68, 31.18, 30.09 [2xC], 29.89, 24.85, 24.67, 23.45 (-*C*H$_2$-), 14.75 (-*C*H$_3$), 13.52, 13.34 (-Si*C*H$_2$-). **^{19}F-NMR** (378 MHz, Pyridine-d_5): δ / ppm = -138.41 − -138.77 (m, C_{Aryl}-F), -156.68 − -157.08 (m, C_{Aryl}-F). **^{29}Si-NMR** (100 MHz, Pyridine-d_5): δ / ppm = 3.06 (*Si*). **HRMS** (m/z): [M]+Cl$^-$ calc. for $C_{102}H_{146}F_8O_8Si_2Cl$: 1743.0142, found: 1743.0186.

1,4-Bis[6-(trioctylsilyl)hexyloxy]-2,5-bis{4-[2,3,5,6-tetrafluoro-4-(2,3-dihydroxyprop-1-yloxy)phenylethynyl]phenylethynyl}benzene (1F6/8):
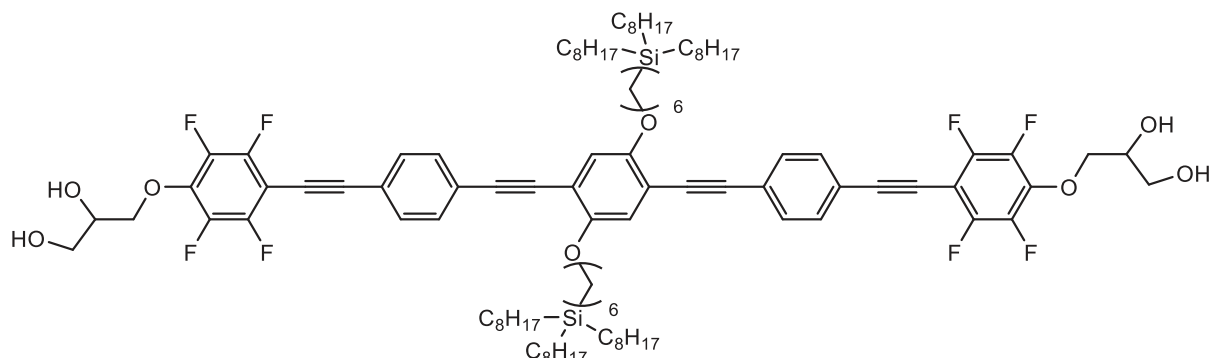
Synthesized according to GP8 from **1F6/8A** (220 mg, 0.12 mmol), PPTS (61 mg, 0.24 mmol) in MeOH/THF (1:1; 30 mL : 30 mL), purification by column chromatography (eluent: CHCl$_3$); yellow solid, yield: C$_{104}$H$_{150}$F$_8$O$_8$Si$_2$ M = 1736.49 g/mol, 173.3 mg (83 %), mp = 93 °C, **^{1}H-NMR** (400 MHz, Pyridine-d_5): δ / ppm = 7.80 (d, $^3J_{H,H}$ = 8.3 Hz, 4H, Aryl-*H*), 7.73 (d, $^3J_{H,H}$ = 8.4 Hz, 4H, Aryl-*H*), 7.50 (s, 2H, Aryl-*H*), 4.90 (dd, $^2J_{H,H}$ = 10.2, $^3J_{H,H}$ = 4.1 Hz, 2H, -Ar$_F$OC*H$_A$*H$_B$), 4.80 (dd, $^2J_{H,H}$ = 10.1, $^3J_{H,H}$ = 6.2 Hz, 2H, -Ar$_F$OCH$_A$*H$_B$*), 4.60 – 4.53 (m, 2H, -C*H*OH), 4.25 – 4.16 (m, 8H, -C*H$_2$*OH, -OC*H$_2$*-), 2.03 – 1.92 (m, 4H, -C*H$_2$*-), 1.81 – 1.70 (m, 4H, -C*H$_2$*-), 1.65 – 1.25 (m, 80H, -C*H$_2$*-), 0.91 (t, $^3J_{H,H}$ = 6.8 Hz, 18H, -C*H$_3$*), 0.78 – 0.68 (m, 16H, -SiC*H$_2$*-). **^{13}C NMR** (101 MHz, Pyridine-d_5) δ / ppm = 154.87 (*C$_{Aryl}$*-O), 147.09 – 146.64, 143.29 – 142.87 (m, *C$_{Aryl}$*-F), 140.90 – 140.48 (m, *C$_{ArylF}$*-O), 132.84, 132.57 (*C$_{Aryl}$*-H), 125.54, 122.54 (*C$_{Aryl}$*-quart), 117.91 (*C$_{Aryl}$*-H), 115.00 (*C$_{Aryl}$*-quart), 100.68 (-*C*≡*C*-), 98.05 – 97.93 (m, C$_{ArylF}$-quart.), 95.62, 90.36 (-*C*≡*C*-), 78.28 (t, $^4J_{C,F}$ = 3.4 Hz, C$_{ArylF}$-O-*C*H$_2$-), 77.10 (t, $^3J_{C,F}$ = 4.1 Hz, -*C*≡*C*-), 72.41, 70.23, 64.21 (-O*C*H-, -O*C*H$_2$-), 34.72, 34.46, 32.68, 30.15, 30.10, 30.08, 26.66, 24.96, 24.85, 23.44 (-*C*H$_2$-), 14.75 (-*C*H$_3$), 13.35, 13.32 (-Si*C*H$_2$-). **^{19}F-NMR** (376 MHz, Pyridine-d_5): δ / ppm = -138.42 – -138.79 (m, C$_{Aryl}$-*F*), -156.57 – -157.21 (m, C$_{Aryl}$-*F*). **^{29}Si-NMR** (79 MHz, Pyridine-d_5): δ / ppm = 3.04 (*Si*). **HRMS** (m/z): [M]+Cl$^-$ calc. for C$_{104}$H$_{150}$F$_8$O$_8$Si$_2$Cl: 1771.0455, found: 1771.0422.

1,4-Bis[8-(trihexylsilyl)octyloxy]-2,5-bis{4-[2,3,5,6-tetrafluoro-4-(2,3-dihydroxyprop-1-yloxy)phenylethynyl]phenylethynyl}benzene (1F8/6):

Synthesized according to GP8 from **1F8/6A** (290 mg, 0.17 mmol), PPTS (86 mg, 0.34 mmol) in MeOH/THF (1:1; 30 mL : 30 mL), purification by column chromatography (eluent: CHCl$_3$); yellow solid, yield: C$_{96}$H$_{134}$F$_8$O$_8$Si$_2$ M = 1624.28 g/mol, 144.6 mg (52 %), mp = 95 °C, **^{1}H-NMR** (502 MHz, Pyridine-d_5): δ / ppm = 7.79 (d, $^3J_{H,H}$ = 8.0 Hz, 4H, Aryl-*H*), 7.71 (d, $^3J_{H,H}$ = 8.0 Hz, 4H, Aryl-*H*), 7.49 (s, 2H, Aryl-*H*), 4.90 (dd, $^2J_{H,H}$ = 10.1, $^3J_{H,H}$ = 4.6 Hz, 2H, -Ar$_F$OC*H$_A$*H$_B$), 4.79 (dd, $^2J_{H,H}$ = 10.8, $^3J_{H,H}$ = 5.0 Hz, 2H, -Ar$_F$OCH$_A$*H$_B$*), 4.61 – 4.53 (m, 2H, -C*H*OH), 4.22 (d, $^3J_{H,H}$ = 5.3 Hz, 4H, -C*H$_2$*OH), 4.16 (t, $^3J_{H,H}$ = 6.4 Hz, 4H, -OC*H$_2$*-), 1.98 – 1.88 (m, 4H, -C*H$_2$*-), 1.72 – 1.65 (m, 4H, -C*H$_2$*-), 1.54 – 1.28 (m, 64H, -C*H$_2$*-), 0.93 (t, $^3J_{H,H}$ = 6.9 Hz, 18H, -C*H$_3$*), 0.74 – 0.65 (m, 16H, -SiC*H$_2$*-). **^{13}C NMR** (126 MHz, Pyridine-d_5) δ / ppm = 154.86 (*C$_{Aryl}$*-O), 147.30 – 146.81, 143.07 – 142.48 (m, *C$_{Aryl}$*-F), 141.10 – 140.65 (m, *C$_{ArylF}$*-O), 132.83, 132.58 (*C$_{Aryl}$*-H), 125.52, 122.54 (*C$_{Aryl}$*-quart), 117.96 (*C$_{Aryl}$*-H), 114.99 (*C$_{Aryl}$*-quart), 100.68 (-*C*≡*C*-), 98.13 – 97.82 (m, C$_{ArylF}$-quart.),

95.62, 90.33 (-$C\equiv C$-), 78.28 (t, $^4J_{C,F}$ = 3.6 Hz, C_{ArylF}-O-CH_2-), 77.10 (t, $^3J_{C,F}$ = 3.6 Hz, -$C\equiv C$-), 72.42, 70.21, 68.30, 64.22 (-OCH-, -OCH_2-), 34.66, 34.36, 32.29, 30.15 [2xC], 30.13, 26.95, 24.86, 24.78, 23.41 (-CH_2-), 14.79 (-CH_3), 13.35, 13.32 (-SiCH_2-). **^{19}F-NMR** (473 MHz, Pyridine-d_5): δ / ppm = -138.52 − -138.77 (m, C_{Aryl}-F), -156.70 − -157.02 (m, C_{Aryl}-F). **^{29}Si-NMR** (100 MHz, Pyridine-d_5): δ / ppm = 3.02 (Si). **HRMS** (m/z): [M]+Cl$^-$ calc. for $C_{96}H_{134}F_8O_8Si_2Cl$: 1658.9203, found: 1658.9223.

1,4-Bis[9-(tripentylsilyl)nonyloxy]-2,5-bis{4-[2,3,5,6-tetrafluoro-4-(2,3-dihydroxyprop-1-yloxy)phenylethynyl]phenylethynyl}benzene (1F9/5):
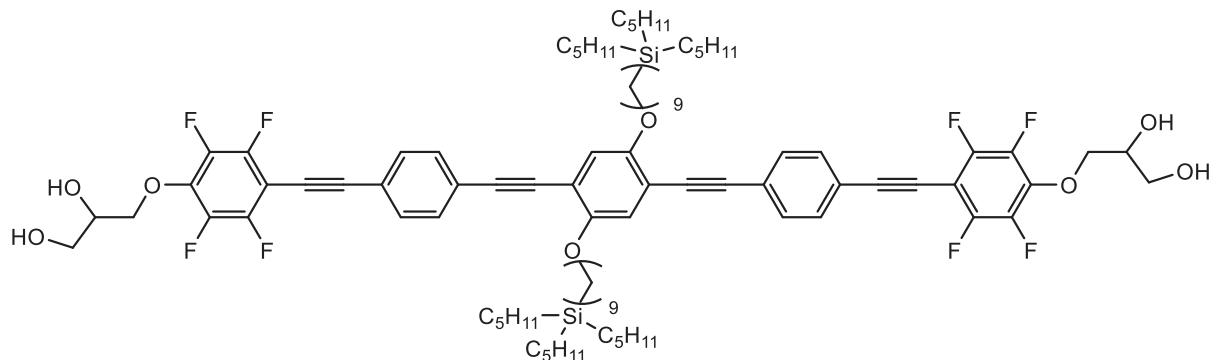
Synthesized according to GP8 from **1F9/5A** (290 mg, 0.18 mmol),PPTS (89 mg, 0.36 mmol) in MeOH/THF (1:1; 30 mL : 30 mL), purification by column chromatography (eluent: CHCl$_3$); yellow solid, yield: $C_{92}H_{126}F_8O_8Si_2$ M = 1568.17 g/mol, 84.1 mg (31 %), mp = 96 °C, **^{1}H-NMR** (402 MHz, Pyridine-d_5): δ / ppm = 7.79 (d, $^3J_{H,H}$ = 8.0 Hz, 4H, Aryl-H), 7.71 (d, $^3J_{H,H}$ = 8.0 Hz, 4H, Aryl-H), 7.50 (s, 2H, Aryl-H), 4.90 (dd, $^2J_{H,H}$ = 10.2, $^3J_{H,H}$ = 4.0 Hz, 2H, -Ar$_F$OCH_AH_B), 4.80 (dd, $^2J_{H,H}$ = 10.2, $^3J_{H,H}$ = 6.5 Hz, 2H, -Ar$_F$OCH_AH_B), 4.61 − 4.51 (m, 2H, -CHOH), 4.22 (d, $^3J_{H,H}$ = 4.8 Hz, 4H, -CH_2OH), 4.16 (t, $^3J_{H,H}$ = 6.4 Hz, 4H, -OCH_2-), 2.02 − 1.87 (m, 4H, -CH_2-), 1.72 − 1.61 (m, 4H, -CH_2-), 1.58 − 1.31 (m, 56H, -CH_2-), 0.94 (t, $^3J_{H,H}$ = 7.2 Hz, 18H, -CH_3), 0.74 − 0.61 (m, 16H, -SiCH_2-).**^{13}C NMR** (101 MHz, Pyridine-d_5) δ / ppm = 154.87 (C_{Aryl}-O), 147.07 − 146.66, 143.33 − 142.77 (m, C_{Aryl}-F), 140.81 − 140.31 (m, C_{ArylF}-O), 132.83, 132.58 (C_{Aryl}-H), 125.51, 122.53 (C_{Aryl}-quart), 117.97 (C_{Aryl}-H), 115.00 (C_{Aryl}-quart), 100.67 (-$C\equiv C$-),98.23 − 97.65 (m, C_{ArylF}-quart.), 95.63, 90.32 (-$C\equiv C$-), 78.28 (t, $^4J_{C,F}$ = 3.6 Hz, C_{ArylF}-O-CH_2-), 77.04 (t, $^3J_{C,F}$ = 4.1 Hz, -$C\equiv C$-), 72.42, 70.25, 64.22 (-OCH-, -OCH_2-), 36.85, 34.73, 30.46, 30.22, 30.14, 30.08, 26.95, 24.83, 24.42, 23.06 (-CH_2-), 14.69 (-CH_3), 13.31, 13.20 (-SiCH_2-). **^{19}F-NMR** (378 MHz, Pyridine-d_5): δ / ppm = -138.55 − -138.91 (m, C_{Aryl}-F), -156.74 − -157.10 (m, C_{Aryl}-F). **^{29}Si-NMR** (80 MHz, Pyridine-d_5): δ / ppm = 2.89 (Si). **HRMS** (m/z): [M]+Cl$^-$ calc. for $C_{92}H_{126}F_8O_8Si_2Cl$: 1602.8577, found: 1602.8591.

1,4-Bis[9-(trihexylsilyl)nonyloxy]-2,5-bis{4-[2,3,5,6-tetrafluoro-4-(2,3-dihydroxyprop-1-yloxy)phenylethynyl]phenylethynyl}benzene (1F9/6):
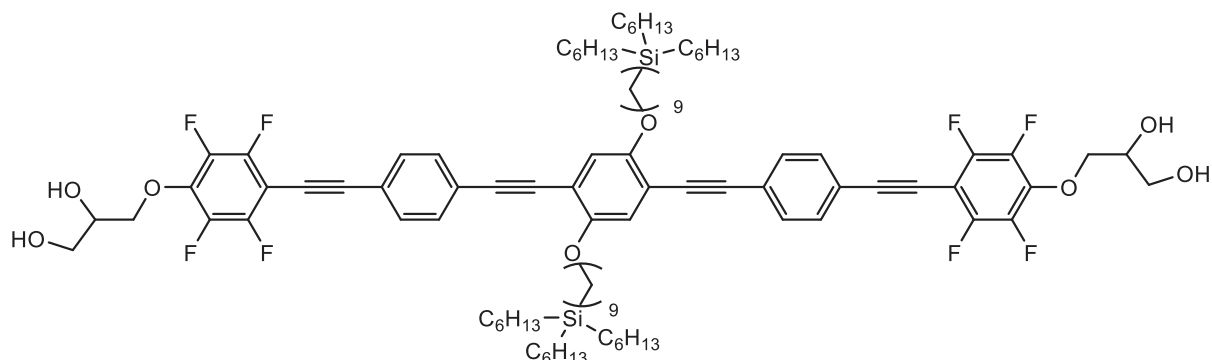
Synthesized according to GP8 from **1F9/6A** (260 mg, 0.15 mmol),PPTS (75 mg, 0.30 mmol) in MeOH/THF (1:1; 30 mL : 30 mL), purification by column chromatography (eluent: CHCl$_3$); yellow solid, yield: $C_{98}H_{138}F_8O_8Si_2$ M = 1652.33 g/mol, 208.9 mg (84 %), mp = 101 °C, **^{1}H-NMR** (402 MHz, Pyridine-d_5): δ / ppm = 7.79 (d, $^3J_{H,H}$ = 8.3 Hz, 4H, Aryl-H), 7.72 (d, $^3J_{H,H}$ = 8.3 Hz, 4H, Aryl-H), 7.50 (s, 2H, Aryl-H),

4.90 (dd, $^2J_{H,H}$ = 10.2, $^3J_{H,H}$ = 4.1 Hz, 2H, -Ar$_F$OCH$_A$H$_B$), 4.80 (dd, $^2J_{H,H}$ = 10.1, $^3J_{H,H}$ = 6.3 Hz, 2H, -Ar$_F$OCH$_A$H$_B$), 4.60 – 4.53 (m, 2H, -CHOH), 4.22 (d, $^3J_{H,H}$ = 5.5 Hz, 4H, -CH$_2$OH), 4.16 (t, $^3J_{H,H}$ = 6.4 Hz, 4H, -OCH$_2$-), 1.97 – 1.88 (m, 4H, -CH$_2$-), 1.70 – 1.62 (m, 4H, -CH$_2$-), 1.55 – 1.29 (m, 68H, -CH$_2$-), 0.94 (t, $^3J_{H,H}$ = 7.0 Hz, 18H, -CH$_3$), 0.74 – 0.65 (m, 16H, -SiCH$_2$-). **^{13}C NMR** (101 MHz, Pyridine-d_5) δ / ppm = 154.87 (C$_{Aryl}$-O), 147.05 – 146.60, 143.25 – 142.87 (m, C$_{Aryl}$-F), 140.75 – 140.17 (m, C$_{ArylF}$-O), 132.83, 132.58 (C$_{Aryl}$-H), 125.51, 122.53 (C$_{Aryl}$-quart), 117.97 (C$_{Aryl}$-H), 115.00 (C$_{Aryl}$-quart), 100.66 (-C≡C-), 98.22 – 97.63 (m, C$_{ArylF}$-quart.), 95.62, 90.32 (-C≡C-), 78.27 (t, $^4J_{C,F}$ = 3.3 Hz, C$_{ArylF}$-O-CH$_2$-), 77.08 (t, $^3J_{C,F}$ = 4.6 Hz, -C≡C-), 72.42, 70.25, 64.22 (-OCH-, -OCH$_2$-), 34.75, 34.36, 32.28, 30.46, 30.21, 30.12, 30.09, 26.93, 24.85, 24.78, 23.40 (-CH$_2$-), 14.78 (-CH$_3$), 13.34, 13.32 (-SiCH$_2$-). **^{19}F-NMR** (378 MHz, Pyridine-d_5): δ / ppm = -138.50 – -138.81 (m, C$_{Aryl}$-F), -156.71 – -157.08 (m, C$_{Aryl}$-F). **^{29}Si-NMR** (80 MHz, Pyridine-d_5): δ / ppm = 2.89 (Si). **HRMS** (m/z): [M]+Cl$^-$ calc. for C$_{98}$H$_{138}$F$_8$O$_8$Si$_2$Cl: 1686.9516, found: 1686.9525.

(S,S)-1,4-Bis(2-tetradecylhexadecyl-1-oxy)-2,5-bis{4-[2,3,5,6-tetrafluoro-4-(2,3-dihydroxyprop-1-yloxy)phenylethynyl]phenylethynyl}benzene *5F1/14
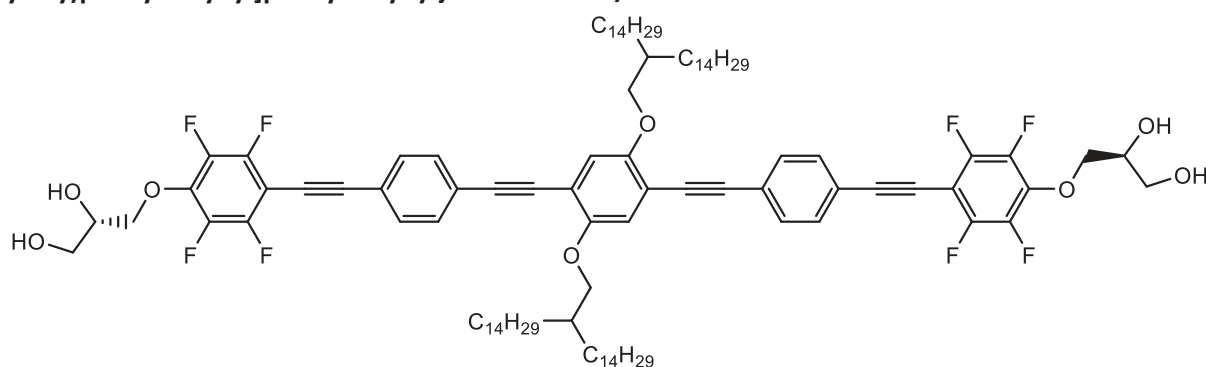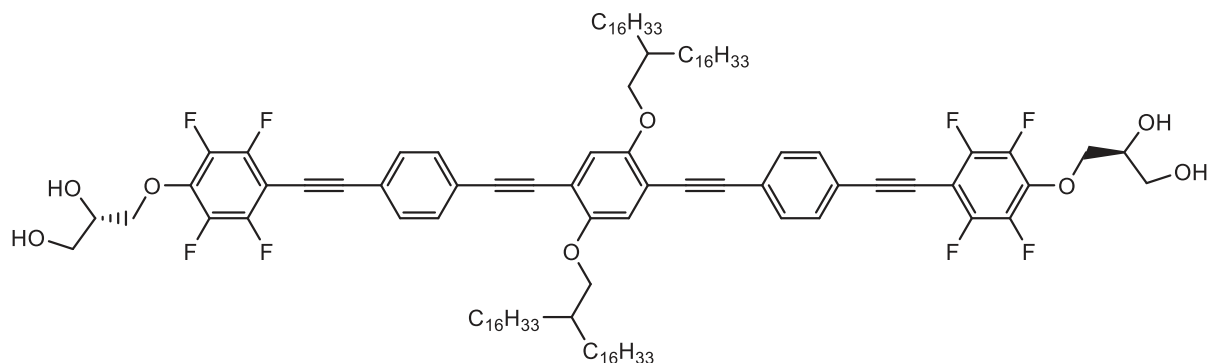

Synthesized according to GP8 from ***5F1/14A** (312 mg, 0.18 mmol),PPTS (89 mg, 0.35 mmol) in MeOH/THF (1:1; 30 mL : 30 mL), purification by column chromatography (eluent: CHCl$_3$); yellow solid, yield: C$_{104}$H$_{146}$F$_8$O$_8$ M = 1676.29 g/mol, 208.7 mg (70 %), mp = 97 °C, **^{1}H-NMR** (400 MHz, Pyridine-d_5): δ / ppm = 7.84 (d, $^3J_{H,H}$ = 8.3 Hz, 4H, Aryl-H), 7.76 (d, $^3J_{H,H}$ = 8.3 Hz, 4H, Aryl-H), 7.59 (s, 2H, Aryl-H), 7.13 (s, 2H, -OH), 6.65 (s, 2H, -OH), 4.90 (dd, $^2J_{H,H}$ = 10.8, $^3J_{H,H}$ = 4.4 Hz, 2H, -Ar$_F$OCH$_A$H$_B$), 4.81 (dd, $^2J_{H,H}$ = 10.2, $^3J_{H,H}$ = 6.2 Hz, 2H, -Ar$_F$OCH$_A$H$_B$), 4.61 – 4.52 (m, 2H, -CHOH), 4.23 (d, $^3J_{H,H}$ = 5.5 Hz, 4H, -OCH$_2$-), 4.16 (d, $^3J_{H,H}$ = 5.5 Hz, 4H, -CH$_2$OH), 2.11 – 1.99 (m, 2H, -CH-), 1.85 – 1.73 (m, 4H, -CH$_2$-), 1.71 – 1.17 (m, 100H), -CH$_2$-, 0.89 (t, $^3J_{H,H}$ = 7.0 Hz, 12H, -CH$_3$). **^{13}C NMR** (101 MHz, Pyridine-d_5) δ / ppm = 155.11 (C$_{Aryl}$-O), 147.08 – 146.71, 143.22 – 142.90 (m, C$_{Aryl}$-F), 140.45 – 140.03 (m, C$_{ArylF}$-O), 132.89, 132.59 (C$_{Aryl}$-H), 125.57, 122.58 (C$_{Aryl}$-quart), 117.77 (C$_{Aryl}$-H), 114.96 (C$_{Aryl}$-quart), 100.69 (-C≡C-), 98.24 – 97.71 (m, C$_{ArylF}$-quart.), 95.68, 90.35 (-C≡C-), 78.29 (t, $^4J_{C,F}$ = 3.2 Hz, C$_{ArylF}$-O-CH$_2$-), 77.11 (t, $^3J_{C,F}$ = 4.4 Hz, -C≡C-), 73.09, 72.43, 64.23 (-OCH-, -OCH$_2$-), 39.10 (-CH-), 32.61, 32.44, 30.95, 30.52 [2xC], 30.50, 30.49, 30.46, 30.43, 30.11, 27.79, 23.42 (-CH$_2$-), 14.74 (-CH$_3$). **^{19}F-NMR** (376 MHz, Pyridine-d_5): δ / ppm = -138.58 – -138.82 (m), -156.85 – -157.05 (m). **HRMS** (m/z): [M]+Cl$^-$ calc. for C$_{104}$H$_{146}$F$_8$O$_8$Cl: 1711.0607, found: 1711.0579.

1,4-Bis(2-pentadecylhetadecyl-1-oxy)-2,5-bis{4-[2,3,5,6-tetrafluoro-4-(2,3-dihydroxyprop-1-yloxy)phenylethynyl]phenylethynyl}benzene 5F1/15:
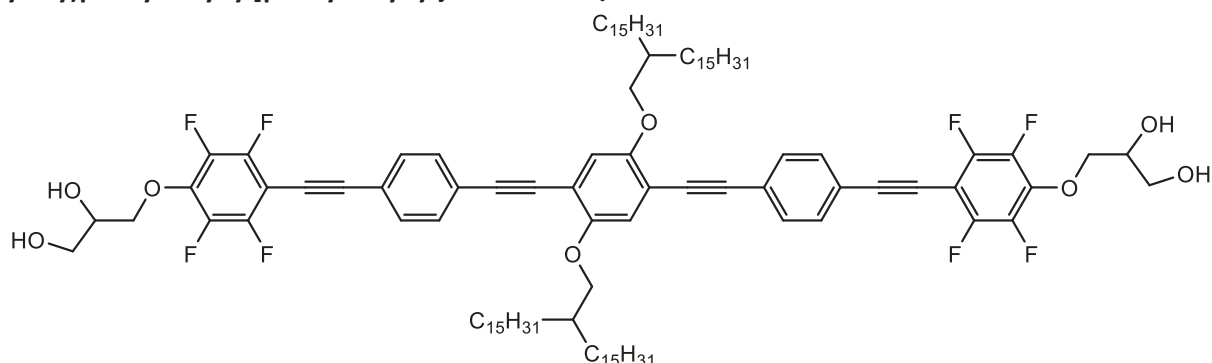
Synthesized according to GP8 from **5F1/15A** (220 mg, 0.12 mmol),PPTS (61 mg, 0.24 mmol) in MeOH/THF (1:1; 30 mL : 30 mL), purification by column chromatography (eluent: CHCl$_3$); yellow solid, yield: C$_{108}$H$_{154}$F$_8$O$_8$ M = 1732.40 g/mol, 181.9 mg (87 %), mp = 121 °C, **^{1}H-NMR** (400 MHz, Pyridine-d_5): δ / ppm = 7.84 (d, $^3J_{H,H}$ = 8.2 Hz, 4H, Aryl-H), 7.76 (d, $^3J_{H,H}$ = 8.1 Hz, 4H, Aryl-H), 7.59 (s, 2H, Aryl-H), 4.90 (dd, $^2J_{H,H}$ = 10.1, $^3J_{H,H}$ = 4.1 Hz, 2H, -Ar$_F$OCH_AH$_B$), 4.80 (dd, $^2J_{H,H}$ = 10.1, $^3J_{H,H}$ = 6.2 Hz, 2H, -Ar$_F$OCH$_A$H$_B$), 4.59 − 4.51 (m, 2H, -CHOH), 4.22 (d, $^3J_{H,H}$ = 5.5 Hz, 4H, -OCH_2-), 4.16 (d, $^3J_{H,H}$ = 5.5 Hz, 4H, -CH_2OH), 2.11 − 1.99 (m, 2H, -CH-), 1.85 − 1.73 (m, 4H, -CH_2-), 1.72 − 1.21 (m, 108H, -CH_2-), 0.90 (t, $^3J_{H,H}$ = 7.0 Hz, 12H, -CH_3). **^{13}C NMR** (101 MHz, Pyridine-d_5) δ / ppm = 154.40 (C_{Aryl}-O), 146.36 − 145.89, 142.57 − 142.19 (m, C_{Aryl}-F), 140.02 − 139.68 (m, C_{ArylF}-O), 132.17, 131.88 (C_{Aryl}-H), 124.87, 121.87 (C_{Aryl}-quart), 117.04 (C_{Aryl}-H), 114.25 (C_{Aryl}-quart), 99.98 (-C≡C-), 97.47 − 97.06 (m, C$_{ArylF}$-quart.), 94.96, 89.64 (-C≡C-), 77.58 (t, $^4J_{C,F}$ = 3.3 Hz, C$_{ArylF}$-O-CH$_2$-), 76.40 (t, $^3J_{C,F}$ = 4.3 Hz, -C≡C-), 72.37, 71.71, 63.52 (-OCH-, -OCH$_2$-), 38.39 (-CH-), 31.91, 31.73, 30.25, 29.82 [4xC], 29.80, 29.78, 29.76, 29.72, 29.40, 27.09, 22.71 (-CH$_2$-), 14.04 (-CH$_3$). **^{19}F-NMR** (376 MHz, Pyridine-d_5): δ / ppm = -138.49 − -138.81 (m), -156.76 − -157.05 (m). **HRMS** (m/z): [M]+Cl$^-$ calc. for C$_{108}$H$_{154}$F$_8$O$_8$Cl: 1767.1233, found: 1767.1250.

(S,S)-1,4-Bis(2-hexadecyloctadecyl-1-oxy)-2,5-bis{4-[2,3,5,6-tetrafluoro-4-(2,3-dihydroxyprop-1-yloxy)phenylethynyl]phenylethynyl}benzene *5F1/16:

Synthesized according to GP8 from ***5F1/16A** (290 mg, 0.16 mmol),PPTS (78 mg, 0.32 mmol) in MeOH/THF (1:1; 30 mL : 30 mL), purification by column chromatography (eluent: CHCl$_3$); yellow solid, yield: C$_{112}$H$_{162}$F$_8$O$_8$ M = 1788.51 g/mol, 175.8 mg (63 %), mp = 125 °C, **^{1}H-NMR** (400 MHz, Pyridine-d_5): δ / ppm = 7.84 (d, $^3J_{H,H}$ = 8.3 Hz, 4H, Aryl-H), 7.76 (d, $^3J_{H,H}$ = 8.3 Hz, 4H, Aryl-H), 7.59 (s, 2H, Aryl-H), 4.91 (dd, $^2J_{H,H}$ = 10.1, $^3J_{H,H}$ = 4.1 Hz, 2H, -Ar$_F$OCH_AH$_B$), 4.81 (dd, $^2J_{H,H}$ = 10.2, $^3J_{H,H}$ = 6.4 Hz, 2H, -Ar$_F$OCH$_A$H$_B$), 4.61 − 4.52 (m, 2H, -CHOH), 4.23 (d, $^3J_{H,H}$ = 5.5 Hz, 4H, -CH_2OH), 4.16 (d, $^3J_{H,H}$ = 5.5 Hz, 4H, -OCH_2-), 2.10 − 2.01 (m, 2H, -CH-), 1.86 − 1.73 (m, 4H, -CH_2-), 1.71 − 1.22 (m, 116H, -CH_2-), 0.90 (t, $^3J_{H,H}$ = 7.0 Hz, 12H, -CH_3). **^{13}C NMR** (101 MHz, Pyridine-d_5) δ / ppm = 155.10 (C_{Aryl}-O), 147.12 − 146.44, 143.38 − 142.70 (m, C_{Aryl}-F), 140.82 − 140.33 (m, C_{ArylF}-O), 132.87, 132.57 (C_{Aryl}-H), 125.56, 122.56 (C_{Aryl}-quart), 117.74 (C_{Aryl}-H), 114.94 (C_{Aryl}-quart), 100.67 (-C≡C-), 98.10 − 97.81 (m, C$_{Aryl}$-quart.), 95.66, 90.34 (-C≡C-), 78.28 (t,
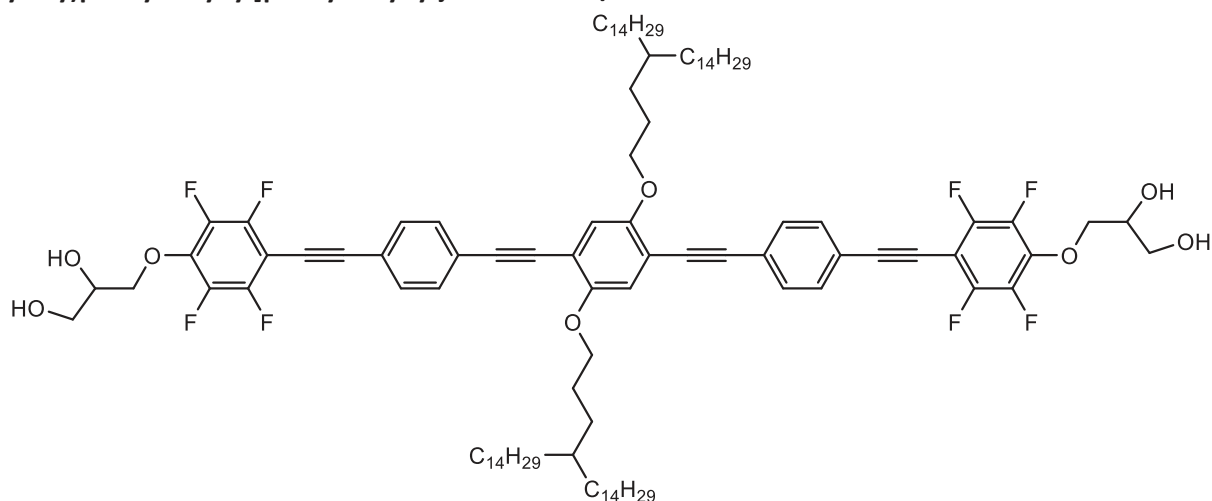
$^4J_{C,F}$ = 3.3 Hz, C_{ArylF}-O-CH_2-), 77.09 (t, $^3J_{C,F}$ = 4.2 Hz, -$C\equiv C$-), 73.06, 72.41, 64.21 (-OCH-, -OCH_2-), 39.08 (-CH-), 32.59, 32.42, 30.93, 30.50 [4xC], 30.48, 30.47, 30.45, 30.40, 30.09, 27.77, 23.40 (-CH_2-), 14.72 (-CH_3). **^{19}F-NMR** (376 MHz, Pyridine-d_5): δ / ppm = -138.48 − -138.78 (m, C_{Aryl}-F), -156.76 − -157.00 (m, C_{Aryl}-F). **HRMS** (m/z): [M]+Cl$^-$ calc. for $C_{112}H_{162}F_8O_8Cl$: 1823.1859, found: 1823.1886.

1,4-Bis(4-tetradecylnonadecyl-1-oxy)-2,5-bis{4-[4-(2,3-dihydroxyprop-1-yloxy)phenylethynyl]phenylethynyl}benzene 5H1/14:
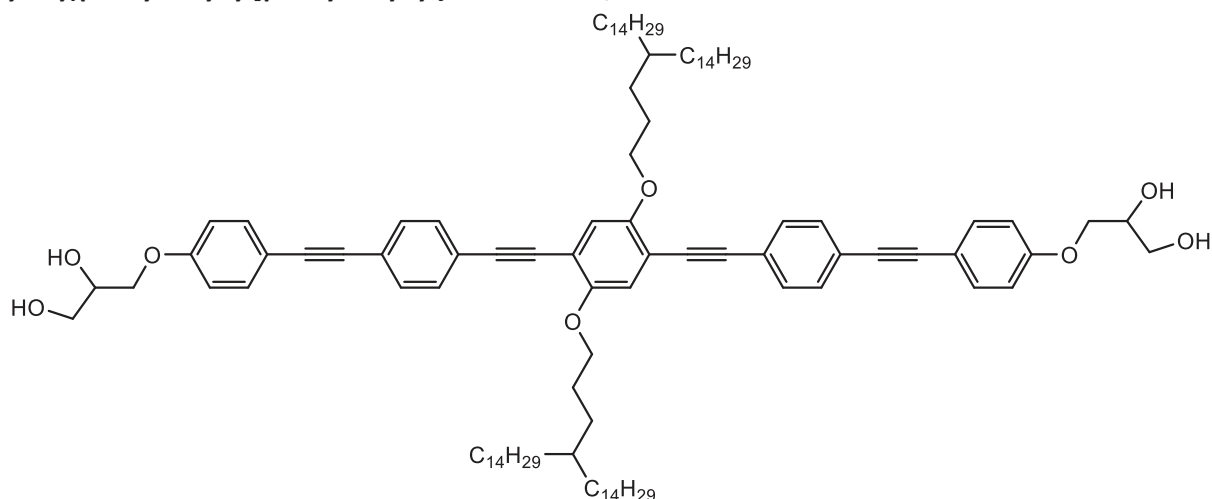
Synthesized according to GP8 from **5H3/14A** (230 mg, 0.14 mmol),PPTS (68 mg, 0.27 mmol) in MeOH/THF (1:1; 30 mL : 30 mL), purification by column chromatography (eluent: CHCl$_3$); yellow solid, yield: $C_{108}H_{162}O_8$ M = 1588.48 g/mol, 138.3 mg (64 %), mp = 84 °C, **^{1}H-NMR** (400 MHz, Pyridine-d_5): δ / ppm = 7.80 (d, $^3J_{H,H}$ = 8.3 Hz, 4H, Aryl-H), 7.72 (d, $^3J_{H,H}$ = 8.1 Hz, 4H, Aryl-H), 7.66 (d, $^3J_{H,H}$ = 8.8 Hz, 4H, Aryl-H), 7.53 (s, 2H, Aryl-H), 7.12 (d, $^3J_{H,H}$ = 8.9 Hz, 4H, Aryl-H), 4.61 − 4.54 (m, 2H, -CHOH), 4.52 (dd, $^2J_{H,H}$ = 9.5, $^3J_{H,H}$ = 4.3 Hz, 2H, -ArOCH_AH$_B$), 4.43 (dd, $^2J_{H,H}$ = 9.6, $^3J_{H,H}$ = 6.2 Hz, 2H, -ArOCH$_A$$H_B$), 4.27 − 4.16 (m, 8H, -CH_2OH, -OCH_2-), 2.03 − 1.93 (m, 4H, -CH_2-), 1.75 − 1.64 (m, 4H, -CH_2-), 1.60 − 1.50 (m, 2H, -CH-), 1.50 − 1.18 (m, 104H, -CH_2-), 0.89 (t, $^3J_{H,H}$ = 6.7 Hz, 12H, -CH_3). **^{13}C NMR** (101 MHz, Pyridine-d_5) δ / ppm = 160.75, 154.78 (C_{Aryl}-O), 134.06, 132.54, 132.44 (C_{Aryl}-H), 124.68, 123.41 (C_{Aryl}-$quart$), 117.98, 115.86 (C_{Aryl}-H), 115.67, 115.03 (C_{Aryl}-$quart$), 95.88, 93.14, 89.61, 89.00 (-$C\equiv C$-), 71.80, 71.55, 70.59, 64.72 (-OCH-, -OCH_2-), 37.99 (-CH-), 34.50, 32.60, 30.98, 30.83, 30.55, 30.53 [2xC], 30.52, 30.49, 30.48, 30.41, 30.09, 27.51, 27.39, 23.41 (-CH_2-), 14.74 (-CH_3). **HRMS** (m/z): [M]+Cl$^-$ calc. for $C_{108}H_{162}O_8Cl$: 1623.1987, found: 1623.1970.

1,4-Bis(4-tetradecylnonadecyl-1-oxy)-2,5-bis{4-[2,3,5,6-tetrafluoro-4-(2,3-dihydroxyprop-1-yloxy)phenylethynyl]phenylethynyl}benzene 5F3/14:

Synthesized according to GP8 from **5F3/14A** (280 mg, 0.16 mmol),PPTS (78 mg, 0.31 mmol) in MeOH/THF (1:1; 30 mL : 30 mL), purification by column chromatography (eluent: CHCl$_3$); yellow solid, yield: C$_{108}$H$_{154}$F$_8$O$_8$ M = 1732.40 g/mol, 192.1 mg (72 %), mp = 95 °C, **^{1}H-NMR** (400 MHz, Pyridine-d_5): δ / ppm = 7.81 (d, $^3J_{H,H}$ = 8.2 Hz, 4H, Aryl-H), 7.74 (d, $^3J_{H,H}$ = 8.1 Hz, 4H, Aryl-H), 7.55 (s, 2H, Aryl-H), 4.90 (dd, $^2J_{H,H}$ = 10.1, $^3J_{H,H}$ = 4.1 Hz, 2H, -Ar$_F$OCH_AH$_B$), 4.80 (dd, $^2J_{H,H}$ = 10.2, $^3J_{H,H}$ = 6.2 Hz, 2H, -Ar$_F$OCH$_A$$H_B$), 4.60 − 4.52 (m, 2H, -CHOH), 4.25 − 4.17 (m, 8H, -CH_2OH, -OCH_2-), 2.03 − 1.94 (m, 4H, -CH_2-), 1.75 − 1.68 (m, 4H, -CH_2-), 1.58 − 1.51 (m, 2H, -CH-), 1.49 − 1.21 (m, 104H, -CH_2-), 0.90 (t, $^3J_{H,H}$ = 7.3 Hz, 12H, -CH_3). **^{13}C NMR** (101 MHz, Pyridine-d_5) δ / ppm = 154.84 (C_{Aryl}-O), 132.84, 132.62 (C_{Aryl}-H), 125.53, 122.56 (C_{Aryl}-quart), 117.99 (C_{Aryl}-H), 114.99 (C_{Aryl}-quart), 95.61, 90.34 (-C≡C-), 78.28 (t, $^4J_{C,F}$ = 3.3 Hz, C$_{ArylF}$-O-CH$_2$-), 77.10 (t, $^3J_{C,F}$ = 4.5 Hz, -C≡C-), 72.42, 70.59, 64.22 (-OCH-, -OCH$_2$-), 38.00 (-CH-), 34.51, 32.61, 30.99, 30.83, 30.56, 30.55, 30.53, 30.52, 30.50, 30.49, 30.42, 30.11, 27.52, 27.38, 23.41 (-CH$_2$-), 14.74 (-CH$_3$). **^{19}F-NMR** (376 MHz, Pyridine-d_5): δ / ppm = -138.48 − -138.85 (m), -156.58 − -157.26 (m). **HRMS** (m/z): [M]+Cl$^-$ calc. for C$_{108}$H$_{154}$F$_8$O$_8$Cl: 1767.1233, found: 1767.1241.

6 References

[1] A. Lavoisier, *Elements of Chemistry*, **1796**, pp. 186.

[2] A. Velasco Abadia, K. M. Herbert, V. M. Matavulj, T. J. White, D. K. Schwartz, J. L. Kaar, *J., Am. Chem. Soc.*, **2021**, 143, 16740.

[3] W. A. Held, B. Ballou, S. Mizushima, M. Nomura, *J. Biol. Chem.*, **1974**, 249, 3103.

[4] J. Nishikawa, T. Ohyama, *Nucl. Acids Res.*, **2013**;41, 1544.

[5] a) J. C. Rochet, R. T. Lansbury., *Curr. Opin. Struct. Biol.*, **2000**, 10, 60; b) Makin OS, Serpell LC, *FEBS J.*, **2005**, 272, 5950.

[6] A. Pohorille, D. Deamer, *Res. Microbiol.*, **2009**, 160, 449.

[7] J. W. Goodby, J. P. Collings, T. Kato, C. Tschierske, H. F. Gleeson, P. Raynes, (Eds) *Handbook of Liquid Crystals 2nd Ed*. Wiley-VCH, Weinheim, **2014**, Vol. 5.

[8] M. Bremer, P. Kirsch, M. Klasen-Memmer, K. Tarumi, *Angew. Chem. Int. Ed.*, **2013**, 52, 8880.

[9] J. Wang, L. Bergquist, J.-I. Hwang, K.-J. Kim, J.-H. Lee, T. Hegmann, A. Jákli, *Liq. Cryst.*, **2018**, 45, 333.

[10] R. R. Shah, N. L. Abbott, *Science*, **2001**, 293, 1296.

[11] M. E. Prévôt, A. Nemati, T. R. Cull, E. Hegmann, T. Hegmann, *Adv. Mater. Technol.*, **2020**, 5, 2000058.

[12] M. Kumar, S. Kumar, *Polym. J.*, **2017**, 49, 85.

[13] a) R. A. Reddy, C. Tschierske, *J. Mater. Chem.*, **2006**, 16, 907; b) S. Sergeyev, W. Pisula, Y. H. Geerts, *Chem. Soc. Rev.*, **2007**, 36, 1902.

[14] F. Reinitzer, *Monatsh. Chem.*, **1888**, 9, 421.

[15] O. Lehmann, *Z. Phys. Chem.*, **1889**, 4, 462.

[16] M. Baron, *Pure Appl. Chem.*, **2001**, 5, 845.

[17] R. Sueyoshi, K. Tada, M. Goto, N. Tamai, H. Matsuki, S. Kaneshina, *Colloids Surf. B: Biointerfaces*, **2006**, 50, 85.

[18] D. Demus, *Mol. Cryst. Liq. Cryst. Incorp. Nonlinear Opt.*, **1988**, 165, 45.

[19] S. Chandrasekhar, G. S. Ranganath, *Rep. Prog. Phys.*, **1990**, 53, 57.

[20] T. Wöhrle, I. Wurzbach, J. Kirres, A. Kostidou, N. Kapernaum, J. Litterscheidt, J. C. Haenle, P. Staffeld, A. Baro, F. Giesselmann, S. Laschat, *Chem. Rev.*, **2016**, 116, 1139.

[21] S. Sergeyev, W. Pisula, Y. H. Geerts, *Chem. Soc. Rev.*, **2007**, 36, 1902.

[22] T. Niori, T. Sekine, J. Watanabe, T. Furukawa, H. Takezoe, *J. Mater. Chem.*, **1996**, 6, 1231.

[23] A. Jákli, O. D. Lavrentovich, J. V. Selinger, *Rev. Mod. Phys.*, **2018**, 90, 045004.

[24] B. Sezgin, J. Liu, D. P. N. Gonçalves, C. Zhu, T. Tilki, M. E. Prévôt, T. Hegmann, *ACS Nanoscience Au*, **2023**, 3, 295.

[25] T. Hegmann, J. Kain, S. Diele, G. Pelzl, C. Tschierske, *Angew. Chem. Int. Ed.*, **2001**, 5, 887.

[26] G. Castruita, V. García, E. Arias, I. Moggio, R. Ziolo, A. Ponce, V. González, J. E. Haley, J. L. Flikkema, T. Cooper, *J. Mater. Chem.*, **2012**, 22, 3770.

[27] W. Maier, A. Saupe, *Z. Naturforsch. A: Phys. Sci.*, **1959**, 14, 882.

[28] W. Maier, A. Saupe, *Z. Naturforsch. A: Phys. Sci.*, **1960**, 15, 287.

[29] C. Tschierske, *Angew. Chem.*, **2013**, 125, 8992.

[30] C. Tschierske, *J. Mater. Chem.*, **2001**, 11, 2647.

[31] C. Tschierske, *Chem. Sov. Rev.*, **2007**, 36, 1930.

[32] V. Percec, M. Peterca, M. J. Sienkowska, M. A. Ilies, E. Aqad, J. Smidrkal, P. A. Heiney, *J. Am. Chem. Soc.*, **2006**, 128, 3324.

[33] M. A. Shcherbina, A. V. Bakirov, A. N. Yakunin, V. Percec, U. Beginn, M. Möller, S. N. Chvalun, *Crystallogr. Rep.*, **2012**, 57, 151.

[34] F. S. Bates, *Science,* **1991**, 251, 898.

[35] K. Borisch, C. Tschierske, P. Göring, S. Diele, *Chem. Commun.*, **1998**, 2711.

[36] F. Liu, M. Prehm, X. Zeng, G. Ungar, C. Tschierske, *Angew. Chem.*, **2011**, 123, 10787.

[37] K. Borisch, C. Tschierske, P. Göring, S. Diele, *Langmuir*, **2000**, 16, 6701.

[38] C. Tschierske, C. Nürnberger, H. Ebert, B. Glettner, M. Prehm, F. Liu, X.-B. Zeng, G. Ungar, *Interface focus*, **2012**, 2, 669.

[39] I. W. Hamley, *The physics of block copolymers*, Oxford Univ. Press, Oxford, **2003**.

[40] V. Abetz, P. F. W. Simon, *Block Copolymers I*, Springer. Berlin und Heidelberg **2005,** Vol. 189.

[41] A. Nishizawa, Y. Takanishi, J. Yamamoto, A. Yoshizawa, *Liquid Crystals*, **2011**, 38, 793.

[42] Z. Luo, G. Yao, Z. Gao, X. Cheng, *Chin. J. Chem.*, **2009**, 27, 1942.

[43] B. Chen, X. B. Zeng, U. Baumeister, S. Diele, G. Ungar, C. Tschierske, *Angew. Chem. Int. Ed.*, **2004**, 43, 4621.

[44] M. Poppe, *Dissertation*, Martin-Luther-Universität Halle-Wittenberg, Halle (Saale), **2018.**

[45] S. Poppe, *Dissertation*, Martin-Luther-Universität Halle-Wittenberg, Halle (Saale), **2018**.

[46] S. Hauche, *Dissertation*, Martin-Luther-Universität Halle-Wittenberg, Halle (Saale), **2021**.

[47] A. Lehmann, *Diplomarbeit*, Martin-Luther-Universität Halle-Wittenberg, Halle (Saale), **2008**.

[48] X. Cai, S. Hauche, S. Poppe, Y. Cao, L. Zhang, C. Huang, C. Tschierske, F. Liu, *J. Am. Chem. Soc.,* **2023**, 145, 2, 1000.

[49] M. Poppe, C. Chen, H. Ebert, S. Poppe, M. Prehm, C. Kerzig, F. Liu, C. Tschierske, *Soft Matter*, **2017**, 13, 4381.

[50] S. Poppe, M. Poppe, H. Ebert, M. Prehm, C. Chen, F. Liu, S. Werner, K. Bacia and C. Tschierske, *Chem. Commun.*, **2017**, 9, 471.

[51] C. Chen, M. Poppe, S. Poppe, M. Wagner, C. Tschierske and F. Liu, *Angew. Chem. Int. Ed.*, **2022**, 61, e202203447.

[52] X. Zeng, R. Kieffer, B. Glettner, C. Nürnberger, F. Liu, K. Pelz, M. Prehm, U. Baumeister, H. Hahn, H. Lang, G. A. Gehring, C. H. M. Weber, J. K. Hobbs, C. Tschierske, G. Ungar, *Science*, **2011**, 331, 1302.

[53] X. Cheng, M. Prehm, M. K. Das, J. Kain, U. Baumeister, S. Diele, D. Leine, A. Blume, C. Tschierske, *J. Am. Chem. Soc.*, **2003**, 125, 10977.

[54] X. H. Cheng, M. K. Das, U. Baumeister, S. Diele, C. Tschierske, *J. Am. Chem. Soc.*, **2004**, 126, 12930.

[55] B. Chen, U. Baumeister, G. Pelzl, M. K. Das, X. B. Zeng, G. Ungar, C. Tschierske, *J. Am. Chem. Soc.*, **2005**, 127, 16578.

[56] M. Prehm, F. Liu, U. Baumeister, X. Zeng, G. Ungar, C. Tschierske, *Angew. Chem. Int. Ed.*, **2007**, 46, 7972.

[57] M. Prehm, C. Enders, M. Y. Anzahaee, B. Glettner, U. Baumeister, C. Tschierske, *Chem. Eur. J.*, **2008**, 14, 6352.

[58] F. Liu, M. Prehm, X. Zeng, G. Ungar, C. Tschierske, *Angew. Chem. Int. Ed.*, **2011**, 50, 10599.

[59] X. Zeng, M. Prehm, G. Ungar, C. Tschierske, F. Liu, *Angew. Chem. Int. Ed.*, **2016**, 55, 8324.

[60] S. Poppe, M. Poppe, H. Ebert, M. Prehm, C. Chen, F. Liu, S. Werner, K. Bacia, C. Tschierske, *Polymers*, **2017**, 9, 471.

[61] M. Poppe, C. Chen, F. Liu, S. Poppe, C. Tschierske, *Chem. Eur. J.* **2017**, 23, 7196.

[62] M. Poppe, C. Chen, F. Liu, M. Prehm, S. Poppe, C. Tschierske, *Soft Matter*, **2017**, 13, 4676.

[63] S. Poppe, A. Lehmann, A. Scholte, M. Prehm, X. Zeng, G. Ungar, C. Tschierske, *Nature Communications*, **2015**, 6, 8637.

[64] H. Ebert, *Dissertation*, Martin-Luther-Universität Halle-Wittenberg, Halle (Saale), **2014**.

[65] A. Achilles, R. Bärenwald, B.-D. Lechner, S. Werner, H. Ebert, C. Tschierske, A. Blume, K. Bacia, K. Saalwächter, *Langmuir*, **2016**, 32, 673.

[66] R. Penrose, *Bull. Inst. Math. Appl.*, **1974**, 10 266.

[67] D. Shechtman, I. Blech, D. Gratias, J. Cahn, *Phys. Rev. Lett.*, **1984**, 53, 1951.

[68] D. V. Louzugine-Luzgin, A. Inoue, *Annu. Rev. Mater. Res.*, **2008**, 38, 403.

[69] G. Ungar, Y. Liu, X. Zeng, V. Percec, W. D. Cho, *Science*, **2003**, 299, 1208.

[70] D. V. Talapin, E. V. Shevchenko, M. I. Bodnarchuk, X. Ye, J. Chen, C. B. Murray, *Nature,* **2009**, 461, 964.

[71] A. J. Mueller, A. P. Ashish, T. P. Lodge, M. K. Mahanthappa, F. S. Bates, *Macromolecules*, **2021**, 54, 6, 2647.

[72] K. Hayashida, T. Dotera, A. Takano, Y. Matsushita, *Phys. Rev. Lett.* **2007**, 98, 195502.

[73] X. Zeng, B. Glettner, U. Baumeister, B. Chen, G. Ungar, F. Liu, C. Tschierske, *Nat. Chem.*, **2023**, 15. 625.

[74] Y. Cao, A. Scholte, M. Prehm, C. Anders, C. Chen, J. Song, L. Zhang, G. He, C. Tschierske, F. Liu, *Angew. Chem. Int. Ed.*, **2024**, 63, e202314454.

[75] R. van Rijsbergen, M. J. O. Anteunis and A. De Bruyn, *J. Carbohydr. Chem.*, **1983**, *2*, 395.

[76] A. P. Krapcho, *Synthesis*, **1982**, 805.

[77] R. F. Nystrom, W. G. Brown, *J. Am. Chem. Soc.*, **1947**, *69*, 1197.

[78] N. Iranpoor, H. Firouzabadi, Gh. Aghapour, A. R. Vaez zadeh, *Tetrahedron*, **2002**, *58*, 8669.

[79] A. Williamson, *The London, Edinburgh, and Dublin Philosophical Magazine and Journal of Science*, **1850**, *37*, 350.

[80] Y. N. Loponosov, D. O. Balakirev, I. V. Dyadishchev, A. N. Solodukhin, M. A. Obrezakova, E. A. Svidchenko, N. M. Surin, S. A. Ponomarenko, *J. Mater. Chem. C*, **2020**, *2*,17074.

[81] Y. C. Chiang, H. C. Wu, H. F. Wen, C. C. Hung, C. W. Hong, C. C. Kuo, T. Higashihara, W. C. Chen, *Macromolecules*, **2019**, *52*, 4396.

[82] a) S. Santra, R. Bean, B. Heckert, Z. Shaw, V. Jain, L. Shrestha, R. Narayanam and Q. Austin, *Polym. Chem.*, **2020**, *11*, 3723; b) C. Anders, M. Wagner, M. Alaasar, V. M. Fischer, R. Waldecker, Y. Zhao, T. Tan, Y. Cao, F. Liu, C. Tschierske, *Chem. Commun.*, **2024**, 60, 1023.

[83] G. Nagarjuna, A. Kokil, J. Kumar, D. Venkataraman, *J. Mater. Chem.* **2012**, *22*, 16091.

[84] *G. Johansson, V. Percec, G. Ungar, J. P. Zhou, Macromolecules,* **1996**, 29, 646*.

[85] Jr. Lever, O. W. Bell, L. N. Hymna, C. McGuire, R. Ferone, M. Ferone, *J. Med. Chem.* **1986**, *29*, 665.

[86] a) S. Werner, H. Ebert, B.-D. Lechner, F. Lange, A. Achilles, R. Bärenwald, S. Poppe, A. Blume, K. Saalwächter, C. Tschierske, K. Bacia, *Chem. Eur. J.*, **2015**, 21, 8840; b) M. Poppe, C. Chen, F. Liu, S. Poppe, C. Tschierske, *Chem. Eur. J.*, **2017**, 23, 7196.

[87] L. Brunsveld, H. Zhang, M. Glasbeek, J. A. J. M. Vekemans, E. W. Meijer, *J. Am. Chem. Soc.,* **2000**, *122*, 6175.

[88] K. Sonogashira, Y. Tohda, N. Hagihara, *Tetrahedron Lett*, **1975**, *50*, 4467.

[89] W. B. Austin, N. Bilow, W. J. Kelleghan, K. S. Y. Lau, *J. Org. Chem.*, **1981**, *46*, 2280.

[90] A. Lehmann, A. Scholte, M. Prehm, F. Liu, X. Zeng, G. Ungar, C. Tschierske, *Adv. Funct. Mater.*, **2018**, 28, 1804162.

[91] A. Saeed, M. Poppe, M. B. Wagner, S. Hauche, C. Anders, Y. Cao, L. Zhang, C. Tschierske, *Chem. Commun.*, **2022**, 58, 7054.

[92] M. Poppe, C. Chen, S. Poppe, F. Liu, C. Tschierske, *Commun. Chem.*, **2020**, 3, 70.

[93] X. Cheng, H. Gao, X. Tan, X. Yang, M. Prehm, H. Ebert, C. Tschierske, *Chem. Sci.*, **2013**, 4, 3317.

[94] Y. Cao, A. Scholte, M. Prehm, C. Anders, C. Chen, J. Song, L. Zhang, G. He, C. Tschierske and F. Liu, *Angew. Chem. Int. Ed.*, **2023**, e202314454.

[95] C. Anders, M. Wagner, M. Alaasar, V. M. Fischer, R. Waldecker, Y. Zhao, T. Tan, Y. Cao, F. Liu, C. Tschierske, *Chem. Commun.*, **2024**, 60, 1023.

[96] a) K. Borisch, S. Diele, P. Göring, C. Tschierske, *Chem. Commun.*, **1996**, 237; b) V. S. K. Balagurusamy, G. Ungar, V. Percec, G. Johannsson, *J. Am. Chem. Soc.*, **1997**, 119, 1539, c) K. D. Dorfman, *Macromolecules*, **2021**, 54, 10251.

[97] C. Anders, T. Tan, V.-M. Fischer, R. Wang, M. Alaasar, R. Waldecker, Y. Cao, F. Liu, C. Tschierske, *Aggregate*, **2024**, Accepted Manuscript. DOI:10.1002/agt2.728.

[98] A. Immirzi, B. Perini, *Acta Cryst. A*, **1977,** 33, 216.

[99] A. I. Kitaigorodski, *Molekülkristalle*, Akademie-Verlag Berlin, **1979**.

[100] Y. Cao, F. Liu, et al., unpublished results.

[101] V. M. Fischer, R. Waldecker, unpublished results.

[102] C. Anders, V.-M. Fischer, T. Tan, M. Alaasar, R. Waldecker, Y. Ke, Y. Cao, F.Liu and C. Tschierske, *J. Mater. Chem. C*, **2024**, Accepted Manuscript. DOI: 10.1039/D4TC04076G.

[103] S. Poppe, A. Lehmann, M. Steimecke, M. Prehm, Y. Zhao, C. Chen, Y. Cao, F. Liu, C. Tschierske, *Giant*, **2024**, 18, 100254.

[104] H. G. O. Becker, *Organikum*, Wiley-VCH, Weinheim, **2001**.

[105] M. Wagner, C. Tschierske, unpublished results.

[106] M. Poppe, C. Tschierske, unpublished results.

[107] X. Zeng, S. Poppe, A. Lehmann, M. Prehm, C. Chen, F. Liu, H. Lu, G. Ungar, C. Tschierske, *Angew. Chem. Int. Ed.*, **2019**, 58(22), 7375.

[108] S. Barik, S. Valiyabeettil, *J. Polym. Sci., Part A: Polym. Chem.*, **2014**, 52, 2217.

[109] J. Wen, M. Tian, Q. Chen, *J. Fluorine Chem*., **1994**, 68, 117.

Appendix

Appendix-1: Publications

The following section lists all publications A–C on which this work is based.

1. C. Anders, M. Wagner, M. Alaasar, V.-M. Fischer, R. Waldecker, Y. Zhao, T. Tan, Y. Cao, F. Liu, and C. Tschierske, „*Highly branched bolapolyphilic liquid crystals with a cubic A15 network at the triangle-square transition*", *Chem. Commun.*, **2024**, 60, 1023 – 1026. DOI: 10.1039/D4TC04076G. (**Publication A**)
   The SI is available at https://www.rsc.org/suppdata/d3/cc/d3cc05247h/d3cc05247h1.pdf.

2. C. Anders, T. Tan, V.-M. Fischer, R. Wang, M. Alaasar, R. Waldecker, Y. Cao, F. Liu, C. Tschierske, „*Engineering "meso-Atom" bonding: Honeycomb-Network Transitions in Reticular Liquid Crystals*", *Aggregate*, **2024**, Accepted Manuscript. DOI:10.1002/agt2.728. (**Publication B)**
   The SI is available at https://doi.org/10.1002/agt2.728.

3. C. Anders, V.-M. Fischer, T. Tan, M. Alaasar, R. Waldecker, Y. Ke, Y. Cao, F.Liu and C. Tschierske, „*Modifying the liquid crystalline chessboard tiling - Soft reticular self-assembly of side-chain fluorinated polyphiles*", *J. Mater. Chem. C*, **2024**, Accepted Manuscript. DOI: 10.1039/D4TC04076G. (**Publication C**)
   The SI is available at https://www.rsc.org/suppdata/d4/tc/d4tc04076g/d4tc04076g1.pdf.

Highly branched bolapolyphilic liquid crystals with a cubic A15 network at the triangle-square transition
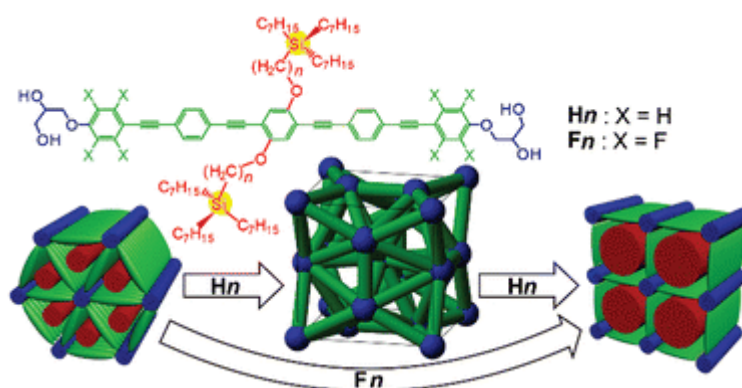
C. Anders,[a] M. Wagner,[a] M. Alaasar, V.-M. Fischer,[b] R. Waldecker,[b] Y. Zhao,[c] T. Tan,[c] Y. Cao,[*c] F. Liu[c] and C. Tschierske[*a]

*Corresponding authors
[a]Institute of Chemistry, Martin Luther University Halle-Wittenberg, Kurt-Mothes Str. 2, Halle 06120, Germany
[b]Institute of Mathematics, Martin Luther University Halle-Wittenberg, Theodor-Lieser-Str. 5, Halle 06120, Germany
[c]Shaanxi International Research Center for Soft Matter, Xi'an Jiaotong University, Xi'an 710049, P. R. China

Abstract

Rod-like bolapolyphiles with highly branched carbosilane-based side-chains self-assemble into several honeycomb structures if the oligo(*p*-phenylene ethynylene) core is polyfluorinated, whereas for the non-fluorinated series an A15 type cubic network of rod-bundles was observed instead, suggesting a brand new pathway for the transition between triangular and square honeycomb phases.

ChemComm

Check for updates

Highly branched bolapolyphilic liquid crystals with a cubic A15 network at the triangle-square transition†

Christian Anders, [ID] [a] Matthias Wagner, [a] Mohamed Alaasar, [ID] [a]
Virginia-Marie Fischer, [b] Rebecca Waldecker, [ID] [b] Yangyang Zhao, [ID] [c]
Tianyi Tan, [ID] [c] Yu Cao, [ID] *[c] Feng Liu [ID] [c] and Carsten Tschierske [ID] *[a]

Rod-like bolapolyphiles with highly branched carbosilane-based side-chains self-assemble into several honeycomb structures if the oligo(*p*-phenylene ethynylene) core is polyfluorinated, whereas for the non-fluorinated series an A15 type cubic network of rod-bundles was observed instead, suggesting a brand new pathway for the transition between triangular and square honeycomb phases.

Liquid crystalline (LC) systems represent perfect examples to show how nature creates well-defined structures by soft matter self-assembly.[1,2] Particularly successful examples are provided by T-shaped[3] and X-shaped bolapolyphilic block molecules (Fig. 1h),[3–5] *i.e.* amphiphiles with two polar ends at a lipophilic unit and combining more than two incompatible units. These molecules are composed of a π-conjugated rod with sticky hydrogen bonding at both ends and flexible side-chains. Depending on the rod-length, side-chain number, length and volume, these molecules form a wide range of columnar liquid crystalline phases with honeycomb structures (Fig. 1). In the honeycombs, the π-conjugated rod-like cores lie perpendicular to the column long axis, held together at the edges by columns involving the hydrogen bonded glycerol ends. The resulting prismatic cells are filled by the flexible side-chains. Depending on the side-chain volume and the length of the rigid rod-like core, different types of honeycombs were observed, such as triangular, square, pentagonal, and hexagonal, while compounds with even larger chains tend to form giant honeycombs,[6] lamellar phases[7] and cubic network structures (see also Section S3.1, ESI†).[8]

The transition from triangular ($Col_{hex}/p6mm$) to square honeycombs ($Col_{squ}/p4mm$, Fig. 1a and g) is of particular
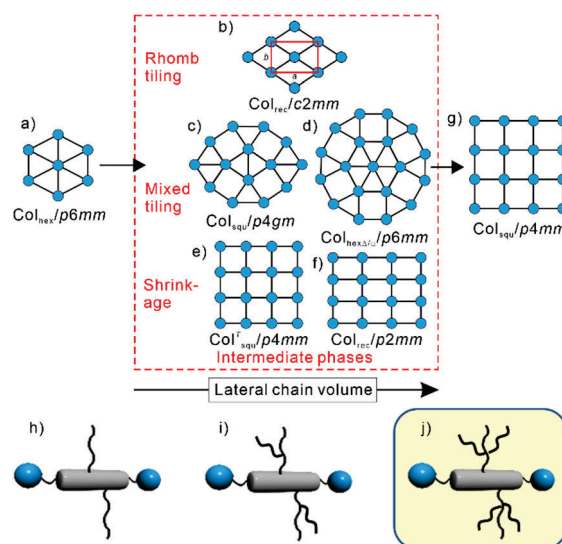

Fig. 1 (b)–(f) Selected intermediate phases at the transition between (a) triangular and (g) square LC honeycombs; the shown nets represent cuts through the honeycombs perpendicular to the *c*-axis (see Fig. 3c.i for spatial models), the rod-like cores are organized along the dark lines and the blue dots represent the polar columns of the end groups, the side chains fill the cells; (h) and (i) bolapolyphiles forming these tiling patterns and (j) compounds under discussion herein.

interest owing to the large cell volume jump between them and the huge number of possible tiling patterns involving rectangular[9] and rhombic cells (Fig. 1b and f)[10] as well as combinations of squares with equilateral triangles (Fig. 1c and d),[11,12] the latter being of special interest as they could possibly provide a source of liquid quasicrystals.[13]

While in previous work linear and simply branched alkyl chains have been used (Fig. 1h and i), we discuss here, for the first time, bolapolyphiles with triply branched side-chains (Fig. 1j), where silicon acts as branching point.[14] An oligo-(*p*-phenylene ethynylene) (OPE) unit was used as rod-like core,[4,5,10,15,16] and the total chain volume was chosen to fit into the triangle-square transition region. The volume was

[a] Institute of Chemistry, Martin Luther University Halle-Wittenberg, Kurt-Mothes Str. 2, Halle 06120, Germany. E-mail: Carsten.tschierske@chemie.uni-halle.de
[b] Institute of Mathematics, Martin Luther University Halle-Wittenberg, Theodor-Lieser-Str. 5, Halle 06120, Germany
[c] Shaanxi International Research Center for Soft Matter, Xi'an Jiaotong University, Xi'an 710049, P. R. China. E-mail: yu.cao@xjtu.edu.cn
† Electronic supplementary information (ESI) available: Synthesis, methods, analytical data, additional data and discussions. See DOI: https://doi.org/10.1039/d3cc05247h
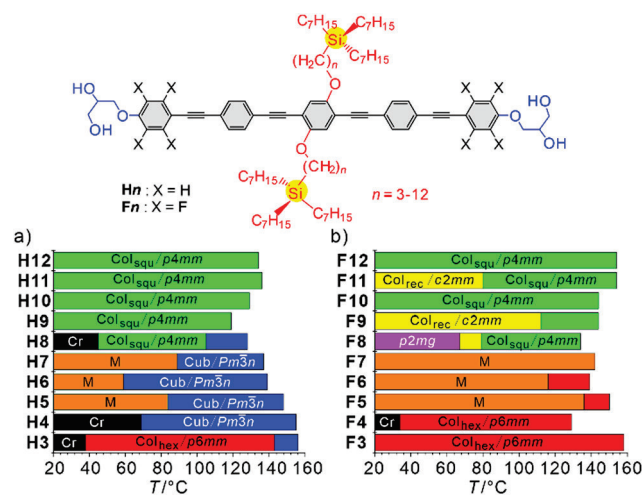
Fig. 2 Molecular structure and LC phases of (a) **H***n* and (b) **F***n* as observed on cooling with 10 K min^{-1}; abbreviations: Cr = crystalline solid; Col$_{hex}$/$p6mm$ and Col$_{squ}$/$p4mm$ = triangular and square LC honeycombs, respectively; Col$_{rec}$/$c2mm$ and $p2mg$ = tilings by rhombic and non-regular triangular honeycombs, respectively; Cub/$Pm\bar{3}n$ = cubic network phase with $Pm\bar{3}n$ space group; M = unknown LC phases; isotropic liquid is at the right side of the columns; for numerical data, transitions on heating and enthalpies, see Table S1a, b, for DSCs Fig. S1 and S2, for textures Fig. S3–S6, for SAXS/WAXS data Fig. S7–S10, Tables S2–S29 (ESI†).
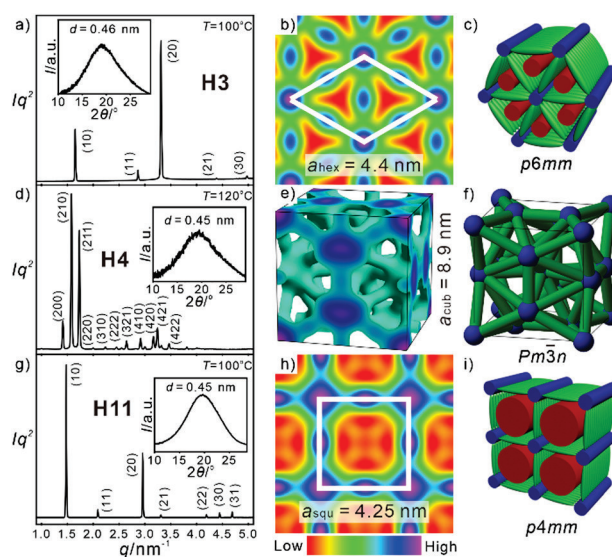

Fig. 3 (a), (d) and (g) SAXS diffractograms with WAXS (insets), (b), (e) and (h) reconstructed ED maps, and (c), (f) and (i) schematic illustrations of the organization of the molecules in the (a)–(c) Col$_{hex}$/$p6mm$ phase of **H3** at $T = 100$ °C; (d)–(f) Cub/$Pm\bar{3}n$ phase of **H4** at $T = 120$ °C and (g)–(i) Col$_{squ}$/$p4mm$ phase of **H11** at $T = 100$ °C.

fine-tuned by modifying the spacer unit between core and tri-*n*-heptylsilyl unit from $n = 3$ to 12. Two series were studied, the non-fluorinated compounds **H***n* (X = H) and the compounds **F***n* with the outer benzene rings being perfluorinated (X = F). The synthesis is described in Scheme S2 and Section S4 (ESI†), and investigation was conducted by differential scanning calorimetry (DSC), polarized optical microscopy (POM) and small- and wide-angle X-ray scattering (SAXS, WAXS) as described in Section S1 (ESI†).

Three different LC phases were observed for the series **H***n* (Fig. 2a). Compound **H3** with the shortest spacer forms a hexagonal columnar phase with $a_{hex} = 4.3$ nm between 70 and 147 °C (Fig. 3a). The lattice parameter corresponds to the molecular length ($L_{mol} = 4.0$–4.4 nm, depending on the conformation of the glycerol groups), suggesting a triangular honeycomb as confirmed by the reconstructed electron density (ED) map in Fig. 3b, showing triangular low ED regions (red/yellow) filled by the aliphatic side-chains which are separated by medium electron density walls (green) of the OPE cores and high ED dots (purple/blue) involving the glycerol groups at the junctions. The number of molecules in each unit cell with an assumed height of $h = 0.45$ nm is $n_{cell} = 3.2$, meaning that a single rod-like core is found in the lateral cross section of the walls ($n_{wall} = n_{cell}/3$; Table S27, ESI†). The diffuse character of the WAXS (insets in Fig. 3a, d and g) indicates the absence of fixed positions of individual molecules, thus confirming a highly dynamic LC honeycomb. Upon heating to 147 °C a transition to a viscous optically isotropic mesophase is observed, which becomes fluid at 160 °C. This transition is associated with an enthalpy of 1.5 kJ mol^{-1}, indicating a cubic mesophase occurring between 147 and 160 °C (Fig. S1a, ESI†).

For the next homologue **H4** the range of this cubic mesophase is expanded and the triangular honeycomb is completely removed. With further growing n it is retained up to $n = 8$ (Fig. 2a). All cubic mesophases show the same typical pattern of three strong peaks in the SAXS (Fig. 3d) indicative for the (200), (210) and (211) reflections of a $Pm\bar{3}n$ lattice; the WAXS is diffuse, confirming the LC state. This type of cubic LC phase was recently analysed in detail for a series of compounds related to **H***n*, but having two simply branched alkyl chains (see Fig. 1i and Scheme S1 and discussion in Section S3.2, ESI†).[17] The $Pm\bar{3}n$ phase, shown in Fig. 3e and g, is formed by a network of rod-bundles interconnected at the junctions by spheres or oblate spheroids involving the polar glycerol groups while the continuum is filled by the side chains. The positions of the spheres at the edges, in the centre, and pairs of spheroids on the 6 faces of the unit cell corresponds to that observed for the A15 Frank Kasper phases,[18] however, in this case representing a dense packing of tetrahedra formed by bundles of rods interconnected by the glycerol spheres/spheroids at the edges. The lattice parameter $a_{cub} = 8.6$–9.2 nm, increases with growing n from 3 to 6 and then remains almost constant, and 5–6 molecules are organized in the cross-section of the bundles of single molecular length (Table S28, ESI†).[17]

For compounds **H***n* with $n = 5$–8 the cubic phase is accompanied by birefringent mesophases at lower temperature (Fig. S3c and d, ESI†) and for the following homologues with $n = 9$–12 the cubic phase is completely removed. For compounds **H5–H7** a complicated diffraction pattern (M) is found, which needs to be solved in future work. In contrast, a simple square lattice with $p4mm$ plane group and $a_{squ} = 4.1$–4.3 nm (Fig. 3g), again corresponding to the molecular length, is observed for **H8–H12** (Table S29, ESI†). This indicates a square honeycomb, as also obvious from the ED map

ChemComm

(Fig. 3h and i). No further transition is observed for the Col$_{squ}$ phases until crystallization.

The interesting and new observation in the series of compounds **Hn** depending on the spacer length n is, that a cubic phase occurs at the transition between two columnar LC phases, only having different honeycomb shapes. This means that it is not preliminary caused by changing interface curvatures, but by a destabilization of the honeycombs due to steric and geometric frustration during the triangle-square transition. Hence, it is a new intermediate structure at this transition (see also Section S3.2, ESI†).[12]

The situation changes for the series of core-fluorinated compounds **Fn** where the $Pm\bar{3}n$ phase is completely removed (Fig. 2b and Tables S1a, b, ESI†), while the range of the triangular honeycomb with $p6mm$ plane group is expanded up to n = 6, indicating that a bit more space is available in the polygonal cells formed by compounds **Fn**. The lattice parameters of the Col$_{hex}$ and Col$_{squ}$ phases (a_{hex} = 4.1–4.3 nm, a_{squ} = 4.2–4.4 nm) are almost identical to those observed for the series **Hn** (Tables S27, S29, ESI†). There is a general mesophase stabilization by core fluorination, with a tendency to increase with growing side chain length (Fig. 2). There is also an odd–even effect of the spacer length with a tendency to higher mesophase stabilities for compounds with odd numbered n (or an even total numbers of connecting atoms n + 1 including the ether oxygen). This is because of the effect of spacer parity on the side chain conformation (linear *vs.* bent, Fig. S16, ESI†) which modulates the packing of the bulky trialkylsilyl end group. This leads to a non-continuous development of the phase stabilities, lattice types, and lattice parameters depending on n, and to a more complicated sequence of different LC phases for the series **Fn**. The WAXS is still diffuse for all the mesophases, thus representing true LCs (Fig. 4c, f and Fig. S8, ESI†).

There are additional mesophases accompanying the square honeycombs of some of the compounds **F8**–**F12** at lower temperature (Fig. 2b). Upon cooling the $p4mm$ phase of compound **F8** a LC phase with centred rectangular lattice and $c2mm$ plane group is formed below 80 °C (Fig. 4a–c). The ED map in Fig. 4b shows a honeycomb based on rhombic cells with a = 5.0 and b = 7.0 nm, *i.e.* a distorted square honeycomb, formed by 4.3 nm long walls. On cooling it is followed below 64 °C by a further

change of the SAXS pattern which can now be indexed to a $p2mg$ lattice (Fig. 4d–f, Table S20, ESI†). The ED map shows that this honeycomb is composed of acute triangular cells where two walls are slightly expanded to 4.5 nm while the third is 4.0 nm. Optical investigations support the proposed phase structures (see Fig. S5, ESI†). The transition $p4mm \rightarrow c2mm$ is attributed to an increasing contribution of *all-trans* alkyl chains conformations at lower temperature, which prefer rhombic cells for easier chain expansion, while division of the rhombi into two triangles at the $c2mm \rightarrow p2mg$ transition is attributed to the simultaneously occurring shrinkage of the side chain volume due to reduced thermal motions.

While the following homologues **F10** and **F12** with even numbered n form exclusively the square honeycomb, for the odd numbered **F9** and **F11** the $c2mm$ phase is found and gradually suppressed with growing n by the $p4mm$ phase (Fig. 2b). For the $p4mm$ phases, the side lengths of 4.1–4.3 nm corresponds to L_{mol}, making any tilted organization of the rods in the honeycomb walls unlikely, even at low temperature to about 40 °C (Table S29 and Fig. S15, ESI†). However, in the $c2mm$ phase of **F9** the side length starts decreasing from 4.2 nm around 80 °C to 3.95 nm at 40 °C, indicating the development of a small tilt due to continuing side chain volume shrinkage upon cooling (see Fig. S14, ESI†). This tilt shrinks the rhombi of **F9** without splitting into two triangles as observed for **F8**.

Here the question of the origin of the effects of core fluorination on the LC self-assembly arises, which can be subdivided into steric and polar effects. The larger size of F (0.13 nm³) compared to H (0.07 nm³, crystal volume increments)[19] can reduce or increase the space available for the side-chains, depending on the preferred orientation of the planes of the benzene rings (Fig. 5a–c). Benzenes aligned with their faces perpendicular to the column axis (Fig. 5c) reduce the available space by fluorination due to the reduced height h of the (hypothetical) 3D unit cell along the π-stacking direction and by the accommodation of the larger fluorines inside the prismatic cells. Benzene rings aligned almost parallel or only slightly tilted to the c-direction increase h and thus provide additional space if H is replaced by F (Fig. 5b). Though there is still an almost free rotation of the OPEs in the honeycomb walls, the polar effects influence the preferred orientation of the π-planes along the honeycomb walls by electrostatic interactions. Compounds **Hn**, having electron rich benzenes, for which only one diffuse SAXS around 0.45 nm is observed in all LC phases (Fig. 3a, d and g and Fig. S7, ESI†), are known to
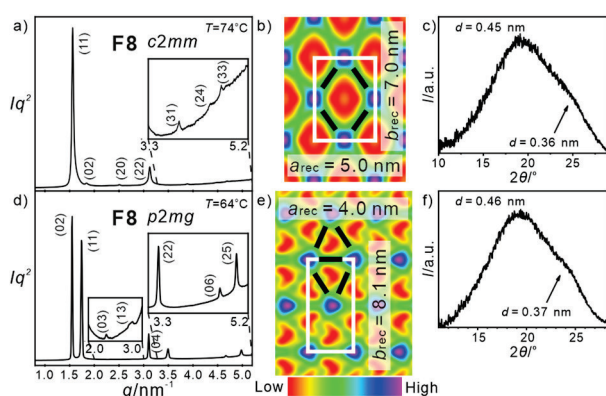

Fig. 4 SAXS diffractograms (left) with WAXS (right), and reconstructed ED maps (middle) of the honeycomb phases of compound **F8** (see Tables S18–S20, ESI†).
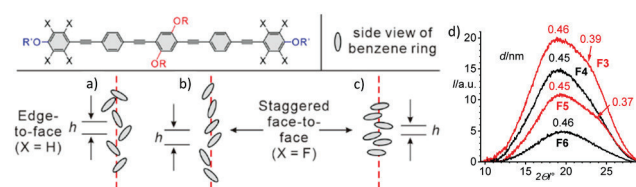

Fig. 5 (a)–(c) Schematic presentation of the stacking modes in the honeycomb walls; the grey ellipses represent side view on the benzene rings if viewed along the OPE long axis; the red dashed line is the c-axis and h the intermolecular stacking distance; (d) shows the odd–even effect of the WAXS of compounds **F3**–**F6** at 120 °C; intensities are not scaled.

prefer an edge-to-face orientation (Fig. 5a and Fig. S17a, ESI†), while the electron deficit π-systems of the perfluorinated rings in **Fn** tend to align face-to-face (Fig. 5b and c).[20] This difference is evident in the WAXS profiles of compounds **Fn** where a weak broad shoulder around 0.36–0.39 nm is found beside the diffuse scattering maximum at 0.44–0.46 nm (Fig. 4c, f and 5d and Fig. S8, ESI†). The very broad and weak shoulder indicates a poor order and short correlation length of π-stacking as found in the stacking mode in Fig. 5b, while that in Fig. 5c is expected to lead to a stronger scattering. This additional scattering is the strongest for compounds **Fn** with odd-numbered n (see Fig. 5d). This odd–even effect becomes weaker with growing n and the intensity of the shoulder rises with lowering temperature (Fig. S8, ESI†). Face-to-face stacking is known to preferably take place by alternation of the electron-rich benzenes or acetylenes and the polyfluorinated benzenes,[20] which in our case would lead to a significant longitudinal shift between the cores, causing a tilt of the rods in the walls, thus reducing the effective value of L_{wall} of the honeycombs (Fig. S17b–d, ESI†).[15,16] However, this shift would distort the segregation of the polar glycerols from the aromatic cores. In the present case the reduction of L_{wall} due to this mode of tilting is not observed in most cases (except $c2mm$ of **F9**, see above) and a face-to-face packing of the electron deficit fluorinated rings with some transversal shift appears more likely (Fig. 5b, c and Fig. S17e, ESI†).[21] This face-to-face stacking increases the core–core attractive interactions, thus supporting the quasi infinite stacking along the honeycomb walls. This provides a higher stability for the honeycombs (and the M phase) of compounds **Fn** and favours the honeycombs over the shorter stacks in the $Pm\bar{3}n$ networks of compounds **H3–H8**. The transversal shifted face-to-face stacking increases h if the benzenes preferably arrange with their planes parallel to the honeycomb main axis (see Fig. 5b), thus leading to more space for the side-chains and this shifts the triangle → square transition towards larger chain volume (**H3** → **F8**), in line with the experimental observations. This packing mode is obviously supported by odd-numbered n (**F9**, **F11**), favouring the formation of the smaller rhombic honeycombs replacing the larger square of the even numbered compounds **F10** and **F12**.

In summary, a new type of polyphilic block-molecules with highly branched carbosilane-based side-chains is reported. For the non-fluorinated series an A15-type cubic network phase composed of tetrahedra of rod-bundles was observed as a new mode of transition between triangular and square honeycombs. Peripheral core fluorination was found to be an efficient tool to suppress the $Pm\bar{3}n$ network formation and provides triangular and rhombic honeycombs with reduced symmetry. This could pave the way towards new periodic and quasiperiodic honeycombs based on mixed triangle/square tilings.[11,12] If the unknown M phase belongs to these complex honeycombs or represents another complex tiling by rod-bundles remains to be investigated in future work.

Conflicts of interest

There are no conflicts to declare.

Notes and references

1 T. Kato, J. Uchida, T. Ichikawa and T. Sakamoto, *Angew. Chem., Int. Ed.*, 2018, **57**, 4335; M. Lehmann, M. Dechant, M. Lambov and T. Ghosh, *Acc. Chem. Res.*, 2019, **52**, 1653; J. W. Goodby, S. J. Cowling, C. K. Bradbury and R. J. Mandle, *Liq. Cryst.*, 2022, **49**, 908; J. Voskul and M. Giese, *Aggregate*, 2023, **3**, e124; H. K. Bisoyi and Q. Li, *Chem. Rev.*, 2022, **122**, 4887.

2 R. Zhang, Z. Su, X.-Y. Yan, J. Huang, W. Shan, K.-H. Dong, X. Feng, Z. Lin and S. Z. D. Cheng, *Chem. – Eur. J.*, 2020, **26**, 6741.

3 (*a*) C. Tschierske, *Chem. Soc. Rev.*, 2007, **36**, 1930; (*b*) C. Tschierske, C. Nürnberger, H. Ebert, B. Glettner, M. Prehm, F. Liu, X. B. Zeng and G. Ungar, *Interface Focus*, 2012, **2**, 669; (*c*) Y. Sun and F. A. Escobedo, *J. Chem. Theory Comput.*, 2023, DOI: 10.1021/acs.jctc.3c00395.

4 M. Poppe, C. Chen, H. Ebert, S. Poppe, M. Prehm, C. Kerzig, F. Liu and C. Tschierske, *Soft Matter*, 2017, **13**, 4381.

5 S. Poppe, M. Poppe, H. Ebert, M. Prehm, C. Chen, F. Liu, S. Werner, K. Bacia and C. Tschierske, *Polymers*, 2017, **9**, 471.

6 A. Scholte, S. Hauche, M. Wagner, M. Prehm, S. Poppe, C. Chen, F. Liu, X. Zeng, G. Ungar and C. Tschierske, *Chem. Commun.*, 2020, **56**, 62.

7 M. Prehm, C. Enders, X. Mang, X. Zeng, F. Liu, G. Ungar, U. Baumeister and C. Tschierske, *Chem. – Eur. J.*, 2018, **24**, 16072.

8 X. Zeng, S. Poppe, A. Lehmann, M. Prehm, C. Chen, F. Liu, H. Lu, G. Ungar and C. Tschierske, *Angew. Chem., Int. Ed.*, 2019, **58**, 7375; S. Poppe, X. Cheng, C. Chen, X. Zeng, R.-B. Zhang, F. Liu, G. Ungar and C. Tschierske, *J. Am. Chem. Soc.*, 2020, **142**, 3296; C. Chen, M. Poppe, S. Poppe, C. Tschierske and F. Liu, *Angew. Chem., Int. Ed.*, 2020, **59**, 20820; X. Cai, S. Hauche, S. Poppe, Y. Cao, L. Zhang, C. Huang, C. Tschierske and F. Liu, *J. Am. Chem. Soc.*, 2023, **145**, 1000.

9 A. Lehmann, A. Scholte, M. Prehm, F. Liu, X. Zeng, G. Ungar and C. Tschierske, *Adv. Funct. Mater.*, 2018, **28**, 1804162.

10 A. Saeed, M. Poppe, M. B. Wagner, S. Hauche, C. Anders, Y. Cao, L. Zhang, C. Tschierske and F. Liu, *Chem. Commun.*, 2022, **58**, 7054.

11 M. Poppe, C. Chen, S. Poppe, F. Liu and C. Tschierske, *Commun. Chem.*, 2020, **3**, 70.

12 X. Cheng, H. Gao, X. Tan, X. Yang, M. Prehm, H. Ebert and C. Tschierske, *Chem. Sci.*, 2013, **4**, 3317.

13 X. Zeng, B. Glettner, U. Baumeister, B. Chen, G. Ungar, F. Liu and C. Tschierske, *Nat. Chem.*, 2023, **15**, 625; Y. Cao, A. Scholte, M. Prehm, C. Anders, C. Chen, J. Song, L. Zhang, G. He, C. Tschierske and F. Liu, *Angew. Chem., Int. Ed.*, 2023, e202314454; M. Imperor-Clerc, A. Jagannathan, P. Kalugin and J.-F. Sadoc, *Soft Matter*, 2021, **17**, 9560; U. Tu Lieu and N. Yoshinaga, *Soft Matter*, 2022, **18**, 7497.

14 A. Kreyes, A. Masoud, I. Lieberwirth, R. Mauer, F. Laquai, K. Landfester and U. Ziener, *Chem. Mater.*, 2010, **22**, 6453.

15 M. Poppe, C. Chen, F. Liu, M. Prehm, S. Poppe and C. Tschierske, *Soft Matter*, 2017, **13**, 4676.

16 (*a*) M. Poppe, C. Chen, S. Poppe, C. Kerzig, F. Liu and C. Tschierske, *Adv. Mater.*, 2020, 202005070; (*b*) M. Poppe, C. Chen, F. Liu, S. Poppe and C. Tschierske, *Chem. Commun.*, 2021, **57**, 6526.

17 C. Chen, M. Poppe, S. Poppe, M. Wagner, C. Tschierske and F. Liu, *Angew. Chem., Int. Ed.*, 2022, e202203447.

18 (*a*) K. Borisch, S. Diele, P. Göring and C. Tschierske, *Chem. Commun.*, 1996, 237; (*b*) V. S. K. Balagurusamy, G. Ungar, V. Percec and G. Johannsson, *J. Am. Chem. Soc.*, 1997, **119**, 1539; (*c*) K. D. Dorfman, *Macromolecules*, 2021, **54**, 10251.

19 A. Immirzi and B. Perini, *Acta Cryst. Sect. A*, 1977, **33**, 216.

20 (*a*) C. A. Hunter and J. K. M. Sanders, *J. Am. Chem. Soc.*, 1990, **112**, 5525; (*b*) G. A. Coates, A. R. Dunn, L. M. Henling, D. A. Dougherty and R. H. Grubbs, *Angew. Chem., Int. Ed. Engl.*, 1997, **36**, 248; (*c*) K. Kishikawa, *Isr. J. Chem.*, 2012, **52**, 800.

21 M.-M. Zhou, J. He, H.-M. Pan, Q. Zeng, H. Lin, K.-Q. Zhao, P. Hu, B.-Q. Wang and B. Donnio, *Chem. – Eur. J.*, 2023, 3202301829.

Publication B

# Engineering "meso-Atom" bonding: Honeycomb-Network Transitions in Reticular Liquid Crystals

C. Anders,[a+] T. Tan,[b+] V.-M. Fischer,[c] R. Wang,[b] M. Alaasar, [a] R. Waldecker,[c] Y. Cao,[b]* F. Liu,[b] C. Tschierske[a]*

[a]Institute of Chemistry, Martin-Luther University Halle-Wittenberg, Kurt-Mothes Str. 2, D-06120 Halle/Saale, German.
[b]Shannxi International Research Center for Soft Matter, State Key Laboratory for Mechanical Behavior of Materials, Xi'an Jiaotong University, Xi'an 710049, P. R. China.
[c]Institute of Mathematics, Martin-Luther University Halle-Wittenberg, Theodor-Lieser-Str. 5, 06120 Halle, Germany.
[+]These two authors contributed equally to this paper.
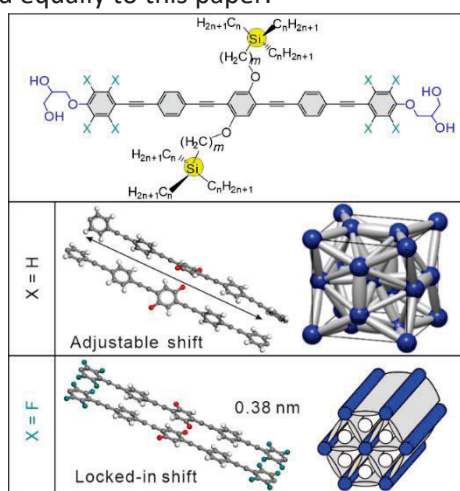
Abstract

A library of rod-like bolapolyphiles with sticky hydrogen bonded glycerol groups at their ends and having highly branched side-chains with a quaternary carbosilane based branching point, all based on the same oligo *p*-(phenylene ethynylene) core, has been synthesized and investigated. For these compounds a A15 type Frank Kasper phase is formed upon side-chain elongation in the steric frustration range at the transition from the triangular to the much larger square honeycombs. In contrast to the previously known tetrahedral sphere packings the A15 phase is in this case formed by tetrahedral networks of aggregates of parallel organized p-conjugated rods. It is found that the total side chain length and the distance between the rod-like core and the Si-branching point are the key issues determining the mode of self-assembly, often overriding the volume effects. This allows the design of compounds with wide ranges of the A15 network down to room temperature. However, its formation becomes strongly disfavored by core fluorination which is attributed to a changing mode of core-core interaction which also modifies the square honeycombs by deformation of the squares into rectangular or rhombic cells, either with or without emergence of tilt of the rods.

Engineering "meso-Atom" bonding: Honeycomb-Network Transitions in Reticular Liquid Crystals

Christian Anders,[a+] Tianyi Tan,[b+] Virginia-Marie Fischer,[c] Ruoyu Wang,[b] Mohamed Alaasar, [a] Rebecca Waldecker,[c] Yu Cao,[b*] Feng Liu,[b] Carsten Tschierske[a*]

[a]Institute of Chemistry, Martin-Luther University Halle-Wittenberg, Kurt-Mothes Str. 2, D-06120 Halle/Saale, German. E-mail: carsten.tschierske@chemie.uni-halle.de

[b]Shannxi International Research Center for Soft Matter, State Key Laboratory for Mechanical Behavior of Materials, Xi'an Jiaotong University, Xi'an 710049, P. R. China. E-mail: yu.cao@xjtu.edu.cn

[c]Institute of Mathematics, Martin-Luther University Halle-Wittenberg, Theodor-Lieser-Str. 5, 06120 Halle, Germany.

[+]These two authors contributed equally to this paper.

Abstract

A library of rod-like bolapolyphiles with sticky hydrogen bonded glycerol groups at their ends and having highly branched side-chains with a quaternary carbosilane based branching point, all based on the same oligo(phenylene ethynylene) core, has been synthesized and investigated. For these compounds a A15 type Frank Kasper phase is formed upon side-chain elongation in the steric frustration range at the transition from the triangular to the much larger square honeycombs. In contrast to the previously known tetrahedral sphere packings the A15 phase is in this case formed by tetrahedral networks of aggregates of parallel organized π-conjugated rods. It is found that the total side chain length and the distance between the rod-like core and the Si-branching point are the key issues determining the mode of self-assembly, often overriding the volume effects. This allows the design of compounds with wide ranges of the A15 network down to room temperature. However, its formation becomes strongly disfavored by core fluorination which is attributed to a changing mode of core-core interaction which also modifies the square honeycombs by deformation of the squares into rectangular or rhombic cells, either with or without emergence of tilt of the rods.

Introduction

The aggregation of π-conjugated molecules into well-defined structures and their precise programmed arrangement in space represents a contemporary challenge of importance for numerous applications like photovoltaics,[1] induced and polarized emission[2-6] and the design of light harvesting systems.[7,8] Liquid crystals (LC) combining rigid polyaromatic units with flexible chains provide the possibility to organize such π-conjugated units into ordered arrays under thermodynamic control in a bottom-up approach.[9-12] In addition, the mobility of the molecules in these LC phases allows easy manipulation of the local and macroscopic structures by external stimuli, as for example used in display technology.[13] Previous LCs were found to form relatively simple structures like nematic phases,[14] layers and columns, mainly depending on the shape of the aromatic core structure. More complex super-structures - allowing more sophisticated future applications of LCs[15] - were achieved by so-called polyphilic molecules,[16] among them the so-called bolapolyphiles.[17-19] These bolapolyphiles represent molecules combining a rigid polyaromatic rod with more than just two incompatible segments, while "bola"[20] means molecules having highly polar groups at both ends of a less polar central unit. In our case this unit is a rod-like π-conjugated system and polar glycerol groups at both ends provide cooperative and dynamic hydrogen bondings[21-24] between them, giving rise to end-to-end attractions (rods with sticky ends,[25,26] see for example Fig. 1b). However, the naturally preferred parallel alignment of the long rods is distorted by the attached flexible side-chains, giving rise to various new states of aggregation. Typically, in these LC phases the polyaromatic cores aggregate into ribbons of parallel organized rods which are interconnected at the junctions by strings of the H-bonding networks of the glycerols to honeycombs with their polygonal cells filled by the flexible side chains (Fig. 1c).[17,18,27,28] The shape of the honeycomb cells can be modified in a wide range from triangular via square (Fig. 1c) and pentagonal to hexagonal, including those with non-regular shapes[29,30] and mixtures of different types of polygonal cells.[31,32]
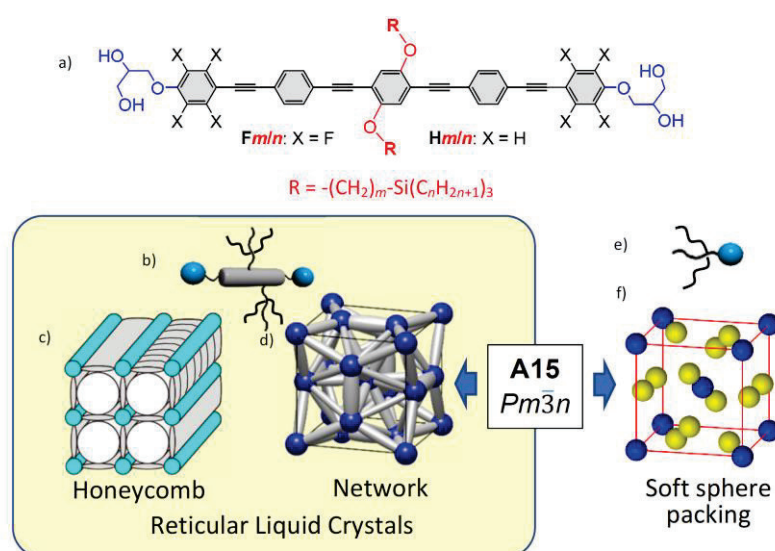

Figure 1. (a) Structure and nomenclature of compounds **H***m*/*n* and **F***m*/*n* with the side-chains shown in red. The first letter **H** or **F** indicates molecules with non-fluorinated OPE or semiperfluorinated FOPE core, respectively, while the combination *m*/*n* indicates the length *m* of the alkylene spacer connecting the (F)OPE core with the Si branching points in the side chains, and *n* is the length of the three alkyl

chains attached to Si. (b) shows a schematic sketch of the considered bolapolyphiles; (c, d) show the phase structures; reticular LC can be divided into (c) honeycombs and (d) 3D networks which can both be described within the meso-atom concept as outlined in ref. [87] c) shows a square honeycombs and (d) the segmented FK-type tetrahedral network with $Pm\bar{3}n$ space group; (e) shows a dendritic amphiphile known to form (f) the $Pm\bar{3}n$ sphere packing without interconnecting junctions (blue and yellow indicate the crystallographic different positions of the spheres).

For larger side-chains the number of polyaromatic rods forming the ribbons becomes limited, leading to a splitting into rod-bundles. These smaller aggregates of polyaromatic rod-bundles form struts with the glycerols at the junctions interconnecting them into 3D-networks.[33-37] Among them the recently discovered tetrahedral network with $Pm\bar{3}n$ space group is a unique structure (Fig.1d)[38] due to its close relationship with Frank-Kasper type sphere packings,[39-42] specifically, the A15 phase (Fig. 1f). Huge efforts have been made to design and investigate the A15 sphere packing in solid state modifications of metals, alloys and intermetallic compounds,[43] in aqueous lyotropic systems,[44-47] in the soft mesophases of different types of amphiphilic[48-50] and dendritic molecules,[47,51-78] as well as in block copolymer morphologies,[79-83] and to understand their formation under the aspect of minimizing the interfaces in soft sphere packings (Fig. 1g,h).[84,85] However, in the new type of FK phase formed by polyphiles the focus is on the engineering of the struts interconnecting the spherical aggregates at the junctions. In this case the spheres at the junctions can be considered as a kind of "superatoms"[86] or "meso-atoms"[87-89] which are interconnected by bonds between them ("meso-atom" bonds).[90]

Here we report about engineering of meso-atom bonding in such reticular[91] (net-like) LCs. For this purpose we use bolapolyphiles with oligo(phenylene ethynylene) (OPE)[92] rods and sticky ends having two highly branched carbosilane based side-chains with the silicon acting as a tetravalent branching point in these chains.[93,94] The side-chain effects, as well the effects of core fluorination[95] on the aggregation of the OPE rods[27,30,38,96-100] into different reticular LC, either into honeycombs, or alternatively, into network structures (Fig. 1c, d) are investigated. In these compounds X*m/n* (Fig. 1a) X = **H** means a non-fluorinated OPE core and X = **F** indicates an FOPE core with perfluorinated benzene rings at both peripheries, besides the glycerol groups. The numbers *m/n* give the aliphatic spacer length *m* and the alkyl chain length *n* in each branch, respectively (Fig. 1a). In a previous short communication we have reported the effect of spacer length *m* at constant chain length on the LC phase formation for a series of compounds with fixed *n* = 7.[94] Here we provide a much wider study of a larger library of OPE based bolapolyphiles depending on the side-chain volume, side-chain length and core-fluorination in order to fully understand their soft self-assembly, especially the conditions for A15 phase formation in the perspective of polyaromatic core aggregation. It is found that the A15 FK-type network phase represents an intermediate structure in the frustration range at the transition between triangular and square honeycombs (mainly determined by the side-chain length and volume), but only if an easy longitudinal shift between the individual polyaromatic rods can take place. Any restriction of this shift by specific core-core interactions removes the A15 phase which is then replaced by different types of deformed honeycombs.
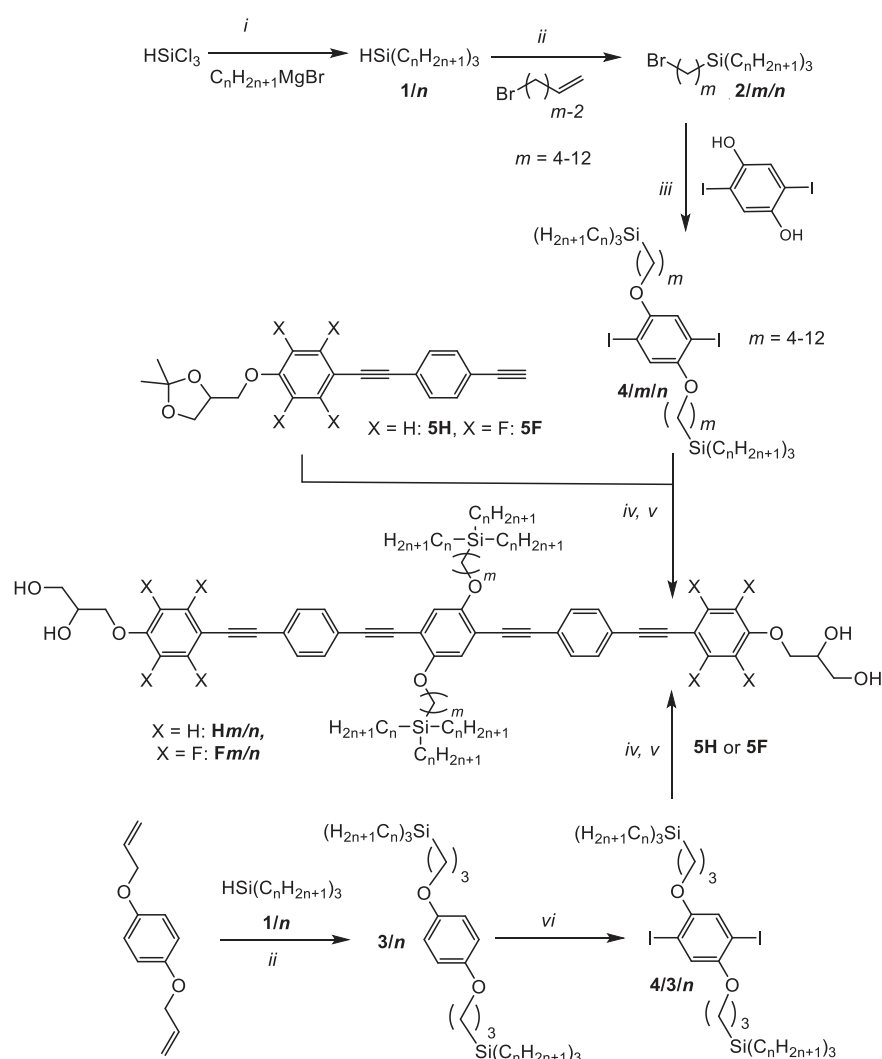
Experimental

Materials

Figure 2. Synthesis of compounds **H*m/n*** and **F*m/n***. *Reagents and conditions*: i: THF, LiCl, 20 °C, 24 h; ii: CH$_2$Cl$_2$, Karstedts cat., 20 °C, 1d, iii: K$_2$CO$_3$, Bu$_4$NI, DMF, 80 °C, 3d; iv: Pd(PPh$_3$)$_4$, CuI, Et$_3$N, 80 °C, 1d; v: PPTS, MeOH / THF, 50 °C; vi: PhI(OCOCF$_3$)$_2$, I$_2$, DCM, 60 °C, 1d.

All compounds were synthesized as shown in Figure 2 by Sonogashira coupling[101] of the 2,5-dialkylated 1,4-diiodobenzenes **4/*m/n*** with the acetylene terminated building blocks **5H** or **5F**.[27,99,100] For compounds with spacer lengths *m* = 4-12 the carbosilane chains were attached by alkylation of diiodohydroquinone with the bromosubstituted carbosilanes **2/*m/n***, while for compounds with *m* = 3, 1,4-diallyloxybenzene was hydrosilylated[102] with the *H*-carbosilanes **1/*n***[103] and then iodinated with a hypervalent iodination reagent[104] to yield the diiodohydroquinone ethers **4/3/*n***. The bromosubstituted carbosilanes **2/*m/n*** were prepared by hydrosilylation of ω-bromoalkenes with **1/*n*** and In the final step the glycerol groups of the bisacetonides of **H*m/n*** and **F*m/n*** (**H*m/n*A** and **H*m/n*A**), were deprotected under mild acidolytic conditions using pyridinium p-toluene sulfonate[105] to give the final compounds

4

which were purified by repeated column chromatography. The experimental details and the analytical data and details of the synthesis of the ethynyltolanes **5H** and **5F** are provided in the Synthesis Section of the Supporting Information file (SI).

Methods

Investigation of the compounds was performed by differential scanning calorimetry (DSC), polarizing optical microscopy (POM), small-angle and wide-angle X-ray scattering (SAXS and WAXS) and UV-vis and fluorescence measurements in thin films under the conditions and with the equipment described in the methods section in the SI.

Results and Discussion

Series of non-fluorinated compounds H*m*/*n*.

Table 1. LC phases, transition temperatures, transition enthalpies and lattice parameters of compounds H*m*/*n*.[a]
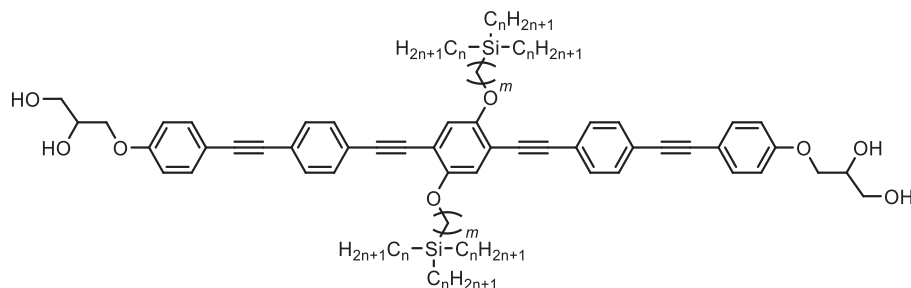
Compd.	m	n	T/°C [ΔH/kJ mol^{-1}]	a/nm@T/°C	V_C	L_C
H3/6	3	6	Cr 93 [24.1] *p6mm* 163 [5.0] Iso	4.27@130	44	10
H3/7[b]	3	7	Cr 70 [13.6] *p6mm* 147 [3.5] *Pm$\bar{3}$n* 160 [1.5] Iso	4.39@101 8.62@151	50	11
H6/6	6	6	Cr 59 [31.3] *p6mm* 108 [2.8] *Pm$\bar{3}$n* 155 [1.6] Iso	4.38@69 9.09@119		13
H4/7[b]	4	7	Cr 91 [41.5] *Pm$\bar{3}$n* 159 [1.3] Iso	8.89@119	52	12
H8/6	8	6	Cr 67 [23.4] M 109 [2.2] *Pm$\bar{3}$n* 139 [0.5] Iso	9.13@119	54	15
H3/8	3	8	Cr 75 [14.6] *p6mm* 120 [4.4] *Pm$\bar{3}$n* 162 [1.8] Iso	4.45@69 4.29@110 8.84@120	56	12
H6/7[b]	6	7	Cr 54 [16.3] M 85 [1.1] *Pm$\bar{3}$n* 146 [0.5] Iso	9.19@92		14
H9/6	9	6	Cr 87 [18.3] *p4mm* 118 [3.3] Iso	4.14@96		16
H4/8	4	8	Cr 74 [29.5] *Pm$\bar{3}$n* 157 [1.8] Iso	8.85@110	58	13
H5/8	5	8	Cr 74 [24.0] M 104 [4.5] *Pm$\bar{3}$n* 157 [1.6] Iso	9.06@119		14
H8/7[b]	8	7	Cr 45 [1.5] *p4mm* 105 [3.0] *Pm$\bar{3}$n* 128 [0.4] Iso	4.12@64 9.13@105	60	16
H11/6	11	6	Cr 85 [17.2] *p4mm* 142 [5.2] Iso	4.54@120		18
H3/9	3	9	Cr 67 [19.8] *p6mm* 101 [4.3] *Pm$\bar{3}$n* 157 [1.8] Iso	4.44@74 8.89@110		13
H6/8	6	8	Cr 68 [13.1] *Pm$\bar{3}$n* 147 [0.8] Iso	9.15@101	62	15
H9/7[b]	9	7	Cr 80 [11.1] *p4mm* 127 [4.0] Iso	4.16@101 3.93@121		17
H4/9	4	9	Cr 50 [23.7] *Pm$\bar{3}$n* 155 [2.1] Iso	8.86@119	64	14
H10/7[b]	10	7	Cr 83 [11.1] *p4mm* 134 [5.4] Iso	4.18@110		18
H11/7[b]	11	7	Cr 78 [11.8] *p4mm* 142 [5.4] Iso	4.25@92	66	19
H3/10	3	10	Cr 88 [53.4] *Pm$\bar{3}$n* 156 [2.2] Iso	8.81@128		14
H6/9	6	9	Cr 59 [28.5] *p4mm* 64 [-] *Pm$\bar{3}$n* 128 [0.3] Iso	3.99@54 9.01@101	68	16
H4/10	4	10	Cr 55 [14.7] *Pm$\bar{3}$n* 146 [1.7] Iso	8.98@101	70	15

[a] peak temperatures as determined by DSC (10 Kmin^{-1}) on cooling; ordered according to growing V_C values and for identical V_C with growing spacer length m; abbreviations: V_C = total number of C- and Si-atoms in both side chains, $V_C = 2(m+3n+1)$; L_C = number of C- and Si-atoms along each side-chain between ether oxygen and most distant CH$_3$ group, $L_C = m + n + 1$; Cr = crystalline solid (in the case of different crystalline modifications only the highest melting one is given here), *p6mm* = triangular honeycomb (Col$_{hex}$/*p6mm*), *p4mm* = square honeycomb

(Col$_{squ}$/$p4mm$), $Pm\bar{3}n$ = cubic network phase with $Pm\bar{3}n$ space group (Cub$_{net}$/$Pm\bar{3}n$, for model see Fig. 1d), Iso = isotropic liquid; M = unknown birefringent mesophases; for data on cooling, see Fig. 5 and Table S1; for DSC traces, see Fig. S1; additional structural data can be found in Tables S31-S33 in the SI. [b] see ref. 94.
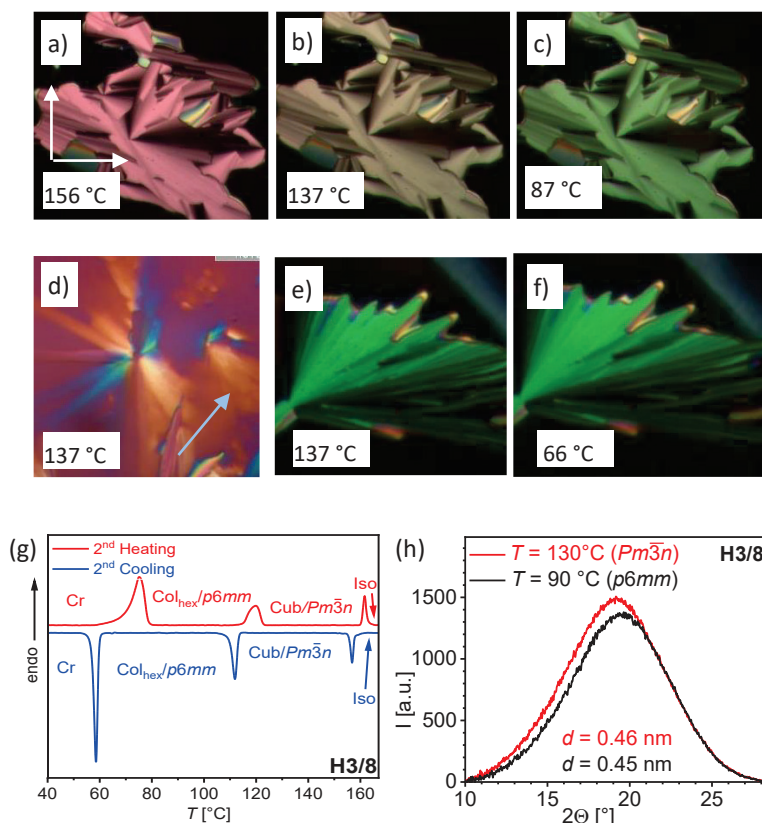

Figure 3. a-c) Textures of the Col$_{hex}$/$p6mm$ phase of **H3/6** as observed between crossed polarizers (arrows in (a)) on cooling at the given temperatures; the changing color of the fan-like domains shows the decreasing Δn; d-f) textures of the Col$_{squ}$/$p4mm$ phase of **H11/6**, d) shows the texture with λ-retarder plate, indicating negative Δn (blue shift along the indicatrix slow axis indicated by the arrow); dark areas in a-c, e, f) represent homeotropic aligned areas with the columns perpendicular to the substrates; g), DSC traces and h) WAXS scans of **H3/8**.

Three different reticular LC phases, Col$_{hex}$/$p6mm$, Cub$_{net}$/$Pm\bar{3}n$ and Col$_{squ}$/$p4mm$ were identified (Table 1). Two of them form birefringent spherulite-like and fan-like textures between crossed polarizers (Fig. 3a-f) as typical for columnar LC phases (Col). POM Investigation with an additional λ-retarder plate (Fig. 3d) show negative birefringence by the blue shift of the fans along the slow indicatrix axis, meaning that the major conjugation pathway of the π-conjugated rods lays perpendicular to the column long axis, as typical for honeycomb LC phases. In contrast, the cubic phases (Cub) are optically isotropic and can be distinguished from the isotropic liquid only by the significantly higher viscosity and the presence of sharp scatterings in the SAXS patterns. In addition, the Cub-Iso transition is associated with a small DSC peak (0.3-1.8 kJ mol^{-1}, see Table 1 and Fig. 3g).
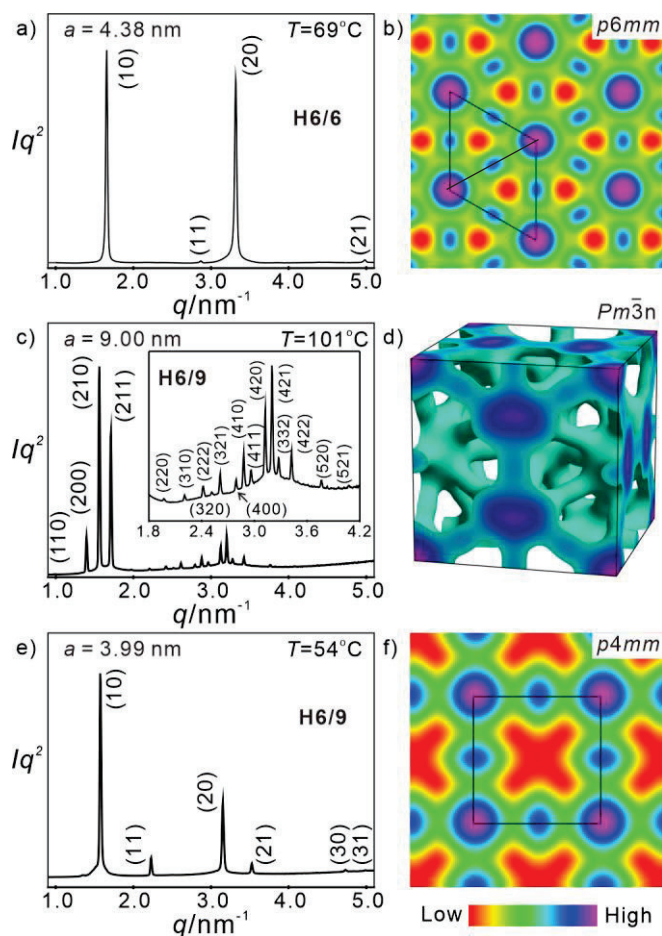
Figure 4. SAXS patterns of compounds **H*m*/*n*** with a non-fluorinated OPE core: a, c, e) SAXS patterns, b, d, f) the corresponding ED maps, a, b) in the Col_{hex}/*p6mm* phase of **H6/6** at 69 °C (triangular honeycomb), c, d) in the Cub_{net}/*Pm$\bar{3}$n* phase of compound **H6/9** at 101 °C (A15 phase), e, f) in the Col_{squ}/*p4mm* phase of **H6/9** at 54 °C (square honeycomb); in b,f) the positions of the OPE rods in one unit cells are shown as black lines, for a model of d), see Fig. 1d; for additional SAXS patterns and ED maps, see Figs. S6, S8; the origin of the enhanced intensity of the (20) reflection in the columnar phases is explained in Fig. S8b.

The WAXS patterns of the columnar and cubic mesophases of compounds **H*m*/*n*** are diffuse with a single maximum around 0.45-0.46 nm (Fig. 3h), indicating the absence of positional order between individual molecules and thus confirming the LC state. The SAXS patterns of the birefringent colmnar phases can be indexed either to a hexagonal *p6mm* lattice (ratio of reciprocal *d*-spacing is 1: √3: 2: √7….. see Fig. 4a) or to a square *p4mm* lattice (ratio of reciprocal *d*-spacing is 1: √2: 2 …., see Fig. 4e). The triangular and square honeycomb structures of the LC phases are confirmed by the reconstructed electron density (ED) maps (see Figs. 4b, f), where the red areas represent the low ED centers of the columns, formed by the alkyl side chains filling the polygonal prismatic cells (triangular or square, respectively). These are enclosed by the OPE cores as sides and the high ED polar glycerol groups (blue/purple) as junctions of the honeycomb cells. The light blue high ED dots in the middle of the honeycomb walls are due to the two electron-rich ether oxygens connecting the side chains to the middle

benzene rings. The lattice parameter in the Col_{hex} phases is $a_{hex} = 4.2\text{-}4.5$ nm (Table S31) which is close to the maximum value of the molecular length (L_{mol}) as measured between the ends of the glycerol groups ($L_{mol} = 4.0\text{-}4.4$ nm) and typical for triangular honeycombs.[27] Likewise, the lattice parameters of the square phase ($a_{squ} = 3.9\text{-}4.5$ nm, Table S33) are in line with a square honeycomb, though there is a wider variation of a_{squ} depending on side chain volume. There is also a temperature dependence of the lattice parameter in both phases which is however small (<0.1 nm in the phase ranges, see Fig. S9). The number of molecules organized side-by-side in the lateral cross section of the honeycomb walls (n_{wall}) is around 0.9-1.1 ("single molecule walls") in the triangular and a bit larger, around 1.2-1.7 (shifted towards "double molecule walls"), in the square honeycombs (these are no integer numbers due to molecular staggering and molecular dynamics in the LC state, see Tables S31 and S33). This difference is due to the different valence (ν) of the junctions connecting the cylinder walls, being $\nu=6$ in Col_{hex} and only $\nu=4$ in Col_{squ}. Due to the larger valence of the junctions, the cross section of the polar glycerol columns would be larger in the triangular honeycombs. However, this difference is compensated by the tendency of the polar columns to retain their diameter in a narrow range and this requires an increase of n_{wall} in the square honeycomb. Thus, in both honeycomb phases the diameter of the polar columns remains in the range between 4.8 and 6.6 glycerols in the cross section. These limits appear to be the result of two competing forces. On the one hand the columns are stabilized by increasing the number of cooperative (polarization enhanced) and dynamic H-bonding interactions between the glycerols,[21-24] providing a tendency for lattice-expansion, while on the other hand the limited size of the polar glycerol units restricts the possible column expansion without distorting nano-segregation by significant overlapping of lipophilic OPE cores and polar glycerols upon shifting the molecules with respect to each other. Outside this range the honeycombs become instable and are replaced by other modes of self-assembly.

The absence of a temperature dependence of the birefringence (see Fig, 3e, f), and a larger variation of n_{wall} in the square honeycombs indicates that adjustment of the cell volume to the space actually required by the side-chain volume (depending on m, n and T) is in this case mainly achieved by lattice shrinkage/expansion due to variation of n_{wall}. In contrast, in the triangular honeycombs the variation in n_{wall} is much smaller and a decrease of birefringence with rising temperature is observed (color change from green, via reddish green to red see textures of **H3/6** in Fig. 3a-c). This means that in this case the main contribution to the adjustment of cell volume and chain volumes is provided by a changing orientational order parameter of the rods in the walls (random tilt of the rods in the walls), i.e. due to a changing of the effective molecular length. It seems that the relatively long spacer units in the molecules forming the square honeycombs allows an easy adjustment of n_{wall}, which is more difficult for the triangular honeycombs, mainly formed by molecules having shorter spacers, where the bulky $-SiR_3$ groups close to the core reduce their capability of forming double molecular walls. Hence, long spacers allow an easy compensation of differences between prismatic cell volume and effective chain volume by changing n_{wall}, while this becomes more difficult as the spacer length decreases, then requiring a change of the orientational order parameter or tilting of the rods to adjust the cell size. It is noted that the change of the orientational order parameter and tilt are also affected by the core-core interactions as discussed further below for compounds **F*m/n***.
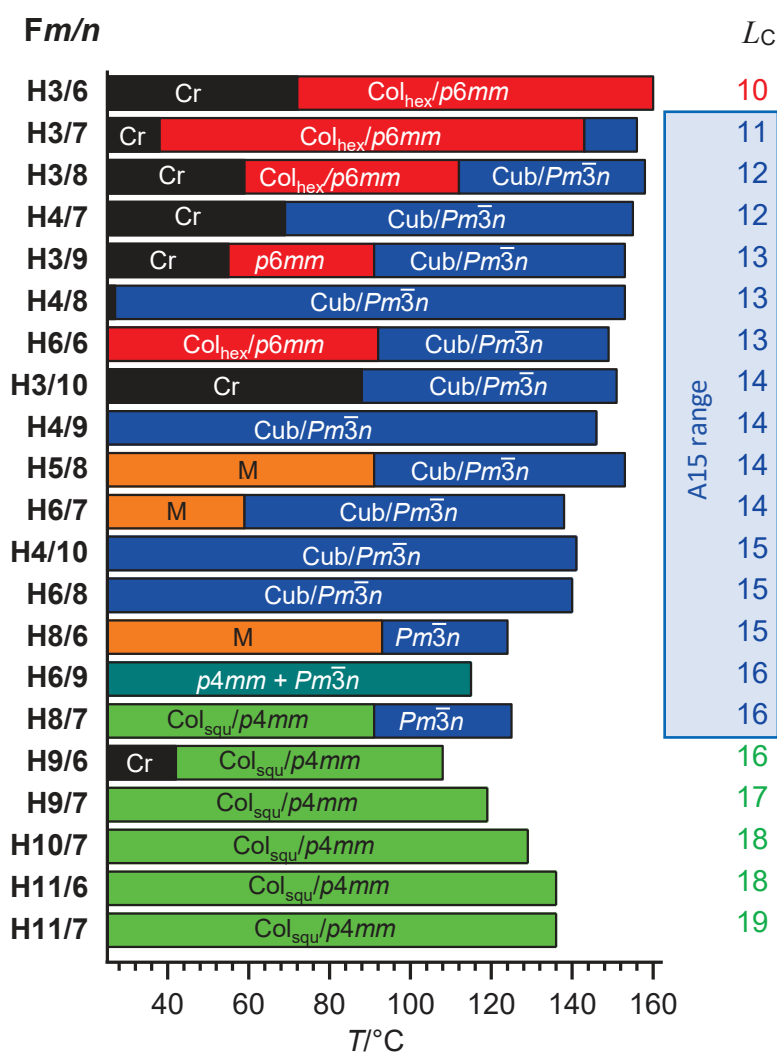
Figure 5. Bar diagram of series **H***m/n* ordered according to increasing $L_C = m + n + 1$ and for identical L_C with growing number of CH_2 units (m) in the spacer. The temperatures were recorded on cooling with 10 K min^{-1}.

Most investigated compounds **H***m/n* form a cubic mesophase above one of the honeycomb phases or even as the only observable mesophase. The SAXS patterns show three strong reflections which can be indexed to (200), (210) and (211) reflections of a lattice with $Pm\bar{3}n$ space group (Fig. 4c). All remaining weaker reflections can be indexed to this space group, too. The ED-map indicates a packing of high ED spheres at the corners, in the center and as pairs of spheres on the faces of the unit cell of the cubic lattice, as typical for the A15 phase (Fig. 4d). Moreover, the high ED glycerol spheroids are interconnected by a tetrahedral network of medium ED bonds, indicating struts formed by bundles of parallel OPE rods (see also Fig. 1d). The low ED alkyl chains, filling the continuum around them, are omitted for clarity. Because there are two different types of spheroids with different valence (12+14), size and shape, also the bond lengths are different and assume the values 0.5 a_{cub}, 0.56 a_{cub}, and 0.61 a_{cub}.[38] The lattice parameters are a_{cub} = 8.6-9.2 nm from which the length of the bonds can be calculated

10

to be L_{bond} = 4.3 to 5.5 nm, i.e. their length exceeds that of the individual molecules **Hm/n** which is attributed to the significant size of the glycerol spheroids interconnecting 12 and 14 rod-bundles, respectively. The number of molecules per unit cell is between 240 and 320 ($n_{cell;LC}$, see Table S32) which are distributed among the 54 bonds interconnecting the spheroids, meaning that there are on average 4.4-5.9 molecules organized side-by-side in the bundles of parallel aligned OPEs. This number decreases with growing n and tends to increase with elongation of m (Table S32). Around 53-71 glycerols are organized in the smaller spheroids with ν = 12 (V_{sph} = 6.5-8.7 nm³, as estimated using Immirzi's crystal volume increments[106]) in the center and at the corners, whereas the larger spheroids with ν = 14 on the faces of the unit cell are each formed by 62-83 glycerols (V_{sph} = 7.6-10.1 nm³). Assuming a spherical shape their diameters would be 2.3-2.6 nm and 2.4-2.7 nm, respectively. Considering $L_{OPE-core}$ = 3.1 nm the distance between the centers of the spheres should be 5.4-5.8 nm, being just around the upper limit of the bond length of 5.5 nm. This indicates some intercalation of OPE cores and glycerols requiring some longitudinal shift of the OPE cores (see discussion of **Fm/n** further below).

The overall sequence of phases is affected by the side-chain volume V_C, calculated from the total number of C- and Si-atoms in the side chains as V_C =2(m+3n+1). This leads to the sequence Col$_{hex}$/$p6mm$ (V_C = 44-50) → Cub$_{net}$/$Pm\overline{3}n$ (V_C = 50-70) → Col$_{squ}$/$p4mm$ (V_C = 60-70). However, as obvious from Table 1, this sequence is not strict, there are several cases for which the observed phases do not follow this rule, as for example the Col$_{hex}$ phases of **H3/8** with V_C = 56 and **H3/9** with V_C = 62 occur for much larger side-chain volumes while the Col$_{squ}$ phase of **H9/6** with V_C = 56 is found for a smaller volume than expected. If one compares, for example, the three compounds with constant chain volume V_C = 56 then with growing spacer length the sequence Col$_{squ}$/$p6mm$ → Cub$_{net}$/$Pm\overline{3}n$ → Col$_{hex}$/$p4mm$ is observed from **H3/8** via **H6/7** to **H9/6**. The same sequence is found for the series of compounds **H3/9, H6/8** and **H9/7** with V_C = 62. This means that at identical V_C long spacers prefer the square honeycomb and short spacers the triangular honeycombs, and the cubic $Pm\overline{3}n$ phase is found as intermediate structure at the transition between them. Both series occur upon increasing the spacer length (m) while simultaneously decreasing the length of the three alkyl branches (n) to keep the total chain volume V_C constant. This means that it is not sufficient that the chain volume fits with the cell volume, but the chains must also be sufficiently long to efficiently fill the most distant spaces in the selected structure. Increasing the spacer length m contributes more to an increase of the total L_C = m + n + 1, while increasing the length of the 3 branches (n) contributes mostly to V_C and less to L_C. Ordering the compounds **Hm/n** according to the side-chain length L_C, and for identical side chain length according to growing spacer length m, as shown in the bar diagram in Fig. 5, provides a much clearer picture showing a transition Col$_{squ}$/$p6mm$ → Cub$_{net}$/$Pm\overline{3}n$ → Col$_{squ}$/$p4mm$ with growing side chain length L_C. In the series **Hm/n** the $Pm\overline{3}n$ phase becomes the dominating phase for compounds with relatively short spacers (m ~ 3-8) and medium length of the branches (n ~ 8-9) within the chain length range between L_C = 11-16, corresponding to L_{chain} = 1.5-2.1 nm.

The dV/dr curves in Fig. 6 support the observed phase sequence. For each curve, the intersection with the x-axis refers to the furthest distance required to fill the lattice, and the area occupied by the curves represents the volume requirement for each molecule. The shape of the curves provides information

about the development of the chain volume depending on the distance from the core (r). The $Pm\overline{3}n$ phase (blue) requires short side chain length (r), large side chain volume (given as areas V/r in Fig. 6) and a strong volume increase (dV/dr) close to the OPE core which is provided by the compounds **Hm/n** with short spacers m and longer n, while the formation of the triangular honeycomb (red) is favored for molecules with limited side chain volume and a smaller increase of dV/dr. However, as shown in Fig. 6 the curves of $p6mm$ and $Pm\overline{3}n$ cross each other and the areas occupied are close, thus both structures can compete with each other and the majority of the $Pm\overline{3}n$ phase occurs close to the $p6mm$ phase (Fig 5). There is a transition $p6mm$-$Pm\overline{3}n$-$p4mm$ with growing spacer length m, and for any m, larger n favors $Pm\overline{3}n$ due to larger chain volume and more possibilities of chain folding. On top of this, there appears to be an odd-even effect. A bent-shaped odd numbered $m+1$ (1 stands for the ether oxygen) contributes to a steeper dV/dr growth, favoring $Pm\overline{3}n$ more than a related linear even numbered. In all cases with $p6mm$-$Pm\overline{3}n$ dimorphism higher chain flexibility supports chain folding and thus additionally favors $Pm\overline{3}n$ at high temperature above $p6mm$. Moreover, the increased possibilities of chain orientations and conformations makes the $Pm\overline{3}n$ phase also entropically more favorable. Further increasing m favors $p4mm$ (green line in Fig. 6; the other yellowish green lines are explained further below).
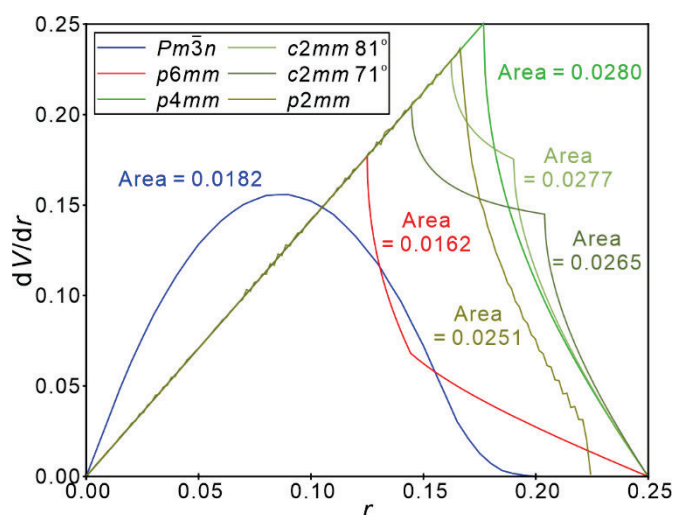

Figure 6. dV/dr curve of the LC phases formed by **Hm/n** and **Fm/n**. The aromatic core length is taken as 0.5 to normalize all phases. The given area values are the areas under the curves as a measure of the total chain volume. The calculation of the curves is described in the SI.

Honeycomb vs. network competition in the series of fluorinated compounds Fm/n.

In a next step a series of related core-fluorinated compounds **Fm/n** with almost the same chain volume range (V_C = 44-68) was investigated (Table 2, Fig. 7), where clear trends can also be identified. First of all, the probability of finding the $Pm\overline{3}n$ phase is dramatically reduced by core fluorination. The existence range of the $p6mm$ phase is significantly expanded and among the investigated compounds there are only two compounds with L_C = 14 (**F3/10** and **F4/9**) with a small $Pm\overline{3}n$ range of about 10-20 K. However, even in this case the Cub-Iso transition temperature is reduced strongly by 17 and 33 K in comparison with the non-fluorinated compounds **H3/10** and **H4/9**, respectively. Thus, the molecular structural space for $Pm\overline{3}n$ phase formation is much narrower and the stability of this phase is

considerably reduced by core fluorination. In contrast, there appears to be a general stabilizing core-fluorination effect for the honeycomb phases (Fig. 7) which acts against the steric distortion of core packing provided by fluorination.[95,107,108] This effect, giving rise to a mesophase stabilization by about 10-20 K upon core-fluorination is only observed for compounds with optimal space filling in the prismatic cells ($L_C < 11$ for *p6mm* and $L_C > 16$ for *p4mm*, see Fig. 7). All compounds between these limits, experience some steric frustration leading in most cases to a decrease of the LC → Iso transition temperature by up to 33 K upon fluorination (see frustration range in Fig. 7).

Table 2. LC phases, transition temperatures transition enthalpies and lattice parameters of compounds **F*m/n*** [a]
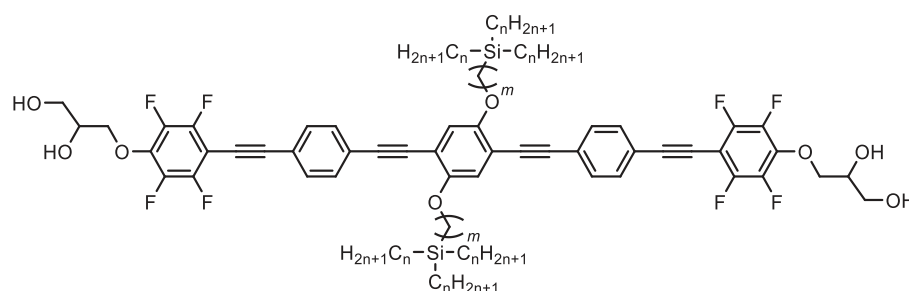
F*m/n*	*m*	*n*	*T*/°C [Δ*H*/kJ mol⁻¹]	*a,b*/nm @*T*/°C	V_C	L_C
F3/6	3	6	Cr 41 [3.3] *p6mm* 173 [11.1] Iso	4.48@83	44	10
F3/7[b]	3	7	Cr 44 [2. 8] *p6mm* 160 [6.3] Iso	4.43@120	50	11
F6/6	6	6	Cr <20 *p6mm* 156 [5.3] Iso	4.51@151		13
F4/7[b]	4	7	Cr 50 [9.2] *p6mm* 134 [2.8] Iso	4.29@64	52	12
F3/8	3	8	Cr 39 [5.9] *p6mm* 156 [8.9] Iso	4.35@115	56	12
F6/7[b]	6	7	Cr < 20 M 131 [0.3] *p6mm* 146 [5.4] Iso	4.30@92		14
F4/8	4	8	Cr 30 [6.9] *p6mm* 135 [4.9] Iso	4.33@83	58	13
F11/6	11	6	Cr 74 [8.4] *c2mm* 115 [-] *p4mm* 164 [11.1] Iso	*a* = 5.14; *b* = 6.82@78 4.24@124	60	18
F3/9	3	9	Cr 37 [7.8] M 105 [0.9] *p6mm* 143 [4.5] Iso	4.43@55		13
F9/7[b]	9	7	Cr 59 [8.2] *c2mm* 115 [-] *p4mm* 148 [8.8] Iso	*a* = 4.92; *b* = 6.92@60 4.14@119	62	17
F4/9	4	9	Cr 64 [1.8] *p6mm* 103 [2.6] *Pm$\bar{3}$n* 122 [0.5] Iso	4.30@74 8.98@101	64	14
F10/7[b]	10	7	Cr 94 [22.0] *p4mm* 150 [4.8] Iso	4.14@74		18
F11/7[b]	11	7	Cr 67 [10.2] *c2mm* 80 [-] *p4mm* 158 [9.1] Iso	*a* = 5.25; *b* = 6.64 @46 4.26@119	66	19
F3/10	3	10	Cr 105 [3.3] M1 118 [0.8] M2 129 [6.8] *Pm$\bar{3}$n* 139 [1.1] Iso	8.70@136		14
F6/9	6	9	Cr < 20 *p2mm* 108 [1.5] *p4mm* 124 [6.6] Iso	*a* = 4.16; *b* = 3.64@92 4.00@105	68	16
F12/7[b]	12	7	Cr 94 [18.5] *p4mm* 159 [10.8] Iso	4.23@137		20

[a] Ordered according to growing V_C values and for identical V_C with growing spacer length *m*. Peak temperatures as determined by DSC (10 Kmin⁻¹) on heating; abbreviations, *c2mm* = rhombic honeycomb

(Col$_{rec}$/*c2mm*), *p2mm* = rectangular honeycomb (Col$_{rec}$/*p2mm*), M1, M2 = different unknown birefringent mesophases; for all other abbreviations, see Table 1; for data on cooling, see Fig. 5 and Table S1; for DSC traces, see Fig. S2; additional structural data can be found in Tables S31-S33 in the SI. [b] see ref. 94.
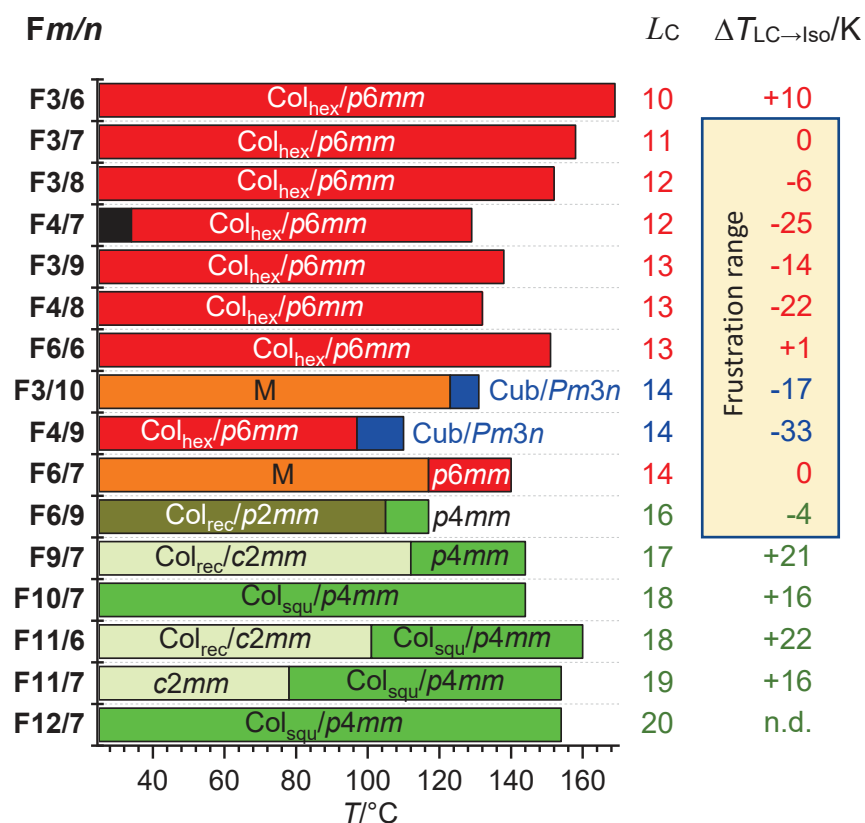

Figure 7. Bar diagram of series **F*m/n*** ordered according to increasing side-chain length L_C and growing *m,* as observed on *cooling* with 10 K min⁻¹; at the right the differences between the LC→Iso transition temperatures: $\Delta T_{LC\rightarrow Iso} = T_{LC\rightarrow Iso}$ (**F*m/n***) - $T_{LC\rightarrow Iso}$ (**H*m/n***) based on the data on *heating* (Tables S1, S2) with 10 K min⁻¹; for abbreviations, see Tables 1, 2.

The SAXS patterns of the *p6mm*, *p4mm* and *Pm$\bar{3}$n* phases of compounds **F*m/n*** indicate lattice parameters in the ranges of a_{hex} = 4.2-4.5 nm, a_{squ} = 4.0-4.3 nm and a_{cub} = 8.7-9.0 nm, being almost identical with those of compounds **H*m/n*** (compare Figs. 4a, c, e, and. 8a, c, e). Hence, their phase structures are almost identical and there is no recognizable effect of core fluorination on these parameters (for a discussion of the textures, see Fig. S3). Slight differences in the ED maps are caused by differences in the intensity distribution of the reflections compared to **H*m/n*** due to the enhanced ED of the perfluorinated ends of the FOPE cores. (see Fig. 8b, d and f).
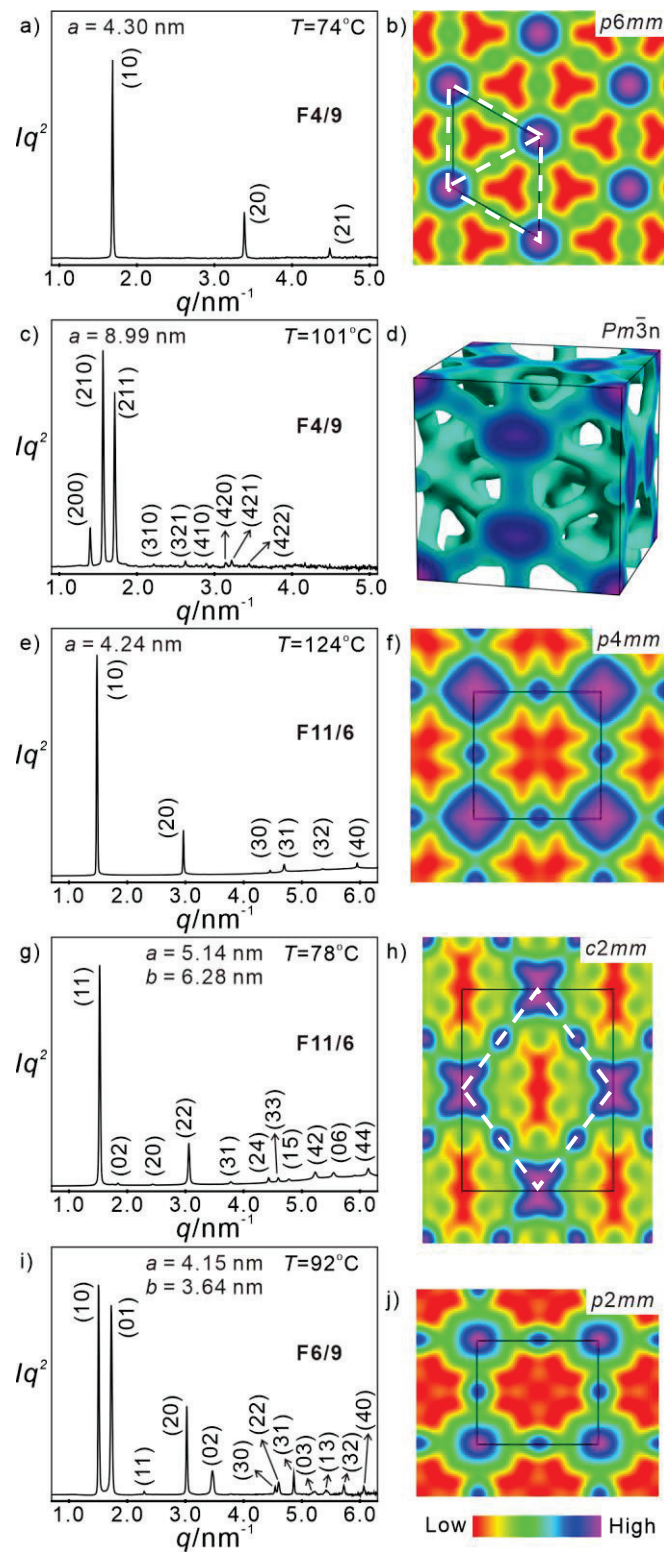
Figure 8. SAXS patterns (left) and ED maps (right) of representative compounds **F***m/n* in their mesophases. The black lines indicate the unit cells, which coincide with the honeycomb cells, except for b, h) where the honeycomb cells are indicated by the white dotted lines; for additional SAXS patterns and ED maps, see Figs. S7, S8a.
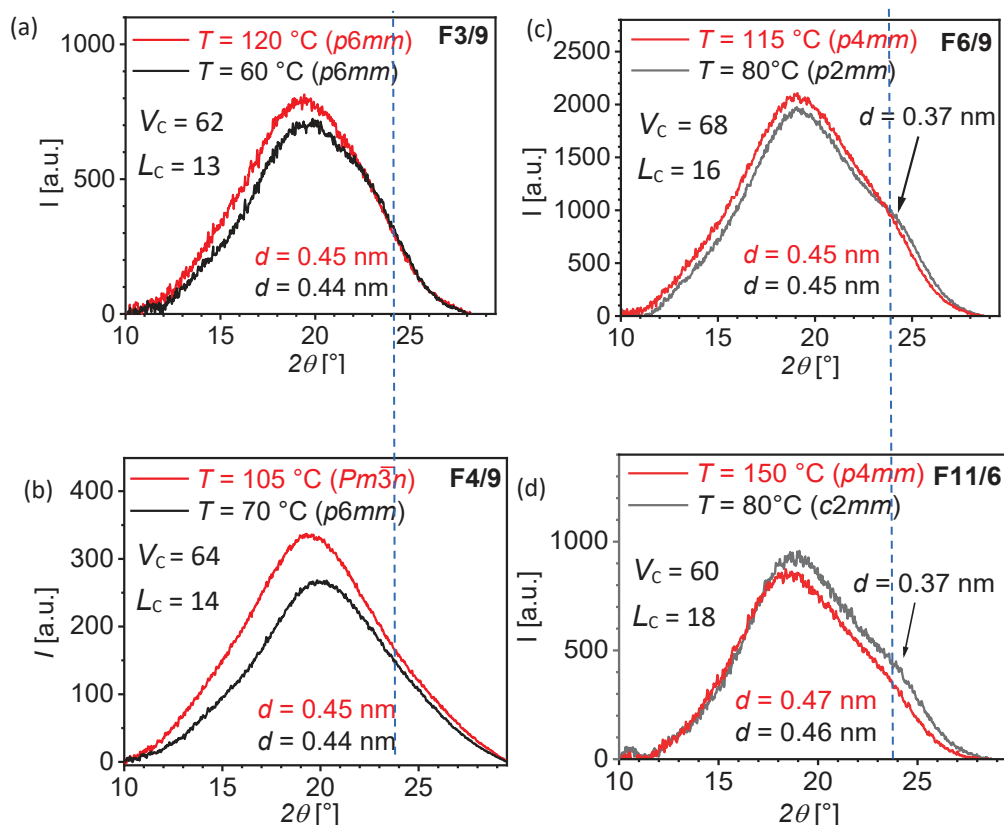
Figure 9. WAXS patterns of compounds **F***m*/*n* depending on the V_C and L_C-values, in the different LC phases and depending on spacer length. The dash line indicates the peak position of $\pi-\pi$ stacking around 0.37 nm; for more WAXS patterns, see Fig. S4-S5.

A major difference between the series **H***m*/*n* and **F***m*/*n* is found in the WAXS patterns (Fig. 9). For most core fluorinated compounds there is an additional weak shoulder around $d = 0.36$-0.38 nm besides the main diffuse scattering, being absent for the non-fluorinated compounds (Fig. 3h). We attribute it to a contribution of closer face-to-face stacking interactions between neighboring FOPE cores, while for the electron rich OPE compounds **H***m*/*n* the larger core-core distance around 0.45 nm (in the WAXS overlapping with the mean alkyl chain distances, see Fig. 3h) allows an almost free rotation around the rod long axes. Thus, the OPE cores can assume different stacking modes, including face-to-face[109] and edge-to-face arrangements.[110] In the series of compounds **F***m*/*n* the contribution of the shoulder around 0.36-0.38 nm increases with growing spacer length *m* (Fig. 9), because longer spacers allow a closer packing of the FOPE cores, while short spacers lead to a significant disturbance of face-to-face core packing by the bulky R_3Si units in closer proximity. For the *p6mm* phases of the compounds with short spacers, this steric suppression of π-stacking is especially pronounced (Fig. 9a, b). The relative intensity of the shoulder increases with lowering temperature (Fig. 9a, c, d), indicating an improved packing, in line with the growing order parameter (Fig. S3a, b). The very diffuse character of this shoulder indicates an only short coherence length of this stacking over only few molecules, in line with the significant molecular dynamics in the LC phases. It is not visible in the $Pm\bar{3}n$ phase range of **F4/9** and **F3/10** (Figs. 9b, S5d) because of the limited length of π-stacking in the rod-bundles.

UV-Vis absorption and emission spectra were recorded for representative compounds in the *p6mm* and *Pm$\bar{3}$n* phases of compounds **H3/9** and **F4/9**, as shown in Fig 10. For the absorption spectra of **H3/9** (Fig. 10a), two main absorptions centered around 338 nm and 388 nm at low temperature can be assigned as the HOMO$_2$ to LUMO and HOMO to LUMO transitions of the OPE core (Fig. S12).[111] Upon heating, minor red shift of 10-15 nm can be found for the two main absorptions, which is attributed to an increasing intramolecular twist along the OPE core. However, only a minor difference between **H3/9** and **F4/9** can be found in the absorption spectra. Compound **F4/9** mainly exhibits a blue shift of ~15 nm compared with **H3/9** which is attributed to the effects of fluorination on the frontier orbitals energy. One striking feature of the **H3/9** emission spectra (Fig. 10c) is that it emits round 480 nm and minor blue shift (~10 nm) can be found upon heating up to the cubic phase. **F4/9** gives a very different feature with emission around 510 nm and stronger blue shift (~20 nm) upon heating (Fig. 10d). Such difference can be attributed to the effect of aggregation. For OPEs, there're two types of planarization due to aggregation. One is from loose packing (aggregation induced coplanarization) and another one is from ordered packing (co-facial planar aggregation) (Fig. S13).[112] The more ordered packing induces red shift of the emission as well as extension of Stokes shift due to stronger intermolecular π−π interaction. This further support the improved planarization and denser packing of the FOPEs compared with the OPEs. Overall, the OPE cores assume a loose aggregation in the LC range, whose planar conformation gradually turns into more twisted conformation upon heating. FOPE with stronger intermolecular interaction has reduced twist and stacks into more ordered packing.
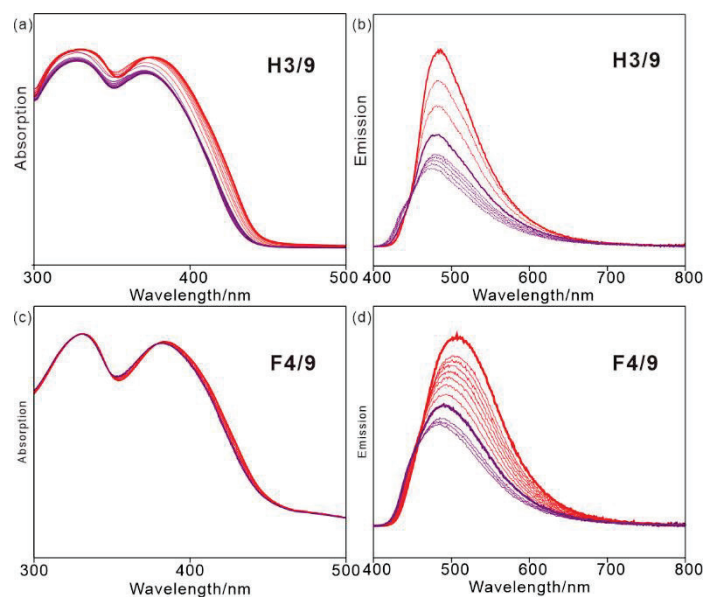

Figure 10. UV-Vis absorption and emission spectra of (a-b) **H3/9**; (c-d) **F4/9.** Color code: red: *p6mm*; purple: *Pm$\bar{3}$n*; the thick lines indicate the phase transition temperatures; for additional examples, see Fig. S10.

This explains the stabilization of the triangular (+10 K) and especially the square honeycomb (+20 K) by core fluorination, observed as long as the side chain volume fits with the prismatic cell volume and

the chain have the appropriate length to reach the centers of the cells (Fig. 7). The non-shifted side-by-side packing of the electron deficit perfluorinated rings in these honeycombs (Fig. 11c(A)) requires some lateral offset of the interacting rings (tangential shift), leading to some out of-plane twist of the benzene rings to optimize the face-to-face interaction (Fig. 11d).[113-116] As the coherence length of the twist direction is only short the scattering corresponding to the π-stacking distance is broad and weak (Fig. 9).
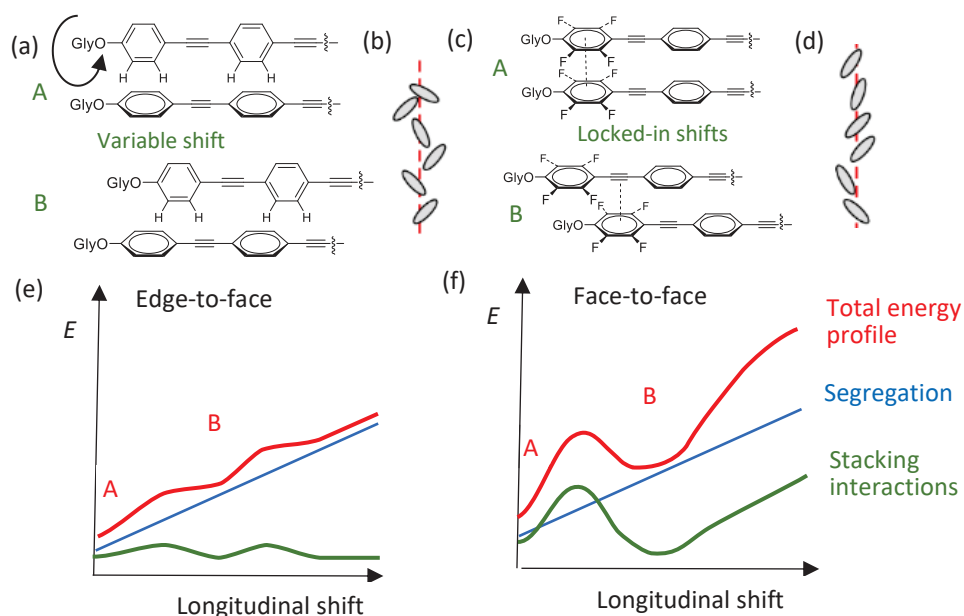
Figure 11. (a-d) Schematics of the rod-packing and (e,f) sketches of their tentative energy profiles depending on longitudinal shift (a-d) views on the packing of the rods in the honeycombs (a, c) view along a short axis (only the two outer rings at one end of the molecules are shown) and (b, d) side-views along the long axes of the rod-like (F)OPE cores, and (e, f) the effects of stacking interactions and glycerol-(F)OPE segregation on the energy profiles of the longitudinal shift between neighboring molecules; (a, b, e) there is an easy longitudinal sliding of the rotationally less ordered non-fluorinated OPE cores due to larger core-core distances (only edge-to-face packing is shown although also face-to-face and other arrangements contribute) and twisted conformations must be considered, while (c, d, f) for the FOPEs the reduced twist allows a denser packing with distinct preferred longitudinal shifts for the distinct face-to-face stacking motifs; Gly = glycerol end groups.

In the region with intermediate side-chain length L_C (Fig. 7) there is a frustration between the spaces and distances provided by the honeycomb framework with fixed side lengths and the volumes and lengths of the side chains, which leads to a reduced stability of the triangular and square honeycombs, thus allowing alternative modes of self-assembly to take place. For most of them the honeycombs are retained albeit with reduced LC-Iso transition temperature (frustration range in Fig. 7). This means that due to the stronger core-core interactions the spitting of the honeycombs into a network of rod-bundles becomes disfavored. Nevertheless, if compared with compounds **H***m/n*, the limited phase range and phase stability of the $Pm\bar{3}n$ phase in the series **F***m/n* is surprising. We attribute the easier formation of the $Pm\bar{3}n$ network in the case of the series **H***m/n* to the larger lateral stacking distance of the OPE cores

18

of compounds **H*m*/*n***, allowing an easy and non-restricted longitudinal shift of adjacent OPE cores (Fig. 11a, e). In contrast, the shorter stacking distance and a preference of face-to-face stacking of the **F*m*/*n*** compounds provides more pronounced energetic minima and maxima for the longitudinal shift (Fig. 11c, f).[117] There is a minimum for the side-by-side packing of the electron deficit perfluorinated benzenes without longitudinal shift as noted above, and a second minimum for the significant shift required for the donor-acceptor packing of the fluorinated benzenes besides the π-electron rich acetylene[118,119] or benzene units of adjacent molecules (Fig. 11c(B)).[120-126] In the $Pm\bar{3}n$ network there are different lengths for the strut bonds connecting the polar glycerol spheroids, requiring a length ratio 1: 1.12: 1.22 which is achieved by deformation of the spheres to spheroids and by some longitudinal shifting of the polyaromatic rod in the bundles to modify the bond length. In the case of compounds **H*m*/*n*** with wider lateral distances between the OPEs a slight shift of neighboring OPEs with respect to one another is easily possible, and thus, the length of the rod-bundles can be precisely adjusted to the required distances. However, for the FOPE cores with a significant contribution of closer face-to-face stacking there are distinct preferred values of the shift which do not fit with the required values, and this provides an energetic penalty for $Pm\bar{3}n$ formation. Due to this mismatch and the small correlation length of the rods in the bundles of the A15 phase (n_{bundle} = 4.1 for **F3/10** and 4.8 for **F4/9**, Tab. S32) face-to-face stacking is difficult to develop and therefore cannot contribute to network stabilization, in line with the absence of a shoulder in the WAXS patterns (Figs. 9b, S5d). Hence, $Pm\bar{3}n$ phase stability is reduced by core-fluorination and in most cases the competing honeycomb phases are preserved.

Honeycomb deformation in the series of fluorinated compounds F*m*/*n*.

Finally, we focus on the deformed square honeycomb phases ($p2mm$ and $c2mm$) induced by core fluorination (Table 2, Fig. 7). One is the angular deformation of the square to a rhombic honeycomb as observed for the low temperature Col_{rec}/$c2mm$ phase of compounds **F11/6**, **F9/7** and **F11/7** with side lengths corresponding to the full molecular length and inner angle of 71-81° (for SAXS patterns and ED maps, see Fig. 8g, h). It is found for compounds with long odd-numbered m (m = 9, 11), i.e. overall even numbered spacers (m+1) considering the ether oxygen. Under the polarizing microscope the transition from $p4mm$ to $c2mm$ is detected by the emergence of biaxiality in the homeotropically aligned areas and a slight increase of Δn of the spherulitic domains (Fig. S3e, f), the first confirms the onset of phase biaxiality and the latter indicating some improvement of the orientational order parameter of the rods in the honeycomb walls during the square to rhomb transition. The rhombic honeycomb is removed for compounds with even number m (i.e. odd numbered m+1; **F10/7, F12/7**)[94] and its stability is reduced as the side-chain length n is increased. The latter is due to the improved space filling in the square cells of long chain compounds, thus reducing the driving force of cell deformation. Hence, there is a preference of rhombic cells for molecules with a linear even numbered spacer m+1 while for bent odd numbered m+1 formation of square cells is supported. It is assumed that the spacer linearity allows a denser parallel chain packing in the rhombic cells, while more disordered chains prefer the square cells with higher symmetry.

For compound **F6/9**, the molecule with the shortest spacer length m and smallest L_C among the $p4mm$ phase forming compounds, being located at the transition to the smaller triangular honeycomb, another mode of prismatic cell deformation is observed (Fig. 8i, j). In this case retaining the 90° angles but modifying the length of two opposite sides of the square honeycomb leads to a $p4mm \to p2mm$ transition on cooling. The parameter $a_{rec} = 4.15$ is in the range of L_{mol}, while $b_{rec} = 3.64$ nm (at $T = 92$ °C) is significantly shorter. There are two different possible types of this kind of transition. One is based on the elliptical deformation of the glycerol columns without tilting, giving rise to a lattice shrinkage in one and a similar expansion in the orthogonal direction, as previously observed for molecules with relatively short core units (e.g. p-terphenyl).[127,128] The second type is caused by the emergence of a tilt in two opposite sides of the square cells.[129] In the case of **F6/9** the length of two opposite sides is almost retained while only the two sides in the orthogonal direction shrink significantly. The transition $p4mm$-$p2mm$ is associated with a decrease of birefringence as indicated by the color change in the spherulitc domains (Fig. S3h-j). Together with the large decrease of one lattice parameter from $a_{squ} = 4.0$ nm to $b_{rec} = 3.64$ nm it is concluded that the cell size shrinkage takes place by tilting the OPE cores out of the crystallographic plane. According to $\beta = \cos^{-1}(b_{rec}/L_{mol})$ and assuming $L_{mol} = 4.4$ nm a tilt angle $\beta = 36°$ can be estimated. This strong tilt which is required for assuming an alternating donor-acceptor core packing reduces the space available in the rectangular cells too much and requires a simultaneous lattice expansion in the orthogonal direction. This leads to a slight elongation of a_{rec} from 4.0 to 4.15 nm in order to adjust the prismatic cell volume to the chain volume by an increasing orientational order parameter of the rods. Because a smaller tilt than 36° is disfavored by the specific core-core interaction between the FOPEs,[129] a simultaneous shrinkage of all honeycomb walls by retaining the square lattice (as found for **H9/6**, Fig. S9g) and assuming a smaller tilt (= longitudinal shift)[97] is obviously not possible. Thus, retaining a non-tilted organization in half of the walls and emergence of a significant tilt in the other half is in line with the proposed restrictions of the intermolecular shift between the FOPE cores (Fig. 10c, f)

It can be concluded that the rhomb tiling ($c2mm$) is replaced by a rectangular tiling ($p2mm$) if the spacer length m falls below a certain limit. Such result is also supported by the dV/dr curves in Fig 6, where $p2mm$ exhibits a shorter tailing than $c2mm$. For longer spacers a difference in space filling is easily compensated by modification of n_{wall} or angular deformation. However, this angular deformation is associated with the tightening of two of the four vertices, which is unfavorable for the packing of the bulky -SiR₃ groups, especially if relatively short spacers restrict their possible arrangements. For these compounds the transition to rectangular cells, retaining the 90° angles and reducing the space in the prismatic cells by tilting some molecules, becomes favorable.

M-phases

In both series **H***m*/*n* and **F***m*/*n* there are additional birefringent mesophases with mosaic-like textures (M) all having yet unsolved complex SAXS patterns and occurring in small temperature ranges or as metastable phases within the steric frustration range associated with the triangle-square transition. At this cross-over several periodic mixed triangle-square tilings and quasicrystalline dodecagonal tiling

patterns are expected to occur.[31,130] The discovery of an A15 tetrahedral rod-sphere packing at the triangle-square cross-over raises the question if there could be a cross-over between the dodecagonal quasicrystals representing sphere packings [131] and those derived from tessellations by polygonal prismatic cells,[132-135] obviously competing with each other in the triangle-square frustration range. If these unknown intermediate phases represent alternative modes of Frank Kasper type networks combining spheres and rods, or complex honeycombs with super-tiling patterns combining different cell shapes is subject of ongoing work.

Conclusions

Segmented network phases, recently predicted for block copolymers[136] and experimentally observed for rod-like bolapolyphiles having bulky side-chains[33-36] represent a new mode of soft self-assembly combining features of bicontinuous and micellar assemblies in a single structure, i.e. they represent sphere (mesoatom) packings interconnected by struts forming the bonds between them. Among them, a Frank Kasper type segmented network phase consisting of tetrahedral rod-packing combined with spheres on a $Pm\overline{3}n$ lattice was found for rod-like bolapolyphiles with properly designed flexible side-chains (Fig. 2c, e).[38,94] It occurs upon increasing side-chain length and side-chain volume as intermediate structure in the sequence $Col_{hex}/p6mm \rightarrow Cub_{net}/Pm\overline{3}n \rightarrow Col_{squ}/p4mm$ at the transition from triangular to square honeycombs (Figs. 5, 7 and 12). It turned out that the side-chain length L_C and especially the length of the oligomethylene spacer m separating the bulky -SiR$_3$ units from the core, i.e. the capability of distant space filling without entropically unfavorable chain stretching, represent the main parameters selecting the phase structure.
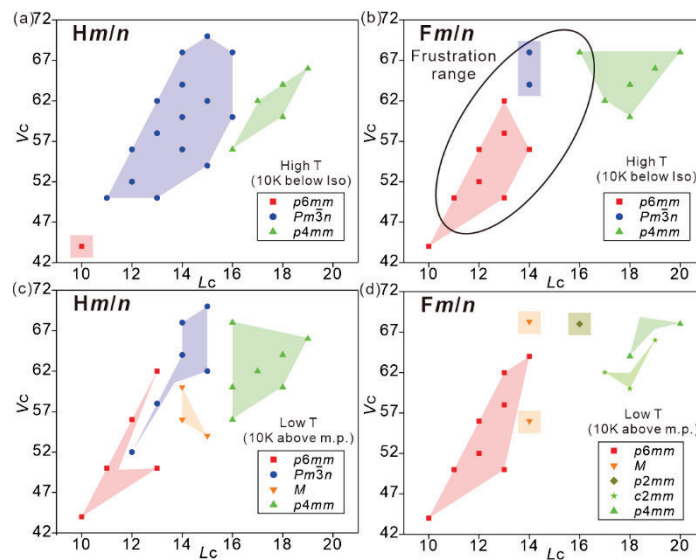

Figure 12. 2D-plots of the phase ranges in the two series **Hm/n** and **Fm/n** depending on side chain volume (V_C) and side chain length (L_C).

Broad ranges of the network type A15 phase were found for compounds with a nonfluorinated OPE core, while for the core-fluorinated compounds there is only a small molecular structural window for A15 phase formation (Fig. 12). This is attributed to a destabilization by the mismatch between required and available length of the bonds interconnecting the meso-atoms. While OPEs allows a continuous adjustment of the bond length by longitudinal shift of the polyaromatic rods with respect to each other (Fig. 10, left side), for the FOPE cores, there are distinct energetic minima restricting the possible degrees of shift (Fig. 10, right side), thus destabilizing the meso-atom bonds in the A15 phase and reducing its range of existence. This restriction in longitudinal shift also affects the organization of the core fluorinated molecules in the honeycomb walls and thus is responsible for the formation of either rhombic or rectangular honeycombs replacing the square honeycombs of some FOPE compounds at lower temperature.

Overall the work highlights the effects of aggregation of π-conjugated rods on self-assembly in reticular LCs. It also provides clues for the rational design of related soft and solid-state materials towards new and more complex architectures, eventually leading to still illusive quasiperiodic networks.[137]

Data Availability

The data that support the findings of this study are available in the supplementary material of this article.

Conflict of interest

None of the authors have a conflict of interest to disclose.

References

1   M. Kumar, S. Kumar, *Polym. J.* **2017**, *49*, 85.

2   Y. Hong, J. W. Y. Lam, B. Z. Tang, *Chem. Soc. Rev.* **2011**, *40*, 5361.

3   Liu, L. H. You, F. X. Lin, K. Fu, W. Z. Yuan, E.-Q. Chen, Z. Q. Yu, B. Z. Tang, *ACS Appl. Mater. Interf.* **2019**, *11*, 3516.

4   Y. Wu, M. Li, Z.-G. Zheng, Z.-Q. Yu, and W.-H. Zhu, *J. Am. Chem. Soc.* **2023**, *145*, 12951.

5   Z.-L. Gong, X. Zhu, Z. Zhou, S.-W. Zhang, D. Yang, B. Zhao, Y.-P. Zhang, J. Deng, Y. Cheng, Y-X. Zheng, S.-Q. Zang, H. Kuang, P. Duan, M. Yuan, C.-F. Chen, Y. S. Zhao, Y.-W. Zhong, B. Z. Tang, M. Liu, *Sci. Chin. Chem.* **2021**, *64*, 2060.

6   J. Liu, Y. Molard, M. E. Prévot, T. Hegmann, *ACS Appl. Mater. Interf.* **2022**, *14*, 2939.

7   Y.-X. Hu, W.-J. Li, P.-P. Jia, X.-Q. Wang, L. Xu, H.-B. Yang, *Adv. Opt. Mater.* **2020**, *8,* 2000265.

8   M. R. Wasielewski, *Acc. Chem. Res.* **2009**, *42*, 1910.

9   J. W. Goodby, J. P. Collings, T. Kato, C. Tschierske, H. F. Gleeson, P. Raynes (Eds,), *Handbook of Liquid Crystals*, 2nd. Ed. Wiley-VCH, Weinheim **2014**.

10   P. J. Collings and J. W. Goodby, *Introduction to Liquid Crystals: Chemistry and Physics* 2nd ed., CRC Press, Boca Raton, FL, **2019**.

11   E.-K. Fleischmann, R. Zentel, *Angew. Chem. Int. Ed.* **2013**, *52*, 8810.

12   H. K. Bisoyi and Q. Li, *Chem. Rev.* **2022**, *122***, 4887.

13   N. Koide, Ed., The Liquid Crystal Display Story, Springer, Tokyo **2014.**

14   R. Iwai, H. Yoshida, Y, Arakawa, S, Sasaki, Y, Iida, K, Igawa, T, Sakurai, S. Suzuki, M, Tokita, J. Watanabe, G. Konishi, *Aggregate* **2024**, e660.

15   J. Uchida, B. Soberats, M. Gupta, T. Kato, *Adv. Mater.* **2022**, 2109063.

16   C. Tschierske, *Angew. Chem. Int. Ed.* **2013**, *52,* 8828.

17   C. Tschierske, *Chem. Soc. Rev.* **2007**, *36*, 1930.

18   C. Tschierske, C. Nürnberger, H. Ebert, B. Glettner, M. Prehm, F. Liu, X. B. Zeng, G. Ungar, *Interface Focus* **2012**, *2*, 669.

19   Z. He, X. Wang, P. Zhang, A.-C. Shi, K. Jiang, *Macromolecules* **2024**, *57*, 2154.

20   R. M. Fuoss, D. Edelson, *J. Am. Chem. Soc.* **1951**, *73,* 269.

21   G. A. Jeffrey, W. Saenger, *Hydrogen Bonding in Biological Structures*, Springer, Berlin, **1994**.

22   E. G. Atovmyan, S. V. Koshchii, T. N. Fedotova, *J. Appl. Spec.* **1988**, *48*, 202.

23   J. S. Lomas, *Magn. Reson. Chem.* **2020**, *58*, 666.

24   C. P. Brock, *Aca Cryst.* B **2002**, *58*, 1025.

25   R. Chelakkot, R. Lipowsky, T. Gruhn, *Macromolecules* **2006**, *39*, 7138.

26   T. D. Nguyen, S. C. Glotzer, *ACS Nano* **2010**, *4*, 2585.

27   S. Poppe, M. Poppe, H. Ebert, M. Prehm, C. Chen, F. Liu, S. Werner, K. Bacia, C. Tschierske, *Polymers* **2017**, *9*, 471.

28   R. Kieffer, M. Prehm, B. Glettner, K. Pelz, U. Baumeister, F. Liu, X. Zeng, G. Ungar, C. Tschierske, *Chem. Commun.* **2008**, 3861.

29   A. Saeed, M. Poppe, M. B. Wagner, S. Hauche, C. Anders, Y. Cao, L. Zhang, C. Tschierske, F. Liu, *Chem. Commun.* **2022**, *58*, 7054.

30   M. Poppe, C. Chen, S. Poppe, C. Kerzig, F. Liu, C. Tschierske*, Adv. Mater.* **2020**, 2005070.

31   B. Glettner, F. Liu, X. Zeng, M. Prehm, U. Baumeister, M. A. Bates, M. Walker, P. Boesecke, G. Ungar, C. Tschierske, *Angew. Chem*. *Int. Ed.* **2008**, *47*, 9063.

32   M. Poppe C. Chen, S. Poppe, F. Liu, C. Tschierske, *Comms. Chem.* **2020***, 3,* 70.

33 X. Cai, S. Hauche, S. Poppe, Y. Cao, L. Zhang, C. Huang, C. Tschierske, F. Liu, *J. Am. Chem. Soc.* **2023**, *145*, 1000.

34 X. Zeng, S. Poppe, A. Lehmann, M. Prehm, C. Chen, F. Liu, H. Lu, G. Ungar, C. Tschierske, *Angew. Chem. Int. Ed.* **2019**, *58*, 7375.

35 S. Poppe, X. Cheng, C. Chen, X. Zeng, R.-B. Zhang, F. Liu, G. Ungar, C. Tschierske, *J. Am. Chem. Soc.* **2020**, *142*, 3296.

36 C. Chen, M. Poppe, S. Poppe, C. Tschierske, F. Liu, *Angew. Chem. Int Ed*. **2020**, *59*, 20820.

37 Y. Sun, F. A. Escobedo, *J. Chem. Theory Comput.* **2024**, *20,* 1519.

38 C. Chen, M. Poppe, S. Poppe, M. Wagner, C. Tschierske, F. Liu, *Angew. Chem. Int. Ed.* **2022**, *61*, e202203447.

39 F. C. Frank, J. S. Kasper, *Acta Cryst.* **1958**, *11*, 184.

40 F. C. Frank, J. S. Kasper, *Acta Cryst*. **1959**, *12*, 483.

41 X.-Y. Liu, X.-Y. Yan, Y. Liu, H. Qu, Y. Wang, J. Wang, Q.-Yun Guo, H. Lei, Xing-Han Li, F. Bian, X.-Y. Cao, R. Zhang, Y. Wang, M. Huang, Z. Lin, E. W. Meijer, T. Aida, X. Kong, S. Z. D. Cheng, *Nature Materials,* **2024**, 23, 570.

42 X.-H. Li,, X. Kuang, X.-Y. Liu, H. Lei, X.-Y. Yan, W. Li, Y. Deng, Y. Wu, Q.-Y. Guo, S. Z.D. Cheng, *Giant* **2023**, 100196.

43 G. R. Stewart, *Physica* C **2015**, *514*, 28.

44 K. Fontell, *Colloid Polym. Sci.* **1990**, *268*, 264.

45 Balmbra, R. R., Clunie, J. S. & Goodman, J. F. *Nature* **1969**, *222*, 1159.

46 V. Luzzati, R. Vargas, P. Mariani, A. Gulik, H. Delacroix, *J. Mol. Biol.* **1993**, *229*, 540.

47 A. Jayaraman, M. K. Mahanthappa, *Langmuir* **2018**, *34*, 2290.

48 K. Borisch, S. Diele, P. Göring, C. Tschierske, *J. Chem. Soc., Chem. Commun*. **1996**, 237.

49 K. Borisch, S. Diele, P. Göring, H. Kresse, C. Tschierske, *Angew. Chem. Int. Ed. Engl.* **1997**, *36*, 2087.

50 M. Huang, C.-H. Hsu, J. Wang, S. Mei, X. Dong, Y. Li, M. Li, H. Liu, W. Zhang, T. Aida, W.-B. Zhang, K. Yue, S. Z. D. Cheng, *Science* **2015,** *348*, 424.

51 V. S. K. Balagurusamy, G. Ungar, V. Percec and G. Johansson, *J. Am. Chem. Soc*., **1997**, *119*, 1539.

52 H.-J. Sun, S. Zhang, V. Percec, *Chem. Soc. Rev.* **2015**, *44*, 3900.

53 X. H. Cheng, K. Das, S. Diele, C. Tschierske, *Langmuir* **2002**, *18*, 6521.

54 T. Jun, H. Park, S. Jeon, S. Jo, H. Ahn, W.-D. Jang, B. Lee, D. Y. Ryu, *J. Am. Chem. Soc.* **2021**, *143,* 17548.

55 B.-K. Cho, *Polym. J.* **2012**, *44*, 475.

56 S. Yazaki, Y. Kamikawa, M. Yoshio, A. Hamasaki, T. Mukai, H. Ohno, T. Kato, *Chem. Lett.* **2008**, *37*, 538.

57 T. Noguchi, K. Kishikawa, S. Kohmoto, *Liq. Cryst.* **2008**, *35*, 1043.

58 X. H. Cheng, S. Diele, C. Tschierske, *Angew. Chem. Int. Ed. Engl.* **2000**, *39*, 592.

59 C. M. Wentz, K. K. Lachmayr, E. H. R. Tsai, L. R. Sita, *Angew. Chem. Int. Ed.* **2023**, *62*, e202302739.

60 I. Bury, B. Heinrich, C. Bourgogne, D. Guillon, B. Donnio, *Chem. Eur. J*. **2006**, *12*, 8396.

61 A. Kohlmeier, D. Janietz, *Chem. Mater.* **2006**, *18,* 1483.

62 N. Komiyama, T. Ohkubo, Y. Maeda, Y. Saeki, N. Ichikuni, H. Masu, H. Kanoh, K. Ohara, R. Takahashi, H. Wadati, H. Takagi, Y. Miwa, S. Kutsumizu, K. Kishikawa, M. Kohri, *Adv. Sci.* **2024**, 2309226

63 D. Sahoo, M. Peterca, M. R. Imam, B. E. Partridge, Q. Xiao, V. Percec, *Giant* **2022**, *10*, 100096.

64 T. Hatano, T. Kato, *Chem. Commun*. **2006**, 1277.

65   Y. Sagara, T. Kato, *Angew. Chem. Int. Ed*. **2008**, *47*, 5175.

66   H. Mukai, M. Yokokawa, M. Ichihara, K. Hatsusaka, K. Ohta *J. Porphyrins Phthalocyanines* **2010**, *14*, 188.

67   V. Percec, M. R. Imam, M. Peterca, D. A. Wilson, R. Graf, H. W. Spiess, V. S. K. Balagurusamy, P. A. Heiney, *J. Am. Chem. Soc*. **2009**, *131*, 7662.

68   M. R. Imam, M. Peterca, Q. Xiao, V. Percec, *Giant* **2022**, *10*, 100098.

69   J. Huang, Z. Su, M. Huang, R. Zhang, J. Wang, X. Feng, R. Zhang, R. Zhang, W. Shan, X.Y. Yan, Q.-Y. Guo, T. Liu, Y. Liu, Y. Cui, X. Li, A.-C. Shi, S. Z. D. Cheng, *Angew. Chem. Int. Ed*. **2020**, *59*, 18563.

70   B. M. Rosen, D. A. Wilson, C. J. Wilson, M. Peterca, B. C. Won, C. Huang, L. R. Lipski, X. Zeng, G. Ungar, P. A. Heiney, V. Percec, *J. Am. Chem. Soc.* **2009**, *131*, 17500.

71   X. Liu, R. Zhang, Y. Shao, L. Xu, G. He, J. Huang, Z.-H. Guo, W.-B. Zhang, W. Tang, K Yue, *ACS Macro Lett.* **2021**, *10*, 844.

72   C.-J. Jang, J.-H. Ryu, J.-D. Lee, D. Sohn, M. Lee, *Chem. Mater.* **2004**, *16,* 4226.

73   X. Cheng, X. Bai, S. Jing, H. Ebert, M. Prehm, C. Tschierske, *Chem. Eur. J.* **2010**, *16*, 4588.

74   S. H. Seo, J. H. Park, G. N. Tew, J. Y. Chang, *Tetrahedron Lett.* **2007**, *48*, 6839.

75   X. Tan, L. Kong, H. Dai, X. Cheng, F. Liu, C. Tschierske, *Chem. Eur. J.* **2013**, *19*, 16303.

76   T. Yasuda, H. Ooi, J. Morita, Y. Akama, K. Minoura, M. Funahashi, T. Shimomura, T. Kato, *Adv. Funct. Mater*. **2009**, *19*, 411.

77   T. Hatano, T. Kato, *Tetrahedron* **2008**, *64*, 8368.

78   X. Feng, R. Zhang, Y. Li, Y.-L Hong, D. Guo, K. Lang, K.-Y. Wu, M. Huang, J. Mao, C. Wesdemiotis, Y. Nishiyama, W. Zhang, W. Zhang, T. Miyoshi, T. Li, S. Z. D. Cheng, *ACS Cent. Sci.* **2017***, 3,* 860.

79   S. Lee, C. Leighton, F. S. Bates, *Proc. Natl Acad. Sci. USA* **2014**, *111*, 17723.

80   A. Reddy, M. B. Buckley, A. Arora, F. S. Bates, K. D. Dorfman, G. M. Grason, *Proc. Natl Acad. Sci. USA* **2018**,*115*, 10233.

81   K. D. Dorfman, *Macromolecules* **2021**, *54*, 10251.

82   K. Kim, M. W. Schulze, A. Arora, R. M. Lewis III, M. A. Hillmyer, K. D. Dorfman, F. S. Bates, *Science* **2017**, *356,* 520.

83   Z. Xu, Q. Dong, W. Li, *Macromolecules* **2024**, *57*, 1869.

84   P. Ziherl, R. D. Kamien, *J. Phys. Chem. B*, **2001**, *105*, 10147.

85   H. Lee, J. Kim, M. J. Park, *Phys. Rev. Mater.* **2024**, *8*, 020302.

86   D. A. Tomalia, S. N. Khanna, *Chem. Rev*. **2016**, *116*, 2705.

87   G. M. Grason, E. L. Thomas, *Phys. Rev. Mater* **2023**, *7*, 045603.

88   X.-Y. Yan, Y. Liu, X.-Y. Liu, H. Lei, X.-H. Li, Y. Wang, W. Li, Q.-Y. Guo, M. Huang, S. Z. D. Cheng, *Phys. Rev. Mater*. **2023**, *7*, 120302.

89   Y. Liu, Q.-Y. Guo, Z. Huang, H. Lei,T. Liu, X.-Y. Yan, F.-G. Bian, Z. Lin, G. Liu, W. Zhang, M. Huang, R. Zhang, S. Z. D. Cheng, *CCS Chem.* **2024**, DOI: 10.31635/ccschem.024.202404791.

90   S. Wang, S. Lee, J. S. Du, B. E. Partridge, H. F. Cheng, W. Zhou, V. P. Dravid, B. Lee, S. C. Glotzer, C. A. Mirkin, *Nat. Mater.* **2022**, *21*, 580.

91   O. M. Yaghi, M. O'Keeffe, N. W. Ockwig, H. K. Chae, M. Eddaoudi, J. Kim, *Nature* **2003**, *423*, 705.

92   U. H. F. Bunz, *Macromol. Rapid Commun.* **2009**, *30*, 772.

93   A. Kreyes, A. Masoud, I. Lieberwirth, R. Mauer, F. Laquai, K. Landfester and U. Ziener, *Chem. Mater.* **2010**, *22*, 6453.

94   C. Anders, M. Wagner, M. Alaasar, V.-M. Fischer, R. Waldecker, Y. Zhao, T. Tan, Y. Cao, F. Liu, C. Tschierske, *Chem. Commun.* **2024**, *60*, 1023.

95   M. Hird, *Chem Soc. Rev.* **2007**, *36*, 2070.
96   M. Poppe, C. Chen, H. Ebert, S. Poppe, M. Prehm, C. Kerzig, F. Liu, C. Tschierske, *Soft Matter* **2017**, *13*, 4381.
97   M. Poppe, C. Chen, F. Liu, M. Prehm, S. Poppe and C. Tschierske*, Soft Matter* **2017**, *13*, 4676.
98   M. Poppe, C. Chen, F. Liu, S. Poppe, C. Tschierske, *Chem. Commun.* **2021**, *57*, 6526.
99   S. Werner, H. Ebert, B.-D. Lechner, F. Lange, A. Achilles, R. Bärenwald, S. Poppe, A. Blume, K. Saalwächter, C. Tschierske, K. Bacia, *Chem. Eur. J.* **2015**, *21*, 8840.
100   M. Poppe, C. Chen, F. Liu, S. Poppe and C. Tschierske, *Chem. Eur. J.* **2017**, *23*, 7196.
101   K. Sonogashira, Y. Tohda and N. Hagihara, *Tetrahedron Lett*, **1975**, *50*, 4467.
102   Y.-C. Chiang, H.-C. Wu, H.-F. Wen, C.-C. Hung, C.-W. Hong, C.-C. Kuo, T. Higashihara and W.-C. Chen, *Macromolecules* **2019**, *52*, 4396.
103   Y. Duan, J.-H. Lin, J.-C. Xiao and Y.-C. Gu, *Org. Chem. Front.* **2017**, *4*, 1917.
104   G. Nagarjuna, A. Kokil, J. Kumar, D. Venkataraman, *J. Mater. Chem.* **2012**, *22*, 16091.
105   R. van Rijsbergen, M. J. O. Anteunis and A. De Bruyn, *J. Carbohydr. Chem.* **1983**, *2*, 395.
106   A. Immirzi, B. Perini, *Acta Cryst. A* **1977**, *33*, 216.
107   C. Tschierske, *Top. Curr. Chem.* **2012**, *318*, 1
108   Y. Xu, Y. Hu, Q. Chen, J. Wen, *J. Mater. Chem.* **1995**, *5*, 219.
109   G. N. Patwari, P. Venuvanalingam, M. Kolaski, *Chem. Phys.* **2013**, *415*,150.
110   S. E. Wheeler, K. N. Houk, *Mol. Phys.* **2009**, *107,* 749.
111   P. V. James, P. K. Sudeep, C. H. Suresh, K. G. Thomas, *J. Phys. Chem. A* **2006**, *110,* 4329.
112   M. Levitus, K. Schmieder, H. Ricks, K. D. Shimizu, U. H. F. Bunz, M. A. Garcia-Garibay, *J. Am. Chem. Soc.* **2001**, *123,* 4259.
113   C. A. Hunter and J. K.M. Sanders, *J. Am. Chem. Soc*. **1990**, *112*, 5525.
114   S. E. Wheeler, *Acc. Chem. Res*. **2013**, *46*, 1029.
115   K. Carter-Fenk, J. M. Herbert, *Phys. Chem. Chem. Phys*. **2020**, *22*, 44870.
116   K. Kishikawa, *Isr. J. Chem*. **2012**, *52*, 800.
117   K. Kishikawa, S. Aikyo, S. Akiyama, T. Inoue, M. Takahashi, S. Yagai, H. Aonuma. S. Kohmoto, *Soft Matter* **2011**, *7*, 5176.
118   A. Kundu, S. Sen, G. N. Patwari, *J. Phys. Chem*. **2020**, *124*, 7470.
119   S. Yamada, M. Morita, T. Agou, T. Kubota, T. Ichikawa. T. Konno, *Org. Biomol. Chem*. **2018**, *16*, 5609.
120   G. W. Coates, A. R. Dunn, L. M. Henling, D. A. Dougherty, R. H. Grubbs, *Angew. Chem. Int. Ed. Engl.* **1997**, *36*, 248.
121   S. A. Sharber, R. N. Baral, F. Frausto, T. E. Haas, P. Müller, S. W. Thomas III, *J. Am. Chem. Soc*. **2017**, *139*, 5164.
122   C. Dai, P. Nguyen, T. B. Marder, A. J. Scott, W. Clegg*,* C. Viney, *Chem. Commun.* **1999**, 2493.
123   C, E. Smith, P. S. Smith, R. L. Thomas, E. G. Robins, J. C. Collings, C. Dai, A. J. Scott, S. Borwick, A. S. Batsanov, S. W. Watt, S. J. Clark, C. Viney, J. A. K. Howard, W. Clegg, T. B. Marder, *J. Mater. Chem*. **2004**, *14*, 413.
124   K. B. Woody, J. E. Bullock, S. R. Parkin, M. D. Watson, *Macromolecules* **2007**, *40,* 4470.
125   L. Shua. M. Mayor, *Chem. Commun.* **2006**, 4134.
126   S. Yamada, T, Konno, *Chem. Rec.* **2023**, *23*, e202300094.
127   A. Lehmann, A. Scholte, M. Prehm, F. Liu, X. Zeng, G. Ungar, C. Tschierske, *Adv. Funct. Mater.* **2018**, *28*, 1804162.

26

128 S. Poppe, A. Lehmann, M. Steimecke, M. Prehm, Y. Zhao, C. Chen, Y. Cao, F. Liu, C. Tschierske, *Giant* **2024**, *18*, 100254.

129 C. Anders, V.-M. Fischer, T. Tan, M. Alaasar, R. Waldecker, Y. Ke, Y. Cao, F. Liu, C. Tschierske, *J. Mater. Chem. C.* **2024**, DOI: 10.1039/d4tc04076.

130 P. A. Stampfli, *Helv. Phys. Acta* **1986**, *59*, 1260.

131 X. Zeng, G. Ungar, Y. Liu, V. Percec, A. E. Dulcey, J. K. Hobbs, *Nature* **2004**, *428*, 157.

132 K. Hayashida, T. Dotera, A. Takano, Y. Matsushita, *Phys. Rev. Lett.* **2007**, *98*, 195502.

133 X. Zeng, B. Glettner, U. Baumeister, B. Chen, G. Ungar, F. Liu, C. Tschierske, *Nat. Chem*. **2023**, 15, 625.

134 Y. Cao, A. Scholte, M. Prehm, C. Anders, C. Chen, J. Song, L. Zhang, G. He, C. Tschierske, F. Liu, *Angew. Chem. Int. Ed.* **2023**, *63*, e202314454.

135 M. Imperor-Clerc, P. Kalugin, S. Schenk, W. Widdra, S. Förster, *Phys. Rev. B* **2024**, *110*, 144106.

136 L. Li, Q. Dong, W. Li, *Macromolecules* **2023**, *57*, 409.

137 J. J. Oppenheim, G. Skorupskii, M. Dinca, *Chem. Sci.* **2020**, *11*, 11094.

Publication C

Modifying the liquid crystalline chessboard tiling - Soft reticular self-assembly of side-chain fluorinated polyphiles

C. Anders,[a] V.-M. Fischer,[b] T. Tan,[c] M. Alaasar,[a] R. Waldecker,[b] Y. Ke,[d] Y. Cao,[c*] F. Liu,[c] C. Tschierske[a*]

[a]Institute of Chemistry, Martin-Luther University Halle-Wittenberg, Kurt-Mothes Str. 2, D-06120 Halle/Saale, German.
[b]Institute of Mathematics, Martin-Luther University Halle-Wittenberg, Theodor-Lieser-Str. 5, 06120 Halle, Germany.
[c]Shannxi International Research Center for Soft Matter, State Key Laboratory for Mechanical Behavior of Materials, Xi'an Jiaotong University, Xi'an 710049, P. R. China.
[d]China Spallation Neutron Source, Institute of High Energy Physics, Chinese Academy of Science, Dongguan 523000, P. R. China.
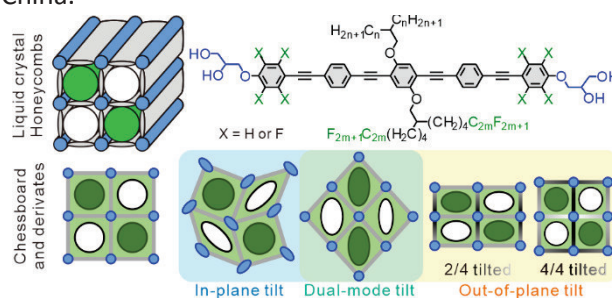
Abstract

Development of new functional materials requires the understanding of the fundamental rules of complex superstructure formation in self-assembling systems. Here we report new liquid crystalline honeycombs based on reticular self-assembly of bolapolyphilic rods with two mutually incompatible and branched side-chains, one a semiperfluorinated, the other one a non-fluorinated alkyl chain, all derived from the chessboard tiling by cell deformation due to distinct modes of tilting of π-conjugated rods within or out of the crystallographic plane. Among them the new square + rhomb tiling and a stretched rectangular "chessboard" tiling, both with alternately filled prismatic cells, are constructed. Out of plane tilting leads to cell shrinking and cell deformation. Nonfluorinated polyaromatic cores allow a continuously changing tilt, retaining the square cells by simultaneously tilting all molecules, associated with an inversion of the birefringence via an optically isotropic state. In contrast, fluorinated cores with different discrete face-to-face stacking modes can assume only discrete tilt angles, which provides rectangular cells with only two walls being tilted. The system offers even more phases including single-color cells with sparingly packed "voids" and a three-color rhomb tiling with additional mixed cells. The research uncovers basic rules of reticular self-assembly by formation of soft multifunctional liquid-crystalline materials.

Check for updates

Modifying the liquid crystalline chessboard tiling – soft reticular self-assembly of side-chain fluorinated polyphiles†

Christian Anders,[a] Virginia-Marie Fischer,[b] Tianyi Tan,[c] Mohamed Alaasar, [ID][a] Rebecca Waldecker,[b] Yubin Ke,[d] Yu Cao, [ID]*[c] Feng Liu [ID][c] and Carsten Tschierske [ID]*[a]

Development of new functional materials requires the understanding of the fundamental rules of complex superstructure formation in self-assembling systems. Here we report new liquid crystalline honeycombs based on reticular self-assembly of bolapolyphilic rods with two mutually incompatible and branched side-chains, one a semiperfluorinated, the other one a non-fluorinated alkyl chain, all derived from the chessboard tiling by cell deformation due to distinct modes of tilting of π-conjugated rods within or out of the crystallographic plane. Among them the new square + rhomb tiling and a stretched rectangular "chessboard" tiling, both with alternatingly filled prismatic cells, are constructed. Out of plane tilting leads to cell shrinking and cell deformation. Nonfluorinated polyaromatic cores allow a continuously changing tilt, retaining the square cells by simultaneously tilting all molecules, associated with an inversion of the birefringence *via* an optically isotropic state. In contrast, fluorinated cores with different discrete face-to-face stacking modes can assume only discrete tilt angles, which provides rectangular cells with only two walls being tilted. The system offers even more phases including single-color cells with sparingly packed "voids" and a three-color rhomb tiling with additional mixed cells. The research uncovers basic rules of reticular self-assembly by formation of soft multi-functional liquid-crystalline materials.

1. Introduction

Liquid crystals (LC) are important advanced materials for application in many fields of modern technology, such as electro-optics, adaptable optics, photonics,[1,2] for biomedical sensing[3] and engineering, for telecommunication devices[4] and in displays for augmented reality[5] to mention only a few.[6–9] Conventional LCs were based on rigid rod-like or disc-like molecules decorated with soft alkyl chains, leading to the classical LC phases such as nematic, smectic and columnar.[6] After recognition of the importance of amphiphilicity and nano-segregation for soft self-assembly[10] attempts were made to create new LC phases and to increase the

complexity of LC self-assembly[11,12] towards that required for development of prebiotic structures[13–15] and for novel functions useful in materials science. Early work in this direction was pioneered by H. Ringsdorf, who pointed out the importance of liquid-crystalline self-assembly for structure formation as required in materials science and life science by the unique combination of order with mobility in this state of matter.[16] His group also pioneered the idea of micro-segregation of siloxane-[17] and perfluoroalkyl units[18] as building blocks to modify the properties of LC materials. A part of this work was conducted in collaboration between his group at Mainz University and the LC research groups at Halle University already in the 1980's as an example of east–west collaboration during the Cold-War before the re-unification of Germany[19]. Such farsighted, integrative and charismatic persons like Prof. Ringsdorf would be highly beneficial in today's world.

Inspired by these early contributions of H. Ringsdorf, we developed the concept of polyphilic self-assembly as a tool to organize π-conjugated rods into well-defined complex LC superstructures combining order and mobility. One class of such compounds is provided by the T-shaped, X-shaped, Π-shaped *etc.* molecules based on a simple rod-like unit with sticky hydrogen bonded glycerols at each end and one, two or more flexible side-chains (see for example Fig. 1(a)).[6,20,21] Depending on the rod-length, side-chain number, their length and volume,

[a] *Institute of Chemistry, Martin-Luther University Halle-Wittenberg, Kurt-Mothes Str. 2, D-06120 Halle/Saale, Germany. E-mail: Carsten.tschierske@chemie.uni-halle.de*

[b] *Institute of Mathematics, Martin-Luther University Halle-Wittenberg, Theodor-Lieser-Str. 5, 06120 Halle, Germany*

[c] *Shannxi International Research Center for Soft Matter, State Key Laboratory for Mechanical Behavior of Materials, Xi'an Jiaotong University, Xi'an 710049, P. R. China. E-mail: yu.cao@xjtu.edu.cn*

[d] *China Spallation Neutron Source, Institute of High Energy Physics, Chinese Academy of Science, Dongguan 523000, P. R. China*

† Electronic supplementary information (ESI) available. See DOI: https://doi.org/10.1039/d4tc04076g
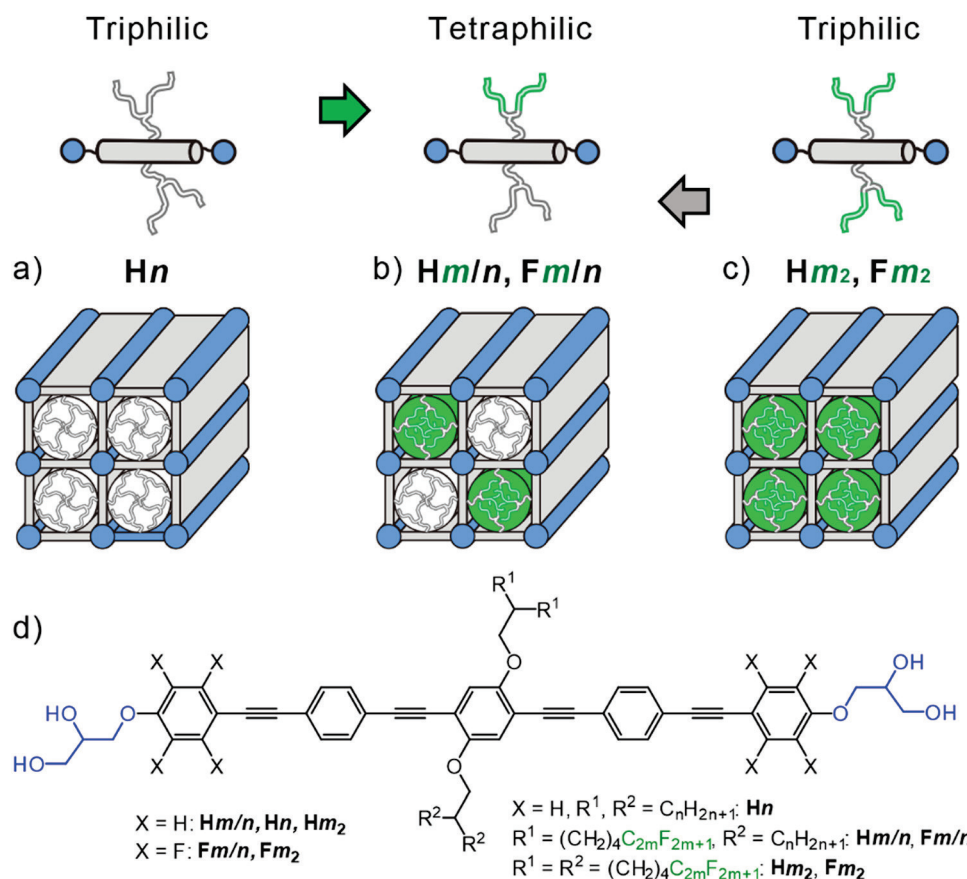
Fig. 1 (a)–(c) Schematics of the bolapolyphiles under discussion and the different types of square honeycomb LC phases; (a) and (c) simple square tilings and (b) chessboard tiling; aromatic cores are in grey, hydrophilic ends are in blue, alkyl side chains are in white and perfluorinated side chains are in green, the cylinders indicate the core shell structure inside the honeycombs cells; (d) shows the structure of the compounds under discussion and used abbreviations; the capital letters **H** and **F** indicate non-fluorinated (OPE) and fluorinated cores (FOPE), respectively; **H**n stands for the previously reported compounds with two branched alkyl side-chains (R_H with n = length of each branch);[25] compounds **H**m_2 and **F**m_2 have both side-chains with perfluorinated end groups (R_F chains, m = length of the R_F segment, the aliphatic spacer length is $(CH_2)_4$ in all cases), while compounds **H**m/n and **F**m/n combine R_H and R_F chains.

these molecules form LC networks[22,23] and LC honeycomb structures.[24,25] In the honeycombs, the π-conjugated rod-like cores lie perpendicular to the column long axis, held together at the edges by columns formed by the hydrogen bonded glycerol end groups. The resulting prismatic cells are filled by the flexible side-chains.[20,21] Depending on the side-chain volume and the length of the rigid rod-like core, different types of honeycombs were observed, such as triangular, square, pentagonal, and hexagonal, among them also giant honeycombs,[26] superlattices with dodecagonal[27] and octagonal motifs[28,29] and liquid quasicrystalline phases.[30,31] Some of these honeycombs with uniform filling of their prismatic cells have recently also been reproduced by different simulation techniques[32–41] and were found for block copolymers and giant molecules on a larger length scale.[42–47]

Different types of side chains can be used to further increase the structural diversity and complexity of honeycomb LCs by tiling patterns where different chains segregate into distinct prismatic cells, thus leading to so-called multi-color tilings where the cells, arranged in a regular periodic manner, are filled by different materials (Fig. 1(b)); the "color" stands for different contents of the prismatic cells.[28,48–56]

Here we report a new class of tetraphilic star-shaped compounds named as **H**m/n. These newly synthesized compounds are based on a rod-like OPE core[57–61] having glycerol end-groups and different branched chains at opposite sides, one being an alkyl chain (R_H) and the other one with perfluorinated ends (R_F), see Fig. 1(b). As aromatic fluorination is known to have a significant effect on LC self-assembly by introducing polarity[62–64] and modifying the core–core interactions,[65–67] two series of compounds were prepared, one with a non-fluorinated OPE core (**H**m/n) and a second one with an OPE core having perfluorinated outer benzene rings[61,68] (FOPEs, compounds **F**m/n, Fig. 1(d)). In addition, the compounds **H8**$_2$ and **F8**$_2$ with two identical R_F side-chains were synthesized and investigated for comparison purposes.

The new LC phases involve a square + rhomb tiling and a stretched rectangular "chessboard" tiling, both with alternating prismatic cells filled by either fluorinated or hydrocarbon chains and a three-color rhomb tiling with additional mixed cells. All structures are derived from the simple chessboard tiling by tilting of the molecular rods, either in the crystallographic plane, or out-of-plane, leading to cell deformation and cell shrinking, respectively. Non-fluorinated polyaromatic rod-like cores allow a continuously changing tilt, retaining the square cells by

simultaneously tilting all molecules, associated with an inversion of the birefringence *via* an optically isotropic state. In contrast, fluorinated cores with different discrete face-to-face stacking modes can assume only discrete tilt angles, which provides rectangular cells with only two walls being tilted. This work provides a guide for bottom-up preparation of complex soft functional arrays of π-conjugated rods at the sub-5 nm scale for use in soft lithography[69] for programmable metafilm[70] and selective absorber.[71] The gained knowledge is also of importance for the construction of new solid-state hydrogen bonded and covalent organic frameworks,[45,72,73] where preparation of multiporous structures combining different cells is still a challenge.[74–76]

2. Results and discussion

2.1 Compound H8₂ with two fluorinated side-chains at the non-fluorinated OPE core – emerging tilt, inversion of birefringence and "void" spaces

Compound **H8₂** with two identical branched fluorinated chains (Fig. 2(a)) was investigated as reference compound for the

evaluation of the specific effects provided by the R_F/R_H combination. The optical texture of **H8₂** between crossed polarizers indicate spherulite-like domains with isotropic areas as typical for optical uniaxial columnar LC phases (Fig. 2(c)). Upon cooling there is a strong change of the birefringence as indicated by a color change in the spherulite-like areas, starting around 180 °C. The birefringence (Δn) changes from being negative to $\Delta n = 0$ at 40 °C, at which temperature the texture becomes completely dark (isotropic) and then assumes a deep blue birefringence color after Δn inversion to positive (see Fig. 2(c) and Fig. S8, ESI†). Such a behavior is due to the emergence and growth of a tilt of the rod-like π-conjugated OPE cores in the cylinder walls around the prismatic honeycomb cells, crossing the tilt angle of 35.3° at the Δn inversion point.[27,57] This boundary between negative and positive birefringence is observed if the slow optical axis of the π-conjugated rods assumes the magic angle of 54.7° with respect to the column long axis, *i.e.* 90°–54.7° = 35.3° tilt with respect to the lattice plane.

In the whole LC temperature range on heating and on cooling down to 30 °C the WAXS is diffuse (inset in Fig. 2(e)), as typical for mesophases with no fixed positions of the
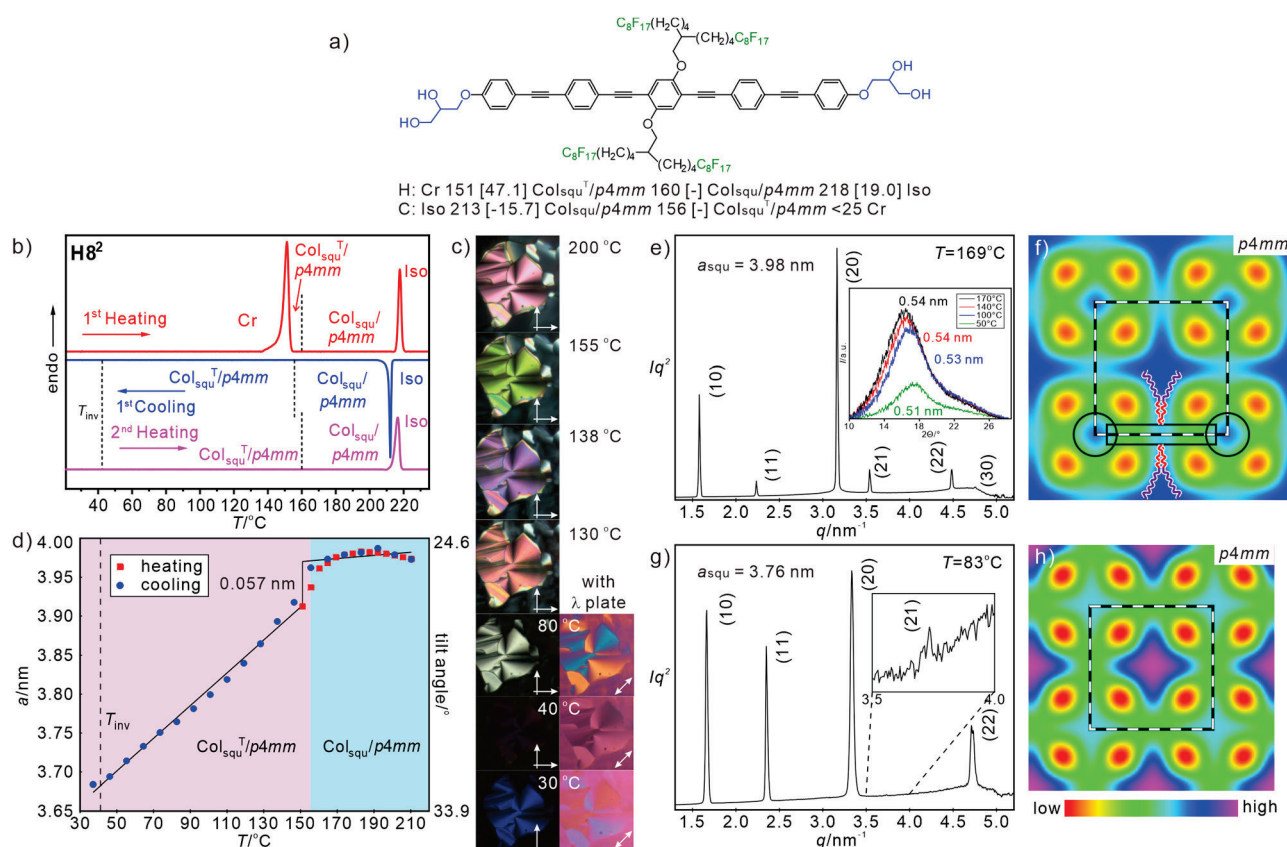

Fig. 2 (a) Formula of **H8₂** with transition temperatures (T/°C) and transition enthalpies (ΔH/kJ mol⁻¹), (b) DSC traces, (c) textures as observed between crossed polarizers at the given temperatures, those at the very right are with additional λ-retarder plate, where blue fans in SW−NE direction indicate negative Δn and in NW−SE direction indicate positive Δn, for additional and enlarged textures, see Fig. S8 (ESI†); (d) $a_{squ} = f(T)$ plot, the transition between tilted/non-tilted squares is indicated; (e) and (g) SAXS patterns at the given temperatures (for numerical data, see Tables S10 and S11, ESI†), inset in (e) shows the WAXS (for numerical data, see Table S2, ESI†) and (f), (h) ED maps reconstructed from these patterns (phase choices 000ππ for the first five peaks); lattice is shown by white dashed lines, tiles with molecules along edges are in black dashed lines and in (f) a molecular model is drawn according to the shape and size of **H8₂**, black rectangle indicates the aromatic core and the black circles indicate the glycerol nodes.

individual molecules. Together with the fluidity of the compounds this confirms the LC state. The diffuse scattering has a significant tailing towards larger 2θ-values (inset in Fig. 2(e)) and can be separated into a major scattering with maximum at 0.51–0.54 nm, corresponding to the mean distance between the R_F chain segments, and a wider diffuse scattering with a maximum around 0.48 nm (Fig. S10a, c, ESI†). The latter is attributed to the mean distance between the hydrocarbon segments (oligomethylene spacers and polyaromatic OPE cores) and the glycerol of the molecules. The absence of a distinct scattering around 0.36–0.38 nm shows that the OPE cores have a relatively loose packing and can rotate almost freely around their long axes, thus assuming different core–core interaction motifs with different distances, including edge-to-face,[77] face-to-face and other intermediate geometries, separated by relatively small energy barriers.[78]

The SAXS pattern can be indexed to a square lattice with $p4mm$ plane group (ratio of d-spacings: $1:1/\sqrt{2}:1/2:1/\sqrt{5}:1/\sqrt{8}\ldots$, see Fig. 2(e) and (g)). The lattice parameter at $T = 169\ °C$ is $a_{squ} = 3.97$ nm which is only slightly smaller than the value typically found for the previously reported R_H substituted compounds $\mathbf{H}n$ ($a_{squ} \sim 4.1$ nm)[25] and is in the range of the molecular length ($L_{mol} = 4.0–4.4$ nm as measured between the ends of the glycerols, depending on the assumed glycerol conformation), thus confirming a square honeycomb with the prismatic cells filled by the side-chains.

Just below the Iso-to-$Col_{squ}/p4mm$ phase transition there is a relatively broad orientational order parameter distribution for the OPE rods in the walls, leading to an effective molecular length of about 4.0 nm. In the $Col_{squ}/p4mm$ range between 210 and 156 °C there is no significant change of birefringence (Fig. S8a–e, ESI†) and a_{squ} (Fig. 2(d)). Upon cooling to ~ 190 °C a tiny increase of a_{squ}, indicates an improving order parameter and below ~ 180 °C a_{squ} starts decreasing. The decrease is small to 156 °C and we attribute it to the development of short-range tilt domains growing in size (Fig. S15, ESI†). At 156 °C there is a small but clearly visible jump to smaller a_{squ}, where the molecules assume a long range correlated tilt with further increasing angle (β) on cooling. This transition to $Col_{squ}^{T}/p4mm$ (T stands for tilted) is not associated with a visible DSC peak (Fig. 2(b)) and therefore considered as a weakly first order phase transition, similar to the SmA–SmC transitions in smectic LCs. On further cooling, the lattice parameter decreases almost linearly to a value of $a_{squ} = 3.68$ nm at 37 °C (Fig. 2(d)), corresponding to the temperature of the inversion of birefringence. The calculated tilt of the OPE rods in the honeycomb walls at this temperature is $\beta = 33.2°$ according to $\beta = \cos^{-1}(a_{squ}/L_{mol})$ with $L_{mol} = 4.4$ nm, which is close to the Δn inversion angle of 35.3°.[57] The slight difference is due to uncertainties about the assumed molecular length used for tilt angle calculation, to the uncertainties concerning the orientational order parameter in the walls formed by tilted molecules, and to small contributions of other molecular parts and "form-birefringence" (caused by the columnar structure itself[79]) to the total birefringence. It is noted, that the inversion takes place within the $Col_{squ}^{T}/p4mm$ range and is not associated with the $Col_{squ} \rightarrow Col_{squ}^{T}$ transition or any other phase transition.

It indicates the temperature of $\sim 35°$ tilt crossing and the higher this inversion temperature, the larger is the driving force for tilting.

The electron density (ED) map of the $Col_{squ}/p4mm$ phase, reconstructed from the SAXS pattern at 169 °C (Fig. 2(e) and (f)) shows a square grid with high ED (blue, purple) which is filled by green medium ED areas with high ED dot (light blue) in the middle, and four low ED dots (yellow/red) in the corners. The light blue dots are assigned to the columns of the glycerols which are interconnected by the OPE rods, while the cells are filled by the high ED areas of the R_F chains together with the medium ED areas resulting from the mixing of R_F segments with the aliphatic spacer units. There is highest ED in the middle of the cells where the R_F chains are concentrated. Somewhat enhanced ED is also found in the middle of the aromatic rods due to the central benzene rings with two electron-rich oxygens. The red low ED dots in the corners of the square honeycomb can only partly be attributed to the low ED aliphatic spacers and mainly to a reduced packing density in the periphery around the R_F cores, because the relatively short and rigid fluorinated chains[52,53] cannot pack sufficiently dense to completely fill the space in the corners of the square cells (see Fig. S18a, ESI†). A related phenomenon was observed in the confined space of micellar aggregates of taper shaped dendritic molecules with relatively rigid peptide based polar groups[80] and in the LC phases of rigid star-shaped molecules.[81] In our case the "voids" are tolerated, because the cohesive energy density of perfluorinated chains is low,[52,53] and hence, the energetic penalty caused by these sparingly packed spaces becomes relatively small. Upon further cooling, the shrinkage of side chains induces a transition to $Col_{squ}^{T}/p4mm$ (Fig. 2(g) and (h)). Due to a stronger restriction of the packing of the rigid fluorinated chain segments and the further R_F chain rigidification, the packing problem is retained (compare red dots in the ED maps in Fig. 2(f) and (h)). Such problem provides a driving force for partial chain mixing and core–shell formation in the honeycomb LC phases of compounds $\mathbf{H}m/n$ as will be discussed in the following section.

2.2 Compound H8/16 with different side chains at the non-fluorinated OPE core – tilted and non-tilted chessboard tilings

To construct tunable multicolor tilings, applicable as functional materials, one of the semiperfluorinated chains is replaced by a longer alkyl chain of approximately the same volume, generating the $\mathbf{H}m/n$ compounds. The transition temperatures and observed mesophases of the three synthesized tetraphilic compounds $\mathbf{H}m/n$, together with the corresponding transition enthalpy values and major structural data of the mesophases are collated in Table 1. The LC-Iso transition temperatures, i.e. the stability of the LC phases against thermal agitation increases in the order $\mathbf{H16}^{[25]}$ (141 °C) $\ll \mathbf{H8/16}$ (212 °C) $< \mathbf{H8_2}$ (218 °C) by increasing degree of side-chain fluorination. This is mainly due to the stronger incompatibility of the R_F segments with the polyaromatic cores and the glycerol units compared to the aliphatic side chains, and the additional incompatibility between R_F chains and hydrocarbon units (R_H chains and $(CH_2)_4$ spacers), both enhancing the stability
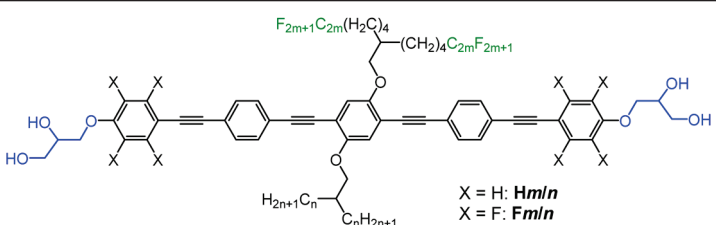
Journal of Materials Chemistry C

Paper

of the self-assembled LC phase.[53,82,83] The relatively small stability increase from **H8/16** to **H8₂** is partly due to the reduced contribution of R_F/R_H segregation and the formation of loosely packed ''voids'' in the $Col_{squ}/p4mm$ phase of **H8₂** (see above).

For compound **H8/16** with mixed side-chains of approximately identical side-chain volume at both sides and also similar side-chain volume as **H16**[25] and **H8₂**, an optically uniaxial columnar LC phase with spherulite-like texture and large optically isotropic (dark) areas is observed by POM in the whole LC phase range below 202 °C (Fig. S4, ESI†). On cooling, the LC phase is retained down to RT and recrystallization cannot be observed in the second and following heating/cooling DSC scan (Fig. S1d, ESI†), as also found for **H8₂**. The SAXS pattern indicates a square lattice (ratio of d-spacings: $1:1/\sqrt{2}:1/2:1/\sqrt{5}:1/\sqrt{8},\ldots$) with a lattice parameter of $a_{squ} = 5.6$ nm at 169 °C (see Fig. 3(a)). The molecular length corresponds approximately to half of the diagonal of the square lattice of $1/2\sqrt{2} \times a_{squ} = 4.0$ nm. This square lattice can thus be interpreted as a chess-board two-color tiling with alternating fluorine rich and hydrocarbon rich square cells ($Col_{squ}/p4mm^L$, where the superscript ''L'' indicates the larger superlattice due to two-color tiling), as confirmed by the reconstructed ED map in Fig. 3(b), where purple/blue areas indicate high ED provided by the R_F chains and red/yellow low ED provided by the alkyl chains located in the middles of the alternating square prismatic cells. We note that the decreasing ED in the center of R_F columns (purple → blue) is due to the insufficient length of semifluorinated chain as illustrated by the space filling molecular models in Fig. S18a (ESI†). The square network with medium ED (green color) is formed by the end-to-end connected OPE rods interconnected by the hydrogen bonding networks in the polar columns of the glycerols at the 4-way junctions. Both, the R_F and R_H chain columns are surrounded by uniform medium ED shells (green) without any indication of additional (red) low ED regions. The partial mixing of R_F and R_H chains provides a similar ED as the aromatic cores and the glycerol columns, all together forming a green medium ED continuum. This R_F/R_H chain mixing is obviously required to achieve optimal and uniform space filling in all cells. Especially the space filling around the R_F columns where the alkylene spacers of the semifluorinated side-chains are located is difficult to achieve with exclusively R_F chains. In order to improve space filling, some R_H side chains are required to be incorporated into the aliphatic periphery around the R_F chains and mixed between the aliphatic spacer units, thus removing any loosely packed areas (Fig. S18c, ESI†). Because R_H and R_F chains are fixed to opposite sides of the OPE cores, this partial mixing of the R_H chains into the R_F cells requires the mixing of their R_F chains at the opposite side into the adjacent R_H-filled cells. Thus, also a mixed R_F/R_H shell develops around the R_H cores.

Table 1 LC phases, transition temperatures, associated enthalpy values, lattice parameters and major structural data of compounds **H***m/n* and **F***m/n*[a]

H*m/n*	Phase sequence T/°C [ΔH kJ mol⁻¹]	T_{inv}/°C	a, b/nm (T/°C)	n_{wall}	L_{wall}
H8/16	H: Cr 96 [48.5] $Col_{squ}^T/p4mm^L$ 160 [–] $Col_{squ}/p4mm^L$ 212 [24.9] Iso	73	5.55 (169)	1.2	3.92
	C: Iso 202 [–20.2] $Col_{squ}/p4mm^L$ 160 [–] $Col_{squ}^T/p4mm^L$ < 20 Cr		5.02 (46)	1.0	3.55
H8/14	H: Cr 104 [47.1] $Col_{squ}^T/p4mm^L$ 162 [1.2] $Col_{squ}/p4mm^L$ 200 [18.3] Iso	105	5.57 (183)	1.3	3.94
	C: Iso 197 [–18.7] $Col_{squ}/p4m m^L$ 161 [–0.8] $Col_{rec}^T/p2mm^L$ 119 [–] $Col_{squ}/p4mm^L$ < 20 Cr		10.41; 5.20 (119)	1.1	3.67
			4.99 (74)	1.0	3.53
H7/14	H: Cr < 20 $Col_{squ}^T/p4mm^L$ 151 [2.3] $Col_{squ}/p4gm$ 194 [16.4] Iso	118	8.08 (169)	1.37	4.27
	C: Iso 188 [–14.7] $Col_{squ}/p4gm$ 137 [–3.9] $Col_{squ}^T/p4mm^L$ < 20 Cr		8.21 (142)	1.42	4.34
			4.96 (101)	1.0	3.51
F8/16	H: Cr 78 [53.6] $Col_{rec}^{T/2}/c2mm$ 193 [4.0] $Col_{squ}/p4mm^L$ 197 [29.5] Iso	—	5.61 (192)	1.2	3.97
	C: Iso 193 [–34.8] $Col_{squ}/p4mm^L$ 191[b] $Col_{rec}^{T/2}/c2mm$ 26 [–24.0] Cr		8.32, 6.77 (146)	1.1	4.16/3.38
F8/14	H: Cr 81 [49.4] $Col_{rec}^{T/2}/c2mm$ 191 [4.4] $Col_{squ}/p4gm + p4mm^L$ 195 [26.7] Iso	—	5.54 (189)	1.2	3.92
	C: Iso 192 [–27.4] $Col_{squ}/p4gm + p4mm^L$ 189 [–4.4] $Col_{rec}^{T/2}/c2mm$ 25 [–17.7] Cr		8.09 (189)	1.3	4.29
			8.17, 6.43 (156)	1.1	4.09/3.21
			7.86, 6.22 (74)	1.0	3.93/3.11
F7/14	H: Cr 35 [21.5] $Col_{rec}^{T/2}/c2mm$ 183 $Col_{squ}/p4gm + M1$ 186 [27.8][b] Iso	—	8.20 (178)	1.4	4.33
	C: Iso 182 [–22.6] $Col_{squ}/p4gm + M1$ 177 [–5.0][c] $Col_{rec}^{T/2}/c2mm$ 24 [–21.5] Cr		8.10, 6.02 (156)	1.0	4.06/3.01

[a] Transition enthalpies and peak temperatures from 1st DSC heating (H)/cooling (C) scans at 10 K min⁻¹ (see Fig. 4(a) and Fig. S1a and d, ESI for DSC traces); abbreviations: n_{wall} = average number of molecules in the lateral cross section of the honeycomb walls with a height of 0.45 nm; L_{wall} = distance between the centers of the polar glycerol columns along the honeycomb walls; Cr = crystalline solid; $Col_{squ}/p4mm^L$, $Col_{squ}/p4mm^L$ = two color chessboard tiling; superscript ^{L} indicates a large lattice due to the multicolor tiling; superscript ^{T} indicates a tilted organization in the honeycomb walls; $Col_{squ}/p4gm$ = two color square-rhomb tiling; $Col_{squ}^T/p2mm^L$ = 3-color tiling by slightly rhombic cells, see Fig. 4(d); $Col_{rec}^{T/2}/c2mm$ = two color tiling by rectangular cells, formed by a combination of tilted and non-tilted walls; M1 = unknown birefringent mesophase; Iso = isotropic liquid; SAXS data were recorded in cooling scans; for more structural data, see Table S22 (ESI). [b] Transitions are not resolved, the enthalpy value includes both transitions. [c] The transition M1 to $Col_{rec}^{T/2}/c2mm$ is slow and takes place between 177 and 140 °C, see Fig. S5c–f.
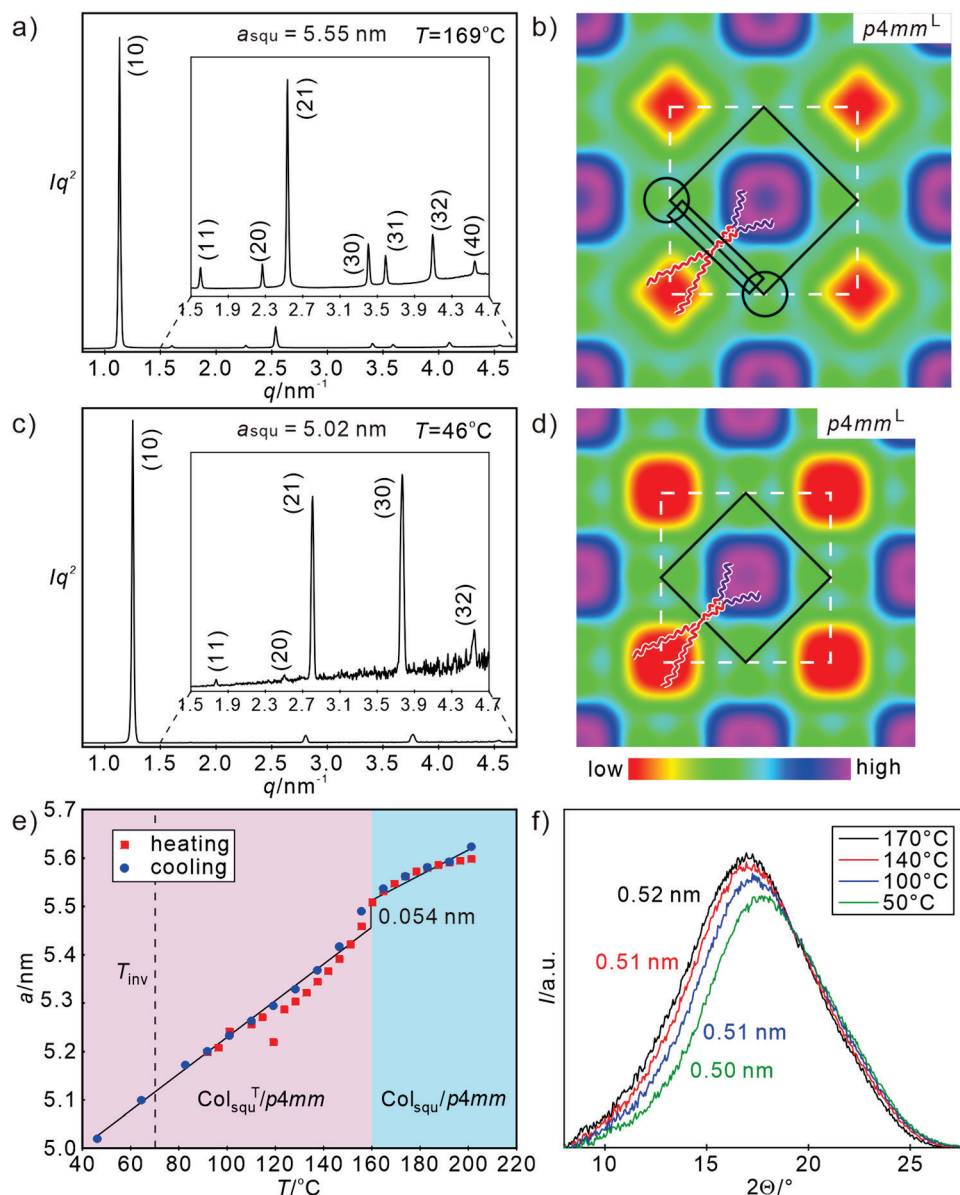
Fig. 3 (a) and (c) SAXS patterns (for numerical data, see Tables S8 and S9, ESI†) and (b) and (d) reconstructed ED maps of the $Col_{squ}/p4mm^L$ phase of **H8/16** at 169 °C and 46 °C, respectively (phase choices $00\pi0\pi\pi\pi\pi$ and $00\pi0\pi\pi$); white dashed lines indicate the unit cell and solid black lines the shape of one honeycomb cell, in (b) a molecular model is drawn, black rectangle indicates the aromatic core and the black circles indicate the glycerol nodes; (e) shows the temperature dependence of a_{squ}; (f) shows the diffuse WAXS scatterings at different temperatures (for numerical WAXS data, see Table S1, ESI†). For DSC data and textures, see Fig. S1d and S4 (ESI†).

The mixing allows optimized space filling in both types of cells and increases the entropy, both stabilizing the chess board tiling. However, chain mixing also creates additional interfaces, leading to a kind of core–shell structure of the prismatic cells in the honeycombs. Hence, the chessboard has differently colored cores surrounded by mixed shells.

The diffuse WAXS pattern, confirming the LC state has its maximum around 0.50–0.52 nm (Fig. 3(f)), being slightly shifted to shorter distances compared to **H8₂**, in line with a partial R_F/R_H chain mixing. The presence of the alkyl chains changes the shape of the WAXS scattering a bit, showing a smoother declination towards larger 2θ values (shorter distances). The absence of

any shoulder or additional scattering at larger 2θ-values corresponding to a distance around 0.36–0.38 nm again indicates the absence of a close face-to-face stacking (see also Fig. S9a–c, ESI†). Notably, the chessboard tiling is directly formed from the isotropic liquid state without passing any region with a simple (color-mixed or only short-range segregated) square honeycomb, as previously reported for all other multi-color square tilings.[49,51] The side-by-side organization of R_F segments in the branched chains obviously provides a cooperativity, supporting the R_F/R_H segregation.

The lattice parameter a_{squ} of the square honeycomb of **H8/16** decreases from 5.6 nm at 201 °C to 5.0 nm at 46 °C,

corresponding to a reduction of the honeycomb wall length from L_{wall} = 3.98 to 3.55 nm (Fig. 3(e)) and development of a 36.2° tilt, very similar to **H8₂**. The discontinuity in the $a_{squ} = f(T)$ diagram in Fig. 3(e) indicates the onset of uniform tilt around 160 °C, *i.e.* close to the temperature observed for **H8₂**. Again, this transition is not associated with any transition enthalpy (see DSC traces in Fig. S1d, ESI†), in line with the almost continuous and reversible character of this $Col_{squ}/p4mm^L$–$Col_{squ}^T/p4mm^L$ transition (see Fig. 3(e)). Also similar to **H8₂**, there is an inversion of Δn in the $Col_{squ}^T/p4mm^L$ range around 73 °C (Fig. S3, ESI†). The enhanced inversion temperature and the larger tilt angle at 45 °C indicate a slightly stronger tilt of the OPE cores in the case of compound **H8/16**, which is assumed to be (at least partly) due to the chain mixing in the periphery around the R_F chains which avoids the sparingly packed areas in the corners of the squares (Fig. 3(b)); thus, an overall denser packing is achieved.

2.3 Reduction of R_H side chain length – three-color tiling

For compound **H8/14** with a shorter alkyl side chain the same sequence $Col_{squ}^T/p4mm^L$–$Col_{squ}/p4mm^L$, as found for **H8/16**, is observed with a transition between them at 162 °C on heating, in this case associated with a DSC endotherm (1.2 kJ mol^{-1},

see Fig. 4(a)). Though the lattice parameters are similar (a_{squ} = 5.6 nm at 183 °C in $Col_{squ}/p4mm^L$ and a_{squ} = 5.0 nm at 74 °C in $Col_{squ}^T/p4mm^L$, for SAXS patterns and ED maps, see Tables S5–S7 and Fig. S11a, b, S12, ESI†) if compared with **H8/16** (Fig. 3(e)), this first order transition is associated with a much larger jump of the cell size (Fig. 4(b)), and hence, tilt angle. Such stronger tilt, also indicated by the increasing birefringence inversion temperature from 73 to 105 °C (Fig. S3, ESI†) originates from side-chain volume reduction.

While a direct transition from $Col_{squ}^T/p4mm^L$ to $Col_{squ}/p4mm^L$ is observed on heating compound **H8/14**, on cooling the reverse transition from $Col_{squ}/p4mm^L$ to $Col_{squ}^T/p4mm^L$ is associated with the formation of an intermediate biaxial columnar phase between 161 and 119 °C (Fig. 4 and Fig. S3, ESI†). In the DSC cooling traces there is a relatively broad peak at 150–160 °C, while the second transition to the uniaxial $Col_{squ}^T/p4mm^L$ phase is not observed, probably, because the transition is too slow. The SAXS pattern of this biaxial LC phase is indexed to a rectangular lattice with $p2mm$ plane group and parameters a_{rec} = 10.4 and b_{rec} = 5.26 nm (Fig. 4(c)), where b_{rec} is only slightly smaller than a_{squ} in the adjacent $Col_{squ}/p4mm^L$ phase and a_{rec} being almost twice as large as b_{rec}. This means that the number of tiles per unit cell increases from only two in the
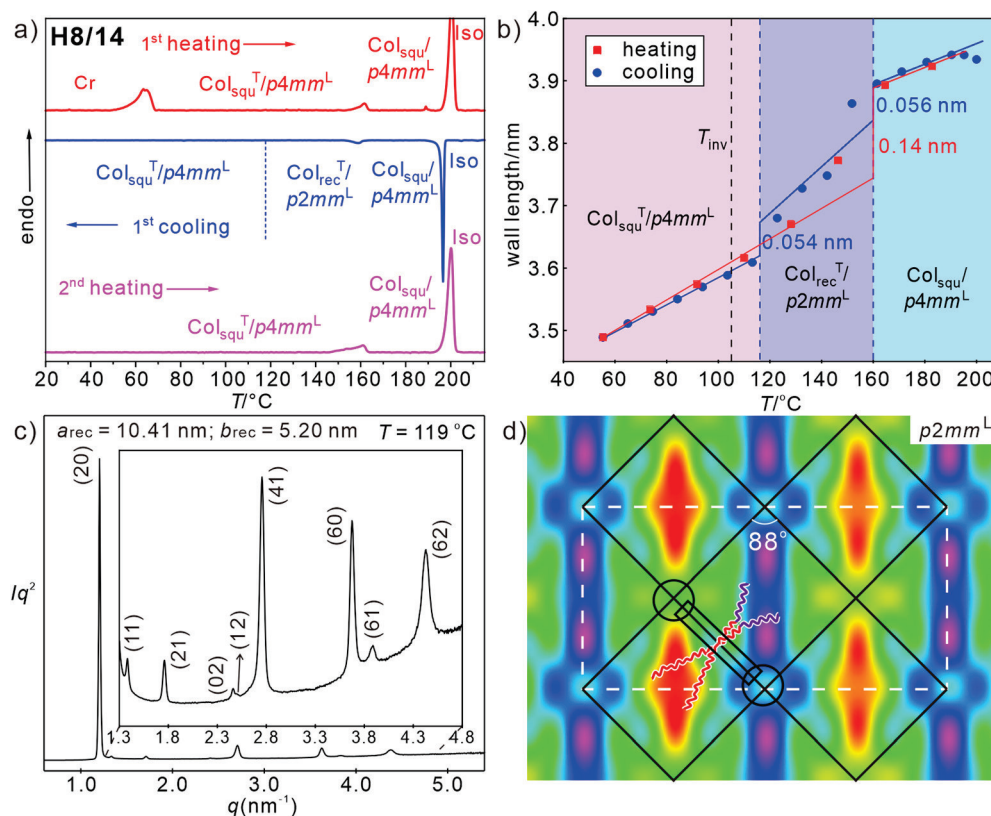

Fig. 4 Compound **H8/14**: (a) DSC traces, (b) wall length depending on temperature diagram on heating (red) and on cooling (blue); the dashed blue lines indicate the $Col_{rec}^T/p2mm^L$ range on cooling, T_{inv} is the birefringence inversion temperature; (c) SAXS pattern and (d) reconstructed ED map of the $Col_{rec}^T/p2mm^L$ phase at 119 °C (ππππππ00, except for (12)) with the lattice shown by white dashed lines and the tiles with molecules along the edges shown as black solid lines; overlaid is a sketch of the organization of the molecules, black rectangle indicates the aromatic core and the black circles indicate the glycerol nodes; SAXS data and ED maps of the square phases, see Tables S5–S7, Fig. S11a,b and S12 (ESI†), for WAXS data, see Fig. S9b and Table S1 (ESI†) and for POM textures Fig. S3 (ESI†).

chessboard phase ($p4mm^L$) to four in $Col_{rec}^T/p2mm^L$. The ED map in Fig. 4(d) shows three different types of almost square cells. Those with high ED are mainly filled with the R_F chains and the other two with low ED cores are mainly filled by the alkyl chains. There is a slight difference in ED between the two types of low ED cells, indicating a different degree of mixing of the R_F chains into the R_H domains, thus leading to a three-color tiling. The formation of this intermediate phase upon cooling is associated with a reduction of L_{wall} from 3.9 to 3.7 nm *i.e.* with the onset of a tilt of $33°$, which is a bit smaller than found at the same temperature in the $Col_{squ}^T/p4mm^L$ phase (L_{wall} = 3.6 nm, β = $35°$) on heating (see Fig. 4(b)). This onset of uniform tilt leads to a decreasing birefringence of the spherulite-like texture which further decreases at the transition to the low tempera-ture $Col_{squ}^T/p4mm^L$ phase (see Fig. S3, ESI†). The ED map in Fig. 4(d) indicates a preferred organization of the R_F and R_H chains along one of the square diagonals, reducing the sym-metry and leading to a slight rhombic deformation of the almost square cells (rhombic angle of $88°$).

It appears that there are two options for the developing tilt, occurring either out of the crystallographic *a–b* plane, in this way shrinking all square sides simultaneously and retaining the square cells as found in the $Col_{squ}^T/p4mm^L$ phase, or tilt within the crystallographic plane, leading to a reduction of the cell size by deformation of the squares to rhombs (see Fig. 8(b) in Section 4). In the present case both tendencies compete with each other in a certain temperature range. On heating exclusive the out-of-plane tilt is found with a direct $Col_{squ}^T/p4mm^L$ to $Col_{squ}/p4mm^L$ transition, while on cooling the reduced side-chain volume of **H8/14** allows some in-plane tilt with only minimal rhombic cell deformation, reducing the required out of plane tilt in the temperature range of the $Col_{rec}^T/p2mm^L$ phase, *i.e.* both modes of tilt are combined, though the out of plane tilt is dominating. At a certain critical temperature, however, the out-of-plane tilt wins over the in-plane tilt and strong tilt develops in the $Col_{squ}^T/p4mm^L$ phase with square cells (Fig. S11b and S12, ESI†). The slight rhombic deformation of the cells is obviously favored by the reduced side-chain volume compared to **H8/16**.

2.4 Reduction of R_F side chain length – angular square deformation

The in-plane tilt becomes more evident upon further side-chain shrinkage. For compound **H7/14** in addition to the alkyl chain shortening also the length (and volume) of the two R_F branches is reduced by one CF_2 group in each branch (Table 1). For this compound an optical uniaxial LC phase with spherulitic texture develops on cooling at 188 °C which in this case does not decrease, but slightly increases in birefringence down to $\sim$140 °C (Fig. S2a–d, ESI†). The SAXS pattern in this temperature range is again indexed to a square lattice, but in this case with $p4gm$ plane group and a_{squ} = 8.07–8.21 nm (Fig. 5(a)). The reconstructed ED maps show a periodic tessellation by square and rhombic cells with a rhombic angle around $52°$ ($Col_{squ}/p4gm$ phase, Fig. 5(b)). The larger squares contain the high ED R_F chains while the rhombic cells are filled by the low ED alkyl chains, also

in this case with core–shell structure. The in-plane tilt with deformation of the squares to rhombs is obviously supported by the reduced total chain volume, favoring the formation of the smaller (rhombic) cells and the volume difference between the R_H and R_F side-chains, supporting the development of different – larger and smaller – cells. It appears that the reduction of the total chain volume is the dominating effect, because the rhombic cells are formed despite the fact that at the transition **H8/14** to **H7/14** the chain volume difference between R_F and R_H side-chains is reduced. Nevertheless, the slightly larger (5%) R_F-chain volume is obviously sufficient to select the larger square cells for the R_F-chains.

It is worth noting that the $p4gm$ phase reported here is the first one combining squares and rhombs[58] in a dihedral tiling pattern, instead of the usually observed combination of squares and pairs of triangles.[49,76,84,85] This is evident from the ED maps showing the lowest ED in the middle of the rhombs (Fig. 5(b)). If there would be additional OPE cores dividing the rhombic cells into two triangles, there should be medium electron density in the middle of the rhombs. Moreover, if there would be an additional wall separating the rhombs into two triangles the triangular cells would become overcrowded as the chains of the additional molecules must be accommodated in the smaller triangular cells (see Fig. S14, ESI†).

It is remarkable that in contrast to the $Col_{squ}/p4mm^L$ phases the lattice parameter of the $Col_{squ}/p4gm$ phase increases quite a bit from a_{squ} = 8.06 nm to a = 8.23 nm upon lowering the temperature from 174 °C to 137 °C (Table 1 and inset in Fig. 5(e)). This is in line with the increase of the birefringence upon cooling in this temperature range (birefringence color changes from bluish green to yellowish green, see Fig. S2a–d, ESI†). Both effects are attributed to an increasing order para-meter of the OPE rods with lowering temperature. The distance between the nodes in this tiling pattern increases from 4.2 to almost 4.4 nm on cooling, corresponding to the fully stretched molecular length. This is surprising, because in the square honeycombs ($p4mm$ and $p4mm^L$) the longest achievable side length is only 3.9–4.0 nm. Moreover, changing the distance from 4.2 to 4.4 nm would simultaneously change the small inner rhombic angle between 43 and $52°$ (see Fig. S13a and b, ESI†), thus becoming too small at higher temperature. In fact, no change of the rhombic angle can be indicated in the ED maps where this angle remains fixed to $52°$ at all temperatures and for the $p4gm$ phases of all compounds (see ED maps in Fig. S12, ESI†). This can be explained by a structure where the OPE cores of the molecules are shifted a bit towards the inside of the square cells (Fig. 5(d)), as previously observed for a columnar liquid quasicrystal.[30] This would require an elliptic deformation of the polar glycerol columns. To confirm the molecular packing in the $p4gm$ phase, small angle neutron scattering (SANS) was conducted and the scattering length density is reconstructed in Fig. 5(c) and (d). Unlike ED maps, in which the ED sequence of different components is $R_F >$ glycerols $\cong$ OPE $> R_H$, neutron scattering depends on the density of hydrogen atoms. Thus, the scattering density of the glycerols becomes lower than the OPE core and the sequence
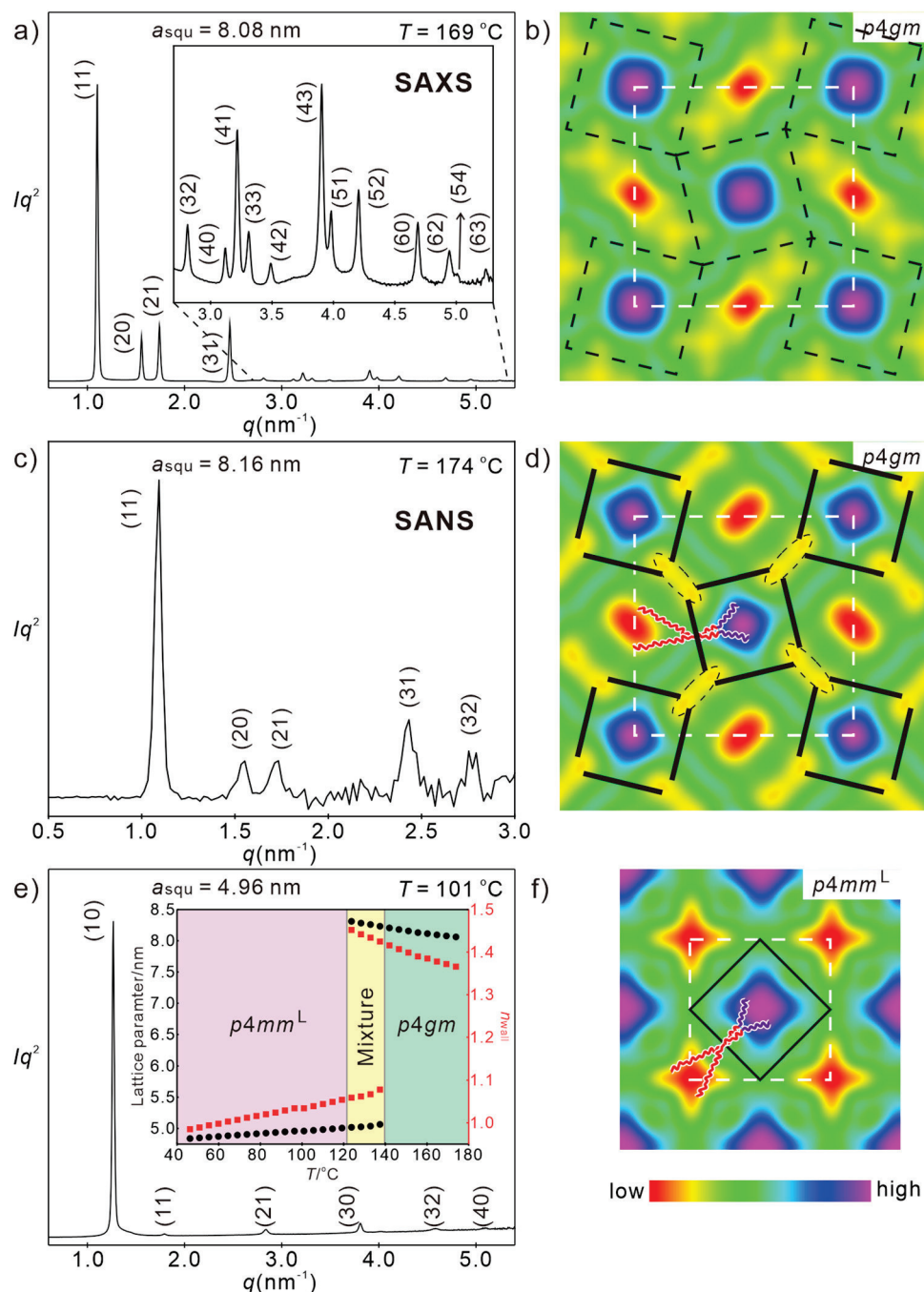
Fig. 5 Investigation of **H7/14**. (a) and (b) SAXS pattern (for numerical data, see Table S3, ESI†) and reconstructed ED map of the Col$_{squ}$/$p4gm$ phase at 169 °C (00π0 for the first four peaks), lattice is shown by white dashed line, tiles are in black dashed lines, (c) and (d) SANS pattern (for numerical data, see Table S20, ESI†) and scattering length density of the Col$_{squ}$/$p4gm$ phase at 174 °C (phase combination as 00000), lattice is shown by white dashed lines, glycerol nodes are shown by black dashed ellipses, tiles with molecules along edges are in black solid lines, (e) and (f) SAXS pattern (for numerical data, see Table S4, ESI†) and reconstructed ED map of the Col$_{squ}$/$p4mm^L$ phase at 101 °C (0000$\pi\pi$); lattice is shown by white dashed lines, tiles with molecules along edges are in black solid lines, the inset in (c) shows the temperature dependence of a_{squ} (black) and n_{wall} (red); for WAXS data, see Fig. S9a and Table S1 (ESI†), for POM textures Fig. S2 (ESI†) and for DSCs, see Fig. S1a, (ESI†).

becomes $R_F >$ OPE $>$ glycerols $> R_H$ (Table S21, ESI†). The dashed ellipses in Fig. 5(d) highlight the edges of the deformed yellow hydrogen bonding columns. This deformation allows a shift of the OPE cores, leading to a shrinkage of the square side length, thus allowing an effective length of only 3.9–4.0 nm

(see Fig. 5(d)) the same length as typically found in the $p4mm$ phases. The shrinkage of the square cells and the simultaneous expansion of the rhombic cells reduces the volume difference between square and rhombic prismatic cells (remember, there is only 5% volume difference between R_H and R_F chains). In

this structure the centers of the square cells can more easily be reached and filled by the shorter fluorinated chains of **H7/14**, in line with the absence of blue dots with reduced ED in the centers of the R_F column (compare Fig. 3(b), (d) and 5(b), (f)). The elliptical glycerol column deformation is also associated with an increase of the wall diameter becoming 1.4 molecules on average, compared to only 1.0 in the square honeycombs (see Table 1). The additional molecules in the thicker walls fill some of the space in the rhombic cells, adjusting it to that actually required by the R_H chains.

Below a certain limiting temperature, the rhomb-square tessellation of the $p4gm$ phase becomes unstable, then all angles become 90° and a transition to a square honeycomb (Fig. S1a, ESI†) with $p4mm$ plane group and a_{squ} = 5.06 nm is observed at 137 °C, in line with a transition to a square chessboard tiling (see Fig. 5(e) and (f)). This transition is associated with a significant DSC peak (ΔH = 3.9 kJ mol^{-1}, Table 1 and Fig. S1a, ESI†), a reduction of n_{wall} from 1.4 to 1.0 and a strong decrease of birefringence with an inversion of birefringence at 116 °C (see Fig. S2c–e, ESI†), being the highest inversion temperature in the series **Hm/n**. This is in line with the strongest tilt in this $Col_{squ}^T/p4mm^L$ phase and the smallest a_{squ} value reaching a_{squ} = 4.83 nm (corresponding to L_{wall} = 3.4 mm and β = 39.4°) at 45 °C for this compound with the smallest side-chain volume (inset in Fig. 5(e)). Due to the significant molecular reorganization the $Col_{squ}/p4gm$ – $Col_{squ}^T/p4mm^L$ transition is not fully reversible but associated with a significant hysteresis, thus taking place at 137 °C on cooling and at 151 °C on heating (Table 1, for DSC, see Fig. S1a, ESI†). The WAXS remains diffuse, confirming that a fluid LC state is retained at the transition from in-plane to out-of-plane tilt. It appears that the in-plane tilt, retaining a non-tilted rod organization in the walls is entropically favored at higher temperature (reduced orientational order parameter). However, the out-of-plane tilt allows development of even smaller prismatic cells with minimized steric frustration of side chain packing by removing the tight vertices of the rhombs. Moreover, it allows a denser packing of OPE cores and chains, in line with the shift of the WAXS maximum from 0.53 at 170 °C to 0.51 nm at 50 °C (Fig. S9a and Table S1, ESI†), presumably driving this transition.

2.5 Compounds F*m*/*n* with a peripherally fluorinated FOPE core – transition from square to rectangular cells

Perfluorination of the outer benzene rings of the OPE core leads to a reduction of the LC-iso transition temperatures by 5–15 K (see Table 1). This can be attributed to (i) the larger fluorine atoms, to some extend distorting the parallel rod-alignment and hindering the hydrogen bonding networks of the adjacent glycerols, and (ii) the changing degree of incompatibility between the fluorinated cores and the R_H and R_F chains, respectively. In the series of compounds **Fm/n** the $p4mm^L$ phase is found only for compound **F8/16**, having the longest side-chains, in a small temperature range (Fig. 6(a), (c) and (d)), while for **F8/14** it coexists in a certain temperature range with the $p4gm$ phase and it has disappeared and is completely replaced by the $p4gm$ phase for **F7/14** with the smallest

side-chain volume (see Table 1). So, the development of the high temperature phase from $p4mm^L$ to $p4gm$ with decreasing chain volume is the same as found for the series **Hm/n**, only shifted a bit towards larger total side-chain volume. The lattice parameter of the $p4mm^L$ phase of **F8/16** (a_{squ} = 5.5–5.6 nm, Fig. 6(a) and (b)) is very similar to that found for **H8/16**, being in line with a two-color chessboard structure and a non-tilted organization of the molecules in the honeycomb walls (L_{wall} = 4.0 nm) with approximately the same orientational order parameter as compounds **Hm/n**.

The $p4gm$ phases of **F8/14** and **F7/14** have almost the same lattice parameters (a_{squ} = 8.1–8.2 nm) as found for **H7/14**. The ED maps (Fig. S12, ESI†) confirm that also for these compounds the high ED R_F chains (blue) fill the squares, while the low ED alkyl chains (red) are in the cores of the rhombic prismatic cells. The inner rhombic angles have the same typical value of 52°.

However, the thermal range of the mesophases without out-of-plane tilt ($p4mm^L$ and $p4gm$) is relatively small for all three compounds **Fm/n** (3–4 K, see Table 1 and Fig. 6(a), Fig. S1b, c, ESI†) and a biaxial mesophase becomes the dominating LC phase at lower temperature. That the LC state is retained in this biaxial phase is supported by the diffuse WAXS (Fig. 6(b) and Fig. S9d–f, ESI†), supported by the WAXS (Fig. 6(b) and Fig. S9d–f, ESI†). The SAXS pattern of the biaxial low temperature phase of **F8/16** is indexed to a rectangular columnar phase with $c2mm$ plane group and parameters a_{rec} = 8.32 nm and b_{rec} = 6.77 nm at 147 °C (Fig. 6(e)). The reconstructed ED map in Fig. 6(f) shows a two-color tiling by two types of rectangular instead of square tiles, *i.e.* a chessboard tiling being compressed along direction b. At 191 °C the transition from the $p4mm^L$ to the $c2mm$ phase is indicated in the DSC traces of **F8/16** by a transition enthalpy of around 4 kJ mol^{-1} (Fig. 6(a)) and optically it is indicated by the emergence of significant birefringence in the homeotropic regions of the texture (insets in Fig. 6(c) and (e)). Areas with spherulite-like texture show a decrease of the birefringence, due to the onset of a tilt (see Fig. S7, ESI†). On further cooling the birefringence continuously decreases, but a relatively large negative birefringence is retained down to 40 °C without inversion of birefringence (Fig. S7, ESI†). This means the tendency to assume a tilted arrangement in the honeycomb walls is reduced for the fluorinated FOPE cores. Probably the aromatic fluorines contribute to the space filling in the prismatic cells and thus reduce the space available for the side chains and the tilt required to adjust the cell size is also reduced.

The formation of rectangular cells with only two opposite cell walls being tilted, while the others have no uniform tilt ($Col_{rec}^{T/2}/c2mm$, where T/2 indicates tilt of half of the walls) is unexpected. It appears that the FOPE cores cannot assume any arbitrary tilt angle, but there are two preferred modes of organization. Either without tilt which is favored by the face-to-face stacking of the electron deficit fluorinated rings on top of each other (Fig. S16b, ESI†) or a tilt around ∼35–50° which is supported by the stacking interactions between the fluorinated benzenes and the electron rich triple bonds of adjacent molecules (Figs. S16d and S17, ESI†). The latter leads
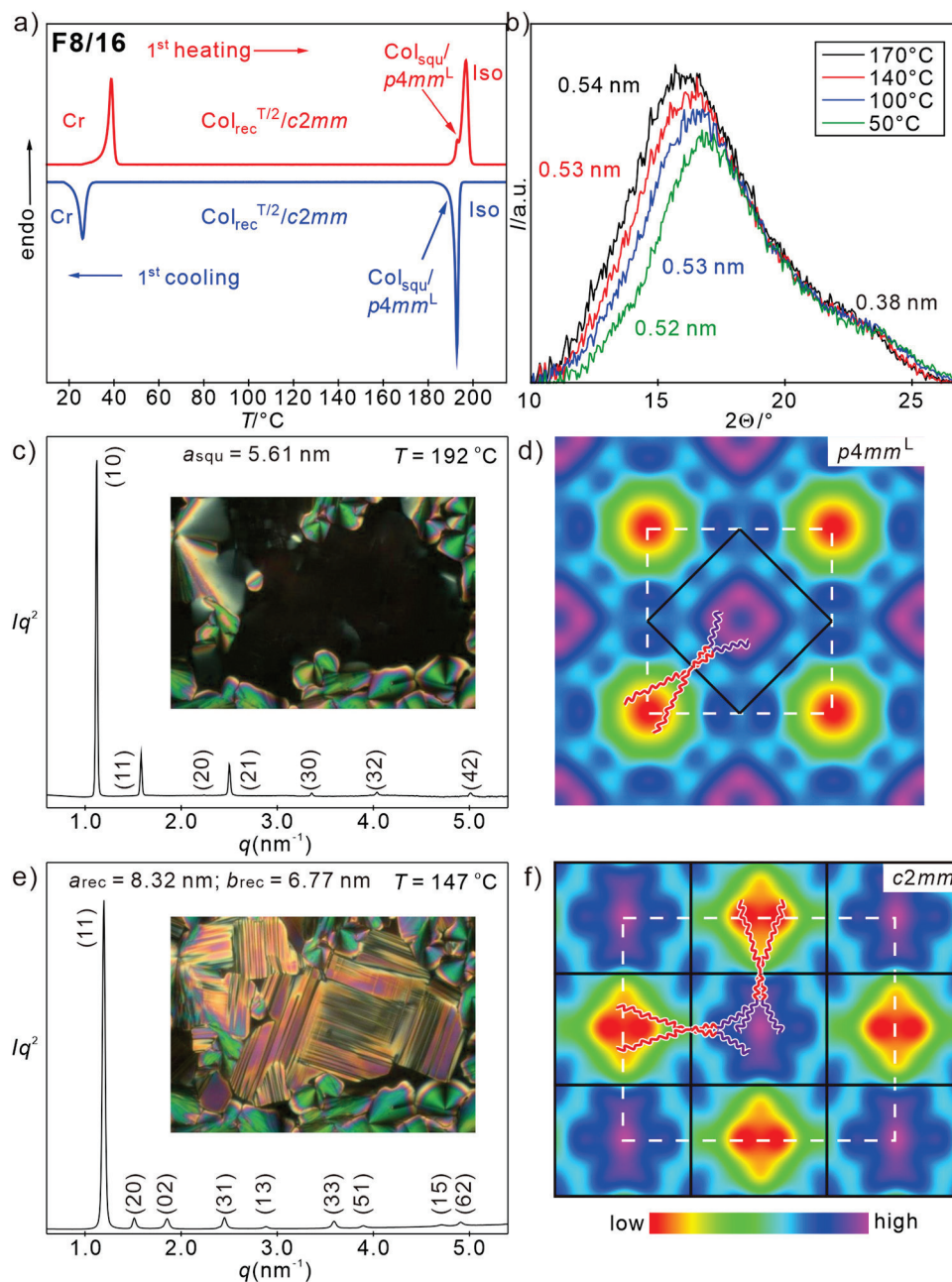
Fig. 6 Investigation of **F8/16**. (a) DSC traces and (b) WAXS patterns; (c) and (e) SAXS pattern (for numerical data, see Tables S16 and S17, ESI†) and POM textures insets (see also Fig. S7, ESI†); (d) and (f) reconstructed ED maps of (c) and (d) the $Col_{squ}/p4mm^L$ phase at 192 °C ($0\pi0\pi\pi$, except for (20)) and (e) and (f) the $Col_{rec}^{T/2}/c2mm$ phase ($0\pi\pi0\pi00$, except for (22), (13), (51) and (71)) at 147 °C; the ED of the perfluorinated benzenes contributes to the enhanced ED around the glycerol columns; lattice is shown by white dashed lines, tiles with molecules along edges are in black solid lines.

to a longitudinal shift of the OPE cores to each other,[66,86–90] providing a tilt of 35–50° if the shift takes place with uniform direction. However, increasing tilt distorts the segregation between glycerols and FOPE cores, which restricts the tilt to 30–40° in most cases. The presence of face-to-face stacking between the FOPE cores is indicated by the presence of a WAXS shoulder with a maximum corresponding to a stacking distance of $d = 0.38$ nm (Fig. 6(b)). However, this scattering is very diffuse, indicating only a short-range correlation of this stacking periodicity. The change of the preferred mode of core packing of

compounds **F***m*/***n*** compared to compounds **H***m*/***n***, thus explains the differences between their mesophase structures and their phase sequences. In the perspective of the temperature dependence of the lattice parameters, for **F8/16**, the longer sides along direction a correspond almost to the full molecular length ($a_{rec}/2 \sim 4.0$–4.2 nm, Fig. S19a, ESI† red). The remaining two sides are significantly shorter ($b_{rec}/2 = 3.4$–3.6, Fig. S19a, ESI† red), requiring a significant tilt of about 38°. Because only 1/2 of the walls becomes significantly tilted, the average tilt over the whole structure is smaller than the Δn inversion angle of 35.3° and

H: Cr 128 [24.7] Col$_{squ}^{T}$/$p4mm$ 156 [-] Col$_{squ}^{T/2}$/$p2mm$ 195 Col$_{squ}$/$p4mm$ 197 [24.1]^{a} Iso
C: Iso 193 [-22.8] Col$_{squ}$/$p4mm$ 191^{a} Col$_{squ}^{T/2}$/$p2mm$ 146 [-] Col$_{squ}^{T}$/$p4mm$ <25 Cr
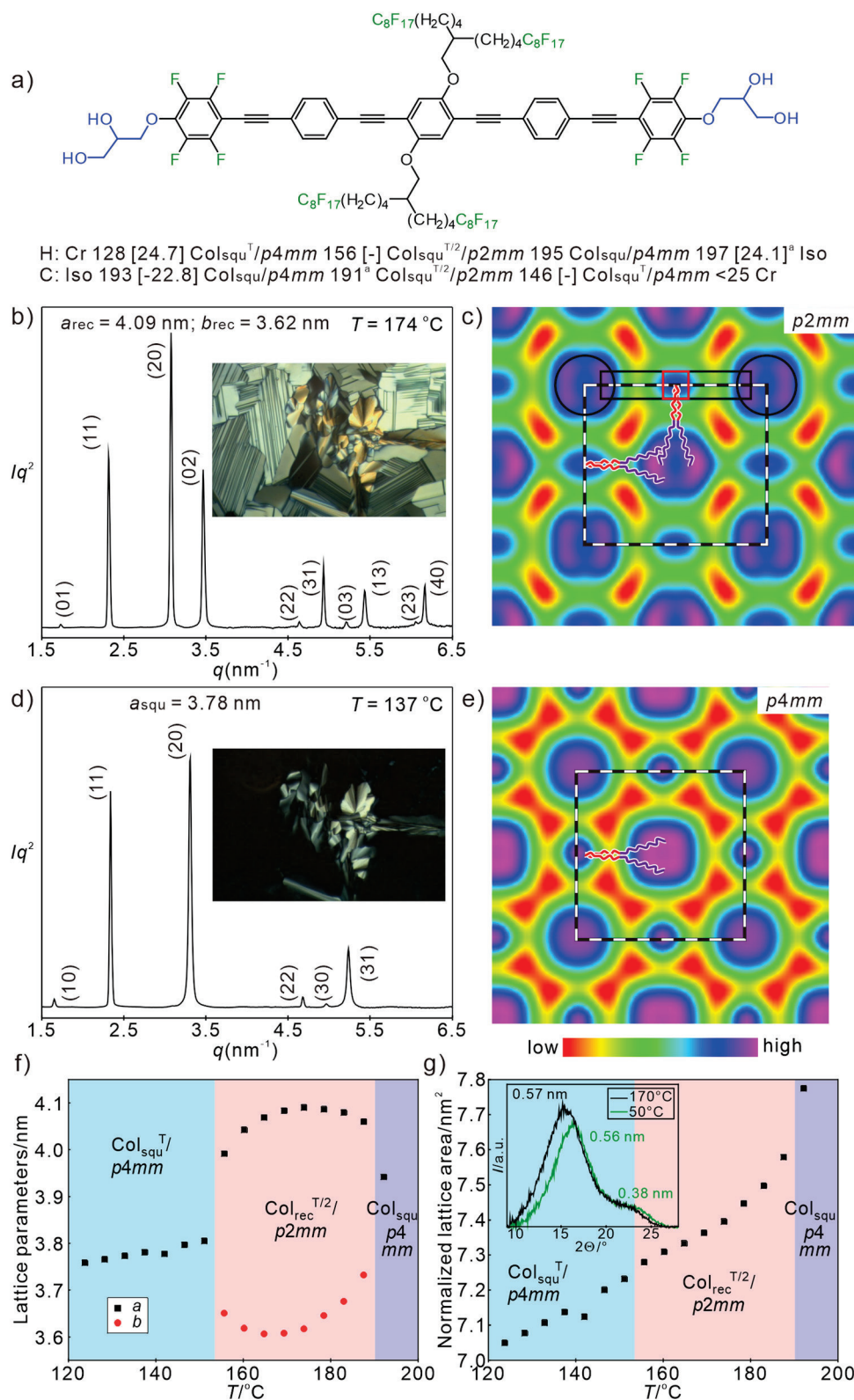
Fig. 7 Data of compound **F8$_2$**. (a) Formula and transition temperatures, (b) and (d) SAXS patterns at the indicated temperatures (for numerical data, see Tables S18 and S19, ESI†) and in the insets typical POM textures of (b) the Col$_{rec}^{T/2}$/$p2mm$ phase and (d) the low temperature Col$_{squ}^{T}$/$p4mm$ phase. (c) and (e) ED maps reconstructed from $p2mm$ pattern (phase choice: 0000ππ0ππ0) and $p4mm$ pattern (phase choice: 0000ππ), dashed lines indicate the unit cell as well as one honeycomb cell, in (c) the position of one molecule is drawn, black rectangle indicates the aromatic core, red rectangle the central benzene ring and the black circles indicate the glycerol nodes; (f) and (g) temperature dependence of (f) lattice parameter and (g) normalized lattice area upon second heating and WAXS diffractograms at high (170 °C) and low temperatures (50 °C). ^{a}The high temperature Col$_{squ}$/$p4mm$ is formed only in a very small temperature range (see Fig. S11c−e, ESI†) and immediately transforms into Col$_{rec}^{T/2}$/$p2mm$, the enthalpy value for both transitions cannot be separated; for WAXS pattern, see Fig. S10b and Table S1 (ESI†).

in line with the fact that for these compounds no inversion of the birefringence can be observed (Fig. S7, ESI†). Details of the development of order parameter and tilt in the distinct sides of compounds **Fm/n** are described in Section S2.2.7 and Fig. S19 of the ESI.†

Though tessellations by rectangular prismatic cells have previously been found in $p2mm$ phases occurring below the $p4mm$ square honeycombs,[91] in all previously reported cases these were single color tilings and the lattice deformation was due to an elliptical deformation of the hydrogen bonding columns at the junctions along one direction and not to an emerging tilt.[91]

For **F7/14** with the smallest side-chain volume there is an additional birefringent mesophase with mosaic-like texture and unknown structure (M1) coexisting and competing with the $p4gm$ and $c2mm$ phases in the temperature range between the LC-Iso transition and 140 °C (see Fig. S5, ESI†). However, the structure of this mesophase has not been resolved yet, because it cannot be obtained as a pure phase.

2.6 Compound F8₂ with two fluorinated side-chains at the peripherally fluorinated FOPE core – square and rectangular honeycombs with inverted sequence

Finally, let's consider the FOPE compound **F8₂** with two identical fluorinated side chains (Fig. 7(a)). Upon cooling it forms a tiny $\mathrm{Col_{squ}}/p4mm$ phase region (single color square honeycomb) of 1–2 K (a_{squ} = 3.94 nm, see Fig. S11c, ESI†), which immediately transforms into a biaxial mesophase. At this transition the homeotropic areas become birefringent, forming a 90° grid pattern as typical for a transition to a rectangular honeycomb (Fig. 7(b) inset). The diffraction pattern of this biaxial mesophase was indexed to a $p2mm$ lattice with the parameters a_{rec} = 4.09 and b_{rec} = 3.62 nm (Fig. 7(b)), being about half of the corresponding values of the $c2mm$ phase of **F8/16**. The parameter a_{rec} corresponds to the single molecular length and b_{rec} to a single molecule tilted by 34.6°. In line with the ED map in Fig. 7(c), this $\mathrm{Col_{rec}^{T/2}}/p2mm$ phase can be considered as the single-color version of the $\mathrm{Col_{rec}^{T/2}}/c2mm$ phase, i.e. it is formed by rectangular cells which are in this case all filled by the R_F side chains. Similar to the single color $p4mm$ phase of **H8₂** (Fig. 2(f) and (h)), the ED map of the $p2mm$ phase of **F8₂** shows high ED areas (blue, purple) in the middle of the cells (R_F-chains) at the corners (glycerols and perfluorinated benzenes) and in the middle of the FOPE cores (dialkoxy substituted middle benzene rings). The R_F columns are surrounded by medium ED shells (green) and low ED areas (yellow/red, Fig. 7(c) and (e)). These low ED areas can again be understood as regions having reduced packing density due to the difficulty to fill these spaces by the R_F segments (Fig. S18b, ESI†).

As shown in Fig. 7(f), on cooling to 170 °C the b_{rec} parameter decreases to 3.6 nm i.e. the tilt in these shorter walls increases to 35°, while the walls along the longer sides a_{rec} become slightly longer (up to 4.1 nm) due to increasing orientational order parameter. This is in line with the locking mode of FOPE organization. However, on further cooling the parameter a_{rec} decreases and b_{rec} increases until they merge at the next transition at 148 °C. At this temperature the birefringence in the

homeotropic domains (columns perpendicular to the substrate surfaces) disappears, in line with a transition to a uniaxial mesophase (Fig. 7(d), inset) and in the SAXS pattern the transition to a square phase with $p4mm$ lattice is observed (Fig. 7(d)). There is no DSC peak associated with this transition (see Fig. S1e, ESI†) and the lattice parameter is 3.78 nm at 137 °C, corresponding to a single-color square honeycomb with a tilt of 30.3°; the Δn inversion is reached around 30 °C. The WAXS scattering remains diffuse in the whole investigated temperature range with its maximum shifting from 0.57 to 0.54 nm on cooling, in line with an increasing packing density (see inset in Fig. 7(g), Fig. S10b, d and Table S2, ESI†), being in line with the decreasing unit cell area with lowering temperature (Fig. 7(g)). The second diffuse scattering with clear maximum at 0.38 nm confirms the pronounced face-to-face packing in all mesophases.

Overall, on cooling the $p4mm$ phase of **F8₂** assumes a maximum tilt of 35° in half of the honeycomb walls, leading to a rectangular honeycomb with $p2mm$ plane group. On further cooling thermal chain shrinkage requires the development of a stronger tilt which obviously cannot be achieved by tilting only half of the molecules and the tilt in all honeycomb walls is required to adjust the cell size. As shown in Fig. 7(f) the tilt in the shorter walls starts expanding around 170 °C which is attributed to a decreasing tilt. This expansion is compensated by a decrease of the longer side length from 4.1 to 4.0 nm, in line with decreasing orientational order parameter. Thus, the side length difference is reduced and finally their lengths merge by assuming uniform tilt of ∼30° in all four walls at the transition to the square honeycomb with uniform tilt in all walls. However, as shown for compounds **Fm/n** (Fig. S19a, ESI†), an angle of 35° is by far not the maximal possible tilt of the FOPE based molecules. Anyhow, the absence of the alkyl chains and the formation of a single-color tiling ($p2mm$) instead of the two-color structure ($c2mm$) disfavors rectangular and favors square cells. It seems that the absence of the longer R_H chains (16–18C, compared to the shorter R_F side-chains with only 13–14C) favors the smaller square cells by removing the longer non-tilted walls. Moreover, the formation of rectangular cells could be supported by the parallel alignment of the R_H chains in the rectangular R_H-filled cells of compounds **Fm/n**.[91] The absence of this additional rectangle stabilizing effect and the preference of the square cells by the shorter R_F chains leads for **F8₂** to the unusual observation of the re-entrance of the square lattice and a transition from a rectangular honeycomb with lower symmetry at higher temperature ($\mathrm{Col_{rec}^{T/2}}/p2mm$) to a square honeycomb ($\mathrm{Col_{squ}^{T}}/p4mm$) with higher symmetry at lower temperature. For the OPE based compounds **H8₂** and **Hm/n** with non-fluorinated cores there are no rectangular cells, because there is no restriction for the tilt angle and therefore the main driving force of rectangular cell formation is absent.

3. Conclusions

In total six different self-assembled LC honeycomb structures have been identified, including 4 chessboard tiling and its derivatives (see Fig. 2, 7 and 8a). Among them the single color ($\mathrm{Col_{squ}}/p4mm$) and two-color square tiling ($\mathrm{Col_{squ}}/p4mm^L$) with
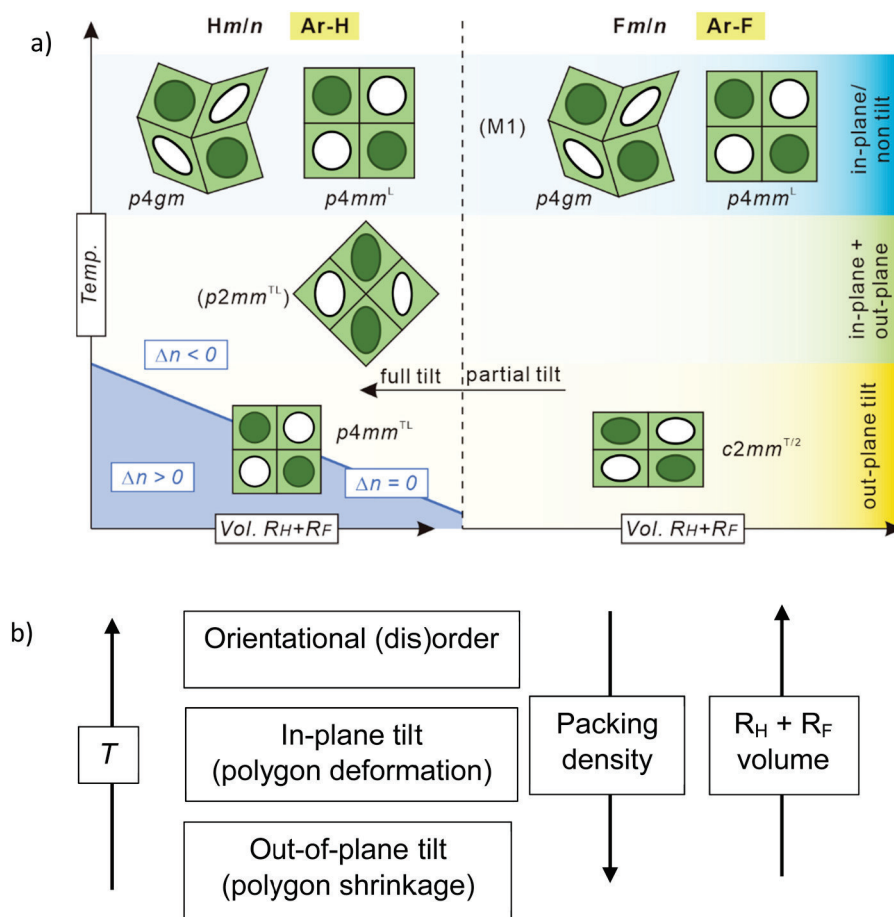
Fig. 8 (a) LC self-assembly of compounds **H**m/n and **F**m/n depending on side-chain volume, temperature, core-fluorination and degree of tilt of the OPE cores in the honeycomb walls. Dark green indicates domains of R_F chains, white R_H chains, and pale green areas are mixed areas; phases in parentheses are metastable or coexisting phases. (b) Development of different tilt-modes of the rod-like cores in polygonal honeycomb LC phases.

and without tilted organization of the rods in the walls and four new phases with reduced symmetry, all involving non-regular quadrangles. Three of them are derived from the chessboard (two-color square) tiling by cell deformation, namely the two-color square-rhomb tiling ($Col_{squ}/p4gm$), the three-color rhomb tiling ($Col_{rec}^T/p2mm^L$) and the stretched chessboard with rectangular cells ($Col_{rec}^{T/2}/c2mm$). The fourth one is the single-color version of the rectangular chessboard ($Col_{rec}^{T/2}/p2mm$). Remarkably, the two rectangular tessellations combine tilted and non-tilted rods in different directions of a uniform rectangular lattice.

There are two competing tilt modes, either within the crystallographic plane, leading to the deformation of square to rhombic tiles, or out of this plane, leading to cell shrinkage (Fig. 8b). Both are affected by the side-chain volume and the distinct modes of "π-stacking" interactions, tuned by aromatic core fluorination.

Packing constraints of the relatively rigid R_F segments lead to "voids" with reduced packing density in the honeycombs of the single color tilings of compounds with R_F chains at both sides and support core–shell formation with partial chain mixing in the shells for the two color tilings of compounds combining R_H and R_F side-chains.

It is also notable that in all cases the two-color tilings with segregated side chains form directly from the isotropic liquid state in a first order phase transition without an intermediate state where the side chains are still mixed, followed by an Ising transition *via* a structure with only local segregation to the long-range two-color structure, as found in all previously reported cases of chessboard tilings.[49,51] We attribute this to the pre-organization of two R_F segments in the branched side chains. This architecture also allows the use of two shorter R_F segments instead of only one with doubled length in the analogous compound with non-branched chains. This design concept is advantageous as shorter perfluorinated building blocks are more easily available and provide less solubility problems during synthesis. In addition, branched chains with shorter R_F segments have lower melting points of the crystalline phases, thus widening the LC phase ranges.

Overall, this work uncovers the importance of specific core–core interactions and space filling effects on the emergence of tilt and lattice deformation modes in multi-color quadrangular honeycomb structures achieved by soft reticular self-assembly. Modification of out-of-plane tilt by tailoring the "π-stacking" interactions is also a potential way to adjust distances between

the nodes in the related solid-state hydrogen bonded and COF-based honeycombs-like networks, especially for the creation of the still elusive quasiperiodic networks based on reticular chemistry.[72] Taking advantage of the special multicolor tiling, the rich variety of different tiling modes we found is of potential use in generating diverse soft programmable metafilm materials, which naturally requires ordered array of multi-components to interact with electromagnetic waves for light modulation and information storage. The possibility to change the birefringence from negative *via* an optically isotropic state to a positive by adjusting the tilt is of additional potential practical interest for applications in optical devices.[92]

4. Experimental

4.1 Synthesis

The synthesis (Scheme S1, ESI†) and the used procedures, together with the analytical data of all compounds are described in full detail in the ESI,† Section S3.

4.2 Investigations

Investigations were conducted by polarizing optical microscopy (POM), differential scanning calorimetry (DSC), small-angle and wide-angle X-ray scattering (SAXS and WAXS) and in one case by additional small angle neutron scattering (SANS) as described in more detail in the ESI,† Section S1.

Data availability

The data supporting this article have been included as part of the ESI.†

Conflicts of interest

There are no conflicts of interest.

Acknowledgements

References

1 J. Uchida, B. Soberats, M. Gupta and T. Kato, *Adv. Mater.*, 2022, **34**, 2109063.

2 H. K. Bisoyi and Q. Li, *Chem. Rev.*, 2022, **122**, 4887–4926.

3 Y.-K. Kim, X. Wang, P. Mondkar, E. Bukusoglu and N. L. Abbott, *Nature*, 2018, **557**, 539–544.

4 J. Ma, J. Choi, S. Park, I. Kong, D. Kim, C. Lee, Y. Youn, M. Hwang, W. Hong and W. Kim, *Adv. Mater.*, 2023, **45**, 2302474.

5 K. Yin, E. L. Hsiang, J. Zou, Y. Li, Z. Yang, Q. Yang, P.-C. Lai, C.-L. Lin and S. T. Wu, *Light: Sci. Appl.*, 2022, **11**, 161.

6 P. J. Collings and J. W. Goodby, *Introduction to Liquid Crystals: Chemistry and Physics*, CRC Press, Boca Raton, FL, 2nd edn, 2019.

7 *Handbook of Liquid Crystals*, ed. J. W. Goodby, J. P. Collings, T. Kato, C. Tschierske, H. F. Gleeson and P. Raynes, Wiley-VCH, Weinheim, 2nd edn, 2014.

8 E.-K. Fleischmann and R. Zentel, *Angew. Chem., Int. Ed.*, 2013, **52**, 8810–8827.

9 S. Sergeyev, W. Pisula and Y. H. Geerts, *Chem. Soc. Rev.*, 2007, **36**, 1902–1929.

10 C. Tschierske, *J. Mater. Chem.*, 1998, **8**, 1485–1508.

11 C. Tschierske, *Angew. Chem., Int. Ed.*, 2013, **52**, 8828–8878.

12 B. M. Rosen, C. J. Wilson, D. A. Wilson, M. Peterca, M. R. Imam and V. Percec, *Chem. Rev.*, 2009, **109**, 6275–6540.

13 C. Tschierske and C. Dressel, *Symmetry*, 2020, **12**, 1098.

14 G. T. Stewart, *Liq. Cryst.*, 2004, **31**, 443–471.

15 D. Deamer, *Chem. Soc. Rev.*, 2012, **41**, 5375–5379.

16 H. Ringsdorf, B. Schlarb and J. Venzmer, *Angew. Chem., Int. Ed. Engl.*, 1988, **27**, 113–158.

17 F. Kuschel, A. Mädicke, S. Diele, H. Utschick, B. Hisgen and H. Ringsdorf, *Polym. Bull.*, 1990, **23**, 373–379.

18 U. Dahn, C. Erdelen, H. Ringsdorf, R. Festag, J. H. Wendorff, P. A. Heiney and N. C. Maliszewskyj, *Liq. Cryst.*, 1995, **19**, 759–764.

19 S. Diele, S. Oekiner, F. Kuschel, B. Hisgen, H. Ringsdorf and R. Zentel, *Makromol. Chem.*, 1987, **188**, 1993–2000.

20 C. Tschierske, *Chem. Soc. Rev.*, 2007, **36**, 1930–1970.

21 C. Tschierske, C. Nürnberger, H. Ebert, B. Glettner, M. Prehm, F. Liu, X.-B. Zeng and G. Ungar, *Interface Focus*, 2012, **2**, 669–680.

22 X. Cai, S. Hauche, S. Poppe, Y. Cao, L. Zhang, C. Huang, C. Tschierske and F. Liu, *J. Am. Chem. Soc.*, 2023, **145**, 1000–1010.

23 S. Poppe, A. Lehmann, M. Steimecke, M. Prehm, Y. Zhao, C. Chen, Y. Cao, F. Liu and C. Tschierske, *Giant*, 2024, 100254.

24 G. Ungar, C. Tschierske, V. Abetz, R. Holyst, M. A. Bates, F. Liu, M. Prehm, R. Kieffer, X. Zeng, M. Walker, B. Glettner and A. Zywocinski, *Adv. Funct. Mater.*, 2011, **21**, 1296–1323.

25 S. Poppe, M. Poppe, H. Ebert, M. Prehm, C. Chen, F. Liu, S. Werner, K. Bacia and C. Tschierske, *Polymers*, 2019, **7**, 471.

26 A. Scholte, S. Hauche, M. Wagner, M. Prehm, S. Poppe, C. Chen, F. Liu, X. Zeng, G. Ungar and C. Tschierske, *Chem. Commun.*, 2020, **56**, 62–65.

27 M. Poppe, C. Chen, S. Poppe, F. Liu and C. Tschierske, *Commun. Chem.*, 2020, **3**, 70.

28 F. Liu, R. Kieffer, X. Zeng, K. Pelz, M. Prehm, G. Ungar and C. Tschierske, *Nat. Commun.*, 2012, **3**, 104.

29 S. Poppe, A. Lehmann, A. Scholte, M. Prehm, X. Zeng, G. Ungar and C. Tschierske, *Nat. Commun.*, 2015, **6**, 8637.

30 X. Zeng, B. Glettner, U. Baumeister, B. Chen, G. Ungar, F. Liu and C. Tschierske, *Nat. Chem.*, 2023, **15**, 625–632.

31 Y. Cao, A. Scholte, M. Prehm, C. Anders, C. Chen, J. Song, L. Zhang, G. He, C. Tschierske and F. Liu, *Angew. Chem., Int. Ed.*, 2024, **63**, e202314454.

32 A. J. Crane, F. J. Martínez-Veracoechea, F. A. Escobedo and E. A. Müller, *Soft Matter*, 2008, **4**, 1820–1829.

33 M. Bates and M. Walker, *Soft Matter*, 2009, **5**, 346–353.

34 X. Liu, K. Yang and H. Guo, *J. Phys. Chem. B*, 2013, **117**, 9106–9120.

35 F. Liu, P. Tang, H. Zhang and Y. Yang, *Macromolecules*, 2018, **51**, 7807–7816.

36 S. D. Peroukidis, *Soft Matter*, 2012, **8**, 11062–11071.

37 M. Fayaz-Torshizi and E. A. Müller, *Mol. Syst. Des. Eng.*, 2021, **6**, 594–608.

38 Y. Sun, P. Padmanabhan, M. Misra and F. A. Escobedo, *Soft Matter*, 2017, **13**, 8542–8555.

39 T. D. Nguyen and S. C. Glotzer, *ACS Nano*, 2010, **4**, 2585–2594.

40 Z. He, X. Wang, P. Zhang, A.-C. Shi and K. Jiang, *Macromolecules*, 2024, **57**, 2154–2164.

41 Y. Sun and F. A. Escobedo, *J. Chem. Theory Comput.*, 2024, **20**, 1519–1537.

42 J. Suzuki, M. Suzuki, A. Takano and Y. Matsushita, *Macromol. Theory Simul.*, 2021, 2100015.

43 X.-Y. Yan, Q.-Y. Guo, Z. Lin, X.-Y. Liu, J. Yuan, J. Wang, H. Wang, Y. Liu, Z. Su, T. Liu, J. Huang, R. Zhang, Y. Wang, M. Huang, W. Zhang and S. Z. D. Cheng, *Angew. Chem., Int. Ed.*, 2021, **60**, 2024–2029.

44 B. Hou, W.-B. Zhang and Y. Shao, *Chin. J. Polym. Sci.*, 2023, **41**, 1508–1524.

45 S.-We Kuo, *Giant*, 2023, **15**, 100170.

46 R. Zentel, *Macromol. Chem. Phys.*, 2021, **222**, 2100216.

47 W.-Y. Chang, D. Shi, X.-Q. Jiang, J.-D. Jiang, Y. Zhao, X.-K. Ren, S. Yang and E.-Q. Chen, *Polym. Chem.*, 2020, **11**, 1454–1461.

48 X. Zeng, R. Kieffer, B. Glettner, C. Nürnberger, F. Liu, K. Pelz, M. Prehm, U. Baumeister, H. Hahn, H. Lang, G. A. Gehring, C. H. M. Weber, J. K. Hobbs, C. Tschierske and G. Ungar, *Science*, 2011, **331**, 1302–1306.

49 C. Nürnberger, H. Lu, X. Zeng, F. Liu, G. Ungar, H. Hahn, H. Lang, M. Prehm and C. Tschierske, *Chem. Commun.*, 2019, **55**, 4154–4157.

50 B. Glettner, F. Liu, X. Zeng, M. Prehm, U. Baumeister, M. A. Bates, M. Walker, P. Boesecke, G. Ungar and C. Tschierske, *Angew. Chem., Int. Ed.*, 2008, **47**, 9063–9066.

51 W. S. Fall, C. Nürnberger, X. Zeng, F. Liu, S. J. Kearney, G. A. Gehring, C. Tschierske and G. Ungar, *Mol. Syst. Des. Eng.*, 2019, **4**, 396–406.

52 M. P. Krafft and J. G. Riess, *Chem. Rev.*, 2009, **109**, 1714–1792.

53 C. Tschierske, *Top. Curr. Chem.*, 2012, **318**, 1–108.

54 L. de Campo, M. J. Moghaddam, T. Varslot, N. Kirby, R. Mittelbach, T. Sawkins and S. T. Hyde, *Chem. Mater.*, 2015, **27**, 857–866.

55 G. Johansson, V. Percec, G. Ungar and J. P. Zhou, *Macromolecules*, 1996, **29**, 646–660.

56 A. Walther and A. H. E. Müller, *Soft Matter*, 2008, **4**, 663–668.

57 M. Poppe, C. Chen, F. Liu, M. Prehm, S. Poppe and C. Tschierske, *Soft Matter*, 2017, **13**, 4676–4680.

58 A. Saeed, M. Poppe, M. B. Wagner, S. Hauche, C. Anders, Y. Cao, L. Zhang, C. Tschierske and F. Liu, *Chem. Commun.*, 2022, **58**, 7054–7057.

59 M. Poppe, C. Chen, S. Poppe, C. Kerzig, F. Liu and C. Tschierske, *Adv. Mater.*, 2020, **47**, 202005070.

60 M. Poppe, C. Chen, F. Liu, S. Poppe and C. Tschierske, *Chem. Commun.*, 2021, **57**, 6526–6529.

61 M. Poppe, C. Chen, H. Ebert, S. Poppe, M. Prehm, C. Kerzig, F. Liu and C. Tschierske, *Soft Matter*, 2017, **13**, 4381–4392.

62 M. Hird, *Chem. Soc. Rev.*, 2007, **36**, 2070–2095.

63 J. Li, H. Nishikawa, J. Kougo, J. Zhou, S. Dai, W. Tang, X. Zhao, Y. Hisai, M. Huang and S. Aya, *Sci. Adv.*, 2021, **7**, eabf5047.

64 J.-C. Liu, H. Peng, X.-G. Chen, H.-P. L, X.-J. Song, R.-G. Xiong and W.-Q. Liao, *JACS Au*, 2023, **3**, 1196–1204.

65 K. Kishikawa, *Isr. J. Chem.*, 2012, **52**, 800–808.

66 G. W. Coates, A. R. Dunn, L. M. Henling, D. A. Dougherty and R. H. Grubbs, *Angew. Chem., Int. Ed. Engl.*, 1997, **36**, 248–251.

67 M. Weck, A. R. Dunn, K. Matsumoto, G. W. Coates, E. B. Lobkovsky and R. H. Grubbs, *Angew. Chem., Int. Ed.*, 1999, **38**, 2741–2745.

68 M. Poppe, C. Chen, F. Liu, S. Poppe and C. Tschierske, *Chem. – Eur. J.*, 2017, **23**, 7196–7200.

69 C. Tang, E. M. Lennon, G. H. Fredrickson, E. J. Kramer and C. J. Hawker, *Science*, 2008, **322**, 429–432.

70 T. J. Cui, M. Q. Qi, X. Wan, J. Zhao and Q. Cheng, *Light: Sci. Appl.*, 2014, **3**, e218.

71 M. Paquay, J. C. Iriarte, I. Ederra, R. Gonzalo and P. de Maagt, *IEEE Trans. Antennas Propag.*, 2007, **55**, 3630–3638.

72 F. Haase and B. V. Lotsch, *Chem. Soc. Rev.*, 2020, **49**, 8469–8500.

73 S. B. Alahakoon, S. D. Diwakara, C. M. Thompson and R. A. Smaldone, *Chem. Soc. Rev.*, 2020, **49**, 1344–1356.

74 Y. Jin, Y. Hu and W. Zhang, *Nat. Rev. Chem.*, 2017, **1**, 0056.

75 R.-R. Liang, S.-Y. Jiang, R.-H. A and X. Zhao, *Chem. Soc. Rev.*, 2020, **49**, 3920–3951.

76 F. Haase, G. A. Craig, M. Bonneau, K. Sugimoto and S. Furukawa, *J. Am. Chem. Soc.*, 2020, **142**, 13839–13845.

77 S. E. Wheeler and K. N. Houk, *Mol. Phys.*, 2009, **107**, 749–760.

78 G. N. Patwari, P. Venuvanalingam and M. Kolaski, *Chem. Phys.*, 2013, **415**, 150–155.

79 M. Born and E. Wolf, *Principles of Optics*, Pergamon, Oxford, 1980.

80 V. Percec, A. E. Dulcey, V. S. K. Balagurusamy, Y. Miura, J. Smidrkal, M. Peterca, S. Nummelin, U. Edlund, S. D. Hudson, P. A. Heiney, H. Duan, S. N. Magonov and S. A. Vinogradov, *Nature*, 2004, **430**, 764–768.

81 M. Lehmann, M. Dechant, M. Lambov and T. Ghosh, *Acc. Chem. Res.*, 2019, **52**, 1653–1664.

82 C. Tschierske, Microsegregation in Liquid Crystalline Systems: Basic Concepts, in *Handbook of Liquid Crystals*, ed. J. W. Goodby, J. P. Collings, T. Kato, C. Tschierske, H. F. Gleeson and P. Raynes, Wiley-VCH, Weinheim, 2014, vol. 5, pp. 1–43.

83 C. Tschierske, *Isr. J. Chem.*, 2012, **52**, 935–959.

84 B. Chen, X. Zeng, U. Baumeister, G. Ungar and C. Tschierske, *Science*, 2005, **307**, 96–99.

85 X. Cheng, H. Gao, X. Tan, X. Yang, M. Prehm, H. Ebert and C. Tschierske, *Chem. Sci.*, 2013, **4**, 3317–3331.

86 J. W. Steed and J. L. Atwood, *Supramolecular Chemistry*, Wiley, Chichester, UK, 2nd edn, 2009.

87 C. A. Hunter and J. K. M. Sanders, *J. Am. Chem. Soc.*, 1990, **112**, 5525–5534.

88 S. E. Wheeler, *Acc. Chem. Res.*, 2013, **46**, 1029–1038.

89 K. Carter-Fenk and J. M. Herbert, *Phys. Chem. Chem. Phys.*, 2020, **22**, 44870–44886.

90 A. Kundu, S. Sen and G. N. Patwari, *J. Phys. Chem.*, 2020, **124**, 7470–7477.

91 A. Lehmann, A. Scholte, M. Prehm, F. Liu, X. Zeng, G. Ungar and C. Tschierske, *Adv. Funct. Mater.*, 2018, **28**, 1804162.

92 S. Lagerwall, A. Dahlgren, P. Jägemalm, P. Rudquist, K. D'have, H. Pauwels, R. Dabrowski and W. Drzewinski, *Adv. Funct. Mater.*, 2001, **11**, 87–94.

Declaration of the author's share

Publication A: C. Anders, M. Wagner, M. Alaasar, V.-M. Fischer, R. Waldecker, Y. Zhao, T. Tan, Y. Cao, F. Liu and C. Tschierske, "*Highly branched bolapolyphilic liquid crystals with a cubic A15 network at the triangle-square transition*", *Chem. Commun.*, **2024**, 60, 1023 – 1026. DOI: 10.1039/D4TC04076G.
I conducted the synthesis and evaluation of the analytical, spectroscopic, and differential scanning calorimetry (DSC) data. The DSC measurements were conducted by Roy Gyger. The optical polarization microscopy (POM) texture recording and evaluation was conducted by myself. The preliminary studies of SAXS and WAXS were conducted and evaluated by me. The GISAXS and synchrotron experiments and electron density map reconstruction were performed and evaluated by the group of Dr. Yu Cao and Prof. Dr. Feng Liu. High-resolution mass spectrometry was performed by Susanne Tanner from the group of Prof. Dr. Wolfgang Binder. Prof. Dr. C. Tschierske provided supervision in both the practical and theoretical aspects of the work.

Publication B: C. Anders, T. Tan, V.-M. Fischer, R. Wang, M. Alaasar, R. Waldecker, Y. Cao, F. Liu, C. Tschierske, "*Engineering "meso-Atom" bonding: Honeycomb-Network Transitions in Reticular Liquid Crystals*", *Aggregate*, **2024**, Accepted Manuscript. DOI:10.1002/agt2.728.
I conducted the synthesis and evaluation of the analytical, spectroscopic, and differential scanning calorimetry (DSC) data. The DSC measurements were conducted by Roy Gyger. The optical polarization microscopy (POM) texture recording and subsequent evaluation were conducted by myself. The preliminary studies of SAXS and WAXS were conducted and assessed by me. The GISAXS and synchrotron experiments were conducted and evaluated by Dr. Yu Cao, Prof. Dr. Feng Liu, and me, during my research stay in China. The electron density map reconstruction was conducted and evaluated by Dr. Yu Cao and Prof. Dr. Feng Liu. The UV-Vis and fluorescence studies were conducted and evaluated by Dr. Yu Cao and Prof. Dr. Feng Liu. The high-resolution mass spectrometry was conducted by Susanne Tanner, from Prof. Dr. Wolfgang Binder's research group.

Publication C: C. Anders, V.-M. Fischer, T. Tan, M. Alaasar, R. Waldecker, Y. Ke, Y. Cao, F.Liu and C. Tschierske, "*Modifying the liquid crystalline chessboard tiling - Soft reticular self-assembly of side-chain fluorinated polyphiles*", *J. Mater. Chem. C*, **2024**, Accepted Manuscript. DOI: 10.1039/D4TC04076G.
I conducted the synthesis and evaluation of the analytical, spectroscopic, and differential scanning calorimetry (DSC) data. The DSC measurements were conducted by Roy Gyger. The optical polarization microscopy (POM) texture recording and evaluation were conducted by myself. The preliminary studies of SAXS and WAXS were conducted and evaluated by myself. The SANS, synchrotron experiments, and electron density map reconstruction were performed and evaluated by the group of Dr. Yu Cao and Prof. Dr. Feng Liu. High-resolution mass spectrometry was performed by Susanne Tanner from the group of Prof. Dr. Wolfgang Binder. Prof. Dr. C. Tschierske and M. Alaasar provided supervision in both the practical and theoretical aspects of the work. V. M. Fischer and Prof. R. Waldecker contributed to the selection of the compounds based on geometrical models.

Appendix-2: Unpublished DSC data

The following section lists selected additional DSC and XRD data on which unpublished work is based.

2.1   DSC traces of the 1H*m/n* and 1F*m/n* compounds
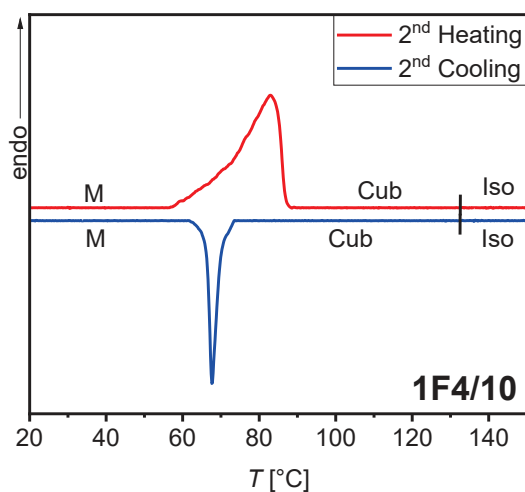
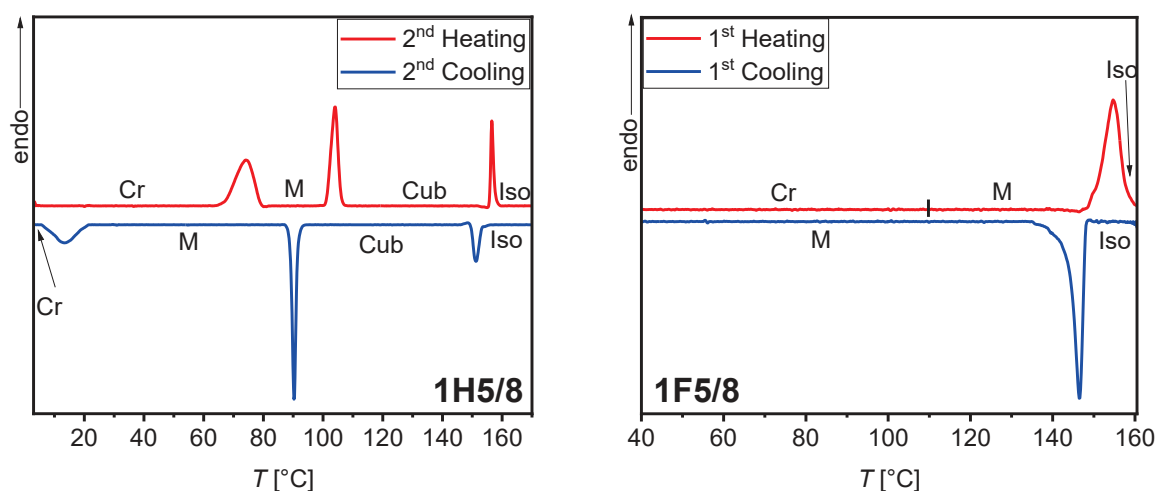**Figure S1:** DSC heating and cooling traces of compounds **1F4/10** recorded at 10 K min^{-1}.

Figure S2: DSC heating and cooling traces of compounds **1H5/8** (left) and **1F5/8** (right) recorded at 10 K min^{-1}.
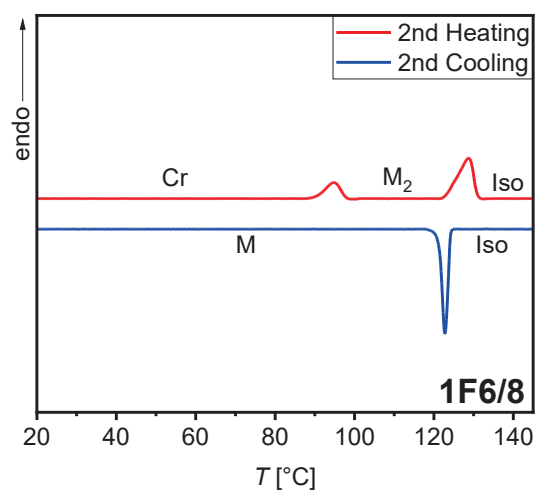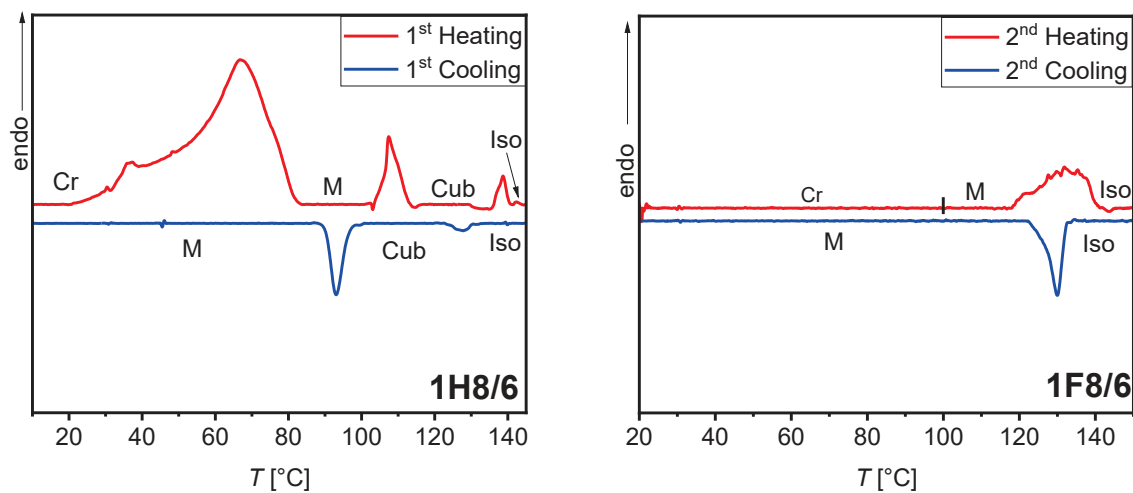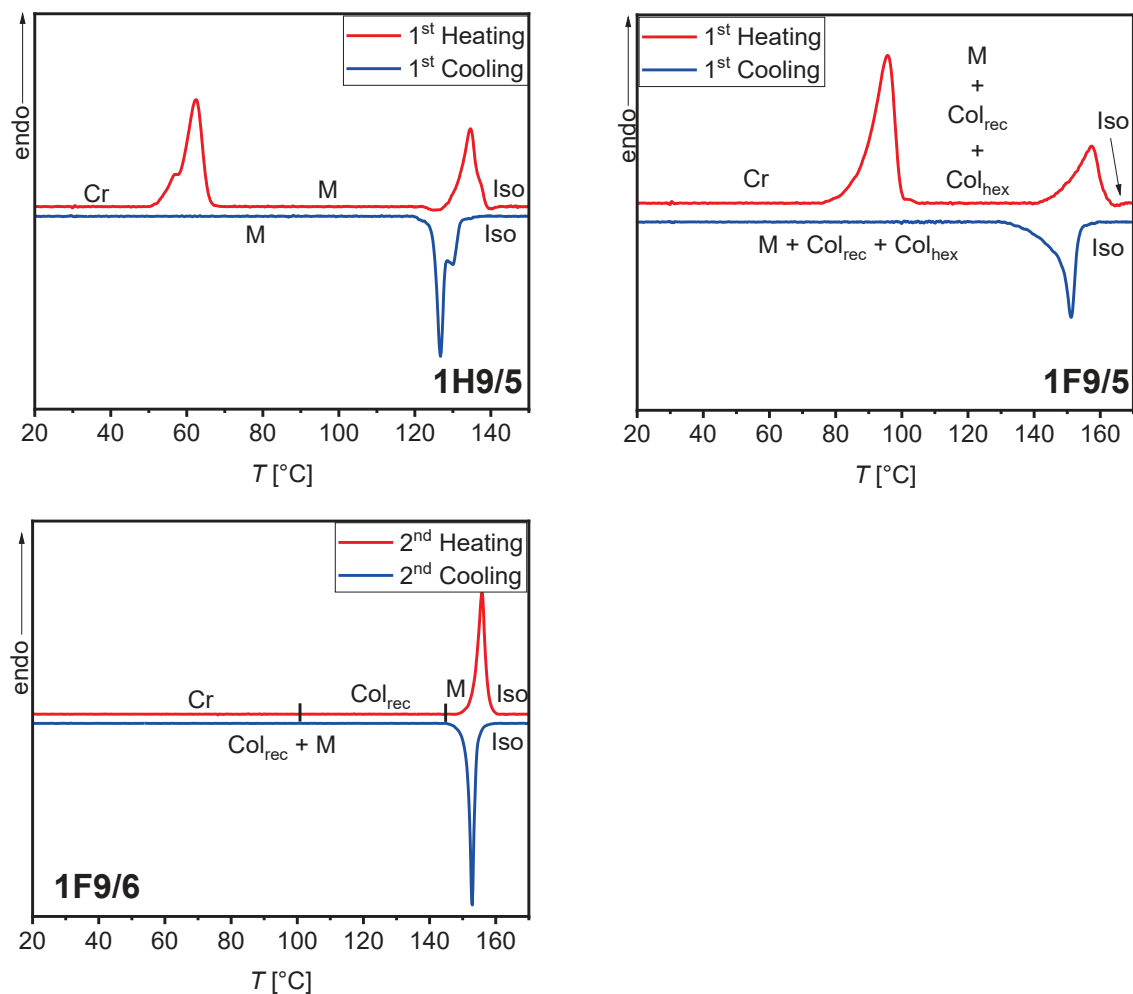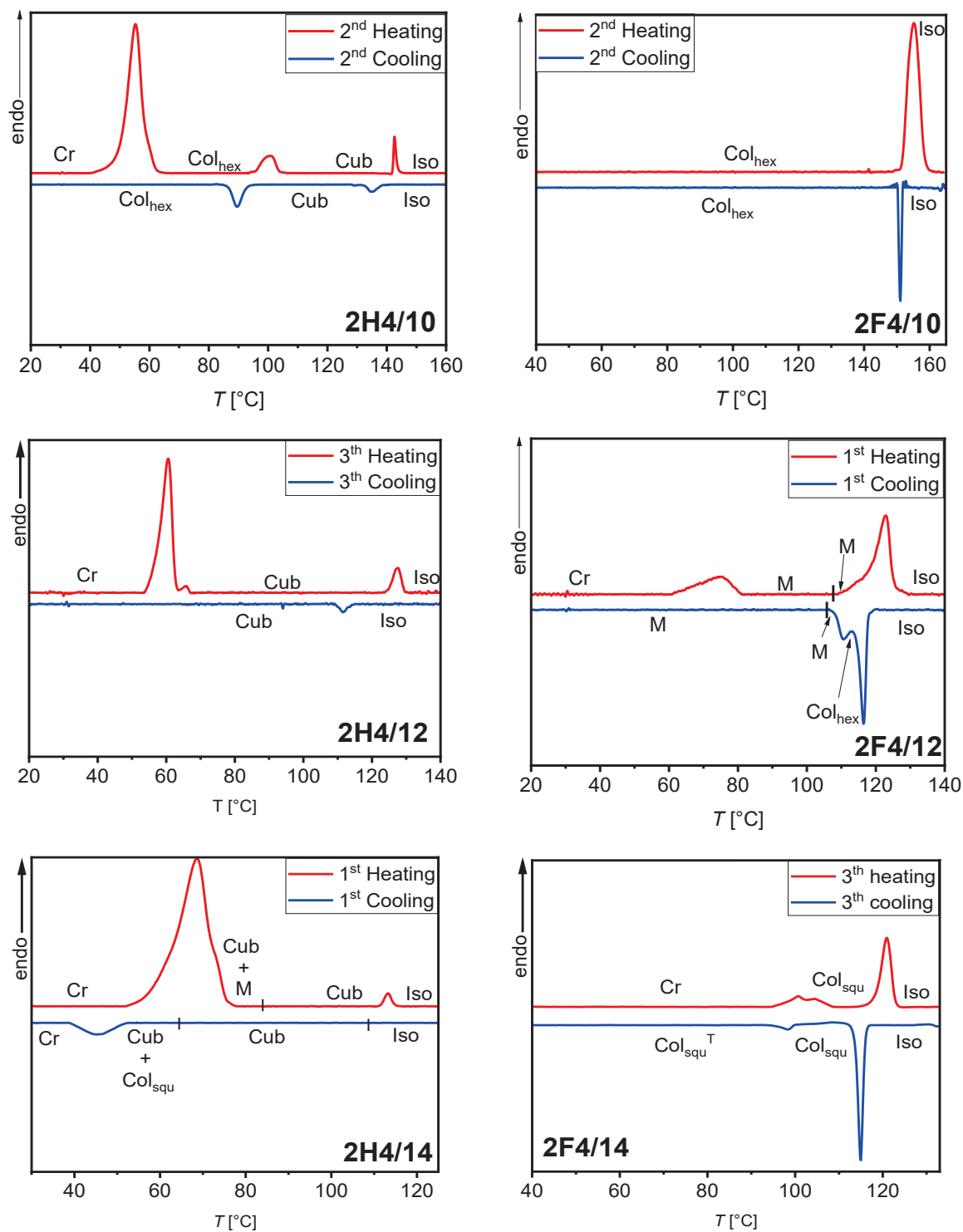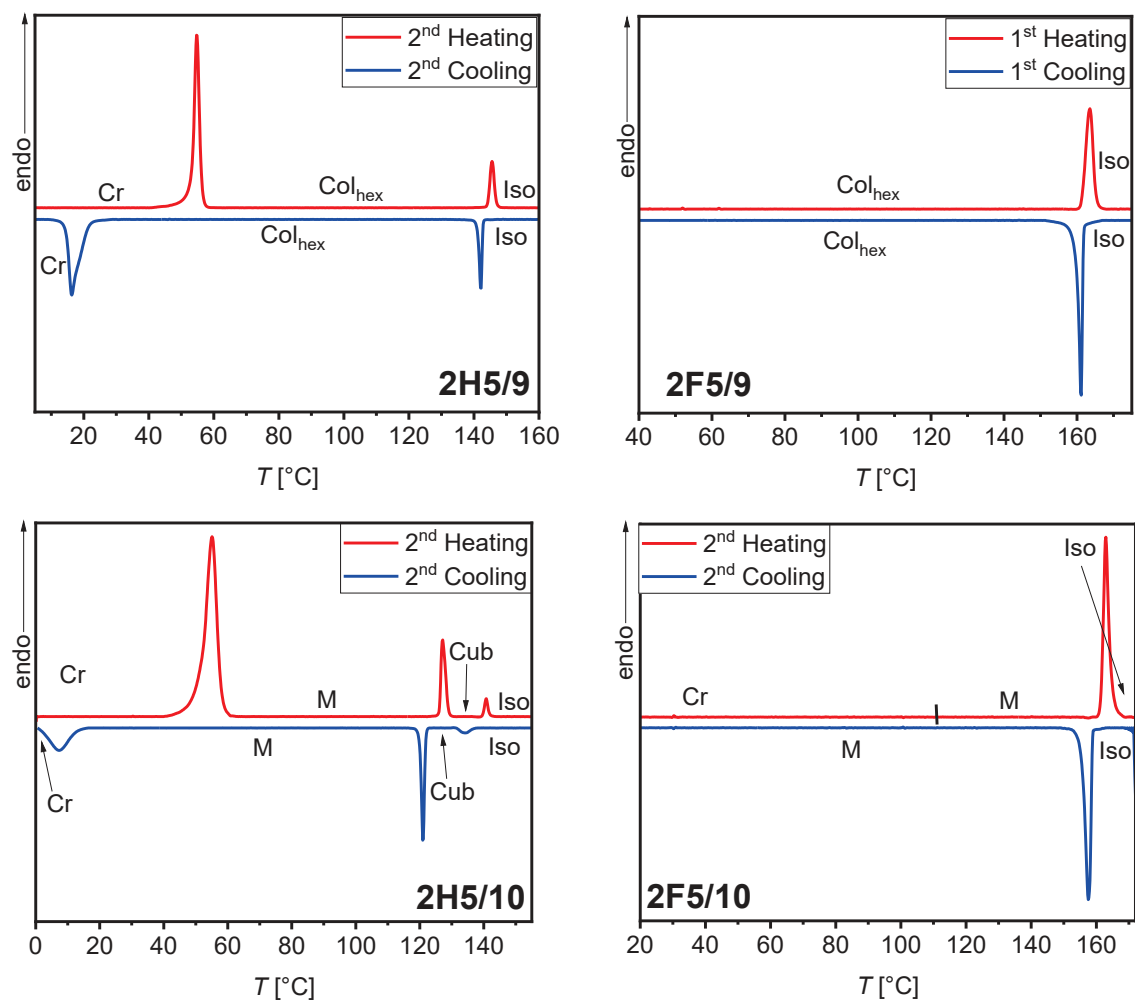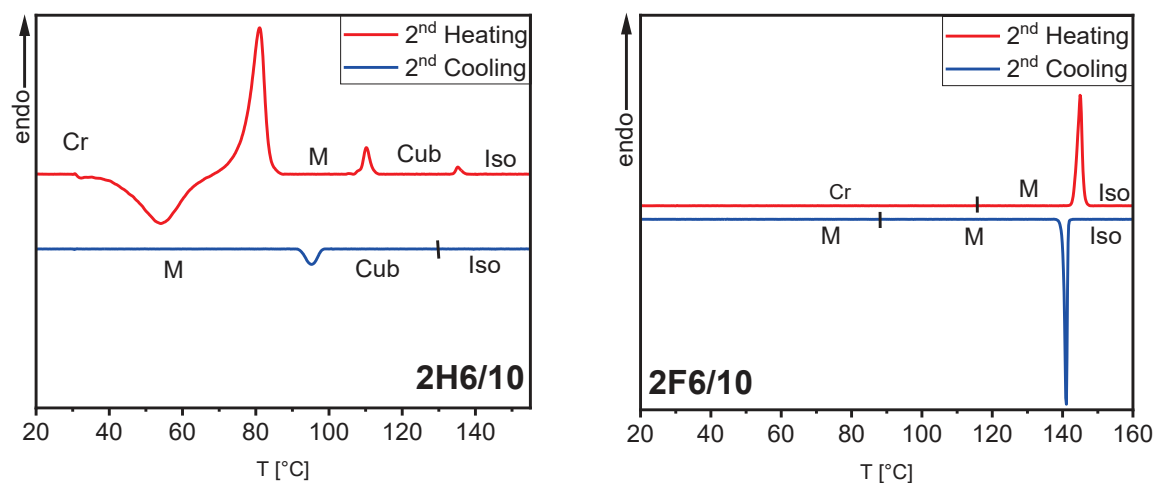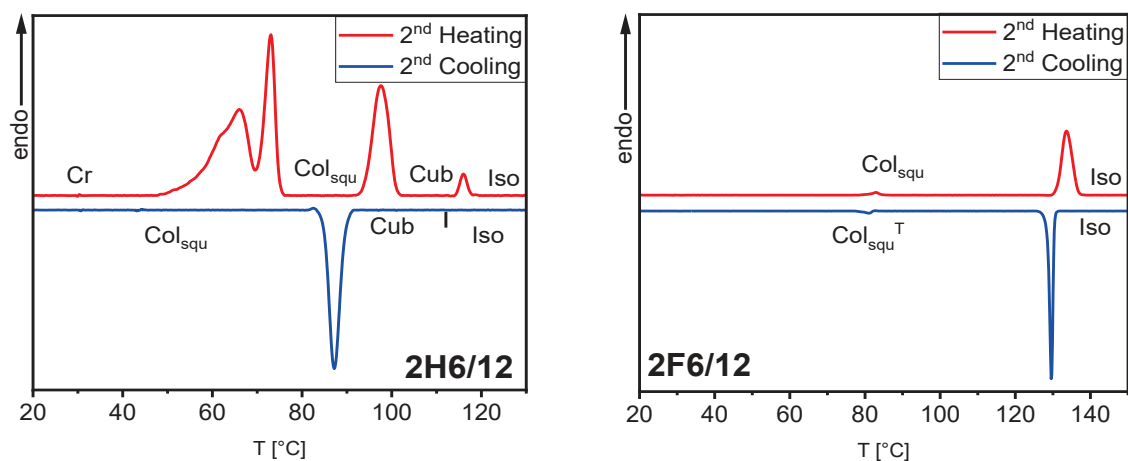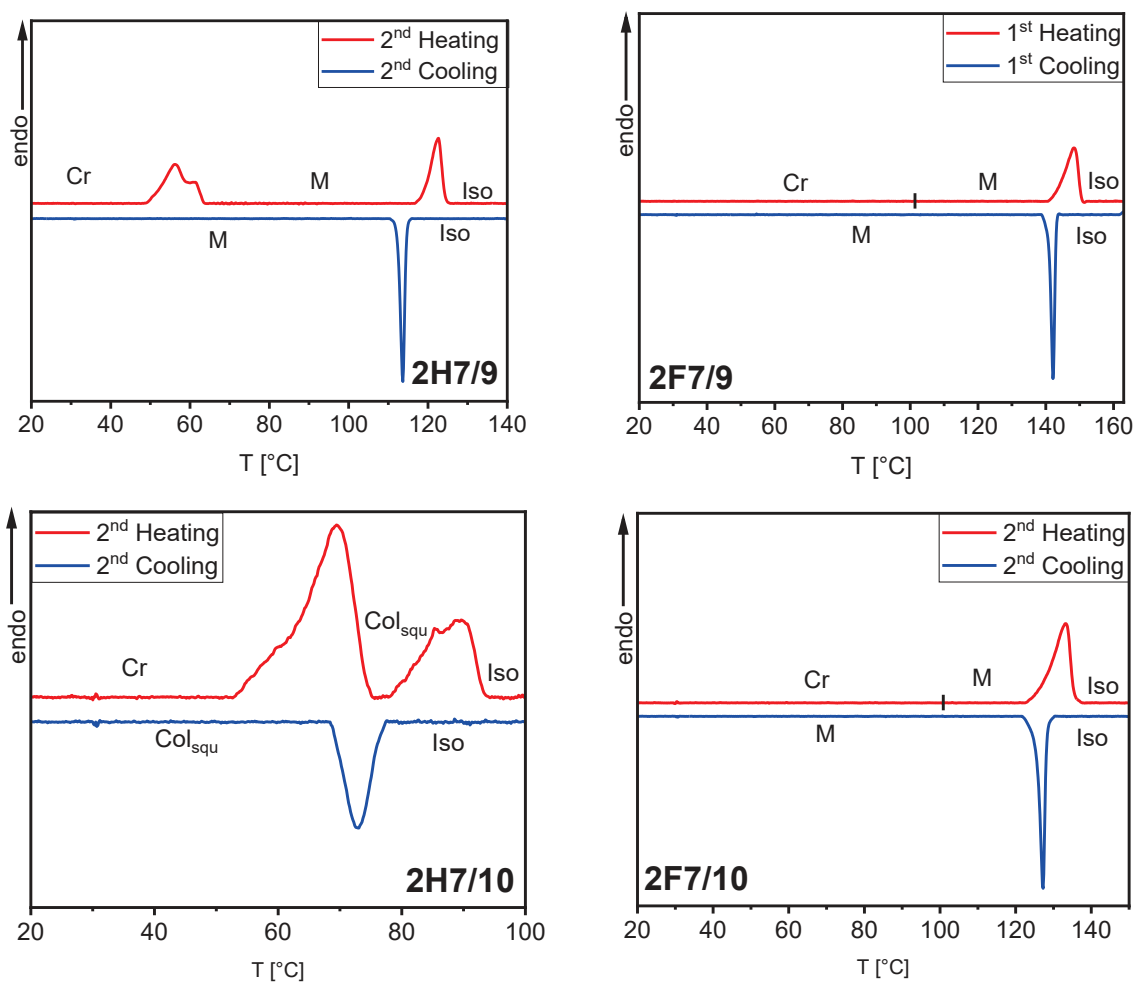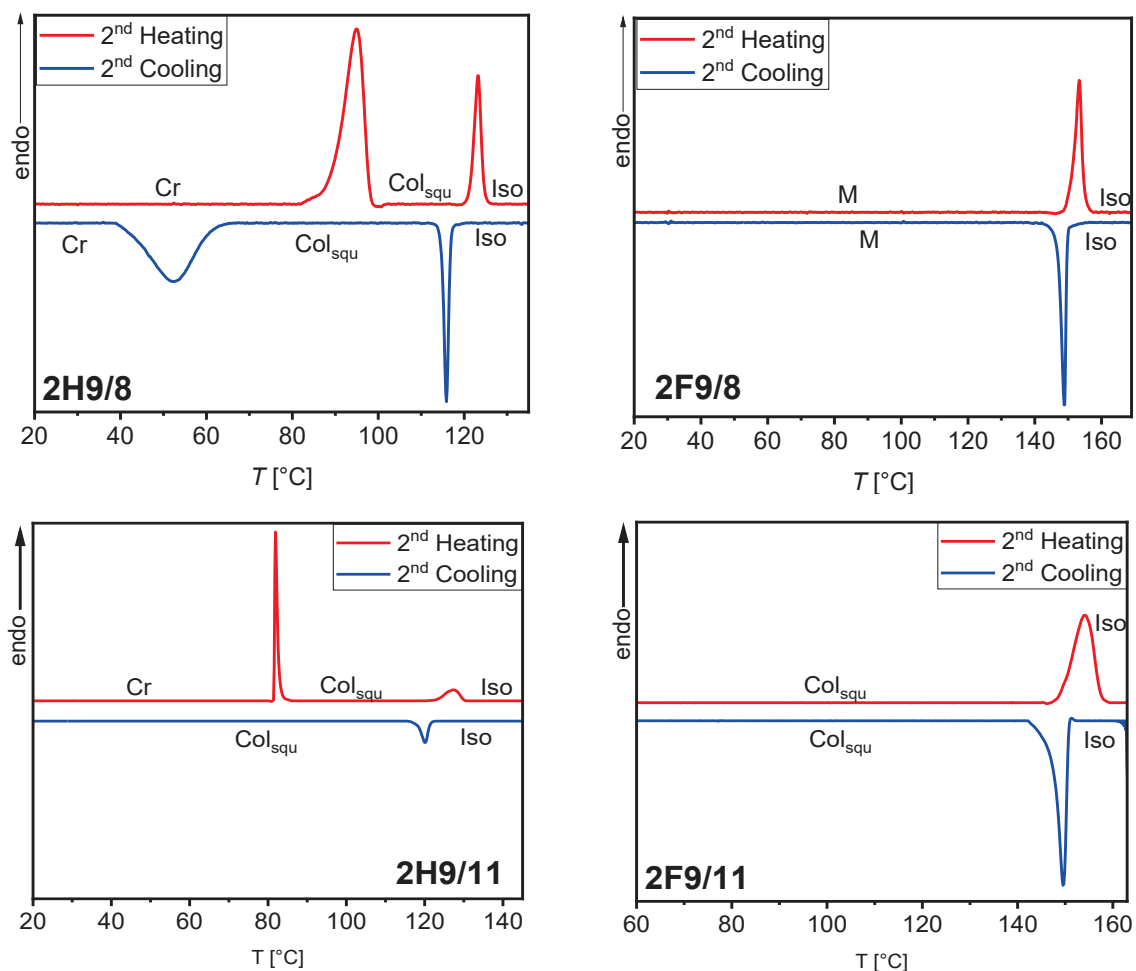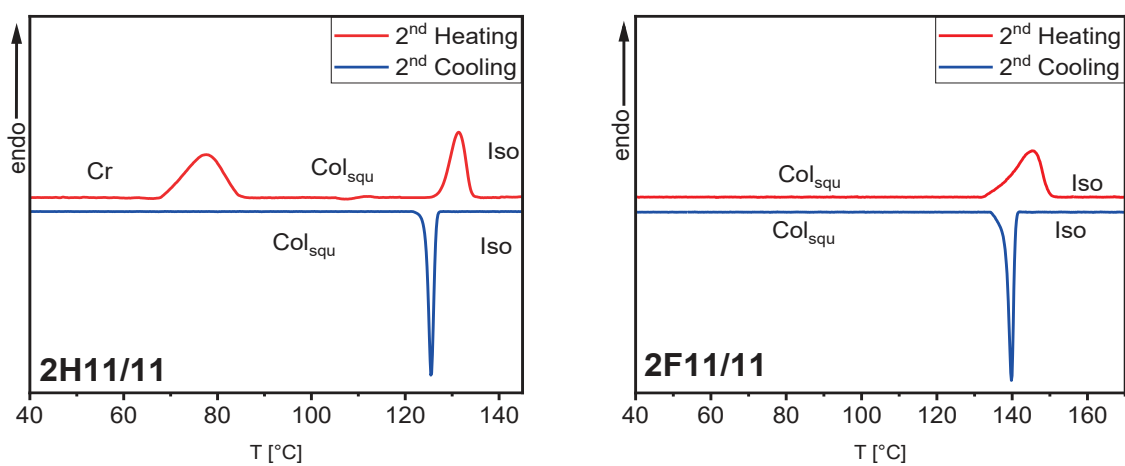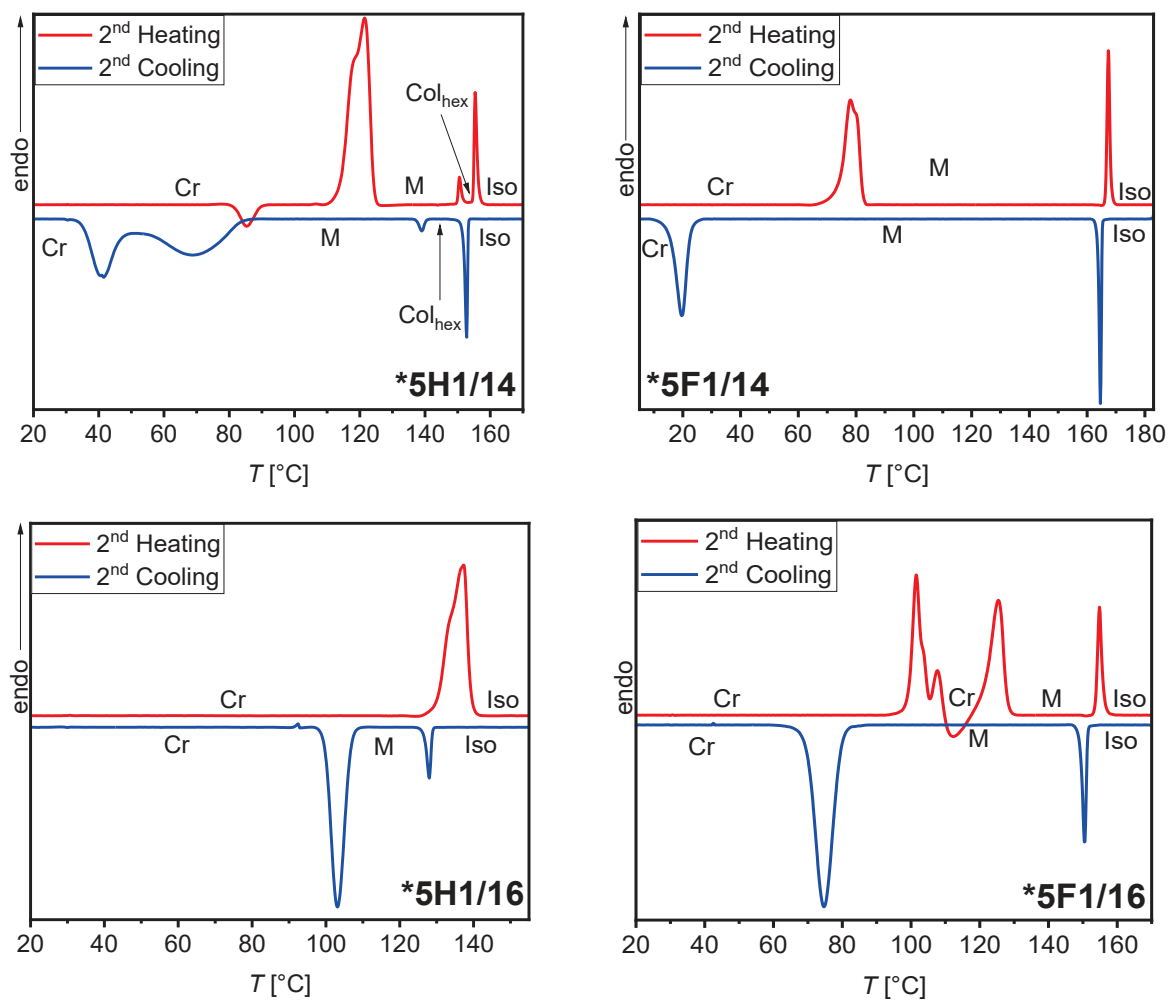

Figure S3: DSC heating and cooling traces of compounds **1F6/8** recorded at 10 K min^{-1}.

Figure S4: DSC heating and cooling traces of compounds **1H8/6** (left) and **1F8/6** (right) recorded at 10 K min^{-1}.

Figure S5: DSC heating and cooling traces of compounds **1H9/*m*** (left) and **1F9/*m*** (right) recorded at 10 K min^{-1}.

2.2 DSC traces of the 2H*m/n* and 2F*m/n* compounds
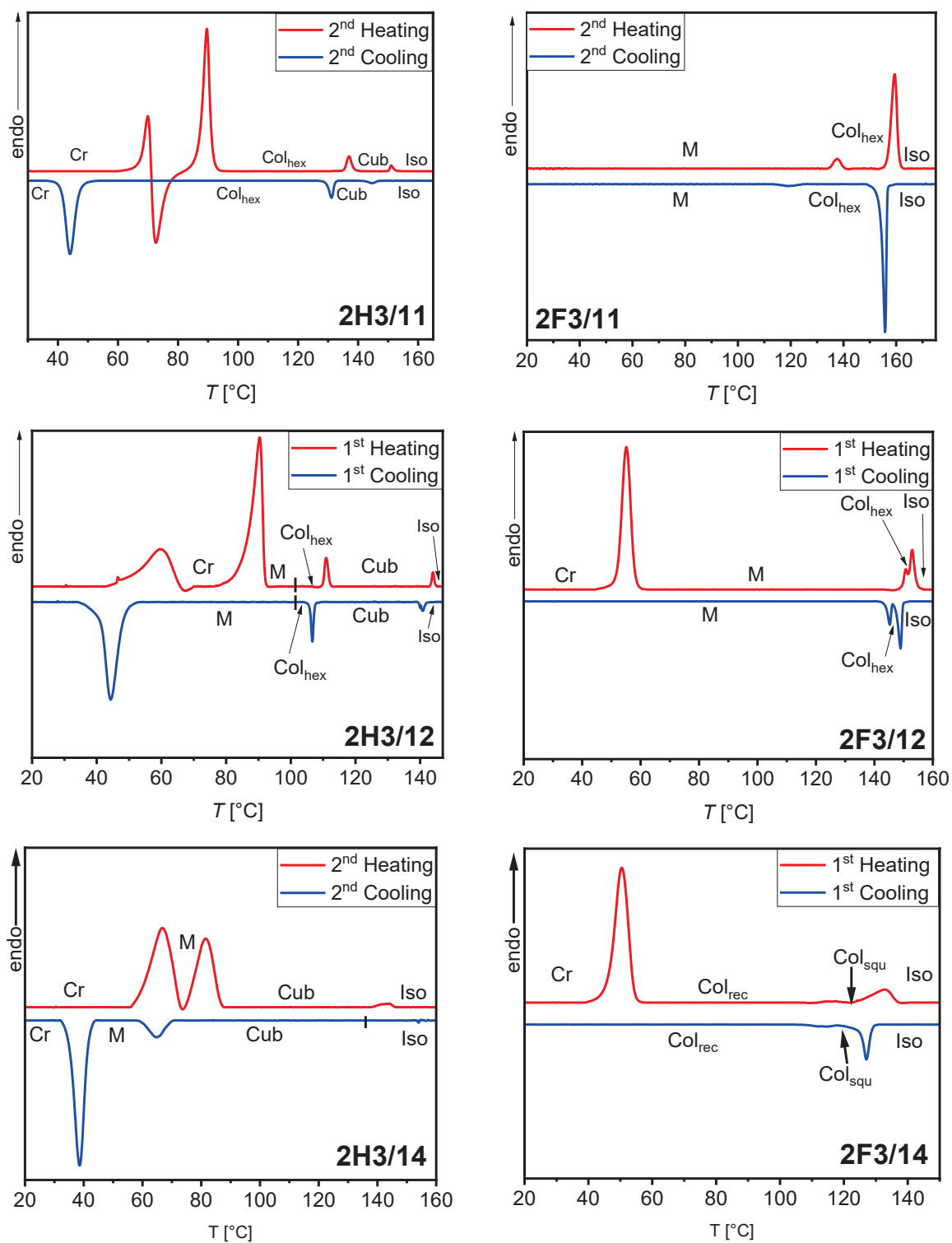
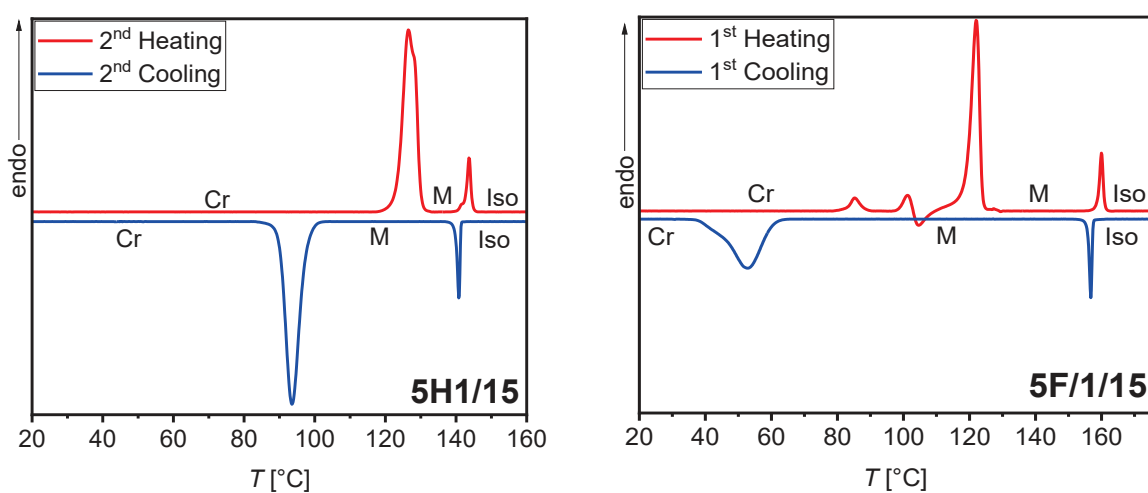**Figure S6:** DSC heating and cooling traces of compounds **2H3/*m*** (left) and **2F3/*m*** (right) recorded at 10 K min^{-1}.

Figure S7: DSC heating and cooling traces of compounds **2H4/*m*** (left) and **2F4/*m*** (right) recorded at 10 K min⁻¹.

Figure S8: DSC heating and cooling traces of compounds **2H5/*m*** (left) and **2F5/*m*** (right) recorded at 10 K min⁻¹.

Figure S9: DSC heating and cooling traces of compounds **2H6/*m*** (left) and **2F6/*m*** (right) recorded at 10 K min⁻¹.

Figure S9 (cont.): DSC heating and cooling traces of compounds **2H6/*m*** (left) and **2F6/*m*** (right) recorded at 10 K min^{-1}.

Figure S10: DSC heating and cooling traces of compounds **2H7/*m*** (left) and **2F7/*m*** (right) recorded at 10 K min^{-1}.

Figure S11: DSC heating and cooling traces of compounds **2H9/11** (left) and **2F9/11** (right) recorded at 10 K min⁻¹.

Figure S12: DSC heating and cooling traces of compounds **2H11/11** (left) and **2F11/11** (right) recorded at 10 K min⁻¹.

2.3　　DSC traces of the 5X*m/n* and *5X*m/n* compounds

Figure S13: DSC heating and cooling traces of compounds ***5H1/*n** (left) and ***5F1/*n** (right) recorded at 10 K min⁻¹.

Figure S14: DSC heating and cooling traces of compounds **5H1/15** (left) and **5F1/15** (right) recorded at 10 K min⁻¹.

Appendix-3: Unpublished XRD data

3.1   Additional WAXS patterns
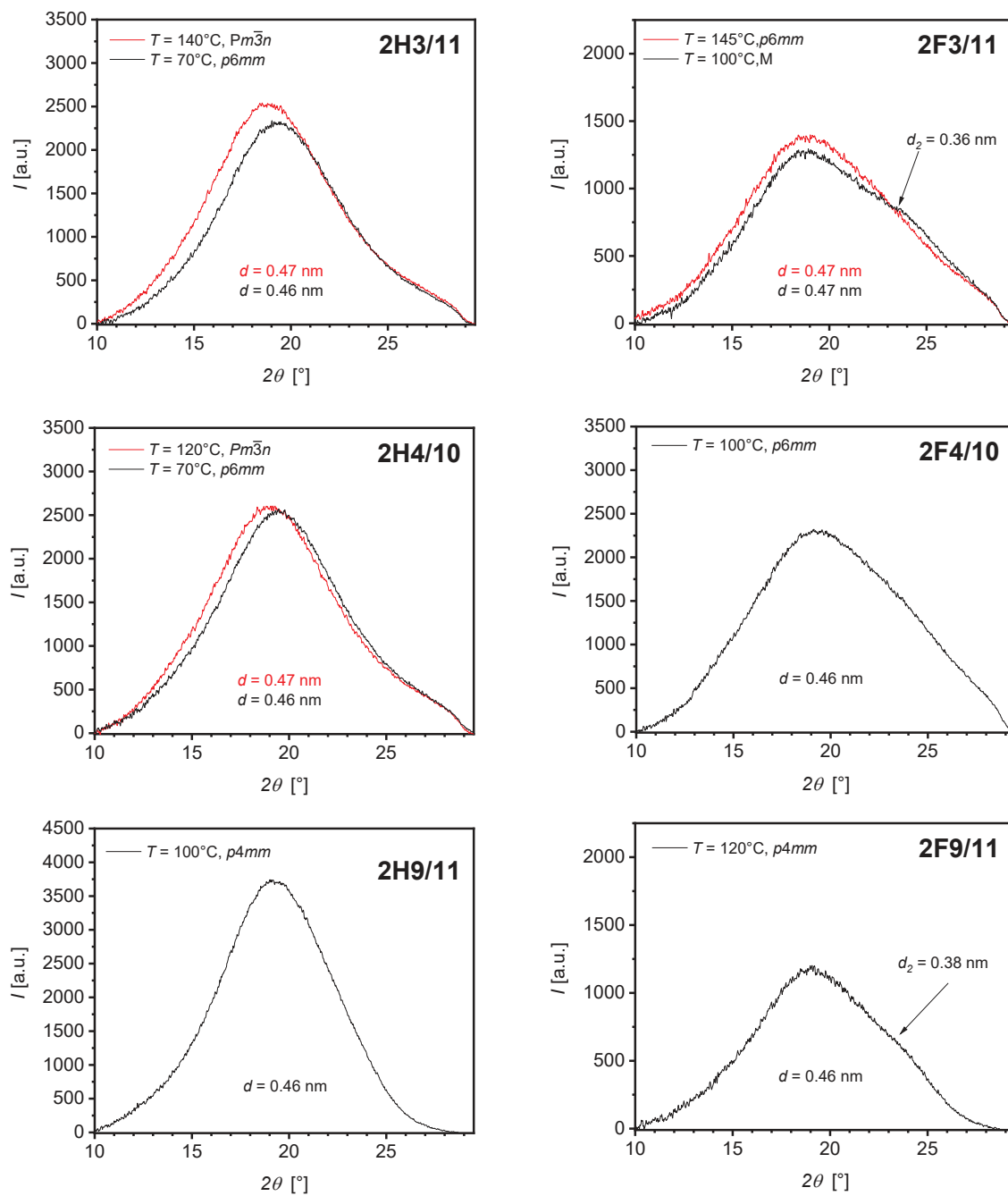
Figure S15: WAXS diffractograms of compounds **2H*m/n*** (left) and **2F*m/n*** (right) at the indicated temperatures measured upon cooling.

3.2   Additional SAXS patterns
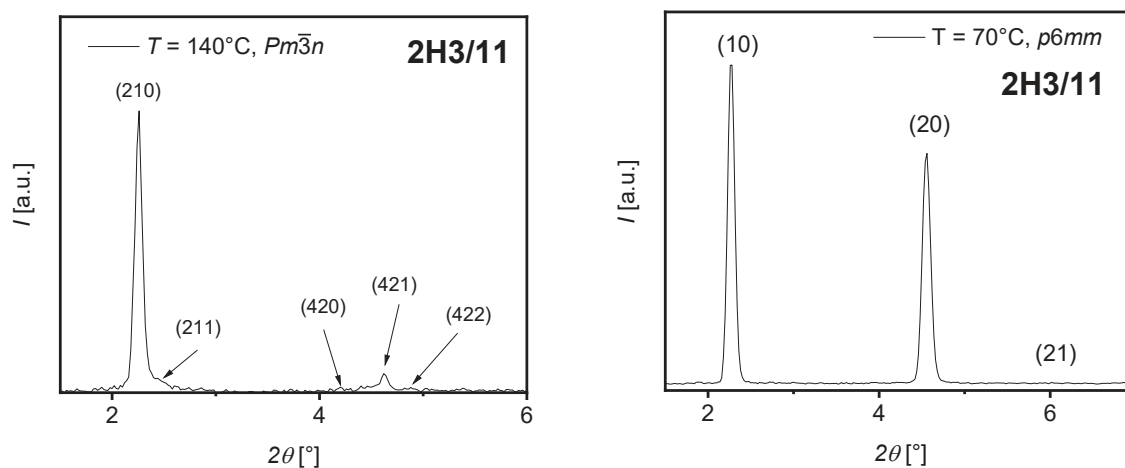
Figure S16: SAXS diffractograms of compound **2H3/11** at the indicated temperatures.
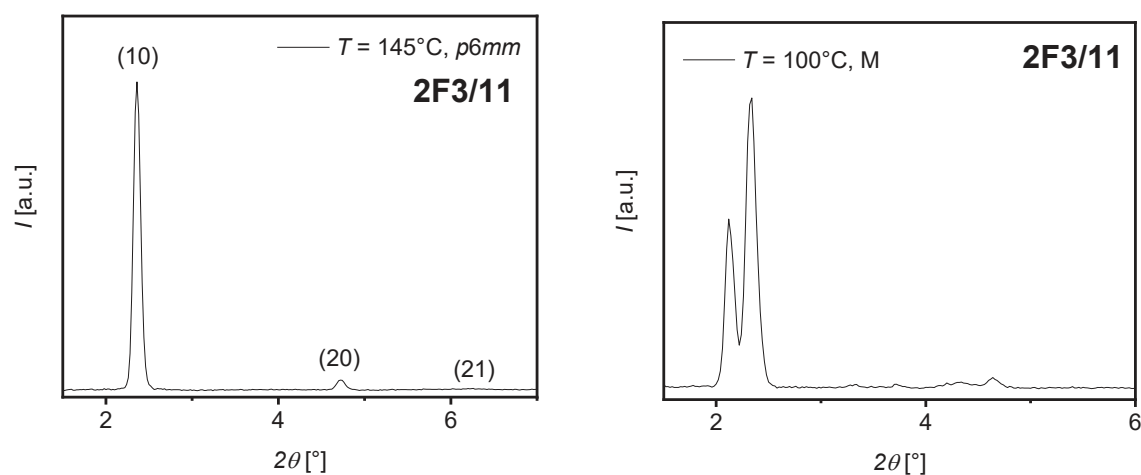
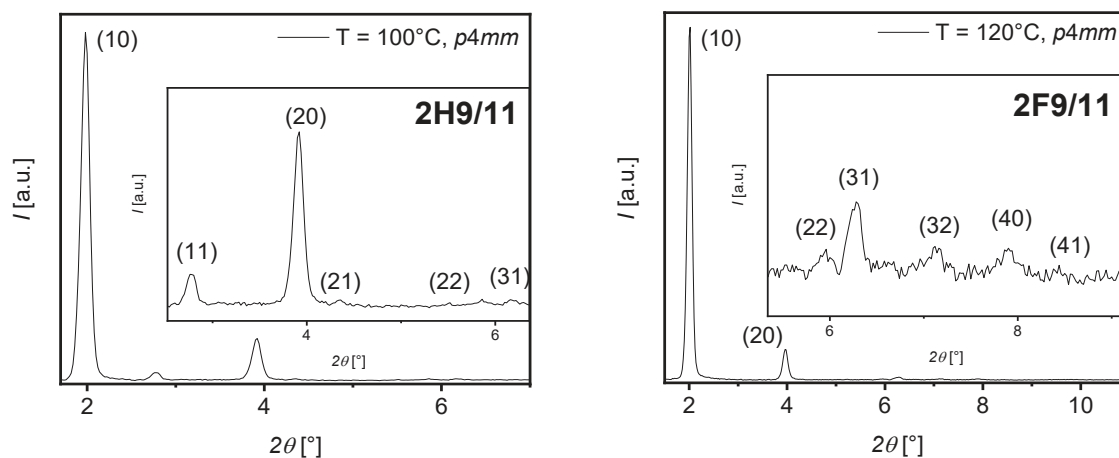**Figure S17:** SAXS diffractograms of compound **2F3/11** at the indicated temperatures.
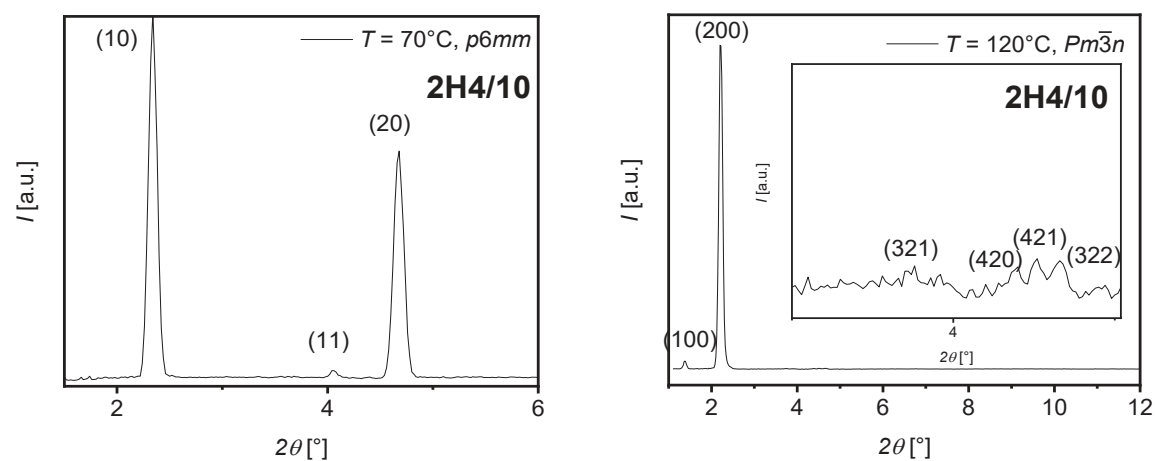
Figure S18: SAXS diffractograms of compound **2H4/10** at the indicated temperatures.
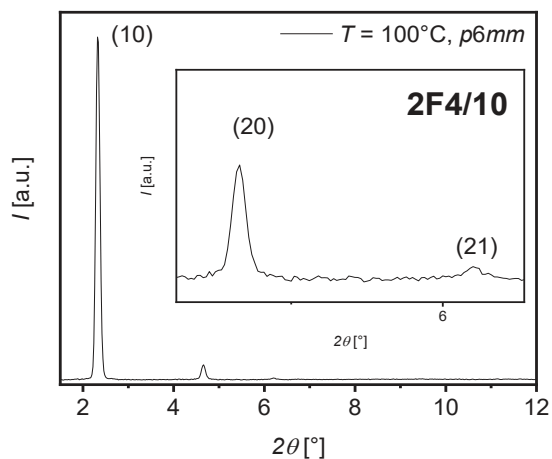
Figure S19: SAXS diffractograms of compound **2F4/10** at the indicated temperatures.

Figure S20: SAXS diffractograms of compounds **2H9/11** (left) and **2F9/11** (right) at the indicated temperatures.

3.3   Numerical SAXS data

Table S1: Experimental and calculated d-spacing for the observed SAXS reflections of the Cub/$Pm\overline{3}n$ phase of compounds **2H3/11** at T = 140°C.

2θ [°]	d_{obs} [nm]	d_{calc} [nm]	Δ	hk
2.258	3.913	3.913	0.00	210
2.457	3.596	3.572	0.02	211
4.441	1.990	1.956	0.03	420
4.625	1.911	1.909	0.00	421
4.858	1.819	1.786	0.03	422
a = 9.05 nm				

Table S2: Experimental and calculated *d*-spacing for the observed SAXS reflections of the Col$_{hex}$/*p6mm* phase of compounds **2H3/11** at *T* = 70°C.

2θ [°]	d$_{obs}$ [nm]	d$_{calc}$ [nm]	Δ	hk	Phase
2.273	3.887	3.887	0.00	10	0
4.562	1.937	1.943	0.01	20	0
6.014	1.470	1.469	0.00	21	Π
a = 4.49 nm					

Table S3: Experimental and calculated *d*-spacing for the observed SAXS reflections of the Cub/*Pm$\overline{3}$n* phase of compounds **2H4/10** at *T* = 120°C.

2θ [°]	d$_{obs}$ [nm]	d$_{calc}$ [nm]	Δ	hk
1.380	6.402	6.402	0.00	100
2.198	4.019	4.049	0.03	200
3.751	2.355	2.420	0.06	321
4.396	2.010	2.024	0.01	420
4.519	1.955	1.976	0.02	421
4.652	1.899	1.930	0.03	332
a = 8.75 nm				

**Table S4:** Experimental and calculated *d*-spacing for the observed SAXS reflections of the Col$_{hex}$/*p6mm* phase of compounds **2H4/10** at *T* = 70°C.

2θ [°]	d$_{obs}$ [nm]	d$_{calc}$ [nm]	Δ	hk	Phase
2.340	3.775	3.775	0.00	10	0
4.057	2.178	2.180	0.00	11	π
4.676	1.890	1.888	0.00	20	0
a = 4.36 nm					

Table S5: Experimental and calculated *d*-spacing for the observed SAXS reflections of the Col$_{hex}$/*p6mm* phase of compounds **2F3/11** at *T* = 145°C.

2θ [°]	d$_{obs}$ [nm]	d$_{calc}$ [nm]	Δ	hk	Phase
2.359	3.745	3.745	0.00	10	0
4.724	1.871	1.873	0.00	20	0
6.242	1.416	1.415	0.00	21	0
a = 4.33 nm					

Table S6: Experimental and calculated *d*-spacing for the observed SAXS reflections of the Col$_{hex}$/*p6mm* phase of compounds **2F4/10** at *T* = 100°C.

2θ [°]	d$_{obs}$ [nm]	d$_{calc}$ [nm]	Δ	hk	Phase
2.321	3.806	3.806	0.00	10	0
4.658	1.897	1.903	0.01	20	0
6.198	1.426	1.439	0.01	21	0
a = 4.40 nm					

Table S7: Experimental and calculated *d*-spacing for the observed SAXS reflections of the Col$_{squ}$/*p4mm* phase of compounds **2H9/11** at *T* = 100°C

2θ [°]	d_{obs} [nm]	d_{calc} [nm]	Δ	hk	Phase
1.980	4.462	4.462	0.00	10	0
2.784	3.172	3.155	0.02	11	0
3.916	2.256	2.231	0.03	20	0
4.352	2.030	1.995	0.03	21	π
5.791	1.526	1.577	0.05	22	-
6.162	1.434	1.411	0.02	31	-
a = 4.49 nm					

Table S8: Experimental and calculated *d*-spacing for the observed SAXS reflections of the Col$_{squ}$/*p4mm* phase of compounds **2F9/11** at *T* = 120°C.

2θ [°]	d_{obs} [nm]	d_{calc} [nm]	Δ	hk	Phase
2.020	4.373	4.373	0.00	10	0
3.963	2.230	2.187	0.04	20	0
5.973	1.480	1.546	0.05	22	0
6.257	1.413	1.383	0.03	31	π
7.122	1.241	1.213	0.02	32	-
7.918	1.117	1.093	0.02	40	-
8.464	1.045	1.061	0.02	41	-
a = 4.20 nm					

3.4   Additional electron density maps
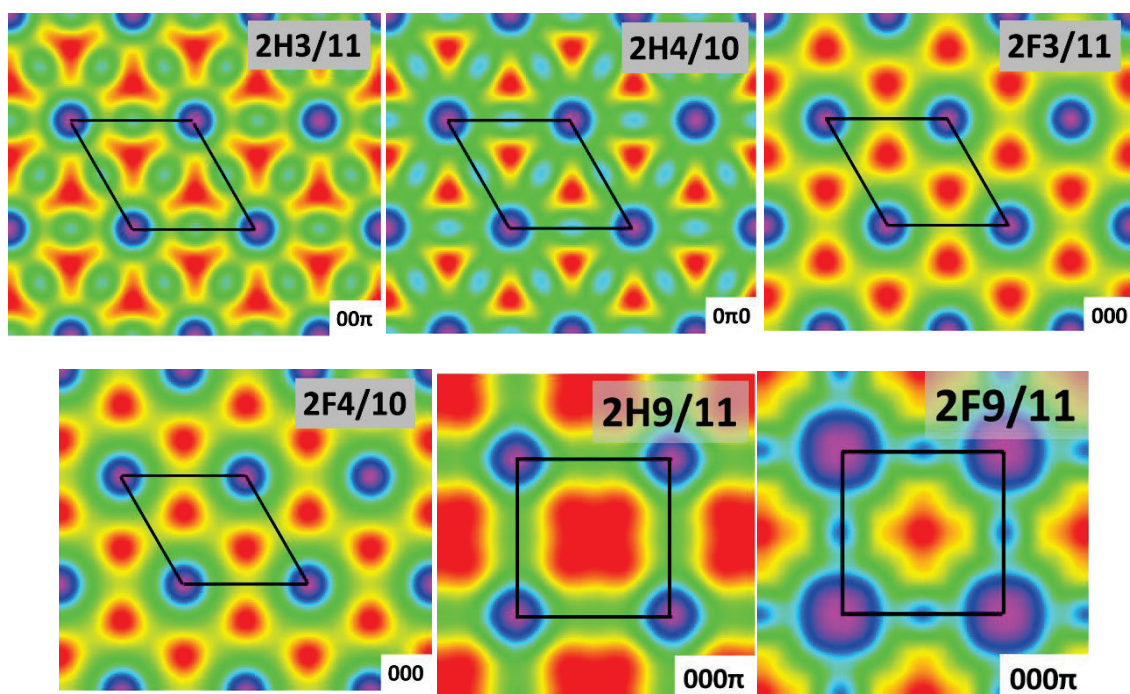
Figure S21: Reconstructed EDMs of columnar phases.

Appendix-4: Representative NMR-spectra of unpublished compounds
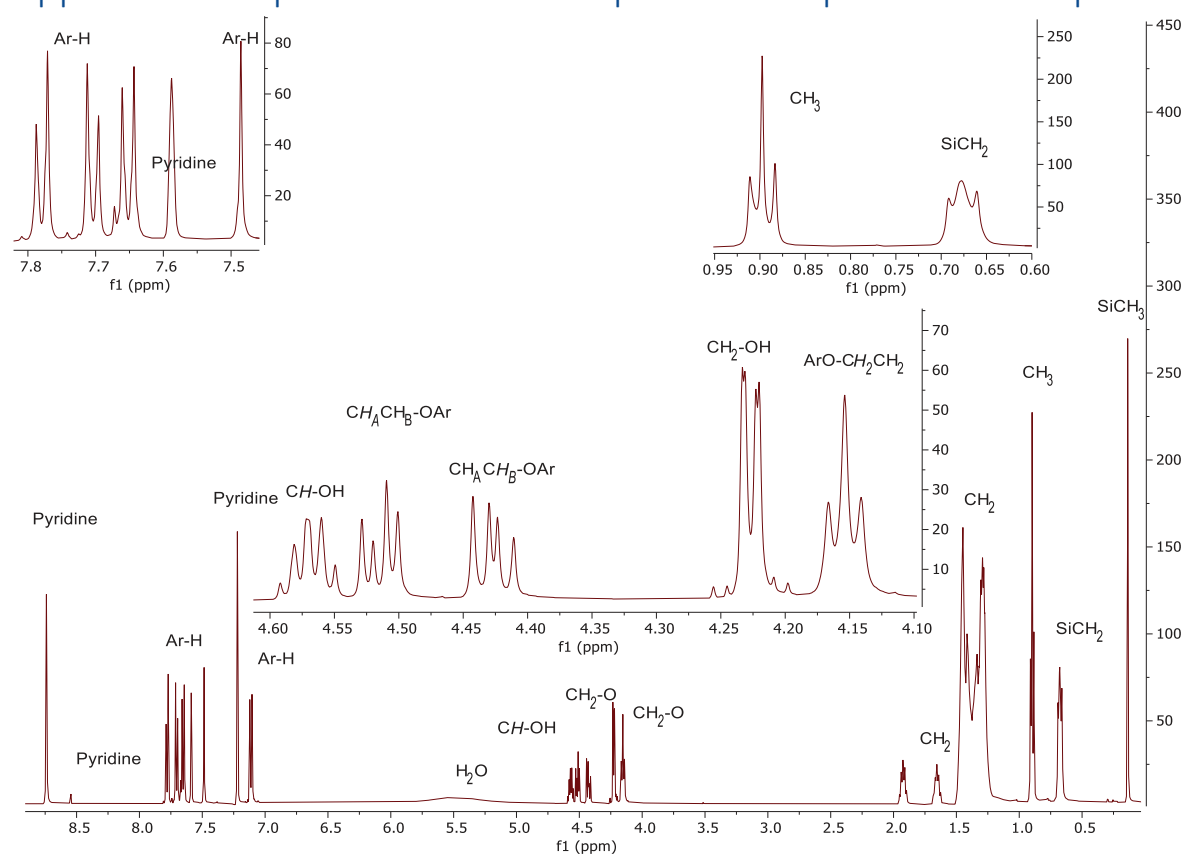
Figure S22: ^{1}H-NMR of compound **2H9/11** (500 MHz, pyridine-d$_5$).
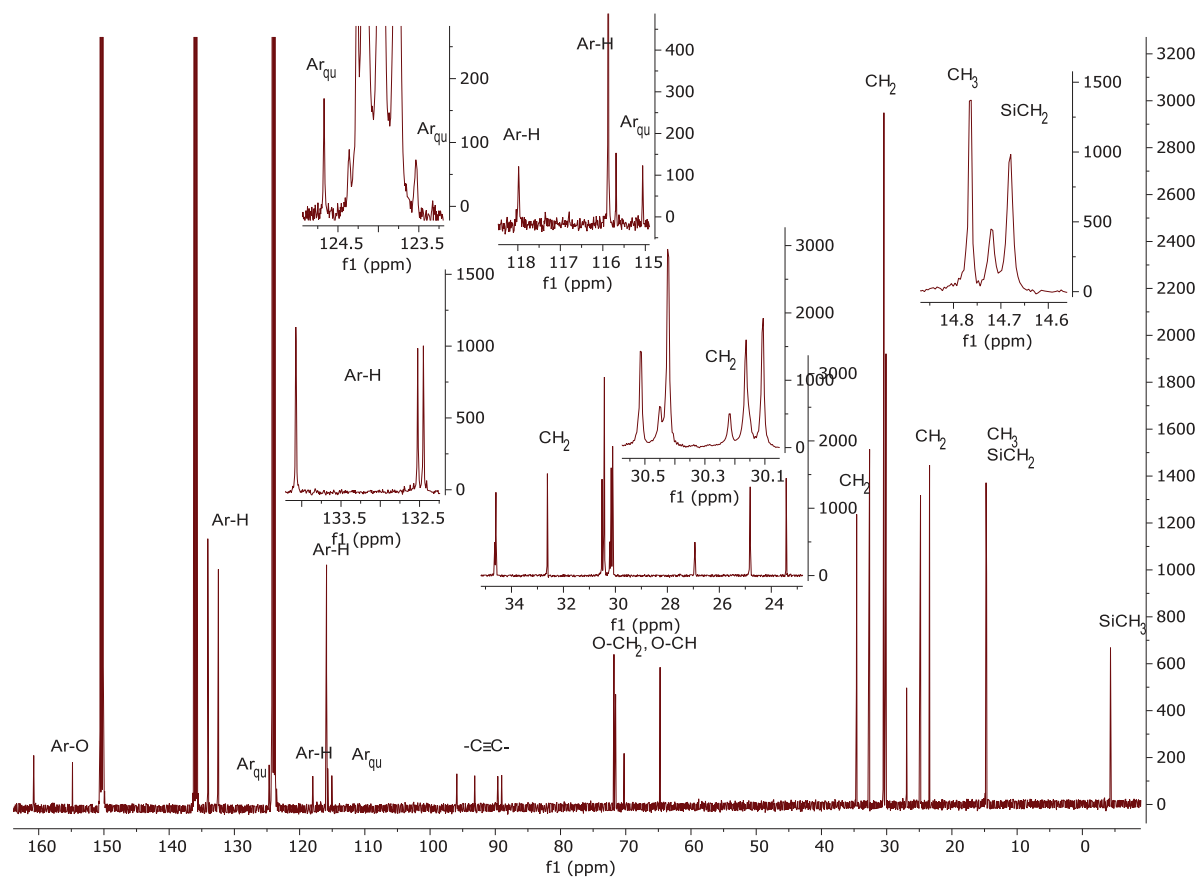
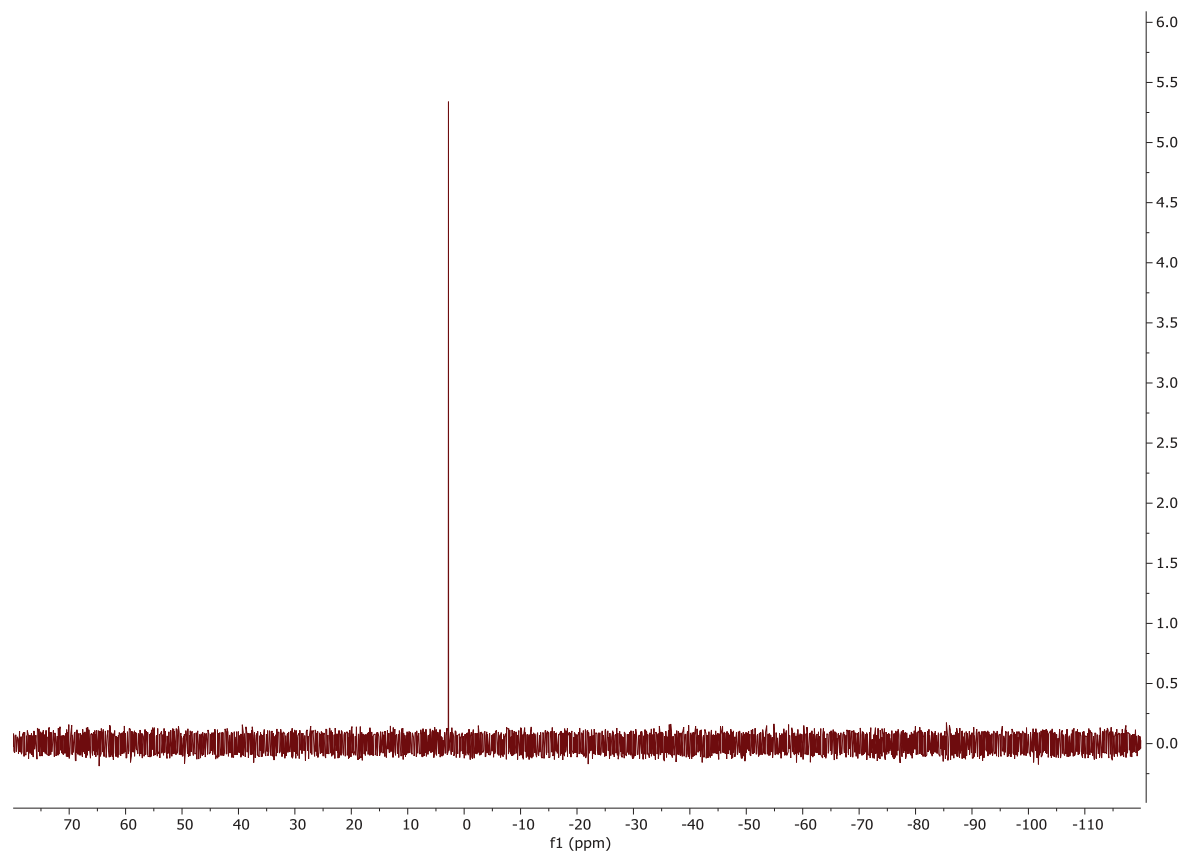**Figure S23:** ^{13}C-NMR of compound **2H9/11** (126 MHz, pyridine-d$_5$).

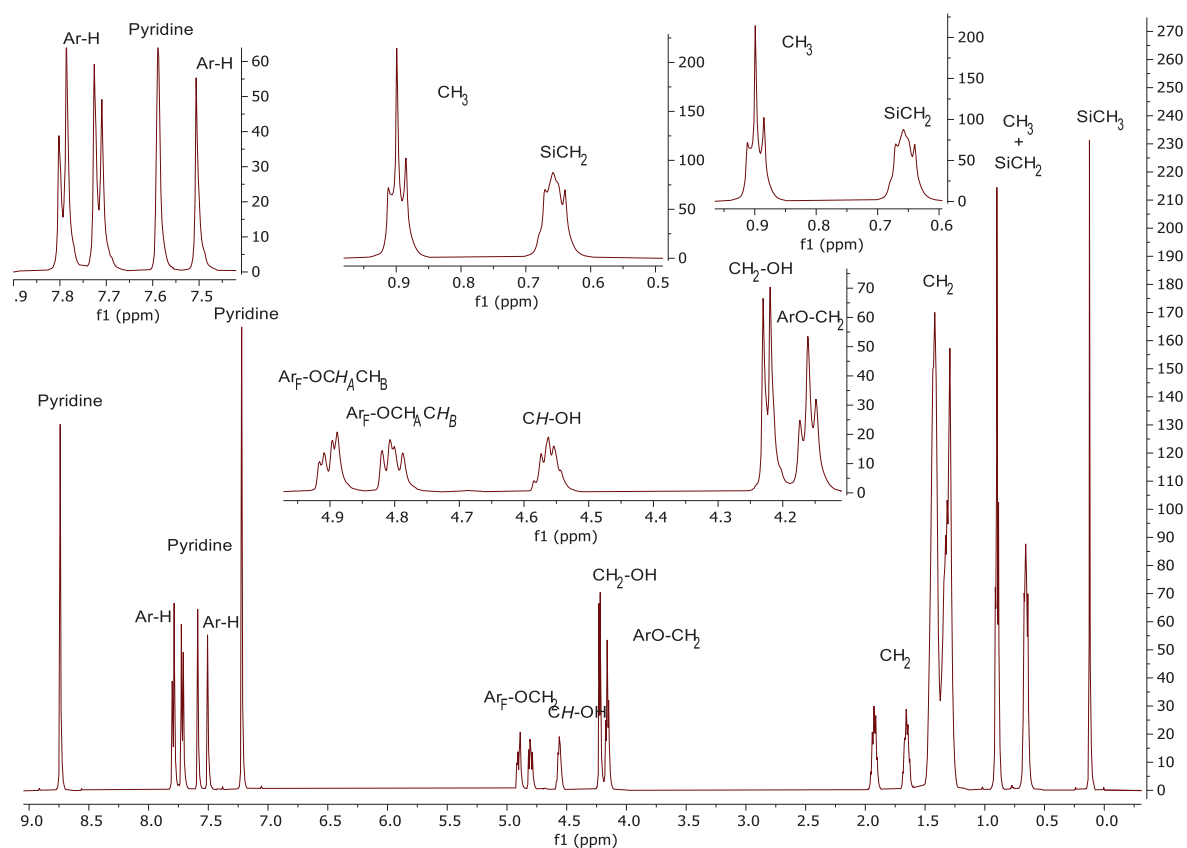**Figure S24:** ^{29}Si-NMR of compound **2H9/11** (99 MHz, pyridine-d$_5$).

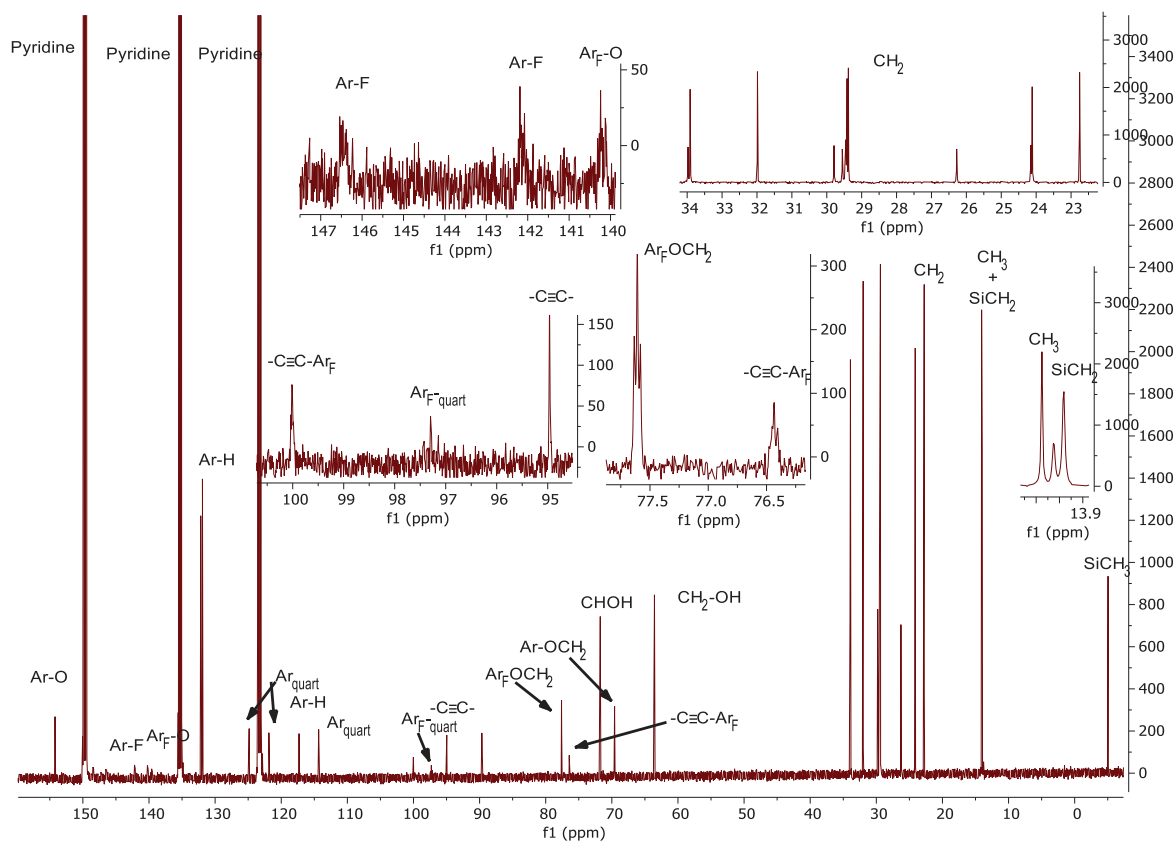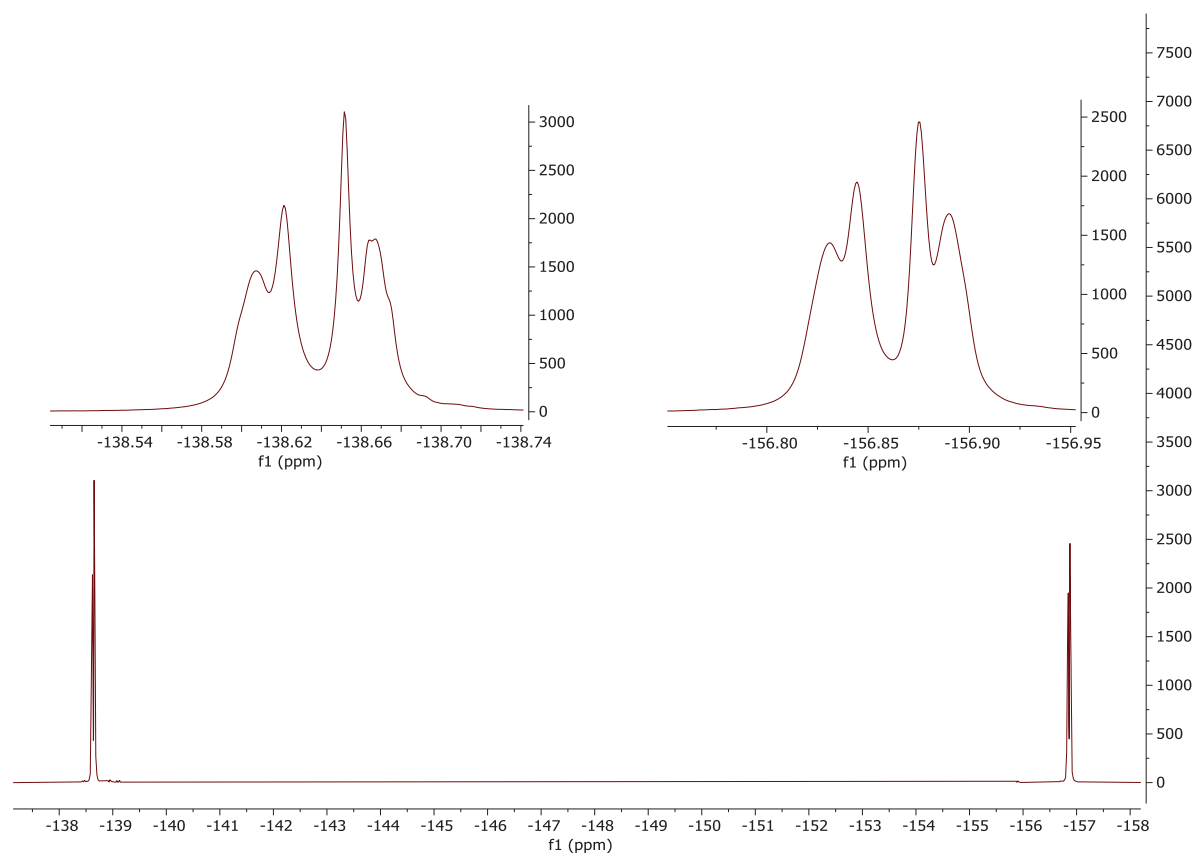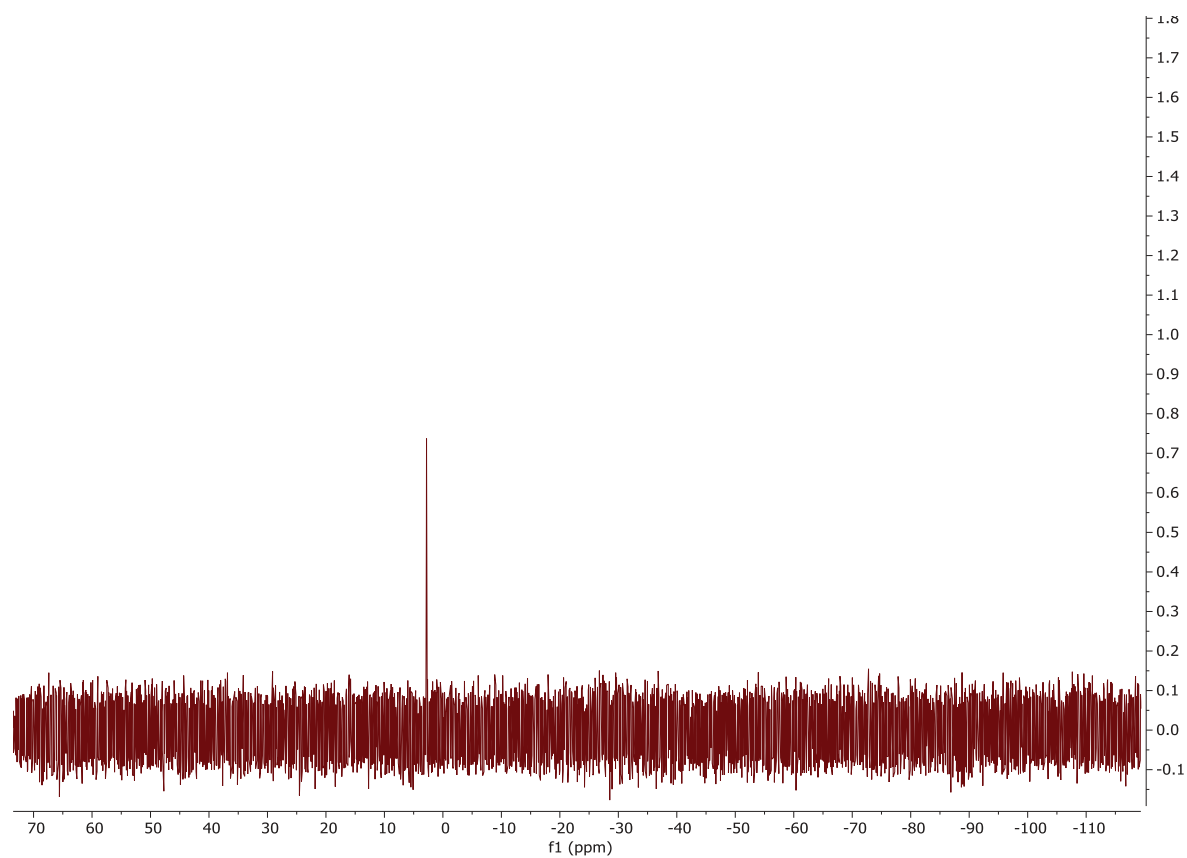**Figure S25:** ^{1}H-NMR of compound **2F9/8** (402 MHz, pyridine-d$_5$).

Figure S26: ^{13}C-NMR of compound **2F9/11** (126 MHz, pyridine-d$_5$).

Figure S27: ^{19}F-NMR of compound **2F9/11** (473 MHz, pyridine-d$_5$).

Figure S28: ^{29}Si-NMR of compound **2F9/11** (80 MHz, pyridine-d$_5$).
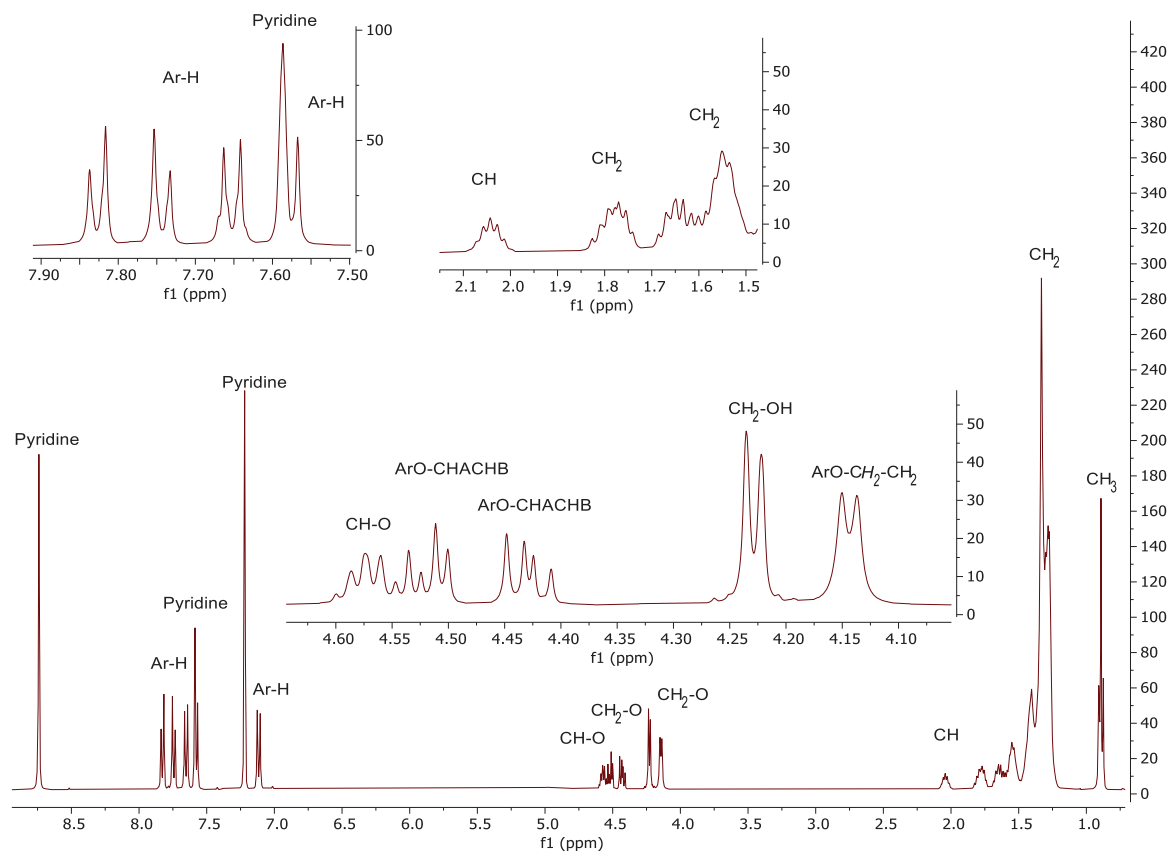
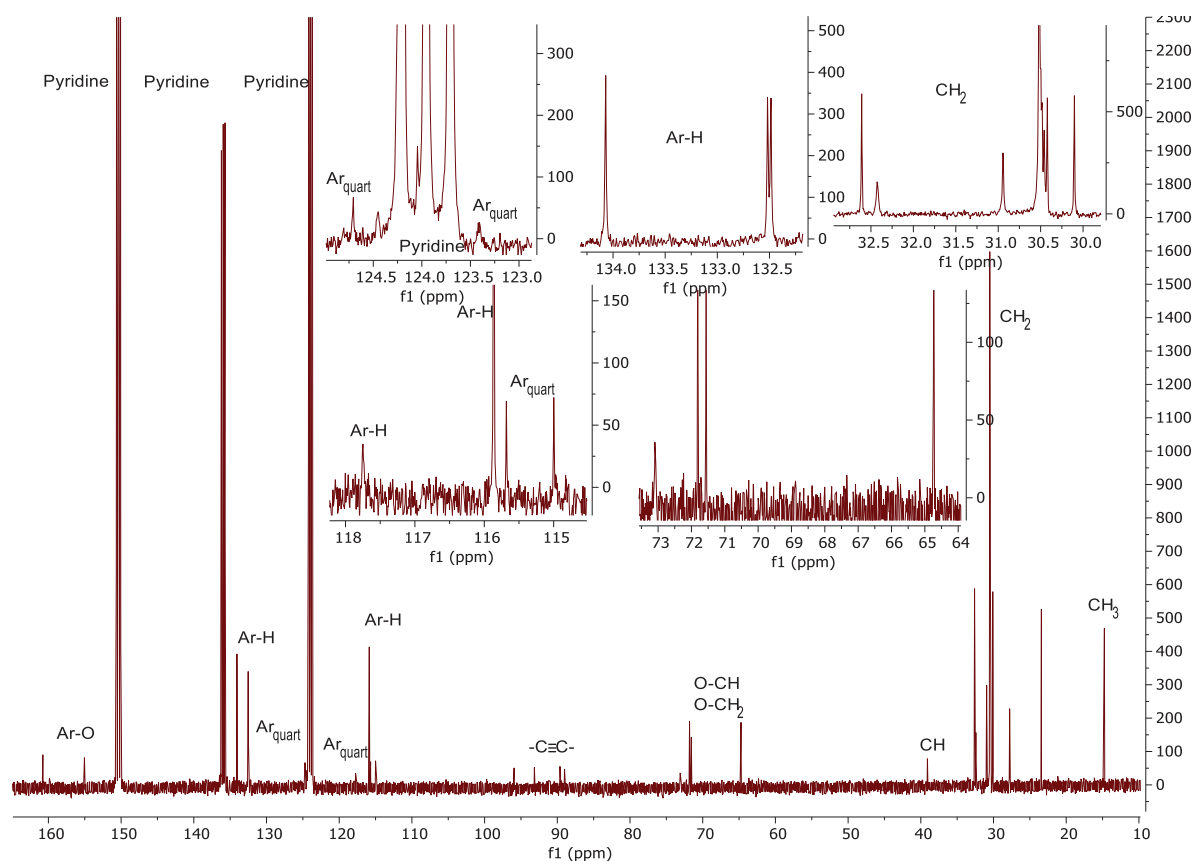**Figure S29:** ^{1}H-NMR of compound **5H1/15** (400 MHz, pyridine-d$_5$).

Figure S30: ^{13}C-NMR of compound **5H1/15** (101 MHz, pyridine-d$_5$).

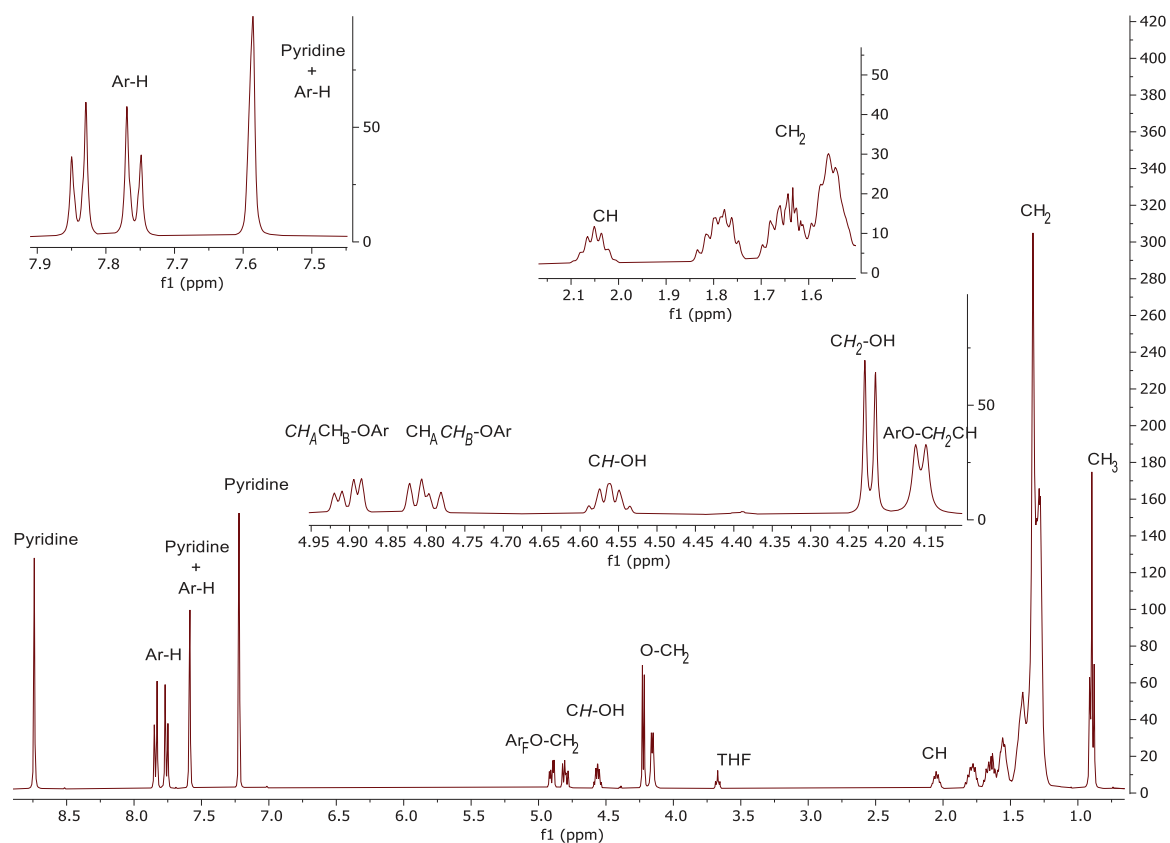**Figure S31:** ^{1}H-NMR of compound **5F1/15** (400 MHz, pyridine-d$_5$).
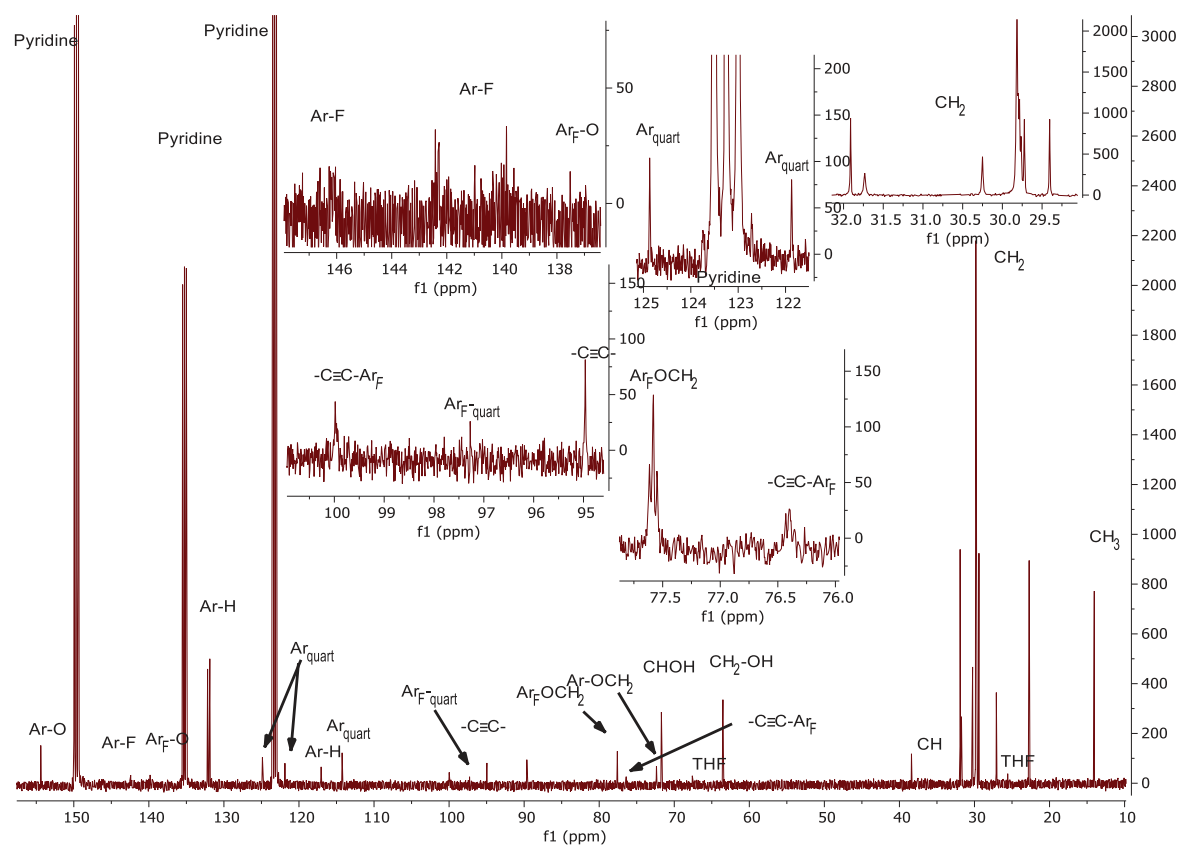

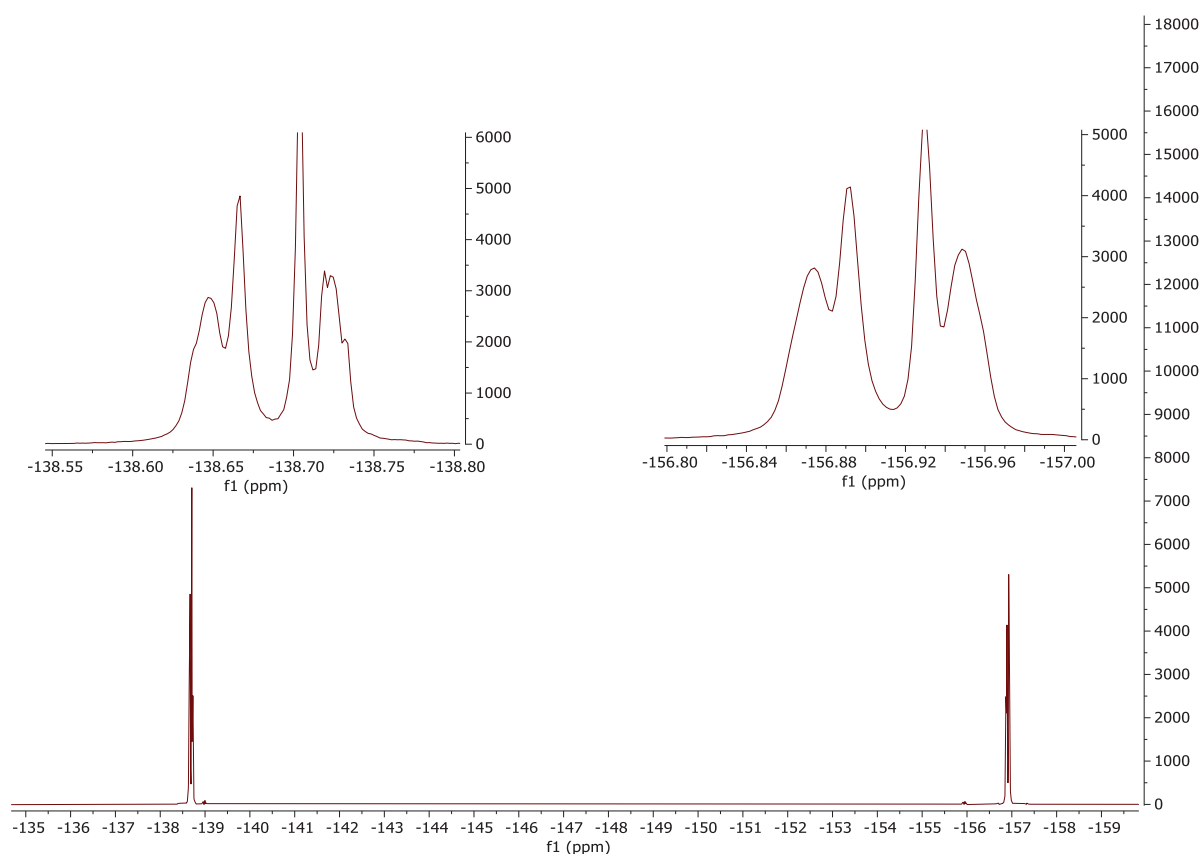**Figure S32:** ^{13}C-NMR of compound **5F1/15** (101 MHz, pyridine-d$_5$).

Figure S33: ^{19}F-NMR of compound **5F1/15** (473 MHz, pyridine-d$_5$).

Figure S34: ^{1}H-NMR of compound **5H3/14** (400 MHz, pyridine-d$_5$).

Figure S35: ^{13}C-NMR of compound **5H3/14** (101 MHz, pyridine-d$_5$).

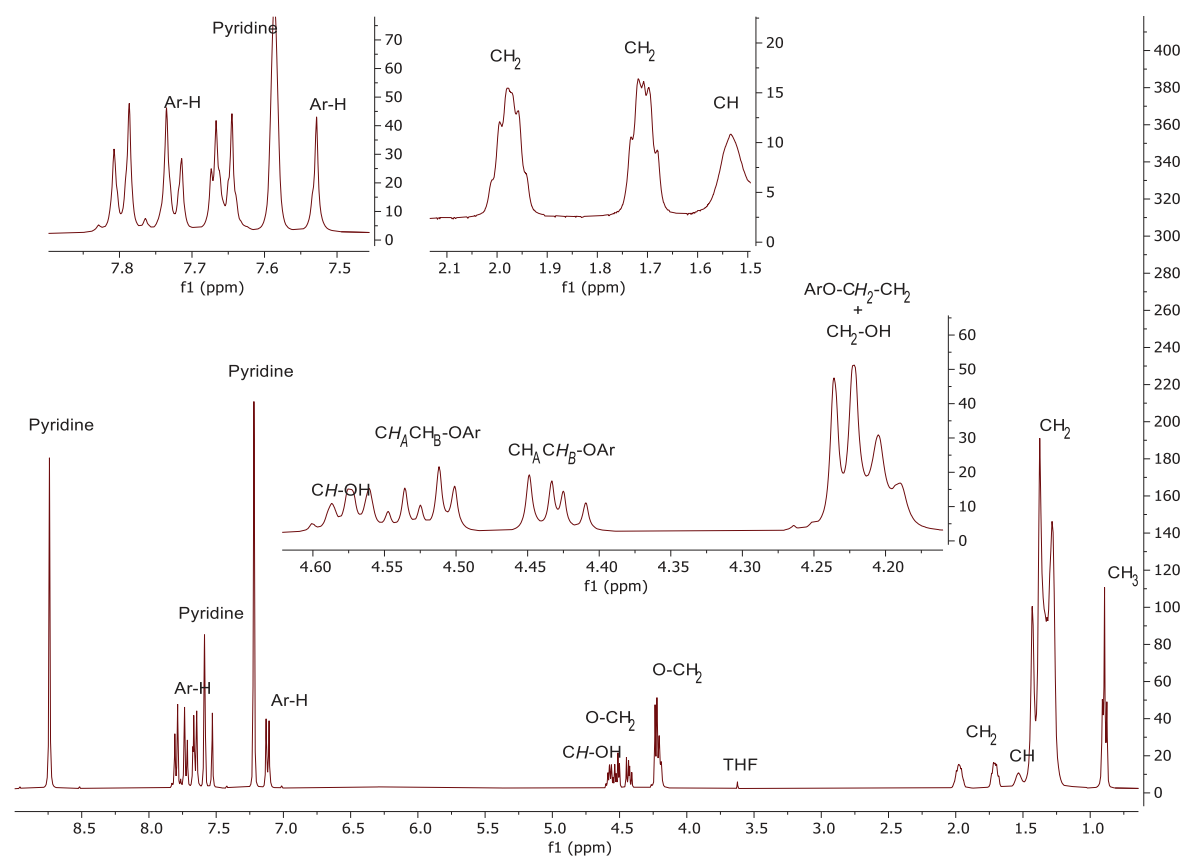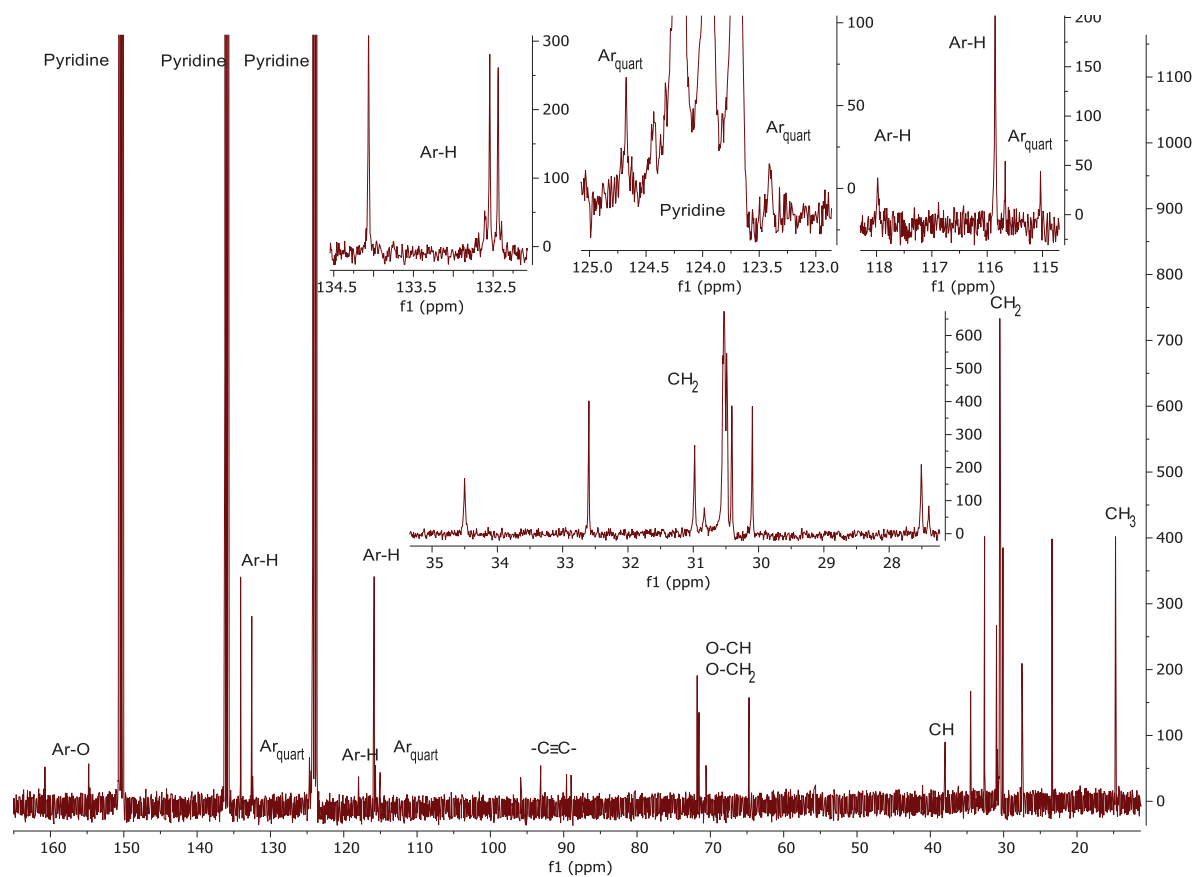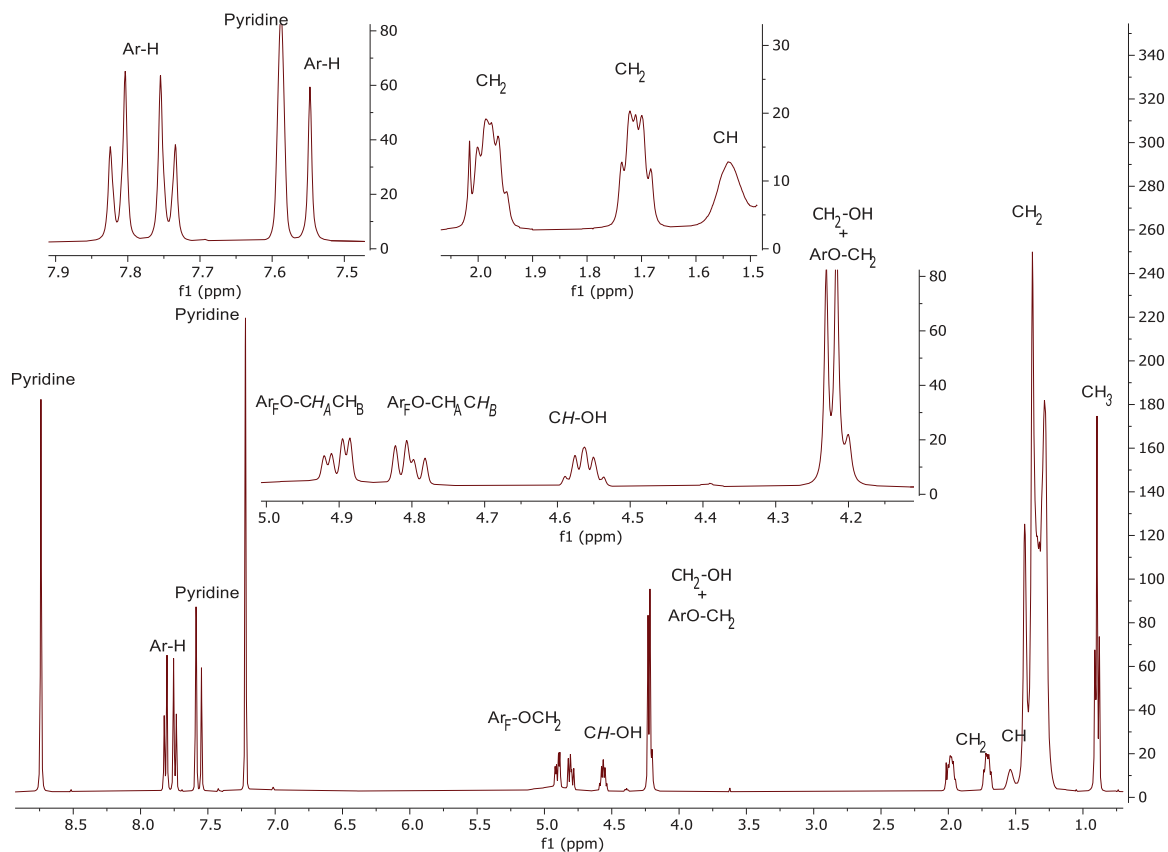**Figure S36:** ^{1}H-NMR of compound **5H3/14** (400 MHz, pyridine-d$_5$).

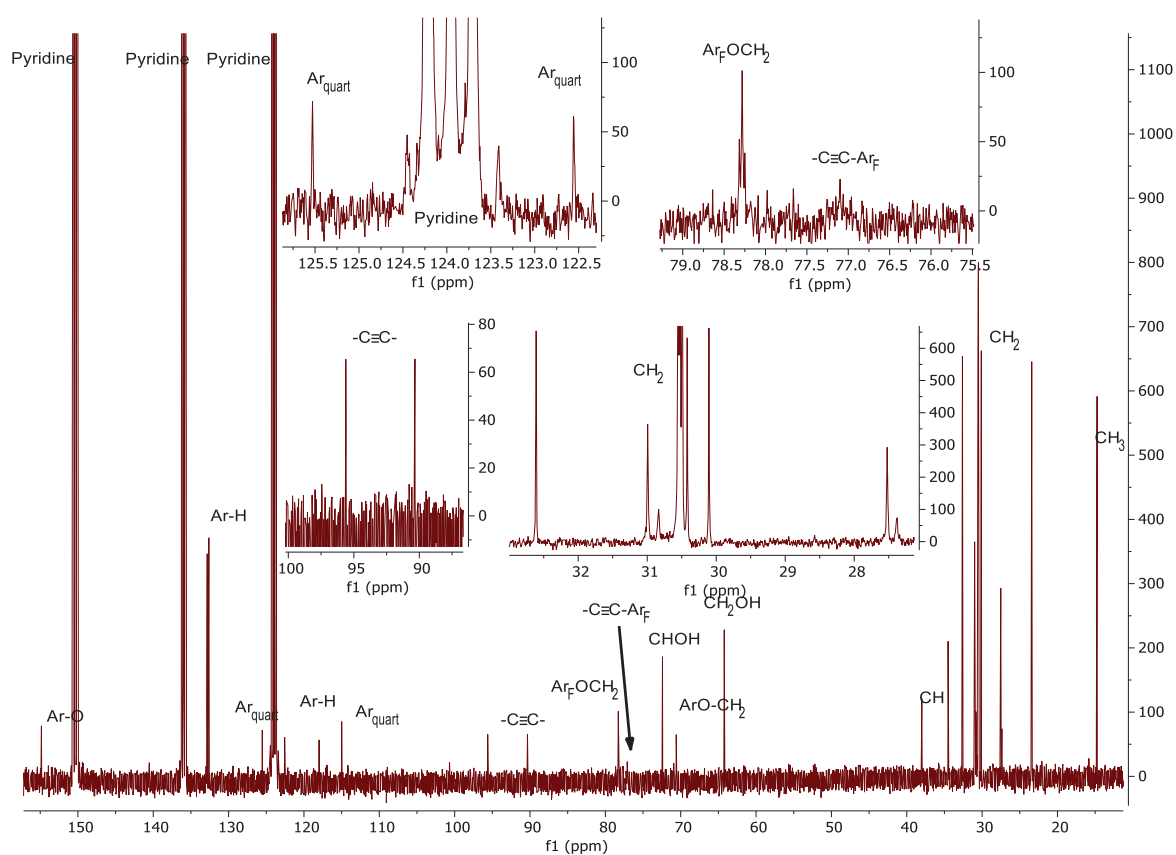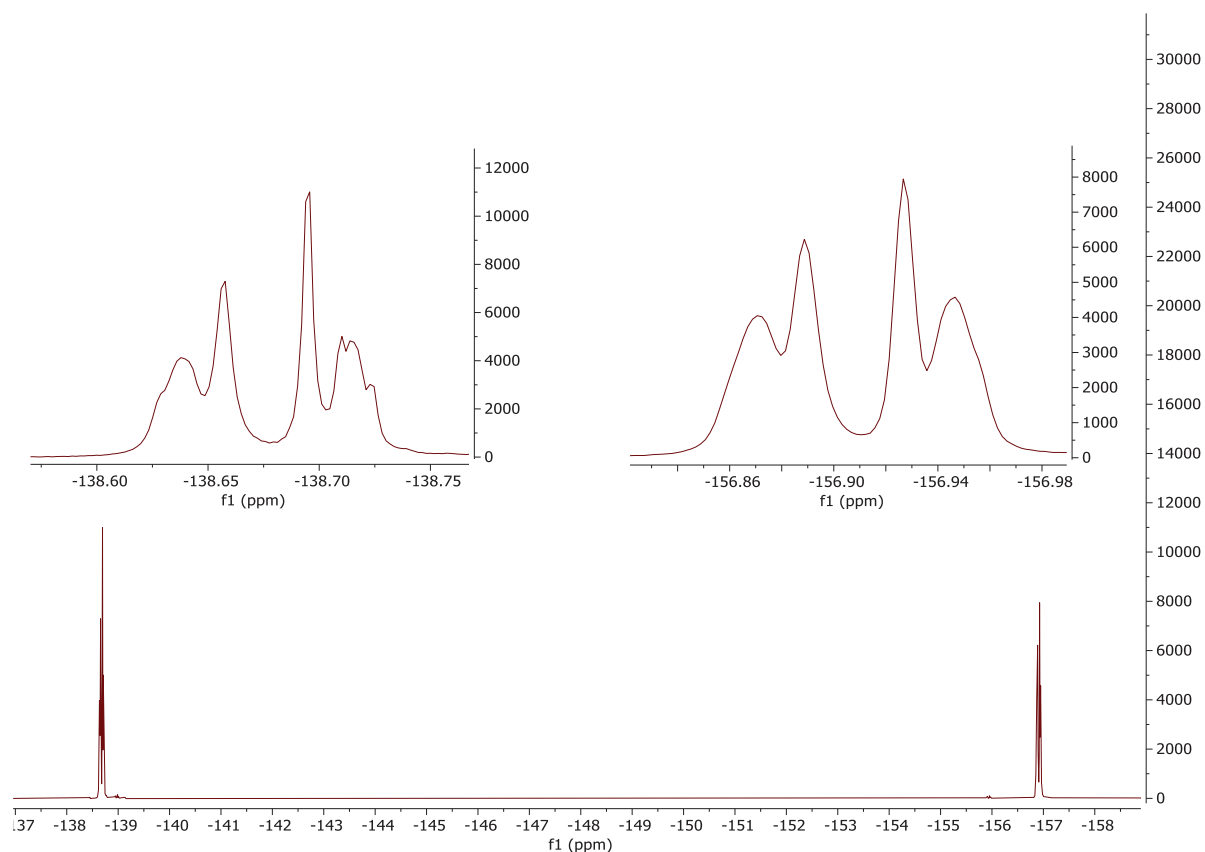**Figure S37:** ^{13}C-NMR of compound **5H3/14** (101 MHz, pyridine-d$_5$).

Figure S38: ^{19}F-NMR of compound **5F3/14** (473 MHz, pyridine-d$_5$).

Appendix-5: List of publications

5.1   Publications as first author

C. Anders, M. Wagner, M. Alaasar, M. V. Fischer, R. Waldecker, Y. Zhao, T. Tan, Y. Cao, F. Liu, C. Tschierske,
„Highly branched bolapolyphilic liquid crystals with a cubic A15 network at the triangle-square transition"
Chem. Commun., 2024, **60**, 1023 – 1026. DOI: 10.1039/D3CC05247H

C. Anders, V.-M. Fischer, T. Tan, M. Alaasar, R. Waldecker, Y. Ke, Y. Cao, F.Liu and C. Tschierske,
„Modifying the liquid crystalline chessboard tiling - Soft reticular self-assembly of side-chain fluorinated polyphiles"
J. Mater. Chem. C, 2024, Accepted Manuscript. DOI: 10.1039/D4TC04076G

C. Anders, T. Tan, V.-M. Fischer, R. Wang, M. Alaasar, R. Waldecker, Y. Cao, F. Liu, C. Tschierske,
„Engineering "meso-Atom" bonding: Honeycomb-Network Transitions in Reticular Liquid Crystals"
Aggregate, 2024, Accepted Manuscript. DOI: 10.1002/agt2.728

5.2   Publications as co author

M. Alaasar, T. Nirgude, **C. Anders**
„The influence of bromine substitution and linking groups on the phase behaviour of light-responsive rod-like molecules"
J. Mol. Liq., 2024, **414**, 126174. DOI: 10.1016/j.molliq.2024.126174

M. Alaasar, A. F. Darweesh, **C. Anders**, K. Iakoubovskii, Y. Yoshio
„Luminescent and photoconductive liquid crystalline lamellar and helical network phases of achiral polycatenars"
Mater. Adv., 2023, **5:2**, 561 – 569. DOI: 10.1039/d3ma00841j

M. Alaasar, **C. Anders**, R. Pashameah, A. F. Darweesh
„Azopyridine-based hydrogen-bonded liquid crystals with thioether tail"
Liq. Cryst., 2023, 0267 – 8292. DOI: 10.1080/02678292.2023.2253199

A. Saeed, M. Poppe, M. B. Wagner, S. Hauche, **C. Ander**s, Y. Cao, L. Zhang, C. Tschierske, F. Liu
„The rhombic honeycomb – a new mode of self-assembly in liquid crystalline soft matter"
Chem. Commun., 2022, 58, 7054 – 7057. DOI: 10.1039/d2cc01907h

Y. Cao, A. Scholte, M. Prehm, **C. Anders**, C. Chen, J. Song, G. He, C. Tschierske, F. Liu
„Understanding the Role of Trapezoids in Honeycomb Self-Assembly – Pathways between a Columnar Liquid Quasicrystal and its Liquid-Crystalline Approximants"
Angew. Chem. Int. Ed., 2024*, e202314454. DOI: 10.1002/anie.202314454*

5.3   Conference and workshop contributions

Oral presentations

1.   **C. Anders**, V. M. Fischer, Y. Cao, F. Liu, M. Alaasar, R. Waldecker, C. Tschierske, 29th International Liquid Crystal Conference, 2024, Rio Deja Nairo – Brazil.
2.   **C. Anders**, V. M. Fischer, Y. Cao, F. Liu, M. Alaasar, R. Waldecker, C. Tschierske, 50th German Liquid Crystal Conference, 2024, Essen – Germany.

Poster presentations

1.   **C. Anders**, V. M. Fischer, Y. Cao, F. Liu, M. Alaasar, R. Waldecker, C. Tschierske, 29th International Liquid Crystal Conference, **2024**, Rio Deja Nairo – Brazil.
2.   V. M. Fischer, **C. Anders**, Y. Cao, F. Liu, R. Waldecker, C. Tschierske, 50th German Liquid Crystal Conference, **2024**, Essen – Germany.
3.   **C. Anders**, V. M. Fischer, M. Alaasar, Y. Cao, F. Liu, C. Tschierske, R. Waldecker, 49th German Liquid Crystal Conference, **2023**, Stuttgart – Germany.
4.   **C. Anders**, V. M. Fischer, Y. Cao, F. Liu, C. Tschierske, R. Waldecker, 28th International Liquid Crystal Conference, **2022**, Lisbon – Portugal.

Talks and poster presentations as part of GRK2670

1.   **C. Anders**, V. M. Fischer, M. Alaasar, Y. Cau, F. Liu, C. Tschierske, R. Waldecker, *3th BEAM Redtreat*, **2024**, Dessau – Germany, Talk.
2.   **C. Anders**, V. M. Fischer, M. Alaasar, Y. Cao, F. Liu, C. Tschierske, R. Waldecker, *1st BEAM Symposium*, **2023**, Halle Saale – Germany, Talk.
3.   V. M. Fischer, **C. Anders**, M. Alaasar, Y. Cao, F. Liu, C. Tschierske, R. Waldecker, *1st BEAM Symposium*, **2023**, Halle Saale – Germany, Poster.
4.   **C. Anders**, V. M. Fischer, Ml Alaasar, R. Waldecker, C. Tschierske, *2nd Beam Retreat*, **2023**, Weimar – Germany, Talk.
5.   **C. Anders**, M. Alaasar, C. Tschierske, *2nd BEAM Progress Meeting*, **2023**, Halle Saale – Germany, Poster.
6.   **C. Anders**, V. M. Fischer, M. Alaasar, R. Waldecker, C. Tschierske, *1st BEAM Retreat*, **2022**, Dessau – Germany, Talk.
7.   **C. Anders**, C. Tschierske, *1st Beam Progress Meeting*, **2022**, Halle Saale – Germany, Poster.
8.   **C. Anders**, C. Tschierske, *1st Beam Social Kick-off Meeting*, **2021**, Halle Saale – Germany, Poster.

5.4   Research Stay:

11/2023 – 01/2024   MOE Key Laboratory for Nonequilibrium Synthesis and Modulation of Condensed Matter, School of Physics, Xi'an Jiaotong University, Xi'an 710049, P. R. China, Research group of Prof. Dr. F. Liu

Curriculum Vitae

Personal Info
Name: Christian Anders

Experience:

06/2021 – today   **Martin-Luther-University Halle-Wittenberg**
Research Assistant
- Organic synthesis of liquid crystals
- X-ray diffraction measurements on liquid crystalline materials
- Characterization of liquid crystalline materials
- Documentation and publication

02/2021 – 05/2021   **I. K. Hofmann**
Chemical laboratory by RP Compounds
- Physical test laboratory
- Measurement of physical parameters of polymers
- Density determination, melt flow index, ash content, soot distribution, test specimen tests
- Documentation and evaluation of measurement results

02/2011 – 06/2011   **Total Raffinerie Mitteldeutschland GmbH**
Chemical production Technician
- Monitoring and control of production plants
- Sampling and measurement testing of wastewater and tank farms
- Reported abnormal conditions developing during work processes
- Taking corrective measurements

08/2007 – 01/2011   **Total Raffinerie Mitteldeutschland GmbH**
Chemical production Technician
- Monitoring and control of production plants
- Sampling and measurement testing of wastewater and tank farms

Education:

06/2021 - today	**Martin-Luther-University Halle-Wittenberg** **PhD Student** - Organic synthesis of liquid crystals - X-ray diffraction measurements on liquid crystalline materials - Characterization of liquid crystalline materials - Documentation and publication
10/2018 – 02/2021	**Martin-Luther-University Halle-Wittenberg** **Master of Science Chemistry** - Specialization in organic chemistry - Master thesis: Synthesis and characterizations of silylated T-shaped bolapolyphiles - Grade of the Master's thesis: 1.1
10/2015 – 09/2018	**Martin-Luther-University Halle-Wittenberg** **Bachelor of Science Chemistry** - Bachelor thesis: Synthesis and characterizations of X-shaped bolapolyphiles - Grade of the Bachelor's thesis: 2.2
10/2014 – 09/2015	**Martin-Luther-University Halle-Wittenberg** **Bachelor of Science Physic**
07/2011 – 07/2014	**Kolleg und Abendgymnasium Halle (Saale)** **Schule des Zweiten Bildungsweges Halle (Saale)** **A-Levels** Grade of A-Levels: 2.5
08/2005 – 07/2007	**Sekundarschule August-Hermann-Francke** **Secondary school** Grad: extended secondary school graduation

Languages:

German	Native language
English	Excellent written and spoken language skills

Supervised Theses

2023	Jonathan Jende, Bachelor thesis, peer review

Eidesstattliche Erklärung

Hiermit erkläre ich, dass ich die vorliegende Arbeit selbständig und nur unter Verwendung der angegebenen Quellen und Hilfsmittel angefertigt habe.

Diese Arbeit habe ich bisher an keiner anderen Universität oder Hochschule vorgelegt und mich zu keinem früheren Zeitpunkt um den Doktorgrad beworben.

Kabelsketal, den 17.12.2024

Christian Anders